GREEN EME 2023

GREEN EME 2023

VIET NAM NATIONAL UNIVERSITY HO CHI MINH CITY
VIET NAM METEOROLOGICAL AND HYDROLOGICAL ADMINISTRATION

Proceedings of the Sixth International Scientific Conference
EARTH AND ENVIRONMENTAL SCIENCES, MINING FOR DIGITAL TRANSFORMATION, GREEN DEVELOPMENT AND RESPONSE TO GLOBAL CHANGE

SCIENCE AND TECHNICS PUBLISHING HOUSE

ORGANIZATIONS

ISBN: 978-604-67-2826-9

DO NOT SALE

THE STATE COUNCIL FOR PROFESSORSHIP
THE INTERDISCIPLINARY EARTH - MINING SCIENCES COUNCIL FOR PROFESSORSHIP

VIET NAM NATIONAL UNIVERSITY HO CHI MINH CITY

VIET NAM METEOROLOGICAL AND HYDROLOGICAL ADMINISTRATION

Proceedings of the Sixth International Scientific Conference

EARTH AND ENVIRONMENTAL SCIENCES, MINING FOR DIGITAL TRANSFORMATION, GREEN DEVELOPMENT AND RESPONSE TO GLOBAL CHANGE



GREEN EME 2023

SCIENCE AND TECHNICS PUBLISHING HOUSE

GREEN EME 2023

THE STATE COUNCIL FOR PROFESSORSHIP
THE INTERDISCIPLINARY EARTH - MINING SCIENCES COUNCIL FOR PROFESSORSHIP

VIET NAM NATIONAL UNIVERSITY HO CHI MINH CITY

VIET NAM METEOROLOGICAL AND HYDROLOGICAL ADMINISTRATION

Proceedings of the Sixth International Scientific Conference

EARTH AND ENVIRONMENTAL SCIENCES, MINING FOR DIGITAL TRANSFORMATION, GREEN DEVELOPMENT AND RESPONSE TO GLOBAL CHANGE

SCIENCE AND TECHNICS PUBLISHING HOUSE

FOREWORD

The fields of Earth, Mines, and Environmental sciences (EME) have emerged and evolved alongside with the evolution of human society, and have created a profound impact on all aspects of life and socio-economic development through utilizing natural resources, impacting the environment, and driving global change. The robust development of these areas serves as the foundation for various other fundamental and applied sciences, and concurrently act as a catalyst for technological advancements worldwide, contributing to the common prosperity and safety of humankind as well as the conservation of the blue Earth.

Global change, rapid development of science and technology, and the fourth industrial revolution (Industry 4.0) create many opportunities and challenges for sustainable development. Vietnam, being one of the most vulnerable countries to climate change and natural disasters, is devoting great efforts to achieve sustainable development goals and achieve net zero emissions by 2050 as well as to improve productivity and national competitiveness. In this context, innovation, digital transformation in training, basic and applied research on EME become more urgent than ever for green, circular development and response to global change, sustainable development, prosperity, and safety of the country, the region and the world.

Against such considerations, Viet Nam National University Ho Chi Minh City, in collaboration with Viet Nam Meteorological and Hydrological Administration, the Interdisciplinary Council for Professorship of Earth - Mining Sciences, as well as various research institutes and local and international higher education institutions, jointly co-organizes the International Conference "Earth Science, Mining, Environment for Digital Transformation, Green Development, Circular Growth, and Response to Global Change" (GREEN EME 2023).

The GREEN EME 2023 is a forum for scientists, administrators, and businesses, who are passionate about Earth Science and Environment, Mining (EME) to meet, present and share their research findings, to engage in discussions, and to exchange solutions for a wide range of overall academic issues in these fields. The specific objectives include:

- Publishing outstanding research results and sharing, replicating achievements and experiences in innovation and digital transformation in fundamental and applied research and technology development in Earth Science, Mining, Environment, and related fields in

order to advance economic efficiency, national competitiveness, sustainable development, national, regional and international safety.

- Proposing solutions to promote innovation in the fields of Earth Science, Mining, and Environment (institutions, policies, promoting educational science and technology, training of high-quality human resource, digital transformation, engagement, and enhancing collaboration with stakeholders, etc.) to meet the requirements of green, circular growth, and response to global changes.

During the preparation for GREEN EME 2023, the Organizing Committee has received 86 scientific manuscripts. After a rigorous reviewing process, 30 highly valued articles were selected for publication in the conference proceedings and other 22 articles will be published in the "IOP Conference Series: Earth and Environmental Science". The Organizing Committee highly appreciates the efforts of the Editorial Board, domestic and international scientists and experts in either submitting their manuscripts or contributing valuable time to review and editing the articles. We would also like to thank the Secretariat for their efforts in preparing and organizing the conference as well as the sponsors for their important contribution. We believe that the GREEN EME 2023 will be successful and all the participants will have opportunities to meet, exchange ideas, and collaborate to propose sustainable development goals for the development of EME sectors.

GREEN EME 2023 CONFERENCE ORGANIZING COMMITTEE

Steering Committee	
Assoc. Prof. Dr. Vu Hai Quan	Chancellor of Viet Nam National University, Ho Chi Minh City
Prof. Dr. Tran Hong Thai	Deputy Minister of Ministry of Science and Technology
International Scientific Committee	
Chairs:	
Prof. Dr. Mai Trong Nhuan	University of Science, Viet Nam National University (VNU), Ha Noi, Chairman of the Council of Interdisciplinary Professors Earth Science and Mining (EME)
Prof. Dr. Le Thanh Hai	Institute for Environment and Resources, Viet Nam National University, Ho Chi Minh City
Prof. Dr. Tran Hong Thai	Viet Nam Meteorological and Hydrological Administration, Ministry of Natural Resources and Environment (MONRE)
Associate chairperson and members:	
Prof. Dr. Tran Thanh Hai	President of Hanoi University of Mining and Geology
Prof. Dr of Science. Pham Hoang Hai	Institute of Geography, Viet Nam Academy of Science and Technology (VAST)
Prof. Dr. Nguyen Van Phuoc	Chairman of Ho Chi Minh City Union of Science and Technology Associations
Prof. Dr. Nguyen Phuoc Dan	Faculty of Civil Engineering, Ho Chi Minh City University of Technology, VNUHCM
Prof. Dr. James Shulmeister	Canterbury University, New Zealand
Prof. Dr. Ken Fukushi	Tokyo University, Japan
Prof. Dr. Nobuo Mimura	Ibaraki University, Japan
Prof. Dr. Carsten Drebenstedt	Freiberg University of Mining and Technology, Germany
Prof. Dr. Katsuaki Koike	Kyoto University, Japan

Prof. Dr. Jaecheol Nam	Korea Meteorological Administration - KMA
Prof. Dr. Kei Yoshimura	Tokyo University, Japan
Dr. Ji Whan Ahn	Korea Institute of Geoscience and Mineral Resources - KIGAM
Prof. Dr. Ngo Huu Hao	University of Technology Sydney (UTS), Australia
Assoc Prof. Dr. Tran Minh Triet	Vice-Rector of Ho Chi Minh City University of Science, VNUHCM
Assoc Prof. Dr. Lam Quang Vinh	Director of Department of Science and Technology, VNUHCM
Assoc Prof. Dr. Nguyen Thi Hoai Nga	Head of International Office, Hanoi University of Mining and Geology
Assoc. Prof. Dr. Vo Le Phu	Faculty of Environment and Natural Resources, Ho Chi Minh City University of Technology (VNUHCM)
Prof. Dr. Bui Xuan Nam	Hanoi University of Mining and Geology
Assoc Prof. Dr. Doan Quang Tri	Deputy Director of Information and Data Center/Acting Editor-in-Chief at Journal of Hydro-Meteorology
Assoc Prof. Dr. Nguyen Van Cong	Dean of College of Environment and Natural Resources, Can Tho University
Assoc Prof. Dr. Vo Van Minh	Faculty of Biology & Environmental Science, The University of Education, Danang University
Assoc Prof. Dr. Nguyen Manh Khai	Dean of Faculty of Environmental Sciences, University of Science, VNU-HUS
Dr. Ngo Thi Thu Trang	Dean of Faculty of Geology, Ho Chi Minh City University of Social Sciences and Humanities, VNUHCM
Dr. Nguyen Thi Thuy	Vice-Dean of School of Chemical and Environmental Engineering, International University, VNUHCM
Assoc. Prof. Dr. Nguyen Hong Quan	Institute for Circular Economy Development, VNUHCM
Assoc. Prof. Dr. Chau Nguyen Xuan Quang	Institute for Environment and Resources, VNUHCM

Assoc. Prof. Dr. Dao Nguyen Khoi	Faculty of Environment, Ho Chi Minh City University of Science, VNUHCM
Assoc. Prof. Dr. Pham Trung Hieu	Faculty of Geology, Ho Chi Minh City University of Science, VNUHCM
Dr. Bui Trong Vinh	Faculty of Petroleum Geology, Ho Chi Minh City University of Technology, VNUHCM
Dr. Nguyen Tran Nhan Tanh	Climate Change Institute, An Giang University, VNUHCM
Prof. Dr. Truong Quang Hai	Institute of Vietnamese Studies and Development Science, Viet Nam National University, Ha Noi
Prof. Dr. Vo Trong Hung	Hanoi University of Mining and Geology
Prof. Dr. Tran Nghi	Viet Nam Union of Geological Sciences, Viet Nam Union of Science and Technology Associations
Prof. Dr. Bui Cong Que	Viet Nam Association of Geophysicists, Viet Nam Union of Science and Technology Associations
Prof. Dr. Tran Duc Thanh	Institute of Marine Environment and Resources, Viet Nam Academy of Science and Technology
Prof. Dr. Tran Tan Tien	Center for Science, Technology, Meteorology, Hydrology and Environment, Viet Nam Union of Science and Technology Associations
Conference Organizing Committee	
Chair:	
Assoc. Prof. Dr. Lam Quang Vinh	Director of Department of Science and Technology, VNUHCM
Members:	
Assoc. Prof. Dr. Nguyen Dinh Tu	Director of VNUHCM Office, VNUHCM
Dr. Bui Thi Hong Hanh	Director of Department of External relations and Project development, VNUHCM
Assoc Prof. Nguyen Van Hieu	Deputy-Director of Department of Science and Technology, VNUHCM
Assoc Prof. Huynh Thanh Cong	Deputy-Director, Department of Science and Technology, VNUHCM

Assoc Prof. Nguyen Nhat Huy	Vice-Dean of Faculty of Environment and Natural resources, Ho Chi Minh City University of Technology, VNUHCM
Assoc Prof. Doan Quang Tri	Deputy Director of Information and Data Center/Acting Editor-in-Chief at Journal of Hydro-Meteorology
Dr. Do Thi Thu Huyen	Head of Department of Science Management and External Relations, Institute for Environment and Resources, VNUHCM
Conference Secretariat	
MS. Tran Quoc Phong	Head of Organization – Administration Department, VNUHCM Office
MS. Tran Tuan Phuong	Head of Communications Department, VNUHCM Office, VNUHCM
MS. Cao Minh Tam	Head of Communications and Corporate Relations, VNUHCM Development Fund, VNUHCM
Mr. Ngo Thanh Nam	Head of Equipment Management Department, VNUHCM Office
Ms. Tran Thi Nhung	Head of Planning and Finance Department, VNUHCM Office
Ms. Le Thi Hong My	Chief Accountant of VNUHCM Development Fund
Dr. Le Thi Quynh Ha	Expert of Department of Science and Technology, VNUHCM
MS. Bùi Phương Anh	Senior expert, Department of Science and Technology, VNUHCM
MS. Phan Thi Huong	Expert of Department of Science and Technology, VNUHCM
MS. Nguyen Thi Bich Thi	Expert of Department of Science and Technology, VNUHCM

Table of Contents

Page

Foreword iii

DIGITAL TRANSFORMATION AND TECHNOLOGY IN EARTH, MINING AND ENVIRONMENTAL SCIENCES (BIG DATA, ML, AND AI)

Application of Cluster Analysis (CA) and Principle Component Analysis (PCA) for surface water quality assessment on main rivers of mining districts in Lao Cai province 3

Cuc Nguyen Thi and Hoa Nguyen Anh

Research on behavior of rock/soil mass during underground parking excavation in multi-layered soils in urban areas 15

Dang Van Kien, FORNONI Benjamin, Mai Xuan Thanh Tuan, Doan Quang Tri, Nguyen Khoa Linh

Identifying solutions for enhancing electrical safety in underground mines by analyzing parameters influence on leakage current 28

Le Xuan Thanh, Nguyen Dinh Tien

Spatial-temporal convolution neural networks for tropical cyclone detection from geostationary satellite images 38

L Q Dao, T H Hoang, L V Hung, B Q Hung, L R Hole, P T Hang, M K Hung and D D Tien

Prediction of Specific Charge in Tunnel Blasting 45

Nguyen Chi Thanh, Nguyen Viet Nghia

Research on the biodiversity and landscape values for the development of green tourism linked to experiential activities in the Kon Ha Nung Plateau Biosphere Reserve, Gia Lai province 56

Nguyen Huu Xuan, Nguyen Trong Doi, Nguyen Thi Huyen

Developing a three-dimensional model of the open pit mine and the industrial yard of nui Beo coal mine 70

Nguyen Quoc Long, Luu The Anh, Bui Ngoc Quy, Le Thi Thu Ha, Le Van Canh, Pham Van Chung

Research on application of electric submersible pumps to increase oil recovery field Y, lot 05-1a, the Nam Con Son basin 79

Nguyen Thi Minh Thu , Pham Nguyen Duy Phuong and Huynh Tan Tuan

Microplastic pollution in aqueous environment at coastal areas in Ha Long and Cam Pha cities, Quang Ninh province, Viet Nam 94

P H Son, T T Cuong, P A Hung, V D Tuan, T V Thuy, N H Huan, N X Hai and P T Thuy

Monitoring land surface temperature by integrating landsat 8 and sentinel 2 in Dau Tieng district, Binh Duong province 103

Phuong Ha Tran, Tuan Cuong Ha, Thi Thuy Huong Nguyen, Ngoc Thy Nguyen, Duong Ba Man, Tuan Nhi Pham

Preliminarily applying Microsoft Azure AI Custom Vision to classify image data of the rice growth stage 113

T-D Ha and O T N Bui

Utilizing remote sensing and GIS to design a database of road transpotation in Thanh Hoa province of Vietnam: A pilot in Dong Son and Thieu Hoa district 119

Thao Vu Thi Phuong, Ha Le Thi, Thao Do Thi Phuong

SUSTAINABLE AND GREEN ENERGY TRANSITION CIRCULAR ECONOMY IN RESOURCE-MINERAL MANAGEMENT AND SUSTAINABLE DEVELOPMENT

(Wind power, solar power, gas power, geothermal, garbage power, hydrogen, etc.; low carbon emission technologies; resource-mineral management and sustainable development)

Research to identify types of microplastics, their shapes, and trends over space and time, and to propose solutions to reduce microplastic pollution from plastic waste in the surface water of the Saigon - Dong Nai River, Vietnam 132

Han H T N, Phu H, Hue N T

The optimal solution for domestic water on the Dongvan karst plateau, Hagiang, Vietnam 146

Le Canh Tuan, Pham Trung Hieu, Cao Minh Thuỷ

Formula for assessing the loading capacity of the tourism environment and results of applying the world natural heritage Phong Nha - Ke Bang area, Vietnam 152

Le Nam, Tran Nghi, Dinh Xuan Thanh, Trinh Hoai Thu, Nguyen Dinh Thai, Dao Bui Dinh

Marine landscape analysis for resource management and biodiversity conservation in Truong Sa Islands, Vietnam 164

Nguyen Dang Hoi, Nguyen Cao Huan, Ngo Trung Dung, Phan Dong Pha and Vu Le Phuong

CLIMATE CHANGE AND DISASTER MITIGATIONINNOVATION MEASURES FOR EARTH, MINING AND ENVIRONMENTAL SCIENCES (innovative measures for earth, mining and environment sciences to meet sustainable development goals)

Flood Early Warning Systems in Ho Chi Minh City, Vietnam: Current Status, Challenges and Way Ahead 180

Anh Cao, Vo Le Phu, Luu Dinh Hiep, Nguyen Danh Thao, Yoshimura Kei

The status of karst springs degradation in the water-scarce high mountain areas of Northern Vietnam and solutions to management for sustainable development 194

Dao Duc Bang, Tran Thi Thanh Thuy, Nguyen Van Trai, Nguyen Minh Viet, Vu Thu Hien and Duong Thi Thanh Thuy

Assessment of marine pollution loads from land-based activities: A case study in Hai An district, Hai Phong city 204

Dao Van Hien, Nguyen Thi Ngoc Huong, Nguyen Manh Khai and Bui Dac Thuyet

Application of deep learning and remote sensing to assess the riverbank change: A case study at Nhat Le river mouth, Vietnam 215

Doan Quang Tri, Nguyen Van Nhat and Vu Dinh Cuong

Inventory of Landslides Triggered by Extreme Rainfall in August 2023 along the National Road No. 32, Mu Cang Chai district, Yen Bai province 227

Duong Thi Toan, Oneta Soulinthone, Nguyen Trung Thanh, Nguyen Viet Ha, Dang Quang Khang, Bui Van Dong, Do Minh Duc

Monitoring land cover change based on multi-scale analysis: A case study in Lao Cai province, Vietnam 240

Hoang Thi Thu Huong, Vu Kim Chi, Anton Van Rompaey

Applying 3D geospatial data and proposed solutions to support the administration, management, and monitoring of coastal smart cities adapting to climate change in Vietnam 261

L T T Ha, N V Trung, N Q Long

Coupled evaluation of polymer-cement modified soil mixture used for the improvement of haul road performance at a coal mining site 270

Lam Phuc Dao, Hung Trong Vo, Manh Van Nguyen, Thuc Van Luu, Tuoc Ngoc Do, Khoa Cong Dam, Piotr Osinski and Duc Van Bui

Shoreline changes from Quang Ninh to Thai Binh in the period 1987 to 2021 using GIS technology and remote sensing data 280

Nguyen Thi Anh Nguyet, Tran Tuan Duong, Nguyen Dac Ve, Tran Anh Tuan, Pham Viet Hong

Interaction of surge and wave on strong/super typhoon in the northern coastal area of Vietnam 292

Pham Van Tien, Nguyen Ba Thuy, Pham Khanh Ngoc, Bui Manh Ha, Vu Hai Dang, Nguyen Kim Cuong, Nguyen Viet Hang

Prediction of incremental cases of death due to high temperature in Ho Chi Minh City, Vietnam based on RCP4.5 and RCP8.5 scenarios 303

Phung Duc Nhat, Tran Ngoc Dang, Duong Thi Minh Tam, Dang Van Chinh, Phu L Vo

Data processing in analysing landslide in the mountainous area by geodetic methods 312

Quoc Khanh Pham and Thi Kim Thanh Nguyen

Monitoring environmental reclamation at coal mines in the territory of Ha Long City using Landsat data 320

Quyet Chien Nguyen, Vu Khac Dang, Thi Anh Cuc Nguyen, Thi Huong Giang Chu, Quynh Trang Phung

Identification of weighting event caused by underground coal mining at Quang Ninh coal field, Vietnam 338

T D Le and P H Nguyen

Determination of the rock pressure by numerical modeling method when digging roadways under the open-pit mine area at the Ha Lam Coal Mine, Quangninh 346

Tien Trung Vu, Doan Viet Dao, Son Anh Do

Managing environmental conflicts for sustainable tourism development 357

Tran Duy Minh

Assessment of oil degrading ability in drilling mud by biosurfactants of strain Brevibacterian celere 365

Tran Thi Thu Huong

DIGITAL TRANSFORMATION AND TECHNOLOGY IN EARTH, MINING AND ENVIRONMENTAL SCIENCES (Big Data, ML, and AI)

APPLICATION OF CLUSTER ANALYSIS (CA) AND PRINCIPLE COMPONENT ANALYSIS (PCA) FOR SURFACE WATER QUALITY ASSESSMENT ON MAIN RIVERS OF MINING DISTRICTS IN LAO CAI PROVINCE

Cuc Nguyen Thi[1,2] and Hoa Nguyen Anh[1]

[1] Ha Noi University of Mining and Geology; [2] PhD HUS, VNU - University of Science

E-mail: nguyencuc.humg@gmail.com

Abstract: This research aims at investigating the application of cluster analysis (CA), principal component analysis (PCA) methods and WQI index to evaluate and group surface water quality in rivers and streams flowing through copper, gold, and apatite ore mining and processing areas in Lao Cai Province. The results show that the 8 rivers and streams included in the evaluation include Chan stream, Nam Xay stream (flowing through Minh Luong gold mine), Ngoi Duong stream, Dong Ho stream and Chu O stream (flowing through Apatite mine), Ngoi Phat stream , Red River (flowing through Sin Quyen Copper mine), Khe Chom stream (flowing through apatite processing factory - Tang Loong industrial park) can be divided into 3 main groups. Group 1 has a total explained variance of 61.9%, including Chan stream and Nam Xay stream. The characteristics of surface water in this cluster are copper (Cu) content, TSS suspended solids content and BOD_5 and COD content. Group 2 has a total explained variance of 27.5% including S. O, S. Dong Ho, S.Hong, S. Ngoi Duong, S. Ngoi Phat flowing through the copper and apatite mining and processing area. The surface water quality characteristics in this group are TSS suspended solids content and copper (Cu) content. Group 3 is Khe Chom stream with the characteristic content of iron (Fe), PO_4^{3-}, NH_4^+ and NO_2^- The results of cluster analysis (CA) and principal component analysis (PCA) also show that the surface water quality is greatly affected by dust emitted during the mining process, shown by the very high TSS suspended solids content. In contrast, the surface water quality in the processing area is mainly affected by the chemical composition of the ore, shown by the relatively high PO_4^{3+} content at Khe Chom stream. The quality of surface water on rivers and streams flowing through the mining and mineral processing area of Lao Cai province is average to good, as shown by the results of calculating the WQI index mainly ranging from 50 to 90. In which, Khe Chom stream flowing through the apatite ore processing area has poorer quality than the quality of the remaining rivers and streams due to the influence of PO_4^{3-}, NH_4^+ and NO_2^- components. Meanwhile, surface water quality in rivers and streams flowing through the mining area is mainly affected by total suspended solids (TSS).

1. INTRODUCTION

In recent years, statistical analysis methods were used widely in environmental applications, including assessments and monitoring of quality variation groundwater, surface water, testing results water quality forcast model in space and time, determine the chemical factors involved to hydrological conditions, and evaluate indicators environmental quality. PCA and CA methods belong to the group of multivariate statistical analysis methods that are increasingly widely applied in many environmental fields such as assessing changes in environmental quality over space and time, interpreting relationships between environmental components and pollution sources. In China [1], Turkey [2], Brazil [3], India [4], these studies used combination of cluster analysis (CA), principal component analysis

(PCA) to assess quality and interpretation of sources of surface and underground water pollution in river basins based on the relationship between monitoring parameters and aquifer characteristics, thereby proposing typical parameters water quality for effective monitoring and management. In Vietnam, Nguyen Hai Au, Phan Nguyễn Hồng Ngọc, 2017 [5,6] used PCA and CA methods to determine the spatial and temporal variation of groundwater quality in Tan Thanh district, Ba Ria - Vung Tau province. Le Van Du, 2019 [7] using PCA and CA analysis methods to evalution surface water quality according to soil depth in U Minh Ha - Ca Mau national forest. Nguyen Phương, 2020 [8] applied PCA and CA methods to assess the level of heavy metal pollution in soil and surface water in copper and apatite ore mining areas, Lao Cai. The research results allow quality clustering, identifying the main components of each cluster and explaining the causes of differences between clusters. Results of processing environmental data using multivariate statistical analysis to extract necessary information, helping to improve the effectiveness of environmental management.

Mineral mining and processing is one of the main industrial activities in Lao Cai province. Besides economic benefits, the quality of surface water in rivers and streams flowing through or adjacent to mineral exploitation and processing areas is also more or less affected. The results of calculating the water quality index WQI on 8 main rivers and streams flowing through the mining and mineral processing area of Lao Cai province in 2022 show that water quality variation strongly from very heavy pollution levels (WQI=8) to very good (WQI = 93), mainly in the average and good range (WQI ≥ 50-90). In which, surface water is mainly affected by suspended solids (TSS), to a lesser extent NH_4^+, NO_2^-, PO_4^{3-}, COD and BOD_5. Heavy metal components in water such as Cd are mainly < 0.001mg/l; Lead (Pb) ranges from 0.002 to 0.029 mg/l; Zinc (Zn) ranges from 0.020 to 0.089 mg/l and does not affect human health according to QCVN 08:2023/BTNMT standards. Copper (Cu) and iron (Fe) content are locally high in some rivers and streams flowing through copper and apatite mining areas. Specifically, copper (Cu) ranges from 0.028 to 0.220 mg/l and iron (Fe) content ranges from 0.05 to 1.421 g/l.

This study applies cluster analysis (CA), principal component analysis (PCA) methods and WQI index to evaluate the quality and clustering of surface water quality on some main rivers and streams in mineral exploitation and processing areas in Lao Cai Province. This method would determine the typical components for each cluster, explain the causes as a basis for providing solutions to improve the quality of surface water environment in the study area.

2. MATERIAL AND METHODOLOGIES

2.1. Material

The object evaluated in the study is the surface water in rivers and streams flowing through the apatite, copper, gold mining area and Tang Loong industrial park (Figure 1). Specifically:

- Khe Chom Stream behind the apatite ore processing factory in Tang Loong industrial park, Bao Thang district, Lao Cai province.

- Ngoi Duong, Dong Ho, and O streams flow through apatite mine, Bat Xat district, Lao Cai city, Lao Cai province.

- Red River and Ngoi Phat stream flow through Sin Quyen copper mine, Bat Xat district, Lao Cai province.

- Suoi Chan and Nam Xay flow through Minh Luong gold mine, Van Ban district, Lao Cai province.

The data used for analysis are the results of continuous monitoring from 2017 to 2022 which were collected from the Lao Cai Provincial Monitoring Center in the months of March, May, August and November [9]. Statistical parameters including average value, maximum value, minimum value, standard deviation and coefficient of variation of observed parameters are summarized in Table 1.

Table 1. Summary of results of water quality parameters in the study area

River/Stream	Parameters	*COD*	BOD_5	*TSS*	*Cu*	*Fe*	NH_4^+	NO_2^-	PO_4^{3-}
Chan	Mean (mg/l)	26.6	11.2	32.8	0.052	0.616	0.279	0.040	0.074
	Standard Deviation	12.8	4.9	37.4	0.061	0.282	0.224	0.039	0.075
	Minimum (mg/l)	8.3	4.0	3.4	0.006	0.087	0.040	0.003	0.004
	Maximum (mg/l)	60.5	24.4	202.3	0.220	1.310	0.894	0.137	0.260
	Coefficient of variation (%)	**48.3**	**43.6**	**114.0**	**118.0**	**45.8**	**80.2**	**96.1**	**101.5**
Khe Chom	Mean (mg/l)	27.0	11.0	40.2	0.043	1.656	2.185	0.468	1.577
	Standard Deviation	11.9	5.4	34.8	0.036	2.079	2.933	0.354	1.824
	Minimum (mg/l)	4.4	2.1	12.2	0.006	0.106	0.136	0.062	0.007
	Maximum (mg/l)	58.6	26.7	158.3	0.133	8.560	12.400	1.230	6.330
	Coefficient of variation (%)	**44.2**	**49.2**	**86.5**	**83.9**	**125.6**	**134.3**	**75.8**	**115.7**
Nam Xay	Mean (mg/l)	23.6	10.1	26.0	0.043	0.609	0.221	0.031	0.095
	Standard Deviation	12.6	4.9	11.8	0.032	0.216	0.167	0.028	0.095
	Minimum (mg/l)	3.0	1.0	4.6	0.008	0.274	0.042	0.003	0.019
	Maximum (mg/l)	46.0	19.2	48.6	0.126	0.960	0.740	0.100	0.325
	Coefficient of variation (%)	**53.2**	**48.7**	**45.4**	**73.7**	**35.6**	**75.5**	**87.7**	**99.3**
Chu O	Mean (mg/l)	17.6	7.1	47.7	0.037	0.507	0.242	0.036	0.085
	Standard Deviation	7.5	3.5	18.4	0.015	0.285	0.229	0.049	0.116
	Minimum (mg/l)	7.6	2.4	17.6	0.010	0.050	0.015	0.003	0.023
	Maximum (mg/l)	46.2	17.4	85.0	0.071	1.185	0.885	0.251	0.540
	Coefficient of variation (%)	**42.6**	**48.7**	**38.7**	**39.6**	**56.2**	**94.7**	**136.7**	**137.3**
Dong Ho	Mean (mg/l)	16.9	6.9	43.5	0.037	0.447	0.239	0.028	0.073
	Standard Deviation	5.0	2.8	19.9	0.017	0.286	0.227	0.026	0.093
	Minimum (mg/l)	8.0	3.2	10.0	0.010	0.050	0.056	0.003	0.034
	Maximum (mg/l)	25.4	13.7	100.0	0.094	1.250	1.160	0.134	0.485
	Coefficient of variation (%)	**29.4**	**41.3**	**45.8**	**47.4**	**63.9**	**95.1**	**95.2**	**127.4**
Hong	Mean (mg/l)	18.8	6.9	44.4	0.042	0.262	0.186	0.043	0.047
	Standard Deviation	7.1	3.9	20.7	0.032	0.235	0.168	0.043	0.045

	Minimum (mg/l)	6.8	3.4	22.0	0.012	0.034	0.035	0.008	0.010
	Maximum (mg/l)	38.2	16.8	132.4	0.140	1.039	0.754	0.162	0.190
	Coefficient of variation (%)	**37.8**	**55.7**	**46.8**	**76.7**	**89.7**	**90.4**	**100.0**	**93.8**
Ngoi Duong	Mean (mg/l)	20.0	7.8	57.0	0.039	0.514	0.257	0.024	0.045
	Standard Deviation	4.3	3.2	44.1	0.019	0.291	0.283	0.011	0.022
	Minimum (mg/l)	11.2	2.7	21.7	0.010	0.050	0.036	0.008	0.010
	Maximum (mg/l)	30.0	14.6	222.0	0.104	0.950	1.350	0.055	0.096
	Coefficient of variation	**21.7**	**41.1**	**77.4**	**49.2**	**56.7**	**110.4**	**47.0**	**47.9**
Ngoi Phat	Mean (mg/l)	17.5	6.6	35.6	0.046	0.260	0.148	0.023	0.039
	Standard Deviation	6.9	3.9	13.9	0.033	0.297	0.140	0.012	0.031
	Minimum (mg/l)	5.2	2.4	18.5	0.014	0.055	0.036	0.003	0.011
	Maximum (mg/l)	32.6	15.4	90.8	0.167	1.421	0.730	0.060	0.160
	Coefficient of variation (%)	39.3	58.4	39.0	72.8	114.3	94.4	52.3	78.1
QCVN 08:2023/BTNMT, column A		**≤ 10**	**≤ 4**	**≤ 25**	-	-	-	-	-
QCVN 08:2023/BTNMT, column B		**≤ 15**	**≤ 6**	**≤ 100**	-	-	-	-	-

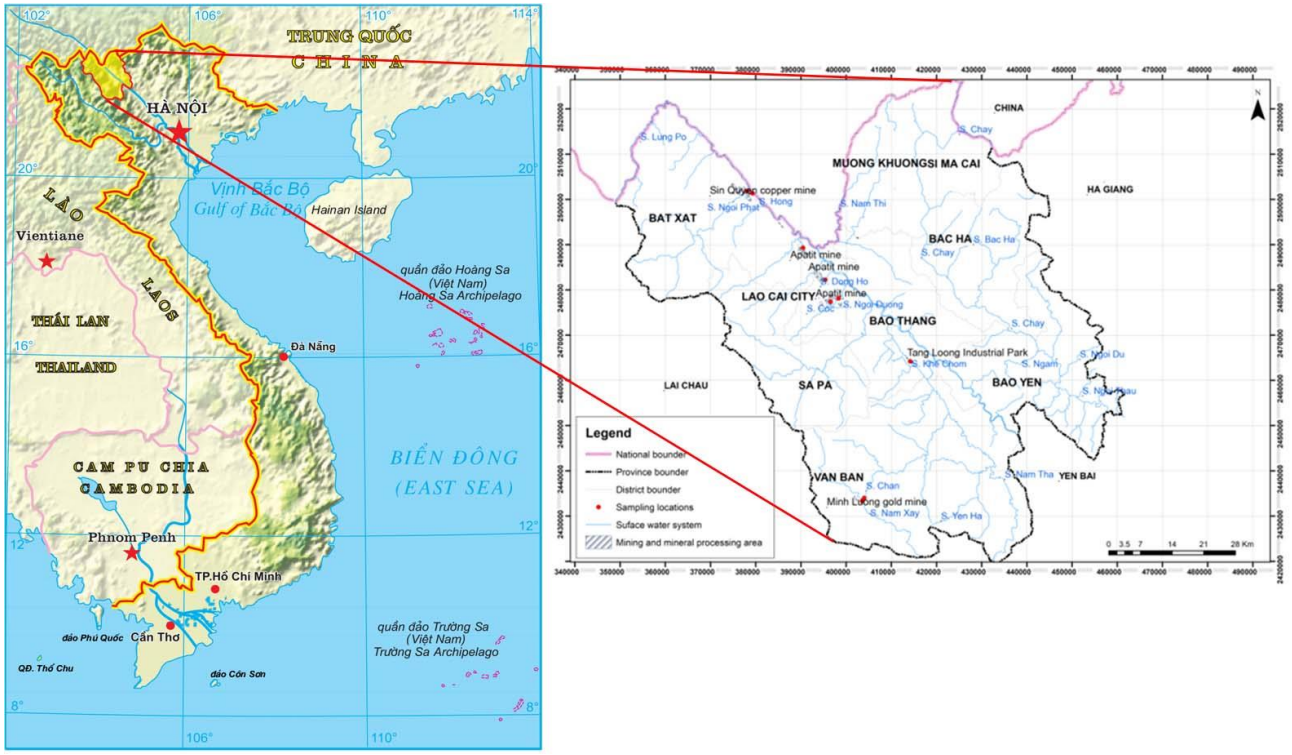


Figure 1. *Location of mineral mining and processing, Lao Cai province*

The results of statistical processing of 184 surface water samples taken from 8 rivers and streams flowing through copper, gold and apatite mining and processing areas from 2017 to 2022 show that the average value of the content of NH_4^+, NO_2^-, PO_4^{3-}on the stream flowing through the apatite processing factory (Khe Chom stream) is very high. In contrast, in streams flowing through copper, apatite, and gold ore mining areas, the TSS suspended solids content is higher than in processing areas. Surface water is polluted mainly by TSS,

COD and BOD_5 content. The TSS content ranges from 3.4 g/ml to 222 mg/l; however, in some samples the TSS content exceeds 8 times the standard 08:2003/BTNMT in column A and exceeds 2 times the standard in column B. The COD content ranges from 3mg/l to 60.5mg/l but some samples exceed 2 to 6 times the standard 08:2003/BTNMT in column A and exceed 1.5 to 4 times the standard in column B. The BOD_5 content ranges from 1.0 mg/l to 26.7 mg/l but some samples exceed 4 to ~7 times the standard 08:2003/BTNMT in column A and exceed 2 to ~ 4 times compared to the standard in column B. The content of parameters NH_4^+, NO_2^- and PO_4^{3-} in water samples varied strongly, especially the NH4+ component (coefficient of variation mainly fluctuated above 90%).

2.2. Methodologies

2.2.1. Cluster Analysis method (CA)

Cluster Analysis was proposed by McQueen (1967) to divide n observed values into different clusters so that the total number of fluctuations in each cluster is minimum (each fluctuation in the cluster is determined by Euclidean distance) [10]. There are many clustering methods, but they can be divided into two groups of methods. The first group of method is to select the optimal number of clusters and conduct clustering according to the smallest distance algorithm, typically the Kmeans method. The second group of method is the hierarchical clustering method. According to this method, the clustering data can be collected by grouping objects into hierarchical clusters which were based on the similarity of objects in the data. The hierarchical order of these clusters forms a dendrogram tree structure. In clustering using the Kmeans method, finding the optimal number of clusters in cluster analysis is very important. Currently, there are many statistical methods to determine the optimal number of clusters such as Elbow method, Average silhouette method and Gap statistical method. In this study, we use the Gap statistic method proposed by Tibshirani, Walther, Hastie (2001) [11] to select the optimal number of clusters and the Kmeans method to cluster the surface water quality in the study area. Specifically, the steps to perform cluster analysis using the Kmeans method include:

Step 1: Data standardization

$$Z = \frac{X_i - \bar{X}}{S}$$

X_i: observed value

$\bar{X}$: Average value

S: Standard deviation

Step 2: Determining the optimal number of clusters according to the Gap statistic method

The algorithm used to determine the number of clusters is Gap statistic (G) proposed by Tibshirani, Walther, Hastie (2001) [11].

$$G = \frac{1}{K}\sum_{K=1}^{k} log\left(W_{ref}\right) - log(WSS)$$

WSS: Total variation value corresponding to each value of K (number of clusters)

Wref: Total expected variation value corresponding to each value of K

Choose K so that G is within the standard deviation of K and K+1

Step 3: Cluster Analysis (CA)

Determine the range (distance) from the observed value to the mean value of each cluster. Conduct clustering for the total variation (Euclidean distance) within each cluster is minimum.

2.2.2. Principal component analysis (PCA)

The principal component analysis (PCA) method was proposed by Karl Pearson (1901) and Hotelling (1933) [12,13]. The goal of this method is to "compress" a data set characterized by many different variables into fewer variables than the original without losing the characteristics of the data. In particular, each new component after "compression" is called the main component. Specifically, the content of the PCA method is as follows:

Assuming the original data is a set X with k objects and p properties, we must find new variables PC_1, PC_2, ... PC_k as follows:

$PC_1 = \delta_{11}X_1 + \delta_{21}X_2 + \ldots + \delta_{p1}X_p$

$PC_2 = \delta_{12}X_1 + \delta_{22}X_2 + \ldots + \delta_{p2}X_p$

...

$PC_k = \delta_{1k}X_1 + \delta_{2k}X_2 + \ldots + \delta_{pk}X_p$

δ_{pk}: is the vector of regression coefficients:

$\delta_1^2 + \delta_2^2 + \ldots + \delta_p^2 = 1$

The number of principal components PCs is selected so that the total cumulative variance is maximized.

2.2.3. Water quality index (WQI)

The water quality index (WQI) is used to quantitatively describe the water quality and usability of that water source. The WQI index is calculated by 05 groups of parameters including: group I (pH); Group II (pesticide parameters); group III (heavy metal parameters); group IV (organic parameters); Group V (microbiological parameters). WQI index calculation data must include at least 3/5 parameter groups. The WQI index value ranges from 0 to 100. In which, WQI < 10 corresponds to very heavy pollution, WQI from 10 to 25 corresponds to very poor water quality, WQI from 26 to 50 corresponds to poor water quality, WQI from 51 to 75 corresponds to fair water quality, WQI from 76 to 90 corresponds to good water quality, and WQI from 91 to 100 corresponds to very good water quality. Specifically, the WQI index is guided in detailed calculation in No. 1460/QĐ-TCMT of the General Department of Environment dated November 12, 2019 [14]. In which, the final WQI index is calculated according to the formula:

$$WQI = \frac{WQI_I}{100} x \frac{(\prod_{i=1}^{n} WQI_{II})^{1/n}}{100} x \frac{(\prod_{i=1}^{m} WQI_{III})^{1/m}}{100} x \left[\left(\frac{1}{k}\sum_{i=1}^{k} WQI_{IV}\right)^2 x \frac{1}{l}\sum_{i=1}^{l} WQI_V\right]^{1/3}$$

Where: WQI_I: Calculation results for group I parameters

WQI_{II}: Calculation results for group II parameters

WQI_{III}: Calculation results for group III parameters

WQI_{IV}: Calculation results for group IV parameters

WQI_V: Calculation results for group V parameters

In this study, the collected database was only calculated for WQI groups I, III and group IV. Parameters in group II and group V do not have enough parameters to calculate. Therefore, the WQI index in this study used the equation:

$$WQI = \frac{WQI_I}{100} x \frac{(\prod_{i=1}^{m} WQI_{III})^{1/m}}{100} x \frac{1}{k} \sum_{i=1}^{k} WQI_{IV}$$

Where: WQI_I: Calculation results for group I parameters

WQI_{III}: Calculation results for group III parameters; WQI_{IV}: Calculation results for group IV parameters

3. RESULTS AND DISCUSSION

Post-processed data were analyzed using the Gap statistic method to select the optimal number of groups. The results show that with the data included in the analysis, the appropriate number of groups to cluster the data is 3 (Figure 2).

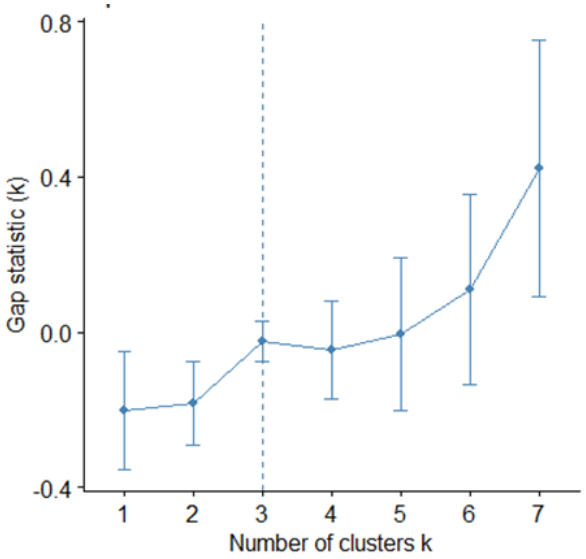


Figure 2. *Analysis chart for selecting the number of clusters according to the Gap statistic method*



Figure 3. *Cluster analysis chart using the Kmeans method*

1. Chan stream; 2. Khe Chom stream; 3. Nam Xay stream; 4. Chu O stream; 5. Dong Ho stream; 6. Hong river; 7. Ngoi Duong stream; 8. Ngoi Phat stream

From Figure 3, it shows that 8 rivers and streams distributed near mineral exploitation and processing areas in Lao Cai province can be divided into 3 groups, of which group 1 and group 2 can explain 89% of the data. Specifically:

Group 1: Chan and Nam Xay streams flow through Minh Luong gold mining area in Van Ban district, Lao Cai province.

Group 2: River Chu O, Dong Ho, Red River, Ngoi Duong S, Ngoi Phat flow through the copper and apatite mining and processing area of Bat Xat district and Lao Cai city.

Group 3: Khe Chom stream flows through the apatite processing factory in Tang Loong industrial park, Bao Thang district, Lao Cai province.

The characteristics of each group were analyzed by principal component analysis PCA method. The results are shown in Figure 4 and Table 2.

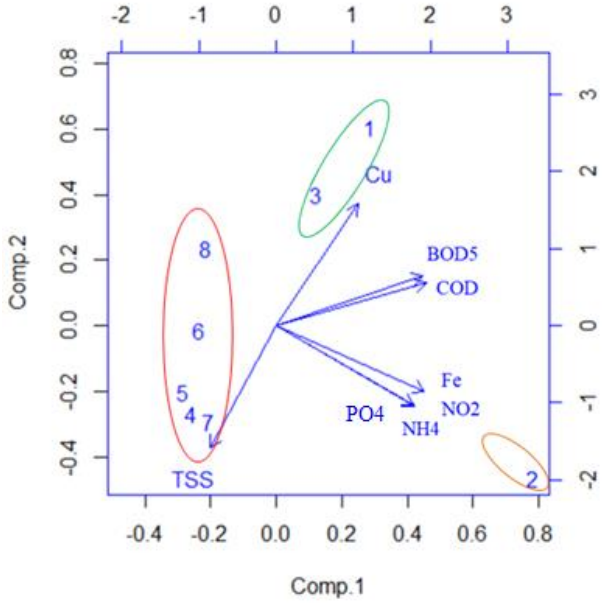


Figure 4. *PCA Biplot plot*

Table 2. Table of principal components analysis PCA results

	Comp.1	Comp.2	Comp.3	Comp.4	Comp.5	Comp.6	Comp.7	Comp.8
Standard deviation	2.12	1.36	0.62	0.52	0.11	0.03	0.02	0.00
Proportion of Variance	0.64	0.26	0.06	0.04	0.00	0.00	0.00	0.00
Cumulative Proportion	0.64	0.90	0.96	1.00	1.00	1.00	1.00	1.00
Eigenvalue	4.4759	1.8489	0.3892	0.2726	0.0125	0.0007	0.0003	0.0000

From table 2, it can be seen that the principal component analysis PCA also gives similar clustering results as the group analysis using the Kmeans method: the first three principal components have an equivalent to 96% cumulative variance that can explain 96% of the variation in the data.

From figure 4 it can be seen that:

Group 1: Chan and Nam Xay streams flow through Minh Luong gold mining area in Van Ban district, Lao Cai province. Characteristics of the surface water in this group are relatively

high levels of copper (Cu), TSS and BOD_5, COD. In particular, the content of copper (Cu) and suspended solids TSS have a strong negative correlation. The high copper content can be partly explained by the oxidation of copper-containing sulfur minerals located in the quartz-sulfur-gold ore-bearing formation of Minh Luong gold mine. In addition, the surface water in this area is also affected by domestic wastewater because the sampling location is close to residential areas, so the BOD_5 and COD contents are also very high.

Group 2: Streams Chu O, Dong Ho, Red River, Ngoi Duong, Ngoi Phat flow through the copper and apatite mining and processing area of Bat Xat district and Lao Cai city. High levels of suspended solids (TSS) and copper (Cu) are characteristic of the water quality of this group. This is also where many copper and apatite mining fields are concentrated such as Ngoi Dum - Dong Ho, Coc mine, field 20 -22, opening of the East and West areas of Sin Quyen copper mine .... in Van Ban district, Lao Cai city, Lao Cai province. Mining activities take place simultaneously on mining sites, leading to the generation of large amounts of dust from mining processes such as blasting, loading, and transporting ore, waste rock, and ore. Wind-blown dust and rainwater runoff entering surface water are the causes of high TSS levels in water.

Group 3: Khe Chom stream flows through the apatite ore processing factory in Tang Loong industrial park, Bao Thang district, Lao Cai province. Characteristics of the surface water in this cluster are very high concentrations of PO_4^{3-}, NH_4^+ and NO_2^-. The high PO_4^{3-} content is due to the influence of wastewater from DAP and fused phosphate fertilizer production. In addition, because the industrial park is densely populated, the surface water is also affected by domestic wastewater and excess fertilizer in agricultural cultivation, so the content of NH_4^+, NO_2^- is also very high.

Research results show that the surface water quality is influenced by mining and mineral processing activities and the chemical composition characteristics of ore-bearing rocks. Dust generated during the mining and processing of apatite ore is the main cause of TSS and PO_4^{3-} content pollution in the surface water. In addition, the surface water in the study area is also affected by domestic wastewater and agricultural activities, leading to the increased levels of NH_4^+, NO_2^-, BOD_5, and COD.

The results of calculating the surface water quality index WQI in the study area from 2017 - 2022 are shown in Table 3:

Table 3. Table of Calculation of WQI

Rivers/Streams	WQI		
	Min	Max	Mean
Chan	9	90	77
Khe Chom	8	76	57
Nam Xay	66	92	79
Chu O	50	89	68
Dong Ho	45	93	71
Hong	60	90	70
Ngoi Duong	8	83	63
Ngoi Phat	44	95	77

Suoi Chan stream: WQI values range from 62 to 90, especially at the sampling location in March 2022, the WQI index is 9, equivalent to a very heavy pollution level due to the TSS suspended solids content of 202,3 mg/l.

Khe Chom stream: WQI values range from 49 to 76, especially at the sampling location in November 2022, the WQI index is 8, equivalent to a very heavy pollution level due to the TSS suspended solids content of 158 .3 mg/l and NH_4^+ content is 12.4 mg/l.

Nam Xay stream: WQI values range from 66 to 92, corresponding to average to good water quality.

Chu O stream: WQI values range from 50 to 89, corresponding to average to good water quality.

Dong Ho Stream: WQI values range from 45 to 93, corresponding to average to very good water quality.

Red River: WQI values range from 60 to 90, corresponding to average to good water quality.

Ngoi Duong Stream: WQI values fluctuate mainly from 50 to 80, corresponding to average to good water quality. Particularly at some sampling locations in November 2017 and August 2018, the WQI index was very low at 8 and 9, corresponding to very seriously polluted water quality due to TSS suspended solids content up to 222mg/l and 117mg/l.

Ngoi Phat Stream: WQI values range from 44 to 95, mainly at 60 to 90, corresponding to average to good water quality.

In general, the quality of surface water on rivers and streams flowing through mineral exploitation and processing areas is average to good, as shown by the results of calculating the WQI index, which fluctuates mainly from 50 to 90. In which , Khe Chom stream flowing through the apatite ore processing area has poorer quality than the quality of the remaining rivers and streams. The main cause is that the water is polluted by the components PO_4^{3-}, NH_4^+ and NO_2^-. The main cause affecting surface water quality in the mining area is mainly due to increased TSS suspended solids concentration.

4. CONCLUSION

Research results show that surface water quality on rivers and streams flowing through the mining and mineral processing area of Lao Cai province is average to good, shown by the results of calculating the WQI index, which fluctuates mainly from 50 to 90. Surface water quality is mainly affected by the components TSS, PO_4^{3-}, NH_4^+ and NO_2^-. The results of cluster analysis (CA) and principal component analysis (PCA) show that the surface water quality characteristics can be divided into 3 clusters. Cluster 1 has a total explained variance of 61.9%, including Chan stream and Nam Xay stream flowing through Minh Luong gold mining area, Van Ban district, Lao Cai province. Characteristics of the surface water in this cluster are copper (Cu) content, TSS suspended solids content and quite high BOD_5 and COD content, which is closely related to the oxidation process of sulfur ore belonging to the quartz - gold-bearing ore system of sulfur - gold. Group 2 has a total data explanation variance of 27.5% including river Chu O, Dong Ho, Red River, Ngoi Duong, Ngoi Phat which flow through the copper and apatite mining area. Characteristics of the surface water in this group are TSS

suspended solids content, copper (Cu) content, and surface water quality which is closely related to dust emissions during the mining process and the oxidation process of sulfur ore release metal copper. Dust moves with rainwater runoff or is carried by wind into surface water sources. Group 3 is Khe Chom stream with the water quality of high levels of iron (Fe), PO_4^{3+}, NH_4^+ and NO_2^- and is closely related to wastewater from apatite ore processing and domestic wastewater of Tang Loong industrial park.

REFERENCES

[1] Xue Li, Pengjing Li, Dong Wang and Yuqiu Wang 2014. Assessment of temporal and spatial variations in water quality using multivariate statistical methods: a case study of the Xin'anjiang River, China. *Frontiers of Environmental Science & Engineering* volume 8, pages895–904 (2014)

[2] Ibrahim Yurtseven, Timothy O and Randhir 2020. Multivariate assessment of spatial and temporal variations in irrigation water quality in Lake Uluabat watershed of Turkey. *Environmental Monitoring and Assessment* volume 192, Article number: 793 (2020)

[3] Somphinith Muangthong and Sangam Shrestha 2015. Assessment of surface water quality using multivariate statistical techniques: case study of the Nampong River and Songkhram River, Thailand. *Environmental Monitoring and Assessment* volume 187, Article number: 548 (2015).

[4] T. A. Khan 2015, "Groundwater Quality Evaluation Using Multivariate Methods, in Parts of Ganga Sot Sub-Basin, Ganga Basin, India," Journal of Water Resource and Protection, vol. 7, p. 769, 2015.

[5] Hai Au Nguyen, Ngan Thi Khanh Phan, Thuy Thi Thanh Hoang and Phan Ngoc 2017. Application of multivariate statistical analysis in the assessment of groundwater quality of Tan Thanh district, Ba Ria – Vung Tau province. *Science & Technology Development Journal - Science of The Earth & Environment* December 2017, p.66-72.

[6] Phan Nguyễn Hồng Ngọc, Hoàng Thị Thanh Thủy và Nguyễn Hải Âu 2017. Applying cluster analysis and discriminant analysis methods to assess salinity in the Pleistocene aquifer in Tan Thanh district, Ba Ria - Vung Tau province. CTU Journal of Innovation and Sustainable Development (2017)(2), p. 129-136.

[7] Lê Văn Dũ, Nguyễn Thu Thùy Anh, Trương Hoàng Đan, Nguyễn Thanh Giao, Phạm Quốc Thái, Trần Văn Sơn and Lê Thị Hồng Nga 2019. Applying multivariate statistics in assessing surface water quality in U Minh Ha National Park - Ca Mau. *Can Tho University Journal of Science*. Vol 55, p.70-76.

[8] Nguyễn Phương, Nguyễn Phương Đông, Vũ Thị Lan Anh and Nguyễn Thị Cúc 2020. Assessing the level of heavy metal pollution in soil and surface water environment in copper and apatite ore mining areas, Lao Cai province. Mining industry Journal, number 5, p. 71-77.

[9] Center for Natural Resources and Environment Monitoring. Results of surface water monitoring in some mineral mining areas from 2017 to 2022, Lao Cai province.

[10] McQueen, J 1967. Some Methods for Classification and Analysis of Multivariate Observations. Computer and Chemistry, vol.4, p.257-272.

[11] Robert Tibshirani, Guenther Walther and Trevor Hastie 2001. Estimating the number of clusters in a data set via the gap statistic. *Journal of the Royal Statistical Society: Series B (Statistical Methodology)*, vol.63, P.411-423.

[12] Pearson and Karl 1901. *On Lines and Planes of Closest Fit to Systems of Points in Space*. Philosophical Magazine, Series 6, 2(11), p.559–572.

[13] Hotelling and Harold 1933. *Analysis of a Complex of Statistical Variables into Principal Components*. Journal of Educational Psychology, 24(6 & 7), 417–441 & 498–520.

[14] The Ministry of Natuaral Resources and Environment 2019. No. 1460/QD-TCMT, dated November 12, 2019 on promulgating Technical Guidelines for calculating and publishing Vietnam water quality index (VN_WQI).

RESEARCH ON BEHAVIOR OF ROCK/SOIL MASS DURING UNDERGROUND PARKING EXCAVATION IN MULTI-LAYERED SOILS IN URBAN AREAS

Dang Van Kien[1,*], FORNONI Benjamin[2], Mai Xuan Thanh Tuan[1], Doan Quang Tri[3], Nguyen Khoa Linh[1]

[1] *Faculty of Civil Engineering, Hanoi University of Mining and Geology (HUMG), Hanoi, Vietnam*

[2] *Institut Polytechntqije de Grenoble-Polytech Grenoble, Untversite Grenoble Alpes, Grenoble, France*

[3]*Viet Nam Meteorological and Hydrological Administration*

[*]*Email: dangvankien@humg.edu.vn*

Abstract: Urban underground space is an important part of densely populated urban areas, helping to solve problems of transportation, water supply and drainage infrastructure, electricity, telecommunications, and other public activities. Urban underground space has been built and operated effectively by developed countries for a long time. In Hanoi, Ho Chi Minh city, Vietnam, the lack of parking facilities space is one of the main causes ncreasingly serious traffic congestions. In order to meet the parking demand in the centre, Hanoi has prepared a plan to develop multi-level and underground parking facilities at the Vietnam-Russia Friendship Palace and Tran Hung Dao station, Thu Le Park, Thong Nhat Park… Earlier, Ho Chi Minh City has also prepared a plan to devolop some underground parking lots on Le Lai Street in District 1, in front of Le Van Tam Park on Hai Ba Trung Street in District 1, in the Cho Lon Bus Station in District 5, and on Hai Thuong Lan Ong Street in District 5.... However, they have never moved past the planning stages. The paper study behavior of rock/soil mass during underground parking excavation in multi-layered soils in urban areas by FEM analysis. The pattern of deformation, stress state, and distribution of plastic areas are analyzed by Plaxis 2D software. The study result provides a reliable way to analyze the stability of underground car parking in multi-layered soils in urban areas and also will help to design or optimize the subsequent support.

Keywords: *Underground car parking, FEM, rock/soil mass, Hanoi, Ho Chi Minh, barrette wall*

1. INTRODUCTION

1.1. Current situation of management and development Urban underground construction upace in Vietnam

In fact, in the past urban development, many underground technical infrastructure works have been built such as water supply, drainage, electrical cables, telecommunications, lighting, technical trenches, tunnels ... especially underground urban traffic works such as: urban railway system, tunnels for automobiles, pedestrian tunnels, underground parking lots,... many high-rise buildings in urban development areas with basements, however, most of them are only used for parking, less used for public service purposes; Currently, some areas in major urban areas such as Hanoi, Ho Chi Minh City, Da Nang... (service and commercial centers combined with high-class housing such as Royal City, Times City, Da Nang Plaza, JW Mariot, Vincom Center Dong Khoi...) has built and put into use a relatively synchronous underground space (currently, only Hanoi prepares and approves the general

planning of underground construction space of the central urban area - Hanoi city to 2030, with a vision to 2050 (Decision 913/QD-UBND dated March 15, 2022). However, in general, most of the underground works are partial, only exploited for a separate purpose, but there is no overall connection for the whole area or an urban area. This shows that the need to exploit and use underground space in urban areas is becoming increasingly necessary to promote urban development, improve people's quality of life and serve economic development [5-7].

In this paper, the traditional urban core where people reside, commercial and business establishments concentrate, government offices and public services such as hospitals, schools, and museums are located using to study. There are is nearly 600 persons/ha of population density in the Ancient Quarter (AQ) and 214 persons/ha in the FQ (French Quarter). As the center and socio-economic hub, a large number of people flows into the area, thus population density is even higher in the daytime (See Table. 1) [3]. The increasing rapidly of the number of private transport vehicles is at a rate of approximately (10÷15)% per year.



Figure 1. *Situation of common traffic congestion in Hanoi*

Table 1. Socio- Economic Profiles in the traditional urban [3]

		Ancient quarter (AQ)	French quarter (FQ)	Total
Area		80	217	297
Night-Time population (000)		47	46	93
Day- Time (000)	Employment	55	54	109
	Student	11	11	22
	Population	77	76	153
Population Density (n^o/ha)	Night - time	585	214	314
	Day - time	958	351	514
Day - Night Ratio		1.87	1.64	1.64

In 2020, there should be 36 million motorbikes and 3 million cars in Hanoi. Correspondingly, a statistic from the Department of Transportation mentioned that Hanoi has 1,178 parking points (see Table 2). However, this parking points accommodated about 8÷10% of Hanoi's parking demand only. Therefore, Many cars have to park on the sidewalk. It makes the situation of common traffic congestion in Hanoi such as Figure 1 [1].

Table 2. Current Situation of Parking in Hanoi by District [3]

District	Car		MC		Total	
	Point	Area (m^2)	Point	Area (m^2)	Point	Area (m^2)
Hoan Kiem	144	18,317	177	12,547	321	30,864
Ba Dinh	121	71,320	102	5,417	223	76,737

Hai Ba Trung	106	22,304	137	4,762	243	27,066
Dong Da	77	11,656	82	3,034	159	14,690
Hoang Mai	18	72,572	8	2,700	26	75,272
Long Bien	9	13,353	18	2,095	27	15,448
Cau Giay	32	55,874	22	11,639	54	67,513
Thanh Xuan	15	679	61	8,815	76	9,494
Tay Ho	20	1,551	11	515	31	2,066
Ha Dong	6	378	7	594	13	972
Tu Liem	5	95,147	0	0	5	95,147
Total	553	363,153	625	52,118	1,178	415,271

Note: Data for Parking administrated by DOT, including On-Street and Off - Street Facilities.

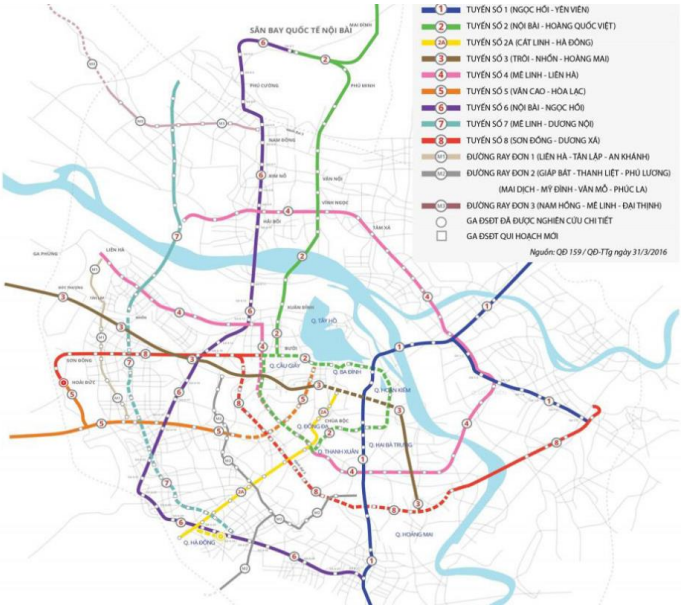


***Figure 2**. Master plan of metro lines in Hanoi [3]*

In fact, in the past urban development, many underground technical infrastructure works have been built such as water supply, drainage, electrical cables, telecommunications, lighting, technical trenches, tunnels ... especially underground urban traffic works such as urban railway system, tunnels for automobiles, pedestrian tunnels, underground parking lots,... many high-rise buildings in urban development areas with basements, however, most of them are only used for parking, less used for public service purposes. Therefore, the planning, design and construction of underground parking lots in big cities like Hanoi and Ho Chi Minh City are very necessary and urgent.

The location of Tran Hung Dao (C10) station is under the intersection of Tran Hung Dao Street and Hue Street in French Quarter area. Hanoi station connected to Tran Hung Dao Street, and Tran Hung Dao Station is a transfer station between Line 3 and Line 2 (Phase -2 section). The station area covers the French Quarter, characterized by its traditional French-style buildings and its wide and grid road network with trees and sidewalks (see Figure 3). An parking area will be constructed underground, above the space where the railway will make a U-turn. This location will devolop the railway terminal after completion of Phase1.

This underground car parking will be contructed by the cut and cover method, hence it is limited additional works to develop an underground parking area [3].

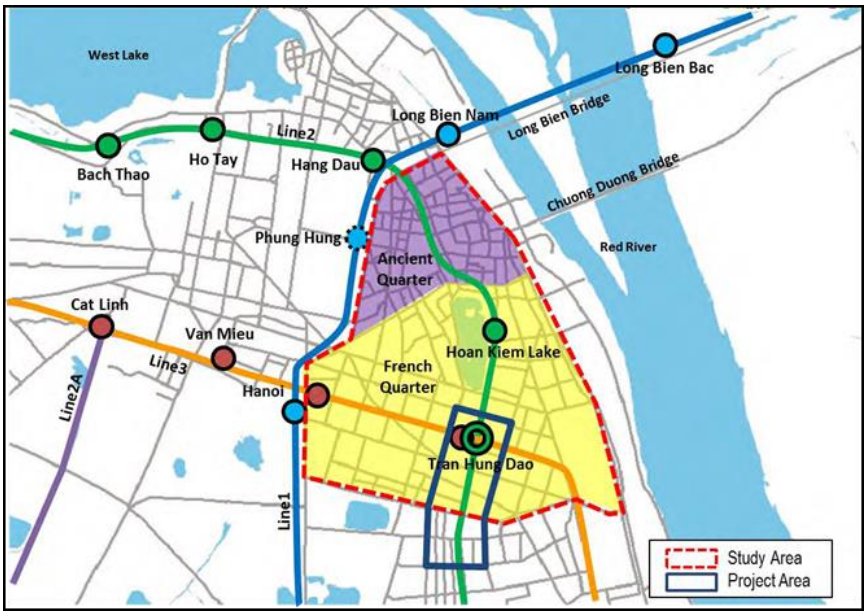


Figure 3. *Location of the study area and the project area*

1.2. Facility Plan

The dimention of underground parking is 255m in long and 21.4 m in wide (see Figure 4). underground parking will constructed in the underground space, above the space where the railway will make a U-turn i.e. the terminal of the Phase 1 section which will be excavated by the cut and cover method, above Line 2. This underground car parking will be designed a self-propelled 2-floor structure with a capacity of about (i) 200 cars for 2 floors, or (ii) 560 lots for motorbikes on the -1 floor and 100 lots for cars on the -2 floor. It'area is 4,900m^2 each floor including machine rooms, toilets, and others. The underground walkway from the -1 floor will directly connect to the concourse of Tran Hung Dao Station. Two emergency exits to Hue Street will be designed.

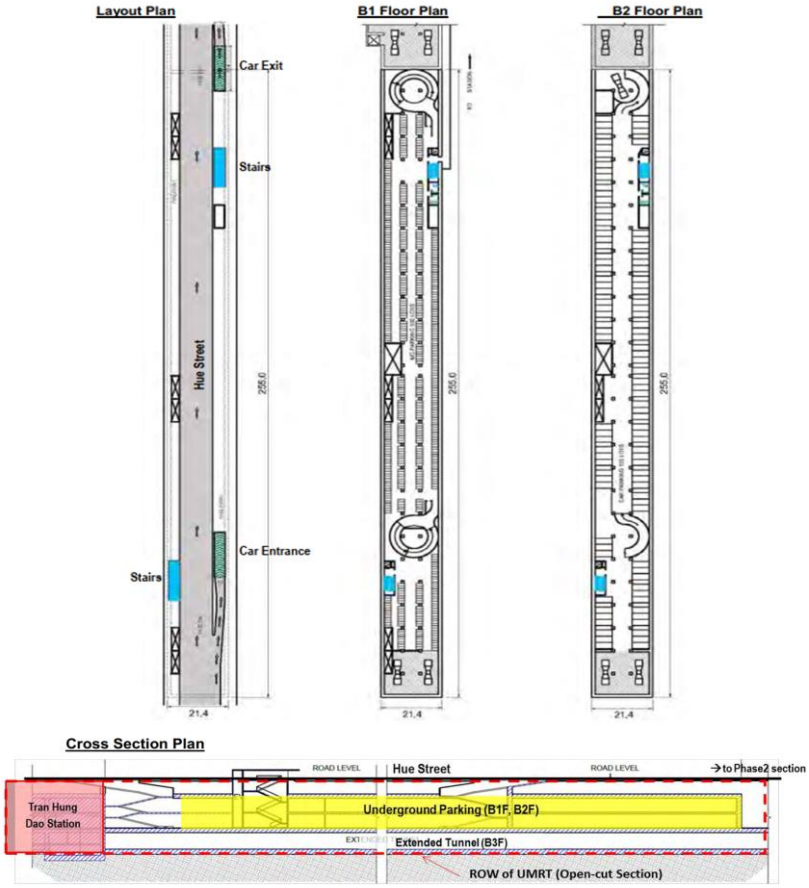


Figure 4. *Tran Hung Dao underground car parking' Facility Plan*

2. NUMERICAL MODELS

2.1. Description of the model

For the numerical simulation, two-dimensional finite element code PLAXIS is used. The Mohr-Coulomb model is used to model soil. Evaluating the behavior of rock/soil mass during underground parking excavation in multi-layered soils in urban areas performed based on Plaxis 2D software. This software allowed to analyze the sequence of underground parking car excavation and install the wall support. The software is also given maximum stress and strength of barrette wall, the concrete slab and the support column. The study is performed the project according to a plane deformation, with elements at 6 nodes, according to (x,y). *The car park is 255.0 m long*, the model is asymmetrical, since on one side of the car park there is a load which corresponds to the stress caused by the road and traffic. I considered a road 1.50 m from the car park. The road in front of the car park is 317.66 m long and 5 m wide. There will be 5 excavation phases for the construction phase of the project. A soil survey was carried out on site and the lithology is made up of 6 apparent layers. Moreover, a water table was detected 2 metres below ground level.

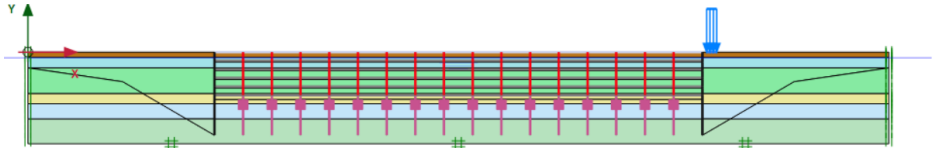


Figure 5. *Numerical model*

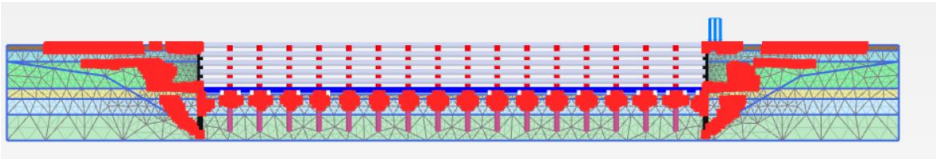


Figure 6. *Meshing of the study area*

Concerning the boundary conditions on the edges, on the vertical edges. The model is blocked vertical movements so that the model doesn't leave the defined zone and this causes problems in the convergence of the calculations. On the bottom horizontal edge. The model is also blocked vertical and horizontal movement. For the top horizontal edge, all movements are free. In addition, in order to understand the behavior of the soil on the structure. All the elements of the structure deformable are left. The model is calculated through 10 phases, in order to have a good understanding of how the soil would behave during the construction of the car park. The phases are as follows:

- Initial phase: Construction of the bar wall, bored piles, steel columns encased in concrete and the first concrete slab.

- Phase 1: Lowering of the water table to -4.0 m from the ground surface then excavation to -3.5 m from the ground surface

- Phase 2 : Construction of the second slab.

- Phase 3: Lowering of the water table to -7.0 m from the ground surface then excavation to -6.5 m from the ground surface.

- Phase 4: Construction of the third slab.

- Phase 5: Lowering of the water table to -10 m from the ground surface then excavation to -9.5 m from the ground surface.

- Phase 6 : Construction of the fourth slab.

- Phase 7: Lowering of the water table to -13 m from the ground surface then excavation to -12.5 m from the ground surface.

- Phase 8: Construction of the fifth slab.

- Phase 9 : Lowering of the water table to -17 m from the ground surface then excavation to -16.5 m from the ground surface.

- Phase 10 : Construction of the sixth slab.

As far as lowering the water table is concerned, the underground ware is located 1.0 m below the future excavation to facilitate working conditions and the installation of the slab. Similarly, the excavation is carried out 0.5 m below the height of the concrete slab, enabling it to be built in good conditions.

2.2. Material Parameter Setting

Various reconnaissance tests have revealed the following lithological parameters. The soil model used for this project and its study is the Mohr-Coulomb model. Given the lithology of the soil, the different soil layers exhibit different behaviours, so it's more appropriate to use the Mohr-Coulomb model. In addition, the soil is predominantly sandy. The parameters of this model are the angle of friction (φ), cohesion (c), angle of expansion (Ψ), Poisson's ratio (ν) and Young's modulus (E). In this project, the Mohr-Coulomb model will be used to assess the forces and stresses exerted on the structure and also to evaluate the stability of the soil-wall model. Soil lithology and its parameters is presented on Table 3. The properties of the embedded beam row are Table 3 as follows:

Table 3. Physical and mechanical parameters of the simplified stratum

Layers	γ (kN/m^3)	γ' (kN/m^3)	C (kN/m^2)	φ (°)	ν	E (MN/m^2)	Thickness (m)
Backfill	18	8	0	30	0.2	22.74	1.8
Sandy Clay	19.4	9.4	60	2	0.3	13.32	3.7
Fine Sand	18	8	0	24	0.2	17.726	9
Sandy Clay	20.1	10.1	60	3	0.3	13.9	3.5
Clayey Sand	19.7	9.7	14	21	0.2	17.614	5.3
Fine to coarse Sand	18	8	0	30	0.2	28.658	8.7

In the case of the barrette wall, the concrete slab and the support column, we resonate at a depth of 1 metre. For each element we consider its weight in the analysis of the results such as Table 4, the properties of the embedded beam row is presented on Table 5.

Table 4. The properties of the plates

Plate	Road	Last concrete slab	Concrete support column	Barrette wall	Concrete slab
Material type	Elastic	Elastic	Elastic	Elastic	Elastic
Thickness (m)	0.2	0.8	0.4	1	0.3
Young's Modulus (MN/m^2)	30000	30000	30000	50000	30000
Poisson's ratio	0.2	0.2	0.2	0.2	0.2

EA (Elastic stiffness) ($kN.m^2/ml$)	6000000	24000000	12000000	50000000	9000000
EI (Bending stiffness) ($kN.m^2/ml$)	70 000	1 280 000	160 000	4167000	67500

Table 5. The properties of the embedded beam row

Identification	Bored piles
Material type	Elastic
Young's Modulus (kN/m^2)	30 000 000
Volume weight (kN/m^3)	25.0
Diameter (m)	1.0
A (m^2)	0.7854
I (m^4)	0.04909
$L_{spacing}$ (m)	1.5
$T_{skin, start, max}$ (kN/m)	188.5
$T_{skin, end, max}$ (kN/m)	188.5

To calculate $T_{skin, start, max}$ and $T_{skin, end, max}$, the following formula (1) is used:

$$T_{skin, start, max} = T_{skin, end, max} = Q_s * 2 * \pi * R \text{ (radius)} \quad (1)$$

Where: the maximum axial skin resistance $T_{skin,max}$. With regard to road and traffic loading, the article by, entitled design and construction experience, predicts a load of 40 kN/m^2 in a traffic jam in front of the car park. This loading is considered in model because it's the most unfavourable for the structure and involves more instability and therefore displacements. In this section, the study is performed to look at the influence of soil behaviour on the structure in terms of the displacements and stresses that this implies for the structure. It's interesting to analyse the stability and safety of the structure with the safety measures that apply in Vietnam in order to find solutions to optimise the project.

2.3. Safety standards

As far as the maximum displacement is concerned, in Vietnam the maximum tolerable displacement $u_{x, max}$ must be less than where H is the height H of the moulded wall.

3. RESULTS AND DISCUSSION

The part of the structure subject to the most displacement is the moulded wall. It's therefore necessary to study the stresses and displacements caused by the ground on the wall. The two moulded walls in the study of displacements is distinguish. Table 6 shows the maximum deformation of the structure caused by the ground:

Table 6. The maximum deformation of the structure

Phase	Maximum displacement of the moulded wall on the park side (cm)	Maximum displacement of the moulded wall on the roadside (cm)
1	1.54	1.85
2	1.58	1.90

3	2.74	3.04
4	2.75	3.06
5	3.92	4.23
6	3.93	4.25
7	4.96	5.25
8	4.96	5.26
9	6.38	6.68
10	6.40	6.72

In fact, the moulded walls are subject to the most stress due to the earth pressure and the hydraulic pressure of the ground. The bending moment in the two moulded walls during the phase 10, as it's during this phase that it's most significant is presented Figure 7. The maximum absolute bending moment is 2578 kN.m/m.

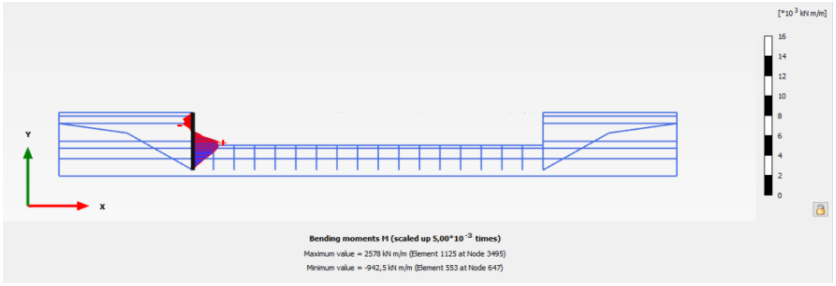


Figure 7. *Bending moment during phase 10 on the park side*

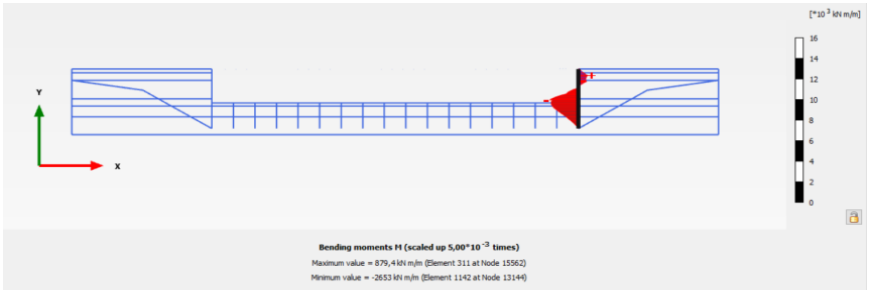


Figure 8. *Bending moment during phase 10 on the roadside*

The maximum absolute bending moment is 2653 kN.m/m. These bending moments are quite significant. When it comes to the water status of the project, there are several things to check, such as flow rate, pore pressure and degree of saturation:

- Interstitial pressure increases with depth;
- In absolute terms, the highest value of interstitial pressure is 320 kN/m^2;
- The flow is zero everywhere in this project.

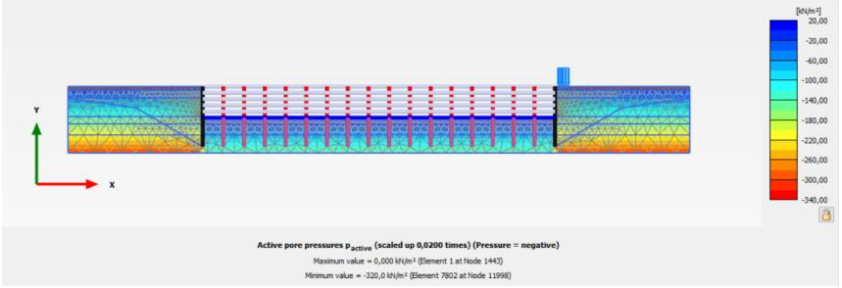


Figure 9. *Interstitial pressure in this project*

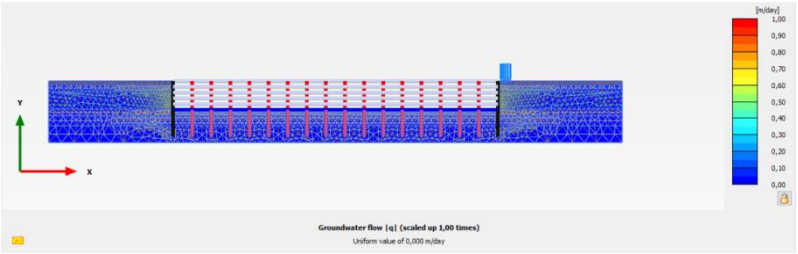


Figure 10. *Water flow in the car park*

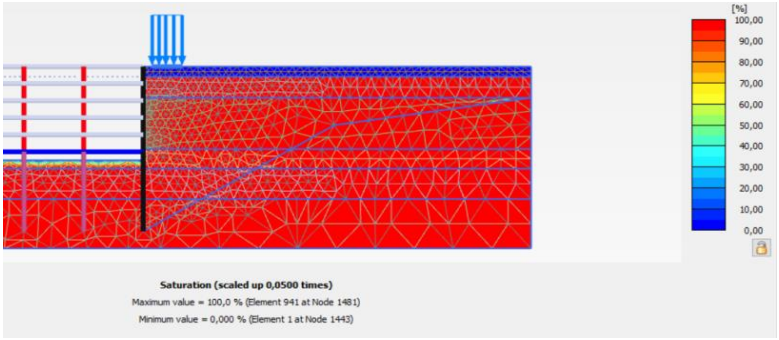


Figure 11. *Representation of soil saturation on the distributed load side*

In fact, the initial state means that the water level is high, which implies that the flow is zero. Soil saturation is as follows. The soil is 100% saturated below the water table on the land side. Similarly, on the excavation side, the soil is 100% saturated below the water table. Suction is the capacity of a soil to retain water inside its pores due to capillary forces. The higher the suction, the more water the soil retains and the more difficult it's for water to move. Suction measures the capillary tension in the soil, which is created by the forces of interaction between the water molecules in the soil. In the suction is very weak or almost non-existent.

3.1. Exploitation of results

Firstly, in terms of displacements in the structure linked to the ground during excavation, the element that moves the most is the moulded wall on the uniformly distributed load side, that is the roadside. The greatest displacement of the moulded wall occurred during the penultimate phase, with a displacement of 6.72 cm. According to the standards in force in Vietnam, this displacement is tolerated. Indeed, the height H of the moulded wall is 19 m, so the maximum permissible displacement is 9.5 cm indeed $\frac{H}{200}$ is equal to 9.5 cm.

These displacements can be explained on the one hand by the presence in the soil of powdery layers, that is granular materials such as sand which, under the application of a load, sees the angle formed by the particles exceed the friction angle, thus causing slippage between the particles and thus causing displacements in the structure. In addition, granular materials are permeable, which means that water can pass through them, altering the mechanical properties of the soil and causing displacement or settlement of the structure. The presence of clay in the sandy soil makes it somewhat coherent but can concentrate hydrostatic pressure on certain points of the structure, destabilising it due to its impermeability. Figure 7 shows that the ground is saturated when the water table falls to 100%, which means that there is no suction, as confirmed by Figure 8. This is because the water fills all the empty spaces between the soil particles, so there is no capillary force to

hold it back. The problem with zero suction in the ground is that it can lead to excessive drainage, allowing a large quantity of water to pass through and thus causing high hydrostatic pressures on the structure. For example, many companies around the world choose to continue pumping groundwater even after the site has been completed. In the case of the Tran Hung Dao underground car park, a large concrete slab is poured at the bottom of the excavation to make it impermeable, and this slab is supported on piles spaced 1.5 m apart to prevent the slab from lifting as a result of the hydrostatic pressures beneath it. So, once the car park is built, they can stop pumping groundwater. However, during the construction phase, a great deal of pumping will be necessary as the soil remains very permeable. In terms of the forces that pass through the moulded walls, it's consistent to find a higher bending moment for the wall on the roadside, as the load linked to the road and traffic increases the vertical and horizontal stress values in the ground. The values obtained for the bending moment were used to design the walls, taking into account the forces due to the different layers of soil, the hydrostatic thrust due to the water table and the distributed load due to road traffic. Having studied the behaviour of the ground on the structure during excavation of the car park, it's worth optimising the project by finding solutions that will reduce displacements in the structure, particularly at the level of the moulded wall, and by reducing the stresses in order to optimise the design.

3.2. Solutions for optimising the structure

The search for solutions to optimise the project will focus primarily on the interaction between the ground and the moulded wall, with the aim of finding various effective ways of reducing displacements and the bending moment in the walls. Various solutions can be implemented, such as changing the dimensions of the wall, external reinforcement, the use of nails…

3.3. Variations in moulded wall dimensions

Increasing the wall thickness increases rigidity and therefore resistance to deformation. In fact, this increases the quadratic moment, allowing the loads to be distributed more evenly over a larger surface area and therefore reducing the stresses applied to the wall. The following Table 7 shows the influence of wall thickness on displacements and bending moment:

Table 7. The influence of wall thickness on displacements and bending moment

/	e = 1 m				e = 2 m			
/	|u|(cm)		M (kN.m/m)		|u|(cm)		M (kN.m/m)	
Phase	Park wall	Roadside wall	Park wall	Roadside wall	Park wall	Roadside wall	Park wall	Roadside wall
1	1.54	1.85	547.9	635.8	1.18	1.50	1344	1457
2	1.58	1.90	536.6	623.4	1.25	1.57	1318	1429
3	2.74	3.04	1161	1262	1.88	2.14	2898	2936
4	2.75	3.06	1155	1254	1.91	2.18	2878	2915
5	3.92	4.23	1734	1827	2.93	3.14	3861	3899
6	3.93	4.25	1725	1815	2.95	3.17	3847	3883
7	4.96	5.25	2145	2237	4.23	4.38	4240	4295

8	4.96	5.26	2129	2221	4.24	4.40	4228	4281
9	6.38	6.68	2565	2600	6.19	6.34	3946	3995
10	6.40	6.72	2579	2657	6.23	6.40	3876	3945

In this section, in the roadside wall is interested. It shows that increasing the thickness of the wall reduces the displacement by around 3 mm in the final phase.

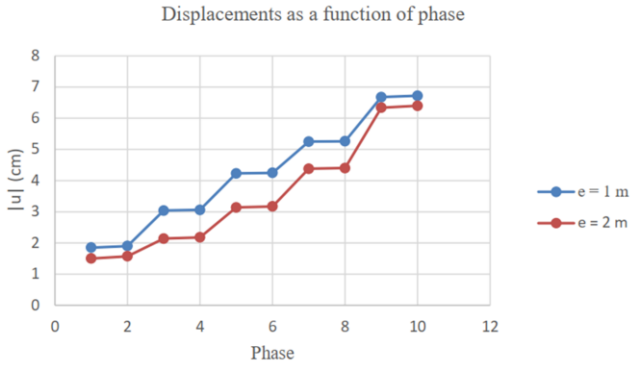


Figure 12. *Graph showing the evolution of displacement as a function of phase with variation in thickness*

Reducing displacements reduces deformation, cracks and therefore damage to materials. However, we can see that on the other hand there is a significant increase in the bending moment. In fact, if we increase the quadratic moment, the bending strength of the cross-section will increase, which means that the structure will have a greater capacity to resist bending moments. This means that the structure will be able to withstand greater bending moments, hence the increase in bending moment. Yet, we can also play with the depth of the wall, and after several simulations with the Plaxis software, It can be found interesting to reduce the moulded walls by 6 m. The wall is now 23 m deep. It's interesting to see how this can affect displacements and efforts. The following Table 8 shows the displacements of the walls on the park and road sides for each phase:

Table 8. The displacements of the walls on the park and road sides for each phase

Phase	Maximum displacement of the moulded wall on the park side (cm)	Maximum displacement of the moulded wall on the roadside (cm)
1	1.88	2.44
2	1.99	2.57
3	2.94	3.46
4	3.00	3.54
5	4.35	4.82
6	4.39	4.89
7	6.19	6.62
8	6.22	6.69
9	8.84	9.62
10	8.99	9.90

It can be seen that the displacements are greater when the depth of the wall is reduced. This is because reducing the depth of the wall results in a reduction in the cross-section, so the wall is less resistant to bending movements and deformations. Displacements are still permissible, they are less than $\frac{H}{200}$ [4÷7], [12], in this case, H equal to 23m. However, reducing the height of the retaining wall can reduce the bending moment applied to the wall.

This is because it reduces the distance between the line of action of the loads and the axis of rotation of the wall. Yet, reducing the height of the wall may reduce its stability to withstand loads and therefore encourage it to topple over. The bending moment in the two moulded walls during the phase 10 is presented on Figure 10, as it's during this phase that it's most significant. The maximum absolute bending moment is 1382 kN.m/m.

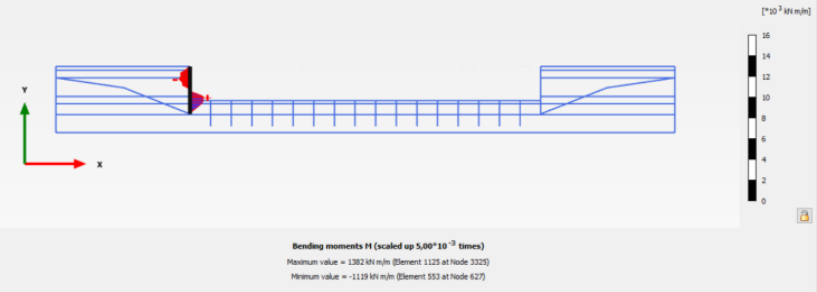


Figure 13. *Bending moment during phase 10 on the park side*

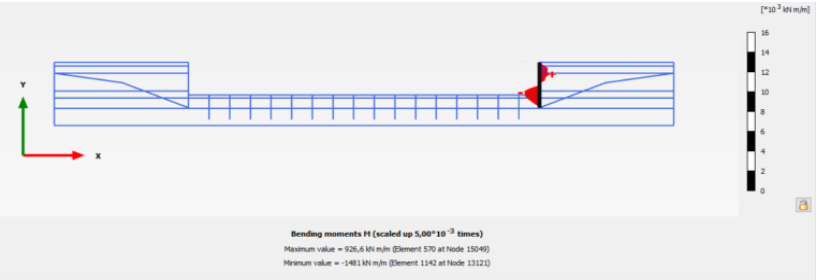


Figure 14. *Bending moment during phase 10 on the roadside*

The maximum absolute bending moment is 1481 kN.m/m (Figure 10). It can be seen that in both cases the maximum bending moment has been reduced, or better distributed in the wall. The retaining wall is keeped this configuration of, that is 23 m deep and 1 m thick.

4. CONCLUSION

1. This paper describes the behavior of rock/soil mass during underground parking excavation in multi-layered soils in urban areas. Based on results of numerical simulation, it is reasonable to conclude that:

2. The pattern of deformation, stress state, and distribution of plastic areas of rock/soil mass during underground parking excavation in multi-layered soils in urban areas can be analyzed by Plaxis 2D software with phases.

3. The maximum vertical displacement and maximum horizontal displacement of the supporting structure are positively correlated with the excavation depth. The the maximum vertical displacement and the maximum horizontal displacement of the support structure are smaller than the allowable limit. The research results summarized in this paper can be used as a means to assess the control risk of foundation pit excavation.

4. The evolution of displacement as a function of phase with variation in thickness. A better understanding of the ground helps to ensure the stability and safety of the structure. Understanding the behaviour of multi-layered soils in urban areas is also very important because it has an environmental impact. The understanding of the soil on which a structure is being built makes adapt the structure to the soil and not the soil to the structure. Improving soil management by optimizing the quantity of soil excavated to limit soil pollution by reducing the number of injections, particularly those used to stabilize, solidify, and consolidate the soil.

REFERENCES

[1] Doc. No.81/KH-UBND "Plan for developing transportation infrastructure of Hanoi, period 2011-2015".

[2] Luong Tu Quyen, Head of Scientific Research task- City level: Research designing system of underground public car park in the city of Hanoi. Code 01C- 04 / 06-2008-2.

[3] JICA Project Team. Project for Studying the Implementation of Integrated UMRT and Urban Development for Hanoi in Vietnam. Final report – main text II. Hanoi. 2008.

[4] Lam Quang Cuong (2006): *Exploitation and developmental management of underground space in Hanoi. Symposium Presentation: Exploiting the advantages of Natural Resources and Socio-economic conditions in the process of urbanization and sustainable development of the capital Hanoi*. Hanoi in 10/2006.

[5] Doan The Tuong (2008): The urban form of background in Hanoi, Ho Chi Minh City and assess them for the construction of underground works. APAVE. Articles Underground.

[6] Doan The Tuong (2000) - Head of research The technical problem of construction of urban underground. The report summarizes the Scientific researches task- State level. Institute of Science and Technology Construction, the Ministry of Construction. Hanoi.

[7] Doan The Tuong (2004)- Head of research: Mastering the technology of construction of underground works in urban soft soil of Vietnam. Final report of Scientific researches task- Ministry level. Institute of Science and Technology Construction, the Ministry of Construction. Hanoi.

[8] ChetanVaidya, KeerthiGowda B.S (2014). Analysis of Underground Parking Structure. International Journal of Emerging Trends in Engineering and Development. Issue 4, Vol.3 (May 2014). ISSN 2249-6149.

[9] http://hanoimetro.net.vn/en/ban-do-8-tuyen/

[10] Midhula Jayanandan (2015). Numerical Simulation of Soil Nailed Structures. nternational Journal of Engineering Research & Technology (IJERT. Vol. 4 Issue 08, August-2015.

[11] Babu G, Singh VP, Simulation of soil nail structures using PLAXIS 2D. Plaxis Bulletin. Spring issue; 2009. p. 16–21.

[12] Luu Nguyen Vu, Pham Quoc Dung. Double diaphragm wall – Design and construction experience. Infrastructure Development, Lecture Notes in Civil Engineering 62. https://doi.org/10.1007/978-981-15-2184-3_57.

[13] Oliaei, M., Norouzi, B., & Binesh, S. M. (2019). Evaluation of soil-nail pullout resistance using mesh-free method. Computers and Geotechnics, 116, 103179. https://doi.org/10.1016/j.compgeo.2019.103179 .

[14] Babu G, Singh VP, Simulation of soil nail structures using PLAXIS 2D. Plaxis Bulletin. Spring issue; 2009. p. 16–21.

[15] Tobias, P., Hugo, C., Eduardo, G., & Alejandro, P. (2012). Imposed Deformations in Concrete: Case Study of an Underground Car Park. Journal of Materials in Civil Engineering, 24(12), 1513–1519. https://doi.org/10.1061/(ASCE)MT.1943-5533.0000542

IDENTIFYING SOLUTIONS FOR ENHANCING ELECTRICAL SAFETY IN UNDERGROUND MINES BY ANALYZING PARAMETERS INFLUENCE ON LEAKAGE CURRENT

Le Xuan Thanh[1], Nguyen Dinh Tien[2]

[1] Faculty of Electromechanic, Hanoi University of Mining and Geology, Hanoi, Vietnam

[1]E-mail: lexuanthanh@humg.edu.vn; [2] Hanoi University of Industry

Abstract: Recent years, electric safety in underground mining is one of top leading priority in manufacturing management of VietNam coal mines. It covers a wide range of areas, including the extraction of coal resources, residential infrastructure, commercial establishments, and public facilities. Because of applying modern and advanced technologies as well as high-tech apparatus, the structure of underground mining networks becomes more complex with higher rated voltage. One key aspect of electrical safety in Vietnam is the adoption of international standards and best practices, particularly those outlined in the International Electrotechnical Commission (IEC) standards. These standards serve as a foundation for the development of Vietnamese electrical safety requirements and help ensure compatibility and interoperability with global electrical systems. To meet this standard, leakage relays working on leakage current in underground mines must operate securely and reliably, hence understanding deeply the parameters influencing on leakage currents is necessary and important. By analyzing all possible structures in low voltage grids of underground mines in VietNam, the paper will identify the most impact parameters which influence on rms of leakage current for generous observation. Some technical solutions will also be proposed for improving the electrical safety which obtaining the reduce of leakage current. The outcomes computing the values of the current will be implemented in MATLAB for verifying the proposed solution.

1. INTRODUCTION ABOUT ELECTRICAL SAFETY IN UNDERGROUND MINES OF VIETNAM

In Vietnam underground coal mines, there are more and more advanced and modern electrical devices are equipped for serving faster and better the demand of increasing coal productivity. The great number of connected apparatuses to main 6kV/660V transformer substation causes changes in the grid's structure and parameters, which also introduces the risk of electrical hazards for electricians [11]. Most electrical networks feature a leakage protection relay, commonly known as УАКИ, installed in the substation. This relay must activate whenever a leakage current occurs within the 660V grid, and its signal is transmitted to the switching protective device, a low-voltage circuit breaker located at the start of the 660V outgoing feeders. Figure 1 illustrates a typical diagram of a 660V electric power system supplying energy to an underground mine area, displaying the connection of the transformer and the leakage relay. Figure 2 exhibits the connection of the relays with 2 separate earthing rods spaced 5m apart.

Not only Vietnamese requirements, but also international ones [1-7], the electrical safety in mining (in specific) and in industry (in general) is the top priority that all the managers

must concern. Enhancing electrical safety in underground mines in Vietnam is of paramount importance due to several following critical reasons:

+ Worker Safety: The primary concern is the safety of underground mine workers. Electricians and miners often work in close proximity to electrical equipment and systems. Ensuring electrical safety is crucial to protect them from potential electrical hazards, including electric shocks, fires, and explosions.

+ Preventing Accidents: Electrical accidents can have catastrophic consequences in underground mines. Fire or explosion incidents can lead to injuries, loss of life, and extensive damage to mining infrastructure. Enhancing electrical safety helps minimize the risk of such accidents.

+ Compliance with Regulations: Adhering to national and international safety standards and regulations is essential. Failure to do so can result in legal repercussions and penalties for mine operators. Enhancing electrical safety ensures compliance with these standards.

+ Operational Continuity: Electrical failures can disrupt mining operations, leading to downtime, production losses, and increased costs. A robust electrical safety framework helps maintain operational continuity by reducing the likelihood of electrical failures.

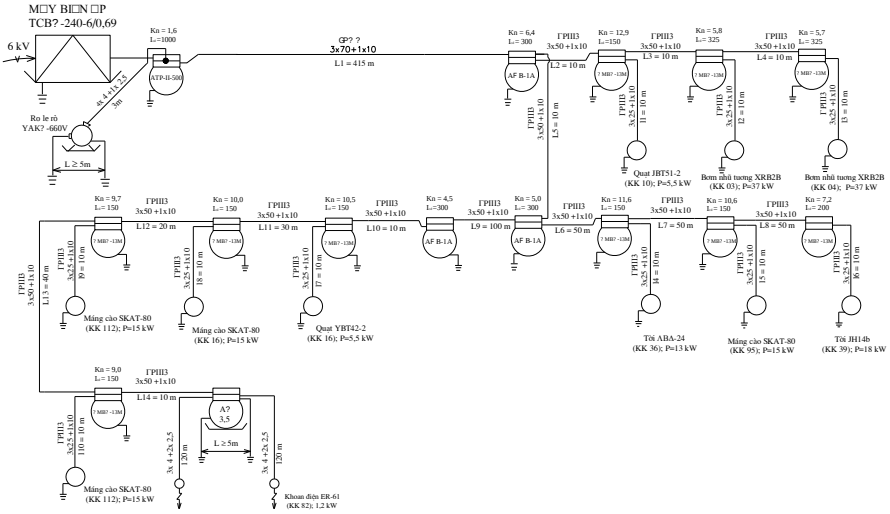


Figure 1. *660V grid in underground mines of VietNam [15], [33]*

+ Economic Viability: Mining is a significant contributor to Vietnam's economy. Ensuring electrical safety in underground mines is essential for sustainable growth. Reducing accidents and operational disruptions safeguards the industry's economic viability.

+ Technological Advancements: The mining industry is evolving with the integration of advanced technologies, such as automation and remote monitoring. These technologies rely heavily on electrical systems. Enhancing electrical safety is crucial to harness the benefits of these innovations while mitigating risks.

+ Environmental Protection: Electrical incidents can lead to environmental pollution and contamination. Leaks, fires, or explosions may release hazardous materials or cause ecological damage. Enhanced electrical safety measures help protect the environment surrounding the mining site.

+ Reputation and Investment: A commitment to electrical safety improves the reputation of mining companies and can attract investment. Investors are more likely to support operations that prioritize safety and sustainability.

+ Long-Term Sustainability: A focus on electrical safety contributes to the long-term sustainability of underground mining in Vietnam. By preventing accidents and ensuring reliable operations, the industry can thrive and continue to provide essential resources.

Because of the importance of electrical safety in mining industry [26-30], many researches [8-10], [22] proposed solutions for precaution or pre-assessment if the accident should sudden arises. Other one recommend equipment for fast detecting or eliminating the cause of accident [12-14], [16-20], [21-26]

In accordance with Vietnamese National safety regulations [11], [12], [15], [32], all metal frames of motors and electrical equipment must be connected to two grounding systems: one is an individual grounding rod, and the other is the centralized grounding system situated at the transformer substation. An illustration of these systems can be found in Figure 3.

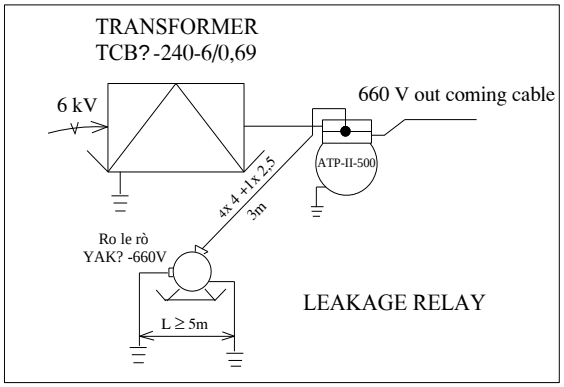


Figure 2. *Leakage relay at transformer substation of underground mining grid in VietNam [15], [33]*

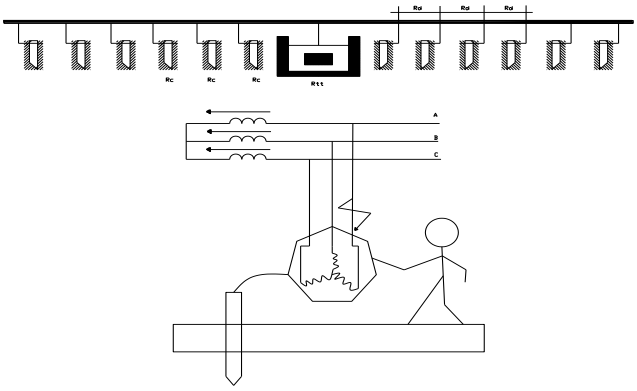


Figure 3. *660V grid in underground mines of VietNam [15], [33]*

In this figure, by earthing the metal parts of uncovered accessories, the accidental leakage current could have easy path to close-circuited back to earthing relay, the excursion of current is presented in figure 4. As described in [15] and [32] the root-means-square (rms) of the current, hence the sensitivity of the relay depends on many internal factors of the grids including: the length of cables, the number of energy supplied equipment, rated voltage… By understanding those factors and their impact on leakage current could assist the mining technicians optimize the operation as well as the reliability of relay [13], [15], [23], [31]. A part from many above mentioned studies, two typical parameters of 660V grids in Vietnam coal mines are eliminated in calculation the earthing current. The main aim of the paper is to focus on the

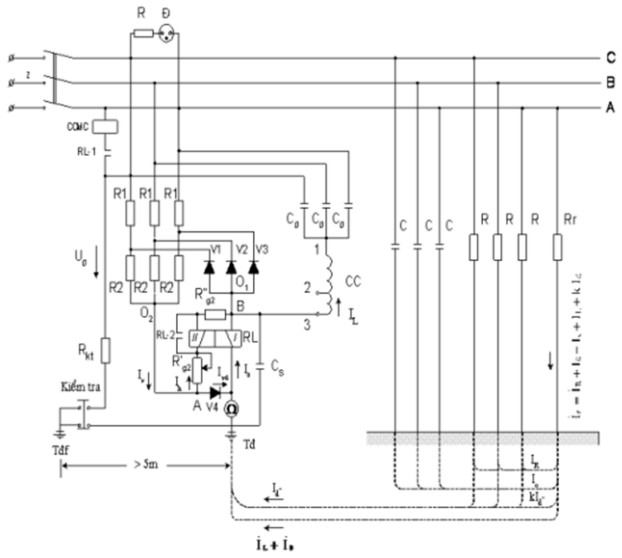


Figure 4. *The expression of leakage current feeding back to leakage relay typed YAKИ*

load ratio and various structure of 660V network to identify their impact on 660V leakage current, then propose solutions for improving the electrical safety.

2. BASIS THEORY OF LEAKAGE CURRENT CALCULATION IN 660V UNDERGROUND MINES

To analyze electrical safety, it is necessary to determine the current that flows through a person upon touching electrically conductive components of the grid. The magnitude of this current is calculated using the following equation (1) [31], [32], [33].

$$I_n = U_f g_n \sqrt{\frac{\left(3g + \frac{r_0}{r_0^2 + \omega^2 L^2}\right)^2 + \left(3\omega C - \frac{\omega L}{r_0^2 + \omega^2 L^2}\right)^2}{\left(3g + g_n + \frac{r_0}{r_0^2 + \omega^2 L^2}\right)^2 + \left(3\omega C - \frac{\omega L}{r_0^2 + \omega^2 L^2}\right)^2}} \quad (1)$$

Where g_n-body's admittance, $g_n = 1/R_{ng}$;

C-compensated capacitance;

L- inductance of compensation coil, the coil is mankind connected to neutral point of the grid;

When the capacitance element of the grid is partially compensated, the current value is calculated by equation (2), and when it is fully compensated, the current is determined using equation (3).

$$I_n = \frac{U_f}{R_n \cdot \sqrt{1 + \frac{R_{cd}(6R_n + R_{cd})}{9R_n^2(1 + \omega^2 C_{cd}^2 . R_{cd}^2)}}} \quad (2)$$

$$I_n = \frac{3U_f}{3R_n + R} \quad (3)$$

In equations (1), (2) and (3) the current running through the human being's body depends strongly on 2 factors:

+ C_{cd}-Capacitance elements of grid (which is proportional to the length of feeders and the numbers of apparatus connected to grid [32], [33];

+ R_{cd}-insulation resistance of grid..

Those quantities in previous researches are supposed to be independent with load ratio and structure of the grids. Hence, the next part of the paper, these factors will be the main aims for analysis to the rms of leakage current.

3. ANALYZING THE IMPACT OF LOAD RATIO AND GRIDS' STRUCTURES ON LEAKAGE CURRENT

3.1. Analyzing the impact of grids' structure on leakage current

According to the accounting data [32], [34] there are three kinds of grid structure in 660V underground mining grids: single routine, two branches and skeleton, the simulation diagrams of those structures are presented in figure 5, 6.

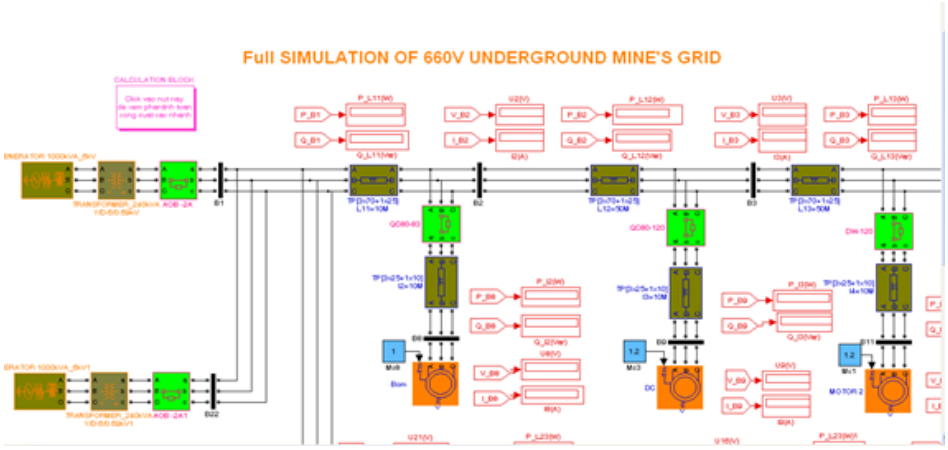


Figure 5. *The diagram of single routine grid*

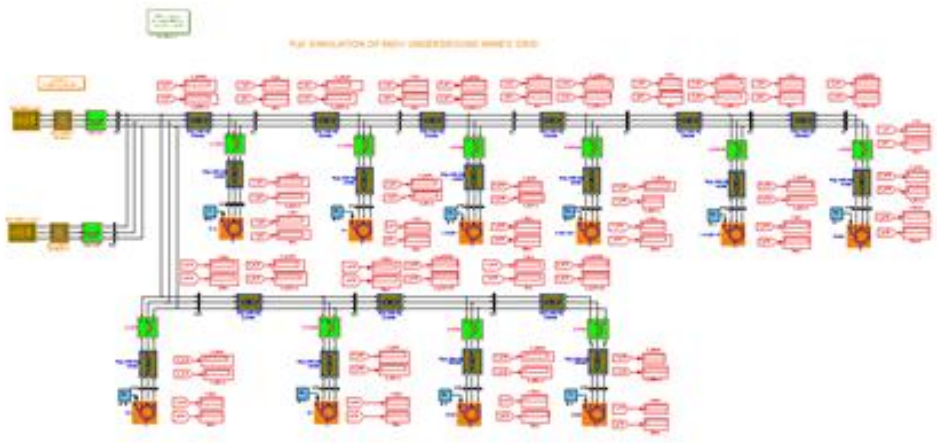


Figure 6. *The diagram of skeleton grid Implementing the simulation in MATLAB, the outcomes are shown in figure 7 and 8*

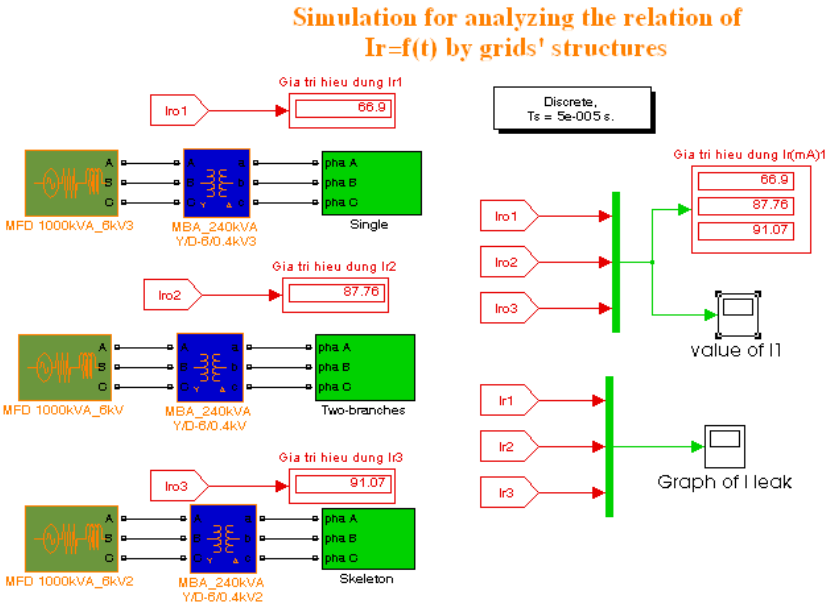


Figure 7. *The block diagram showing the calculation of leakage current I_r in various structure of grid*

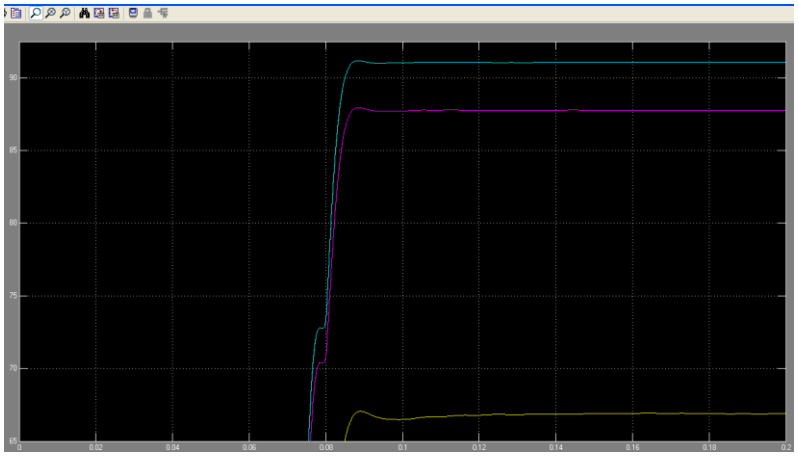


Figure 8. *The graph of $I_r = f(t)$ corresponding to various structure of grid*

The results show that with the same source but different grid's structure, the rms of leakage current has a significant bias (66.9 mA compare to 91.07mA).

3.2. Analyzing the impact of load ratio on leakage current

- Implementing in the same grid with parameters exhibited in

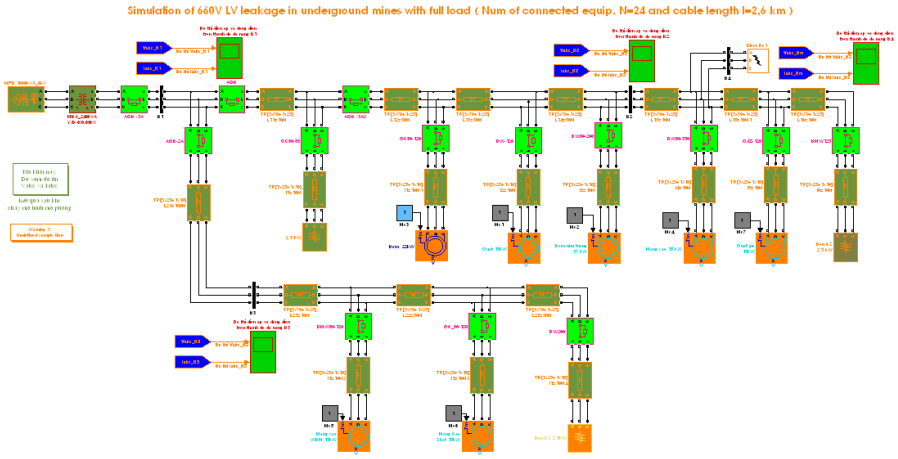


Figure 9. *The block diagram showing the calculation of leakage current I_r with load variation*

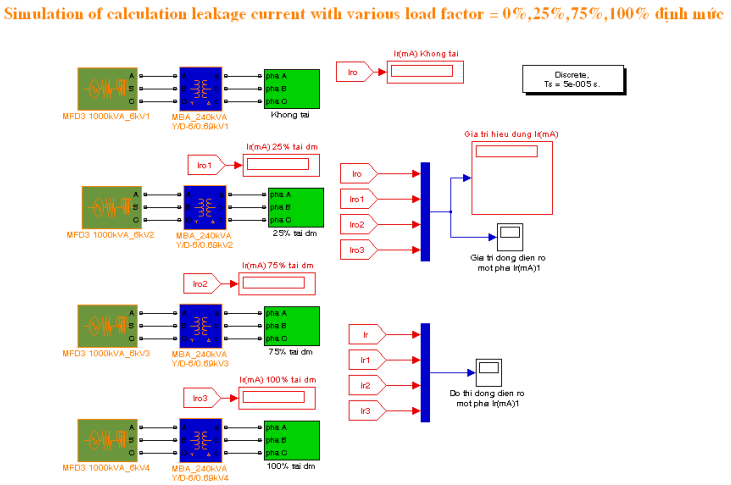


Figure 9. *The block diagram showing the calculation of leakage current I_r with load variation*

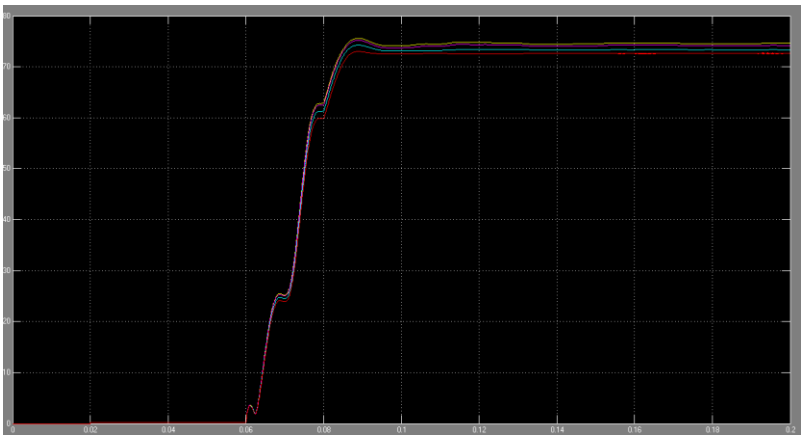


Figure 10. *The graph of I_r with load variation*

3.3. Other results from various underground mines

The simulations are implemented with some typical underground coal mines in QuangNinh of VietNam, the outputs are presented in table 1 to table 2:

Table 1: Results presenting the impact of Load on leakage current

Name	U_{nom} (V)	Structure	Ratio of Load/full load	Rms of leakage current (mA)
QuangHanh	660	Skeleton	20%	41,2
	660	Skeleton	50%	62
	660	Skeleton	70%	87,6
DuongHuy	660	Skeleton	20%	48,2
	660	Skeleton	50%	68
	380	Skeleton	50%	63,6
HaLam	660	Skeleton	20%	49,8
	660	Skeleton	50%	73,6
	660	Skeleton	70%	83,1
	660	Skeleton	95%	98,7
ThongNhat	660	Single-routine	20%	51,4
	660	Single-routine	50%	64
	660	Single-routine	70%	77,6

Table 2: Results presenting the impact of grid's structure on leakage current

Name of Coal mines	U_{nom} (V)	Structure	Ratio of Load/full load	Rms of leakage current (mA)
QuangHanh	660	Skeleton	70%	87,6
	660	Single-routine	70%	71
DuongHuy	660	Skeleton	50%	83,6
	380	Single-routine	50%	68
HaLam	660	Skeleton	50%	83,1
	660	Single-routine	70%	73,6

ThongNhat	660	Skeleton	70%	77,6
	660	Single-routine	70%	61,4

3.4. Conclusion

By utilizing the simulation in MATLAB, the paper investigated the impact of girds' structure and load ratio. The results deducted from the computing process show the following conclusion:

+ Corresponding to 3 typical structure of 660V underground mining grids, there are significant difference of leakage currents, the difference is nearly 50% and all of results are violate the allowance limit [11-13], therefore the manager should consider from designing stage for applying single routine diagram to reduce the rms of leakage current.

+ When the load is varied, the bias of I_r is about 15%, it is not so big, therefore the impact of load ratio could partly ignore in analyzing the electrical safety in underground mines.

+ In both cases, when no capacitance compensation is implemented, the rms of earthing current is violated the domestic and international allowance limit, hence there should be additional technical methods to enhance this unwanted fact.

REFERENCES

[1] NFPA 70E - *Standard for Electrical Safety in the Workplace* https://www.nfpa.org/-/media/Files/Code-or-topic-fact-sheets/70E2021FactSheet.ashx (accessed on 17th October 2023)

[2] IEC 60364-4-41 - *Electrical installations of buildings* - Part 4-41

[3] OSHA 29 CFR 1910 Subpart S – Electrical, USA.

[4] IEEE 1584 - IEEE *Guide for Performing Arc-Flash Hazard Calculations*

[5] IEEE 902 - IEEE *Guide for Maintenance, Operation, and Safety of Industrial and Commercial Power Systems* (Yellow Book)

[6] Richard B. Rubio, Electrical Safety - *A Practical Guide to OSHA and NFPA 70E*, Amazone publisher, 2018.

[7] Dennis K. Neitzel, *Electrical safety Update? OSHA 29 CFR1910.269 and NFPA 70E?-2015 Revisions*. IEEE Transactions on Industry Applications, 2016 http://dx.doi.org/10.1109/TIA.2016.2541098

[8] US department of Labor, *Electrical Safety Precautions Save Miners' lives* https://blog.dol.gov/2023/05/22/electrical-safety-precautions-save-miners-lives (accessed on 17th October 2023)

[9] Lixia Niu, Jin Zhoa and Jinhui Yang, *Risk Assessment of unsafe acts in coal mine gas explosion accidents based on HFACS-GE and Bayesian Networks*, Processes journal, February 2023-11(2), https://doi.org/10.3390/pr11020554

[10] Vlad Mihai Pasculescu, Dragos Pasculescu, Marius Simion Morar, *OHS risk assessment-a case study for underground coal mining electricians*, SWS Journal of Earth and Planetary Sciences, 2020, http://dx.doi.org/10.35603/eps2020/issue1.03

[11] Vietnam National regulation on safety Mining, QCVN 01:2011/BCT, 2011. http://www.kiemdinh.vn/upload/files/QCVN%2001-2011-BCT%20An%20toa%CC%80n%20trong%20khai%20tha%CC%81c%20than%20h%C3%A2%CC%80m%20lo%CC%80.pdf

[12] Coal Mining Safety and Health Regulation 2017, Part 4 *Electrical activities, equipment and installations*. https://www.legislation.qld.gov.au/view/pdf/asmade/sl-2017-0165

[13] *Safety Standards for Electrical Installations and Equipment in explosives facilities*, JSP 482 MOD Explosives Regulations, May 2016. https://assets.publishing.service.gov.uk/government/uploads/system/uploads/attachment_data/file/529168/20160526-JSP_482_Edt4_1_Chapter_8.pdf

[14] Niculescu, T., Arad, V., Marcu, M., Arad, S., & Popescu, F.G. (2020). *Safety barrier of electrical equipment for environments with a potential explosion in underground coal mines*. Mining of Mineral Deposits, *14*(3), 78-86. https://doi.org/10.33271/mining14.03.078

[15] Le Xuan THANH, Ho Viet BUN, *A new approach on AI application for grounding resistor prediction in underground mines of VietNam*, Naukovyi Visnyk Natsionalnoho Hirnychoho Universytetu journal, Vol 5, 2022

[16] Zheng, L., & Liu, S. (2018*). A survey of remote monitoring and fault diagnosis for power equipment based on IoT technology*. IEEE Access, 6, 10491-10502

[17] Ustun, T. S., & Ince, N. F. (2019). *Remote sensing applications for electrical grid safety: A comprehensive review*. IEEE Access, 7, 47498-47513

[18] Dong, X., & Goebel, R. (2018). *Best practices in electrical safety management: A case study of a large industrial facility*. Journal of Loss Prevention in the Process Industries, 55, 202-211

[19] He, Y., & Liu, L. (2019). *Emerging technologies for electrical safety: A review*. Sustainable Energy Technologies and Assessments, 35, 14-22

[20] Chen, X., & Huang, J. (2018). *An overview of electrical safety regulations and standards worldwide. Safety Science*, 105, 19-27

[21] Yan, Y., & Chen, C. (2017). *Analysis of the effectiveness of electrical safety regulations: A case study of the construction industry*. Journal of Construction Engineering and Management, 143(12), 04017105

[22] Khan, F., & Abbasi, S. (2018). *Electrical safety risk assessment in industrial settings: A review. Process Safety and Environmental Protection*, 116, 255-266

[23] Al-Haddad, S. A., & Rahman, M. A. (2018). *Advanced technologies for electrical safety enhancement in smart grids: A review*. IEEE Transactions on Industrial Informatics, 14(3), 1228-1236

[24] Zhang, J., & Zhang, C. (2017). *Electrical safety enhancement through innovative sensor technologies: A review*. IEEE Sensors Journal, 17(18), 5775-5784

[25] Kecojevic, V., Komljenovic, D., & Groves, W. (2007). *Analysis of fatalities and injuries involving mining equipment*. Journal of Safety Research, 38(4), 461-470

[26] Shishvan, S. S., Ataei, M., & Oraee, K. (2007). Modeling risk and its application in the selection of a mining method for an ore deposit in Iran. *Journal of the Southern African Institute of Mining and Metallurgy*, 107(11), 759-766

[27] Zhang, J., & Jee, S. (2018). *Risk assessment and risk management of underground coal mines in China*. Journal of Cleaner Production, 176, 35-45

[28]Brnich, M. J., Veverka, A., Chekan, G., Howerton, D., Hill, T., & Janisko, S. J. (2018). *Analysis of surface and underground coal mine fires involving mobile equipment*. Safety Science, 110, 225-235

[29] The Minerals Council South Africa. (2019*). Guideline for the Compilation of a Mandatory Code of Practice for Risk Based Emergency Care on a Mine*

[30] International Commission on Radiological Protection. (2017). *Occupational Radiological Protection in the Mining and Processing of Raw Materials*. ICRP Publication 132

[31] Xiaoning Qi, Sam C.Lo, Alex Gyure, Yansheng Luo, Mahmoud Shahram, Kishore Singhal and Don B.MacMilen, 2006, *Efficient subthreshold leakage current optimization*, IEEE circuits and devices magazine, September 2006

[32] Kim Ngoc Linh, 2006, "*Research the suitable leakage current protection utilized for Quang Ninh low voltage underground mines*", Unpublished Doctor dissertation, Hanoi University of Ming and Geology

[33] Le Xuan THANH, Ho Viet BUN, *Analyzing and identifying the limits of 660V grid parameters to ensure electrical safety in underground coal mines*, Naukovyi Visnyk Natsionalnoho Hirnychoho Universytetu journal, Vol 6, 2021 https://doi.org/10.33271/nvngu/2021-6/101

[34] Nguyen Anh Nghia, Nguyen Hanh Tien, *Electric power supply for underground mining* book for master of Electrical Engineering, Publication of Hanoi University of Mining and Geology, 2008.

SPATIAL-TEMPORAL CONVOLUTION NEURAL NETWORKS FOR TROPICAL CYCLONE DETECTION FROM GEOSTATIONARY SATELLITE IMAGES

L Q Dao[1], T H Hoang[3], L V Hung[1], B Q Hung[1], L R Hole[5], P T Hang[4], M K Hung[2] and D D Tien[2*]

[1] Center of Multidisciplinary Integrated Technologies for Field Monitoring University of Engineering and Technology, Vietnam National University, Hanoi, Vietnam

[2] National Center for Hydro-Meteorological Forecasting (NCHMF), Vietnam Meteorological and Hydrological Administration, Vietnam

[3]Viettel Cyberspace Center (VTCC), Vietnam; [4]People's Security Academy of Vietnam

[5]Norwegian Meteorological Institute, 5007 Bergen, Norway

Email: duductien@gmail.com

Abstract: In this study, a deep learning approach is investigated to detect and classify tropical cyclones (TCs) according to its stage in an end-to-end manner. A two-stream Convolution Neural Network (CNN) which captures both spatial and temporal features of time-series of geostationary satellite cloud images (SCIs) is proposed. A dataset of Himawari-8 SCIs of 104 TCs over Western North Pacific and Bien Dong Sea from 2014 to 2019 are collected. Additional inputs, namely atmospheric motion vector (AMV), related to tropical cyclone circulation features for the learning processes are derived by tracking clouds through consecutive SCIs. Results show that our proposed model significantly improves the performance of TC detection in comparison to other state-of-the-art based CNN models. Moreover, our case study for the detection of TC Doksuri in 2017 yielded promising results as our proposed model is capable of detecting/warning TC formation 24 hours in advance to the first time reported by the Japanese Meteorological Agency (JMA).

1. INTRODUCTION

Tropical cyclone (TC) as defined by the World Meteorological Organization (WMO) [1] is one of the natural disasters that have the greatest impact on all human socio-economic activities and threaten the lives and properties even when starting to form until decay and ending with consequences (storm surge, heavy rainfall, coastal urban inundation, floods, flash floods, landslides). Studying into tropical cyclones is a paramount concern of meteorologists because tropical cyclones often causes significant damages to human and property when it occurs. Detecting TC early and accurately will bring a lot of efficiency in weather forecasting.

Given the limitations of ground observations over open oceans (purely from buoys or ships), it is clear that the most reliable source of timely information is from Earth observation satellites. With the rapid development of satellite and radar technologies, we have more and more types of input data that can be used for TC detection and identification problems, for example the Geostationary Operational Environmental Satellite (GOES) series of the United States' National Oceanic and Atmospheric Administration (NOAA)'s in 1970s (Lombardi et. al. 2005[2]), The Multi-functional Transport Satellite (MTSAT) series of the Meteorological Satellite Center (MSC) of the Japanese Meteorological Agency (JMA) in 2005 and now as Himawari-8/9 satellites in 2015 (Murata et al 2018[3]).

The most widely analyzed method for TCs using satellite data is the Dvorak technique (DT, or manual DT) which was developed by Vernon Dvorak (Dvorak 1975[4], Dvorak 1984[5]). The DT bases on visible (VIS) and infrared (IR) satellite images and classifies TCs to several cloud patterns and makes a mainly intensity quantification based on the "Tropical Number" concept (T-number). The T- number from one to eight which is identical to the current intensity (CI) number except when cyclones are weakening, e.g. the curved band pattern (T1.0-T4.5), the shear pattern (T1.5–T3.5), central dense overcast (CDO) pattern (T2.5–T5.0), central cold cover (CCC) pattern, banding eye pattern (T4.0–T4.5), and eye pattern (T4.5–T8.0). The DT is then developed to a compute-based methods through automating rules in DT to classify storm clouds, namely the objective Dvorak technique (ODT) or then Advanced Objective Dvorak Technique (AODT)/Advanced Dvorak Technique (ADT) (Velden et. al. 1998[6], Olander et. al. 2004[7], Olander et. al. 2007[8]).

With regard to the rapid growing of volume of satellite data, the application of machine learning and deep learning to solve this issue has proven to be increasingly effective, surpassing the traditional approaches. Research by M. Kim et al. 2019 [9] compared detection of tropical cyclone (TC) formation using three different machine learning (ML) algorithms including decision trees (DT), random forest (RF), and support vector machines (SVM) and a model based on Linear Discriminant Analysis (LDA). The results revealed the superior effectiveness of machine learning over LDA. ML methods demonstrated significantly higher hit rates, ranging from 94% to 96%, compared to LDA's performance (~77%). However, the false alarm rate by MLs was slightly higher (21%–28%) than that of LDA (~13%). Furthermore, MLs detected TC formation as early as 26–30 hours before the first time diagnosed as a tropical depression by the JTWC best track, a margin of 5 to 9 hours earlier than LDA. In a recent study by Thu Zar Hsan et al. [10], a combination of Support Vector Machine and Polynomial Regression was employed to predict TC's track. The authors utilized a Support Vector Machine (SVM) to estimate the center of TCs, yielding better efficiency than conventional image processing techniques in storm detection.

Deep learning algorithms have also found applications in identification and classification tasks. Matsuoka et al. [11] employed a neural network model with a sophisticated architecture comprising 4 convolutional layers, 3 pooling layers, and 3 fully connected layers for binary classification of TCs. The model was trained with 50,000 images containing TCs and their precursors, alongside 500,000 non-TC data. The results indicated detection success rates for precursor identification 2, 5, and 7 days before formation, standing at 91.2%, 77.8%, and 74.8%, respectively, in the Northwestern Pacific. C. Kumler-Bonfanti et al. [12] used U-net model for the detection of regions of interest (ROIs) for tropical and extratropical cyclones. All four U-Net models acted as rapid information extraction tools and exhibited ROI detection accuracy ranging from 80% to 99%. They were further evaluated using Dice and Tversky Crossover-Union (IoU) metrics, yielding Dice coefficient scores within the range of 0.51 to 0.76 and Tversky scores ranging from 0.56 to 0.74. Chong Wang et al. [13] designed a set of deep convolutional neural networks (CNNs) to estimate the intensity of TCs in the Northwestern Pacific using brightness temperature data observed by the Advanced Himawari Imager on the Himawari-8 geostationary satellite. Their model was trained with 97 TCs from 2015 to 2018. The research also highlighted the significant influence of utilizing different infrared (IR) channels on the CNN model's

estimation performance, demonstrating the model's stability even in the presence of image noise. In Wei Tian et al. [14] study, a hybrid model based on CNN was proposed to estimate TCs intensity from satellite images. The TCs intensity was categorized into three levels, with each level employing a distinct model for corresponding intensity regression. Results indicated that this partitioned approach enhanced matching speed on smaller samples.

In this study, a deep learning approach is investigated to detect and classify tropical cyclones (TCs) according to its stage in an end-to-end manner. Our contributions is as follow:

- A two-stream CNN which captures both spatial and temporal features of time-series of geostationary satellite cloud images is proposed. Additional inputs, namely atmospheric motion vector (AMV), represent tropical cyclone temporal features are derived by tracking clouds through consecutive images.

- A dataset of Himawari-8 satellite images of 104 TCs over Western North Pacific and Bien Dong Sea from 2014 to 2019 are collected.

This paper is organized as follows. Section 2 contains the brief descriptions of methods. Section 3 present the experimental results and finally Section 4 is conclusions.

2. PROPOSED METHOD

2.1. Spatial-temporal architecture for Tropical Cyclone Detection

Time series of satellite images can be decomposed into spatial and temporal components. The spatial part, in the form of individual image, carries information about scenes and TCs depicted in the image. The temporal part, in the form of atmospheric motion across the continous images, conveys the wind strength and direction of TCs. We propose architecture accordingly, dividing it into two streams, as shown in Figure 1. In this paper we apply Residual Networks, or ResNets, to learn residual functions with reference to the layer inputs, instead of learning unreferenced functions. ResNets will fit a residual mapping and stacks residual blocks ontop of each other to form network: e.g. a ResNet-54 has fifty four layers using these blocks [15,16]. Each stream is implemented using a ResNet 54 backbone with feature pyramid net learning the spatial and temporal features concurrently, then combined by late fusion using stacked L2-normalised. The concated features is then used as input for header network with two subnetworks, one for classifying anchor boxes and one for regressing from anchor boxes to ground truth following the general architecture of RetinaNet.

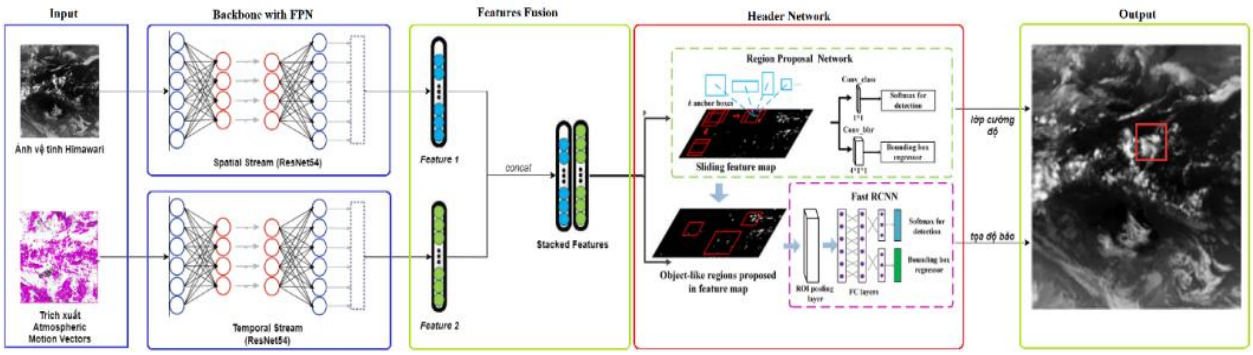


Figure 1: *Spatial-temporal architecture for tropical cyclone detection*

2.2. Temporal stream using Atmospheric Motion Vectors

The input to temporal stream is formed by constructing Atmospheric Motion Vectors (AMVs) between several consecutive satellite images. Such input explicitly describes the wind motion and strength of TCs between images, which makes the recognition easier, as the network does not need to estimate motion implicitly.

AMVs is a satellite-derived product that estimates the altitude and motion vector of clouds from satellite imagery. The AMV is calculated using maximum correlation block matchinhg algorithm using two block sizes which are (7x7) and (28x28). The output of AMVs construction is the wind angle and magnitude. To be used as input for the network, the AMVs output is encoded as HSV color space image with wind angle represent Hue value, and magnitude represent Value.

3. EXPERIMENTAL RESULTS

3.1. Dataset

Himawari-8 satellite image [17] is collected following the best-track data from the Regional Specialized Meteorological Center Tokyo (RSMC-Tokyo) of JMA from 2014 to 2019 over Western North Pacific and Bien Dong Sea with a total of 104 TCs. The RMSC-Tokyo, the WMO's Typhoon Center, provides information on TCs including present and forecast positions as well as the movement and intensity of tropical cyclones. The TC's intensity is divided into six types, including: tropical Depression (TD), tropical storm (TS), severe tropical storm (STS), typhoon (TY), extra tropical cyclone (L) and other.

In this paper, we used infrared data wih the resoltion of 2km x 2km for each pixel. Dataset is then divided into a training set of 60%, a validation set of 20%, and a test set of 20%.

3.2. Evaluation method

Intersection over Union (IoU) is used to evaluate the performance of object detection by comparing the ground truth bounding box to the predicted bounding box. It is often used for evaluation in object detection problems.

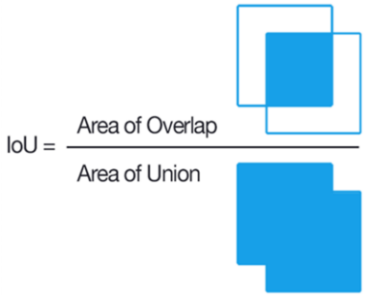


Figure 2: *Formula to calculate IOU*

Evaluation criteria are correctly detected objects (IoU ≥ 0.5), falsely detected objects (IoU < 0.5) and objects not recognized. From the IoU, the rate of correct detection (True Positive -TP), false detection (False Positive -FR), and unrecognizable (False Negative - FN) will be determined to calculate the mAP(mean Average Precision). mAP is also known as Precision-Recall Curve. Precision is a scale that characterizes forecast accuracy. Recall is a scale that characterizes the goodness of the ability to find an accurate prediction region (also known as the sensitivity of the method).

$$Precision = \frac{TP}{TP+FP} \quad (1)$$

$$Recall = \frac{TP}{TP+FN} \quad (2)$$

Suppose there are N thresholds to calculate Precision and Recall, with each threshold for a pair of Precision and Recall values as Pn, Rn, with n=1, 2, …, N. Precision-Recall Curve

is drawn by connecting each coordinate point (Pn, Rn). AP will be calculate by below formula.

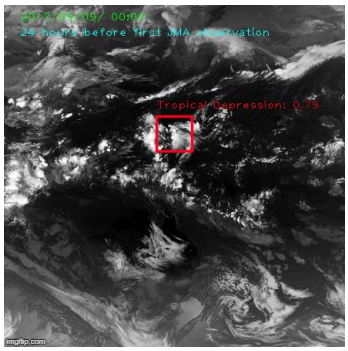
$$AP = \frac{\sum_n R_n - R_{n-1}}{P_n} \quad (3)$$

mAP is the average AP of all classes. mAP is the average reliability of the method. This will be a quantitative method to evaluate the recognition success rate of the identification method using AI.

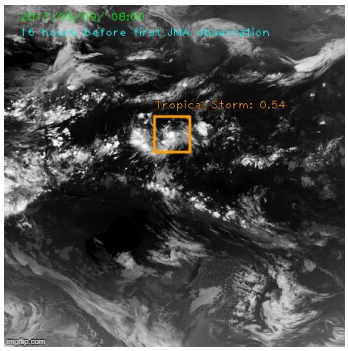
3.3. Results

We compare our proposed methods with 1) RetinaNet model trained on satellite image only, and 2) RetinaNet trained with AMVs only. Quantitative comparisons based on mAP are summarized in Table 1. As expected, our proposed method show significant improvements in compare to two other approaches (mAP of 66.2% in compare to 52.69% and 23.69%). The results validate our assumption that by combining both satellite image and its AMVs can enhance the performance of detection model.

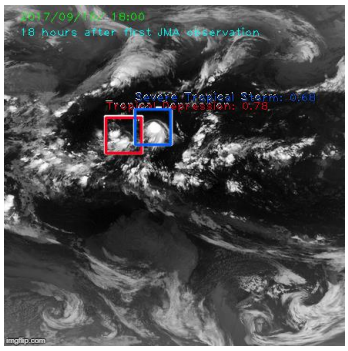
Finally, we give in Figure 3 the tropical cyclone detection results for our proposed model in case study for Doksuri in 2017. Our model achieve the mAP of 93.1% and is able to detect the formation of Doksuri 24 hours before the first warning of JMA.



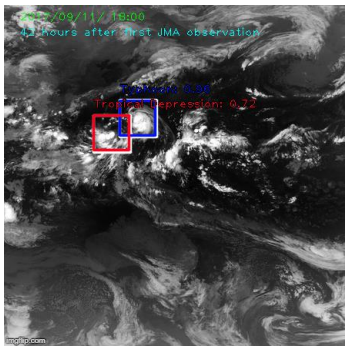
TD (2017/09/09 00:00)



TS (2017/09/09 08:00)



STS (2017/09/10 18:00)



TY (2017/09/11 18:00)

Figure 3. *Case study of Doksuri detection. White box is ground truth from JMA. Red, Orange, Blue boxes are the detection results of our proposed model.*

Table 1. The mean average precision (mAP) of proposed methods

Class	#samples	Satellite image RetinaNet	AMVs RetinaNet	Image + AMVs RetinaNet(proposed)
Tropical Depression (TD)	94	34.51	10.69	60.78

Tropical Storm (TS)	109	52.44	12.87	66.95
Severe Tropical Storm (STS)	45	33.28	19.35	42.30
Typhoon (TY)	103	88.18	60.67	89.13
Extra-tropical Cyclone (L)	76	38.93	7.71	57.24
Weighted average	427	52.69	23.69	66.62

4. CONCLUSION

In this study, we introduce a new CNN-based approach dedicated to tropical cyclone detection using geostationary satellite imagery. Our approach utilizes the use of both spatial and temporal features of the TC in an end-to-end manner. Experiments show that our proposed model outperforms conventional approaches widely used in the literature. Our future work would focus on the augmentation of data using unsupervised learning approach to better utilize large amount of satellite image without the present of TCs.

REFERENCES

[1] https://public.wmo.int/en/our-mandate/focus-areas/natural-hazards-and-disaster-risk-reduction/tropical-cyclones.

[2] Lombardi, Michael A.; Hanson, D. Wayne (March–April 2005). "The GOES Time Code Service, 1974-2004: A Retrospective". Journal of Research of the National Institute of Standards and Technology. 110 (2): 79–96. doi:10.6028/jres.110.008.

[3] Murata, H., K. Saitoh, and Y. Sumida, 2018: True color imagery rendering for Himawari-8 with a color reproduction approach based on the CIE XYZ color system. J. Meteor. Soc. Japan. Doi: 10.2151/jmsj. 2018-049.

[4] Dvorak, V., 1975: Tropical cyclone intensity analysis and forecasting from satellite imagery. Mon. Wea. Rev., 103, 420-430.

[5] Dvorak, V., 1984: Tropical cyclone intensity analysis using satellite data. NOAA Tech. Rep. NESDIS 11, 47 pp. [Available from NOAA/NESDIS, 5200 Auth Rd., Washington, DC 20233].

[6] C.S. Velden, T. Olander, R.M. Zehr: Development of an objective scheme to estimate tropical cyclone intensity from digital geostationary satellite imagery, Wea. Forecasting, 13 (1998), pp. 172-186.

[7] Olander, T.L., C.S. Velden, and J.P. Kossin, 2004: The Advanced Objective Dvorak Technique (AODT) – Latest upgrades and future directions. 26th Conference on Hurricanes and Tropical Meteorology, Miami, FL, Amer. Meteor. Soc., 294-295.

[8] Olander, T.L., and C.S. Velden, 2007: The Advanced Dvorak Technique (ADT) – Continued development of an objective scheme to estimate tropical cyclone intensity using geostationary infrared satellite data. Wea. Forecasting, 22, 287-298.

[9] Minsang Kim, Myung-Sook Park 3, Jungho, Seonyoung Park, Myong-In Lee.

Machine Learning Approaches for Detecting Tropical Cyclone Formation Using Satellite Data. Remote Sens. 2019, 11(10), 1195; https://doi.org/10.3390/rs11101195

[10] Thu Zar Hsan, Myint Myint Sein. Combining Support Vector Machine and Polynomial Regressing to Predict Tropical Cyclone Track. 2021 IEEE 3rd Global Conference on Life Sciences and Technologies (LifeTech). DOI: 10.1109/LifeTech52111.2021.9391780.

[11] Matsuoka, D., Nakano, M., Sugiyama, D., Uchida, S. (2018), Deep learning approach for detecting tropical cyclones and their precursors in the simulation by a cloud-resolving global nonhydrostatic atmospheric model. Prog. Earth Planet. Sci., 5, 80.

[12] C. Kumler-Bonfanti, J. Stewart, D. Hall and M. Govett, "Tropical and extratropical cyclone detection using deep learning", J. Appl. Meteorol. Climatol., vol. 59, no. 12, pp. 1971-1985, Dec. 2020.

[13] C. Wang, G. Zheng, X. Li, Q. Xu, B. Liu and J. Zhang, "Tropical cyclone intensity estimation from geostationary satellite imagery using deep convolutional neural networks", IEEE Trans. Geosci. Remote Sens., Mar. 2021.

[14] W. Tian, W. Huang, L. Yi, L. Wu and C. Wang, "A CNN-based hybrid model for tropical cyclone intensity estimation in meteorological industry", IEEE Access, vol. 8, pp. 59158-59168, 2020.

[15] Pešek, O.; Segal-Rozenhaimer, M.; Karnieli, A. Using Convolutional Neural Networks for Cloud Detection on VENμS Images over Multiple Land-Cover Types. Remote Sens. 2022, 14, 5210. https://doi.org/10.3390/rs14205210

[16] He, K.M.; Zhang, X.Y.; Ren, S.Q.; Sun, J. Deep Residual Learning for Image Recognition. In Proceedings of the IEEE Conference on Computer Vision and Pattern Recognition (CVPR), Boston, CA, USA, 26 June–1 July 2016; pp. 770–778.

[17] Murata, H., K. Saitoh, Y. Sumida, 2018: True color imagery rendering for Himawari-8 with a color reproduction approach based on the CIE XYZ color system. J. Meteor. Soc. Japan. doi: 10.2151/jmsj. 2018-049

ACKNOWLEDGMENTS:

This research is supported by the Ministry of Science and Technology's project titled: "*Reaseach and application of artificial intelligence technique to build the forecasting system of tropical cyclone activity over Bien Dong sea and affecting Vietnam with lead time up to 3 days, Code: KC-4.0-46/19-25*" under “The program for supporting research, development and technology application of Industry 4.0". Hole was supported by the Norwegian Agency for Development Cooperation (NORAD).

PREDICTION OF SPECIFIC CHARGE IN TUNNEL BLASTING

Nguyen Chi Thanh[1,*] , Nguyen Viet Nghia
1 Faculty of Civil Engineering, Hanoi University of Mining and Geology, Hanoi, Vietnam
2 Mine Surveying Departments, Hanoi University of Mining and Geology, Hanoi, Vietnam
*E-mail: nguyenchithanh@humg.edu.vn

Abstract: Currently, tunnel construction extensively utilizes the drilling and blasting method. It is important to calculate the specific charge accurately for this method. The specific charge significantly affects the advancement of tunnel construction, the involved workload, and the stability of the tunnel both during construction and its subsequent operation. In practice, establishing the value of a given charge is intricately tied to rock properties at the explosion site. Empirical formulas are employed to calculate this value. However, accurately determining a specific charge is difficult and requires adjustments based on the prevailing characteristics of the tunnel construction site. This study has developed two AI models that use ANN and ANFIS techniques. These models are designed to predict the specific charge for the Deo Ca tunnel in Phu Yen, Vietnam. The paper employs 100 databases to construct these AI models, enabling accurate prediction of the specific charge required in the construction of the Deo Ca tunnel.

1. INTRODUCTION

The drilling and blasting method is a traditional method, widely used in underground construction, because of its advantages, including: low cost, does not require a high technical level, and low investment cost, the method can be used for tunnels with different features and in different geological conditions... By calculations and results obtained in practice, it can be given it was commented that the effectiveness of blasting for tunneling depends on the rock mass characteristics that surrounding the tunnels and the properties of the explosives used in the blasting method as well as the interactions between them. A number of important parameters can greatly affect the efficiency of the blasting process, including the specific charge, the area of the tunnel face, the mechanical properties of the rock mass where it is stored tunnels, properties of boreholes used in tunnel construction... Among these important parameters, the specific charge is considered one of the most important criteria that can greatly affect the advancement of tunnel construction, the amount of work that needs to be completed during the process of tunnel construction, and also greatly affects the stability of the tunnel during construction and use. Thus, on the basis of the above analysis, it can be seen that it is necessary to accurately determine the value of the specific charge when tunneling by the drilling and blasting method. In fact, at present, to determine the value of the specific charge during the construction of tunnels by drilling and blasting method, empirical formulas [1] are often used. These empirical formulations consider the properties of the explosives and the parameters of the rock mass surrounding the tunnel. In some models studied by authors such as Ryu, C.H et al., 2006 [2]; Han J. et al., 2000 [3]... mentioned the influence of a number of other parameters on the specific charge index value, including the static and dynamic elastic modulus of the rock mass that

surrounding the tunnel. However, the value of the specific charge obtained when using empirical formulas for calculation is often not very accurate and needs to be adjusted in accordance with the actual construction of the tunnel.

Currently, there have been a number of studies using artificial intelligence to determine and predict the amount of the specific charge when using drilling and blasting methods for tunnel construction [4], [5], [6]. Initially, the results obtained from these studies have proved the accuracy of the artificial intelligence models when these models are used to predict the value of the specific charge indicator in the process construction of tunnels using the drilling and blasting method.

In this study, two AI models, specifically the artificial neural network (ANN) and artificial neuro-fuzzy (ANFIS) models, were developed to forecast the precise charge during the construction of tunnels using the drilling and blasting technique. A dataset of 100 variables, gathered from the actual construction of the Deo Ca traffic tunnel in Phu Yen, Vietnam, was utilized to train these AI models. By assessing the determination coefficients R^2 and the root mean square error (*RMSE*) deviation of the predicted values against the actual specific charge values employed in the construction of Deo Ca traffic tunnels, it's clear that utilizing AI models to predict the specific charge of tunnel construction using the drilling and blasting method is practical and essential.

2. CASE STUDY AND DATA PROCESSING

Deo Ca traffic tunnel is located between the two provinces, Phu Yen and Khanh Hoa. The total length of the Deo Ca traffic tunnel is 4.2 km and the tunnel is located in a rocky area with relatively complex geological conditions with mainly igneous and metamorphic rocks. According to geological surveys of the rock mass that surrounds the tunnel, the rock mass rating (*RMR*) has a large amplitude of fluctuations, receiving values from 0 to 73. This tunnel has a constant cross-sectional shape, a vertical-wall arched.



Figure 1. *Deo Ca tunnel project.*

In this study, a database of 100 variables obtained from the actual construction of the Deo Ca tunnel was used to train and test for artificial intelligence models, these capable of predicting the specific charge q for tunnel construction by the drilling and blasting method. In there, which uses 80% of datasets to train the models, and 20% of datasets were used in testing models' performance. By the evaluation and comments, this study used 3 parameters as input variables for artificial intelligence models built to predict the specific charge (*Q*), including rock mass rating RMR; the design area of the tunnel face (S_d); the average boreholes length (*L*). The output variable of the built artificial intelligence models is the specific charge *Q*. The data in this study were normalized using the following equation, resulting in a range of [-1÷1] [7], [8], [9]:

$$Y_n = \frac{Y - Y_{min}}{Y_{max} - Y_{min}} \quad (1)$$

Where Y and Y_n: the measured and normalized values, respectively. Y_{min}: the minimum measured variable, Y_{max} is the maximum measured variable, respectively.

Table 1 represents the value regions of the input and output variables of the artificial intelligence models. In this paper, all datasets used to build artificial intelligence models are divided to conduct the 5-fold cross-validation, random datasets. Build AI models using these datasets to predict the specific charge (*Q*). Compare models' prediction results to select optimal models.

Table 1. The input and output variables.

The variables	Symbols	Unit	Role	Min	Max
Rock Mass Rating	*RMR*	-	Input	4.9833	72.0142
The design area of tunnel face	S_d	m^2	Input	48.6126	63.9853
The average boreholes length	*L*	m	Input	1.0403	3.2089
Specifc Charge	*Q*	kg/m^3	Output	0.4193	2.3415

3. MODELING

2.1. ANN modeling

Artificial neural networks (ANNs) are built and developed by McCulloch and Pitts, 1943 [10]. ANNs operate similarly to human neurons. The multi-layer perceptron (MLP), designed by Haykin, 1999 [11] is a widely utilized and advanced artificial neural network. Consisting of input layer, hidden layers, and output layer, MLP's neurons are interconnected via weights. Typically, number of hidden layers and number of neurons in these hidden layers are determined through trial and error [12], [13]. In an ANN, each input parameter is initially assigned a weight between 0 and 1. The input is multiplied by the weight, and the sum of these values is given to the hidden layer(s). This result is then added to the bias (neuron weight), typically set as one.

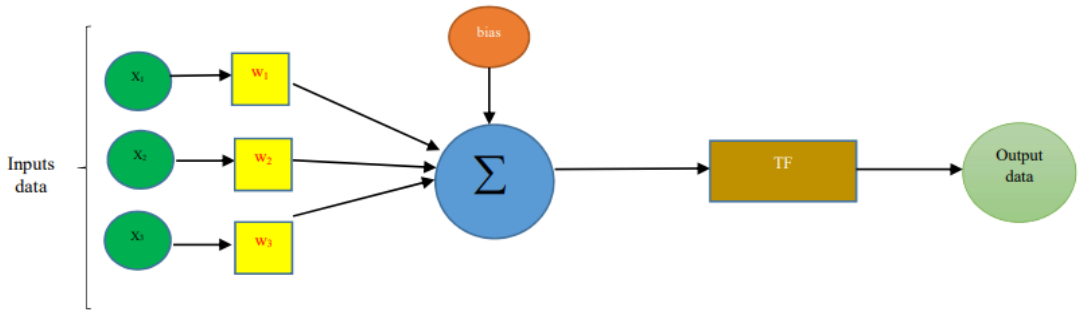


Figure 2. *The architecture of the ANN model.*

The process continues with a new weight assigned to the obtained value, moving to the next layer (output layer). The sum of all values obtained from each layer represents the final step of ANN modeling. In a feed-forward-backpropagation (FF-BP) algorithm, signals pass from the input layer to the output layer during the forward pass. The system's results are then compared to the actual values to calculate the error [7], [8]. This error is then sent backward through the network to update the weights during the backward pass. This

procedure helps reduce errors for both the training and testing datasets. The feed-forward-backpropagation process repeats until the error converges to a defined level determined by a cost function like mean square error (*MSE*) or root mean squared error (*RMSE*) [14], [15]. However, constructing a suitable ANN model requires a database with an adequate number of datasets.

In this paper, MLP has been used in the ANN model to predict the specific charge in tunnel construction by the drilling and blasting method. In this study, a hidden layer of neurons is utilized. As per certain authors, the hidden layer's neuron count significantly affects the model's predictions. Typically, the hidden layer's neuron count should not exceed "2*N+1", with N representing the input variables' count [16]. To assess the quality of AI models, 5-fold cross-validation is employed. The 5 sub-datasets, each of equal size, are divided to conduct the 5-fold cross-validation. Using 5 models for 5 randomly generated datasets derived from the original dataset. Tables 2 and 3 present the results obtained for models with varying hidden layer neuron counts. This study examined ANN models with 1 to 9 neurons in the hidden layer and identified an optimal architecture: the ANN (3x5x1) model with N=5 neurons in the hidden layer. The activation function is tangent sigmoid function. This model yields the best results (highest R^2 and lowest *RMSE*) among the surveyed ANN models. The results of the respective models are shown in Tables 2 and 3.

Table 2. Selecting the number of optimal neurons for the hidden layer of the ANN model based on R^2.

Number nerouns in hidden layer	Network result														
	The determination coefficients R^2														
	Iteration 1		Iteration 2		Iteration 3		Iteration 4		Iteration 5		Average		Rank		
	Train	Test	Train	Test	Train	Test	Train	Test	Train	Test	Train	Test	Rank Train	Rank Test	Sum Rank
1	0.6419	0.5327	0.7178	0.4871	0.6221	0.8411	0.7216	0.4539	0.6243	0.7919	0.6656	0.6213	3	7	10
2	0.5854	0.2301	0.6174	0.0415	0.6703	0.8347	0.7572	0.3005	0.6516	0.7924	0.6564	0.4398	2	1	3
3	0.6802	0.4352	0.7235	0.5765	0.3023	0.6521	0.7872	0.2638	0.6786	0.8765	0.6344	0.5608	1	3	4
4	0.7135	0.6649	0.7067	0.4308	0.6365	0.7792	0.7904	0.3968	0.5872	0.7922	0.6869	0.6128	4	6	10
5	0.6962	0.6352	0.7920	0.4513	0.6820	0.7992	0.7675	0.3374	0.7035	0.9124	0.7282	0.6271	6	8	14
6	0.7949	0.5240	0.7918	0.4513	0.6743	0.7678	0.8007	0.2993	0.7113	0.8842	0.7546	0.5853	8	4	12
7	0.6416	0.3800	0.7305	0.5570	0.6358	0.7520	0.7812	0.1920	0.6562	0.8233	0.6891	0.5409	5	2	7

According to Tables 2 and 3, following Chi Thanh Nguyen et al., 2022 [9] ranking principle, the chosen ANN model for predicting specific charge (*Q*) during the construction

of the Deo Ca tunnel using drilling and blasting is 5th model, there are 5 neurons in the hidden layer of this model.

Table 3. Selecting the number of optimal neurons for the hidden layer of the ANN model based on RMSE

Number nerouns in hidden layer	Network result														
	The root mean square error *RMSE*														
	Iteration 1		Iteration 2		Iteration 3		Iteration 4		Iteration 5		Average		Rank		
	Train	Test	Train	Test	Train	Test	Train	Test	Train	Test	Train	Test	Train	Test	Sum Rank
1	0.0066	0.0087	0.0061	0.0080	0.0067	0.0055	0.0063	0.0074	0.0070	0.0054	0.0065	0.0070	3	6	9
2	0.0070	0.0114	0.0072	0.0085	0.0064	0.0064	0.0060	0.0083	0.0068	0.0058	0.0067	0.0081	1	1	2
3	0.0063	0.0093	0.0061	0.0073	0.0091	0.0091	0.0055	0.0077	0.0064	0.0041	0.0067	0.0075	2	2	4
4	0.0058	0.0074	0.0063	0.0082	0.0067	0.0066	0.0055	0.0065	0.0074	0.0057	0.0063	0.0069	4	7	11
5	0.0060	0.0078	0.0053	0.0084	0.0005	0.0059	0.0059	0.0069	0.0061	0.0037	0.0048	0.0065	9	9	18
6	0.0049	0.0089	0.0054	0.0077	0.0063	0.0064	0.0055	0.0082	0.0061	0.0060	0.0056	0.0074	8	3	11
7	0.0067	0.0101	0.0060	0.0074	0.0066	0.0066	0.0056	0.0082	0.0067	0.0048	0.0063	0.0074	5	4	9

3.2. ANFIS modeling

ANFIS is a hybrid intelligent system that combines fuzzy logic and artificial neural networks to process data and make predictions, integrating their learning and reasoning capabilities to enhance prediction compared to using either method alone. Its objective is to establish a mapping that accurately associates input values with target values. ANFIS employs a fuzzy inference system (FIS) where each fuzzy rule defines a local system behavior. The ANFIS model consists of 5 layers: input, rule, normalization, defuzzification, and output. The ANFIS model used the BP back-propagation algorithm with least square estimation to adjust the nonlinear parameters of the MFs. [17].

The ANFIS system has got two fuzzy if-then rules of Takagi-Sugeno's type:

$$\textit{Rule 1: If } (x \text{ is } A_1) \textit{ and } (y \text{ is } B_1) \textit{ then } (f_1 = p_1x + q_1y + r_1) \quad (2)$$

$$\textit{Rule 2: If } (x \text{ is } A_2) \textit{ and } (y \text{ is } B_2) \textit{ then } (f_2 = p_2x + q_2y + r_2) \quad (3)$$

Where A_1 and B_1 are the fuzzy sets (nonlinear parameters of premise part); p_1, q_1 and r_1 are linear parameters of the consequent part (the design parameters); x and y is the inputs.

In the first Layer: The initial layer fuzzifies the input signal via adaptive nodes:

$$i=1, 2\ O_{1,i} = m_{Ai(x)}; \quad (4)$$

$$i=3,4\ O_{2,i} = m_{Bi(y)}. \quad (5)$$

Every node in this layer is an adaptive node. Parameters in this layer are called premise parameters.

Where x and y are the inputs to the first layer. A and B are the fuzzy sets. $O_{1,i}$ is the membership degree of the fuzzy set A according to the "x" input. $O_{2,i}$ is the membership degree of the fuzzy set B according to the "y" input, and m_{Ai} and m_{Bi} are the fuzzy membership function curve.

The Layer 2. Fixed nodes labeled Π multiply incoming signals, representing rule firing strength. In the 2nd layer: Layer 1's output becomes input to IF-THEN rule in Layer 2.

$$w_i = m_{Ai}(y) * m_{Bj}(y)\ i=1, 2 \quad (6)$$

The third Layer layer normalizes Layer 2's output as input to Layer 3.

$$\boldsymbol{w_i} = \frac{\boldsymbol{w_i}}{\boldsymbol{w_1+w_2}} i=1, 2 \quad (7)$$

Fourth layer: The fourth layer defuzzification of Layer 3's output occurs.

Fifth layer: In the fifth layer, Final model output is determined by summing results from previous layer computations (4th layer).

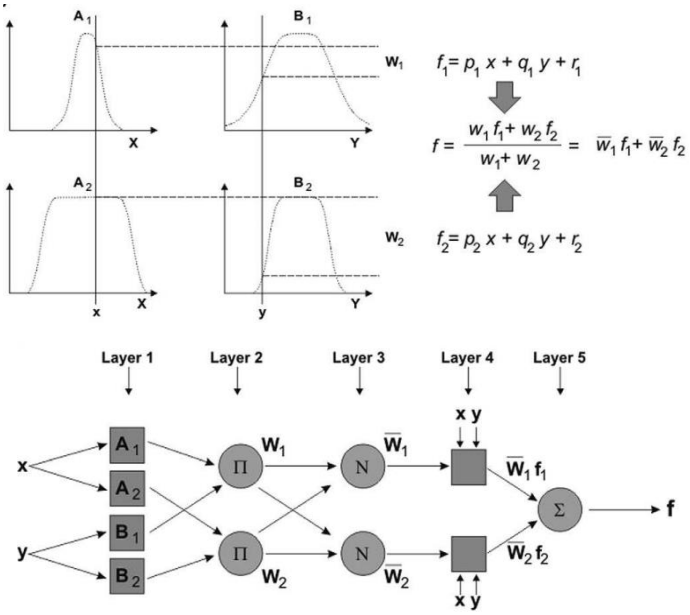


Figure 3. *The ANFIS model has got two fuzzy if-then rules of Takagi-Sugeno's type. [18]*

In this paper, several models were built and trained, each having three input parameters and one output parameter. To evaluate ANFIS models, cross-validation is used with 5-fold cross-validation. The 5 sub-datasets, of equal size, are split to perform the cross-validation. The models were assessed based on their structures (FIS division), with R^2 and *RMSE* used to determine the best model. During the development of an ANFIS model for estimating the specific charge, three membership functions were incorporated for each input parameter along with three rules. Table 4 outlines the additional parameter types and corresponding values used in the artificial neuro-fuzzy (ANFIS). The correlation between measured and predicted values derived from the artificial neuro-fuzzy (ANFIS) model during the testing phase is illustrated in Figure 4.

Table 4. The ANFIS parameters.

ANFIS parameter type	Value
Membership function (MF) type	Gaussia
Number membership function MFs	3
Type of Output function	Linear
Number of nodes	78
Number of linear parameters	27
Total number of parameters	54
Number of training data pairs	80
Number of fuzzy rules	27

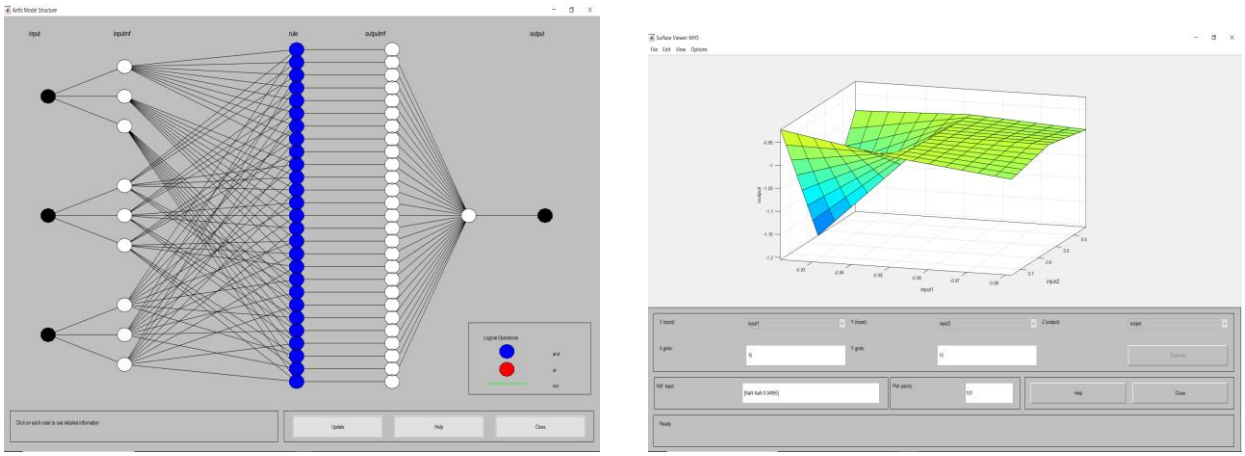


Figure 4. ANFIS model structures.

Based on the trial-and-error method and employing the simple ranking technique, the authors selected the optimal ANFIS model with its architecture and parameters (fuzzy rule count and input membership function type) [19], [20]. It can be concluded that the ANFIS structure with 3 MFs per input yields superior performance when comparing the models' *RMSE*. In the final step, ANFIS models were constructed to forecast the specific charge values. The predictive performances of these ANFIS models are displayed in Tables 5, 6 and 7. Table 5, 6 and 7 demonstrates that the specific charge *Q* values were repeated five times using the same randomly chosen datasets employed in the ANN model. Based on the table's results, 5th model was selected as it outperformed the other models.

4. RESULTS AND DISCUSSION

This paper describes and compares the use of artificial neural network (ANN) and artificial neuro-fuzzy inference system (ANFIS) models for predicting the specific charge. In this study, the authors discussed and compared the utilization of ANN and ANFIS models for predicting the specific charge. The modelling process involved randomly selecting 100 datasets and dividing them into five sets to build models in case of Deo Ca tunnel. To assess the prediction performance, the authors calculated various performance indices such as R^2 and root mean square error (*RMSE*).

Table 5. R^2 of ANFIS models to predict specific charge.

ANFIS Model	Network result									
	The determination coefficients R^2									
	ANFIS Model 1		ANFIS Model 2		ANFIS Model 3		ANFIS Model 4		ANFIS Model 5	
	Train	Test	Train	Test	Train	Test	Train	Test	Train	Test
ANFIS Sugen 3x3x3	0.8141	0.5801	0.8228	0.5264	0.7654	0.8358	0.829	0.3446	0.7702	0.8577
Rank	3	3	4	2	1	4	5	1	2	5
SumRank of R^2	6		6		5		6		7	

Table 6. RMSE of ANFIS models to predict specific charge.

ANFIS Model	Model's result									
	The root mean square error *RMSE*									
	Model 1		Model 2		Model 3		Model 4		Model 5	
	Train	Test	Train	Test	Train	Test	Train	Test	Train	Test
ANFIS Sugen 3x3x3	0.0046	0.0081	0.0048	0.0081	0.0052	0.0053	0.0049	0.0075	0.0053	0.0068
Rank	1	4	2	5	4	1	3	3	5	2
SumRank of *RMSE*	5		7		5		6		7	

Table 7. SumRank ANFIS models

ANFIS Sugen Model 3x3x3	ANFIS Model 1	ANFIS Model 2	ANFIS Model 3	ANFIS Model 4	ANFIS Model 5
SumRank models	11	13	10	12	14

The graphs in Figures 5, 6, and 7 show the predicted specific charge Q using ANN, and ANFIS techniques compared to the measured specific charge for training and testing datasets. From these figures, it is evident that the ANFIS model outperforms other predictive models in predicting the specific charge *Q*. The $R^2_{testing}$ value of 0.8577 for the testing dataset further confirms the superiority of the artificial neuro-fuzzy inference system (ANFIS) model, while the corresponding values for artificial neural networks (ANN) model is $R^2_{testing}$=0.9124, respectively. For the training dataset, $R^2_{training}$value of 0.7702 of the ANFIS model and 0.7035 of the ANN model. With *RMSE*, for the training dataset, $RMSE_{training}$= 0.0053 with the ANFIS model and $RMSE_{training}$= 0.0061 with the ANN model. For the testing dataset, the $RMSE_{testing}$ of the ANFIS model has the value $RMSE_{testing}$= 0.0068; ANN model has $RMSE_{testing}$= 0.0037. It is evident that the ANFIS and ANN models have the higher performance capacity compared to other techniques previously implemented (Table 2, 3, 5, 6 and 7).

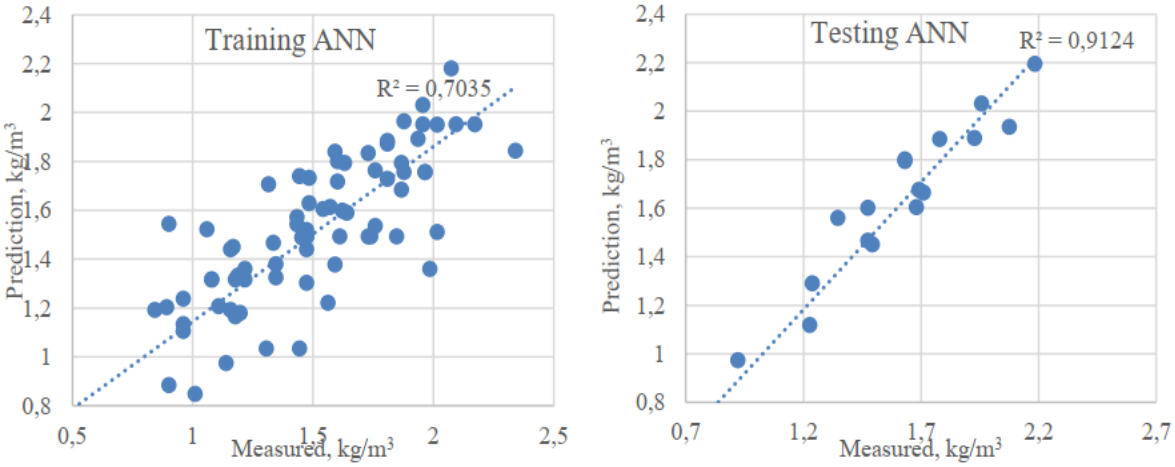


Figure 5. *Correlation coefficient for the ANN model.*

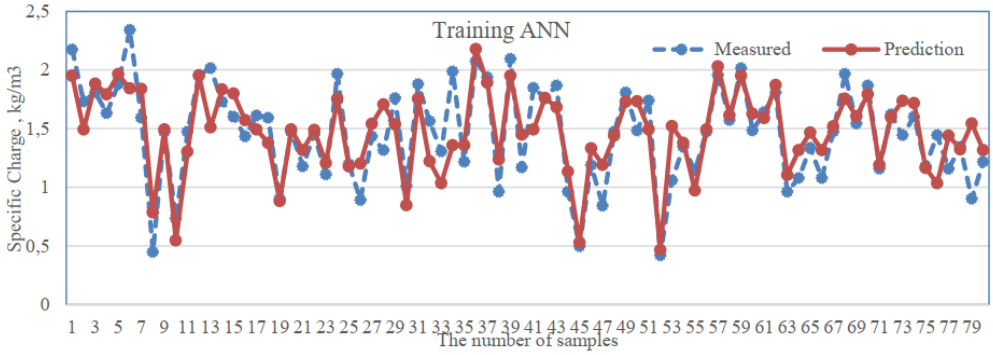


Figure 6. *The simile of measured and predicted specific charge in the training database of Artificial neural network (ANN) model.*

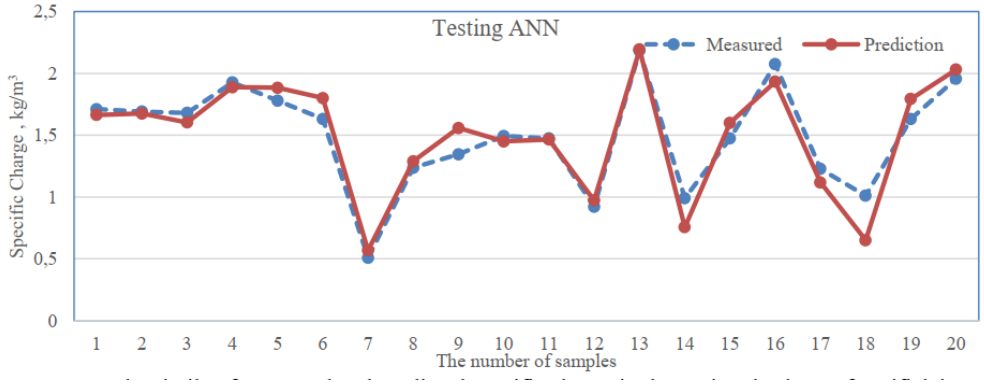


Figure 7. *The simile of measured and predicted specific charge in the testing database of Artificial neural network (ANN) model.*

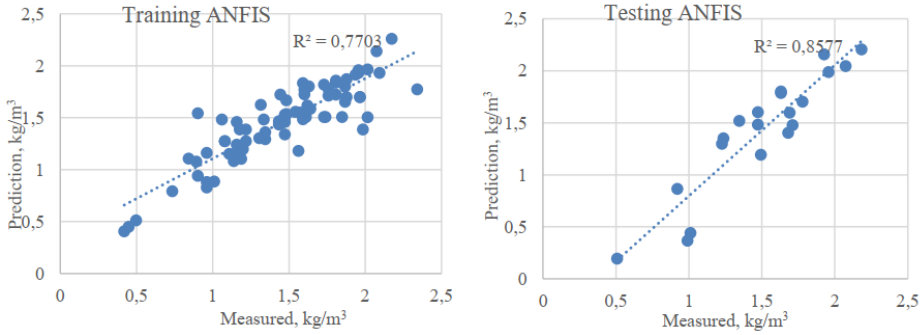


Figure 8. *Correlation coefficient for the ANFIS model.*

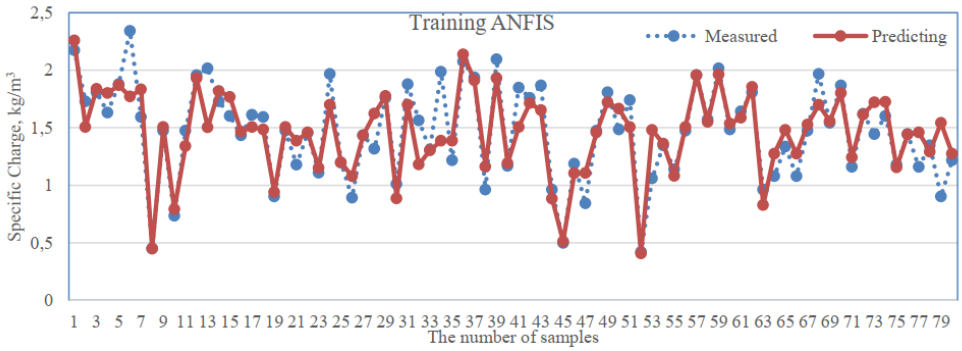


Figure 9. *The simile of measured and predicted specific charge in the training database of Artificial neuro-fuzzy inference system (ANFIS) model.*

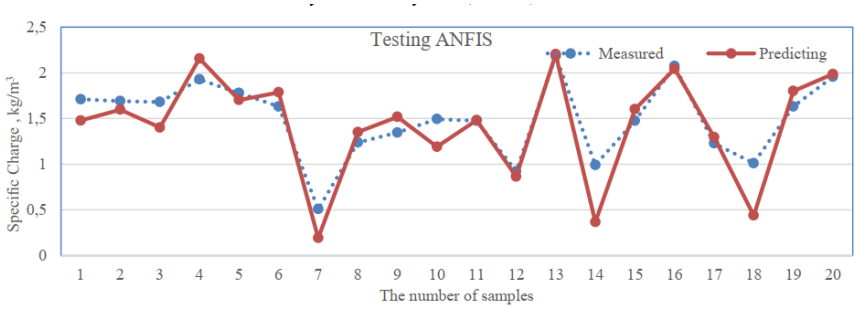


Figure 10. *The simile of measured and predicted specific charge in the testing database of Artificial neuro-fuzzy inference system (ANFIS) model.*

5. CONCLUSIONS

This paper presented how to predict the specific charge in tunneling blasting. Data collected from the Deo Ca tunnel project were used to build the ANN and ANFIS models for the prediction of specific charges in tunnel blasting. Different artificial intelligence models were tested, and three parameters, including rock mass rating *RMR*; the design area of the tunnel face S_d; the average boreholes length *L*, were identified as influential in achieving accurate estimations for specific charges *Q*. These parameters were selected as input variables for the final artificial intelligence models. ANFIS and ANN techniques demonstrate their efficacy in establishing the correlation between rock and tunnel specifications for specific charges. The ANFIS model's results were evaluated and compared with the ANN model's simulation results. Based on the results obtained from the AI models developed in this study, the following conclusions can be drawn:

- The ANFIS and ANN models can be used to predict the specific charge (*Q*) when constructing tunnels by drilling and blasting method with acceptable accuracy;

- It is necessary to study and add some parameters of the rock mass where the tunnel is located, including Young's modulus (*E*), uniaxial compressive strength (*UCS*), Rock Quality Designation (*RQD*) index, exact consumed explosive materials, and applying the details of holes arrangement in drilling and blasting method pattern as input variables of artificial intelligence models, with the aim of improving the accuracy of specific charge prediction results of artificial intelligence models ANN and ANFIS. Adding parameters like *E*, *UCS*, *RQD*, explosive materials, and hole arrangement can improve the accuracy of specific charge prediction;

- Selecting a suitable architecture for ANN and ANFIS models with different research objects is important.

REFERENCES

[1] Pokrovsky, N. M 1980. *Driving horizontal workings and tunnels*, Mir Publishers, Moscow.

[2] Ryu, C.H., Sunwoo, C., Lee, S.-D., Choi, H.-M 2006. Suggestions of rock classification methods for blast design and application to tunnel blasting, *Tunnelling and Underground Space Technology*, **21**(3–4), pp. 401–402.

[3] Han, J., Weiya, X., Shouyi, X 2000. Artificial Neural Network Method of Rock Mass Blastability Classification, In: *Proceedings of the Fifth International Conference on Geo Computation*, London, UK, pp. 23–28.

[4] Rafiai H, Jafari A 2011. Artificial neural networks as a basis for new generation of rock failure criteria. *International Journal of Rock Mechanics and Mining Sciences*. **48**, Issue 7, pp. 1153-1159.

[5] Alipour. A; A. Jafari; and S. M.F. Hossaini 2012. Application of ANNs and MVLRA for Estimation of Specific Charge in Small Size Tunnel. *International Journal of Geomechanics*. **12**, Issue 2 pp. 1-5.

[6] Aref Alipour, Mojtaba Mokhtarian-Asl, Mostafa Asadizadeh 2021. Support Vector Machines for the Estimation of Specific Charge in Tunnel Blasting. *Periodica Polytechnica Civil Engineering*, **65**(3), pp. 967–976.

[7] Jang, J. R 1993. ANFIS: Adaptive-Network-Based Fuzzy Inference System. *IEEE Transactions on Systems*, Man, and Cybernetics. **23**, pp. 665–685.

[8] Iphar, M 2012. ANN and ANFIS performance prediction models for hydraulic impact hammers. *Tunn. Undergr. Space Technol*. **27**, pp. 23–29.

[9] Chi T. N., Do N. A, Pham V. V., Nguyen P. T., Gospodarikov. A. 2022. Prediction of blast-induced the area of the tunnel face in underground excavations using fuzzy set theory ANFIS and artificial neural network ANN. *International Journal of GEOMATE*, **23**(95), pp. 136-143.

[10] Mc Culloch Warren S, Pitts Walter 1943. A logical calculus of the ideas immanent in nervous activity. *Bull Math Biophys.* **5**, pp.115–133.

[11] Haykin S 1999. *Neural networks*. Prentice-Hall, Englewood Cliffs.

[12] Baheer I 2000. Selection of methodology for modeling hysteresis behavior of soils using neural networks. *J Comput Aided Civil Infrastruct Eng.* **5**(6), pp. 445–463.

[13] Poulton MM 2002. Neural networks as an intelligence amplification tool: a review of applications. *J Geophys.* **67(**3), pp. 979–993.

[14] Simpson P.K 1990. *Artificial neural system: foundation, paradigms applications and implementations*. Pergamon, New York.

[15] Garret J.H 1994. Where and why artificial neural networks are applicable in civil engineering. *J Comput Civil Eng.* **8**:129–130.

[16] Sonmez H, Gokceoglu C, Nefeslioglu HA, Kayabasi A 2006. Estimation of rock modulus: for intact rocks with an artificial neural network and for rock masses with a new empirical equation. *Int J Rock Mech Min Sci.* **43**, pp. 224–235.

[17] Iphar M, Yavuz M, Ak H 2008. Prediction of ground vibrations resulting from the blasting operations in an open-pit mine by adaptive neuro-fuzzy inference system. *Environ Geol*. **56**(1), pp. 97–107.

[18] Jang, H., Topal, E 2013. Optimizing over break prediction based on geological parameters comparing multiple regression analysis and artificial neural network. *Tunn. Undergr. Space Technol*. **38**, pp. 161–169.

[19] Armaghani, D.J., Mohamad, E.T., Narayanasamy, M.S., Narita, N 2017. Development of hybrid intelligent models for predicting TBM penetration rate in hard rock condition. *Tunn. Undergr. Space Technol*. **63**, pp. 29–43.

[20] Mottahedi A, Farhang Sereshki F and Mohammad A 2018. Overbreak prediction in underground excavations using hybrid ANFIS-PSO model. *Tunnelling and Underground Space Technology*. **80**, pp. 1-9.

RESEARCH ON THE BIODIVERSITY AND LANDSCAPE VALUES FOR THE DEVELOPMENT OF GREEN TOURISM LINKED TO EXPERIENTIAL ACTIVITIES IN THE KON HA NUNG PLATEAU BIOSPHERE RESERVE, GIA LAI PROVINCE

Nguyen Huu Xuan[1*], Nguyen Trong Doi[1], Nguyen Thi Huyen[2]
[1] Faculty of Natural Sciences, Quy Nhon University, Quy Nhon, Vietnam
[2] Faculty of Social Sciences and Humanities, Quy Nhon University, Quy Nhon, Vietnam
E-mail: nguyenhuuxuan@qnu.edu.vn

Abstract: Green tourism is friendly, responsible tourism, ecological lifestyle and optimization of resources, respecting environmental capacity, and suggests sustainable development of tourist destinations. The article used investigation methods, field surveys, GIS and UAV applications, PRA methods... for research. The results determined: The Biosphere Reserve of the Kon Ha Nung Plateau has an area of 413,511 hectares, a subtropical humid evergreen closed forest ecosystem, with very high biodiversity, typical of the ecosystem forests, fauna and flora of the Central Highlands. This place has extremely attractive landscapes such as K50 waterfall, K40 waterfall, Kon Loc waterfall..., Kon Ka Kinh peak, ethnic villages of Ba Na and E De minority with unique and special cultural values... Current, the travel trend is to return to nature, live slowly and appreciate what you have. That is an opportunity to build and develop activities to explore landscapes, biodiversity, experience indigenous culture and green lifestyle for tourists at Kon Ka Kinh national park and Kon Chu Rang nature reserve.

Keywords: *"Green tourism", " experiential travel", "Central Highland of Vietnam", "Biosphere Reserve", "Kon Ha Nung".*

1. INTRODUCTION

The global and Vietnamese tourism trends following the Covid-19 pandemic are leaning towards a return to nature, embracing a slower pace of life, and cherishing what we have. In this context, to establish and Green tourism and experiential eco-tourism, it is imperative to develop destinations that are in harmony with pristine natural environments, enriched by the distinct local community, committed to conservation efforts, and the preservation of heritage. This approach not only ensures the sustainable growth of Vietnamese tourism but also serves as an attractive proposition for high-spending, responsible tourists who are devoted to preserving Green destinations.

Green tourism is a form of travel with minimal environmental impact, emphasizing the principles of energy conservation and carbon reduction, along with the enjoyment of eco-friendly and human-centered travel experiences (Yi-Huang Tao, Ruei-Yuan Wang, Hsiao-Chi Ling, 2021) [7]. Green tourism, though used interchangeably with environmental-friendly travel, encompasses a variety of meanings. According to Wight (1994), it pertains to eco-nature vacations and distinctive, unfamiliar destinations [10]. Green tourism is characterized by its benign ecological footprint (Font and Tribe, 2001). Green tourism comprises four elements: i) Environmental responsibility, demonstrated through the protection and conservation of the natural environment; ii) Local economic vitality,

supporting the local community for economic development; iii) Cultural diversity, respecting cultural variety; and iv) Experiential richness, providing novel experiences through active individual participation, fostering human connection with nature and culture (Dodds and Joppe, 2001).. In Vietnam, Green tourism involves immersing oneself in the lush natural surroundings, offering a diverse range of activities such as scenic exploration, beachcombing, hiking, hunting, mountain climbing, wellness, and healing. It aligns with the growing trend of rural tourism (Tran Nhan, 1996). Nguyen Van Dinh (2020) has outlined the core values of green tourism, its current state, and development prospects within the country, along with valuable utilization solutions [6]. Nguyen Dinh Thanh (2021) has elucidated the impact of climate change awareness, the concept of green tourism, the demand for green tourism services, environmental conservation attitudes, and intentions to engage in green tourism on the travel choices of tourists in Vietnam [4]. Drawing from Thailand's green tourism development experience, Chien Thang (2019) has emphasized that green tourism should be associated with green certifications and eco-labels for responsible tourism activities. Green tourism is predicated on seven key elements: Green Heart, Green Destination, Green Community, Green Activities, Green Service, and Green Plus, representing an advanced green approach [12].

Landscape plays a pivotal role in the design of discovery and experiential tourism routes. A beautiful and unique landscape significantly contributes to the promotion of tourism and the attraction of visitors. Such captivating landscapes can inspire and raise environmental awareness among tourists. A pristine forest landscape with waterfalls, caves, streams, and rich biodiversity is always an impressive and enticing destination for travelers. Evaluating landscape aesthetics for the development of tourism within national parks and nature reserves involves elucidating the aesthetic values of forest landscapes. This involves highlighting visual preferences and the scenic beauty of nature. Research into tourism development within natural reserves necessitates addressing the aesthetic aspect of forest landscapes [3].

The Kon Ha Nung Biosphere Reserve encompasses an area of 413,511 hectares, incorporating the Kon Ka Kinh National Park, recognized as the "ASEAN Heritage Garden," and the Kon Chư Rang Nature Reserve, known as the "Green Heritage of the Central Highlands." It also includes parts of six districts and towns, specifically Dak Doa District, Mang Yang District, Kbang District, Chư Pah District, Dak Po District, and An Khe Town [5]. This region features a remarkably well-preserved tropical rainforest ecosystem with rich biodiversity, characteristic of the forest ecosystem, fauna, and flora of the Central Highlands. Within this biosphere reserve, numerous scenic and awe-inspiring landscapes abound, such as the K50 waterfall, K40 waterfall, Kon Loc waterfall, Kon Bong waterfall, and the summit of Kon Ka Kinh (1,748 meters). Additionally, it is home to villages inhabited by the Ba Na and E De ethnic communities. Various activities focused on exploring the rainforest ecosystem and understanding nature take place at the Biodiversity Conservation and Development Center of the Kon Ka Kinh National Park. Furthermore, biodiversity research is conducted at the Vietnamese - Russian Tropical Research Center...

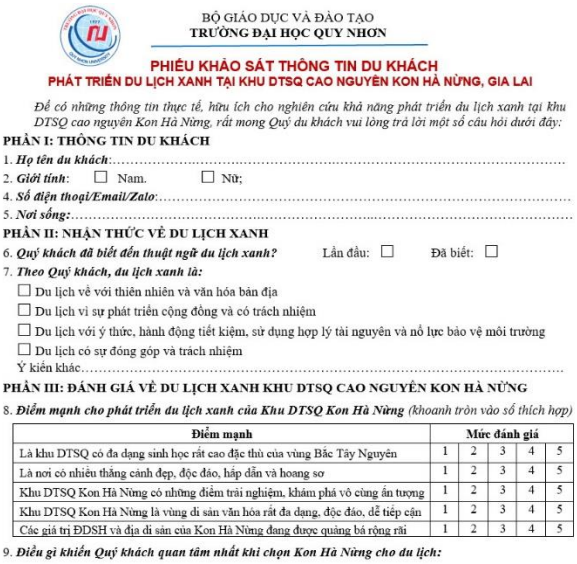
Biodiversity valuation involves assessing the biodiversity value, encompassing conservation value, environmental value, economic value, scientific value, educational value, cultural value, aesthetic value, and recreational value. In this study, the biodiversity

values of the Kon Ha Nung Plateau Biosphere Reserve were evaluated in accordance with the global Convention on Biological Diversity.

Green tourism always focuses on the protection of nature, indigenous cultures, enhancing visitor experiences, and connecting with local communities [6]. Green tourism is inherently tied to responsible tourism. This represents a novel approach, a way to better manage the organization of tourism activities aimed at preserving and developing the values of both natural and indigenous cultural heritage. The core of green tourism is based on the principles of sustainable development, which are defined and adhered to by all parties involved in the tourism product. It involves the responsibility of the community, the responsibility of tourism businesses, the responsibility of tourists, and the responsibility of local tourism management authorities. The Kon Ha Nung Plateau has evolved into a designated global biosphere reserve, thereby affording advantageous prospects for the development of environmentally green tourism.

2. RESEARCH METHODS

Survey and field methods: The research team conducted 03 field trips and surveys at Kon Ka Kinh national park and Kon Chu Rang nature reserve; tour guide with 02 tour groups to participate in experiential activities at K50 waterfall, K40 waterfall, Trại Bò area and the route through the forest and climbing the peak of Kon Ka Kinh mountain. Field and survey data collected are photos, video clips, measurement results and interview recording files.



BỘ GIÁO DỤC VÀ ĐÀO TẠO
TRƯỜNG ĐẠI HỌC QUY NHƠN

PHIẾU KHẢO SÁT THÔNG TIN DU KHÁCH
PHÁT TRIỂN DU LỊCH XANH TẠI KHU DTSQ CAO NGUYÊN KON HÀ NỪNG, GIA LAI

Để có những thông tin thực tế, hữu ích cho nghiên cứu khả năng phát triển du lịch xanh tại khu DTSQ cao nguyên Kon Hà Nừng, rất mong Quý du khách vui lòng trả lời một số câu hỏi dưới đây:

PHẦN I: THÔNG TIN DU KHÁCH

1. ***Họ tên du khách***:.....
2. ***Giới tính***: ☐ Nam. ☐ Nữ;
4. ***Số điện thoại/Email/Zalo***:.....
5. ***Nơi sống***:.....

PHẦN II: NHẬN THỨC VỀ DU LỊCH XANH

6. ***Quý khách đã biết đến thuật ngữ du lịch xanh?*** Lần đầu: ☐ Đã biết: ☐
7. ***Theo Quý khách, du lịch xanh là:***

☐ Du lịch về với thiên nhiên và văn hóa bản địa
☐ Du lịch vì sự phát triển cộng đồng và có trách nhiệm
☐ Du lịch với ý thức, hành động tiết kiệm, sử dụng hợp lý tài nguyên và nỗ lực bảo vệ môi trường
☐ Du lịch có sự đóng góp và trách nhiệm

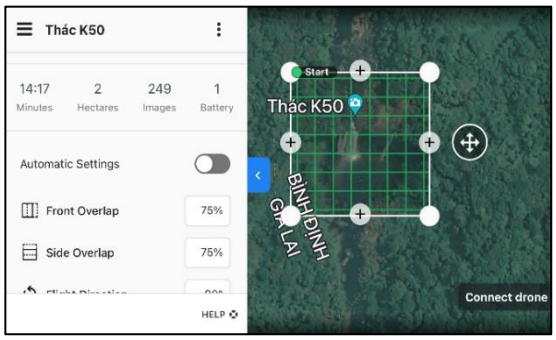
Ý kiến khác.....

PHẦN III: ĐÁNH GIÁ VỀ DU LỊCH XANH KHU DTSQ CAO NGUYÊN KON HÀ NỪNG

8. ***Điểm mạnh cho phát triển du lịch xanh của Khu DTSQ Kon Hà Nừng*** *(khoanh tròn vào số thích hợp)*

Điểm mạnh	Mức đánh giá				
Là khu DTSQ có đa dạng sinh học rất cao đặc thù của vùng Bắc Tây Nguyên	1	2	3	4	5
Là nơi có nhiều thắng cảnh đẹp, độc đáo, hấp dẫn và hoang sơ	1	2	3	4	5
Khu DTSQ Kon Hà Nừng có những điểm trải nghiệm, khám phá vô cùng ấn tượng	1	2	3	4	5
Khu DTSQ Kon Hà Nừng là vùng di sản văn hóa rất đa dạng, độc đáo, dễ tiếp cận	1	2	3	4	5
Các giá trị ĐDSH và địa di sản của Kon Hà Nừng đang được quảng bá rộng rãi	1	2	3	4	5

9. ***Điều gì khiến Quý khách quan tâm nhất khi chọn Kon Hà Nừng cho du lịch:***



The design of UAV flight routes is carried out according to the principle that the flight area must be covered. Based on the flight area boundary, the ground resolution of the image, vertical coverage and horizontal coverage is 80, the flight direction of the UAV is from East-West to South-North.

Figure 1. *Field Survey Investigation Form (Left) and Aerial photography site design for K50 Waterfall (Right)*

Rapid rural interview (PRA) method: The research utilized a questionnaire for conducting direct interviews, specifically targeting 25 tourists, comprising 2 international tourists, 13 students and postgraduate students, 7 tourists from Ho Chi Minh City tour groups, and 3 local tourists. Regarding forest protection forces, the research team interviewed 6 forest protection officers, 3 directors of environmental education centers, rescue and conservation centers, and the director of the Kon Chu Rang nature reserve. The survey questionnaire consisted of 24 questions concerning green tourism, biodiversity value,

landscape, and the potential exploitation of biodiversity and landscape values for experiential, exploratory, and community-based tourism activities (Figure 1).

The method of flying by unmanned aerial vehicle (UAV) and applying GIS: is a new method of collecting real-time surface data in landscape research, helping to determine location. location, scale and analysis of that landscape structure. Using orthogonal aerial photography techniques, processing aerial images with specialized software and GIS applications can create geometrically diverse maps, landscape maps of tourist destinations and travel maps. In this study, the UAV flight method (using the Mavic 2 Pro device) was used to record the location of important points through image coordinates, fly photos, and record video to capture the images. High resolution, panorama photography, 360^0 photos at spots with beautiful and unique tourist landscapes. Image data has super high resolution and high artistic quality for tourism advertising materials. At important locations such as K50 Waterfall, K40 Waterfall, Kon Lốc Waterfall, the core area of the biosphere reserve, orthogonal aerial photography was used to analyze landscape function and structure (Figure 1). In addition, use the high resolution of UAV imaging equipment to classify forest vegetation types in some landscape types of the core and buffer zones in the biosphere reserve.

3. RESEARCH RESULTS

3.1. The essence of green tourism

Green tourism is a form of travel organization that is closely tied to the commitment of all parties involved in tourism activities, aiming to minimize costs and optimize benefits for the natural environment, local communities, and fostering sustainable development.

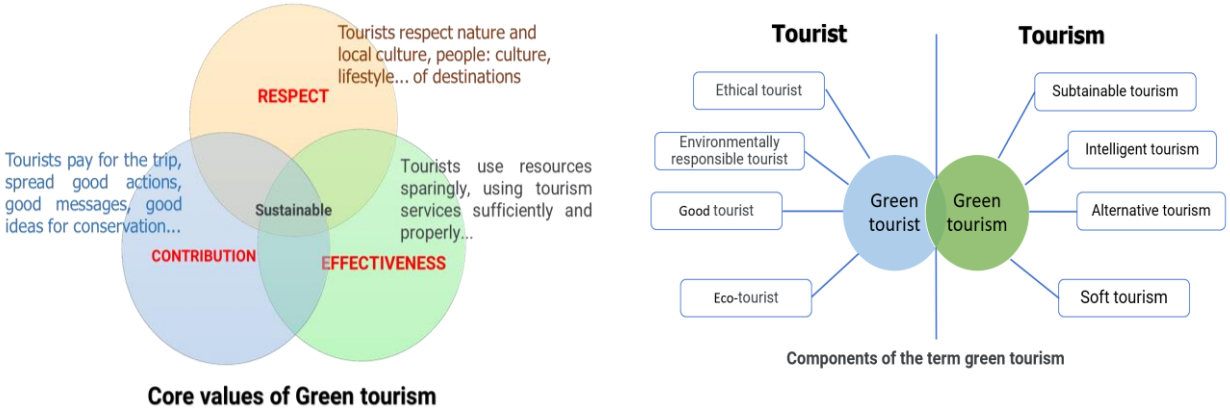


Figure 2. *Core values of green tourism (left) and components that make up the term green tourism (right)*

The core value of green tourism lies in the concept of "green products" [1]. To develop green tourism successfully, the key factors contributing to this endeavor include: i) Preserving and protecting the environment, natural heritage, cultural heritage, and local communities; ii) Enhancing the responsibility of all involved parties to promote sustainable and environmentally friendly activities; iii) Developing infrastructure and tourism facilities that are cost-effective, efficient, and environmentally friendly; iv) The active participation and contribution of tourists; and v) Collaboration among stakeholders in experiential activities and community engagement at tourism destinations [8], [9].

Table 1. Elements and characteristics of green tourism

Element	Featured
Target	Green tourism aims to promote sustainable development at tourist destinations, seeking a balance between economic, environmental, and social sustainability. It strives to minimize the negative impacts of tourism on resources, the environment, and local communities.
In essence	Green tourism endeavors to provide authentic and high-quality travel experiences, reflecting environmental ethics in every action of travelers while respecting the environment and culture of the destination.
Core values	The core values of green tourism include: *Respect:* Travelers respect the values of nature and local culture, lifestyles, at the destination. *Contribution*: Travelers financially support their journey, spreading positive actions, meaningful messages, and good ideas for the conservation of natural resources and the tourism environment. *Efficiency:* Travelers strive to save resources, using them judiciously, and make efficient use of tourism services. The use of tourism services should align with green consumption and ecological lifestyles.
Development platform	The foundation for green tourism development is green lifestyle, green environment and sustainable development. Focus on reducing use and saving resources; Strengthen efforts to protect water sources and reuse water; conserve biodiversity, heritage and community culture; Use renewable energy and ensure environmental green label. - Green tourism aims to implement a green lifestyle and sustainable consumption for tourists at a tourist destination.
Tourism activities	Green tourism activities can encompass a wide range of diverse experiences, from exploring natural areas to immersing in local cultures, participating in community projects, and enjoying environmentally friendly accommodations. These activities emphasize responsible behavior and cultural respect.
Tourism products	- The products of green tourism include nature-based educational tours, cultural experiences involving local communities, participation in Green events and festivals, eco-friendly health and spa services, eco-adventure and eco-tourism activities, and green transportation and local cuisine experiences. - Green tourism offers experiences that emphasize sustainability, responsible travel practices, and environmental friendliness.

3.2. Biodiversity and tourism exploitation value in the Kon Ha Nung plateau biosphere reserve

The Kon Ha Nung plateau biosphere reserve is 413,500 square meters wide ha, including 3 functional areas: Core area, buffer area and transition area. The core area includes core area 1, which is Kon Ka Kinh national park (area of 41,913.8 hectares) and core area 2, which is Kon Chu Rang nature reserve (area of 15,526 hectares). The buffer zone is a

biodiversity corridor, connecting two core zones, with an area of 152,693.9 hectares and a population of 54,884 people. The transition area has a very large area, up to 203,377.86 hectares, with a population of 212,819 people [5].

Table 2. Statistical summary of forest vegetation cover in the Kon Ha Nung Plateau Biosphere Reserve by functional sub-regions Unit of measurement: hectares (ha)

Functional zones of the biosphere reserve	District/ Town	Forest vegetation cover					Agricultural crops area	River, lake	**Total area**
		Seasonal deciduous broad-leaved forest	Mixed broad-leaved and coniferous forest	Tropical evergreen broad-leaved closed forest	Bamboo forest	Planted forest area			
Core zone	Đăk Đoa			3.635		45	60		**3.740**
	KBang		1.781	35.352	240	88	1.991	49	**39.501**
	Mang Yang			4.447	2	173	491	0	**5.113**
	Mang Yang	75		6.407		7.300	18.202	279	**32.265**
Buffer zone	Đăk Đoa	267		13.238		5.877	18.218	37	**37.637**
	KBang			64.693	19	8.859	15.651	1.716	**90.937**
Transition zone	An Khê			574		4.117	14.889	405	**19.984**
	Chư Păh			12.535	4	2.482	15.008	131	**30.160**
	Đăk Đoa	72		1.328		1.186	17.174	62	**19.822**
	Đăk Pơ			15.701		7.408	26.649	603	**50.362**
	KBang			22.047		4.805	25.872	1.012	**53.736**
	Mang Yang	27		13.802	6	7.587	11.558	143	**33.123**
Total area		**442**	**1.781**	**193.768**	**270**	**49.931**	**165.767**	**4.436**	**416.396**

Calculation based on the current map of three types of forests in Gia Lai province in the year 2019

The Kon Ha Nung Biosphere Reserve boasts a highly diverse plant cover, including various forest types such as tropical evergreen broadleaf forests, lowland montane mixed broadleaf-coniferous forests, montane tropical evergreen broadleaf forests, montane sparse broadleaf forests, montane sparse coniferous forests, shrublands, grasslands, and agricultural areas.



Figure 3. *Primeval forest cover observed from a height of 35 m of the forest observation tower of the Vietnam - Russia Tropical Center (left) and wildlife at the National Park biological development and Conservation Rescue center of Kon Ka Kinh (right). NH Xuan's photo.*

Among these, the most characteristic vegetation in the Kon Ka Kinh National Park is the montane mixed broadleaf-coniferous forest, which is situated at elevations above 1,000 meters and characterized by a warm and humid tropical climate, along with a solid foundation on magma rock, creating its distinctiveness. This forest's structure consists of three layers with heights ranging from 20 to 25 meters. The canopy layer includes species such as Dacrydium elatum, Fokienia hodginsii, Pinus dalatensis, Rhodoleia championi, and Elaeocarpus. The sub-canopy and understory layers encompass genera like Rhododendron, Garcinia, coffee, and ginger (Figure 3) [3].

The basalt plateau Kon Ha Nung are part of the biodiversity corridor of the Central Highlands of Vietnam. The central region of this corridor is recognized as the ASEAN Heritage, hosting highly valuable biological resources. The biodiversity corridor between the Kon Ka Kinh National Park and the Kon Chu Rang Nature Reserve is also exceptionally rich in species diversity and various ecosystems, home to many rare and valuable fauna and flora (Table 3).

Table 3. Species diversity in the core zone of Kon Ha Nung plateau biosphere reserve compared to some other national parks and biosphere reserves in Vietnam

Name of national park/natural reserve	Area (ha)	Flora				Animal					Number of rare species
						In there					
		Family	Genus	Species	Total species	Animal	Bird	Reptiles / amphibians	Fish	Insect	
Kon Ka Kinh	41,913	210	761	1738	821	87	265	135	13	321	42
Kon Chu Rang	15,384	162	547	881	719	100	271	104	33	211	64
Kon Ka Kinh - Kon Chu Rang biodiversity corridor	26,000	160	327	836	469	95	124	68	14	168	34
LangBiang Biosphere Reserve *(Lam Dong)*	275,439	1 6 1	658	1475	1087	70	301	169	22	525	62
Phong Nha - Ke Bang *(Quang Binh)*	85,754	198	1007	2952	1394	154	303	151	215	571	47

Source: [2], [3], [5]

The Kon Ka Kinh National Park, covering an expanse of 41,913.78 hectares, resides within the core region of the Kon Ha Nung Biosphere Reserve. The flora and fauna within this area exhibit diversity. Many of these species are of high conservation significance, and they are listed in the Red Data Books of Vietnam and the global [5].

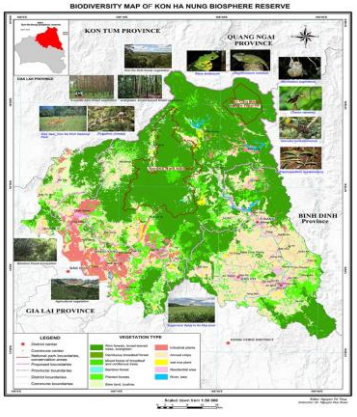


Figure 4. *Biodiversity map of the Kon Ha Nung plateau biosphere reserve*

Kon Chu Rang Nature Reserve has 15,384 hectares of forest (>10,000 hectares of rich forest), It is an A-class region for its biodiversity of international importance. In this has harbors three indigenous mammalian species of Indochina, namely the red-shanked douc langur, gray-shanked douc langur, and large civet.

This area represents an endemism bird areas within the Kon Tum Plateau and has been officially acknowledged as a significant avian habitat in Vietnam.

3.3. Landscape value of Kon Ha Nung plateau international biosphere reserve for green tourism

• Magnificent and impressive waterfall system

Kon Ha Nung Plateau Biosphere Reserve is an area with terrain from the average mountainous area gradually descending to the Kon Ha Nung Plateau. This is the upstream of the Ba River and Kon River system. The edge of the plateau has a very strong gradation and division, so it has formed a very impressive waterfall system with about 30 waterfalls (Kon Nature Reserve alone). Chu Rang has 11 waterfalls) with 5 types of waterfalls: plunge/slope waterfall, curtain waterfall, mantle waterfall, horsetail waterfall and spillway waterfall (Table 4).

Table 4. Some waterfalls and values for tourism in the Kon Ha Nung Plateau Biosphere Reserve

TT	Name	Location	Featured	Ability to exploit tourism	Value
	Hang En Waterfall (K50 waterfall)	Kon Chu Rang Nature Reserve	The waterfall is 54 meters high and its width varies from 20 to 100 meters. It boasts a unique frog-shaped rock formation. The waterfall is incredibly majestic, set against the backdrop of pristine rainforest.	Experiential travel, SUP, camping...	International level
	K40 Waterfall (Hoa Waterfall/ Co Tien Waterfall)	Kon Chu Rang Nature Reserve	The waterfall is 40 meters high and consists of three tiers. The first tier is 30 meters high, the second tier is 7 meters high, and the third tier is 3 meters high. There is a beautiful water reservoir at the base of the waterfall. Structure of columnar basalt of the Dai Nga formation.	Sightseeing, experiencing waterfall wading, stream bathing...	National level
	5-storey waterfall	Kon Chu Rang Nature Reserve	The waterfall is 5 levels, layered, about 45 m high. The 5th floor is up to 20 m high. Structure of columnar basalt of the Dai Nga formation.	Visit and experience primeval forests	National level
	Moss Waterfall (3-tiered Waterfall/Kon Bong)	Dak Rong commune, K'bang district	The waterfall is 30 m high, consists of 3 floors, columnar basalt of the Dai Nga formation. Coniferous and broad-leaved forest, primary.	Sightseeing, camping, experiencing coniferous forests.	National level
	Dak Bok Waterfall (Ong Waterfall)	Cheng village, Dak Rong commune,	Shaped waterfall, wide cleft, columnar basalt of the Dai Nga formation, primeval forest	Visit and experience the old forest	National level

	K'bang district	landscape.		
Bat Waterfall/ Hang Bat Waterfall	K'bang town	Dai Nga formation basalt, small waterfall, little water in dry season. Plunge waterfall shape, below the waterfall there is a frog jaw.	Sightseeing, camping	Local level
K'Bung 1 Waterfall	Dak Beh commune, Mang Yang district	Medium and small-grained biotite granite of the Van Canh Complex. The waterfall is curtain-shaped, with little water.	Sightseeing, camping	Local level

Sources [2], [4] and field survey results

The diversity of waterfall types linked to their formation mechanisms and the values of pristine forest landscapes in the Kon Ha Nung International Biosphere Reserve represent a valuable asset for the tourism development of Gia Lai province.

• *Unique landscape, many impressive destinations to conquer*

The Kon Ha Nung Biosphere Reserve features three distinct topographical regions: a medium-altitude mountainous terrain ranging from 1,200 to 1,500 meters in elevation, the high basalt plateau of Kon Ha Nung, with elevations between 800 and 1,000 meters, and the lowland areas around An Khe, which sit at an altitude of 500 meters.



Figure 5. *Cave En waterfall (K50 waterfall) amidst the primeval forest during the season of changing foliage (left image - Photo by N.T. Doi) and the landscape of Vinh Son B Lake (right image - Photo by T.B. Hoa).*

The Kon Ha Nung plateau is a remnant of the ancient basaltic plateau, covering an estimated area of approximately 2,000 square kilometers. It belongs to the Dai Nga geological stratum (N_2đn) from the late Pliocene, with an absolute geological age of roughly 2.2 to 2.6 million years. Volcanic eruptions primarily occurred along fissures and faults, resulting in the formation of extensive flat lava flows that filled ancient valleys and plains between the mountains. The region is dotted with numerous reservoirs and hydroelectric dams, such as Vinh Son C, Vinh Son B (Figure 5 - left), and KaNak Lake. These are significant hydroelectric reservoirs with stunning and pristine landscapes. Waterfalls are nestled within old-growth forests, either secondary or primary, creating magnificent and breathtaking scenery. Cave Én Waterfall (also known as K50 Waterfall) is particularly remarkable during March and April each year, where the powerful waters of the waterfall are accompanied by the unique red and yellow foliage of the tropical rainforest, creating an enchanting and distinctive sight (Figure 5).

• ***A unique indigenous cultural region with special heritage***

In the East Gia Lai region, apart from the intangible cultural heritage of humanity, which is the Gong Culture space in the Central Highlands, there are other immensely valuable

cultural heritages. Specifically, there are two exceptional national historical relics: the Tay Son Thuong Dao historical relic and the archaeological site of Roc Tung - Go Da (an archaeological site from the Early Stone Age with an estimated age of approximately 800,000 years). Moreover, the Kon Ha Nung plateau serves as the cradle for indigenous communities, consisting of Ba Na and E De ethnic villages. In this area, you can discover communal houses deeply connected to Central Highlands' gong festivals and buffalo stabbing rituals. Additionally, you can observe distinctive production activities and daily life. The Banar ethnic community (including Banar Golar, Banar Ronam, Banar Kon Ko Deh, etc.) has a longstanding presence here. They have established settlements in villages situated along valleys and rivers. Their cultural life revolves around the traditional communal houses. These communities enjoy a rich cultural life enriched by the use of musical instruments such as gongs, cymbals, and traditional string instruments (such as the t'rưng, klông pút, kơni), as well as various types of horns (like the tơ nốt, arơng…). These elements possess a profound appeal to travelers seeking novel experiences in the Kon Ha Nung highland region.

3.4. A number of experience routes/tours are operating on the Kon Ha Nung plateau

Experience Tourism, which emphasizes experiential travel, is a form of tourism that encourages travelers to learn and explore new aspects of nature, life, local culture, and cuisine. This form of tourism can be organized for groups, tours, or individual experiences. Some of the tourism activities that are currently taking place in the Kon Ha Nung Biosphere Reserve include trekking, exploring the ecosystem of primary forests, immersing in the Bahnar people's culture, engaging in SUP paddling within the pristine forest, and experiencing waterfall crossings like K50 and K40. Activities also include environmental education, biodiversity exploration by students at the Environmental Education Center in the Kon Ka Kinh National Park and the Kon Chu Rang Nature Reserve. Some of the main tour options are as follows:

Summiting Mount Kon Ka Kinh: Setting foot on the highest peak in the Kon Ha Nung plateau, with an elevation of 1,748 meters, is a desire of nature enthusiasts and adventure seekers. Referred to as the "roof of Gia Lai," the shortest route to conquer this peak begins at Forest Protection Station No. 5 in Dak Rong Commune, K'bang District. The trekking journey takes approximately 2 days and 1 night, covering a distance of nearly 20 km. The summit of Mount Kon Ka Kinh remains a mystery within the Truong Son mountain range, attracting travelers who appreciate physical challenges and the spirit of self-conquest.



Figure 6. *Some photos of experiential tours at Kon Chu Rang nature reserve in April 2023 (photo N.H. Xuan)*

Cave En Waterfall Experience Tour: Embarking on this journey requires good physical fitness and determination. Starting from the administrative center of the Kon Chu Rang Nature Reserve, travelers can hike to the waterfall (approximately 15 km, taking around 4 to 5 hours) or drive about 8 km and then either walk or ride a motorbike (7 km on steep and winding terrain). Upon completing the experience tour and exploring Hang En waterfall, travelers will have conquered various challenges: trekking through old-growth forests, crossing streams, ascending slippery and steep slopes, camping on the edge of the waterfall, paddleboarding (SUP) on the Say River amidst the ancient forest, witnessing stunning sunrises and rainbows at the base of the waterfall, and even trying their hand at fishing at the waterfall's base (Figure 6).

Various outdoor activities and explorations are available for teachers and students in the Kon Ka Kinh National Park and the Kon Chu Rang Nature Reserve, including: Learning about the local flora in the nature reserve, setting up standardized plant plots; Exploring the impact of human activities on the environment; Visiting waterfalls and scenic spots within the forest. Students can also participate in camping, fishing, group activities, team-building exercises, campfire gatherings, and visiting the Bahnar villages. During these field trips, teachers and students are introduced to various landscapes and scientific research facilities. They encounter unique natural elements such as giant trees, strangler figs, rare and endemic species like gray-shanked doucs, and engage in observations of trees, fruits, various bird and animal species through binoculars. Examining the lives of insects through magnifying glasses adds to the excitement and reinforces their knowledge of the natural environment, instilling a deeper appreciation for their homeland, which is graced with the beautiful and majestic ASEAN Heritage.



Figure 7. *Biodiversity discovery experience activities for teachers and students at the Kon Ha Nung plateau biosphere reserve (photo by N.H.Xuan)*

3.5. Survey results, assessment of biodiversity value

The study processed 35 survey forms, including 25 for tourists and 10 for forest rangers and managers. Each criterion was scored on a scale of 1 to 10, with a maximum total score of 350 and a minimum total score of 35 for each criterion. The assessment results for biodiversity value in the Kon Ha Nung Plateau Biosphere Reserve are as follows (Table 5):

Table 5. Assessment of biodiversity value

Area Value	Core zone			Buffer zone
	Kon Ka Kinh National Park	Kon Chu Rang Nature Reserve	Biodiversity corridor	
Conservation value	328	305	275	179
Environmental value	312	275	280	190
Economic value (including forest carbon credit)	295	270	175	250
Scientific and educational value	340	304	287	187
Cultural, aesthetic, and recreational value	270	290	210	190

The results of the survey, aimed at assessing the awareness, evaluating the value of resources, and identifying strengths for the development of green tourism associated with nature and local culture exploration, indicate the following: For travelers from Ho Chi Minh City participating in experiential journeys, they consistently highly value the natural beauty, diversity, uniqueness, and grandeur of the tourist destinations in Kon Ha Nung. The tourism activities are well-organized, ensuring safety and offering immersive, eco-friendly experiences closely connected to the lush natural surroundings. The frugal and straightforward utilization of services for transportation, dining, and accommodations within the national park is seen as an acceptable approach that contributes to resource conservation and the preservation of the natural heritage. According to the travelers, green tourism represents a correct and distinctive approach, serving as a unique strength for the Kon Ka Kinh National Park and the Kon Chu Rang Nature Reserve on the Kon Ha Nung plateau in Gia Lai province..

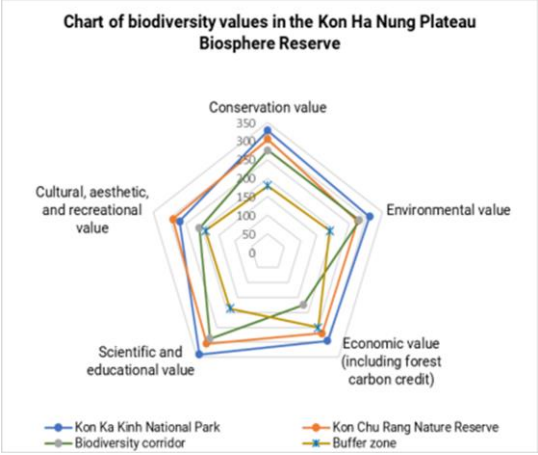


Figure 8. *Chart of biodiversity values in the Kon Ha Nung Plateau Biosphere Reserve*

4. DISCUSSION

Sustainable development is the foundation of green tourism, with a priority on protecting and preserving the environment, culture, economy, and local communities. Green tourism strives to minimize the negative impacts of tourism activities on the local environment

while encouraging environmentally friendly activities, conservation, preservation, and responsible use of natural resources. Here are some suggestions for the development of green tourism and experiential tourism in the Kon Ha Nung International Biosphere Reserve:

- Integrate biodiversity conservation efforts into tourism development. Strengthen proactive partnerships with environmental protection organizations in Vietnam, such as the People and Nature Centre (PanNature), the Frankfurt Zoological Society (Germany), the Vietnam-Russia Tropical Center, and especially UNESCO to promote the "Biosphere and Human" program, focusing on sustainable tourism development.
- Enhance promotion through various media channels to showcase the experiential and memorable moments for tourists in the local and international tourism community.

Conduct detailed research and assessments based on expert surveys to identify the strengths and conditions for exploiting the biodiversity and cultural values for experiential tourism. This should emphasize the conservation and utilization of the region's natural and cultural heritage in East Gia Lai, with a primary focus on the Kon Ka Kinh National Park and the Kon Chu Rang Nature Reserve.

5. CONCLUDE

This research demonstrates that the Kon Ha Nung International Biosphere Reserve is a region with exceptionally high biodiversity, both in terms of ecological diversity, species diversity, and genetic resources of organisms. It boasts a wealth of diverse tourism resources, including numerous beautiful and majestic landscapes, unique cultural and historical sites, and outstanding intangible cultural heritage values in contemporary life. Kon Ka Kinh National Park - an ASEAN Heritage, and the Kon Chu Rang Nature Reserve hold special values for the development of experiential tourism and exploration of nature's beauty and the unique cultural values of ethnic minority communities. This area is a prime location for organizing various experiential tours, nature and local culture exploration tours, and environmental education tours for students.

Establishing a variety of experiential and exploratory tourism models for domestic and international tourists, with careful preparation regarding itineraries, routes, tours, and a focus on utilizing the local residents' skills and knowledge is essential in the Kon Ha Nung International Biosphere Reserve. This approach aims to position the local people as the cornerstone of community-based tourism development, preserving and conserving the community's cultural heritage. It is evident that creating distinctive tourism products associated with scenic spots, outdoor activities, nature exploration, scientific research, cultural experiences, and indigenous knowledge in the Kon Ha Nung International Biosphere Reserve will generate attraction and highlights for the development of conservation-linked tourism. The development of green tourism in Gia Lai province must align with the principle of *"Development for Conservation; Conservation for Development"* for the region..

REFERENCES

1. Nguyen Dinh Thanh (2021). *Factors influencing the behavior of choosing Green tourism in Vietnam*. International Journal of Management and Economics, No. 142 (December 2021). Pages 102-121.

2. Nguyen Thi Thua, 2020. Research on biodiversity value of Kon Ha Nung plateau to serve geography teaching. Master's thesis, Quy Nhon University.

3. Giang Van Trong, 2020. *Landscape assessment for sustainable tourism development in the northern Central Highlands natural reserve - case study of Kon Ka Kinh national park,* doctoral thesis in Natural Resources and Environmental Management, Hanoi National University.

4. Tran Tan Van, 2018. *Investigation, survey, research, and assessment of prospects for establishing a Global geopark.* Provincial-level Science and Technology Project, Code KHGL-07-16.

5. UNESCO Vietnam National Committee, Gia Lai Provincial People's Committee, *Documents Nominated Kon Ha Nung Plateau Biosphere Reserve, Gia Lai Province, Vietnam*

6. Xuan.N.H, Huyen.N.H, 2022, *Research on Green tourism development in Hon Yen national heritage of Phu Yen province*. Social Sciences, 2023, Volume 68, Issue 2, pp. 38-50. DOI: 10.18173/2354-1067.2023-0023

7. Yi-Huang Tao, Ruei-Yuan Wang, Hsiao-Chi Ling…, 2021. *Implementing for innovative management of green tourism and leisure agriculture in Taiwan (China).* The International Journal of Organizational Innovation Volume 13 Number 3, January 2021. Page 210-219.

8. Furqan A., Mat Som AP and Hussin R (2010). *Promoting Green tourism for future. future sustainability*. Theoretical and Empirical Researches in Urban Management 5(8(17)). Pages 64-74.

9. *OECD Tourism Trends and Policies 2022*. OECD Publishing, Paris, https://doi.org/10.1787/a8dd3019-en

10. Xiaocheng Vicky Zhang and Suk Ha Grace Chan (2021). *Do Knowledge and Experience Value Affect Green Tourism Activity Participation and Buying Decision?* A Case Study of Natural Dyeing Experience in China. Sustainability 2021, 13, 8579. https ://doi.org/10.3390/issue13158579

11. https ://business. visitlincolnshire. com/resources/green - tourism -toolkit/? playlist=e68aa91 & video=b1f4a53 (accessed January 16, 2023).

12. https://itdr.org.vn/nghien_cuu/nghien-cuu-trao-doi-ve-du-lich-xanh-tai-viet-nam-hien-nay-bai-hoc- Kinh-nghiem-cua-thai- lan-va-trien-vong-trong-tuong-lai/ (Accessed October 20, 2023).

DEVELOPING A THREE-DIMENSIONAL MODEL OF THE OPEN PIT MINE AND THE INDUSTRIAL YARD OF NUI BEO COAL MINE

Nguyen Quoc Long[1], Luu The Anh[2], Bui Ngoc Quy[2], Le Thi Thu Ha[1], Le Van Canh[1], Pham Van Chung[1,*]

[1] Faculty of Geomatics and Land Administration, Hanoi University of Mining and Geology. No. 18 Pho Vien, Duc Thang Ward, Bac Tu Liem District, Ha Noi City, Viet Nam.

[2] VNU - Central Institute for Natural Resources and Environmental Studies (VNU-CRES). No.19 Le Thanh Tong, Phan Chu Trinh Ward, Hoan Kiem District, Ha Noi City, Viet Nam.

*Corresponding Author: phamvanchung@humg.edu.vn

Abstract: To achieve the goal of building a 3D model of the mine surface area which includes the open pit mine and the industrial yard of an underground coal mine (SCN), an unmanned aerial vehicle (UAV) was used to collect data for the establishment of 3D point cloud (PC) and orthomosaic image of this area, which is about 100 hectares and located at Nui Beo coal mine. The area includes an open pit mine with a depth of 110 m and SCN with a flat terrain, but there are many important works of the mine, especially a mineshaft tower with a height of 50m. To obtain a complete point cloud (PC) for 3D modeling purposes, the terrain characteristics of the area were studied, and three aerial photography scenarios were designed for each location, including: (1) capturing orthogonal images of the entire area, (2) capturing additional images of the industrial mining structures using a 45-degree oblique grid method, and (3) capturing circular path images at 45 and 60 degrees focusing on the well tower. Image processing for each of the above aerial capture scenarios resulted in incomplete and insufficient data for detailed model rendering. The PC was generated by combining images from the three supplementary methods to compensate for each other's deficiencies and provide a comprehensive overall point cloud. The accuracy of the PC was evaluated based on a root mean square error smaller than 3.0 cm, with the maximum deviation in ground position and height of the corresponding model points being 4.5 cm and 4.2 cm, respectively. Using the established PC, a 3D model of the combined area of open pit mining and SCN35 of the Nui Beo coal mine was constructed.

Key words: *Industrial area, Open pit mine, UAV, 3D model, Nui Beo coal mine.*

1. INTRODUCTION

According to Decision 403/QD-TTg regarding the coal industry development plan in Vietnam, by the year 2030, open pit coal mining will only account for 11% of the total production (Prime Minister, 2016) [1]. Mining operations are gradually shifting towards underground mining since coal seams are increasingly deeper, resulting in a higher stripping ratio, which reduces mining efficiency. During the initial construction phase of underground mines and the early operational phase, mines such as Nui Beo, Ha Long, and Ha Lam continue to operate both open pit and underground mining. During this stage, the management of open pit and underground mining operations takes place concurrently.

Creating three-dimensional models is an essential spatial database that significantly improves the efficiency of mining operations and resource management. [2]. Consequently, the establishment of 3D models for mines has been carried out in numerous research studies and practical applications. Integrating point cloud data obtained from Unmanned Aerial

Vehicle (UAV) imagery and Terrestrial Laser Scanning (TLS) data to create 3D models for open pit coal mines was conducted in the research by the author Le Van Canh [3]. In another study, Hao Zhao and colleagues developed a 3D model of an open pit coal mine, which showcased geological features such as cracks and faults on the mine's surface, emphasizing its significance as an essential information platform for mine design and management [4].

UAV technology allows for rapid data collection over a wide area [5]. The nearly featureless terrain of the mining area is advantageous for UAV applications [6]. However, the highly variable terrain of the open pit mine area requires accurate elevation data for mining volume calculations, and 3D modeling efforts focus on terrain features. Therefore, when designing UAV aerial photography for the open pit mine, careful planning of flight paths and positions is essential for both safety and accuracy [7]. In contrast to the open pit mine, the industrial mining site has relatively flat terrain with minimal elevation changes, and the influence of terrain features on elevation accuracy is negligible. However, when creating a 3D model of this area, terrain features become crucial and need to be thoroughly examined [3]. With the different characteristics of terrain features between the open pit mine and SCN, when applying UAV technology for 3D modeling of both areas, detailed studies on elevation differences in the open pit mine and the structure of industrial facilities on SCN are necessary. This involves calculating relevant parameters and developing suitable aerial photography methods for each specific area, ensuring both economic and technical considerations are met.

The terrain of open-pit mine differs from the existing structures on the industrial yard. Therefore, it is crucial to determine suitable UAV flight and image processing methods for both of these objects when establishing a 3D model for this combined area.

2. STUDY AREA

The research area covers 100 hectares within the Nui Beo coal mine in Ha Long, Quang Ninh (Figure 1). Within this area, the open pit coal mines zone occupies 12 hectares, while the rest is designated for highwall mining.

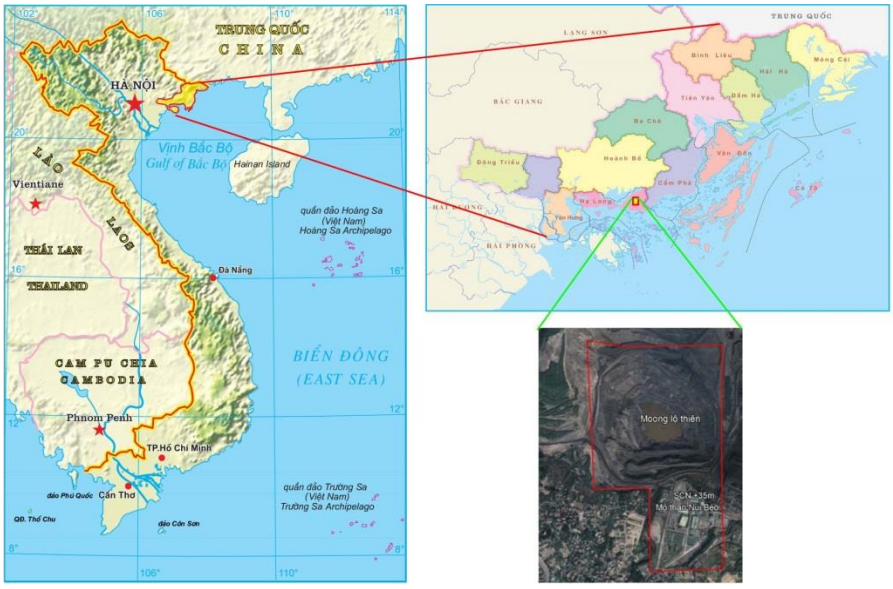


Figure 1. *Study area at Nui Beo Coal Mine, Ha Long, Quang Ninh*

The open pit mine's terrain has a height difference of 110m, ranging from an elevation of +25 meters to -85 meters. The terrain is characterized by terraces and slopes (Figure 2a). In practice, this area proves to be favorable for data collection using UAV (Unmanned Aerial Vehicles) because the terrain is virtually devoid of natural features (Figure 1).

The SCN35m area, on the other hand, has relatively flat terrain at an elevation level of +35 meters. However, this area is home to various industrial mining structures with different sizes, shapes, and structures (Figure 2b). Collecting data using UAV technology in this area requires research to ensure capturing images of the walls and bases of these structures, thereby ensuring the acquisition of complete point cloud data for the construction of a 3D model.

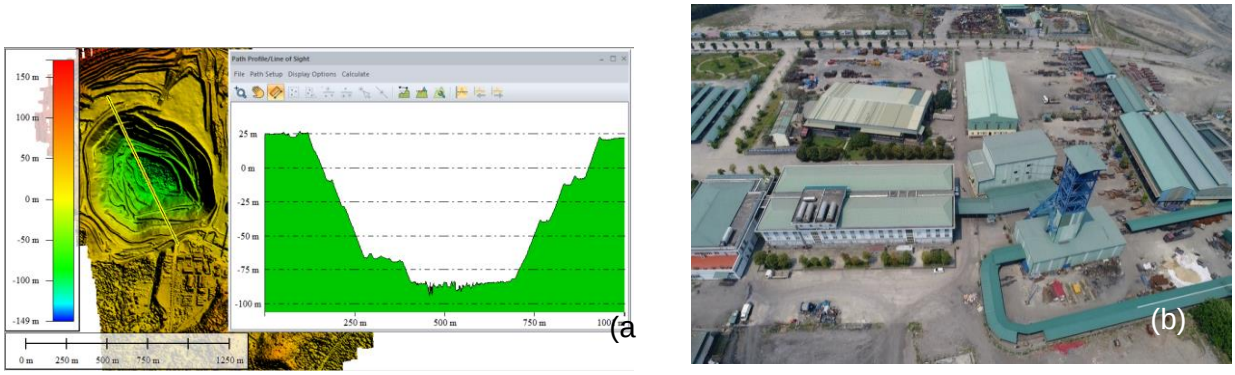


Figure 2. *Topographic features of the study area*

a) Cross-section of the terrain of the open-pit mine; b) Industrial building in SCN35 area

3. MEASUREMENT METHODS AND DATA COLLECTION

3.1. Ground control point determination

Image control points and check points are designed as shown in Figure 3a, consisting of points placed on the terrain surface and points affixed to the object's surface in the vertical direction. Ground points are marked using image control point targets designed as in Figure 3b. These points are evenly distributed throughout the research area, particularly in the lunar landing area, ensuring uniform placement in both position and elevation.

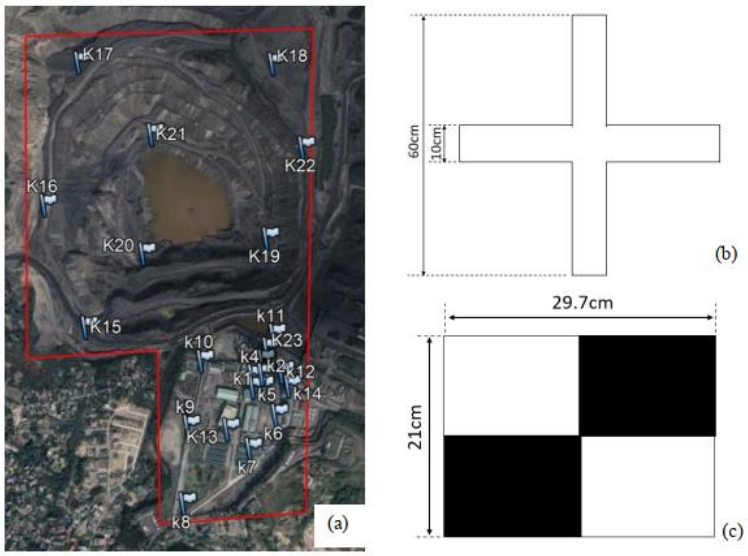


Figure. *3. Control Points and Checkpoints*

a) Designing GCPs on Google Earth; b) Ground Control Targets; c) TLS Control Targets

In order to combine data as well as ensure accuracy in the 3-dimensional space of objects. The dog well tower has a height of 50m, so there are some additional targets posted on the tower wall. Image control and inspection landmarks are located on the well tower wall marked with targets as shown in Figure 3c,



Figure 4. *GCPs determination by GNSS/T300*

The coordinates of the focal points on the ground are connected by a Comnav T300 two-frequency GNSS machine (Accuracy: ground 10mm+0.5ppm; height 20mm+0.5ppm). When measuring, the machine is clamped with a sturdy mirror pole (Figure 4) and measured a minimum of 3 times. Wall decals are measured with coordinates using a Leica TS09 Plus electronic total station (length measurement accuracy 1.5mm+2ppm, angle measurement 1") with a mirrorless laser distance measurement program. Before use, the equipment is inspected to ensure compliance with technical specifications as prescribed.

3.2. UAV Image Capture

The research area was captured using a DJI Phantom 4 Advanced (P4). The P4 is equipped with GPS and Glonass satellite positioning, and it features a 1-inch CMOS sensor with a 20MB resolution. Terrain analysis in Figures 1 and 2 reveals that the surveyed area has unique topography, including open pit mining areas (MO) and industrial yard (SCN). The UAV image capture method was determined as follows:

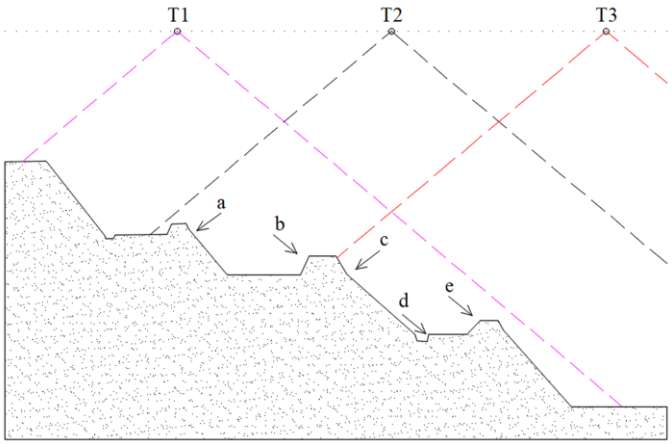


Figure 5. *Feature of open pit Mining Terrance*

Despite having various ground features, including terraces and slopes, it was still possible to obtain complete point cloud data from the image capture. This is because the mining terraces have a relatively small height and always expand gradually from the center of the pit to the mining boundary. Therefore, when flying for image capture, a 75% overlap in both the vertical and horizontal directions was used. Typically, one ground location appeared in nine images. Different ground locations were captured from various angles due to the UAV's changing image capture positions during flight strips. Figure 5 illustrates different UAV image capture locations. Image capture location T1 was suitable for capturing orthogonal and oblique terrain features at positions b, d, and e, but it might not provide data for positions a and c. Conversely, positions T2 and T3 showed the opposite. With this principle in mind, it can be

seen that to establish a 3D model of the mining area, UAV image capture using the B1 orthogonal capture method (2D map) with the parameters listed in Table 1 is sufficient.

In general, the industrial yard (SCN) and specifically at the Nui Beo mining site are typically centered around the mine shaft entrance, which is where various mining industrial structures are located. Figure 6 illustrates that although the images were designed with a large field of view overlap (80%), due to the vertical nature of these structures, the self-obstruction by these structures with considerable height often results in inadequate field of view overlap at certain geographical positions, particularly on the walls and surfaces of these structures (Figure 6, positions L and R). This inadequacy in field of view overlap can lead to insufficient point cloud data at these positions if only the B1 image capture method is employed. Therefore, in the central area of SCN, additional image capture will be conducted using a grid-based image capture method (B2) with a 45-degree oblique capture angle.

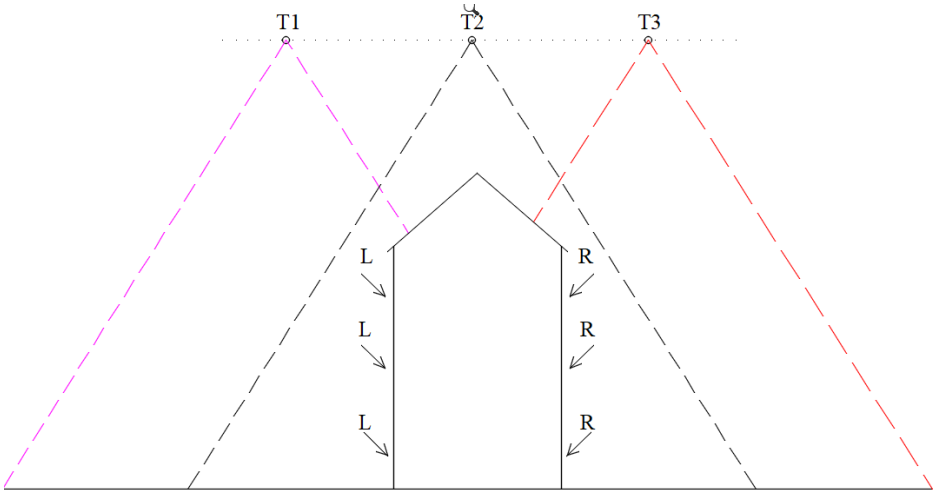


Figure 6. *Occurrence Potential of Ground object in UAV Images*

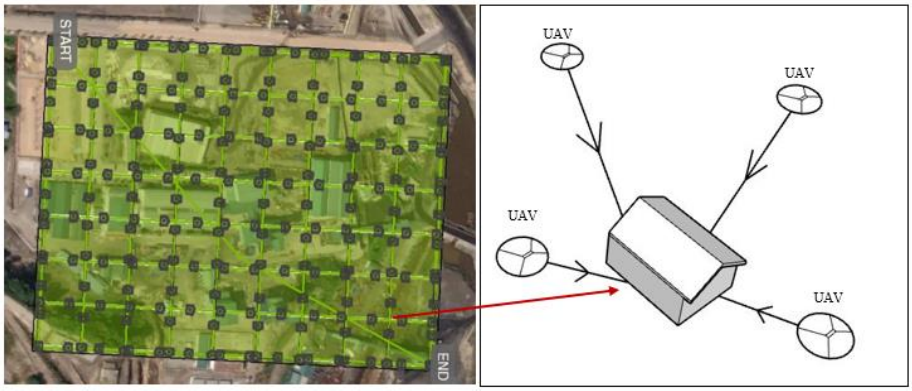


Figure 7. *UAV position for object capture using grid mission.*

With the B2 image capture method and the parameters listed in Table 1, each ground feature within the grid will have four images captured from four different directions (Figure 7) at a 45-degree oblique capture angle.

However, the shaft has a special structure, numerous small details, and is also the tallest structure in SCN35. To obtain a complete point cloud of the well tower for 3D modeling purposes, a circular flight method centered around the structure (B3) is applied to supplement the image capture of the well tower. The flight altitude varies from 50 m to 80 m, with two oblique capture angles of 45 degrees and 60 degrees. The parameters for these image capture methods are summarized and presented in Table 1.

Table 1. Flight plan options

Flight plan	Flight height (m)	Ground Sample Distance (cm)	Front and Side overlap	Capture angle
B1 (2D map)	100	2.74	75%x75%	90°
B2 (Grid)	100	2.74	80%x80%	45°
B3 (Circular)	50÷80	0.5	80%x80%	45° and 60°

When conducting the UAV image capture according to the designed methods, the takeoff location of the UAV is selected based on research [7] to ensure the required ground image resolution as per the design and to ensure the safety of the image capture equipment.

4. Building 3D Point Cloud

The UAV images captured using the B1, B2, and B3 flight methods are processed using Agisoft Metashape software. These images are processed simultaneously to obtain the best overall 3D point cloud (PC) result (Figure 8). The PC is established in accordance with the standard UAV image processing procedures, which include key steps such as image alignment, image correction, bundle adjustment, PC creation, and orthophoto generation, as well as the assessment of the accuracy of the achieved products.



Figure 8. *3D point cloud builded from UAV images*

The accuracy of the PC is assessed based on the Root Mean Square Error (RMSE) using control points within the model. The evaluation method and calculation formulas are referenced from the study by [8].

Table 2. The diffidence of Coordinate of Check Points

Name of point	The diffidence of Coordinate (cm)				Position
	ΔX	ΔY	ΔXY	ΔZ	
K2	-0.5	0.8	0.9	1.1	Shaft
K7	-1.5	1.8	2.3	-2	SCN ground
K9	0.9	1.7	1.9	1.8	
K23	-2.7	-1.5	3.1	-1.9	
K16	1.9	1.3	2.3	-2.5	Open pit mine
K20	-3.1	3.3	4.5	-4.2	
K22	-1.8	-1.5	2.3	-3.1	

The positional deviation of the coordinate points in the model is presented in Table 2. The root mean square error (RMSE) of the PC for the X, Y, and Z coordinate components are 2.0 cm, 1.8cm, and 2.6cm, respectively.

5. ESTABLISHING 3D MODEL

The 3D model of the experimental area is established at the level of detail LOD3. According to 3D format standards, the accuracy of the plan and height of the displayed object must reach 0.5m [9]. Objects with dimensions in three-dimensional space from 2x2x1m will be displayed.

The Industrial mining structures are digitized at various levels of detail, ranging from low detail (LOD0) to high detail (LOD3) based on the point cloud (PC). The dimensions of the structures can be directly measured on the PC, as shown in Figure 9.

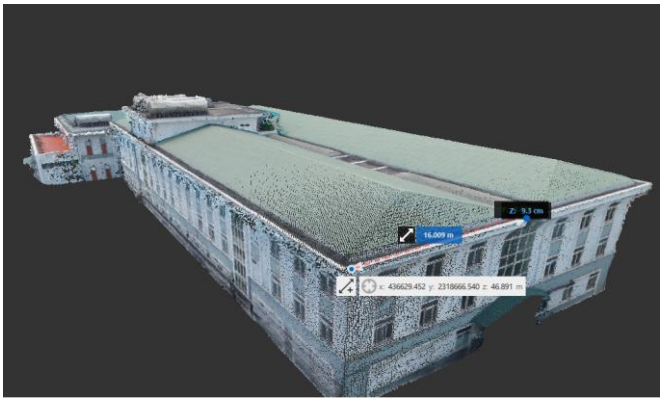


Figure 9. *Determining the dimensions of the structures on the PC*

For the open-pit mining area, the terrain points are extracted from the point cloud (PC) with a point density of < 0.5m. The contour lines and edges of the layers on the pit wall, along with distinctive points, are supplemented with coordinates taken from the PC. The overall PC data is input into SketchUp software, where a triangular TIN (Triangulated Irregular Network) model is automatically generated, creating a 3D surface (Figure 10).

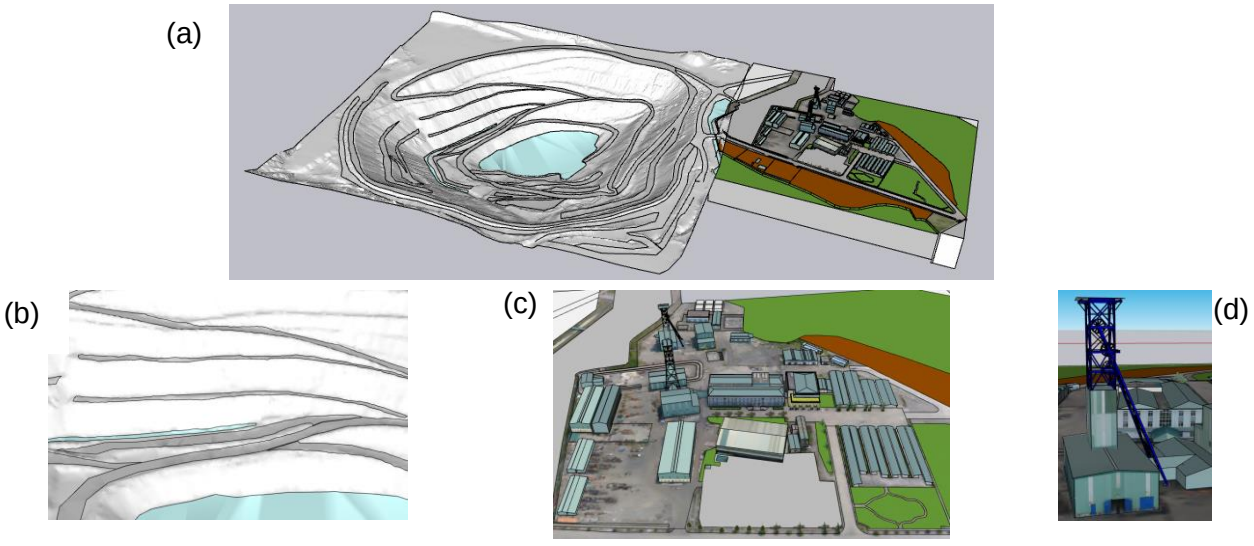


Figure 10. *3D model of the whole area*

a) Entire mining site, b) Working area, c) Mining industry yard, d) Shaft tower

The actual position of the objects is digitized on the orthographic image and referenced to the size on a PC. Pit mineral exploration includes objects such as road networks, mine infrastructure systems connected to the underlying terrain after being directly established on the 3D point cloud after noise filtering (outliers, equipment on the mine surface).

The terrain and geographical features are drawn using Sketchup Pro 2022 software. The results in Figure 10 illustrate the overall model, the Pit terrace area, the Central Processing Plant (SCN) area, and the model of the shaft.

6. RESULTS AND DISCUSSION

The UAV aerial photography method was designed with technical specifications as shown in Table 1, which were suitable for the actual conditions in the survey area. The results indicate that the combination of three flight plans, B1, B2, and B3, provided a complete 3D point cloud (Figure 8) with more details than each individual flight [5]. A high and comprehensive level of detail in the point cloud (PC) can be utilized to create a high-detail 3D model for both the industrial area and the open-pit mining site.

The root mean square error (RMSE) of the PC for both the horizontal and vertical components of the PC was less than 3.0 cm. The component coordinate deviations of the PC control points shown in Table 2 reveal that the positional error at the Pit terrace is greater than at the Central Processing Plant (SCN). The point K20 is located at the base of the Pit pit (corresponding to the greatest capture height), and it has the largest deviation. The industrial yard has a flat terrain, and the control points here have similar capture heights. Additionally, the inclusion of oblique images provides more complete PC data with smaller position errors in the Pit area (Table 2). Notably, point K2, located on the shaft tower, has the smallest deviation due to the addition of images captured along a circular path with a ground sampling distance (GSD) of 0.5 cm. Based on these evaluation results, in accordance with TCVN 16074:2015 standards, the established point cloud achieves the required accuracy for creating a 1:500-scale map corresponding to a LOD3 model.

The smallest identifiable object on the PC, necessary for modeling, is considered to be 1.5 times the ground sampling distance (GSD) [10]. The maximum GSD in the designed UAV photography is 2.74 cm, allowing for the identification of objects with a minimum distinguishable size of 4.11 cm. In theory, it is possible to model all geographical objects at the Central Processing Plant. However, the shaft tower has complex structures with many details smaller than 10 cm, making it impossible to directly measure and model these objects on the PC [3]. The 3D model of the shaft tower is created with objects larger than 20 cm in size.

7. CONCLUSION

The creation of a 3D model for the mining area, which includes the open pit mine, the industrial yard, and the shaft tower, requires a carefully calculated UAV aerial photography method to obtain a comprehensive point cloud and ensure economic and technical feasibility. For the Pit mineral excavation area, where there are minimal geographical features, orthogonal aerial photography is sufficient. In the central processing plant area (SCN), characterized by numerous construction structures, oblique angle images should be added, captured in a grid pattern. The shaft tower's complex structure, with many small

details, allows for the measurement and reconstruction of objects larger than 20 cm using UAV data. Smaller details may require additional aerial photography or integration with other data sources, such as laser scanning.

In the process of creating the 3D model, the Pit mineral excavation can be directly reconstructed from the point cloud data after noise filtering. Geographical features within the SCN are reconstructed based on their real-world positions in orthographic images and measured dimensions on a PC.

However, the upper part of the shaft tower, with its intricate structure and numerous small details, can only be accurately measured, reconstructed, and modeled for objects larger than 20 cm using UAV data. Smaller details may necessitate additional aerial photography or the incorporation of alternative data sources like laser scanning.

ACKNOWLEDGMENTS:

This research was supported by The Ministry of Education and Training of Vietnam (MOET) under grant number B2022-MDA-10.

Conflicts of Interest: The authors declare no conflict of interest.

REFERENCES

1. Prime Minister, Decision No. 403/QD-TTg on approving the adjustment of Vietnam's coal industry development planning to 2020, considering the outlook to 2030. 2016.

2. Nguyen, N.V., L.Q. Nguyen, and L.Q. Vu, *Application of terrestrial laser scanner GeoMax Zoom 300 for 3D mapping of Vietnam's open-pit mines (in Vietnamese).* Journal of Mining and Earth Sciences, 2017. **58**(4): p. 0-0.

3. Canh L.V et al., *Research to establish 3D model of mine industrial site area from terrestrial laser scanning and Unmanned aerial vehicle data.* Journal of Mining and Earth Sciences, 2022. **63**(5): p. 25-36.

4. Zhao, H., R. Bai, and G. Liu, *3D Modeling of Open Pit Based on AutoCAD and Application.* Procedia Earth and Planetary Science, 2011. **3**: p. 258-265.

5. Cuong C.X, et al., *Quality assessment of 3D point cloud of industrial buildings from imagery acquired by oblique and nadir UAV flights.* Naukovyi Visnyk Natsionalnoho Hirnychoho Universytetu, 2021. **5**: p. 131-139.

6. Long N.Q and Canh L.V, *Application of low-cost Unmanned Aerial Vehicle in calculating reserves of open pit mine.* Mining Industry, 2020. **29**(2): p. 79-85.

7. Canh L.V, Cuong C.X, and Ha L.T.T, *Research on optimal takeoff positions of UAV integrated GNSS - RTK in producing large scale topological maps for open - pit mines.* Journal of Mining and Earth Sciences, 2020. **4**.

8. Le Van Canh, et al., *Experimental Investigation on the Performance of DJI Phantom 4 RTK in the PPK Mode for 3D Mapping Open - Pit Mines.* Journal of the Polish Mineral Engineering Society, 2020. **2**: p. 65-74.

9. Consortium, O.G. *OGC City Geography Markup Language (CityGML) Encoding Standard*. 2019.

10. Burdziakowski, P. and A. Zakrzewska, *A New Adaptive Method for the Extraction of Steel Design Structures from an Integrated Point Cloud.* Sensors, 2021. **21**(10): p. 3416.

RESEARCH ON APPLICATION OF ELECTRIC SUBMERSIBLE PUMPS TO INCREASE OIL RECOVERY FIELD Y, LOT 05-1A, THE NAM CON SON BASIN

Nguyen Thi Minh Thu [(1)], Pham Nguyen Duy Phuong [(2)] and Huynh Tan Tuan[(3)]
Faculty of Geology, VNUHCM - University of Science [(1,2,3)]
ntthuminh05@gmail.com[(1)]; phamnguyenduyphuong96@gmail.com[(2)];
httuan@hcmus.edu.vn[(3)]

Abstract: The application method of Electric Submersible Pump increases the oil recovery factor Y at 05-1A block, the Nam Con Son basin, which is affected by many factors such as energy regime, fluid regime, fractures, etc. All these factors are based on the simulation model from Prosper simulation software. The process starts from the appropriate PVT data, exploitation data, selecting necessary parameters, designing wells, and predicting exploitation to find the best case for the Electric Submersible Pump exploitation plan. The results showed that if oil is only exploited by natural energy, it will not be effective, so it is possible to equip a Electric submersible pump system with 2 exploitation wells for the most efficient exploitation. The Electric Submersible Pump is applied and effective in the case of wells with high Water Cut and low Gas Oil Ratio.

Keyword: *Recovery factory; Gas-oil ratio; the Electric Submersible Pump*

1. INTRODUCTION

Y field is located in Block 05-1A in the offshore continental shelf of Southern Vietnam, approximately 262 km southeast of Vung Tau. The seabed depth in the mining area ranges from 110-120 meters. The seabed terrain in most of the mine's area is relatively flat and free from major obstacles, providing favorable conditions for the construction of oil and gas extraction facilities.

According to seismic interpretation results, Oligocene sediments are predicted to be present in the surrounding basins of the Y structure and have been identified through drilling in various structures within the Nam Con Son basin, where the basement is situated much deeper compared to Y field. These sediments consist of clay-rich layers, greenish sandy layers containing thin coal seams, with a total thickness of up to 1000 meters. The predominant rock types at Y field are Miocene middle-aged sandy layers and limestone. They are widely distributed in the southern and central parts, gradually thinning and disappearing towards the north and northeast of the mine.

Thick, stable clay layers, originating from the upper Miocene to Pliocene marine environment, act as a regional sealing layer. Local sealing layers in the reservoirs are heterogeneous sets from the lower Miocene and middle Miocene, primarily formed in a continental environment. Most researchers believe that the organic-rich clay sets from the lower Miocene and Oligocene ages in the vicinity are the source rocks for hydrocarbon generation at Y field.

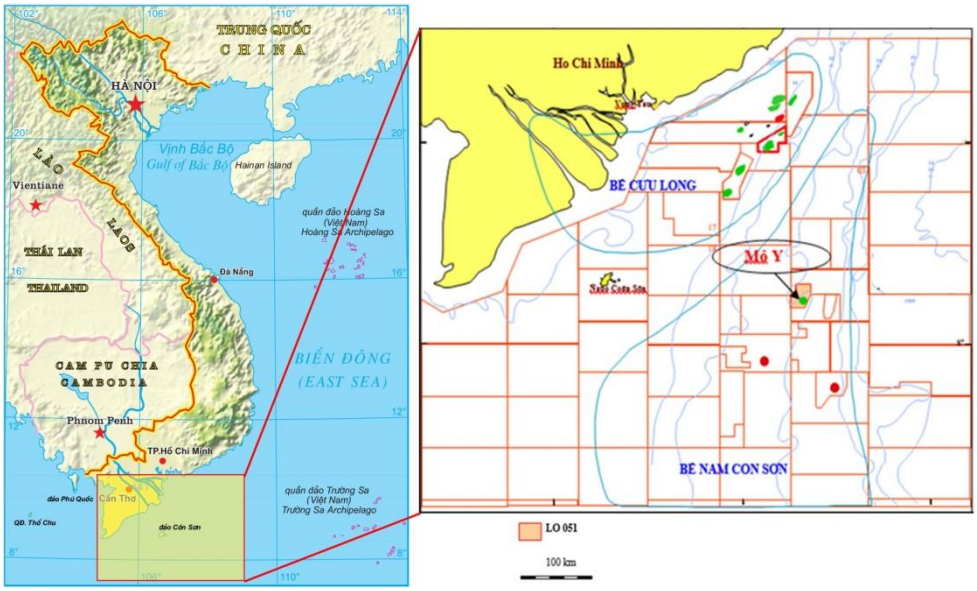


Figure 1. *Geographic Location of Y Mine [PVEP POC].*

2. THEORETICAL BASIS

2.1. Introduction to Electrical Submersible Pump (ESP)

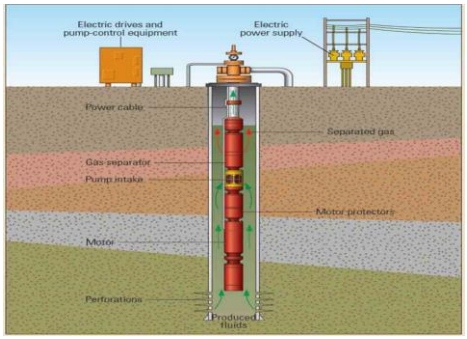


Figure 2. *Typical ESP Configuration [PVEP POC]*

Utilizing Electrical Submersible Pumps (ESPs) is a mechanical extraction method employed when the well cannot naturally produce at the desired flow rate. This is achieved by supplying additional energy from the surface down to the submersible centrifugal pump unit through a three-phase electric cable system running along the OKT (Production Tubing) or suspended freely. The components of the ESP in the wellbore include the motor, protective components, pump components, pump intake, electrical cables, gas handling equipment, and drilling hole sensors (not shown). The surface components consist of the control box and power source. Energy is provided to the electric motor of the submersible centrifugal pump unit, causing the pump impeller to rotate. This generates centrifugal force and increases pressure, facilitating the flow of fluid from the reservoir into the multi-stage pump to be lifted to the surface, then to the collection and processing system.

The ESP is a multi-part centrifugal pump stacked on top of each other; the number of parts will be determined depending on the well operation requirements and completed design work. Each cycle consists of a rotating fan blade and a fixed diffuser typically cast from high-nickel iron to minimize material erosion. As fluid flows into the first cycle of the ESP, it passes through a fan blade, and the centrifuged fluid is directed outwards, obtaining energy in the form of velocity. The centrifugal pump is controlled by an induction motor capable of achieving operating speeds exceeding 5,000 revolutions per minute when using a variable-speed drive.

After exiting the fan blade, the fluid must swirl strongly to enter the diffuser. As it moves through this section, the fluid is diffused, and its velocity is converted into pressure. At this point, the fluid will have slightly higher pressure than when it entered the first cycle,

entering the fan blade and diffuser stage to repeat the process. The fluid passes through all cycles of the pump, gradually increasing pressure in each stage until it reaches the total energy head required to move up to the well surface.

2.2. Design of the Electrical Conditions and Basic Submersible Pumping Method

Table 1. Well Completion Conditions

Well completion conditions/Production conditions	Ideal	Acceptable	Further research needed	Not suitable
Outer Casing Diameter (inch)	≥9	≥7	≥7	<7
Bottomhole Temperature (F)	<250	250 – 350	350 – 400	>400
Productivity Index (bbl/day/psi)	≥6	3 - 6	1 - 3	<1
Pump Depth (ft)	<10.000	10.000 – 14.000	14.000 – 17.000	>17.000
Potential (bbl/day)	5.000 – 40.000	2.500 – 5.000	1.000 – 2.500	<1.000
Gas-to-Pump Depth Ratio (%)	< 20	20 – 40	40 – 70	>70

Electrical submersible pumps can be installed in four different production environments, where design criteria vary as the fluid properties and well conditions change. There are four basic design types of ESP.

The basic designs will vary accordingly and primarily depend on:

- High or low water cut
- High or low gas-oil ratio
- Light or heavy oil (viscous fluid?)
- Uncertain well productivity

Table 2. Reservoir Conditions

Type	Reservoir Condition	Design Type
1	Low GOR / High WCT	High WOR Design
2	Significant Gas Volume	High GLR Design
3	Heavy Oil	Viscous Fluid Design
4	Variable or Uncertain Production Ratio	Speed Variable Design

3. RESEARCH METHODOLOGY

Designing a submersible pump system requires a comprehensive understanding of various data sets at a high level of expertise. Perhaps the most crucial parameter for designing is the well exploitation target, which is used to determine the expected flow rate. The design process is based on input data groups and follows these steps:

Step 1: Gathering basic data

General information (location, well name, reservoir name, mining field name, etc.);

Well's physical data: Well trajectory, inclination, and depth; Perforation depth/zone; Casing levels/cementing depth; Type/size of production tubing.

Well's exploitation parameters: Bottom hole pressure or static hydraulic column pressure; Flowing bottom hole pressure; Productivity index (PI); Water cut index (WTC); Gas-oil ratio (GOR); Flow assurance issues: sand, paraffin deposition, corrosion, etc.

Fluid data: Oil density (API); Gas and water density; Saturation pressure; Viscosity; Gas-oil solubility ratio; Surface parameters (power supply threshold, etc.).

Step 2: Well exploitation capacity

Establish the relationship between Inflow Performance Relationship (IPR) and Vertical Lift Performance (VLP) curves in the design of the ESP centrifugal pump system.

Step 3: Calculate the volume of fluid

Volume of dynamic gas.

(Note: The text continues after this point, please let me know if you'd like me to continue with the translation.)

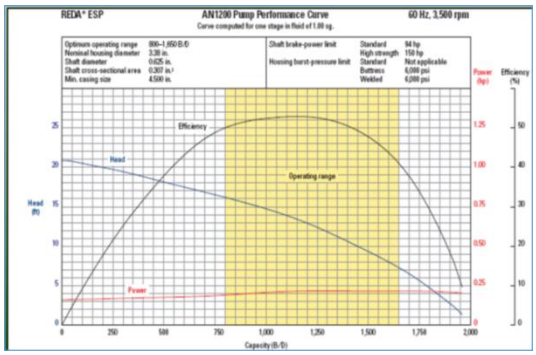
Gas-Oil Ratio - GOR	$$R_s = \gamma_g * \left[\frac{P_b}{18} * \frac{10^{0.0125*API}}{10^{0.00091*T}}\right]^{1.20482}$$
Gas Volume Factor	$$B_g = 5.04\frac{zT}{p}$$
Oil Volume Factor	$$B_o = 0.972 + 0.000147 * \left[R_s * \left(\frac{\gamma_g}{\gamma_o}\right)^{0.5} + 1.25 * T\right]^{1.175}$$
Total Fluid Volume	$$Total\ Gas = \frac{Producing\ GOR * BOPD}{1000} = MCF$$ $$Solution\ Gas = \frac{R_s * BOPD}{1000} = MCF$$ $$Freegas = Total\ Gas - Solution\ gas$$
	$$Volume\ of\ Oil\ @\ Pump\ Intake, \quad V_o = BOPD * B_o$$ $$Volume\ of\ gas\ @\ the\ Pump\ Intake, \quad V_g = Free\ gas * B_g$$ $$Volume\ of\ water\ @\ Pump\ Intake, \quad V_w = BWPD * B_w$$ $$Total\ Fluid\ Volume, \quad V_T = V_g + V_o + V_w$$ $$Percentage\ of\ free\ gas\ to\ total\ volumme,$$ $$\%\ Free\ gas = \frac{V_g}{V_T}$$

This is the amount of gas at the pump intake, with the limit percentage falling in the range of 10-15%. If the gas content at the pump intake exceeds 15%, it is necessary to consider installing an additional gas separator in the design.

Step 4: Calculate the Total Dynamic Head (TY).

TDH = Net well lift (dynamic lift) + Tubing Friction Loss + Wellhead Discharge

$$TDH = H_d + F_t + P_d$$



Step 5: *Selecting the type of centrifugal submersible pump.*

4. RESEARCH RESULTS

4.1. Analysis Results of Y field Oil Characteristics - Block 05-1A

- Rock Composition: The products of Y Mine consist of Greenish Sandy Shale, Limestone, and Fractured Granite. Among these, industrial products are primarily obtained from Greenish Sandy Shale and Limestone. Greenish Sandy Shale exhibits generally good rock quality, with an average porosity of 15-20% and permeability of 50 mD. Average water saturation ranges from 20-50%. The maximum rock content based on core sample analysis of porosity is 11%, corresponding to a permeability of about 1-1.5 mD. This type of rock is primarily water-wet to neutrally wet, with an average remaining oil saturation of 25%. Limestone has better permeability compared to Greenish Sandy Shale. According to core sample analysis and DST reservoir testing, permeability mostly falls in the range of 50-100 mD.

- Porosity-Permeability Relationship: Based on available sample data, routine core analysis (RCA), and special core analysis (SCAL), the porosity-permeability relationship is determined for each Greenish Sandy Shale and Limestone reservoir object.

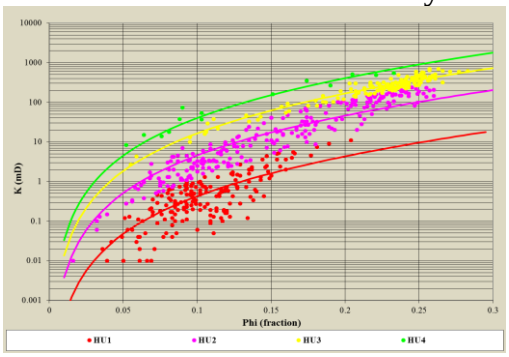


Figure 3. *Porosity-Permeability Relationship of the Exploited Area in Y field [PVEP POC]*

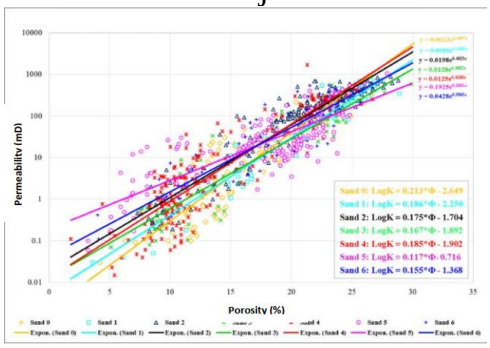


Figure 4. *Porosity-Permeability Relationship of Limestone Layers in the Exploited Area of Y field [PVEP POC]*

Reservoir fluid characteristics: Fluid samples from the reservoir bottom layers in Y Mine are primarily taken from the Limestone and Greenish Sandy Shale layers during DST reservoir testing, using bottom sampling equipment with effective capacities ranging from 600 ml to 2500 ml. Additionally, samples are also collected during RFT/RCI/MDT measurements, but in smaller quantities and volumes, ranging from 450 ml to 700 ml. For multiphase fluid systems, samples are considered satisfactory when the pressure at the sampling depth is higher than the saturation pressure of gas-dissolved oil under reservoir temperature conditions. Furthermore, during reservoir testing, oil and gas samples are also collected at the surface separator for recombination in cases where the bottom samples do not meet the required quality.

PVT characteristics of oil & gas: The Y field reservoir oil, classified according to collected data, can be summarized as follows:

Un-saturated reservoir oil system (P_reservoir > P_bubble) is found in most oil reservoirs in Limestone and Greenish Sandy Shale layers throughout Y field.

Near-saturated reservoir oil system (P_bubble ~ P_reservoir) or bubble-point reservoir oil system (P_bubble > P_reservoir) is predominantly found in the Southern blocks, especially in the Greenish Sandy Shale and occasionally in the Limestone layers.

Gas-condensate reservoir system (P_dew ~ P_reservoir): with dew point pressure close to the reservoir pressure, it accounts for a smaller quantity and is primarily found in the Southern block areas in the Greenish Sandy Shale layer, and to a lesser extent in the Limestone layer.

The PVT analysis results also demonstrate that while the oil properties are quite similar, there is a clear distinction between reservoir product layers within the same wellbore, indicating a non-uniform distribution of oil properties in the reservoir product layer cross-section. By exploration/production region, the oil properties are distinctly separated as follows:

Northern exploitation area of Y field: only exploited in the Greenish Sandy Shale layer, consisting entirely of un-saturated reservoir oil products (except for H137 in Y-4X block D) with a bubble point pressure of ~ 2000-3500 psi, low average oil volume factor Bo ~ 1.25-1.45 rb/stb, low gas-oil ratio Rs ~ 350-700 scf/stb, oil density ~ 26-32 oAPI, and viscosity ~ 0.6-2.6 cP.

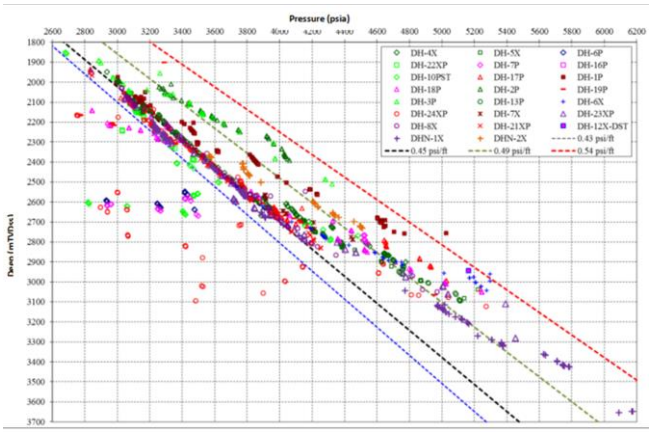


Figure 5. *Reservoir Pressure Regime [PVEP POC]*

Southern exploitation area of Y field: exploits both Limestone and Greenish Sandy Shale layers. In the Limestone layers, the bubble point pressure is ~ 2900-3300 psi, oil volume factor Bo ~ 1.32-1.57 rb/stb, gas-oil ratio Rs ~ 550-1000 scf/stb, oil density ~ 33-37.5 oAPI, and viscosity ~ 0.3-0.5 cP. In the Greenish Sandy Shale layers, the bubble point pressure ranges from 3400-5100 psi, with a high oil volume factor Bo ~ 1.6-2.1 rb/stb, high gas-oil ratio Rs ~ 1000-2000 scf/stb, oil density ~ 35-39 oAPI, and low viscosity ~ 0.2-0.45 cP.

Crude oil characteristics: The crude oil from Y Mine falls within the classification range from medium to heavy, with densities ranging from 0.827 g/cm³ to 0.930 g/cm³. It contains low sulfur content, ranging from 0.05% to 0.152% by weight, and is classified from low asphaltene content to high asphaltene content, with asphaltene content ranging from 3.0% to 21.8% by weight. It also contains a significant amount of paraffin, with paraffin content ranging from 6.9% to 30.0% by weight.

Reservoir water characteristics: Based on the lithological and physicochemical properties of the reservoir water, the water-bearing formations can be divided into two main layers: the intermediate Mioxen water-bearing layer and the upper Mioxen layer (N12+3). According to the water sample analysis results, the water mineralization ranges from 24460 ppm to 30170 ppm (24.46 g/l to 30.17 g/l) in the Mioxen water-bearing layer. In the lower Mioxen water-bearing layer (N11), the water mineralization ranges from 24015 ppm to 28238 ppm (from 24.015 g/l to 28.238 g/l) based on water sample analysis.

Reservoir pressure and temperature regime: With a total of 40 exploratory, appraisal, and production wells drilled across most of the Y Mine area, pressure and temperature data for the reservoir have been collected during surveying processes such as RFT/RCI/MDT, DST, and MPLT. This data has allowed for the basic determination of pressure and temperature profiles for the various product-bearing layers. The initial reservoir pressure of

the Y Mine-bearing formations has been determined using various methods, including pressure measurement along the wellbore during drilling (RFT, RCI, MDT), DST reservoir testing, and PLT reservoir testing during well completion. The pressure results for the entire mine are shown in Figure 3.3.5-1. In general, the initial pressure of the wells is higher than the hydrostatic pressure, especially in wells located in the Early Production area, where the reservoir pressure is 100-400 psi higher than the hydrostatic pressure. The initial reservoir pressure values obtained from RFT/RCI/MDT documentation for each product-bearing layer generally exhibit good linear relationships, following the pressure gradient determined for the type of reservoir fluid. The reservoir fluid analysis results obtained from Y Mine documentation are consistent with log analysis and have been confirmed by DST documentation and production testing after well completion. Additionally, the subdivision of the product-bearing formations into sandstone layers in the Greenish Sandy Shale and Limestone layers is clearly shown in the RFT/RCI/MDT analysis results. These product-bearing formations exhibit distinct pressure gradient differences and reservoir pressures when brought to the same depth.

The MDT measurement results for the newly drilled wells Y-18P and 22XP show that after approximately 03 years of production, most of the formations in the YTT area have experienced pressure reduction (approximately 100-350 psia), except for some unproduced gas formations and newly produced oil formations in the DV1 formation. The pressure reduction in the DV3 formation is less significant due to energy support from the underlying/aquifer.

4.2. Research Results on Well Simulation Models

Criteria for selecting wells for submersible pump installation: Through the analysis of production from the Y fields mentioned above, it is evident that, in general, reservoir pressure is gradually decreasing and water influx is increasing. This necessitates considering the conversion of some oil production wells from the natural flow method to a mechanical extraction method. Based on calculations and applied experience, and considering the deployment in similar mines and the Summary Table of Production History for wells in the southern region of Y Mine (Figure 3.13), two wells, Y-16P and Y-19P, can be selected for experimental research on the Electrical Submersible Pump (ESP) method, based on the following criteria:

Based on the criteria outlined in the paper "Offshore ESP Selection Criteria" SPE 146652, most of the fluid properties in Y Mine fall under the category of "ideal" or "acceptable". This indicates that Y Mine provides suitable conditions for the application of the submersible pump extraction method.

Table 3. Well Completion Conditions/Production Conditions

Well completion conditions/Production conditions	Ideal	Acceptable	Further research needed	Not suitable	Y field
Outer Casing Diameter (inch)	≥ 9	≥ 7	≥ 7	< 7	≥ 7

Bottomhole Temperature (F)	< 250	250 – 350	350 – 400	> 400	< 300
Productivity Index (bbl/day/psi)	≥ 6	3 - 6	1 - 3	<1	2 – 5
Pump Depth (ft)	< 10.000	10.000 – 14.000	14.000 – 17.000	> 17.000	< 8.000
Potential (bbl/day)	5.000 – 40.000	2.500 – 5.000	1.000 – 2.500	< 1.000	200 – 2.000
Gas-to-Pump Depth Ratio (%)	< 20	20 – 40	40 – 70	> 70	20 – 40

Production rate during low days (< 300 barrels/day)
Wells producing from one reservoir (limestone).

4.2.1. Exploitation Scenario with Natural Pressure Depletion

Well Y-16P

The structure of the production well Y-16P

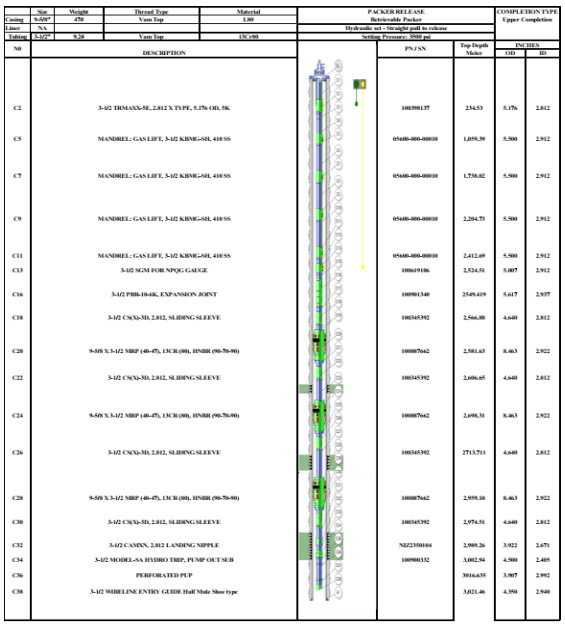


Figure 6. *Wellbore structure of production well Y-16P [PVEP POC]*

Exploitation Dynamics of Well Y-16P

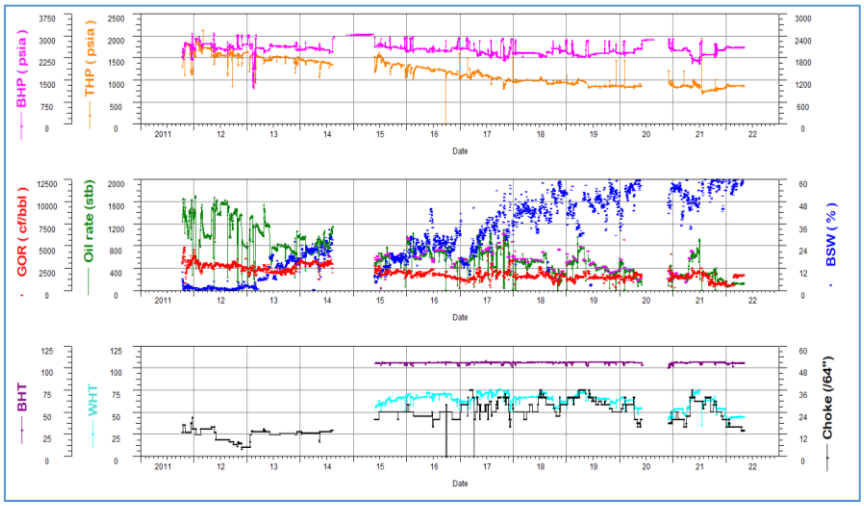


Figure 7. *Exploitation dynamics of well Y-16P*

Forecasted production rate under natural pressure reduction scenario

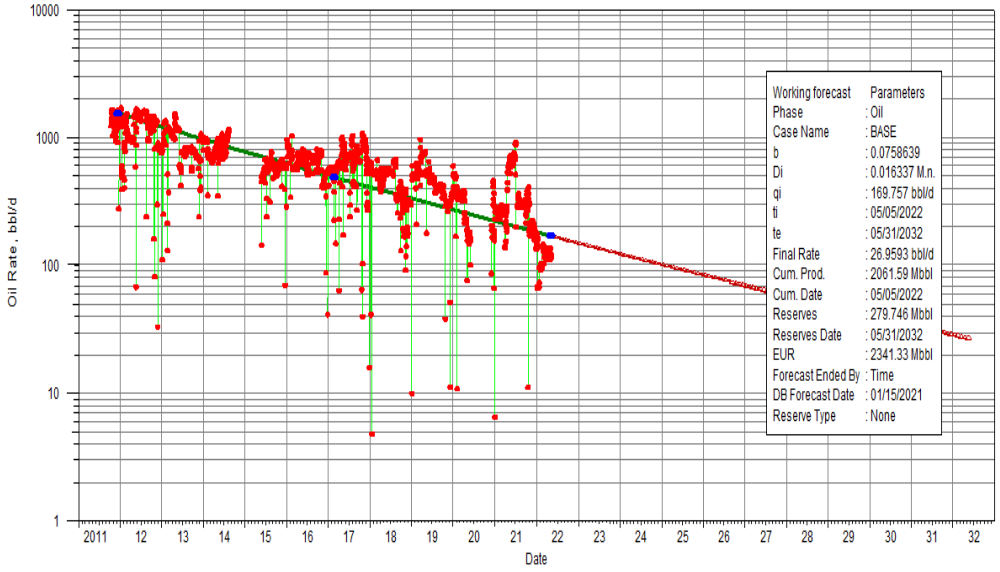


Figure 8. *Production Forecast Under Natural Pressure Reduction*

Well Y-19P

Well Y-19P Exploitation Structure

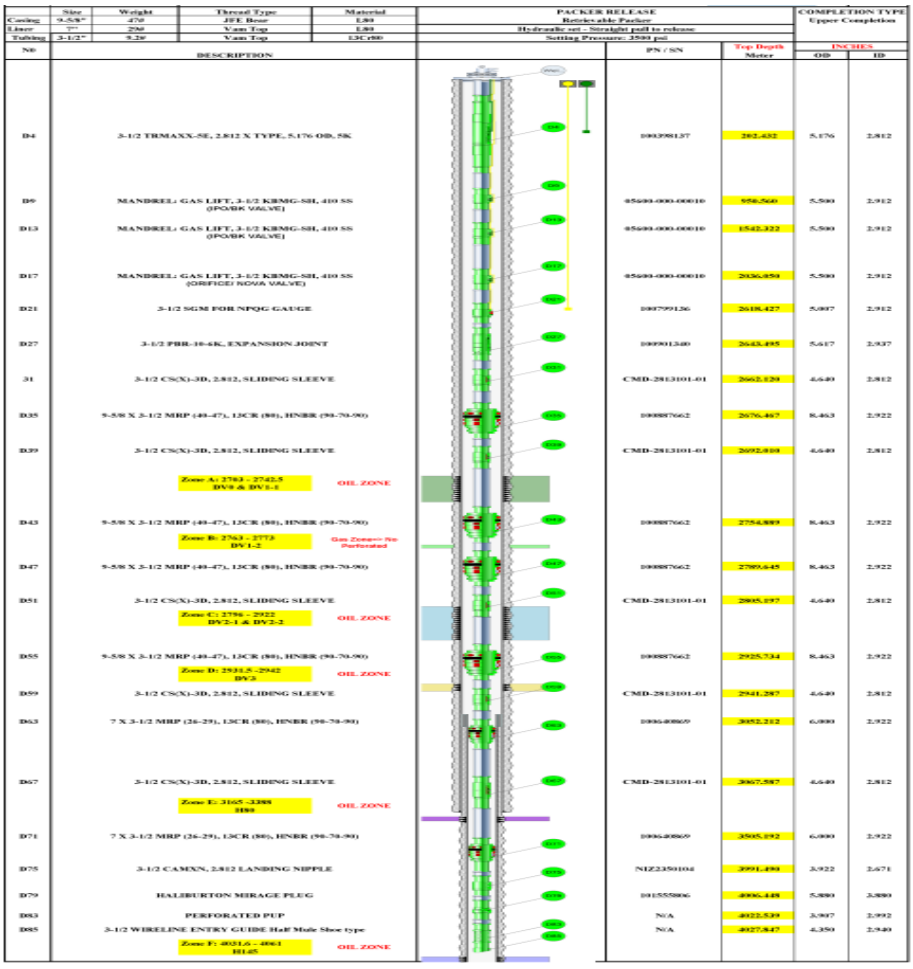


Figure 9. *Well Y-19P Exploitation Structure [PVEP POC]*

Y-19P Well Exploitation Dynamics

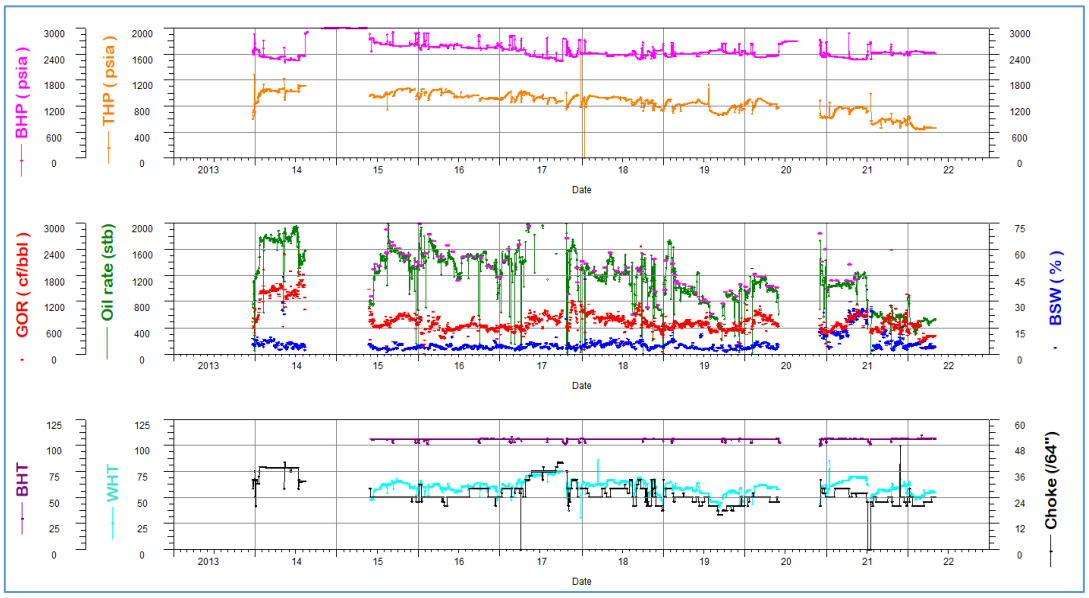


Figure 10. *Production Dynamics of Well Y-19P*

Forecasted Production Output in the Case of Natural Pressure Reduction

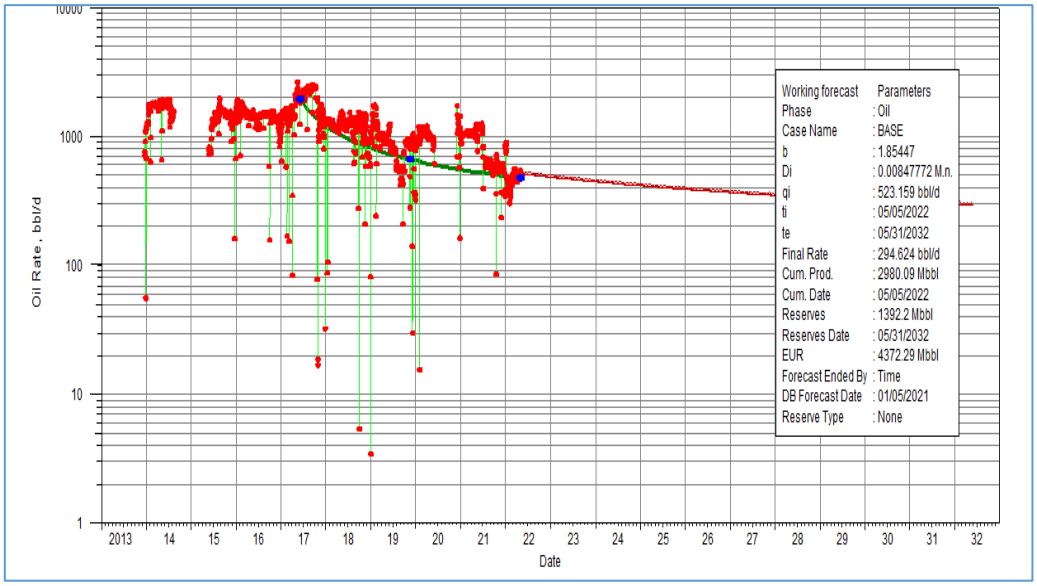


Figure 11. *Production Output in the Case of Natural Pressure Reduction*

4.2.2. Results of Applying ESP on the Well Simulation Model

A common phenomenon observed in production wells is that when water ingress occurs, the water content rapidly increases, and the well stops self-flowing after a short period. Gas lift injection outside the production tubing is an effective, economical, and flexible method to maintain well flow rates in the early stage without incurring significant maintenance costs. However, as time goes on, when the water production rate increases and reservoir energy gradually decreases, the gas lift method cannot sustain the well's production capability. Therefore, it is necessary to explore and apply alternative production methods for wells with high water production rates, aiming to increase production capability and oil recovery efficiency. In this case, submersible pumping is a promising method with the potential for higher recovery rates compared to gas lift under similar operating conditions.

Well Y-16P

• Well Description and Pumping System Structure:

- Well Depth: 4420m
- Drill Hole Diameter: 8.5 inches
- Bottom Rock Type: Sedimentary rock
- Current Well Flow Rate: ~ 250 barrels/day

• Submersible Pumping System Components:

- Submersible Pump: GE_ESP TD387_6000_COMP 3.85 INCHES (1800-7500 RB/day)
- Motor: Centrilift 544 250HP 1905V 82A
- Cable: #1 Aluminium 0.33 (Volts/1000ft) 95 (amps) max

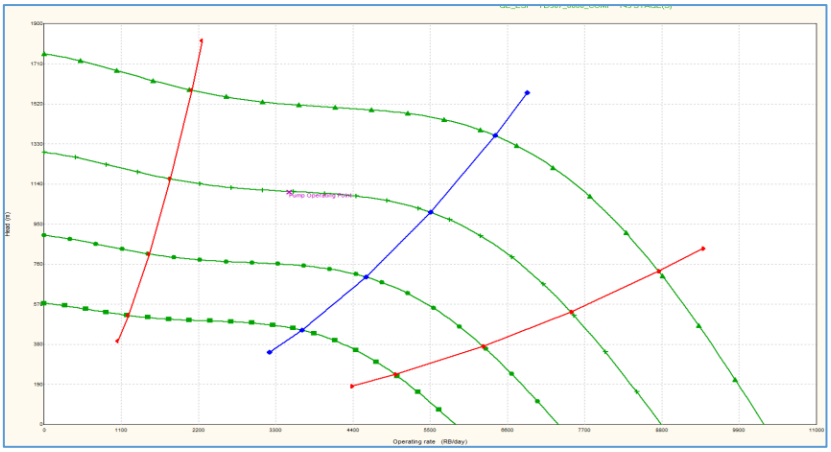


Figure 12. *Pump Design Graph of ESP*

• Pump System Performance:

- Inlet Pressure: 700 - 1400 psi
- Outlet Pressure: 1400 - 4000 psi
- Operating Frequency: 30 - 250 Hz
- Rated Voltage: 456 - 575 V (3-phase)
- Rated Power: 50 - 350 hp
- Pump Installation Depth: 2570 m below sea level

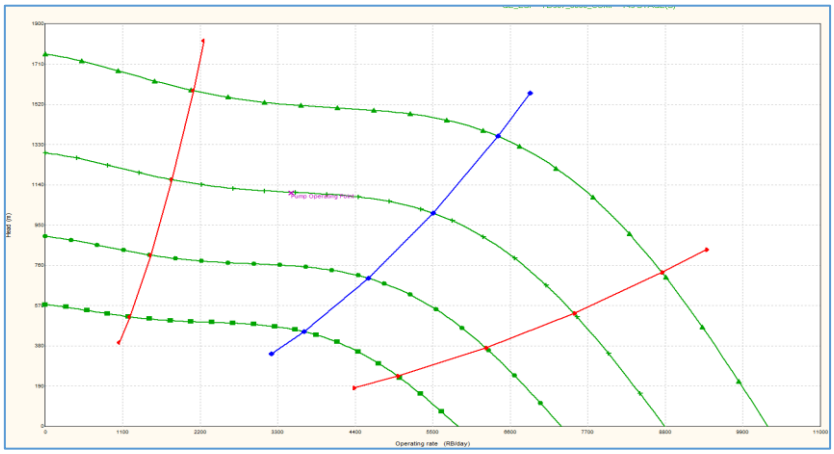


Figure 13. *Pump Design Graph of ESP*

Technical Matters:

The submersible pump system operates 24/7. It operates normally without encountering any technical issues.

• Production Output:

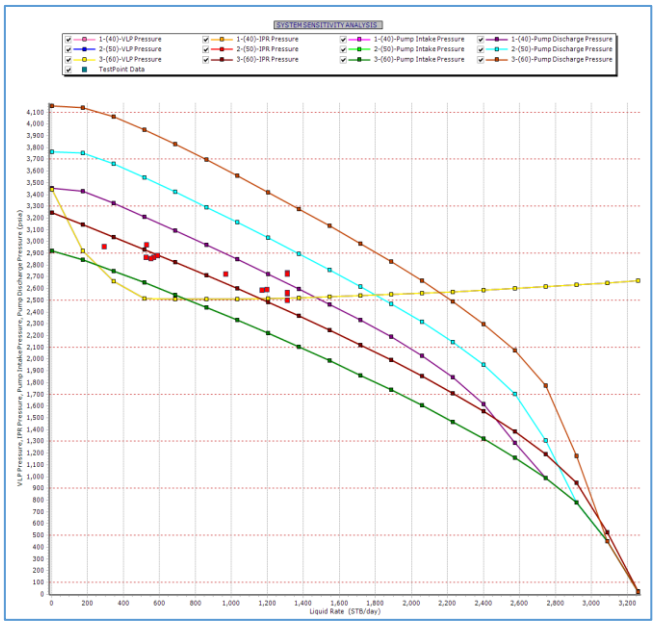


Figure 13. *Production Output of Well Y-16P*

Assessment: Based on the production dynamics when applying ESP as described above, with pump operating frequencies of 40-50-60 Hz, the liquid production rates per day are approximately 1300 barrels/day, 1700 barrels/day, and 1900 barrels/day, respectively. Meanwhile, the highest daily oil production rates at pump operating frequencies of 40, 50, and 60 Hz are approximately 600 barrels/day, 800 barrels/day, and 1000 barrels/day, due to the well having a water production ratio of 65%.

Well Y-19P

• Description of the oil well and pump system structure:

- Well depth: 4027m
- Drill hole diameter: 8.5 inches
- Well bottom type: sedimentary rock
- Production capacity of the well: 500-600 barrels/day

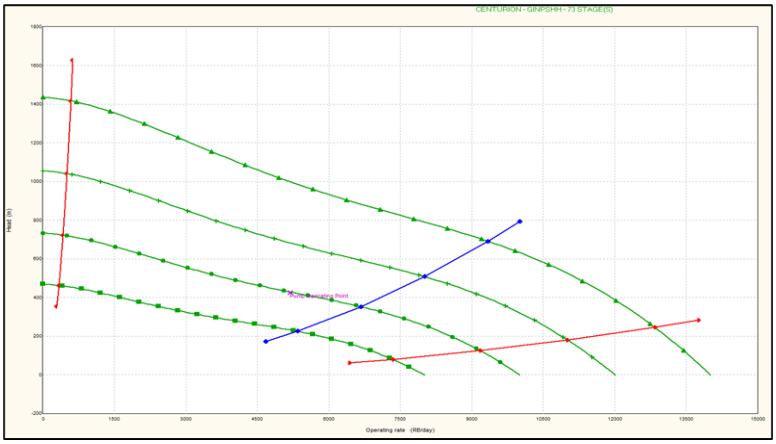


Figure 14. *ESP Pump Design Graph*

- Submersible pump system includes:

- Submersible pump: GE_ESP TD387_6000_COMP 3.85 INCHES (1800-7500 RB/day)
- Motor: Centrilift 544 250HP 1905V 82A
- Cable: #1 Aluminium 0.33 (Volts/1000ft) 95 (amps) max

- Pump system performance:

- Input pressure: 700-1400 psi
- Output pressure: 1400-4000 psi
- Frequency range: 30-250 Hz
- Rated voltage: 456-575 V (3-phase)
- Rated power: 50-200 hp
- Pump installation depth: 2670 m below sea level

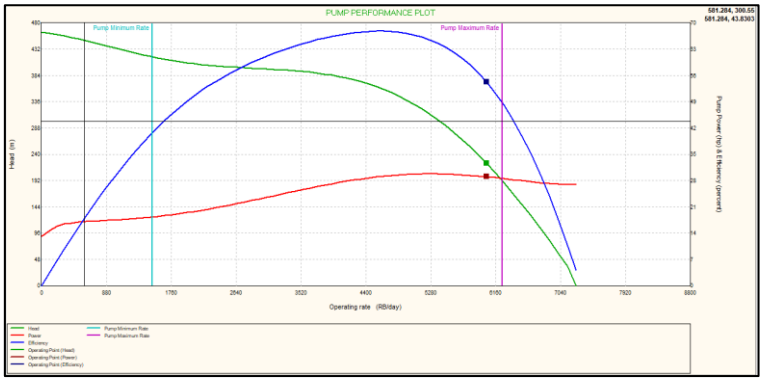


Figure 15. *ESP Pump Design Graph*

- Technical Considerations:

The submersible pump system is operated 24/7. The operation process is normal and does not encounter technical issues.

- Production Rate:

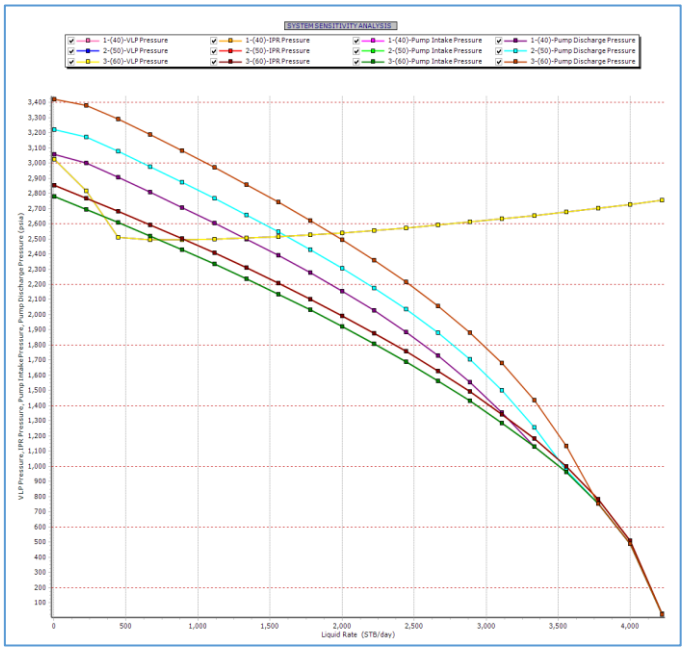


Figure 16. *Production Rate of Well Y-19P*

Evaluation: Based on the production behavior observed when applying ESP as described above, with pump operation frequencies of 40-50-60 Hz, the daily fluid production is approximately 1300 barrels/day, 1600 barrels/day, and 1900 barrels/day, respectively. Correspondingly, the daily oil production is approximateSly 1100 barrels/day, 1360 barrels/day, and 1615 barrels/day, given that the well has a water production ratio of 15%.

4.3.3. Increased Production Efficiency

Table 4. Production Rate Results

Y-16P				
Year	Recoverable Oil Reserves (barrels)			
	Base case	ESP# 40 HZ	ESP# 50 HZ	ESP# 60 HZ
2023	74,737	279,515	365,520	408,522
2024	61,295	229,242	299,778	335,046
	Increased Oil Reserves with ESP Installation			
2023	-	204,778	290,783	333,785
2023 & 2024	-	372,725	529,265	607,536

Y-19P				
Year	Recoverable Oil Reserves (barrels)			
	Base case	ESP# 40 HZ	ESP# 50 HZ	ESP# 60 HZ
2023	201,449	386,336	457,879	543,732
2024	171,367	328,644	389,504	462,535
	Increased Oil Reserves with ESP Installation			
2023	-	184,886	256,430	342,282
2023 & 2024	-	342,163	474,567	633,451

5. CONCLUSION

Evaluation: Based on the production dynamics of well Y-16P when applying ESP as described above, the projected increase in oil production compared to natural extraction from 2023 to 2024 is approximately 372,725 barrels, 529,265 barrels, and 607,536 barrels for operating frequencies of 40, 50, and 60 Hz, respectively. If operated with a high-capacity pump at 60 Hz, the oil production obtained is nearly 5.5 times the natural extraction.

Similarly, for well Y-19P, the projected increase in oil production compared to natural extraction from 2023 to 2024 is approximately 342,163 barrels, 474,567 barrels, and 633,451 barrels for operating frequencies of 40, 50, and 60 Hz, respectively. If operated with a high-capacity pump at 60 Hz, the oil production obtained is nearly 7.4 times the natural extraction.

Preliminary calculations show that the method of using centrifugal submersible pumps is technically effective for wells extracting from the Limestone formation in the Y field, where the formation temperature does not exceed 130°C.

To achieve high efficiency in oil extraction using a combination of centrifugal submersible pumps, it depends on the conditions of each reservoir and each well. The selection of the appropriate type of submersible pump is crucial:

1. For wells with low production rates and unstable product flow, consider applying a combination of centrifugal submersible pumps inside the production tubing.

2. For wells with significant depth and fluid temperature, choose centrifugal submersible pumps with appropriate technical specifications.

Further research is needed on factors affecting the efficiency of oil extraction operations using centrifugal submersible pumps, such as the gas content of the extracted product, wellbore curvature, production tubing structure, etc.

REFERENCES

[1] Huỳnh Thanh Sơn – Lê Phước Hảo, "Công nghệ mỏ ứng dụng", Publishing House of Ho Chi Minh City National University, 2008.

[2] PVEP POC, "Report on simulation model of primary shale, Limestone reservoirs of Well X, lot 051, Nam Côn Sơn basin", 2018.

[3] MSc. Nguyễn Văn Tuân - Assoc. Prof. Dr. Trần Văn Xuân - MSc. Lê Ngọc Sơn - Eng. Nguyễn Văn Quế - MSc. Trương Tuấn Anh, "Application of submersible pumps for wells exploiting fractured reservoirs of Sư Tử Vàng field", 2016.

[4] Michael C.Romer et al. "Offshore ESP selection criteria: An industry study". SPE Paper 146652, SPE Deepwater Drilling and Completions Conference, Galveston, Texas, USA. 20 - 21 June 2012

MICROPLASTIC POLLUTION IN AQUEOUS ENVIRONMENT AT COASTAL AREAS IN HA LONG AND CAM PHA CITIES, QUANG NINH PROVINCE, VIET NAM

P H Son[1], T T Cuong[1], P A Hung[1], V D Tuan[1], T V Thuy[1], N H Huan[1], N X Hai[2] and P T Thuy[1*]

[1] Faculty of Environmental Sciences, University of Science, Vietnam National University, Hanoi, 334 Nguyen Trai, Hanoi, Vietnam; Email: phamthithuy@hus.edu.vn

[2] Department of Science and Technology, Ministry of Natural Resources and Environment, 10 Ton That Thuyet, Hanoi, Vietnam; E-mail: phamthithuy@hus.edu.vn

Abstract: Due to the socio-economic development, the production and consumption of non-biodegradable plastic products tend to increase rapidly, which has been causing a lot of pressure on the environment, especially in aqueous environment. Microplastic pollution is considered to have become one of the serious environmental problems and negative effects on the environment, ecology and human health. This study conducted with the current status of microplastic pollution through some characteristics, physical and chemical properties of microplastics in aqueous environment from coastal areas of Ha Long cities and Cam Pha city in Quang Ninh Province. The results of the study showed that the microplastic composition had the main component is HDPE plastic, which accounts for about 53.5% for the coastal area of Ha Long city and 34.3% for the coastal area of Cam Pha city. The origin of microplastics in the form of flakes, fibers and globules is mainly formed from the fragmentation process from plastic waste from agricultural activities such as ropes, fishing nets and from agricultural activities.

1. INTRODUCTION

Plastic waste become global issue nowadays that poses many severe impacts on ecosystems, social economics and human health. Due to their versatile properties and cheap production, the product of plastics has increased by 23% in 7 years (from 2008 to 2015) [1]. However, only 9% of plastic was recycled of all plastic produced [2]. Five type of plastic that are used most in view of their ease and convenience are (1) polyethylene terephthalate (PET), (2) low density polyeth- ylene (LDPE), (3) high-density polyethylene (HDPE), (4) polypropylene (PP), and (5) polystyrene (PS) [1, 2]. It is estimated that 10% of plastic is discharged directly into the environment and by 2025 the total amount of plastic waste will be equal to 1/3 of the total fish in the ocean [3]. The majority of plastic waste (80%) in ocean originated from land [3] and was disposed to the ocean through human activities such as tourism, fishing, and household waste. and industrial wastes [4]. In addition, natural disasters, the devastation of storms, tsunamis can also transfer plastic from land to the sea. According Jambeck et al (2015), Vietnam is the top 4th country leaking plastic waste into the ocean every year due to mismanagement of waste. The amount of unmanaged plastic waste in coastal areas is up to 1.83 million tons/year, in which, 0.28-0.73 million tons of plastic discharged into the sea, equal to 6% of the total amount of plastic discharged into the sea worldwide [2]. Currently, most wastewater treatment plants cannot remove all microplastics in wastewater [5], also discharged about 65 million microplastic particles daily into the environment [6, 7].

Plastic waste has decomposed under the influence of radiation, UV, sea water, etc., and broken down into microplastics [6]. Microplastic pollution is one of the serious environmental problems and has negative effects on the environment, ecology and human health. Microplastic can penetrate and destroy cells of organisms in freshwater and marine environments. When animals eat microplastics, they will be poisoned, and will be transferred to humans when eating. Vietnam is the fourth country in the world, behind China, Indonesia and the Philippines, in terms of plastic emissions into the ocean [2]. However, there is no assessment of microplastic sources (from cleaning products, cosmetics, laundry activities, textiles, traffic...) or the microplastics distribution in the environment (soil, water). , air) in Vietnam.

In Viet Nam, the study of Emilie et al, 2021 [17] with the monitoring of microplastic in sediments and surface waters of 21 environments (rivers, lakes, bays, beaches) of eight cities or provinces, showed that the concentration of microplastic in aquoues environment varied from 0.35 to 2522 particle/ m3, with the lowest concentrations recorded in the bays and the highest in the rivers. Fibers dominated over fragments in most environments (from 47% to 97%) [17].

Quang Ninh is a coastal province in the Northeast region of Vietnam that plays an important role in the socio-economic development strategy of the Gulf of Tonkin... Quang Ninh not only has great potential for marine tourism development, but also for the development of port traffic and fishing and aquaculture. With such advantages, marine economic development has become an outstanding advantage compared to other coastal areas in Vietnam. However, due to economic and social development, microplastic pollution is also serious problem in some coastal areas of Quang Ninh province.

Hence, this study aims to evaluate the current status of microplastic at coastal area in Ha Long and Cam Pha cities, Quang Ninh Province through the characteristics, physical and chemical properties of microplastics in aqueous environment; thereby serving as a scientific basis for further research on the microplastic generation to coastal areas.

2. MATERIAL AND METHODS

2.1. Sampling sites

To evaluate characteristics, physical and chemical properties, chemical composition, structure, morphology and mass of microplastic particles of microplastics found in aqueous environment in coastal areas in Quang Ninh province, the study conducted water sampling in coastal areas of Ha Long city and Cam Pha city where developed tourism and dense population. The location of water sampling in the coastal areas of Ha Long and Cam Pha city were shown in Table 1 and Figure 1.

Table 1. Water sampling location in the coastal areas of Ha Long and Cam Pha cities

No	No. Sampling	Coordinate		Types and sampling location
		X	Y	
1	NB1-HL	2313140	420273	Sea water sample – Coastal area in Tuan Chau island, Ha Long city

2	NB2-HL	2318200	428711	Sea water sample – Coastal area in Bai Chay ward, Ha Long city
3	NB3-HL	2315825	435997	Sea water sample – Coastal area in Hong Ha ward, Ha Long city
4	NB4-CP	2319801	449856	Sea water sample – Coastal area in Cam Binh ward, Cam Pha city
5	NB5-CP	2324062	460701	Sea water sample – Coastal area in Cua Ong ward, Cam Pha city

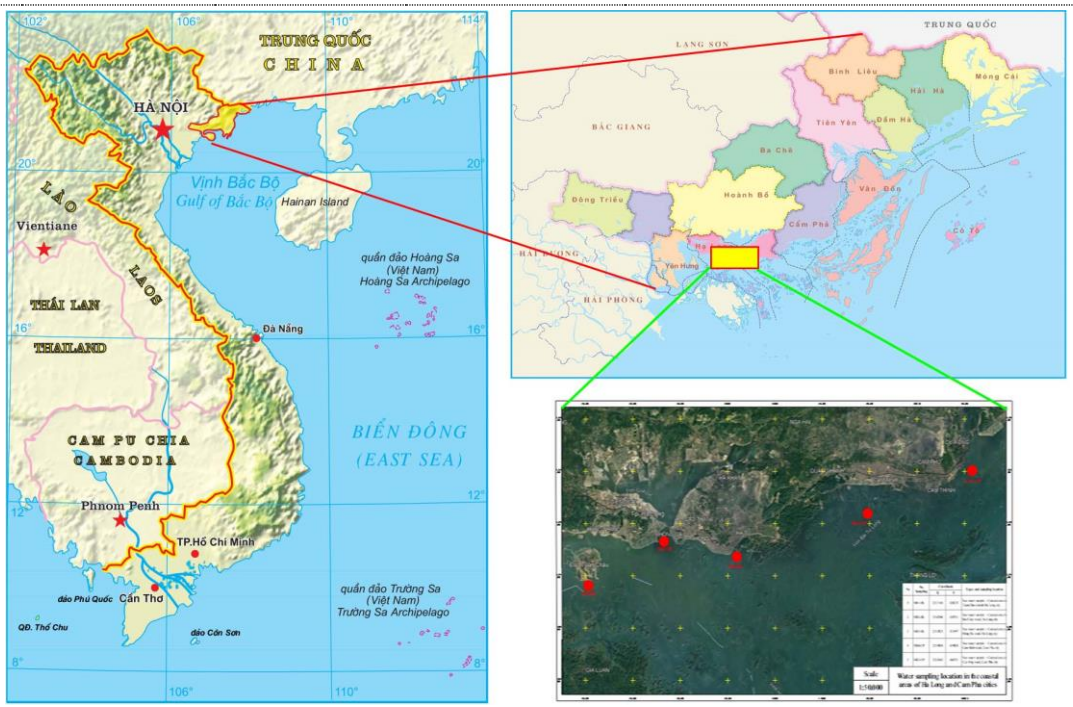


***Figure 1**. Sampling sites in the coastal areas of Ha Long and Cam Pha cities*

2.2. Methodologies

Microplastics sample in seawater were collected using a microorganism net with a mesh size of 20µm, a sampling net of 50cm×50cm, kept 50% buoyant on the surface by a buoy and a boat dragging the net. During the sailing process, a speedometer is used to measure the water flow speed. The method of analysing microplastic samples in seawater was carried out according to NOAA procedures.

This method was applied to analyse plastic debris (secondary microplastics) in the form of suspended solids in water samples. Water samples, after removing all organic matter, went to the separation step based on the density used. Using NaCl, plastic debris floated to the surface based on density. Filtration with a 100µm sieve and drying was yield microplastic fragments [8]. The blank and control samples were also analysed in each measurement for comparison.

Microplastic samples were photographed with an LCD Digital Microscope Terino HDMI-HD 1000X digital microscope, and GIMP software was used to process the images and pass through the particle size measurement step. Dimensions were measured using ImageJ software (Fiji) based on the Feret diameter method. ImageJ software is used to measure the sample according to the Feret diameter, the results obtained include the diagonal length and area of the sample.

The chemical composition of microplastic samples was determined by Fourier transform infrared spectroscopy (FTIR) using a JASCO FTIR Model 4600 with an ATR probe. Microplastic composition was determined by FTIR analysis with an ATR probe. Plastic type identification was based on comparison with standard FTIR spectra with an ATR probe in accordance with the Council of Europe (EC) Guidelines for monitoring marine waste in European waters [14].

3. RESULTS AND DISCUSSION

3.1. Microplastic concentration in sea water sample at coastal areas

The concentration of microplastics in Ha Long and Cam Pha cities ranged from 0.13 particles/m^3 to 1.07 particles/m^3. In which the average concentration of microplastic particles in the coastal area of Ha Long city ranged from 0.13 particles/m^3 to 0.69 particles/m^3. Location NB2-HL (Ha Long city) had high concentration as 3.4 - 5.4 times as location NB1-HL and NB3-HL, because NB2-HL located near the Luc gate area where is the convergence of 6 estuaries from Hoanh Bo district and some small rivers such as Dien Vong river, Troi river, Dong Giang river, etc.

The concentration of microplastic particles in Cam Pha city ranged from 0.49 particles/m^3 to 1.07 particles/m^3, location NB4-CP (Cam Pha city) has microplastic concentration was 2.2 times higher than location in Cam Pha city (location NB5-CP) and was 1.5 - 8.3 times higher than in Ha Long city. It is explained that location NB4-CP is located near the Mong Duong estuary area where polluted by mine dumps and waste disposal in Cam Pha city. The results in this study were consistent with previous research on the density of microplastics in estuaries and coastal areas in coastal areas (Quang Ninh and Hai Phong) [9].

The density of microplastics in the coastal area of Ha Long city and Cam Pha city, Quang Ninh province was only at level of microplastic and is similar to the results of Strady et al. (2020) study [10] and clearly showed the trend of microplastic pollution measured in Vietnam is within about low comparison with China, the Philippines and Indonesia (see Table 2) [11,12,13].

Table 2. Comparison of the microplastic concentration in some estuaries of coastal areas

Case study		Concentration		Reference
National	Estuary, coastal area	Value	Unit	
Indonesia	Southern coastal area in Surabaya	380 ÷ 610	particle/m^3	Cordova et al., 2019 [12]
Philippines	Macajalar bay	2.95 ÷ 33.65	g/L	Esquinas et al., 2020 [13]
China	Yangtze estuary	4137.3 ± 2461.5	particle/m^3	Zhang ey al., 2018 [14]
	Jiaojiang estuary	955.6 ± 848.7		
	Oujiang estuary	680.0 ± 284.6		

Viet Nam	Thuan An estuary, Hue	35 ÷ 175	particle/m^3	Nguyen et al., 2023 [15]
Viet Nam	Tien Giang, Can Gio và Ba Ria estuaríes - Vung Tau	0.04 ÷ 0.82	particle/m^3	Strady et al., 2020 [1]
Viet Nam	Coastal area in Ha Long city, Quang Ninh province	0.13 ÷ 0.69	particle/m^3	This study
	Coastal area in Cam Pha city, Quang Ninh province	0.49 ÷ 1.07		

3.2. Size and morphology of microplastic in coastal areas

Size:

Microplastic particles in coastal areas of Ha Long city and Cam Pha city had diameter (Feret) D50, mainly at 1mm-2mm and 2mm-3mm. For the microplastic particles sizes 1mm-2mm and 2mm-3mm, the coastal area of Ha Long city accounted for about 79.3%; the coastal area of Cam Pha city accounted for 77.7%. For the microplastic particles size < 1 mm, it accounted for the lowest proportion with 1.4% and 6.0% for the coastal areas of Ha Long city and Cam Pha city, respectively. Thus, the microplastics in Ha Long city and Cam Pha city can be assumed that secondary microplastics in these coastal area were still in the process of decomposing into smaller microplastics under the influence of radiation, UV rays, sea water, etc,. (Figure 2).

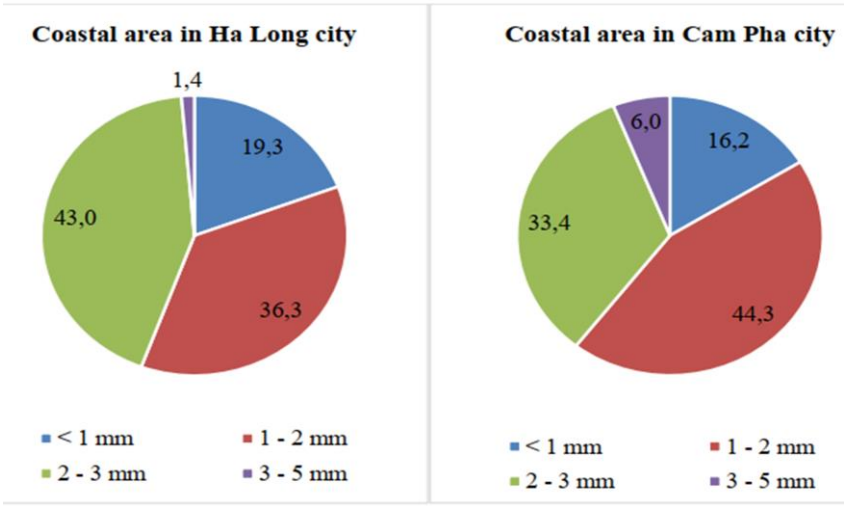


Figure 2. *Microplastic size rate (%)*

Morphology:

Microplastic particles in the coastal areas of Ha Long city and Cam Pha city had the main morphology of pieces, spheres and fibers. The number of microplastic particles with these basic shape accounts for about 92.5% for the coastal area of Ha Long city and 100% for the Cam Pha city area of the total number of samples collected. In the coastal area of Ha Long city, fibers and pieces accounted for the majority with 43.7% and 33.7% respectively; as for the coastal area of Cam Pha city, the thin and spherical shapes account for the majority at 40.4% and 34.6%. (Figure 3).

Fibers and fragments accounted for a large proportion of morphology, especially in water sample locations near coastal estuaries, suggesting that the origin of fibrous microplastics is mainly formed from the fragmentation process from waste. plastic from agricultural activities such as ropes and fishing nets and from industrial activities such as industrial fabrics, industrial cotton fibers, and decorations.

The studied areas also showed a high number of spherical microplastics which were form the source of granular microplastics mainly comes from debris from styrofoam containers,

widely used in aquaculture in the region.Thus, it can be said that signs of microplastic pollution in the coastal areas of Ha Long city and Cam Pha city mainly come from activities related to fishing, aquaculture and coastal production activities.

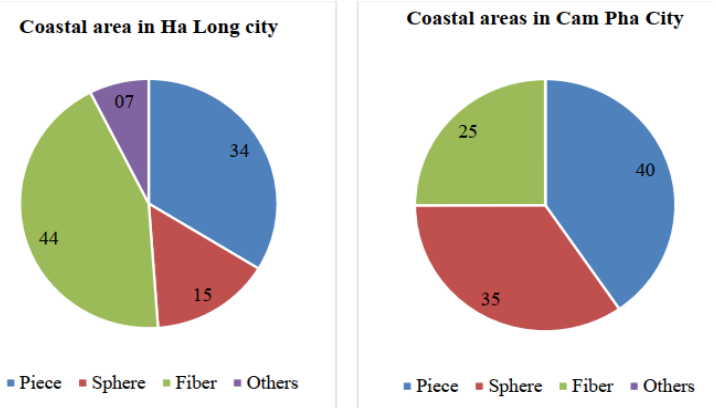


Figure 3. *Microplastic morphology rate (%)*

Color:

The color of microplastics collected in the coastal areas of Ha Long city and Cam Pha city are very diverse, including colors such as green, blue, red, black, white... (Figure 4, Figure 5). However, the majority of color was white or transparent with a rate of 41.8% in the coastal area of Ha Long city and 53.1% in the coastal area of Cam Pha city. It was due to most of the plastic waste is of white origin such as styrofoam, plastic bags, canned and plastic bottles. Besides, plastic pieces last a long time in the seawater environment, gradually decomposing into small pieces and fading over time to their original color, gradually becoming milky white, ivory white or transparent.

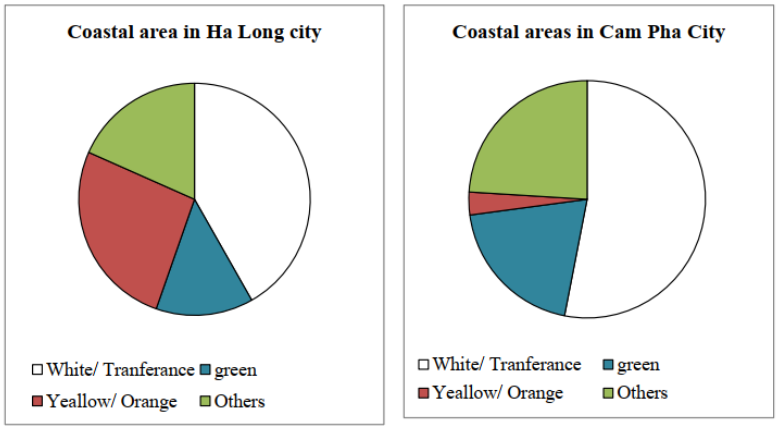


Figure 4. *Microplastic color rate (%)*

Blue color accounted for a relatively large proportion of samples collected in the study area, with 13.6% in the coastal area of Ha Long city and 19.8% in the Cam Pha city area. This was the color commonly found in fishing lines or fishing and aquaculture tools. Yellow also accounted for a relatively large proportion in samples collected in the coastal area of Ha Long city with 26.3%. The xxisting in an alluvial environment (typical of the Quang Ninh area) made this plastic adhered to the surface, causing the microplastic particles to have this color.

In addition, although not in the main quantity, the existence of other colors also shows the diversity of plastic types that exist in the coastal areas of Ha Long city and Cam Pha city such as types of plastic bags, packaging, food containers, bottles, fishing and aquaculture tools, etc.

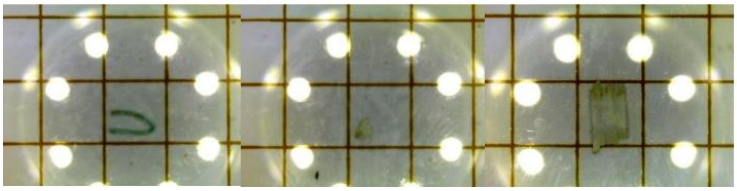


Figure 5. *Color and size of microplastic particles in studied area through a digital microscope LCD Digital Microscope*

3.3. Microplastic composition

Microplastic composition in samples collected in the coastal areas of Ha Long city and Cam Pha city were shown in Figure 6 and Figure 7. The main component of microplastic samples was HDPE plastic, accounting for about 53.5% in coastal area of Ha Long city and 34.3% in coastal area of Cam Pha city. PS, PET, LDPE, PP plastics had lower proportions and were quite similar in the collected samples, fluctuating between 6.0% and 10.6% for the coastal areas of Ha Long city and 10 .2% to 15.5% for the coastal area of Cam Pha city.

HDPE plastic was widely used in the packaging industry of products and consumer goods, and especially due to its high tensile strength, HDPE is widely used for agricultural applications, such as ropes and fishing nets. and sports, mesh as well as industrial and decorative fabrics. HDPE plastic is also recyclable, so it is suitable for multiple uses.

PS plastic is also one of the most commonly used plastics today due to its low price, convenience, short usage time, and quick disposal with diverse applications such as making food containers, plastic cups, single-use plastic eating utensils.

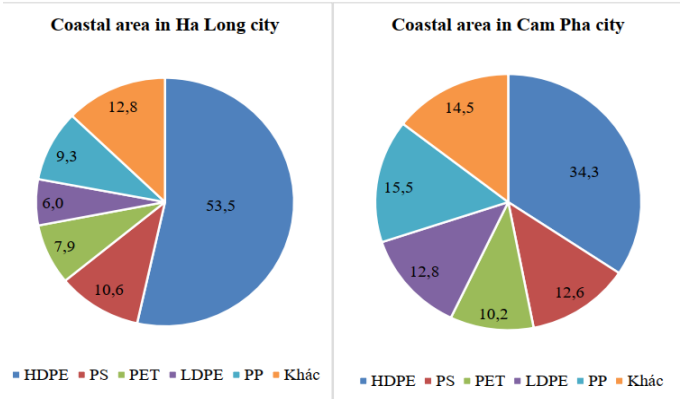
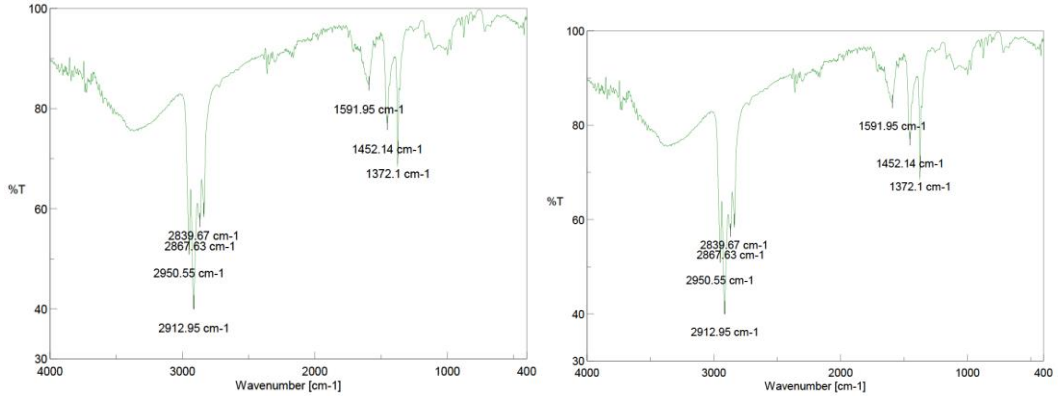


Figure 6. *Microplastic compostion (%)*



a) *b)*

Figure 7. *FTIR of studied area a) HDPE, b) PP*

4. CONCLUSION

The microplastic concentrations in the coastal areas of Ha Long and Cam Pha cities had shown appearance of microplastic pollution. The average concentration of microplastics in the coastal area of Ha Long city ranges from 0.13 particles/m^3 to 0.69 particles/m^3, and in the coastal area of Cam Pha city ranges from 0.49 particles/m^3 to 1 .07 grains/m^3. In coastal seawater samples near estuaries, the concentration of microplastics is 3.4 - 5.4 times higher (Ha Long), 1.5 - 8.3 times (Cam Pha) compared to other locations.

Microplastic particles in the study area with diameter (Feret) D50 at 1mm-2mm and 2mm-3mm predominate with about 79.3% and 77.7% in samples collected respectively in the coastal area of the city. Ha Long and Cam Pha cities.

The morphology of microplastics in water samples is mainly in the form of flakes, fibers and spheres, accounting for 92.5% for the coastal area of Ha Long city and 100% for the Cam Pha city area in the research samples. The color of microplastic particles, white or transparent, accounts for the majority with 41.8% and 53.1% in the coastal areas of Ha Long city and Cam Pha city, respectively.

The microplastic composition had the main component is HDPE plastic. In which HDPE accounts for about 53.5% for the coastal area of Ha Long city and 34.3% for the coastal area of Cam Pha city. HDPE accounts for a large proportion, suggesting that the origin of microplastics in the form of flakes, fibers and globules is mainly formed from the fragmentation process from plastic waste from agricultural activities such as ropes, fishing nets and from agricultural activities. Industrial activities such as industrial fabrics, industrial cotton yarn, and decoration.

REFERENCES

[1] PlasticsEurope 2018 Annual Review 2017–2018. Retrieved from: https://issuu.com/plasticseuropeebook/docs/annualreport2018_plasticseurope_web.

[2] Geyer R, Jambeck J R, Law K L 2017 Production, use, and fate of all plastics ever made. Sci Adv 3:e1700782. https://doi.org/10.1126/ sciadv.1700782 .

[3] Jambeck J R, Geyer R, Wilcox C, Siegler T R, Perryman M, Andrady A, Narayan R, Law K L, 2015. Plastic waste inputs from land into the ocean. *Science* 347, 768–771. https://doi.org/10.1126/science.1260352.

[4] Thompson R C 2016, Plastic debris in the marine environment: consequences and solutions, *Mar. Nat. Conserv. Eur,* 193, pp.107-115.

[5]WHO 2020 Shortage of personal protective equipment endangering health workers worldwide, World Healthy Organization, [Online]. Available: https://www.who.int/news/item/03-03-2020-shortage-of-personal-protective.

[6]Anderson J C, Park B J, Palace V P 2016 Microplastics in aquatic environments: implications for Canadian ecosystems. *Environ. Pollution* 218, 269-280.

[7] Auta H S, Emenike C U, Fauziah S H 2017 Distribution and importance of microplastics in the marine environment a review of the sources, fate, effects and potential solutions. *Environ. Inter.*, 102, 165-176.

[8] Waller C L, Griffiths H J, Waluda C M, Thorpe S E, Loaiza I, Moreno B, Pacherres C O, Hughes K A 2017 Microplastics in the Antartic marine sustem: An emerging area of research. *Sci. Total Environ.*, 598, 220-227.

[9] Masura J, et al. 2015. Laboratory methods for the analysis of microplastics in the marine environment: recommendations for quantifying synthetic particles in waters and sediments. National Oceanic and Atmospheric Administration (NOAA)- Technical Memorandum NOS-OR&R-48.

[10] Institute of Strategy and Policy on Natural Resources and Environment, 2021. Microplastic pollution: Case studies in Vietnam and international experiences. Transportation publishing.

[11] Strady E, Dang T H, Dao T D, Dinh H N, Do T T D, Duong T N, Duong T T, Hoang D A, Kieu-Le T C, Le T Q, Mai H, Trinh D M, Nguyen QH, Tran-Nguyen Q A, Tran Q V, Truong T N S, Chu V H, Vo V C, 2020a. Baseline assessment of microplastic concentrations in marine and freshwater environments of a developing Southeast Asian country, Viet Nam. *Marine Pollution Bulletin* Vol 162, January, 2021. 111870. https://doi.org/10.1016/j.marpolbul.2020.111870) .

[12] Cordova M R, Purwiyanto A I S, Suteja Y 2019. Abundance and characteristics of microplastics in the northern coastal waters of Surabaya, Indonesia. *Marine Pollution Bulletin* 142, 183–188.

[13] Esquinas G G M S, Mantala, A P, Atilano M G, Apugan R P, Galarpe V R K R 2020. Physical characterization of litter and microplastic along the urban coast of Cagayan de Oro in Macajalar Bay, Philippines. Marine Pollution Bulletin 154, 111083. https://doi.org/10.1016/j.marpolbul.2020.111083.

[14] Zhang K, Shi H, Peng J, Wang Y, Xiong, X, Wu C, Lam P K S 2018. Microplastic pollution in China's inland water systems: A review of findings, methods, characteristics, effects, and management. *Sci. Total Environ.*, 630, 1641–1653.

[15] European Commission (EC), 2013, Guidance on Monitoring of Marine Litter in European Seas, doi:10.2788/99475.

[16] Nguyen H N Y, Truong T N H, Phan T T L, Vo V M, Le T M, Trinh D M, Tran NQ A (2023), Distribution of microplastics in surface water and sediment in Thuan An estuary, Thua Thien Hue, Journal of Science and Technology - University of Danang, ISSN 1859-1531, Vol 21, No.3, 2023.

[17]Emilie S, Thi Ha D, Dao T , Dinh H N, Do T T D, Duong T N, Duong T T, Hoang, Le KT C, Le T P Q, Dang H M, Nguyen Q H, Nguyen T Q A, Tran Q V, Truong T N S, Chu V H, Vo V C, 2021, Baseline assessment of microplastic concentrations in marine and freshwater environments of a developing Southeast Asian country, Viet Nam, Marine Pollution Bulletin, 162, 111870.

MONITORING LAND SURFACE TEMPERATURE BY INTEGRATING LANDSAT 8 AND SENTINEL 2 IN DAU TIENG DISTRICT, BINH DUONG PROVINCE

Phuong Ha Tran[1], Tuan Cuong Ha[2], Thi Thuy Huong Nguyen[3], Ngoc Thy Nguyen[4], Duong Ba Man[5], Tuan Nhi Pham[5]

[1]Institute of Applied Mechanics and Informatics, Vietnam Academy of Science and Technology (VAST)

[2]Southern Sub-Institute of Forest Inventory and Planning

[3]Institute of biotechnology, Vietnam Academy Science & Technology (VAST)

[4]Nong Lam University

[5]Ho Chi Minh City Institute of Resources Geography, Vietnam Academy of Science and Technology (VAST)

* Corresponding author: phuonghatran76@yahoo.com, tuancuongdialyk38@gmail.com

Abstract: Dau Tieng district has the largest forest area in Binh Duong province, with a natural forest area of over 3,000 hectares along with a widely distributed rubber forest area. However, the process of urbanization and population growth in Dau Tieng district has caused the decrease in vegetation cover, causing significant change in land surface temperature (LST) and related to changes in local climate. Nowadays, remote sensing technology is increasingly developed and has many applications in many fields, especially in resource management and environment. In this article, we combined Landsat 8 and Sentinel 2 images to enhance the spatial resolution of LST, the method combines Landsat and Sentinel 2 images to calculate LST based on NDVI values and surface emissivity of Sentinel 2 images to extract temperature. From 2016 to 2022, the results showed that the high temperature above 30^0C was concentrated in the urban residential area of Dau Tieng town, An Lap commune, Thanh An commune, etc. and low temperatures were concentrated in areas with the vegetation cover and the water surface. The research results are a basis for planning green spaces and mitigating the impact of urban heat islands in residential areas.

Keywords: *Land surface temperature (LST), Landsat 8, Sentinel 2, Dau Tieng district*

1. INTRODUCTION

The urbanization process is a driving force for socio-economic development, population growth, and environmental change. Urbanization changes agricultural land, vegetation, and water surface to built-up land [1]. Replacement of vegetation by asphalt and concrete for the construction of roads, and buildings leads to the formation of Urban heat islands [2] Establishing land use land cover (LULC) maps is a necessity in monitoring changes in land use cover and the impact of this change on the environment, especially land surface temperature (LST) monitoring [3, 4]. Therefore, in urban areas, studying changes in land surface cover objects is essential in monitoring local climate change, as well as global climate, in which LST plays an important role in urban environments, as well as hydrological, geo-biophysical, and LULC studies [5].

The temperature difference between these two areas could fluctuate from 3 – 6^oC, sometimes up to 11 - 12^oC [6]. The appearance of erratic high-temperature values compared

to the surrounding temperature, forms the urban heat island (UHI) effect, due to impervious surfaces (residential areas, concrete roads) [7]. With the advent of satellites and aircraft, thermal infrared remote sensing has provided new developments for LST as well as UHI research. Nowadays, there are many image datasets used to calculate LST, for example, the medium spatial resolution data from Landsat or MODIS images that are. In particular, the Landsat 8 image has a TIRS sensor with the thermal infrared band used to calculate LST. However, the spatial resolution of thermal infrared (TIR) is relatively low. This is a relatively coarse spatial resolution of TIR datasets; typically, the ground sampling distance of Earth observation TIR sensors ranges from 1000 m (Meteosat, AVHRR, MODIS) to 100 m (Sentinel-3, ASTER, Landsat 8 and 9 TIRS) [8]. Higher spatial resolution of thermal sensing is needed to resolve urban features (streets, roads, buildings) to study microclimate and human comfort in urban areas [9]. This constraint has been addressed by sharpening the TIR satellite imagery to a higher spatial resolution. These sharpening techniques are often termed as downscaling or disaggregation methods in previous publications [8]. Sentinel 2 (S2) image material is one of the most popular solutions for enhancing the resolution of LST values, for example: Sánchez et *al*,. (2020) [10] used S2 data to downscale MODIS data of 1000 m resolution to 10 m resolution, Pu and Bonafoni (2021) [11] argue that the difference between the downscaled LST and LST measured at the same (high) resolution is scale-dependent, i.e., subject to a scaling effect.

Based on data from Landsat 8 satellite images, this article calculated the LST value for Dau Tieng district in the period 2015 - 2022. Because Landsat satellite images have medium resolution (30x30m), so we combined Sentinel 2 images with high resolution (10x10m) to improve accuracy when calculating LST values. From there, this article made an overall assessment of the LST change over each year in the study area, serving as a basis for the arrangement of green space in Dau Tieng, urban planning,...

2. STUDY AREA

Dau Tieng is a Northern district of Binh Duong province, about 50 km from the administrative center of Binh Duong province. The North borders Binh Long district (Binh Phuoc province), the East and Southeast border Ben Cat town (Binh Duong province), the Northwest and Southwest border Duong Minh Chau district (Tay Ninh province), the South borders Cu Chi district (Ho Chi Minh City). With more than 3,000 ha of natural forest, Dau Tieng district is considered as a green lung to regulate the climate for Binh Duong. At the same time, this forest prevents erosion of Dau Tieng lake bed, and protects Dau Tieng dam containing over 1.5 billion m³ of water to provide fresh water for irrigation for the entire Southeast region.

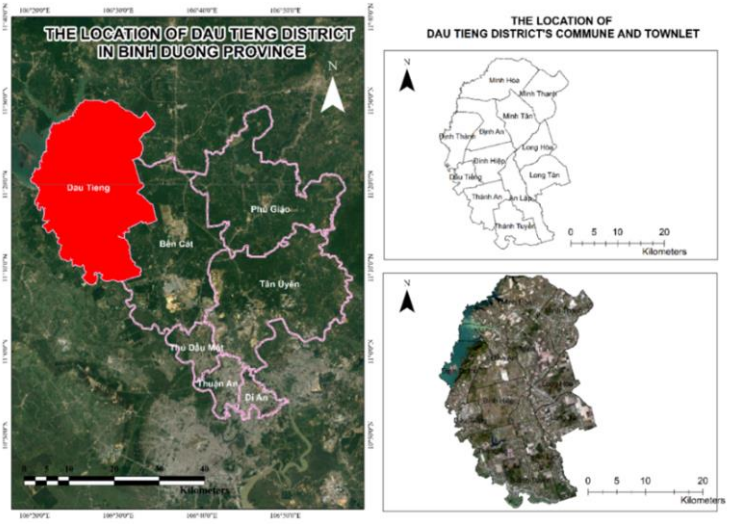


Figure 1. *The location of Dau Tieng district.*

Dau Tieng is a district that has just escaped poverty in a few years and is developing into a new rural district and a green urban area in the period 2021 - 2025. In the process of urban planning and construction, the District People's Committee orients the construction of Dau Tieng district in the direction of a sustainable model, with a synchronous, modern, environmentally friendly technical infrastructure system. All of these will become the driving force for economic restructuring. The economic strength of Dau Tieng district is agriculture. The agricultural economy is dominated by the rubber crop, with accounts for over 87% of the natural land area. The perennial cropland accounts for over 90% of the agricultural land area [12]. Therefore, Dau Tieng also determined a plan to develop a high-tech agricultural economy associated with eco-tourism.

3. DATA AND METHOD

3.1. Data source

This study collected two Earth observation missions, the Landsat mission by NAS and the Sentinel mission by ESA. Landsat's OLI sensor with multi-spectral bands was used to calculate the NDVI index (from band 4 and 5). TIRS sensors with band 10 and 11 were used to calculate the LST value. Landsat 8 was obtained from the USGS website (https://earthexplorer.usgs.gov). All the Landsat images were focus on cloud cover of less 10%, and images data acquired in the dry season for 2016, 2020 and 2022. We should collect Landsat images in the cloud-free environment, to create LST. These Landsat images had stable and clear weather conditions without geometric and atmospheric.

Besides, Sentinel 2 satellite images were chosen to be taken close in time to each other to minimize the influence of changes in emissivity on the surface temperature calculation results [13], and were brought to the UTM coordinate system zone 48 of the Northern Hemisphere. Sentinel 2A was collected from the website (https://apps.sentinel-hub.com/). Because the Sentinel 2 images were launched in June 2015, we could not use images from the rainy season and early dry season of 2015 while the remaining images were collected in February.

Table 1. The information of the satellite images.

Year	Scene ID	Date	Cloud cover
Landsat 8 OLI/TIS	LC08_L1TP_125052_20160228_20160228_02_T1	28/02/2016	2.1%
	LC08_L1TP_125052_20200207_20200823_02_T1	07/02/2020	2.03%
	LC08_L1TP_125052_20220204_20230429_02_T1	04/02/2022	1.3%
Sentinel 2 MSI	2016-02-06-00_00_2016-02-06-23_59_Sentinel-2	06/02/2016	< 10%
	2020-02-20-00_00_2020-02-20-23_59_Sentinel-2	20/02/2020	
	2022-02-11-00_00_2022-02-14-23_59_Sentinel 2	14/02/2022	

Therefore, we collectred images during the period 2016 - 2022 to calculate LST values. On the other hand, collecting these images at this time did not make too much difference in land cover area, because most of the land cover in Dau Tieng district is rubber trees. The first months of the year are when rubber trees change leaves and have not yet had much latex exploited, so when viewed on satellite images, the density of rubber tree cover is very large. The details of time and scene ID were shown in Table 1.

3.2. Calculating LST value from Landsat 8

3.2.1. Enhanced resolution for thermal band (band 10)

Because the resolution of the 2 thermal bands (bands 10 and 11) is 100m, when calculating the next steps with the image channels related to the NDVI index of 30m resolution, it is necessary to synchronize the resolution of the image bands in this study. We used the Resample command in ArcGIS software to increase the resolution of band 10 from 100m to 30m. The Resample command changes the cell size of a raster and can be applied to individual images, raster datasets, and mosaics.

3.2.3. Convert digital number (DN) to Radiance

There are 2 methods of converting DN to TOA: The first method is to convert the DNs to spectral radiance using bias and gain values that it can be acquired from the header file of the images. The other longer method uses L_{Min} and L_{Max} spectral radiance scaling factors [14]. The spectral radiance energy value was calculated according to the formula [15]:

$$L_\lambda = \frac{(L_{MAX\lambda} - L_{MIN\lambda})}{Q_{CALMAX} - QCALMIN} \times (Q_{CAL} - Q_{CALMIN}) + L_{MIN\lambda} \quad (1)$$

Where:

$L_{MAX\lambda}$: is the maximum radiance (Watts/(m^2.srad.µm));

$L_{MIN\lambda}$: is the minimum radiance (Watts/(m^2.srad.µm));

Q_{CAL}: is the DN value of pixel (DN);

Q_{CALMIN}: is the minimum DN value of pixels (MIN);

Q_{CALMAX}: is the maximum DN value of pixels (MAX).

3.2.3. Conversion to brightness temperature (B_T)

The purpose of this step is to convert radiance into degrees Kelvin (0K): From TOA was calculated by the formula in (1), we used the K1 and K2 which was stored at metadata file. The equation for calculating the brightness temperature for Landsat OLI/TIRS [16, 17]:

$$B_T = \frac{K_2}{ln\left(\frac{K_1}{L_\lambda} + 1\right)} \quad (2)$$

Where:

B_T – brightness temperature (^{0}K);

K - thermal constants (W/(m^2.sr.µm) and K), found in METADATA file.

3.2.4. Normalized Difference Vegetation Index (NDVI) and Proportional vegetation (Pv)

NDVI is essential to identify different land cover types of the study area. NDVI ranges between -1.0 to +1.0. NDVI is calculated based on the red band and near - infrared band [18, 19]:

$$NDVI = \frac{NIR - RED}{NIR + RED} \quad (3)$$

Calculation of NDVI was necessary to further calculate proportional vegetation (Pv) and emissivity (ε). Proportion of vegetation (Pv): is defined as the percentage of vegetation occupying the ground area in vertical projection [20]. Changes in vegetation cover directly impact surface water and energy budgets through plant transpiration, surface albedo,

emissivity, and roughness [21]. Pv has a value of 0 for bare land and 1 for bare land with the area covered with vegetation.:

The formula was calculated as follows [22]:

$$Pv = (\frac{NDVI-NDVImin}{NDVImax-NDVImin})^2 \quad (4)$$

3.2.5. Land Surface Emissivity (LSE) calculation

Valor and Caselles [23] proposed a theoretical model that relates the emissivity to the NDVI of a given surface by:

$$\varepsilon = \varepsilon_v Pv + \varepsilon_s (1-Pv) + 4\langle d\varepsilon \rangle Pv (1- Pv) \quad (5)$$

Where: ε_v and ε_s represent the emissivity of vegetation and soil;

d_ε is a term accounting for the cavity effect, which depends on the surface geometry.

As Valor and Caselles [23] suggested, ε_v and ε_s as 0.985 and 0.960, respectively, for unknown emissivity and vegetation structures. Besides, they calculated the mean value for d_ε term as 0.015. The final equation of the LSE model can be given by:

$$LSE = 0.985 \times Pv + 0.960 \times (1 - Pv) + 0.06 \times Pv \times (1 - Pv) \quad (6)$$

3.2.6. Calculate LST in Celsius (^oC)

The actual surface temperature (TC) was calculated by the formula [24]:

$$\boldsymbol{LST} = \frac{BT}{\varepsilon^{\frac{1}{4}}} - 273,1 \quad (6)$$

3.3. Integrate Sentinel 2 images to improve LST calculation values

The combined of Landsat 8 and Sentinel 2 images allowed for increasing the spatial resolution of LST from 30m (if using only Landsat 8 images) to 10m (using a combination of Landsat 8 and Sentinel 2 images) without significantly affecting the accuracy of the results received. The LST value according to Sentinel 2 images was calculated like formula (7).

3.3.1. Calculating NDVI index in Sentinel 2

NDVI is a standard algorithm designed to estimate the quality of terrestrial green vegetation by measuring reflectance at red and near-infrared wavelengths. To calculate the NDVI index, apply the following formula:

$$NDVI = \frac{Band\ 8 - Band\ 4}{Band\ 8 - Band\ 4} \quad (7)$$

3.3.2. Calculating surface emissivity (ε) for Sentinel 2

Sobrino et al. [25], Skoković et al. [26], Yu et al. [27], Li and Jiang [28] estimated LSE from NDVI threshold values considering three different cases as presented in equation (8).

$$\varepsilon_\lambda = \varepsilon_{v\lambda} P_v + \varepsilon_{s\lambda} (1 - P_v) + C_\lambda , \quad (8)$$

Where: ε_v and ε_s are the vegetation and soil emissivities, respectively,

C represents the surface roughness (C = 0 for homogenous and flat surfaces) taken as a constant value of 0.005 [29].

The condition can be represented with the following formula and the emissivity constant values shown [30]

$$\varepsilon_\lambda = \begin{cases} \varepsilon_{s\lambda}, & \text{NDVI} < \text{NDVI}_s, \\ \varepsilon_{v\lambda} P_v + \varepsilon_{s\lambda}(1 - P_v) + C, & \text{NDVI}_s \le \text{NDVI} \le \text{NDVI}_v \\ \varepsilon_{s\lambda} + C, & \text{NDVI} < \text{NDVI}_v, \end{cases} \quad (9)$$

When the NDVI is less than 0, it is classified as water, and the emissivity value of 0.991 is assigned. For NDVI values between 0 and 0.2, it is considered that the land is covered with soil, and the emissivity value of 0.996 is assigned. Values between 0.2 and 0.5 are considered mixtures of soil and vegetation cover and [31] is applied to retrieve the emissivity. In the last case, when the NDVI value is greater than 0.5, it is considered to be covered with vegetation, and the value of 0.973 is assigned. However for this study the mean NDVI value is between 0 and 0.2 therefore the emissivity value of 0.996 was assigned.

2.3.3. LST value according to Sentinel 2

The actual surface temperature (T_C) for sentinel 2 was calculated by this formula:

$$LST_{sentinel\ 2} = (BT_{Landsat\ 8} / \boldsymbol{\varepsilon\ sentinel}^{\frac{1}{4}}) - 273.1 \quad (10)$$

4. RESULTS

4.1. LST calculation results from Landsat 8 image and combined Sentinel 2 image

The comparison between the calculation results of Landsat 8 images itself and Landsat 8 (L8) images combined with Sentinel 2A (S2) in this study only focuses on the difference in values such as LST max, LST min and LST mean. There was no significant difference in the LST results. Thus, it is possible to combine the use of multi-resolution remote sensing image data Landsat 8 and Sentinel 2 to improve the efficiency in extracting information about the Earth's surface temperature.

Table 4. Comparing some LST (^{0}C) statistical parameters.

Parameter	2016		2020		2022	
	L8	L8 & S2	L8	L8 & S2	L8	L8 & S2
Max	36.59	36.54	36.58	36.55	34.59	34.55
Min	18.45	18.85	24.14	24.21	22.38	22.38
Mean	26.68	26.67	28.76	28.76	26.92	26.92

The results confirm that even the use of resolved surface properties, such as spectral indices from S2 in 10m resolution, to derive LST cannot improve the original L8 satellite's capability to resolve some thermal details [26]. Nevertheless, the custom downscaling procedure provided an additional value by improving the spatial resolution with respect to the L8 image and other regressive downscaling techniques.

The spatial distribution of LST values was shown in these following figure 1 and figure 2.

Locations with high temperatures correspond to built-up land, roads and bare land, whereas areas with water surface and vegetation cover (rubber forests, natural forests,...) were low LST value, usually below 26^{0}C.

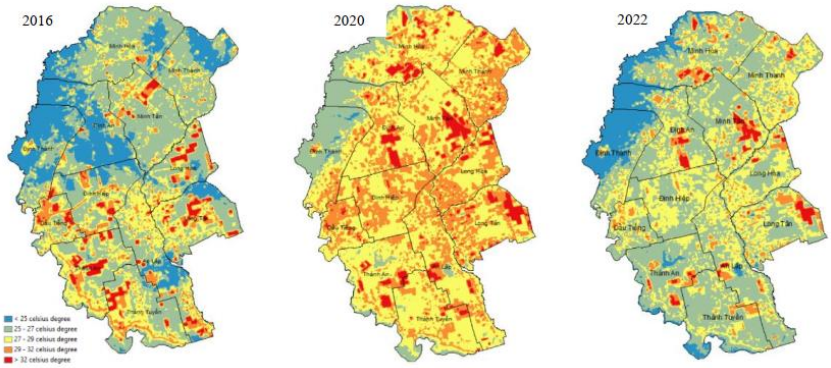


Figure 1. *The changes in LST of Ho Chi Minh City in the period 2016 – 2020 based on L8*

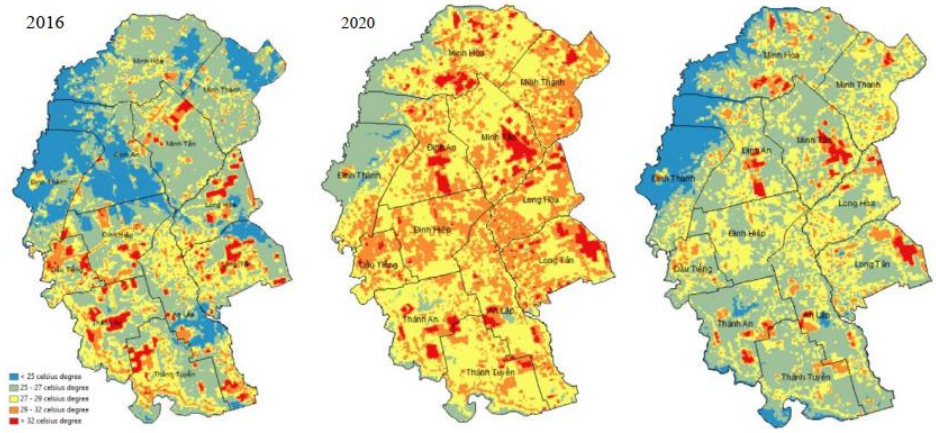


Figure 2. *The changes in LST of Ho Chi Minh City in the period 2016 – 2020 based on L8 which combine S2*

4.2. Spatial distribution of LST and statistics

The maximum value was always above 29^0C, distributed on main traffic routes such as DT744, DT748. DT750, resident areas, and in bare land areas after rubber tree exploitation. The max value always depends on the rubber tree cover in Dau Tieng district.

Table 5. The changes in LST area for Dau Tieng district in 2015, 2020 and 2022

LST range (^{0}C)	Area (ha)					
	2016		2020		2022	
	L8	S2 & L8	L8	S2 & L8	L8	S2 & L8
< 25^0C	141,48	145,08	114,57	115,11	505,26	501,21
25 - 27^0C	1.414,80	1.426,59	7.354,62	7.287,84	2.651,23	2.621,16
27 – 29^0C	5.943,87	5.918,85	37.923,39	37.868,76	1.736,47	1.738,44
29 – 32^0C	16.507,44	16.403,94	22.994,37	22.856,13	388,53	384,93
> 32^0C	14.849,28	14.799,42	3.781,98	3.735,72	104,7	103,86

The minimum value tended to expand in value, due to the decrease of forest land (mainly in rubber tree land), along with the appearance of impervious surfaces, the minimum LST value in 2016 was about 18^0C and in 2022 was 19^0C. The study area was categorized into

five LST zones to explain further LST distribution (below 25^0C, 25 – 27^0C, 27 – 29^0C, 29 – 32^0C, > 32^0C). LST distribution pattern over the study area was demonstrated in Table 4.

The temperature threshold below 25^0C coincided with the distribution of water surface and rubber forests in the mature stage. The area of these two thresholds was shrinking each year.

However, the threshold value below 25^0C – 27^0C, representing forests and agricultural land, generally tended to decrease in area. The temperature threshold of 27 – 29^0C corresponded to bare land after exploiting rubber trees. This temperature threshold always fluctuates because it depends on the time to acquire satellite images. Threshold values above 32^0C represent built-up land, however, it is necessary to clearly determine which is land for rubber trees and which is impervious surfaces.

5. CONCLUSION

With free image resources, Landsat and Sentinel 2 images effectively support the assessment of land surface temperature changes in Dau Tieng district in the period 2016 - 2022. With the formation and expansion of traffic routes from the south of Dau Tieng district to the East and the East along with the formation of residential areas in Binh Phuoc province, it has created a driving force to attract population concentrated in the areas. this area. Because of that, the LST value increased to the threshold value, causing many maximum values to appear. LST results from Landsat images and Landsat images combined with Sentinel 2 were no too much different. The results obtained in the study can be used for the assessment and monitoring of land surface temperature changes, early detection of temperature abnormalities as well as providing input information for meteorological, climate models.

ACKNOWLEDGMENT

This research was financially supported by the VAST under the code CSCL14.01/23-24.

REFERENCES

[1] H. Ding and W. Si 2013 Land-use/land-cover change and its influence on surface temperature: a case study in Beijing City *International Journal of Remote Sensing*, **34**(15), 5503– 5517

[2] Valsson, S. and Bharat, A 2009 Urban Heat Island: Cause for Microclimate Variations *Architecture - Time Space & People*, **2125.**

[3] W. Chen, Y. Zhang, W. Gao, and D. Zhou 2016 The Investigation of Urbanization and Urban Heat Island in Beijing Based on Remote Sensing *Procedia - Social and Behavioral Sciences*, **216**, 141–150.

[4] R. C. Estoque and Y. Murayama 2017 Monitoring surface urban heat island formation in a tropical mountain city using Landsat data (1987–2015) *ISPRS Journal of Photogrammetry and Remote Sensing*, **133**, 18–29.

[5] Zhang, W., Zhu, Y., & Jiang, J 2016 Effect of the Urbanization of Wetlands on Microclimate: A Case Study of Xixi Wetland, Hangzhou, China *Sustainability*, **8**(9), 85.https://doi.org/10.3390/su8090885.

[6] Thi Van T and Duong Xuan Bao H 2010 Study of the Impact of Urban Development on Surface Temperature Using Remote Sensing in Ho Chi Minh City. *Southern Vietnam Geographical Research* **48** 86–96

[7] T C Ha and T P C Nguyen 2023 Application of Multi-Temporal Landsat Images to Analyze the Relationship Between the Land Surface Temperature (LST) and the Land Use Land Cover (LULC) in Ho Chi Minh City *IOP Conf. Ser.: Earth Environ. Sci.* **1170** 012017

[8] Becker F, Li Z 1995 Surface temperature and emissivity at various scales: Definition, measurement and related problems. *Remote Sens. Rev.* 1995, **12**, 225–253.

[9] Onačillová K, Gallay M, Paluba D, Péliová A, Tokarčík O, Laubertová D 2022 Combining Landsat 8 and Sentinel-2 Data in Google Earth Engine to Derive Higher Resolution Land Surface Temperature Maps in Urban Environment. *Remote Sensing* **14**(16):4076.

[10] Sánchez J M, Galve J M, González Piqueras J, López Urrean R, Niclòs R, Calera A 2020 Monitoring 10-m LST from the Combination MODIS/Sentinel-2, Validation in a High Contrast Semi-Arid Agroecosystem. *Remote Sens.* **12**, 1453.

[11] Pu R, Bonafoni S 2021 Reducing Scaling Effect on Downscaled Land Surface Temperature Maps in Heterogeneous Urban Environments. *Remote Sens.* **13**, 5044.

[12] Nguyen Huynh Anh Tuyet et al 2017 Assessing the variation of the dry season's surface temperature in Binh Duong province from 2002 – 2016 by applying thermal remote sensing *Vietnam Journal of Science and Technology*, **55**(4C), 136-141.

[13] Obregón, M.A., Rodrigues, G., Costa, M.J. 2019 Validation of ESA Sentinel-2 L2A aerosol optical thickness and columnar water vapour during 2017-2018. *Remote Sensing* **11**(14), 1649.

[14] Fathian F, A Prasad, Z Dehghan, and S Eslamian 2015 Influence of land use/land cover change on land surface temperature using RS and GIS techniques *Int J Hydrol Sci Tech*. **5**(3): p. 195-207.

[15] Chander, G.; Markham, B.L.; Helder, D.L 2009 Summary of current radiometric calibration coefficients for landsat MSS, TM, ETM+, and EO-1 ALI sensors *Remote Sens. Environ* **113** 893–903.

[16] Mishra, N.; Haque, M.O.; Leigh, L.; Aaron, D.; Helder, D.; Markham, B., 2014. Radiometric cross calibration of Landsat 8 operational land imager (OLI) and Landsat 7 enhanced thematic mapper plus (ETM plus) *Remote Sens*. **6** 12619–12638.

[17] Tran T V, Reef R and Zhu X 2022 A Review of Spectral Indices for Mangrove *Remote Sensing Remote Sensing* **14** 4868.

[18] Zha Y, Gao J and Ni S 2003 Use of normalized difference built-up index in automatically mapping urban areas from TM imagery *International Journal of Remote Sensing* **24** 583–94.

[19] Twumasi, Y.A., Merem, E.C., Namwamba, J.B., Mwakimi, O.S., Ayala-Silva, T., Frimpong, D.B., Ning, Z.H., Asare-Ansah, A.B., Annan, J.B., Oppong, J., Loh, P.M., Owusu, F., Jeruto, V., Petja, B.M., Okwemba, R., McClendon-Peralta, J., Akinrinwoye, C.O. and Mosby, H.J. 2021 Estimation of Land Surface Temperature from Landsat-8 OLI Thermal Infrared Satellite Data. A Comparative Analysis of Two Cities in Ghana *Advances in Remote Sensing* **10** 131-149. https://doi.org/10.4236/ars.2021.104009.

[20] Aman, A., Randriamanantena, H.P., Podaire, A. and Froutin, R 1992 Upscale Integration of Normalized Difference Vegetation Index: The Problem of Spatial Heterogeneity *IEEE Transactions on Geoscience and Remote Sensing* **30** 326-338. https://doi.org/10.1109/36.134082.

[21] Xu Y & Shen Y 2013 Reconstruction of the land surface temperature time series using harmonic analysis. *Computers & Geosciences* **61** 126-132. https://doi.org/10.1016/j.cageo.2013.08.009.

[22] Valor, E.; Caselles, V. 1996 Mapping land surface emissivity from NDVI: Application to European, African, and South American areas *Remote Sens. Environ*. **57** 167–184.

[23] Van de Griend, A.A.; Owe, M. On the relationship between thermal emissivity and the normalized difference vegetation index for natural surfaces *Int. J. Remote Sens.* **14** 1119-1131.

[24] Mallick J, Kant Y, Bharath B.D 2008 Estimation of land surface temperature over Delhi using Landsat-7 ETM+ *J. Ind. Geophys. Union* **12** 131-140.

[25] Sobrino, J.A.; Jimenez-Muoz, J.C.; Soria, G.; Romaguera, M.; Guanter, L.; Moreno, J.; Plaza, A.; Martinez, P 2014 Land surface emissivity retrieval from different VNIR and TIR sensors *IEEE Trans. Geosci. Remote Sens* **46** 316–327.

[26] Skokovic, D.; Sobrino, J.A.; Jiménez Muñoz, J.C.; Soria, G.; Julien, Y.; Mattar, C.; Cristóbal, J. 2014 Calibration and validation of land surface temperature for Landsat8-TIRS sensor TIRS Landsat-8 characteristics *L. Prod. Valid. Evol. ESA/ESRIN*, **27.**

[27] Yu, X.; Guo, X.; Wu, Z 2014 Land surface temperature retrieval from Landsat 8 TIRS-comparison between radiative transfer equation-based method, split window algorithm and single channel method *Remote Sens* **6** 9829–9852.

[28] Li, S.; Jiang, G.-M 2014 Land surface temperature retrieval from Landsat-8 data with the generalized split-window algorithm *IEEE Access* **6** 18149–18162.

[29] Sobrino, J.A. and Raissouni, N 2000 Toward Remote Sensing Methods for Land Cover Dynamic Monitoring: Application to Morocco *International Journal of Remote Sensing* **21** 353-366.

[30] Avdan, U. and Jovanovska, J. 2016 Algorithm for Automated Mapping of Land Surface Temperature Using LANDSAT 8 Satellite Data. *Journal of Sensors*, Article ID: 1480307. https://doi.org/10.1155/2016/1480307.

[31] Barsi, J.A., Schott, J.R., Hook, S.J., Raqueno, N.G 2014 Markham, B.L. and Radocinski, R.G. Landsat-8 Thermal Infrared Sensor (TIRS) Vicarious Radiometric Calibration. *Remote Sensing* **6** 11607-11626.

.

PRELIMINARILY APPLYING MICROSOFT AZURE AI CUSTOM VISION TO CLASSIFY IMAGE DATA OF THE RICE GROWTH STAGE

T-D Ha[1] and O T N Bui[1]

[1] University of Science, Vietnam National University, Ho Chi Minh City, Vietnam

Abstract: This article uses Microsoft Azure AI Custom Vision to classify image data of the rice growth stage in Lang Sen Wetland Reserve, Long An Province, Vietnam. This tool classifies rice field images into four stages with high accuracy (99%): land preparation, vegetative stage, reproductive and ripening stage. In addition, the tool supports determining the rice growth stage of new images uploaded by users after training. We got good classification results. However, there are still some limitations because the images are blurred due to condensation, and the images cannot distinguish between the growing and ripening stages due to sudden changes in lighting conditions at the measuring station due to weather reasons.

Keyword: *Microsoft Azure AI Custom Vision, categorisation of image data, rice growth stage*

1. INTRODUCTION

Agriculture is a vital industry for every country. In 2022, 691 to 783 million people faced global hunger globally **[1].** Therefore, ensuring food security remains a big challenge for the whole world. For Vietnam, in 2022, the agriculture, forestry, and fisheries sectors accounted for nearly 12% of Vietnam's economic structure. In 2022, Vietnam's rice production also was 42.7 million tons of rice. Rice export production was about 7 million tons, ranking second globally **[2].** However, agricultural production in Vietnam, especially the rice industry, still has many difficulties, such as a large area for planting, a lot of water for drainage, and the level of application of science and technology to production activities is not high, which causes low labour productivity**.**

In recent years, there have been many digital and mechanised innovations around the world that have helped increase productivity, reduce poverty, and ensure food security. The application of new technologies such as automation and artificial intelligence (AI) in agriculture is increasing, mainly in high-income countries. However, the limitation is that the infrastructure is still weak, making transmitting information and data difficult in low- and middle-income countries. [3]. AI applications in agriculture include early detection of pests and diseases [4], improving crop productivity, effectively managing water resources, and automating farming [5]. However, the application of AI in agriculture is still at the beginning of individual research and has not been broadly applied. In Vietnam, previously, humans performed agricultural activities such as fertilising, sowing, providing water for irrigation, and detecting pests. In the last ten years, AI-integrated drones have replaced manual actions for sowing, spraying and fertilising in some Mekong Delta localities. Automatic water management systems have been introduced to serve agricultural work, effectively regulating water resources and avoiding wasting water resources. This replacement saves time and human resources and reduces the amount of water, fertiliser, and pesticides used.

Image categorisation technology has been applied in Vietnam in some sectors. It has specific results with an efficiency of over 99% against pests on grapefruit leaves [6], more than 97% effective against pests on rice leaves [7], and practical from 90% to 95% for ripe pineapple [8]... With a large rice growing area, visiting fields on-site and monitoring rice plants' growth period is time-consuming for scientists who are not on site. Categorising of taken image data provides researchers with immediate crop information during the day or helps to retrieve the agricultural calendar as quickly as possible.

This research applies a machine learning algorithm built into the Microsoft Azure AI Custom Vision service to classify the rice growth stage into the agricultural sector. The advantage of technology is that it is simple, easy to use, does not require programming experience, and is easy to deploy with an extensive image repository. Finally, we can quickly obtain information about rice plants' growth period from a captured photo and cut down the time to retrieve growth period information.

2. METHODOLOGY AND DATA

2.1. Methodology

The sequence for processing and classifying images using the Microsoft Azure AI Custom Vision is as follows [9]: Firstly, the image file name is standardised according to ISO 8601:2019 standards and then uploaded to Microsoft Azure AI Custom Vision. Here, the image will be labelled with four labels corresponding to the four stages of a crop: (1) land preparation stage, (2) vegetative phase, (3) reproductive phase, and (4) ripening phase [10]. The images are labelled based on the typical colours and growth density of each stage of rice plant development. For example, the rice plant is green and sparse in the vegetative stage compared to the reproductive stage. Next, when the rice is ripe, the rice plants turn yellow and spread across the field. The characteristics of the land preparation stage are flooded areas, burned fields, or images of stubble after harvesting, so images with those characteristics will be labelled with the land preparation stage. These images are categorised based on the local agricultural calendar.

Next, the labelled image will undergo the training process and export results. The results will then be evaluated through two indicators: Precision and Recall. The Precision index is the ratio of correct images compared to those predicted by the model to be corrected. Recall index is the ratio of accurate images compared to the total number of images in reality. These two indicators are non-negative values, less than or equal to 1. A higher Precision index shows that the categorisation tool is good, and a high Recall index shows that the model does not miss corrected images in reality. From these two indicators users can take steps to improve these two indicators, such as improving the quality of new images, balancing the number of labelled images, and eliminating error images (for example, error image are deposition of dew or rain on cameras; or are with sudden light changes due to cloud cover). The user then retrains the images. This sequence is summarised in Figure 1. The tool interface is familiar and easy to operate.

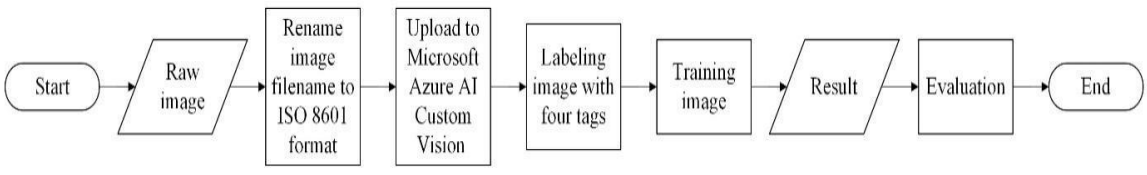


Figure 1: *Sequences of classification images using the Microsoft Azure AI Custom Vision*

2.2. Data

The image data is taken daily at 10:00 and 14:00 (each capture has at least one image) from a greenhouse gas monitoring station located at Lang Sen Wetland Reserve Area, Long An province, Vietnam. The station is located at 10°46'49.6" N, 105°46'01.0" E, established in 2019. This is the first greenhouse gas monitoring station within the framework of a cooperation project between the University of Sciences, Vietnam National University – Ho Chi Minh City (Vietnam) and the Climate Change Research Institute (Czech Globe), Republic of Czech. This monitoring station measures greenhouse gases such as methane (CH_4), carbon dioxide (CO_2), and water vapour. Also, it measures other meteorological factors such as air temperature, soil temperature, air humidity, and soil moisture. The images support the information of crops in the rice field.

6139 images from 2019 to 2021 were uploaded to Microsoft Azure AI Custom Vision. The program is run three times, with the first time using images from 2019, the second time using images from 2019 and 2020, and the third time using images from all three years 2019, 2020, and 2021. Each running time took from 2 hours to 6 hours. The results obtained need to reevaluate the effectiveness of categorisation based on the Recall and Precision index. Figure 2 shows the interface of Microsoft Azure AI Custom Vision.

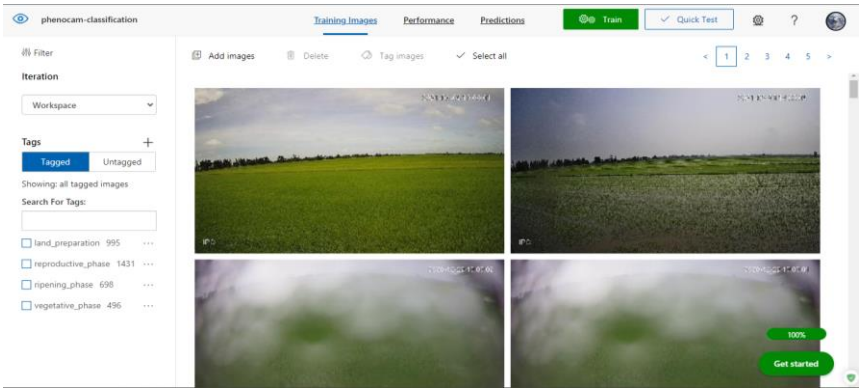


Figure 2: *Interface of training tool in Microsoft Azure AI Custom Vision*

3. RESULT AND DISCUSSION

3.1. Classification images according to the rice growth stage

3.1.1. Classification images in the land preparation stage

As mentioned above, we divided it into four stages, with three main rice growth stages and land preparation. Typical results of land preparation stage classification are shown in Figure 3. The classified results have a high probability of land preparation with flooded fields (83.6%) (Figure 3) ploughing. When the rice field was covered with stubble, the remaining dried rice straw after harvesting and the land preparation of staying rice straw was incomplete, the probability of categorisation was not so reasonable. In this case, those images need to be relabelled and reprocessed. There is an error at different points on the site, so users must do it carefully and accurately. The problem occurs because the input of labelled images in the land preparation stage has a high proportion of flooded field images, few burned rice straw images, and images of non-flooded land combined without burned rice straws. This causes the image data to be visually imbalanced, leading to incorrect classification. The problem can be solved by adding a number of images of burned rice

straw and images of non-flooded soil without burned rice straw to the labelled land preparation stage in subsequent runs.

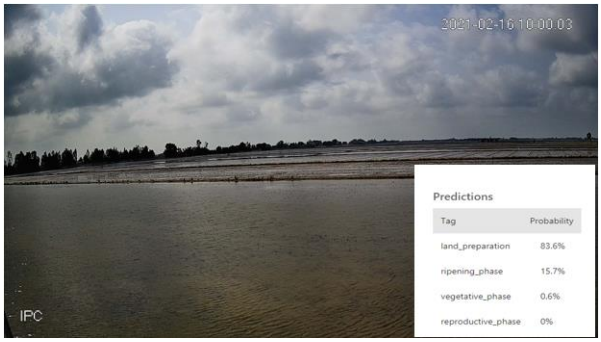


Figure 3: *A representative result of land preparation when flooded rice field*

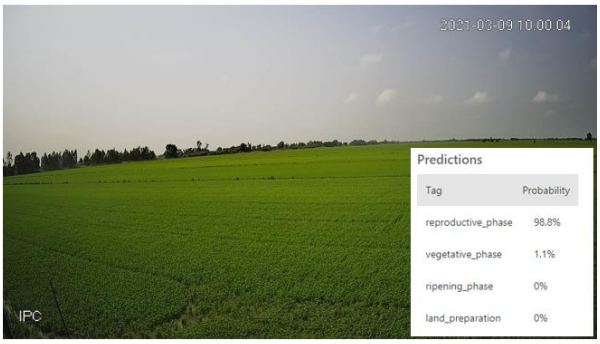


Figure 4. *The result for the classification images in the vegetative stage*

3.1.2. Classification images in the vegetative stage

Figure 4 is a representative result for the classification images in the vegetative stage with a probability of 79.8%; that is an example of classification. If there is sparse growing rice during this period, classified results will be obtained with high accuracy. However, when the rice grows more evenly, it can be classified into the rice reproductive stage or even the ripening stage in case of intense lighting at the time of shooting. This problem can be processed by relabeling according to the local agricultural calendar.

3.1.3. Classification images in the reproductive stage

Figure 5 is a representative result for the classification images in the reproductive stage of 98.8%, an example of classification.

If the image is uniformly green and the height of rice plants is evenly tall, the probability of being classified as the reproductive stage is high. However, if there is intense lighting during shooting, the image will quickly be classified as ripe rice. This problem can be processed by relabeling according to the local agricultural calendar.



Figure 5. *A representative result for the classification images in the reproductive stage*



Figure 6. *A representative result for the classification images in the ripening stage*

3.1.4. Classification images in the ripening stage

Figure 6 is a representative result for classification images in the ripening stage. Here, we add more new images in 2023 and predicted results are more accurate. Similar to the above stage, if the color of rice plants is evenly yellow, the probability of being classified as ripe is high. In some cases, images belonging to other stages are classified as ripening stages, such as classifying the land preparation stage as the ripening stage due to the lack of images of

burning rice straw and images of non-flooded soil combining without burning rice straw, classifying the vegetative stage or the reproductive stage into the ripening stage for when the time of shooting having intense lighting.

3.1.5. Advantages and disadvantages of Microsoft Azure AI Custom Vision as applied in agriculture science

Microsoft Azure AI Custom Vision supports users in classifying the labelled images well. However, suppose the image quality is not good. In that case, the number of images is imbalanced, or it is impossible to distinguish which image should be labelled, which will cause poor classification results. In this study, the land preparation stage lacked images of burning rice straw in the rice field and the unflooded rice field and fields without burning rice straw after harvesting. The vegetative and reproductive stages were sometimes not distinguishable from the ripening stage, causing classification results to be poor and less accurate.

3.2. Application for prediction images

After training with image storage for three years, from 2019 to 2021, Microsoft Azure AI Custom Vision allows users to upload or use images on the Internet to test training programs. Then, the prediction results have been also shown to users analysis (Figure 7).

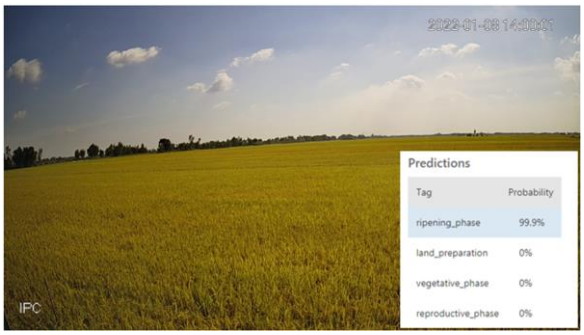


Figure 7. *Demonstrates the test function of Microsoft Azure AI Custom Vision.*

3.3. Further Discussion

Microsoft Azure AI Custom Vision has the advantage of being simple and easy to use, does not require programming experience, and the algorithm is fine-tuned to suit diverse user requirements. The limitation is that the number of images for each label must be large enough (minimum 50 images), and the number of images for each label must not differ too much to make the classification results more accurate. In addition, labelled images also need to be diverse in terms of shooting angle, lighting, and context for more accurate classification and identification results. In addition, the image storage used in this study has several limitations that make the classification results less accurate, such as images being blurred due to dew on the camera and images that cannot distinguish the vegetative stage from the reproductive stage due to sudden changes in lighting conditions at the measuring station. The way to handle poor-quality images is to remove and not add these images in subsequent runs. This work helps the person not on-site to determine the correct rice growth stage just with a rice field photo.

4. CONCLUSION

Applying Microsoft Azure AI Custom Vision to classify images has yielded some accurate, preliminarily results. We have already classified four stages of the rice growth and land preparation of taken images with high accuracy. In addition, the classification results can also be used to determine what stages of new images are uploaded by users. For more

accurate classification and determination results in the future, the quality of input images needs to be improved, error images should be eliminated, and images need to be taken at different times of the day.

ACKNOWLEDGEMENT

This research is funded by the University of Science, VNU-HCM, under grant number T2022-50. Besides that, we would like to thank the Centre of Climate Change and Greenhouse Gases in the University of Science (VNU-HCM) for supplying data to this research.

REFERENCE

[1] Food and Agriculture Organization of the United Nations 2023 *The State of Food Security and Nutrition in the World 2023*. Rome: Food and Agriculture Organization of the United Nations.

[2] General of General Statistics 2022 *Statistical Yearbook of Viet Nam 2022*. Ha Noi: General of General Statistics.

[3] Food and Agriculture Organization of the United Nations 2022 *The State of Food and Agriculture 2022*. Rome: Food and Agriculture Organization of the United Nations.

[4] Singh V, Sharma N, Singh S 2020 *Artif. Intell. Agric.* **4** 229.

[5] Pathan M, Patel N, Yagnik H, Shah M 2020 *Artif. Intell. Agric.* **4** 81.

[6] Triet NM, Bảo TQ, Dinh TQ 2017 Can Tho University Journal of Science **88**.

[7] Thanh TTP, Nghe NT 2022 *Can Tho University Journal of Science* **58** 1.

[8] Hai TT, Cuong NHH, Duy NK 2022 *University of Danang - Journal of Science and Technology* **20** 94.

[9] Microsoft 2023 *Custom Vision documentation* [updated 2023 Jul 18; cited 2023 Nov 8]. Available from: https://learn.microsoft.com/en-us/azure/ai-services/custom-vision-service/.

[10] International Rice Research Institute 2015 *Steps to successful rice production*. Los Baños (Philippines): International Rice Research Institute.

UTILIZING REMOTE SENSING AND GIS TO DESIGN A DATABASE OF ROAD TRANSPOTATION IN THANH HOA PROVINCE OF VIETNAM: A PILOT IN DONG SON AND THIEU HOA DISTRICT

Thao Vu Thi Phuong [*1], Ha Le Thi [1,2], Thao Do Thi Phuong [1,3]

[1] Hanoi University of Mining and Geology, 18 Vien street, Bac Tu Liem district, Hanoi, Vietnam; vuthiphuongthao@humg.edu.vn

[2] Campus in Ho Chi Minh City, University of Transport and Communications, No. 450- 451 Le Van Viet Street, Tang Nhon Phu A Ward, District 9, Ho Chi Minh City, Vietnam;

[3] Research and Development of Geospatial data Management and Analysis Techniques (GMA), Hanoi University of Mining and Geology, Duc Thang, Bac Tu Liem, Hanoi 10000, Vietnam

Abstract. It is necessary to construct a comprehensive and accurate road transport database for Thanh Hoa province, a large province in the North Central region, which ranks third in population and fifth in area of Vietnam. This database will provide an essential overview of the transport infrastructure, enabling effective and precise management. The study utilizes remote sensing in conjunction with GIS technology to develop the road transport system database, with a pilot project focused on Dong Son and Thieu Hoa districts. The database has been successfully established and standardized to include traffic infrastructure objects, such as roads, bridges, signs, traffic signal systems, and lighting systems, for both Thieu Hoa and Dong Son districts. Using this well-structured framework, the road network management can easily expand data coverage to include the remaining districts within the province. In addition to the database creation, the study has developed three groups of tools to facilitate the management and maintenance planning for road infrastructure objects in the province. These tool groups consist of data management and updating tools, tools for generating statistical reports, and tools for planning and estimating maintenance costs. This road network database plays a vital role in providing essential spatial and non-spatial information to support various aspects, such as urban planning, environmental resources management, and more.

Keyword: *Sentinel-2A, Sentinel-2B, GIS technology, road transport database, Model Builder.*

1. INTRODUCTION

The transport system is a crucial component of any economy and serves as a fundamental tool for development. There exists a close relationship between the quantity and quality of transport infrastructure and the level of economic development. Efficient transport systems provide economic and social opportunities and benefits, enabling easy accessibility to markets, employment, and investments. On the other hand, deficient transport systems, whether in terms of capacity or reliability, can lead to economic costs, including reduced or missed opportunities and a lower quality of life [3].

Proper management, operations, and maintenance are essential for a transportation system to remain effective. Strict and systematic management of quantity, quality, condition, maintenance, and operational information is imperative. To achieve an effective

and accurate management, it is crucial to build a complete and accurate database that provides an overview of the transportation infrastructure [9]

In developed countries, the use of remote sensing images has become common practice in urban planning. Currently remote sensing data is being used to create thematic maps and base maps for urban planning, due to it's useful. Over the past few years, many successful applications have demonstrated the feasibility of using remote sensing techniques for traffic infrastructure monitoring purposes such as radar-based remote sensing techniques, interferometric synthetic aperture radar techniques, high-frequency ground-penetrating radar… High-resolution images are helpful for interpreting and monitoring structural changes in infrastructure [4], [8], [11].

Some other studies have aimed at integrating remote sensing and GIS focusing mainly on road feature extraction [19], road network analysis [1]. The application of remote sensing and GIS can be seen as a great support for effective planning, analysis and decision making especially for the development and growth of urban areas.

The above studies have focused on building a database on road traffic infrastructure, but it is not complete. Due to the use of raw data sources, the integration of data and forecast information were not fast, synchronous and timely. Therefore, research on remote sensing and GIS applications in road traffic infrastructure management which provide users with truly useful information, ensuring speed, synchronization and timeliness is an issue that needs to be addressed.

Over the years, remote sensing and GIS technologies have been developed in Vietnam and have made significant contributions in multi-sectoral, multi-field including the transportation industry [5]. It is a fact that in Vietnam, there are quite a lot of remote sensing image materials; from low and medium resolution satellite images such as MODIS, LANDSAT images to ASTER, SPOT 6/7, KOMPSat ... with high resolution covering the territory of Vietnam taken in different times. This is a great advantage of remote sensing data that needs to be exploited, applied well for a large space, reducing the cost of direct measurement of the field to ensure economic efficiency for managers. The use of remote sensing data, with features used by high spike frequency, extended range, multi-time, increasingly high resolution... including remote sensing data and research radar, combined with GIS and actual investigation results is a modern, highly effective method [21]. GIS is built using computer tools and application software to analyze and display on the map the spatial data related to the earth. GIS technology allows efficient integration of common database operations such as analysis, statistics and search functions, with special tools for geographic processing and visualization on maps [4].

Today, the need for planning and development of urban and residential areas is rapidly increasing, leading to the development and expansion of traffic infrastructure and also posing new requirements and challenges in urban traffic infrastructure management, especially database system management. Several studies have, provided database solutions and technical infrastructure solutions to build suitable software for road traffic management [6], [7], [15]… However, these systems only focus on managing the current state of road traffic, not providing much support for network planning management. The system's road traffic has not yet been published on the Internet, some research is only theoretical and implementation requires a very high capital source [6],[15].

In Vietnam today, facilities directly managing transport system mainly store transport system database records on paper, some discrete data on computers and some data are digitized using GIS technology, image files.... However, this digitized data is scattered, incomplete and inaccurate, and not updated regularly. Storage, updating, searching, and statistics still face many difficulties [12]. Therefore, digitizing and building a database of the current state of road traffic infrastructure is very necessary, supporting effective exploitation and improving management.



Figure 1. *Geographical site map of Dong Son and Thieu Hoa districts, Thanh Hoa province*

Thanh Hoa is a significant province located in the North Central region of Vietnam, boasting the third-largest population and the fifth-largest area. Alongside Hanoi, Hai Phong, and Quang Ninh, it serves as a major center for various industries, including energy, processing, and manufacturing. The province also excels in high value-added agriculture, logistics, tourism, education and training, specialized medical services, as well as cultural and sports offerings. As part of the northern development quadrangle of Vietnam, Thanh Hoa represents a new growth pole, contributing significantly to the region's advancement [13].

With a long history of development, Thanh Hoa province now boasts a dense and extensive transportation system to cater to its large population. To effectively support the transportation needs and overall development of the region, there is a pressing need for a modern, up-to-date, and accessible transport database system. Hence, the primary objective of this paper is to construct a comprehensive database for managing road transportation infrastructure in Thanh Hoa province, utilizing a combination of remote sensing and GIS technology through a pilot study in Dong Son and Thieu Hoa districts. The resulting dataset

holds potential for practical application, serving as a platform not only for transportation databases but also for other fields, such as natural resources and environment, construction, and agriculture.

2. MATERIAL AND METHODOLOGY

2.1. Material

Study area: Dong Son and Thieu Hoa, two districts situated in the center of Thanh Hoa province, can be found in specific coordinate regions. Dong Son's coordinates lie between 19°43’ to 19°51’ north latitude and from 105°33’ to 105°45’ east longitude, while Thieu Hoa's coordinates range from 19°51' to 12°50' north latitude and from 105°35' to 105°48' east longitude (Figure1). These districts were chosen as study sites due to their well-established and developed road networks. Both Dong Son and Thieu Hoa boast major national highways traversing through them. National Highway 45 runs from Thanh Hoa city, cutting across the north of Dong Son district, passing through Rung Thong town, and extending to Thieu Hoa district. Similarly, National Highway 47 starts from Thanh Hoa city, crosses the north of Dong Son district, goes through Rung Thong town, and reaches Trieu Son district. Additionally, a trans-Vietnam railway passes through both districts, facilitating economic and cultural exchanges with other localities in the country.

Data: - Remote sensing image data serves to build a geographic database: The Sentinel-2A MSI taken on July 7, 2023; Sentinel-2B MSI taken on July 12, 2023 1 radar satellite images taken on December 21, 2017 and Landsat – 8 OLI/TIRLIGT taken on July 7, 2023 in Thanh Hoa province were used in this study.

- Spatial data and attribute data on road transport system in Dong Son and Thieu Hoa districts of Thanh Hoa province.

2.2. Methodology

This paper used the following methods:

***Collect data:** Spatial data and attribute data in the article are collected from 2 sources:

- Collection of Spatial data is maps from the Department of Surveying and Mapping or the Department of Transport of Thanh Hoa province.

- Attribute data is collected from survey work, collecting locations and characteristics of objects in the field.

After collected data will be analyzed, evaluated, and formatted. In this article, data will be built and stored in ESRI's Geodatabase standard.

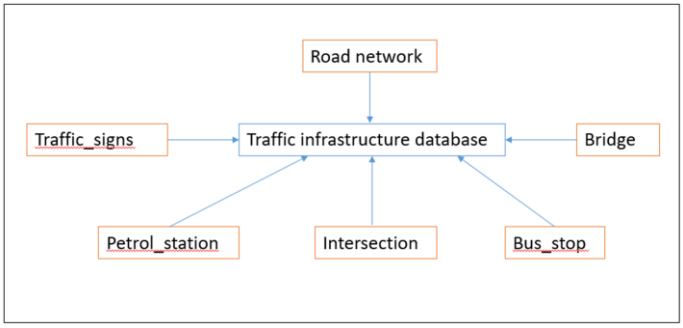


Figure 2. *Traffic infrastructure database management model*

- **Remote sensing data, in combination with GIS and actual investigation results method:** played a pivotal role in fulfilling various tasks, including input data provision, updating, analysis, querying, and information management. The road network extraction was achieved through the utilization of remote sensing data, alongside other

essential background data such as boundary data, population statistics, topography, hydrology, and field data [2]. To construct the road transportation map, spatial data obtained from the satellite image database, coupled with measurement data from Dong Son and Thieu Hoa districts, were integrated using ArcGIS software. GIS technology facilitated the creation of electronic maps, seamless integration of information, visualization of scenarios, resolution of intricate problems, and the swift and efficient generation of innovative solutions [10], 20].

- **Field surveys**: were conducted to supplement and provide further spatial data and object properties.
- **Modeling method:** Model Builder in ArcGIS is used in this study. Models will be constructed based on data conversion between various formats consist of transportation database fields and surface overlays for mapping the road transport system, for example from Kmz format in Google Earth to Gdb spatial layers in ArcGIS. Similary, by passing the output of this model as input to next model, these models consist of a series of combined numerical tools that facilitate automated data processing in ArcGIS.

Based on the characteristics and management objects, propose a data structure design model as shown in Figure 2.

The process of building a road transportation database for Dong Son and Thieu Hoa districts, Thanh Hoa province is summarized in Figure 3 below.

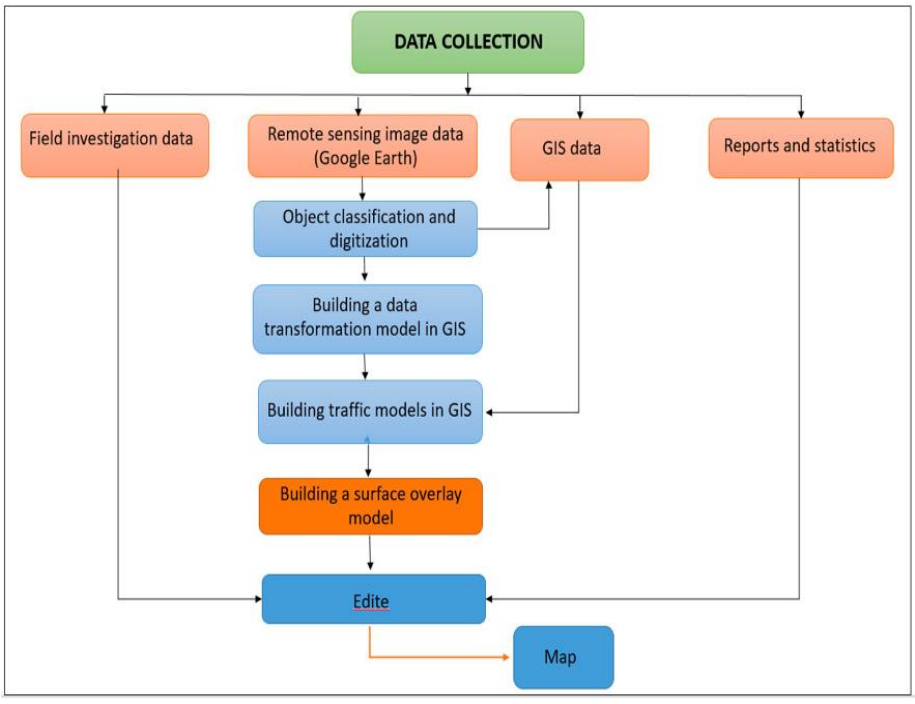


Figure 3. *Using remote sensing and GIS to design the database of road transportation database for Dong Son and Thieu Hoa districts, Thanh Hoa province*

3. RESULT AND DISCUSSION

3.1. The process of building a road network system database for Dong Son and Thieu Hoa districts, Thanh Hoa province

The Model Builder process was chosen to convert kmz format to gdb format data in ArcGIS

due to its agility and convenience [18]. The road transport database of Dong Son and Thieu Hoa districts is conducted as follows:

Step 1: add the boundary layer of Dong Son and Thieu Hoa districts to Google Earth using the Add Path tool to digitize roads. The scope is national highways and provincial roads belonging to two districts (Figure 4).

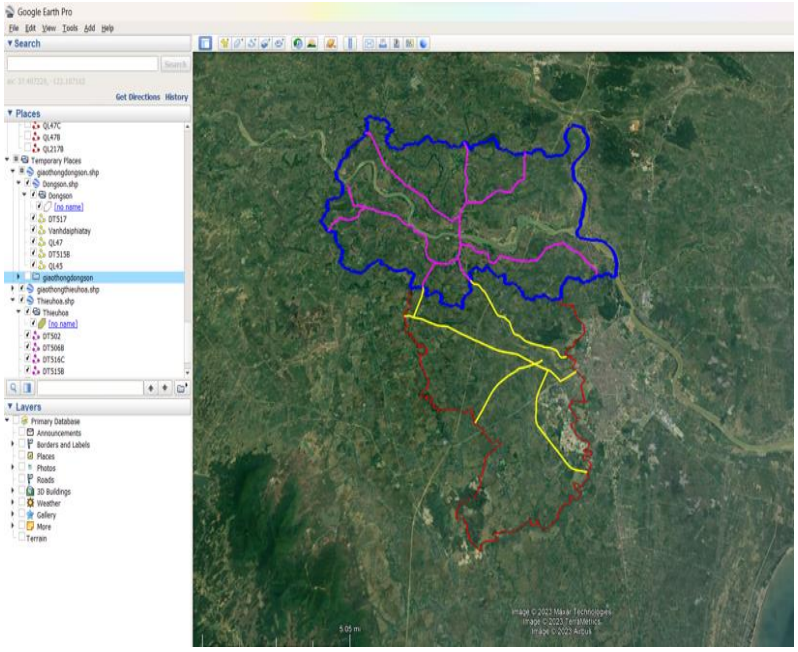


Figure 4. *Digitizing roads on Google Earth.*

- Step 2: After the data is generated as a KMZ file, build a builder model in ArcGIS to convert multiple KMZ files into spatial layers (Figure 5 and Figure 6).

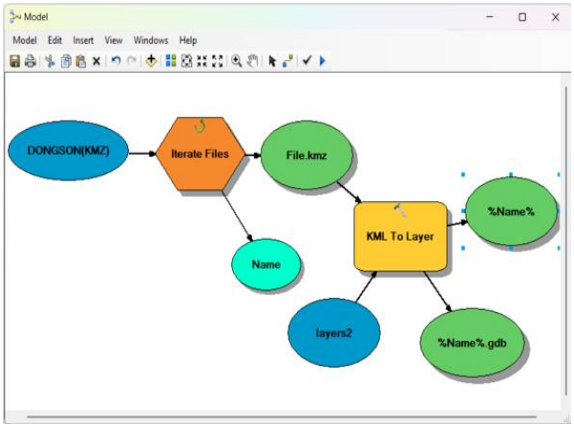


Figure 5. *Build Builder Model converting KMZ file in ArcGIS for Dong Son district.*

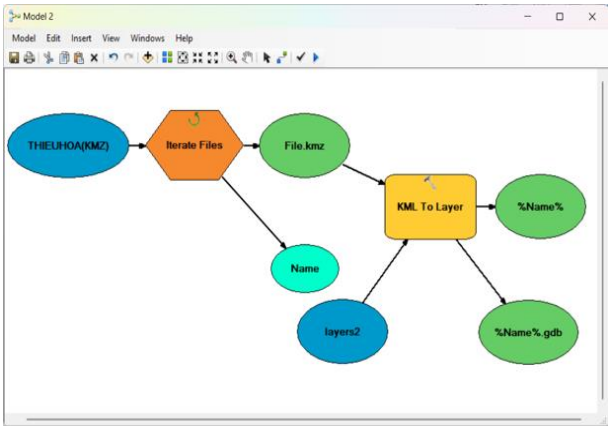


Figure 6. *Building Builder Model to convert KMZ file in ArcGIS for Thieu Hoa district.*

- Step 3: Build a transportation database model (Figure 7 and Figure 8).

Road network is a linear reference system in GIS. Both districts have two levels of road network, the national dataset and the provincial dataset. For this study, provincial and national road networks are used, the unique identifier for route reference in the road network is the segment ID. There is also the type of road, route (primary direction starting and ending) and the length of the road segment. For other objects such as bridges, transport signs, intersections, petrol stations and bus stops the same procedure is applied to the road layer.

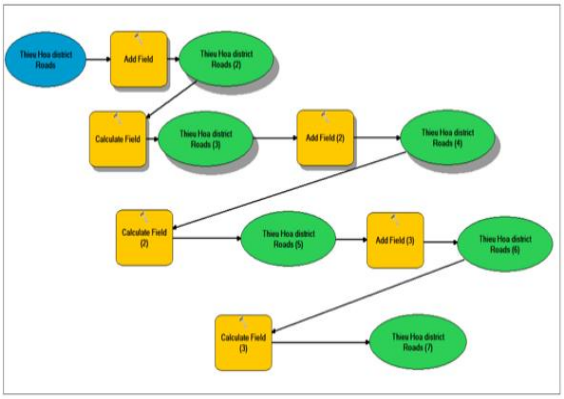


Figure 7. *Construction of Builder Model for transportation in Thieu Hoa district.*

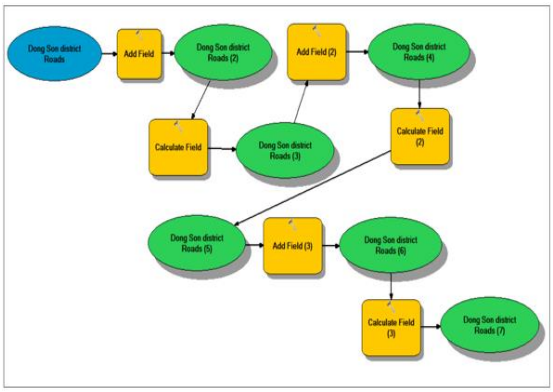


Figure 8. *Construction of Builder Model for transportation in Dong Son district.*

The structure of the road layer attribute database is presented in table 1.

Table 1. The structure of the road layer attribute database

Data layer name	Content interpretation	Data style
ID	Object class classification code	Short Interger
Name	Road names	Text(50)
NameOther	Another name for road	Text(50)
RoadClass	Road classification	Short Interger
WidthRoad	Road width	Float
FirstPoint	The first point of the route	Text(50)
FinalPoint	End point of the route	Text(50)
SurfaceTyp	Road surface material	Text(50)

- Step 4: After construction of the Geodatabase, enter spatial and non-spatial data for road layers such as design, edit and present maps, and obtain a database of road layer maps for research areas.

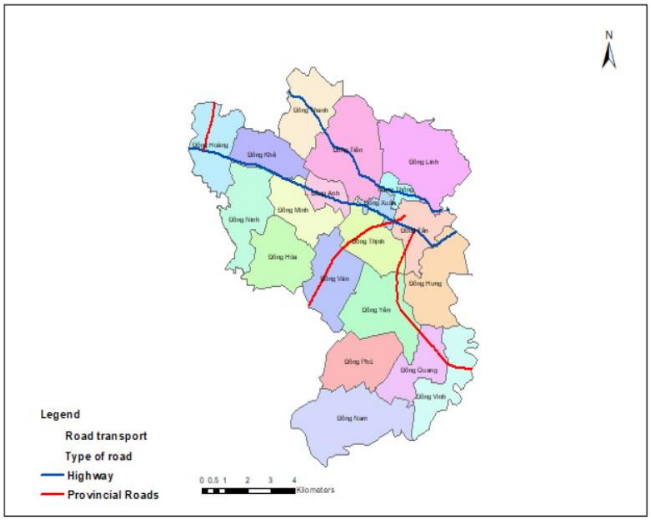


Figure 9. *Road layer after construction for Thieu Hoa district*

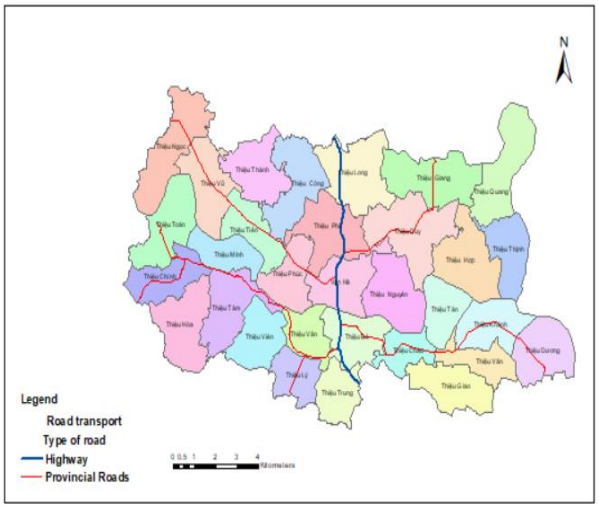


Figure 10. *Road layer after construction for Dong Son district*

3.2. The process of building database of bridges, traffic signs, intersections, gas stations, bus stations in Dong Son and Thieu Hoa districts, Thanh Hoa province

The process of building database of other objects such as bridges, traffic signs, intersections, gas stations, … is applied similar to the road layer. Spatial data of the above point objects is updated from excel files collected and located directly in the field. Attribute data is built based on the data structure for each object. After completing for building of Geodatabase database and entering spatial and non-spatial data for the remaining layers of the transportation infrastructure as designed, proceed to edit and present the map, obtain a road transport system map for the study area as in Figure 11 and Figure 12.

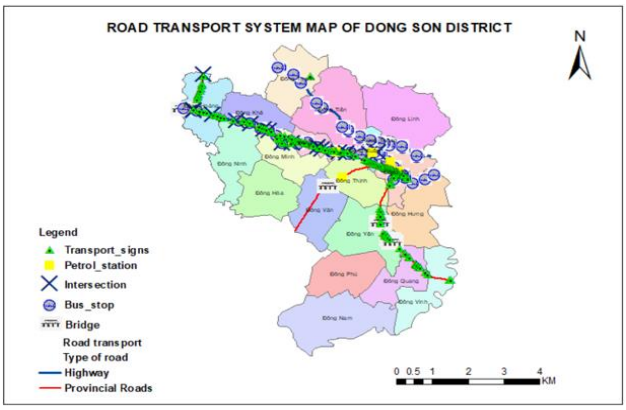


Figure 11. *Complete road transport system map for Thieu Hoa district*

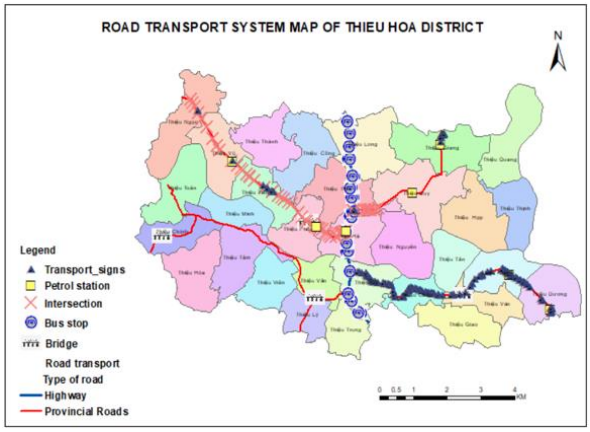


Figure 12. *Complete road transport system map for Dong Son district*

The regional road transport system database, stored as standard data in GIS is GeoDatabase based on applying standards in database construction: standard data format, standard project, standard topology and standard attribute data (Figure 13).

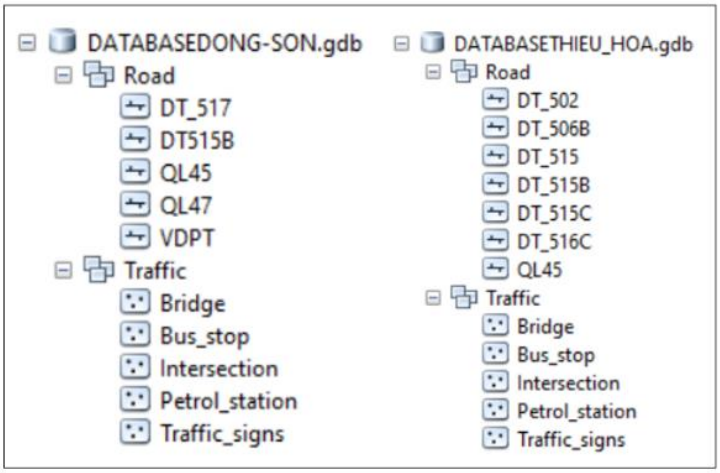


Figure 13. *Structure of road transport system database in 2 districts of Dong Son and Thieu Hoa, Thanh Hoa province*

3.3. Building a base layer database for road transport network maps

To add a base layer to the road transport network map, two methods were chosen. Two studied areas are both agricultural land, so the first method will build an NDVI base layer model for the map as shown in Figure 14 (a) and Figure 14 (b). Input data is from Sentinel - 2 image.



a) *b)*

Figure 14. *NDVI index of Dong Son district (a) and Thieu Hoa district (b)*

In oder to generalize the background layers for the map, Landsat 8 satellite images collected for input data of two districts to classify and improve the accuracy.

3.4. Exploit and use databases to serve road traffic infrastructure management.

Overlaying the GIS data layers, map of road traffic system in Dong Son and Thieu Hoa districts will be obtained (Figure 15).

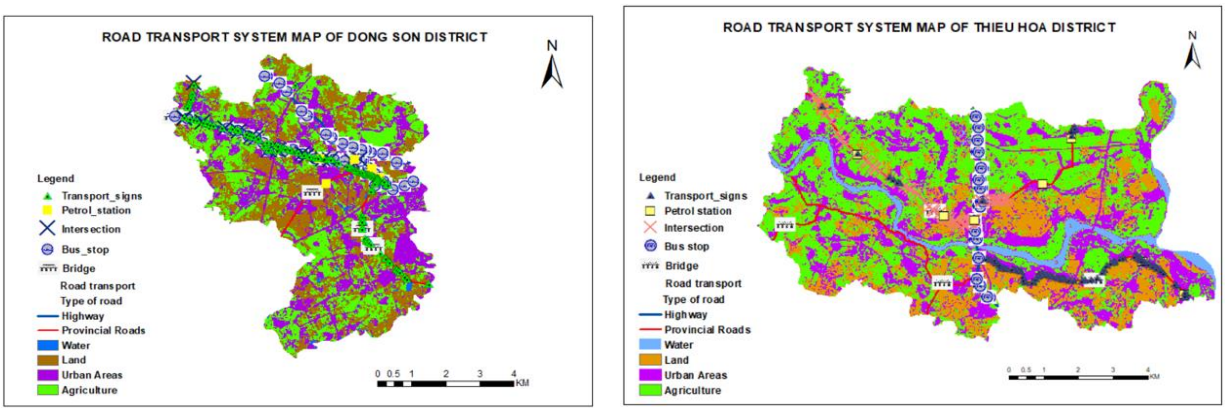


Figure 15. *A road network map of Dong Son district (a) and Thieu Hoa district (b)*

With the advent of geographic information systems (GIS), many studies on road traffic have been conducted in road traffic network analysis [14], [16], [17]. In which, GIS is a very effective approach for building databases, organizing geographical objects in the transportation network, including routes, auxiliary works and all information about the status of objects [22]. The road network database for Dong Son and Thieu Hoa districts has been successfully built and standardized, including the structure of many road infrastructure items, including roads, bridges, signs, traffic signal systems. This framework structure facilitates the effective expansion of data coverage for the remaining districts in the province, thereby benefiting the urban traffic management sector.

Thanh Hoa province is in strong development movement therefore the road network database is so important in providing essential spatial and non-spatial information. This valuable database serves a variety of purposes, supporting urban planning and environmental resource management, and many other purposes.

This study refers to the study management and data update tool group: These tools allow to access and update attribute information for each object of each data layer type. In addition, each object can be located and identified directly on the map.

This group of tools includes:

***Update attribute information directly via the attribute table (Figure 16)**

*** Use the Indentify tool (Figure 17)**

On the toolbar, click on the Indentify tool and click on the object need to look up information about. Then, click on the line layer object. The Identify Results windo wappears.

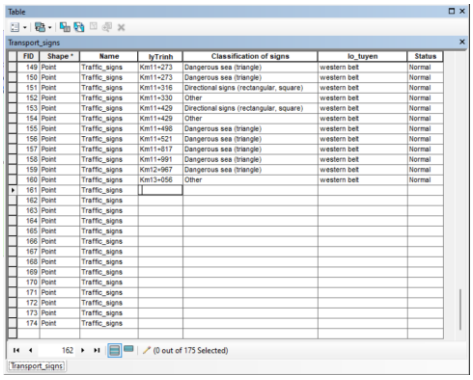


Figure 16. *Attribute table tool*

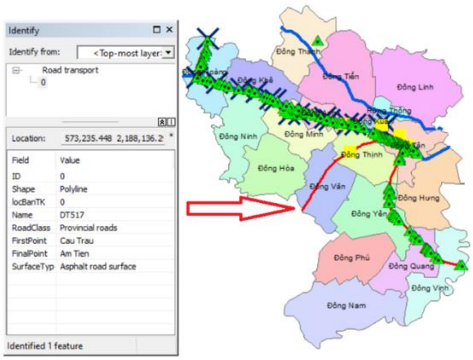


Figure 17. *Indentify information lookup tool*

*** Query objects on the Select by Attributes map:**

From the Menu toolbar, select Selection\ Select by Attributes. The Select by Attributes dialog box appears:

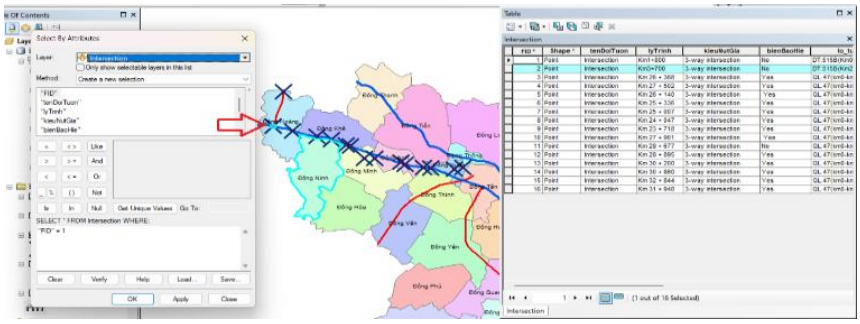


Figure 18. *Objects query tool on Select by Attributes map*

Based on the road transport system database that has been built, using ArGIS's specialized functions, additional functions such as extracting, updating, presenting data, and preparing reports can be provided. The report provides optimal solutions for the purpose of managing the road network of the remaining districts in the province and on a broader scale with other fields.

4. CONCLUSION

Effective transportation systems play a vital role in promoting economic growth and prosperity by enhancing the mobility of citizens and goods. Additionally, they exert significant impacts on road safety and social development. In this study, the database structure, encompassing various traffic infrastructure objects like roads, bridges, trees, signs, traffic signal systems, and lighting systems for both Thieu Hoa and Dong Son districts were successfully constructed and standardized. The framework structure facilitates seamless extension of the road network management data coverage to include the remaining districts within the province.

Furthermore, this study has developed three groups of tools to address the management and maintenance planning of road infrastructure objects in the province, which includes tools for managing and updating data, tools to generate statistical reports, and tools for planning and estimating maintenance costs. These tools contribute significantly to the efficient and effective management of the province's transport infrastructure, ensuring its smooth operation and supporting sustainable development.

REFERENCES

[1] Ajay D N, Gawali B W 2013 *Transportation network analysis by using Remote sensing and GIS a review*, International Journal of Engineering Research and Applications, pp. 70 -76.

[2] Aoying Z, Shuigeng Z 2000 *Approaches for Scaling DBSCAN Algorithm to Large Spatial Database*, Journal of Computer Science and Technology, 15 (6), pp. 509-526.

[3] Choudhary J et al 2015 *Spatial and Statistical Analysis of Road Accidents Hot Spots Using GIS*, Transportation Research Group of India, Kolkata, India, December, pp. 17-20.

[4] Ciampoli LB, Gagliardi V, Clementini C 2020 *Transport Infrastructure Monitoring by InSAR and GPR Data Fusion*, Surveys in Geophysics, 41, pp. 371-394.

[5] Dang Van Duc 2001 *Geographic Information System*, Science and Technology Publishing House, Hanoi.

[6] Dinh Thi Phuong 2012 *Research on GIS application in road traffic network management in Vinh Phuc province*, Master's thesis, Institute of Posts and Telecommunications Technology, Hanoi.

[7] Doan Van Truong 2016, *Application of geographic information system in management of Ho Chi Minh City's main road system*, Sejong University, Korea.

[8] Gagliardi V, Benedetto A, Bianchini C L, D'Amico F, Alani A M, Tosti F (2020), *Health monitoring approach for transport infrastructure and bridges by satellite remote sensing Persistent Scatterers Interferometry (PSI)*, Earth Resources and Environmental Remote Sensing/GIS Applications XI.

[9] Geurts K et al 2004 Identification and Ranking of Black Spots: Sensitivity Analysis, Journal of the Transportation Research Board, 1897(1), pp. 34−42.

[10] Heather Campbell, I Masser 2020 *GIS In Organizations. How Effective Are GIS In Practice*? CRC Press.

[11] Kongyang C, Mingming L, Xiaopeng F, Mingming W, Wu J 2011 *Road condition monitoring using on-board Three-axis Accelerometer and GPS Sensor*, 6th International ICST Conference on Communications and Networking in China, Harbin, pp. 1032-1037.

[12] Le Van Minh 2019 *Hybrid database organization solution for technical infrastructure of traffic works*, Proceedings of the National Scientific Conference, pp. 288-295.

[13] Ministry of Natural Resources and Environment of Vietnam 2022, *Approve and announce the results of land area statistics in 2020*. Decision No. 387/QD-BTNMT.

[14] Morgado P, Costa N 2011, *Geographic networks analysis A graphbased model for analyses the roads networks impact on land cover*, International Conference Virtual City and Territory, PP. 223-229.

[15] Nguyen Van Dang, Cao Thi Xuan My 2017 *Proposed structure of Vietnam's pavement exploitation management system*, Journal of Science and Technology of Danang University, 3(112), p. 15-21.

[16] Nijagunappa R, Sulochana Shekhar S, Gurugnanam BRaju PLN, De P 2007 *Road Network Analysis Of Dehradun City Using High Resolution Satellite Data And GIS*, Journal Of The Indian Society Of Remote Sensing, 35 (3).

[17] Obafemi A A, Eludoyin O S, Opara D R 2011 *Road Network Assessment in Trans-Amadi, Port Harcourt in Nigeria Using GIS*, International Journal for Traffic and Transport Engineering, pp. 257-264.

[18] Raju A, Kaliyaperumal K 2020 *Comparative Study On Methods of Creating Geodatabase Using ARCGIS 10.3*, International Journal of Advanced Research in Engineering and Technology, 11(8), pp. 13-21.

[19] Rock A, Malhoski R (2018), *Mapping with ArcGIS pro*, Parkt Publishing Ltd, Birmingham, UK.

[20] Tomlinson R F 2007 *Thinking about GIS: geographic information system planning for managers* (Vol. 1). ESRI, Inc.

[21] Tsan Mo et al 1984 *Calculations of Radar backscattering coefficient of vegetation – covered soils*, Remote sensing of environment, 15, pp. 119 - 133.

[22] Weiping H, Chi W 2011 *Urban Road Network Accessibility Evaluation Method Based on GIS Spatial Analysis Techniques*, The International Archives of the Photogrammetry, Remote Sensing and Spatial Information Sciences, 38, pp. 114-117.

SUSTAINABLE AND GREEN ENERGY TRANSITION; CIRCULAR ECONOMY IN RESOURCE-MINERAL MANAGEMENT AND SUSTAINABLE DEVELOPMENT

(Wind power, Solar power, Gas power, Geothermal, Garbage power, Hydrogen, etc.; low carbon emission technologies; resource-mineral management and sustainable development)

RESEARCH TO IDENTIFY TYPES OF MICROPLASTICS, THEIR SHAPES, AND TRENDS OVER SPACE AND TIME, AND TO PROPOSE SOLUTIONS TO REDUCE MICROPLASTIC POLLUTION FROM PLASTIC WASTE IN THE SURFACE WATER OF THE SAIGON - DONG NAI RIVER, VIETNAM

Han H T N[1,3*], Phu H[2*], Hue N T[3]

[1] Hochiminh City University of Natural Resources and Environment, Ho Chi Minh City, Vietnam;

[2] HUTECH Institute of Applied Sciences; HUTECH University, Ho Chi Minh City, Vietnam;

[3] Institute of Environmental Technology, Vietnam Academy of Science and Technology.

*Email: h.phu@hutech.edu.vn; htnhan_ctn@hcmunre.edu.vn

Abstract: This study has developed a process for analyzing microplastics in suface water samples using Fourier infrared spectroscopy combined with stereo electron microscopy to determine the types of microplastics, their density, shape in the water of Saigon river and Dong Nai river, Vietnam. Microplastics in the water source were found in fibers, pieces, and particles, according to research results, in both the dry season and rainy seasons of the year. The content of fibrous microplastics from sources affecting river basins was very high. More than 31 types of microplastics have been discovered, confirming the richness of microplastic sources. In addition to substances Propylene, Ethylene, synthetic colloids' Vinyl, MUF, TEFLON, OLEFIN, AMIO, and EVOH have also been discovered. Correlation analysis and principal component determination methods were applied to evaluate trends in the shape of microplastics according to the season of the year, and the rise or fall off the tide. Based on the research results, the abundance of microplastic types and the dominant fiber shapes show that the main source of microplastics in the river water environment are components found in plastic waste. This study's proposal to reduce plastic and microplastic waste with solutions to transition to a circular economy for the plastics industry is considered the most promising path for economists and environmental managers to effectively protect the environment.

Keywords: *Circular Economy, Microplastics, Plastic waste, Saigon–Dong Nai River, Surface water, Water supply*

1. INTRODUCTION

Each year in Vietnam, approximately 1800 x 1000 tons of plastic waste are released into the environment, but only 27% of it is recycled and utilized [1]. The amount of plastic waste in Vietnam is increasing every year, and Vietnam is a group of countries that imports a lot of scrap in the world, including plastic scrap. The increase in plastic waste causes people to face environmental and health pollution problems. Recently, the Prime Minister issued Directive No. 33/CT-TTg dated August 20, 2020, to strengthen the management of reuse, recycling, treatment, and reduction of plastic waste; Directive No. 41/CT-TTg dated December 1, 2020, on a number of urgent solutions to strengthen solid waste management (including microplastics); Environmental Protection Law 2020, with specific regulations related to minimizing plastic waste and ocean plastic waste, regulates the extended

responsibility of manufacturers [2]. Floating plastic waste collected annually on main urban canals in Vietnam accounts for from 2x1000 to 13x1000 tons [3]. Plastic pollution is potentially harmful to human health [4]. Smaller particles, ranging in size from 1 to 5x1000 μm, appears due to the decomposition of plastic waste, further breakdown by UV radiation and turbulence, degradation of textiles and abrasives. Abrasion and washing are concerns because they are the same size as zooplankton, which form the basis of the aquatic food chain and play an important role. are important for climate regulation.

The process of decomposition of plastic is known as the process in which the polymer structure of plastic is broken under the direct impact of sunlight over a certain period. When decomposing, plastic will transform into smaller micro or canonized pieces, not into other substances. Depending on the structure of each type of plastic, the decomposition time ranges from several decades to hundreds of years. However, for plastics that are not directly exposed to sunlight or lack of light and low humidity, the decomposition time is very long, can last up to 1000 years. Under the physical impact of flow, water force, velocity, temperature and water flow, plastic waste is crushed or crushed into powder. This decomposition takes a long time and takes a long time. In addition, substances with oxo-catalytic effects such as Alta, Chitosan, and D2W are available in the environment, weakening the plastic structure and possibly decomposing faster. In addition, when there is the impact of enzymes in the environment, plastic turns into CO_2 gas, water, humus, et cetera. The biological decomposition processes of plastic are very long and depends on environmental factors as well as the type of structure different plastic.

With the current increase in plastic waste, the assessment of microplastics in aquatic environments, especially continental surface waters is urgent. Regarding the current status of microplastic pollution, Vietnam does not have official statistics; However, several recent studies have determined the distribution and content of microplastics in sediment samples and water environments. Huynh Phu et al. (2021) published the first research results on the level of microplastic pollution in the water and sediment of the Saigon river and Dong Nai river, showing the appearance of microplastics in flakes and fibers, and microplastics from 0.1-5 mm in size [5]. Filamentous microplastics ranged from 228120 items.m^{-3} of water to a maximum of 715124 items.m^{-3} of water and in flakes from 11 items.m^{-3} to 222 items.m^{-3} of water, in sediments from 6.47±1.45 mg.kg^{-1} to 52.32±4.92 mg.kg^{-1}, average of 21.77±6.9 mg.kg^{-1}. The majority of these were PVC (accounting for 13.4%), PE (accounting for 51.2%), PP (accounting for 27.1%), and other [5]. In a study by Strady et al. (2020) on the Saigon river, the concentration of artificial fiber microplastics ranged from 22 to 251 items per 1 liter of water, regardless of influencing factors such as rainfall, water flow, and other abiotic factors [6]. It is estimated that from 115164x1012 to 164x1012 fibrous micro-plastics are discharged into the ocean from the Saigon river every year [7]. The Saigon river estuary system flows through major urban areas in Vietnam such as Ho Chi Minh City, analysis results on the Nhieu Loc - Thi Nghe Canal show that the total volume of microplastics is 11-43%. Fibrous and fragmented microplastics are 172000 to 519000 items.m^{-3} of water and 10 items.m^{-3} to 223 items.m^{-3}, respectively [8].

The purpose of the study is to evaluate the correlation of microplastic density according to the rising and falling tides of the day and the rainy and dry seasons of the year, specifically their shape characteristics. From there, we can predict the trend of microplastics according to tides and seasons in the future. Based on the results obtained, we propose a

circular economy model for the plastic industry as a basis, evaluating the feasibility of this model using expert scores through spider chart analysis of SWOT factors.

2. METHODS AND MATERIAL

2.1. Study sites



Figure 1. *Sampling sites*

Water sampling surveys and detailed information collected from spatial and temporal differences in plastic pollution to help identify the direct sources or dispersal sources of plastic particles. Direct sources, such as waste from densely populated areas, transported plastic waste from one river to another in the sampling area. The study was conducted on the Saigon river and Dong Nai river. The Saigon river branch from Dau Tieng Lake to the mouth of the Saigon river (The confluence of the Saigon river and Dong Nai river) and the Dong Nai river branch from Tri An lake to the confluence of the Saigon river and Dong Nai river. Water samples were denoted as follows: for the Saigon River branch in the order SGL.1, SGL.2, SGL.3, SGL.4, SGL.5, SGL.6, SGL.7, SGL.8, SGL.9, SGL.10, SGL.11, SGL.12, SGL.13; and the Dong Nai river was denoted as DNL.1, DNL.2, DNL.3, DNL.4, and DNL.5 (Figure 1). Coordinates of sampling locations are shown specifically in Table 1.

The sampling frequency was 6 months during the dry and rainy seasons per year. Samples were taken at high tide and low tide (twice per day). The dry season is from January to April and the rainy season is from May to December in Vietnam.

Table 1. Coordinates of surface water sampling sites in Saigon river and Dong Nai river

Symbol	X	Y	Symbol	X	Y	Symbol	X	Y
SGL.1	644827	1254580	SGL.7	686313	1199038	SGL.13	690745	1192026
SGL.2	658638	1233625	SGL.8	691208	1197649	DNL.1	738880	1239992
SGL.3	676392	1215574	SGL.9	691142	1195995	DNL.2	714121	1228955
SGL.4	679897	1214384	SGL.10	688430	1196061	DNL.3	702017	1203356
SGL.5	681022	1208298	SGL.11	687240	1192886	DNL.4	702810	1199387
SGL.6	684991	1205652	SGL.12	688430	1189976	DNL.5	701024	1192244

Sampling was carried out at high tide and low tide during the day, during the rainy and dry seasons in 2021 and 2022. A total of 144 water samples were preserved in dark glass bottles to avoid being affected by temperature or natural light and transported to the Nation Lab and Institute of Environment and Circular Economy Southern (IECES).

2.2. Method for determining micro-plastics in surface water samples in the laboratory

2.2.1. Procedure for extracting and analyzing water samples containing microplastics

The extraction and sample processing method was developed from the NOAA method [9]. The identification of microplastics in water samples was carried out according to the main steps (Figure 2), and water samples containing microplastics were removed from coarse impurities (> 5 mm) 300 mm sieve hole made of 304 stainless steel. After removing impurities, branches, and trash larger than 5x1000 µm remaining on the sieve membrane, the samples were dried (60°C). 30% Hydrogen Peroxide (H_2O_2) solution is added until the organic matter is completely decomposed and the solution is clear. Then, $ZnCl_2$ solution (d=1.6 $g.ml^{-1}$) was added to increase the density of the sample solution and separate the microplastic particles floating on top. The sample was transferred to a 15 ml centrifuge tube and centrifuged for 5 minutes. 0.45 µm filter paper was used to filter emerging microplastics. The sample was kept in a petri dish and continued to dry at 40°C for 48 hours, then observed under a microscope to quantify microplastics. Microplastics from each sample were counted and classified based on their shape into fibers, fragments, and particles. Simultaneously, the color of the microplastics was recorded (Picture 1).



Figure 2. *Procedure for analyzing micro-plastics in water samples*



Picture 1. *Sample extraction and drying*

2.3.2. Stereo microscope method

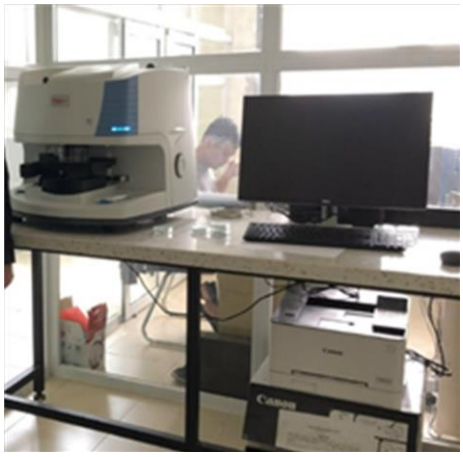
A Leica Stereoscope S6D (magnification 80X) combined with an HD camera was used. Microplastic morphologies (including size and color) were determined using the integrated LAS software.

2.3.3. Method for classifying microplastics

There are many ways to classify microplastics (by size, shape, color, etc.) Principles for classifying by type [7]: i) Microplastic fibers must be long fiber microplastics; ii) Microplastic pieces should be microplastics with any piece shape; iii) Granular microplastics are hard, flexible, angular microplastics or nearly spherical particles. As for the structure, not all microplastics must have an identical structure repeated inside (because it is an organic structure) and must present a clear and uniform color.

2.3.4. Fourier infrared spectroscopy (FTIR)

The types of microplastics were determined by Fourier transform infrared spectroscopy (FTIR). When exposed to infrared radiation, microplastics absorb radiation at specific wavelengths. The visual structure of the FTIR analyzer used to determine types of microplastics in the water samples is shown in Picture 2.



Picture 2. *FTIR analysis equipment*

To minimize the influence of resonance from "false microplastics" and additives, FTIR analysis of samples is 3 stages process: i) The stage one is to record the FTIR spectrum of a new microplastic sample to obtain basic FTIR traces; ii) The second stage is to record the same FTIR spectrum of the used microplastic sample; iii) The third and final stage is to subtract the new microplastic baseline, often called the new reference, from the used microplastic spectrum to obtain the difference spectrum.

2.4. Multivariate correlation analysis method

This method is used to evaluate the correlation between multiple variables at the same time. The coefficient of correlation is denoted in this study as r and is used to measure the magnitude of the relationship between two variables. The correlation coefficient (r) was estimated using Eq. (1) [10]:

$$r = \frac{\sum_{i=1}^{n}(x_i-\bar{x})(y_i-\bar{y})}{\sqrt{\sum_{i=1}^{n}(x_i-\bar{x})^2 \sum_{i=1}^{n}(y_i-\bar{y})^2}} \quad (1)$$

where x and y are two variables from n samples.

The correlation coefficient (r) is meaningful only if and only if the observed significance level is < 0.05.

2.5. Principal Component Analysis (PCA)

Principal component analysis can be used as a dimensionality reduction technique in which we form new variables that are linear combinations of the original variables. The simplest way to reduce the data dimensionality from D to k < D is to retain only the K most important elements.

Finding principal component (PCs) that are function of original variables:

$$PC_k = \delta_{1k}X_1 + \delta_{2k}X_2 + \cdots + \delta_{pk}X_p \quad (2)$$

We have p correlated variables: X_1, X_2, …, X_p obtained from n subjects. We want to find a method of transformation of X (n x p) matrix such that:

$$Y = \delta_1X_1 + \delta_2X_2 + \cdots + \delta_pX_p \quad (3)$$

Where,

Y (vector of k) is called "principal components"; δ (δ1, δ2, …, δp): vacteor of waeights such that:

$$\delta_1^2 + \delta_2^2 + \cdots + \delta_p^2 = 1 \quad (4)$$

→ Maximize the variance of data (X).

Find δ so that:

$$var(\delta^T X) = \delta^T var(X)\delta \quad (5)$$

The matric C=var(X) is actually covariance of X_i

The variance of Y (PC) is called an eigenvalue. According to the Kaiser criterion, PCs with eigenvalues > 1 and the number of PCs with a total variance explained between 50% and 70% were kept constant [10].

2.6. SWOT analysis method

The SWOT is a method of finding internal and external strengths, weaknesses, opportunities and challenges when applying a research model on plastic waste recycling. In addition, the authors used a concurrent expert method to evaluate the applicability of the circular economy model to the plastic products industry. This arcticle applied a scale from 1 to 5 to specifically evaluate the strengths, weaknesses, opportunities and threats.

3. RESEARCH RESULTS

3.1. Results of analysis of trends in their shape and existence over space and time in surface water of the Saigon river and Dong Nai river, Vietnam

Microplastic morphology collected from all sampling locations mainly showed the presence of three forms: fibers, fragments, and particles. The results are shown in Table 2.

Table 2. Shape status of microplastics appearing according to season

Year	Values	Dry season				Rainy season			
		Fiber items.m^{-3}	Fragment items.m^{-3}	Particle items.m^{-3}	Other items.m^{-3}	Fiber items.m^{-3}	Fragment items.m^{-3}	Particle items.m^{-3}	Other items.m^{-3}
2021	Minimum	171066	11939	10738	13279	22112	7532	22112	164543
	Maximum	576707	71495	50148	117670	69707	29545	69707	425126
	Mean	387496	44541	27231	37762	39269	19961	39269	325856
	Median	393327	46986	24579	32569	36739	20869	36739	351376
	Standard deviation	115631	16394	10533	24035	11528	5970	11528	75730
2022	Minimum	185483	12447	7658	7753	170621	11567	8585	20882
	Maximum	561563	82925	42374	87266	587850	59083	31923	91395
	Mean	381998	41773	23254	44233	396274	34335	21114	43848
	Median	405298	35762	23162	41158	406117	33242	22171	31406
	Standard deviation	116057	19484	9262	22192	114699	13072	7305	21804

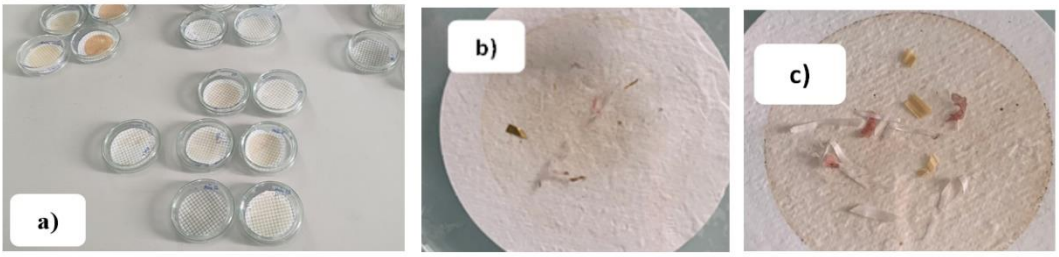
According to the results from Table 2, fibrous microplastics predominate in all seasons of the 2 survey years (average 387496 items.m^{-3}, and 381998 items.m^{-3}, respectively). Fibrous microplastics have many different sources, including laundry, discarded fabrics, unused masks, and abrasion of fibrous plastic products. Microplastics are easily affected by the wind, water currents, tides, temperature and erosion by hard substances (rocks, gravel, structures...) during flow migration. Average hydrological parameters in the rainy season and dry season of 2021 and 2022 in the downstream area of Saigon river and Dong Nai

river; densely populated areas such as Ho Chi Minh City, Binh Duong, and Dong Nai is shown in Table 3.

Table 3. Average seasonal hydrological parameters in the lower reaches of the Saigon river and Dong Nai river

Hydrological parameters	Dry season	Rainy season
Lighting time of day (hours)	11.7	12.2
Number of sunny hours per month (hours)	256	162
Number of sunny hours per day (hours)	8.5	6.6
Highest temperature (^oC)	38	34
Minimum temperature (^oC)	29	25
Relative humidity (%)	78	88
Amount of rain (mm)	14	225
Wind speed (m/s)	2.2	3.5
Highest water level (m)	1.61	1.71
Lowest water level (m)	-0.15	-0.13
Flow (m^3/s)	93.59 (Saigon river branch) and 780.65 (Dong Nai river branch)	

Actual images of the actual shape and color of microplastics in water samples after being dried on filter paper are shown in Picture 3.



Picture 3. *Micro-plastics on filter paper after drying*

a) Micro-plastic samples after drying; b) Micro-plastics on filter paper have many fibers and white particles; c) Plastic pieces with different colors.

The results of correlation analysis of microplastic shape variables and PCA in the 2 years 2021 - 2022 are shown in Figures 3 and 4.

Based on the results obtained after PCA analysis in R language, it has been shown that the first major contributions of microplastic shape in 2021 that satisfy the variance explanation percentage greater than 10% are PC1(56, 6%), PC2(23.8%) and PC3(12.7%). However, this study only selected the first two principal components because the total of these two components explained all 80.5% of the required data set. The blue vectors represent the relationships between the initial variables (microplastic shape) and the PCs, and the lengths of the vectors represent the correlation strengths of the variables with the PCs. According to the rotation matrix analysis results in Figure 3 shows that:

PC1 includes: Fibers (determination coefficient is 49%), fragments (56%) and particles (52.8%)

PC2 includes: Other forms (74.7%)

Representation of main component PC1:

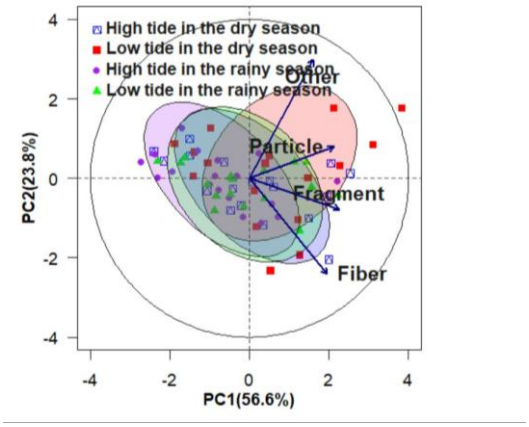
$$PC1 = 0.49Fiber + 0.56Fragment + 0.53Particle \quad (6)$$

Representing the main component PC2:

$$PC2 = 0.75\ other \quad (7)$$

```
> print(pc)
Standard deviations (1, .., p=4):
[1] 1.5049831 0.9764745 0.7116877 0.5244273

Rotation (n x k) = (4 x 4):
              PC1        PC2         PC3        PC4
Fiber     0.4900693  0.6031740  0.03015217  0.6285730
Fragment 0.5645086  0.1953144 -0.52973450 -0.6021326
Particle 0.5285401 -0.1991835  0.78366503 -0.2585351
Other     0.4022530 -0.7472344 -0.32301907  0.4189176
> summary(pc)
Importance of components:
                          PC1    PC2    PC3     PC4
Standard deviation     1.5050 0.9765 0.7117 0.52443
Proportion of Variance 0.5662 0.2384 0.1266 0.06876
Cumulative Proportion  0.5662 0.8046 0.9312 1.00000
```



a) *b)*

Figure 3. *Results of principal component analysis of microplastic shapes in 2021*

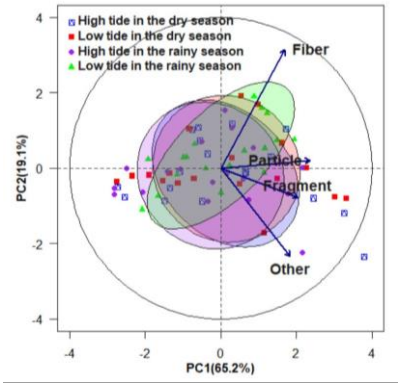
a) Results of correlation analysis between PCs and microplastic morphology in 2021;

b) Results of trend analysis of microplastic shape characteristics status in 2021;

Most types of microplastics at the surveyed sites are related to PC1 and PC2. When the study conducted data visualization using the first 2 components to represent the PCA analysis results for the appearance of microplastics in 2021, microplastics during the high tide of the dry season and at high tide and low tide of the rainy season are highly influenced by PC1 in PC1 values ranging from -2.5 to 2 (blue, green and purple elliptical clusters) and microplastics of the remaining shapes appear in the dry season at low tide.

```
> print(pc)
Standard deviations (1, .., p=4):
[1] 1.6147184 0.8748295 0.7016527 0.3674798

Rotation (n x k) = (4 x 4):
               PC1         PC2          PC3         PC4
Fiber     0.4255148  0.78690590  0.27508579 -0.3521989
Fragment 0.5112127 -0.19430465 -0.73889952 -0.3936175
Particle 0.5907643  0.05233241 -0.03357134  0.8044450
Other     0.4567233 -0.58334048  0.61418912 -0.2718260
> summary(pc)
Importance of components:
                          PC1    PC2    PC3     PC4
Standard deviation     1.6147 0.8748 0.7017 0.36748
Proportion of Variance 0.6518 0.1913 0.1231 0.03376
Cumulative Proportion  0.6518 0.8432 0.9662 1.00000
```



a) *b)*

Figure 4. *Results of principal component analysis of microplastic shapes in 2022*

a) Results of correlation analysis between PCs and microplastic morphology in 2022;

b) Results of trend analysis of microplastic shape characteristics status in 2022;

Mainly influenced by PC2, with PC1 value range from -1.5 to 2 (red elliptical cluster). In addition, PCA analysis results showed that the Saigon river and Dong Nai river basin was

affected by microplastic fibers, fragments and particles in both seasons. The content of fibrous microplastics from sources affecting river basins is very high. From there, this characteristic can be used for further research when analyzing the origin of microplastics and controlling their emissions.

Similar analysis for 2022, PCA results show that the Saigon river and Dong Nai river basin is affected by more fibrous and fine micro-plastics in both seasons of 2022. The content of fibrous micro-plastics from the source has a very high impact on river basins.

According to the rotation matrix analysis results in Figure 4 shows that:

PC1 includes: Fragments (51%), particles(59%) and other forms (45.6%)

PC2 includes: Fibers (78.7%)

Representation of main component PC1:

$$PC1 = 0.51Fragment + 0.59Particle + 0.46Other \quad (7)$$

Representing the main component PC2:

$$PC2 = 0.79Fiber \quad (8)$$

Thus, in the 2 years 2021-2022, the level of microplastic contamination in fibers and pieces is quite superior to other forms in all seasons of the year, 2022 is higher than 2021. There needs to be attention to the source that gives rise to microplastics of this type for timely control and management.

3.2. Results of microplastic analysis in Saigon river and Dong Nai river water samples using FTIR spectroscopy

Applying a combination of methods to more accurately determine microplastic components will be more effective for small-sized microplastic particles that cannot be directly identified optically. The spectrum collected from the device will be compared with spectral libraries to find the best match and determine the chemical composition of the microplastic species.The composition of microplastics in the sample was confirmed through the spectral peak data collected when running the sample (Figure 5).

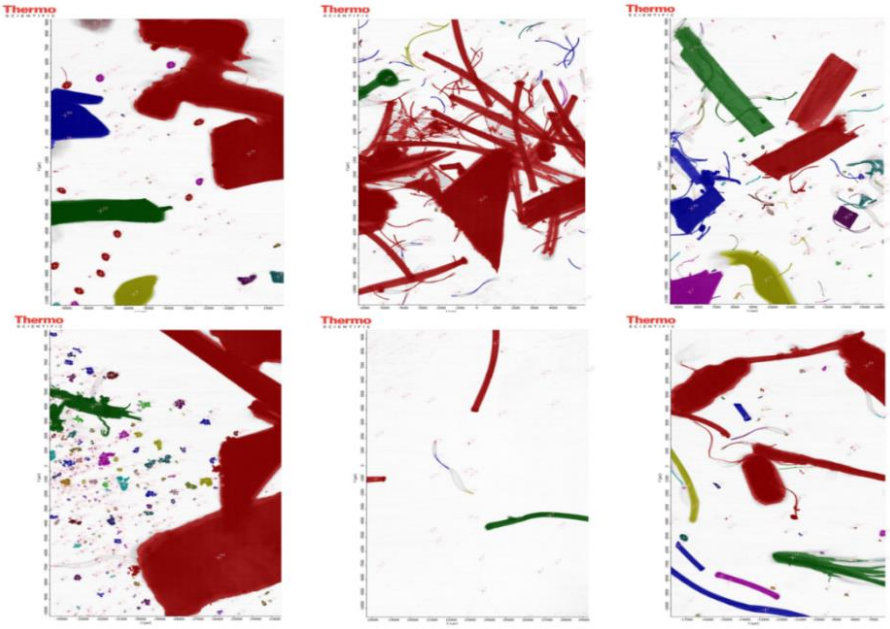


Figure 5. *The colors and shapes of micro-plastics in water samples were detected using an FTIR transform infrared spectroscopy device*

As a result of FTIR transform infrared spectroscopy analysis, the study discovered that 31 types of microplastics were found in water samples. This result is expressed and listed in Figure 6.

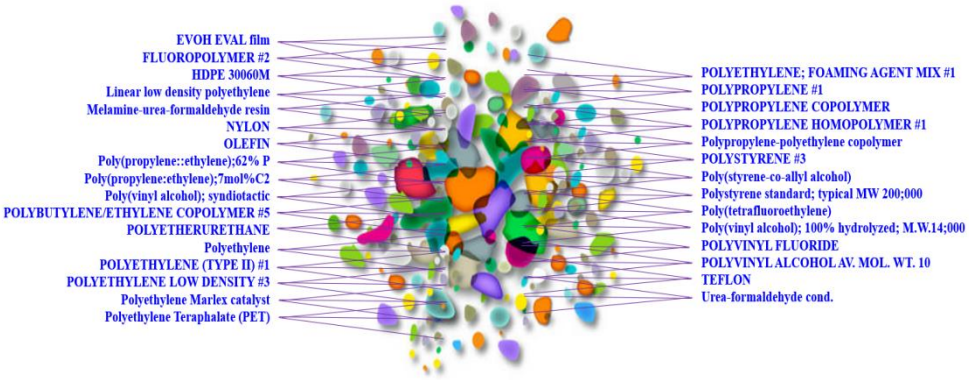


Figure 6. *Summary of plastic catalog detected in water samples under FTIR transform infrared spectroscopy*

3.3. Proposal to apply a circular economy model to reduce products plastic and microplastic

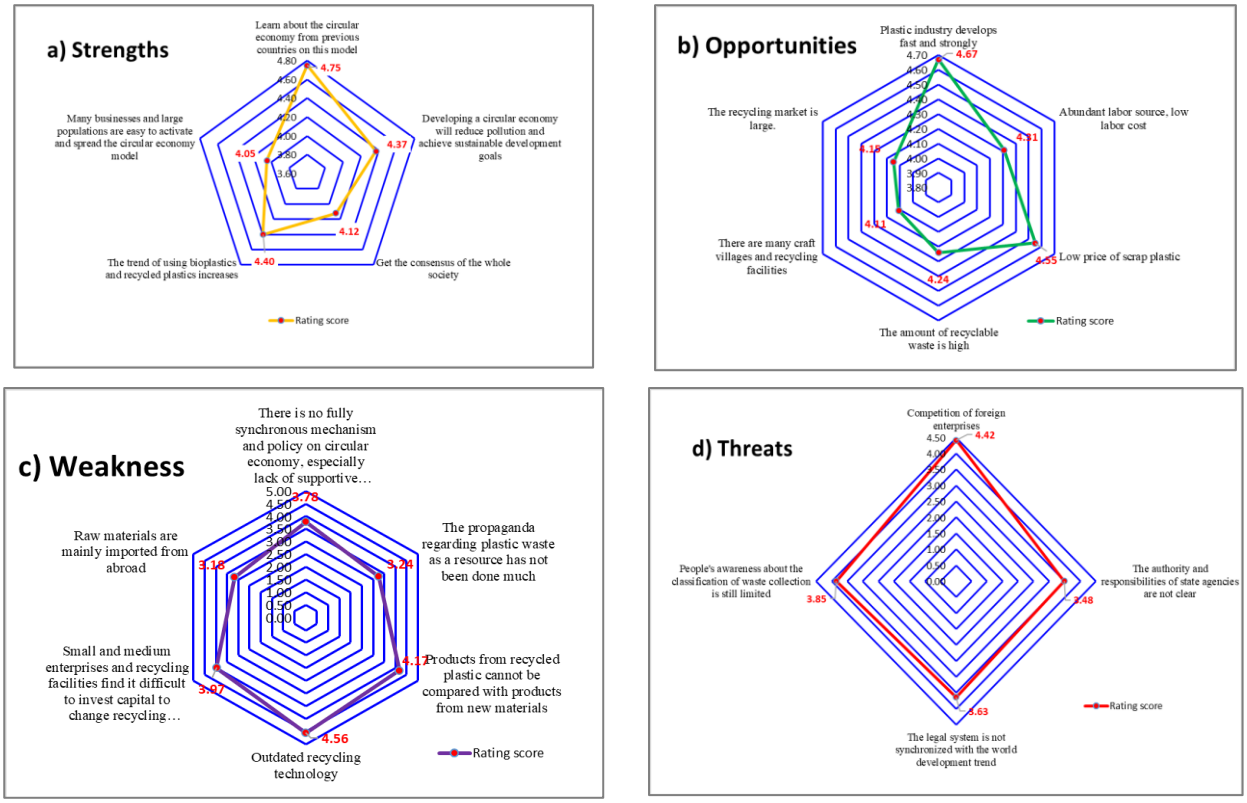
With a processing capacity of about 300 tons of waste/day, factories can create 450 tons of recycled plastic/month [11]. The current price of recycled plastic resins in Vietnam is about more than 10 million VND/ton [12]. This means that plastic waste can bring in a large amount of high profit. The study proposes a CE model for the plastic industry to reduce plastic-waste and micro-plastics generated in the water environment (Figure 7).



Figure 7. *A Circular Economy model for the plastic industry is proposed*

Analyzing the circular plastic economy has six points to note: i) Through redesign, new manufacturing and new distribution processes, plastic products are prioritized for elimination; ii) Models of reusing and reducing the use of single-use plastic products need to be promoted; iii) Plastic products can be reused or recycled 100%; iv) Plastic products are all reused, recycled or biodegradable in practice; v) The use of plastic is completely separate from the consumption of finite resources; vi) Strictly enforce that all plastic

products are free of toxic chemicals and respect the safety and rights of all parties. The opportunities, advantages, difficulties and challenges in applying a circular plastic economy to reduce plastic waste and microplastic pollution in the environment are analyzed in Figure 8. Evaluation results are based on ideas. Expert opinions and SWOT analysis are evaluated on a scale of 1 to 5 reflected on the spider chart (Figure 8).



Figures 8. *Spider chart on SWOT assessment in applying circular economy to plastic industry a) Strengths; b) Opportunities; c) Weakness; d)Threats*

The Rada chart in Figure 8 showed the possibility of favorable factors and the opportunity to apply circular economy in the plastics industry is quite high (Figures 8a and 8b). It should be noted that the plastic product manufacturing industry is a fast-growing and strong industry both now and in the future. Therefore, cheap plastic waste can become a potential raw material for recycled plastic products, providing large financial capital for plastic businesses. Besides, the trend of using cheap recycled plastic products will meet many types of life needs and strongly demonstrate a huge culture of environmental protection. However, the difficult and challenging factors that need to be improved and paid more attention are that domestic recycling technology is outdated, small scale, rudimentary technology, and low recycling efficiency; resulting in low quality products (Figures 8c and 8d).

From the analysis results in Figure 8, regarding the plastic industry's roadmap to transition to a circular economy, it is necessary to establish specific goals regarding the desired results and the main steps or stages to be achieved. It is important to unify stakeholders and partners involved in the plastics value chain and collaborate on the design, use and reuse of plastics. Based on the contents mentioned, create a circular economy for plastic waste and the plastic manufacturing industry, minimize plastic waste into the environment, especially controlling the density of microplastics from this source in future. The roadmap also needs to be clearly defined in the supply chain, looking for internal

opportunities to reduce plastic waste, reuse and recycle materials to continue making plastic products to serve people. The development of new technology and new techniques will create products, services and supporting industries based on circular economy business models.

4. CONCLUSIONS

Plastic products are increasing day by day despite the Government's Decree and many documents from the Ministry of Natural Resources and Environment on minimizing plastic products and moving towards not using plastic packaging. However, because of the convenience of packaging and disposable household items, plastic products continue to increase, thereby increasing the amount of plastic and microplastic waste.

The Saigon River and Dong Nai River basins are densely populated areas, with many industrial parks and industrial clusters, and the consumption level of plastic product packaging can be said to be the largest in the country. Floating plastic waste collected annually on main urban canals in Vietnam accounts for from 2x1000 to 13x1000 tons [3]. Accordingly, the amount of waste also increases. Through research surveys, it has been shown that plastic waste collected and processed for recycling is still very limited, only accounting for about 27%. The amount of waste haphazardly discharged from residential areas in the two river basins is very large. In the dry season, the amount of garbage on both river banks is large, and in the rainy season it flows into the river; Therefore, during the rainy season, microplastics of many different shapes and sizes appear in river water, of which fiber microplastics make up the majority. The majority of these were PVC (accounting for 13.4%), PE (accounting for 51.2%), PP (accounting for 27.1%), and other [5]. In a study by Strady et al. (2020) on the Saigon river, the concentration of artificial fiber microplastics ranged from 22 to 251 items per 1 liter of water, regardless of influencing factors such as rainfall, water flow, and other abiotic factors. Predictive research results have shown that the density of microplastics, especially fibrous microplastics, tends to increase over time. There were seasonal differences, higher in the rainy season and in the dry season of the year, and the amount of microplastics was higher at high tide and in the rainy season.

The research results of the article are the basis for proposing and applying the proposed circular economy model in the plastic industry. With SWOT analysis, the ability to deploy circular economy for the plastic industry is very feasible. The source of scrap plastic products collected at cheap prices and abundant supply is a potential source of raw materials for recycled plastic products, creating a large source of financial capital for businesses. With a processing capacity of about 300 tons of waste/day, factories can create 450 tons of recycled plastic/month [11]. The current price of recycled plastic resins in Vietnam is about more than 10 million VND/ton. The transition to a circular economy is considered the most promising path to reducing plastic and microplastic pollution in the water resources of the Saigon and Dong Nai rivers.

REFERENCES

[1] Barnes, D. K. A., Galgani, F., Thompson, R. C., & Barlaz, M. (2009). Accumulation and fragmentation of plastic debris in global environments. Philosophical Transactions of the Royal Society B: Biological Sciences. Jul 27; 364(1526): 1985–1998.

Doi: 10.1098/rstb.2008.0205;

[2] Report on the current status of plastic waste in 2022. Expert consultation workshop. The Pollution Control Department (Ministry of Natural Resources and Environment) coordinates with the International Cooperation Organization for Nature Conservation (WWF) in Vietnam;

[3] Kieu Le, T. C., Strady, E. & Perset, M. (2016). Life Cycle of Floating Debris in the Canals of Ho Chi Minh City (PADDI);

[4] Phu, H.; Han, H.T.N, Thao, N.L(2022). Plastic waste, microplastics in the Saigon – Dong Nai river basin, the risk of impacts on the health of people. Hydrometeorological Journal. ISSN 2525-2208.DOI: 10.36335/VNJHM.2022(736(1)).14-27;

[5] Phu, H.; Han, H.T.N; Thao, N.L; Dong, DV; Han, T.G. (2021). Study on the level of microplastic pollution in water and sediments of Saigon–Dong Nai river. Hydrometeorological Journal. ISSN 2525-2208. DOI: 10.36335/VNJHM.2021(731).69-81;

[6] Strady, E. et al. (2021). Baseline assessment of microplastic concentrations in marine and freshwater environments of a developing Southeast Asian country, Viet Nam. Marine Pollution Bulletin. Elsevier BV. Doi:10.1016/j.marpolbul.2020.111870;

[7] Strady, E., Dang, T.H., Dao, T.D., Dinh, H.N., Do, T.T.D., Duong, T.N., Duong, T.T., Hoang, D.A., Kieu-Le, T.C., Le, T.P.Q., Mai, H., Trinh, D.M., Nguyen, Q.H., Tran-Nguyen, Q.A., Tran, Q.V., Truong, T.N.S., Chu, V.H., Vo, V.C., (2021). Baseline assessment of microplastic concentrations in marine and freshwater environments of a developing southeast Asian country, Viet Nam. Mar. Pollut. Bull. 162, 111870;

[8] Lahens L, Strady E, Kieu-Le Tc, Dris R, Boukerma Kada, Rinnert Emmanuel, Gasperi J, Tassin B (2018), Macroplastic and microplastic contamination assessment of a tropical river (Saigon River, Vietnam) transversed by a developing megacity, Environmental Pollution, Volume 236 Pages 661-671, http://dx,doi,org/10,1016/j,envpol,2018,02,005;

[9] NOAA. (2015). Methods for the Analysis of Microplastics in the Marine Environmet Recommendations for quantifyling synthetic particles in water and sediments. Technical Menmorandum NOS-OR&R-48

[10] Tuan N. V (2014). Data analysis with R. Publishing House General TP. HCM. pp 145-148;

[11] IFC & World Bank Group (2021). Vietnam market research: plastic circularity, opportunities and barriers. Link: https://www.ifc.org/wps/wcm/connect/7610d60f-eb79-4dca-9592-d1853048792b/Market+Study-Vietnam+Plastic+Circularity-Appendices.pdf?MOD=AJPERES&CVID=nMRr8PX (Accessed updated October 15, 2023);

[12] IANFA (2023). General price list of recycled plastic granules 4/2023. Link: https://ianfa.vn (Accessed updated October 15, 2023);

[13] La, V. P. et al. (2020). Policy response, social media and science journalism for the sustainability of the public health system amid the COVID-19 outbreak: The vietnam lessons. Sustainability (Switzerland), 12(7). https://doi.org/10.3390/su12072931

[14] Phu, H.; Han, H.T.N; Hue, N. T. (2023). Developing a circular economy from plastic waste and identifying microplastics in drinking and domestic water supplies in Ho Chi Minh City and Southeast provinces. The 3rd International Conference on Environment,

Resources and Earth Sciences (ICERES 2023). Green and Nature-based Solutions for Environmental Sustainability and Resources Management. Ho Chi Minh City University of Technology, Vietnam National University-Ho Chi Minh City, October 21st, 2023;

[15] Idumah, C.I.; Nwuzor, I.C. Novel trends in plastic waste management. SN Appl. Sci. 2019, 1, 1–14.Gibb, B.C. Plastics are forever. Nat. Chem. 2019, 11, 394–395;

[16] Goldstein, M.C., Goodwin, D.S., 2013. Gooseneck barnacles (Lepas spp.) ingest microplastic debris in the North Pacific Subtropical Gyre. PeerJ 1, e184. http://dx.doi.org/10.7717/peerj.184.

[17] Kristian Syberg, Maria Bille Nielsen, Nikoline B. Oturai, Lauge Peter Westergaard Clausen, Tiffany Marilou Ramos, Steffen Foss Hansen (2022). Circular economy and reduction of micro(nano)plastics contamination. Journal of Hazardous Materials Advances. Volume 5, February 2022, 100044

[18] Seyed reza seyyedi, Elaheh Kowsari, Seeram Ramakrishna, Mohammad Gheibi, Amutha Chinnappan (2023). Marine plastics, circular economy, and artificial intelligence: A comprehensive review of challenges, solutions, and policies. Journal of Environmental Management Volume 345, 1 November 2023, 118591. https://doi.org/10.1016/j.jenvman.2023.118591

[19] George Bishop, David Styles, Piet N.L. Lens (2020). Recycling of European plastic is a pathway for plastic debris in the ocean. Environment International Volume 142, September 2020, 105893, https://doi.org/10.1016/j.envint.2020.105893

[20] View PDFView articleView in ScopusGoogle ScholarCollins, 2019

[21] Collins, C., 2019. The Global Environmental Recycling Crisis. What Options Exist for Plastic Waste? Washington, DC.

[22] Emmerik and Schwarz, 2020. Plastic debris in rivers. WIREs Water, 7 (2020), 10.1002/wat2.1398

THE OPTIMAL SOLUTION FOR DOMESTIC WATER ON THE DONGVAN KARST PLATEAU, HAGIANG, VIETNAM

Le Canh Tuan[1], Pham Trung Hieu[2,3], Cao Minh Thuỷ[1]
[1]Hanoi University of Natural Resources & Environment
[2]Faculty of geology, University of Science
[3]Vietnam National University Ho Chi Minh city
Corresponding author: lctuan@hunre.edu.vn

Abstract: Karst regions are characterized by their intricate topography, abundance of caverns, challenging access, and regular dry-season water shortages. The Dongvan Karst Plateau (DVKP) region is primarily composed of limestone, according to the findings of our research, and it contains karst landforms ranging in elevation from 300 meters to about 2000 meters. Based on their heights, the 300–600 m, 600–900 m, 900–1200 m, 1200–1500 m, and 1500–2000 m cave floors can be distinguished. There are five distinct levels at which karst caves can be found: 300–600 m; 600–900 m; 900–1200 m; 1200–1500 m; and 1500–2000 m. Because the DVKP region frequently experiences a shortage of water during the dry season, it is also known as "the land of thirst".. Geologists have found that the Ma Le cave system at 1150m always has water. Accordingly, the idea of pumping water based on altitude difference was born. When there is water, the lives of people in DVKP are revived. For the first time, DVKP of Vietnam has successfully applied: the "water pumping solution that does not use electricity. The authors would like to introduce the successful research cooperation of Vietnamese, Belgian and German geologists in the DVKP region. The results of this study can be applied to karst areas with similar structures to the DVKP area.

Key words: Ground water, cave, karst, Ma Le cave, ***Dongvan Karst Plateau.***

1. INTRODUCTION

North Vietnam's Hagiang province is mountainous, covering an area of roughly 7,945.8 km². It shares boundaries with Tuyen Quang province to the southeast, Lao Cai province to the west, Cao Bang province to the east, and China to the north. With a total area of roughly 2380 km2, the DVKP in the province of Hagiang is primarily made of limestone and has a complicated topographical structure with numerous unique cave floors. During the dry seasons, it is commonly

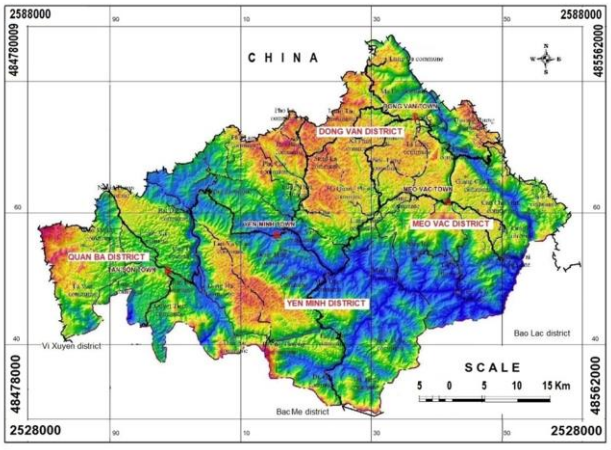


Figure 1. *Location of the Dongvan Karst Plateau in Hagiang Province of Vietnam*

assessed as a place lacking in water (Figure 1). Our purpose is to find water in karst caves, serving the water supply for people in DVKP. Therefore, the limestone area is of particular interest to us.

Research on water resource management for sustainable development has interested many scientists [1, 3, 4, 7, 8, 9]. Finding freshwater in the karst is extremely challenging and sometimes even unsuccessful. There have been many solutions to overcome the water shortage at DVKP, such as building concrete tanks or small hydroelectric dams, but there has been no success so far as building concrete tanks on limestone often causes water to drain out (Figure 2) or water supply for operating small hydroelectric dams is not sufficiently maintained. Geologists have recently found a water source at an altitude of 1150 m in the Ma Le cave system to help DVKP meet water needs for daily life and sustainable development. Finding the existence of karst water at an altitude of 1150m gave geologists an idea: to take advantage of the difference in altitude to design "Water pump does not use electricity".



***Fig 2**. A concrete tank without water during the dry seasons in DVKP*

2. MATERIAL AND METHODS

2.1. Material

The data in this article have been compiled from geological documents on geomorphology, karst hydrogeology, and tectonics of the DVKP region [2, 5, 6, 10, 11].

In addition, the SPOT5 satellite image documents are incorporated as an important input, helping us to build a digital elevation model (DEM).

2.2. Pre-investigations research

This is an important task helping us to orient and locate the important positions that need to be approached when conducting field investigations. Indoor data analysis helps us save time, effort, and money that may be required for field investigations. The indoor approaches include:

- Data acquisition: We reviewed all sources of documents related to the study area. Especially documents related to karst and karst hydrology.
- Analyzing satellite images, geological maps, and topographical maps
- Research geological, hydrogeological, and geomorphological documents and the available results of cave investigations.
- Building DEM

From the DEM model combined with satellite image analysis, we build component maps such as:

- Slope map;
- Lithological map showing the distribution of rock types;
- Terrain sections;

- Distribution of sinkholes and caves.

2.3. field investigations

- We investigated and researched on geological structures, hydrogeological characteristics, and distribution of caves were conducted throughout the study area to classify karst caves according to different elevations.

- From the results obtained, we identify capacity areas of water storage, flow measurement, and investigations of the water quality that were implemented to serve the water supply for DVKP.

2.4. Cave investigations

Fieldwork in our DVKP area includes searching for water in the cave and taking samples.

3. RESULTS

3.1. Geological setting

The DVKP area has a complex geological structure. Participating in the geological structure of the DVKP area includes karst and non-karst rocks. The main karst rocks are limestone of the Bac Son formation (C-P *bs*), Dong Dang formation ($P_3đđ$), the no karst rocks include those of the Chang Pung Formation (€ 3 *cp*), Lutxia (O_1 *lx*), Song Cau (D_1sc), Hong Ngai (T_1 *hn*) and Song Hien Formation (T_1 *sh*) [2; 5].

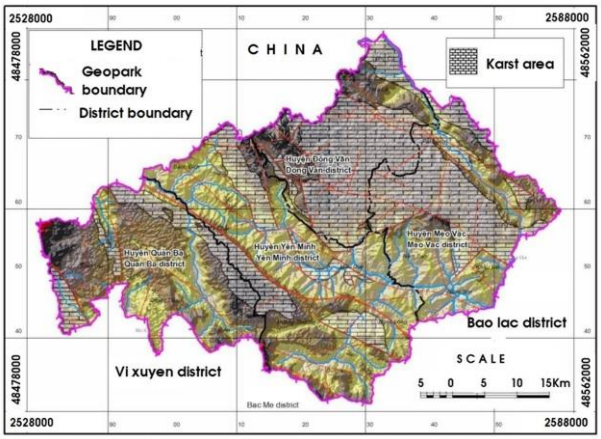


Fig. 3. *Distribution carbornate rocks*

Our research object is the limestone area, so all the above geological formations are divided into 2 groups of rocks: the karst rock group and the non-karst rock group (Figure 3). Figure 3 is obtained from the DEM.

3.2. Distribution of limestone and karst caves

Our purpose is to find water in karst caves, serving the water supply for people in DVKP. Therefore, the limestone area is of particular interest to us. From geological data, combined with satellite images, the limestone distribution area of DVKP is obtained from the DEM (table 1).

Table 1. Statistics of carbonate rocks in the study area.

No	District	Area (km^2)	Areas with carbonat rocks (km^2)
1	Dong Van	460.0	329.7
2	Meo Vac	577.6	287.1
3	Yen Minh	785.2	178.2
4	Quan Ba	557.2	108.5
	Total	2380	903.5

Thus, limestone accounts for 40% of the total area of DVKP.

Based on the available research results, the number of karst caves and sinkholes was also determined by DEM (table 2).

Table 2. Distribution of sinkholes according to height classes

Height class (m)	Number of caves	number of sinkholes
0-300	0	0
300-600	20	15
600-900	17	53
900-1200	31	391
1200-1500	28	652
1500-2000	17	188
Sum	**103**	**1299**

Thus, the karst caves are concentrated at 2 elevation levels: (1) from 900 to 1200m and (2) from 1200 m to 1500 m.

3.3. Results of karst cave investigations

With the efforts of Vietnamese and Belgian geologists, we have found the Ma Le cave system distributed at an altitude of about 1150 m [6, 10, 11]. The wonderful thing is that the Ma Le cave system has water all year round. This is where the freshwater supply serves the needs of the DVKP area. Nho Que river is at an altitude of 350-400 m (depending on different locations), so the height difference between Ma Le cave system and the Nho Que river ranges from 750 to 800 m. People live in the DVKP area where the highest point is about 1200 m. Therefore, Ma Le cave system completely meets our requirements.

Our survey shows that, in the dry seasons, the water flowing from Ma Le cave to Seo Ho Stream reaches 101 l/s to 137 l/s. The water will be collected, flowing into the drainage ditch to return to the clarifier. (fig 4. Fig 5).



Fig 4. *Water from Ma Le cave system flowing into Seo Ho stream in the dry seasons reaches 120 l/s*



Fig 5. *A water channel from Ma Le cave system to clarifier*

Water samples in the Ma Le cave system were also collected during the survey. The results of the analysis of indices such as pH, TDS, $CaCO_3$, Fe, Chlorite, Pb, and COD have been evaluated to meet Vietnam's water standards.

3.4. Water supply plan for DVKP area

Research on karst geology has been conducted by Vietnamese and Belgian geologists since 1995. The idea of finding a karst cave with water at DVKP has been cherished by us

for a long time, now come true. This is the basis for us to implement the science and technology cooperation project with Germany in finding solutions for sustainable water supply in high mountains and for water scarcity in Hagiang province. All work such as designing water pumps, water tanks, and pressure tanks has been done by the Kawatech project and completed since 2019. The KaWaTech project has a power of 19 liters/s, providing about 1,800m3 of water/day, the pressure pipeline is about 2.5km long. The diagram illustrating a non-electric water pump solution at DVKP is presented in figure 6.

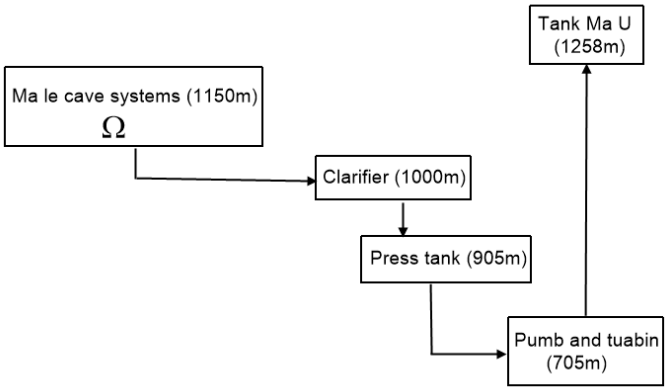


Fig 6. *The diagram illustrating a non-electric water pump solution at DVKP, Hagiang, Vietnam*

3.5. Why does Ma Le cave system at an altitude of 1150m often have water even in the dry season?

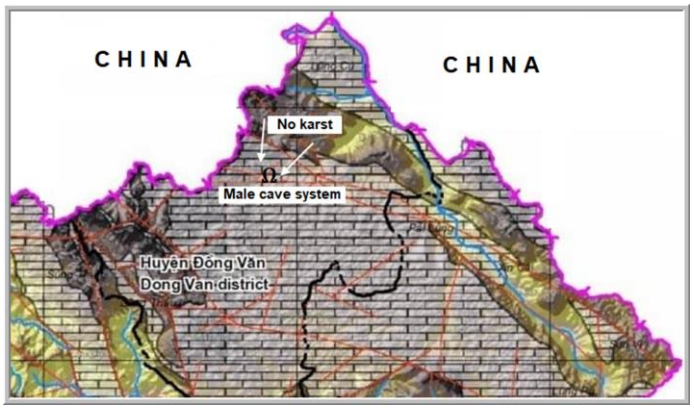


Fig 7*. Male cave system is supplied with water from the no -karst area*

Section 3.1 shows that the DVKP region is an area with a complex geological structure, with many different types of rocks. The no -karst rocks are distributed in the north of the male cave system at altitudes from 800m to 1700m (fig 7). The characteristics of karst areas are water shortage in the dry season and water abundance in the rainy season, but the water drains very quickly through fault systems, caves, fructured, dolines and vertical shafts, going down into underground caves. However, the Male cave system always has water because the water is supplied from the no- karst area.

The no-karst area is located at an altitude of 800m to 1700m, formed from rocks of Mia Le formation, and Song Cau formation, mainly composed of clayish siltstone, marlaceous shale, conglomerate, sandy siltstone, and clay shale. Thus, the diversity and complexity of geology is the reason why Male cave system has water all year round.

4. CONCLUSION

Research on the distribution of karst caves at DVKP serving the search for freshwater has become real. The existence of 5 levels of caves has created enough potential energy to lead water from the Ma Le cave system to a height of 1258m. The Ma U reservoir at this altitude

is where water is distributed to the Dong Van Karst Plateau, overcoming water shortages in the dry season. Currently, Dong Van Karst Plateau has been given the new name "Dong Van Karst Plateau Geopark", Non-electric water pumping solution can be applied to limestone mountain areas with similar geological structures as the Dong Van Karst Plateau. This is an optimal solution, serving environmental protection and sustainable development.

REFERENCES

[1]. Antonov , V. V. (2012). Environmental factors in case of appraisal of groundwater resources. Journal of Mining Institute, 197, 184. Retrieved from https://pmi.spmi.ru/index.php/pmi/article/view/5988

[2]. Dang, T. H et al (2007). Stratigraphical Phanerozoic sediments in the Northeast, storage General Department of Geology and Minerals of Vietnam

[3]. Golovina E. I., Grebneva A. V. (2021). Management of groundwater resources in transboundary territories (on the example of the Russian Federation and the Republic of Estonia). Journal of Mining Institute 2021. Vol 252,p 788 -800 . DOI:10.31897/PMI.2021.6.2

[4]. Kurilenko , V. V., & Zhdanov , S. V. (2013). Problems of water management in Izhora ground water deposit. Journal of Mining Institute, 200, 216. Retrieved from https://pmi.spmi.ru/index.php/pmi/article/view/5792

[5]. Le. V, G et al. (1997). Geology and Minerals of Yen Minh sheet group, scale 1:50,000, storage General Department of Geology and Minerals of Vietnam

[6]. Masschelein, J., Coessens V., Lagrou D., Dusar M., Tran T.V. (2007). Northern Vietnam 1993 – 2006 (Belgian-Vietnamese Speleological Projects in the Provinces of Bac Kan, Hagiang, Hoa Binh, Lai Chau and Son La). Berliner Höhlenkundliche Berichte 22, 1-212.

[7]. Pashkevich , N. V., & Golovina , E. I. (2014). Topical issues of the management of extraction of underground waters on the territory of the Russian Federation. Journal of Mining Institute, 210, 99. Retrieved from https://pmi.spmi.ru/index.php/pmi/article/view/5271

[8]. Ravbar, N., and Košutnik, J. (2014). Variations of karst underground air temperature induced by various factors (Cave of Županova jama, Central Slovenia): Theoretical and Applied Climatology, v. 116, p. 327–341. https://doi.org/10.1007/s00704-013-0955-4

[9]. Shannon D. Williams,William J. Wolfe,James J. (2006). Farmer. Sampling Strategies for Volatile Organic Compounds at Three Karst Springs in Tennessee. https://doi.org/10.1111/j.1745-6592.2006.00044.x

[10]. Tran T, V et, al. (2004). Karst Water Management in Dong Van and Meo Vac Districts, Hagiang Province, Vietnam. Contribution of Geological and Speleological Investigations-Trans- KARST 2004, Proceedings of the International Transdisciplinary Conference on Development and Conservation of Karst Regions, Hanoi, Vietnam, 13-18.9.2004,p. 265-271; Hanoi.

[11]. Tran, T. V et al. (2011). Final report “Investigate, research Geo-heritages and offer to build Geopark in Northern Vietnam”. No KC.08.20/06-10. Storage Vietnam Institute of Geosciences and Minerals Resources.

FORMULA FOR ASSESSING THE LOADING CAPACITY OF THE TOURISM ENVIRONMENT AND RESULTS OF APPLYING THE WORLD NATURAL HERITAGE PHONG NHA - KE BANG AREA, VIETNAM

Le Nam[1], Tran Nghi[2], Dinh Xuan Thanh[2], Trinh Hoai Thu [3*], Nguyen Dinh Thai[2], Dao Bui Dinh[1]

[1]Ministry of Natural Resources and Environment; Email: lenam.monre@gmail.com

[2]VNU-University of Sciences

[3*]Institute of Marine Geology and Geophysics-VAST; Email: *ththu@imgg.vast.vn

Abstract: Any tourist area can be considered a geo-ecosystem, they are limited to a certain geographical space. That system could be a coastal resort area, a mountain resort area, or the Phong Nha-Ke Bang cave heritage area. This report includes 2 contents: (1) establish a formula to evaluate the Load Capacity for all tourism environments: Lc = 1- A/B. In which: Lc is the load capacity value of a member object. Lc is a dimensionless coefficient and varies from 0 (min) to 1 (max). The number 1 refers to the member object that has never had any negative impact on them; A is the value of real negative load; B is the critical standard value allowed by Vietnam. The Load Capacity of an entire geo-ecosystem is calculated according to the following formula: Lcav = 1/n (Lc1+ Lc2+ …+ Lcn). In which: Lcav is the average bearing capacity of the entire geo-ecosystem; Lc1, Lc2... are the medium load capacity value of member objects, n is the number of member objects in the geo-ecosystem. (2) The results of applying the formula for assessing the load capacity of the tourism environment of the World Natural Heritage "Phong Nha-Ke Bang National Park" Quang Binh Vietnam are as follows: (1) the heritage tourist area has Lci value varies from 0.49 to 0.99; Lcav value is 0.78. Thus, compared to Vietnamese standards, the heritage area's tourism Load Capacity has a surplus of 78% to reach the critical capacity (Lcav=0). Balancing the correlation matrix between Lci values of member objects will allow managers to pay attention to increasing the Load Capacity of motel and hotel objects that have the lowest value (<0.5).

Keywords: *Phong Nha – Ke Bang, carrying capacity, load capacity, tourism, environment, geo-ecosystem.*

1. INTRODUCTION

Vietnam is a country with outstanding tourism resources. Currently, Vietnam is developing strong tourism based on the advantage of a 3.260km long coastline with many beautiful high-quality beaches, famous World Natural Heritage sites such as Ha Long Bay and Phong Nha -Ke Bang, Dong Van Karst Plateau Geopark, and a variety of landscapes, historical sites and national parks attract more and more tourists. However, in the period of global climate change, Vietnam is one of the countries most strongly affected by extreme climate change. That makes scientists and managers pay attention to the problem of assessing the carrying capacity of the tourism environment. The general trend in the world as well as in Vietnam is to quantify the carrying capacity of tourist areas.

WTO (1994) defines carrying capacity as follows: “Carrying capacity is the level of living requirements of visitors that an area can provide”. Luc Hens (1998): "Carrying capacity is the maximum number of visitors that a tourist area can serve".

Cifuentes (1992) and Zacaria (2011) have proposed two formulas to calculate the carrying capacity of the tourism environment as follows:

(1) PCC= Ax1/BxRf. In which PCC is the physical carrying capacity (maximum number of passengers per day); A- area used for tourists; B- usable area for 1 tourist;

(2) RCC =PCCxCf1xCf2x…Cfn. Where RCC is the real carrying capacity (Real Carrying Capacity). Cf1…Cfn is a regulatory factor.

In Vietnam, Tran Nghi (2005) applied this formula to calculate the bearing capacity for the Phong Nha - Ke Bang heritage tourist area. However, the calculated results are still semi-quantitative and not convincing. Because the input values according to this formula are not experimental observation or analysis values, they are inaccurate, have low reliability, and depend on the subjective opinions of each different author.

2. METHOD TO ESTABLISH FORMULA FOR CALCULATING ENVIRONMENTAL LOAD CAPACITY

The author's approach to this report is aimed at quantifying the load capacity of the environment in general, so it is not called "Carrying Capacity" but "Load Capacity" calculated according to a formula for each member object of the same geo-ecosystem and according to the formula for an entire geosystem space. As a result, the dimensionless coefficients vary in a finite range from 0 (min) to 1(max). This formula applies to all different areas. The results of applying this formula to calculate the load capacity of the Phong Nha - Ke Bang tourism environment are very positive and convincing to managers. The most important thing about the formula must meet two criteria: (1) the main input quantities are member objects in the geo-ecosystem, including natural and socio-economic objects representing the tourism area; (2) those quantities obtained must be based on observation, statistics and experimental analysis over a certain period of time. Negative factors that damage natural and socio-economic objects are (1) heavy metals polluting the surface water and underground water environment such as Cu, As, Pb, Zn, Cd, Hg...; (2) coastal and river bank erosion due to storms, floods and rising sea levels; (3) the destruction of infrastructure in coastal tourist areas and heritage and conservation areas due to increasing frequency and intensity of floods and storms; (3) arbitrary activities of craft villages pollute surface and underground water sources; (4) building dikes and hydroelectric dams causes ecological imbalance and lack of alluvial sources, increasing riverbank and coastal erosion. Thus, the natural and socio-economic environments are facing increasing negative impacts. This report would like to introduce a formula for calculating the environmental load capacity and possible application results for the tourist area "Phong Nha - Ke Bang National Park Heritage in Quang Binh Vietnam". Hopefully, this research direction will be replicated in other tourist areas in Vietnam to improve effective solutions in responding, minimizing, and adapting to current and long-term extreme climate change.

The scientific basis for formulating the formula to calculate environmental load capacity 1) Formula to calculate the load-bearing capacity of a member object Based on the interactive relationship between the load-bearing capacity of a member object, the negative impact factors and the load-bearing limit threshold according to Vietnam's prescribed standards can be expressed by a formula as follows: Lc = 1- A/B (1) In which: Lc - Load capacity of a member object (Load Capacity); A – Negative load value; B – Limit value of the member object. This value is regulated by Vietnam and internationally. In Vietnam, it is

called QCVN When A=0 then A/B=0◊ Lc=1. That is, the members have not suffered any negative impacts When A/B < 1, Lc > 0: the member object is still able to bear the load; When A/B = 1, Lc = 0: the member object begins to reach the load-bearing threshold and is also capable of self-recovery; When A/B > 1, Lc < 0: the member's load-bearing capacity is exceeded. If there is no positive intervention, the load-bearing capacity will have an increasing negative value. At a certain value and a certain time, the member object will be completely degraded and lose its ability to recover.

When A/B > 1, Lc < 0: the member's load-bearing capacity is exceeded. If there is no positive intervention, the load-bearing capacity will have an increasing negative value. At a certain value and a certain time, the member object will be completely degraded and lose its ability to recover.

The load-bearing capacity of any object from land to sea can be calculated using the above formula. The value Lc is a dimensionless coefficient because A and B are always of the same dimension so the result of the A/B ratio becomes a dimensionless decimal number.

The general formula to calculate the value of the carrying capacity of an entire geo-ecosystem:

$$Lcav = 1/n\ (Lc1 + Lc2 + \ldots + Lcn) \quad (1)$$

In which: Lcav – Average carrying capacity of the entire geo-ecosystem

Lc1, Lc2…Lcn- Load capacity of member objects.

n – Number of member objects

3. THE RESULTS APPLYING TO THE PHONG NHA-KE BANG TOURISM AREA

3.1. Introduction to the World Natural Heritage site "Phong Nha-Ke Bang National Park"

The World Natural Heritage Phong Nha-Ke Bang National Park occupies an area of 200,000 hectares, located in the northwest of Quang Binh province, along the Vietnam - Laos border.

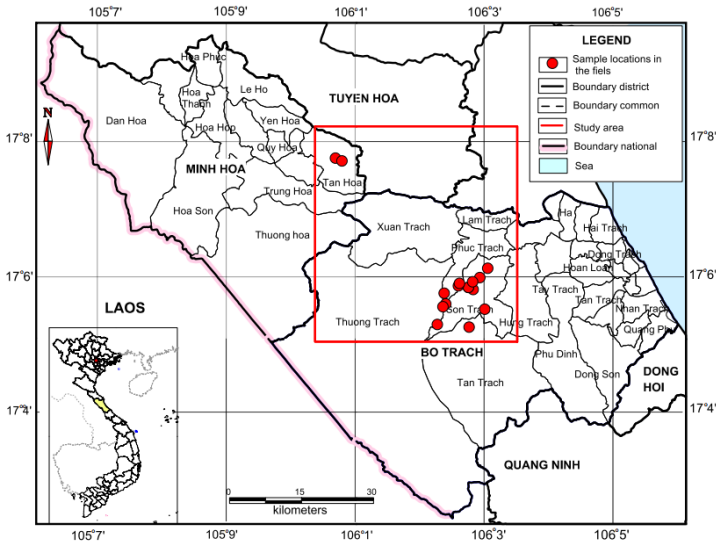


Figure 1. *Geographic location of the World Natural Heritage area of Phong Nha-Ke Bang National Park, Quang Binh, Vietnam (Source: Center for Environmental Monitoring in the Central and Central Highlands, Ministry of Natural Resources and Environment, 2020)*

Geographic coordinates: 17o20'-17o48'N; 105o46-106o24'E

The World Natural Heritage profile of Phong Nha-Ke Bang National Park was built by Professor Tran Nghi from 1999-2001 and in July 2003 was recognized by UNESCO. This is the second World Natural Heritage in Vietnam after Ha Long Bay. Since then, Quang Binh province's tourism industry has developed to a new level. However, National Park and Tourism managers have not yet shaped a sustainable management model. Finding a formula to evaluate the Load Capacity of the Phong Nha-Ke Bang tourist area is an important contribution for tourism managers to build a scientific and effective management model.

There are 6 member objects in the Phong Nha - Ke Bang heritage area as follows:

Lc1: Load Capacity of the soil environment

Lc2: Load Capacity of water environment;

Lc3: load Capacity of Air environment;

Lc4: Load Capacity of infrastructure (motels, hotels, roads, service area) against the effects of tourists and natural disasters (storms, floods, droughts);

Lc5: Load Capacity of the cave environment for cave visitors;

Lc6: Load Capacity of hotels for guests staying and living.

Assessing the average Load Capacity of the tourism environment of the entire geo-ecosystem of Phong Nha - Ke Bang National Park is the algebraic average value of 6 members object values:

$$Lcav = 1/6\ (Lc1+Lc2+ \ldots+Lc6) \quad (2)$$

In which: Lcav is the average load capacity of the entire geo-ecosystem of the heritage area

Lc1, Lc2, …, Lc6 is the load capacity of the member objects constituting a geo-ecological system.

3.2. Load capacity of different member objects in the geo-ecosystem of the Phong Nha - Ke Bang heritage area:

3.2.1. Load Capacity of the Soil Environment

General formula: Lc1 = 1 - (A1/B1) In which: Lc1 is the Load Capacity of the soil environment in the Phong Nha - Ke Bang area; A1 is the real value of pollution of heavy metals and insoluble organic compounds compared to Vietnamese standards (Cu, Pb, Zn, As, Hg); B1 is the threshold for soil environmental pollution according to VNS (Vietnam Standard) 15:2008/BTNMT

- National technical regulation on plant protection substance residues in soil

According to the results of soil environmental monitoring in 2020 conducted by the Center for Natural Resources and Environmental Monitoring of Quang Binh province, plant protection chemical residues are present in the soil in Bo Trach district in general and the National Park area. Phong Nha - Ke Bang in particular is within the allowable threshold according toVNS 15:2008/BTNMT

- National technical regulation on pesticide residues in soil. Thus, it is possible to determine the soil environmental Load Capacity Lc1 = 0.9.

3.2.2. Load capacity of the water environment

General formula: Lc2 = 1 - (A2/B2) In which: Lc1 is the Load Capacity of the water environment in the Phong Nha - Ke Bang area. A2 – Recent real value of water environment, including substances such as (pH, BOD5, COD, Acid, Phosphate, Ammonium): (1) surface water pollution (river water, streams, ponds and lakes); (2) groundwater pollution. B2 is according to VNS 08-MT:2015/BTNMT for surface water and VNS 09-MT:2015/BTNMT for groundwater.

a) Load Capacity of Surface Water Environment

Based on the surface water environmental monitoring report of Son River in 2020 conducted by the Central and Central Highlands Environmental Monitoring Center under the Ministry of Natural Resources and Environment, the research team has compiled water environment monitoring data present at 15 monitoring points (fig.1).

Table 1. Monitoring data of surface water environment in the Son River area flowing through the Phong Nha - Ke Bang tourist area.

Assessment Criteria	Monitoring														
	St 01	St 02	St 03	St 04	St 05	St 06	St 07	St 08	St 09	St 10	St 11	St 12	St 13	St 14	St 15
pH	7,55	6,6	7,4	7,3	7,44	6,98	7,34	7,4	7,76	6,4	7,21	7,46	7,88	7,15	7,4
Solid suspended matter	9	7	10	8	7	11	9	6	9	8	14	12	17	12	7
BOD_5	4,18	4,24	4,5	4,3	4,5	4,4	4,6	4,5	4,1	3,2	5,1	4,8	5,3	4,5	4,56
COD	6,5	6,4	6,1	6,7	6,8	6,5	6,3	6,1	6,8	6,4	6,7	6,9	5,6	6,25	6,85
Fe	0,03	0,02	0,05	0,04	0,02	0,03	0,06	0,04	0,03	0,02	0,06	0,05	0,06	0,042	0,02
Phosphate	0,05	0,04	0,05	0,03	0,06	0,05	0,04	0,05	0,07	0,04	0,033	0,08	0,043	0,012	0,062
Ammonium	0,03	0,06	0,02	0,04	0,04	0,03	0,03	0,02	0,09	0,06	0,051	0,09	0,088	0,058	0,046

(Source: Center for Environmental Monitoring in the Central and Central Highlands, Ministry of Natural Resources and Environment, 2020)

Table 2. Load Capacity of monitoring stations in surface water environment in the Son River area flowing through Phong Nha - Ke Bang tourist area.

Assessment Criteria	Limit value (according to VNS 08-MT:2015/BTNMT)	Load Capacity of monitoring data														
		St 01	St 02	St 03	St 04	St 05	St 06	St 07	St 08	St 09	St 10	St 11	St 12	St 13	St 14	St 15
pH	9	0,16	0,27	0,18	0,17	0,17	0,22	0,18	0,18	0,14	0,29	0,20	0,17	0,12	0,21	0,18
Suspended solid matter	100	0,91	0,93	0,90	0,93	0,93	0,89	0,91	0,94	0,91	0,92	0,86	0,88	0,83	0,88	0,93
BOD_5	15	0,72	0,72	0,70	0,70	0,70	0,71	0,69	0,70	0,73	0,79	0,66	0,68	0,65	0,70	0,70
COD	30	0,78	0,79	0,80	0,77	0,77	0,78	0,79	0,80	0,77	0,79	0,78	0,77	0,81	0,79	0,77
Fe	1,5	0,98	0,99	0,97	0,99	0,99	0,98	0,96	0,97	0,98	0,99	0,96	0,97	0,96	0,97	0,99
Phosphate	0,3	0,83	0,87	0,83	0,80	0,80	0,83	0,87	0,83	0,77	0,87	0,89	0,73	0,86	0,96	0,79

Ammonium	0,9	0,97	0,93	0,98	0,96	0,96	0,97	0,97	0,98	0,90	0,93	0,94	0,90	0,90	0,94	0,95
$Lc_{i\ av}$		0,76	0,79	0,77	0,76	0,76	0,77	0,77	0,77	0,75	0,80	0,76	0,74	0,74	0,78	0,76
Lc_{2av}		0,76														

b) Load capacity of the underground water environment

Based on the groundwater environmental monitoring report in the Phong Nha - Ke Bang area in 2020 conducted by the Central and Central Highlands Environmental Monitoring Center under the Ministry of Natural Resources and Environment, the research team has compiled data with 15 monitoring points (table 2, 3).

Table 3. Monitoring data of underground water environment in the Phong Nha - Ke Bang area.

Pollution Index	Monitoring data														
	St 01	St 02	St 03	St 04	St 05	St 06	St 07	St 08	St 09	St 10	St 11	St 12	St 13	St 14	St 15
pH	6,49	6,1	6,57	7,3	7,44	6,98	7,34	7,4	7,76	6,4	7,21	7,46	7,88	7,15	7,4
Water hardness	115	125	113	183	7	11	9	6	9	8	14	12	17	12	7
Dissolved solids	162,3	152,7	156,2	129	4,5	4,4	4,6	4,5	4,1	3,2	5,1	4,8	5,3	4,5	4,56
Permanganate Index	4	6,4	4,21	3,84	6,8	6,5	6,3	6,1	6,8	6,4	6,7	6,9	5,6	6,25	6,85
Chloride	14,8	12,6	17,2	18	12,6	17,9	14,1	28,2	30,6	15,6	44,6	12,5	49,1	36,5	38,9
Sulfate	24	25	29	64	81	39	32	61	65	59	49	57	64	36	46
Ammonium (Calculated as N)	0,025	0,042	0,02	0,04	0,04	0,03	0,03	0,02	0,09	0,06	0,051	0,09	0,088	0,058	0,046
Fe	0,006	0,0045	0,0072	0,0058	0,0076	0,0065	0,0039	0,0075	0,0067	0,0081	0,0051	0,004	0,0032	0,0074	0,0083
As	0,03	0,057	0,041	0,06	0,038	0,037	0,04	0,057	0,06	0,031	0,059	0,042	0,035	0,046	0,047
Cd	0,0022	0,0035	0,0056	0,0029	0,0039	0,0089	0,0037	0,0029	0,0037	0,0056	0,0041	0,0057	0,0038	0,0075	0,0071
Pb	0,0003	0,00064	0,00069	0,00058	0,00075	0,0006	0,00061	0,0006	0,00075	0,00064	0,00047	0,00021	0,00054	0,00076	0,00046

(Source: Center for Environmental Monitoring in the Central and Central Highlands, Ministry of Natural Resources and Environment, 2020)

Table 4. Load Capacity of groundwater environment in the Phong Nha - Ke Bang area

Pollution Index	Limit Criteria QCVN09-MT:2015/BTNMT (State technical criteria)	Load Capacity of monitoring stations														
		St 01	St 02	St 03	St 04	St 05	St 06	St 07	St 08	St 09	St 10	St 11	St 12	St 13	St 14	St 15
pH	8,50	0,24	0,28	0,23	0,12	0,12	0,18	0,14	0,13	0,09	0,25	0,15	0,12	0,07	0,16	0,13
Water hardness	500	0,77	0,75	0,77	0,99	0,99	0,98	0,98	0,99	0,98	0,98	0,97	0,98	0,97	0,98	0,99
Dissolved solids	1500	0,89	0,90	0,90	1,00	1,00	1,00	1,00	1,00	1,00	1,00	1,00	1,00	1,00	1,00	1,00
Chỉ số permaganate	4	0,00	-0,60	-0,05	-0,70	-0,70	-0,63	-0,58	-0,53	-0,70	-0,60	-0,68	-0,73	-0,40	-0,56	-0,71
Chloride	250	0,94	0,95	0,93	0,95	0,95	0,93	0,94	0,89	0,88	0,94	0,82	0,95	0,80	0,85	0,84
Sulfate	400	0,94	0,94	0,93	0,80	0,80	0,90	0,92	0,85	0,84	0,85	0,88	0,86	0,84	0,91	0,89
Ammonium (calculated as N)	1	0,98	0,96	0,98	0,96	0,96	0,97	0,97	0,98	0,91	0,94	0,95	0,91	0,91	0,94	0,95
Nitrite (calculated as N)	1	0,99	1,00	0,99	0,99	0,99	0,99	1,00	0,99	0,99	0,99	0,99	1,00	1,00	0,99	0,99
Ion	5	0,99	0,99	0,99	0,99	0,99	0,99	0,99	0,99	0,99	0,99	0,99	0,99	0,99	0,99	0,99
Asen	0,05	0,96	0,93	0,89	0,92	0,92	0,82	0,93	0,94	0,93	0,89	0,92	0,89	0,92	0,85	0,86
Cadimi	0,01	0,94	0,87	0,86	0,85	0,85	0,88	0,88	0,88	0,85	0,87	0,91	0,96	0,89	0,85	0,91
Pb	0,01	0,88	0,33	0,39	0,72	0,72	0,61	0,22	0,88	0,33	0,88	0,39	0,55	0,48	0,61	0,55
Load Capacity of groundwater at monitoring stations		0,79	0,69	0,73	0,72	0,72	0,72	0,70	0,75	0,67	0,75	0,69	0,71	0,71	0,71	0,70
Average Load of groundwater		0,72														

The average Load Capacity of both groundwater and surface water is **0,74.**

c) Load capacity of the air environment

General formula: $Lc_3 = (A_3/B_3)$

In which: A_3 is the actual dust concentration load in the air (mg/m^3); B3- VNS

Air environment monitoring data in the Phong Nha - Ke Bang area using data from the 2020 air environment monitoring report conducted by the Center for Environmental Monitoring in the Central and Central Highlands regions is shown (table 4).

Table 5. Air environment monitoring data in the Phong Nha - Ke Bang area

Pollution Index	Load Capacity according to monitoring data of stations														
	St 01	St 02	St 03	St 04	St 05	St 06	St 07	St 08	St 09	St 10	St 11	St 12	St 13	St 14	St 15
Dust	0,06	0,036	0,045	0,067	0,069	0,076	0,064	0,087	0,093	0,04	0,048	0,057	0,032	0,072	0,064
Dust PM_{10}	0,03	0,021	0,046	0,033	0,021	0,012	0,028	0,025	0,031	0,041	0,037	0,012	0,032	0,042	0,038
CO	3	4,9	5	8	3	4	5,3	7	4	5	2	4	5	6,3	14
SO_2	0,06	0,04	0,03	0,034	0,054	0,036	0,054	0,048	0,065	0,076	0,062	0,075	0,045	0,023	0,045
NO_2	0,051	0,077	0,081	0,051	0,059	0,024	0,028	0,047	0,076	0,089	0,094	0,086	0,022	0,086	0,074

(Source: Center for Environmental Monitoring in the Central and Central Highlands, Ministry of Natural Resources and Environment, 2020)

Table 6. Load Capacity of air environment at the Phong Nha - Ke Bang area

Pollution	Pollution limit VNS 09-MT:2015/BTNMT	Load Capacity according to monitoring data of stations														
		St 01	St 02	St 03	St 04	St 05	St 06	St 07	St 08	St 09	St 10	St 11	St 12	St 13	St 14	St 15
Dust	0,30	0,80	0,88	0,85	0,77	0,77	0,75	0,79	0,71	0,69	0,87	0,84	0,81	0,89	0,76	0,79
Dust PM_{10}	0,05	0,33	0,53	-0,02	0,53	0,53	0,73	0,38	0,44	0,31	0,09	0,18	0,73	0,29	0,07	0,16
CO	30,00	0,90	0,84	0,83	0,90	0,90	0,87	0,82	0,77	0,87	0,83	0,93	0,87	0,83	0,79	0,53
SO_2	0,35	0,83	0,89	0,91	0,85	0,85	0,90	0,85	0,86	0,81	0,78	0,82	0,79	0,87	0,93	0,87
NO_2	0,20	0,75	0,62	0,60	0,71	0,71	0,88	0,86	0,77	0,62	0,56	0,53	0,57	0,89	0,57	0,63
Lcav of staions		0,72	0,75	0,63	0,75	0,75	0,82	0,74	0,71	0,66	0,63	0,66	0,75	0,76	0,62	0,60
Lc_{av} of whole area		0,70														

d) Load capacity of tourism infrastructure

General formula: $Lc_4 = 1 - (A_4/B_4)$. In which: A_4 - Percentage of damage and degradation caused by natural disasters (storms, floods). This value is equivalent to a percentage (%) of the budget spent on remediation after 10 years; B_4 - Total investment cost. According to the Report on Sustainable Forest Management Plan for Phong Nha - Ke Bang National Park for the period 2021 - 2030, we have data of the above quantities as follows: $A_4 = 2$ (billion VND); $B_4 = 201$ (billion VND). From the above data, we apply the general formula and get the result of infrastructure load capacity as follows: $Lc_4 = 1 – 2/201 = 0.99$

e) Load capacity of visitors in the cave

General formula: $Lc_5 = 1 - (A_5/B_5)$ In which: A_5 Actual number of visitors; B_5 Maximum number of guests that can be accommodated in the cave.

Table 7. The actual number of visitors and maximum number threshold for the Phong Nha - Ke Bang area in the period 2013-2023

Visiting positions	Limit the number of visitors/year	Number of real visitors (people/year)										
		2013	2014	2015	2016	2017	2018	2019	2020	2021	2022	2023
Son Doong Cave	1.000	842	953	812	833	733	856	786	663	610	126	141
En Cave	14.400	2.178	2.373	2.155	2.253	2.509	2.111	2.406	1.577	573	395	263
Water Cave	2.400	365	326	697	365	797	710	489	256	113	0	0
Tra Ang Cave	14.700	4.579	5.356	4.135	4.436	5.002	3.829	5.991	1.406	20	1.006	1.006
Phong Nha Cave	3.832.500	195.890	295.578	266.435	289.343	319.017	348.985	356.844	126.975	38.530	78.616	55.218
Tien Son Cave	1.200.000	44.686	62.747	28.463	31.675	34.756	25.452	25.452	11.426	0	0	0
Thien Duong Cave	3.832.500	143.062	234.599	165.334	176.765	198.716	254.332	27.858	77.860	18.334	41.221	39.557

(Source: Management of National Park Phong Nha-Ke Bang, 2020)

Table 8. Load Capacity of Caves for Visitors

Visiting sites	Member Load Capacity during the period 2013 – 2023										
	2013	2014	2015	2016	2017	2018	2019	2020	2021	2022	2023
Son Doong	0,16	0,05	0,19	0,27	0,27	0,14	0,21	0,34	0,4	0,87	0,86
Thien Đuong Cave	0,96	0,94	0,96	0,95	0,95	0,93	0,99	0,98	1,0	0,99	0,99
Phong Nha Cave	0,95	0,92	0,93	0,92	0,92	0,91	0,91	0,97	1,0	0,98	0,99
Tien Son Cave	0,96	0,95	0,98	0,97	0,97	0,98	0,98	0,99	1,0	1,00	1,00
Hang En Cave	0,92	0,92	0,93	0,91	0,91	0,93	0,92	0,95	1,0	0,99	0,99
Water Cave	0,98	0,98	0,95	0,95	0,95	0,95	0,97	0,98	1,0	1,00	1,00
Tra Ang Cave	0,79	0,76	0,81	0,77	0,77	0,83	0,73	0,94	1,0	0,95	0,95
Whole Cave	0,82	0,79	0,82	0,82	0,82	0,81	0,81	0,88	0,9	0,97	0,97
Lc_{av} from 2013 to2023	0,86										

f) Load capacity of motels and hotels for resident guests

General formula:

$Lc_6 = 1 - (A_6/B_6)$

In which: A_6- Actual number of guests residing

B_6- Maximum number of guests that can accommodate

Table 9. Calculation of load-bearing capacity of motels and hotels for resident guests

Sets	Visitor customer	Accommodate (people/day)	Number of Real guests (people/day)	Negative Load	Load of hotel (Lc_6)
Phong Nha – Ke Bang	123	3902	2.000	0,51	0,49

(Source: Management of National Park Phong Nha-Ke Bang, 2020)

Bearing capacity of the entire Phong Nha-Ke Bang tourist area

From the above calculation results, we have enough data to put into the following general calculation formula:

$$L_{cav} = \frac{(Lc1+Lc2+Lc3+Lc4+Lc5+Lc6)}{6} = 0.78$$

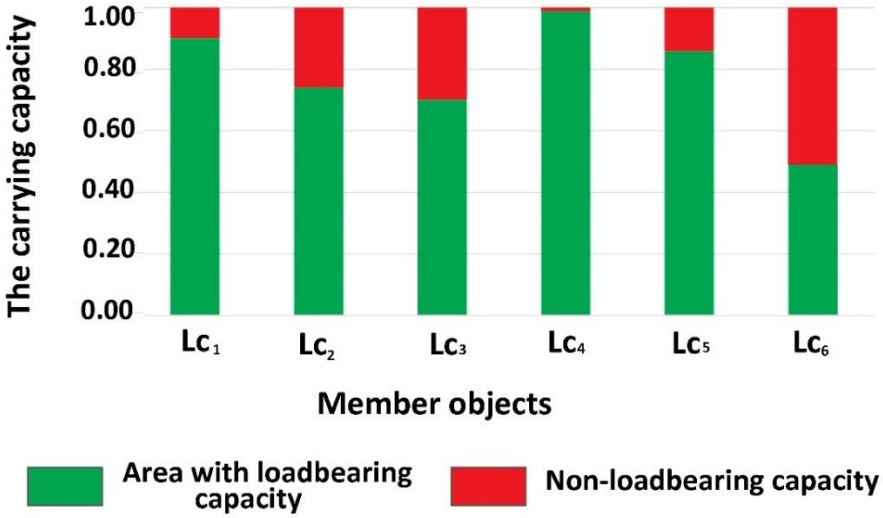


Figure 2. *Diagram showing the carrying capacity of member objects and the average tourism environmental carrying capacity value (Lcav) of the Phong Nha-Ke Bang ecosystem*

Thus, we can see that the calculation results have given the number 0.78<1, so it can be concluded that the carrying capacity of the tourism environment in the Phong Nha - Ke Bang area is within the limit. allow.

4. CONCLUSION

1. Researching and developing a formula to assess the carrying capacity of the environment in general and the tourism environment, in particular, is an urgent task during the challenging period of extreme climate change in Vietnam. The formula Lc = 1- A/B and Lcav is a method that contributes to standard quantification to evaluate the load-bearing capacity of a member object and the entire environment of the study area.

2. The geo-ecosystem of Phong Nha-Ke Bang National Park is made up of 6 member objects, each member object has a different load-bearing capacity and is calculated according to the formula: Lc = 1- A /B;

3. Quantitative values of the carrying capacity of member objects and the average carrying capacity of the entire geosystem-ecosystem vary from 0.49 (motels, hotels) to 0.9 (soil environment); including many objects with values more than 0.7. This proves that the current state of the tourism environment of the Phong Nha-Ke Bang geo-ecosystem still can bear the load above the allowed critical threshold.

4. The carrying capacity of the tourism environment can be increased if the National Park tourism management board pays more attention to organizing infrastructure management and tourism services to meet international standards to increase traffic. Guests have reached the allowable limit.

5. The tourism environment of the geo-ecosystem of Phong Nha-Ke Bang National Park also has great potential in terms of carrying capacity but needs 2 factors: (1) focus on investing in weighted members and having high load capacity; (2) regulating the Load Capacity of a strong and sustainable development system requires investment in building the Phong Nha area as an impressive and attractive destination with resonant and spread power.

ACKNOWLEDGEMENTS

To complete this report, the authors received effective support and facilitation from the National Park Leadership Board, the Department of Natural Resources and Environment, the Department of Science and Technology, and the Department of Natural Resources and Environment, Culture Sports and Tourism of Quang Binh province in the process of collecting documents and data related to the assessment of the Load Capacity of the Phong Nha-Ke Bang tourism environment. On this occasion, the authors sincerely send to individuals and agencies their deepest thanks for their valuable help.

REFERENCES

1. Lime, D. W., & Stankey, G. H. (1971). Carrying capacity: Maintaining outdoor recreation quality. In Recreation symposium proceedings.

2. Graefe, A. R., Kuss, F. R., & Vaske, J. J. (1990). Visitor impact management.

3. The planning framework. Washington, DC: National Parks and Conservation Association.

4. Manning, R. E. (2001). Visitor experience and resource protection: A framework for managing the carrying capacity of national parks. Journal of Park and Recreation Administration, 19(1), 93–108.

5. Simón, F., Narangajavana, Y., & Marqués, D. (2004). Carrying capacity in the tourism industry: A case study of Hengistbury Head. Tourism Management, 25(2), 275–283.

6. Vo, Q. (2008). The use of the formulas of Cifuentes and Ceballos-Lascurain to calculate the carrying capacity of ecotourism sites in Vietnam]. Hanoi: Institute for Tourism Development Research.

7. Tuan Phong Ly & Thi Hong Hai Nguyen (2017) Application of carrying capacity management in Vietnamese national parks, Asia Pacific Journal of Tourism Research, 22:10, 1005-1020, DOI: 10.1080/10941665.2017.1359194.

8. CuiFengjun, LiuJiaming(1998), "A study on the theory and applied on of tourism environmental bearing capacity", ProgressinGeography.Vol.17, pp.86-91.

9. Sun Rui-hong, LiuShi-dong (2009), "Research on Tourism Environmental Carrying Capacity of Chong Ming Island", Proceedings of the 2009 International Conference on Environmental Science and Inform an on Applica on Technology.Vol.3. July 2009.

10. Tran Dinh Gian, 1979. Geomorphological characteristics of the North Central region and some opinions on planning for production. Marine research training route 1/2 Nha Trang.

11. Nguyen Huu Hung, Pham Kim Ngan, Nguyen Dinh Hong, Nguyen Duc Khoa, Doan Nhat Truong, 1980. Discovery of Frasni-Famen limestone (upper Devon) in Quy Dat area (Binh Tri Thien). TC Earth Sciences, 4/2: 27-28. Hanoi

12. Ta Hoa Phuong, Nguyen Huu Hung, 1997. Frasni-Famen boundary (Upper Devonian) in Xom Nha limestone block in Quy Dat region, Quang Binh. TC Geology 283; 5-11. Hanoi 13. Nguyen Quang Trung, 1996. Geology and Minerals, Mahaxay- Dong Hoi newspaper. Vietnam Geological Department. Hanoi.

13. Tran Nghi, Hoang Trong So, 1997. Sedimentary characteristics and evolutionary history of coastal sand formations in Quang Binh. Journal of Science, Natural Sciences XIII/3. Hanoi.

14. Nguyen Quoc Dung, 2000. Phong Nha-Ke Bang. The area is nominated as a World Natural Heritage Site. Journal Forestry. No. 3. Hanoi.

15. Tran Nghi, Dang Van Bao, Nguyen Quang My, Le Huy Cuong Nguyen Quoc Dung, Phan Duy Nga, Ta Hoa Phuong, Vu Van Dung, Vu Van Phai, 2003. World Natural Heritage Phong Nha National Park- Ke Bang Quang Binh, Vietnam. Publisher of Vietnam Geological Department. Hanoi, 202 pages.

16. Tran Nghi, Ta Hoa Phuong, Nguyen Quang My, Vu Van Phai, Dang Van Bao, Phan Duy Nga, 2004. Geological and geomorphological diversity constitutes the Phong Nha-Ke Bang World Natural Heritage site. TC Geology 282; 1-10. Hanoi. Vietnam Department of Geology and Minerals

17. Muhammad Rasidi, Bambang S. Lautt, Yetrie Ludang, Sidik R. Usup, Adi Jaya, 2023 Analysis of the Carrying Capacity and Environmental Capacity of the Bukit Tangkiling Natural Park. International Journal of Multidisciplinary Approach Research and Science E-ISSN 2987-226X. Volume 1 Issue 02, May 2023, PP.179-189.

MARINE LANDSCAPE ANALYSIS FOR RESOURCE MANAGEMENT AND BIODIVERSITY CONSERVATION IN TRUONG SA ISLANDS, VIETNAM

Nguyen Dang Hoi[1], Nguyen Cao Huan[2], Ngo Trung Dung[1], Phan Dong Pha[3] and Vu Le Phuong[2, 3]

[1] Vietnam-Russia Tropical Center, Vietnam Ministry of Defense

[2] University of Science, Vietnam National University

[3] Institute of Marine Geology and Geophysics, Vietnam Academy of Science and Technology

ABSTRACT: Landscape study, exclusively marine landscape, has an insightful significance in both theoretical and practical. The study outcomes could be represented in the form of classification and zonation maps which are the intensive composite of geospatial data used for analysis and evaluation to serve multi-purpose applications. In this article, we introduce the preliminary outcomes of a multi-scale marine landscape study using a novel approach and landscape classification and zonation systems for the territorial area of the Truong Sa Islands, Vietnam. Accordingly, the study area is classified into 1 system, 1 sub-system, 4 classes, 7 sub-classes and 20 kinds of landscape, distributed on 8 subregions of 3 marine landscape regions. Subsequently, we apply DPR and SWOT techniques for regional and subregional marine landscape domains corresponding to national-level guidance to propose a marine landscape scheme for economic development, resource management, and biodiversity conservation associated with national defense and security purposes. The scheme is assembled of 3 prioritized-purpose groups including (i) Administrative, economic and fishery logistics developments; (ii) Marine biodiversity conservation and restricted fishery activities; and (iii) fishery and maritime transport. The specific course of action is proposed for each domain on 2 major issues (a) Economic development and resource management; (b) Environmental protection and biodiversity conservation.

Keywords: *analysis, marine landscape, resource management, solution, Truong Sa Islands.*

1. INTRODUCTION

Resource management and biodiversity conservation associated with economic development, national defense and security are the goals, tasks, and driving forces of the strategy to construct and protect the Socialist Republic of Vietnam in the current stage. The perspectives, approaches and outcomes of science and technology research are significant and gradually becoming direct drivers contributing to major works of the country, following the statement “Novel, advanced and modern scientific achievements are the direct drivers promoting the sustainable development of the marine economy” [1]. Marine landscape research is a new direction of modern geography [8, 15]. In former Soviet Union countries, marine landscape research aims to discover the laws of creation and characteristics of physical marine units. Likewise, the marine landscape has been a concern in the research community of European and North American countries. Among other issues of marine landscape, there were numerous coral reef management studies as it has been considered a pivotal biological resource of tropical marine habitat [2, 9]. Many methods have been

implemented alongside, including the application of remote sensing method and UAV, geophysical methods such as multi/single beam echosounder, side-scan sonar... [6, 7]. Such studies have provided important and adequate data for the management and conservation of marine biodiversity. In Vietnam, there have been a few theoretical studies on establishing classification systems for marine landscapes [12, 13] and application of district and regional scales for some areas, such as the offshore maritime territory of Truong Sa Islands [10, 11, 14], or the coast and littoral zone of Quang Ngai Province, central Vietnam have been carried out [3].

The Truong Sa Islands are under Vietnam's sovereignty, which is in a critical position in terms of national defense and security, marine economy, maritime safety, and foreign affairs as the Vietnam portal to the Vietnam East Sea. Furthermore, the marine domain of Truong Sa Islands contains an assemblage of outstanding and unique values of resources and environment, especially in ecology and marine landscape. The marine landscapes of Truong Sa Islands was kept intact for a long time thanks to the low intensity of anthropogenic activities, therefore it maintained exclusive characteristics and values not only for Vietnam but also at the regional and global scale. However, in the past few decades, human activities have been changing landscape structure and dynamic in the area. Additionally, in the context of gradual changes in global climate and oceanography conditions, anthropogenic interference and landscape evolution would be more intense, unpredictable and complicated, thus creating more challenges in resource management and environmental protection issues, as well as difficulties in national defense and territorial security safeguard activities by maritime law enforcement forces on the remote sea and islands.

As a result, the application and integration of traditional research methods with modern instruments to study the characteristics of marine and island landscapes has both theoretical and practical influence. In this article, we present the results of a landscape study and assessment to serve economic development, resource management, and biodiversity conservation for the Truong Sa Islands, Viet Nam.

2. MATERIAL AND METHODS

2.1. Materials

- Map database: Nautical charts scaled at 1/250,000 of the Truong Sa Islands; thematic maps including geology, seabed substrate, geomorphology, oceanographic conditions, and marine species distribution map established by the authors.

- Acquired field data and research outcomes by the joint scientific team of the Vietnam - Russia Tropical Center - Vietnam Ministry of Defense (MOD-VRTC), and the Institute of Marine Geology and Geophysics - Vietnam Academy of Science and Technology (VAST-IMGG) within the framework of the research project, ID code KCB-TS.03.

- Other literature on the physical conditions, natural resources, socioeconomic conditions provided by specialized agencies.

2.2. Methods

Literature collection and processing. In this study, we collected multiple documents on various disciplinaries of the study subjects, including physical conditions, environment

characteristics and natural resources, statistics and reports on socio-economic issues from many specialized agencies.

We conducted four field trips to the reefs of Truong Sa Islands. In each field trip, we performed several investigations on multiple objects, including questionnaire interviews with military personnel and other forces living in Vietnam outposts, and fishermen to collect data and information on land use, water bodies monitoring, fishery, environmental protection practices and other specific movements. Foreign vessel activities were also acquired during surveys.

Field data acquisition: *the raw data on surface sediment, soil characteristics, biology and environmental conditions was acquired following the transect and point scheme.* Survey transects were plotted using topographic maps, concerning the distribution of islands and shoals in the Truong Sa Island domain and a map of current land use (for islands). Four field trips were implemented in the following periods: October-November 2020, April-May 2021, October-November 2021 and April-May 2022 (Figure 1).

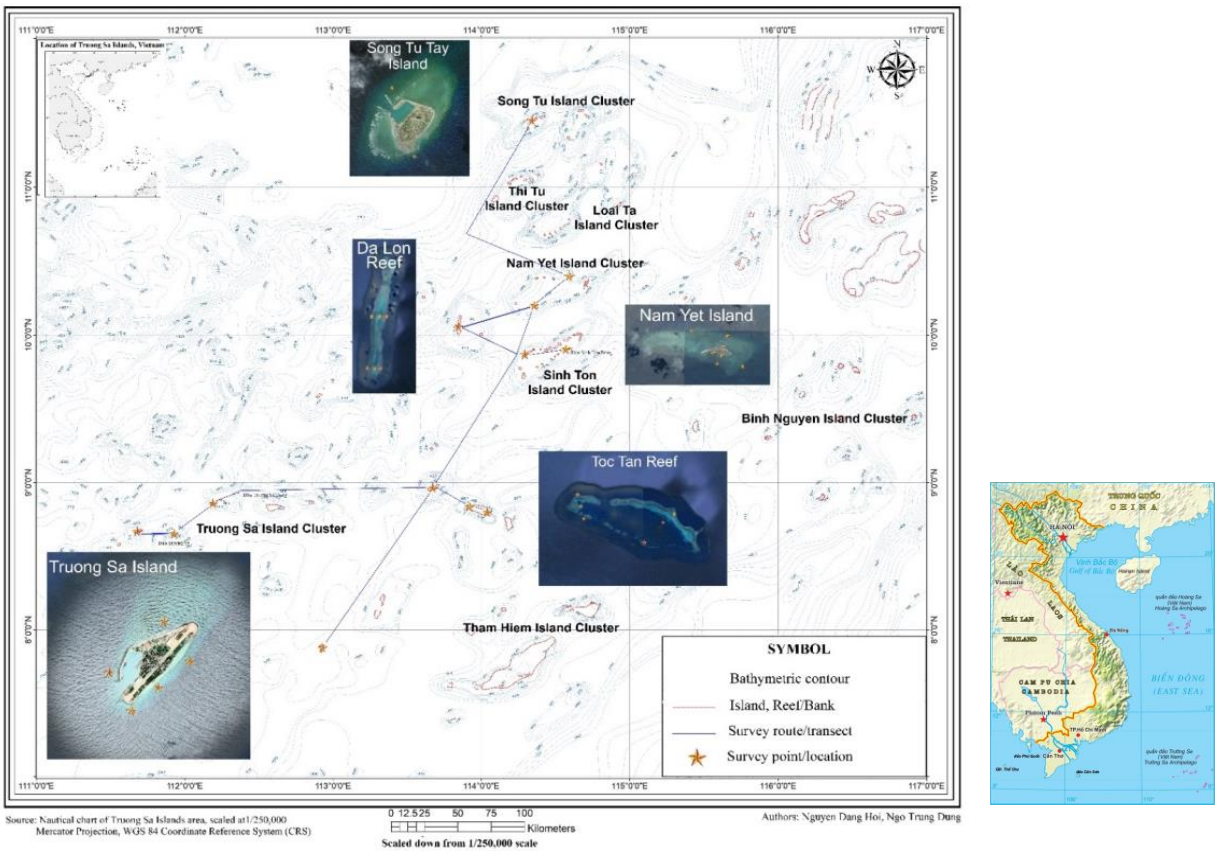


Figure 1. *Diagram of survey routes and points in the Truong Sa Islands area*

Accordingly, the survey scheme was divided into 2 major parts: (i) On cays/islands: acquire data on the topographic structure, morphology, geological characteristics - especially the aggregated coral platform, nearshore hydrographic and oceanographic features, soil composition, vegetation cover and other land cover types. Collected sediment and biological samples were described onsite at the time of acquisition; (ii) On shallow water areas: performed standard SCUBA diving [4] and snorkelling techniques. SCUBA diving team included 3 divers working at a depth from 3-40m to measure and interpret seabed substrate compositions, topographic structure and morphology, sediment characteristics and major marine biological group(s) of the seabed habitat.

Snorkelling was performed in shallow water (less than 10m depth) to specify general seabed morphology, sediments, and typical organism populations (corals, fishes or seagrasses) with their extension along cross-reef transects (or perpendicular to the reef limit). In each survey site, the number and position of survey locations/transects were described in detail on the corresponding satellite imagery and on-site after pilot observation.

Remote sensing image processing, GIS analysis and map establishment. Documents and published maps were collected and fused into a single synchronized database. Analysis and map establishment were taken accordingly to represent research outcomes in the type of thematic maps. The component thematic maps edited and established include geomorphology, seabed sediment, oceanographic conditions, and major marine community distribution in the Truong Sa Islands area. Geo-Object Based Image Analysis (GEOBIA) technique was applied to Pleiades-1A satellite images (2m resolution for R, G, B, and NIR bands, enhanced with a 0.45m panchromatic band) collected in the two years 2019 and 2020 on specific coral reef locations to classify shallow seabed substrate as inputs to establish geomorphological map and vegetation cover - landcover map. Satellite image classification was performed using eCognition software. Component maps and outcome maps were edited and published using PRECISELY MapInfo 15, ESRI ArcGIS Desktop 10.8 and eCognition 9.0 software.

- ***DPR analysis:*** Using 3 parameters Dynamics (D), Pressures (P) and Responses (R) to analyze landscape regions: (a) Dynamics: changes appear in the landscape region, caused by natural and artificial agents (and their synergy) that are causing, either directly or indirectly, pressure on natural resource management, environment protection and biodiversity conservation; (b) Pressures: In resource management and biodiversity conservation, those are changes in landscape structures and functions that cause negative influence to the economy, environment and society; (c) Responses: are the course of action of solutions, policies, planning orientation or practical actions by the communities against the dynamics and pressures...

- ***SWOT analysis:*** the SWOT analysis model includes 4 elements Strengths (S), Weaknesses (W), Opportunities (O) and Threats (T) [5] to analyze landscape subregions in detail to serve as a scientific foundation guidance to orientate territorial use in resource management, environmental protection, biodiversity conservation. Accordingly, based on the characteristics of each subregion, the SWOT technique is applied to analyze and clarify strengths, weaknesses, opportunities and challenges. Input data includes parameters of physical elements and natural resources of each landscape subregion; conservation value; and influencers within the region, domestically and internationally. Analysed outcomes are used to promote strengths, take advantage of opportunities, and overcome weaknesses and limitations for each landscape subregion.

3. RESULTS AND DISCUSSION

3.1. Landscape characteristics of Truong Sa Islands region

3.1.1. Landscape taxonomic units

a) Classification principles and criteria: in compliance with the main principles, including the principle of genetic morphology, the principle of relative uniformity, and the principle of dominant element(s).

b) Classification system and criteria: The landscape classification system of the Truong Sa Islands includes coral island/cay landscapes, shallow water reef/banks and marine landscapes diversified follow water depths. Accordingly, the landscape classification system of the Truong Sa Islands applied to establish a map at a scale of 1/250,000 comprises 5 grades: System - sub-system - class - sub-class - type of landscape.

c) Characteristics of landscape taxonomic units: In the study, following the principles and classification system organized above, and based on the content of a collection of component maps (geological map, geomorphological map, layered salinity and temperature maps, major species group distribution map), a landscape map of the Truong Sa Islands, Viet Nam at the scale of 1/250.000 was established. It included 1 system, 1 sub-system, 4 classes, 7 sub-classes and 20 types of landscape.

The marine landscape of Truong Sa Islands region is classified into four landscape classes, including 1 offshore island landscape class (subaerial landscape) and 3 marine landscape classes (subaqueous landscape). According to the characteristics of the island topography (physical/artificial genetic) and geomorphological processes on coral reef sediment: abrasion on consolidated beach rock, erosion-accumulation on other materials under the influence of waves and wave-induced current, thus the island landscape class is homogenous, with 1 offshore island landscape sub-class contains natural islands/cays and artificial islands. The marine landscapes are classified into 6 sub-classes and 19 types of which the most diverse bathypelagic landscape class consist of 3 sub-classes and 8 types. The shallow marine landscape class includes 9 types of 2 sub-classes, and the abyssalpelagic landscape class has only 1 sub-class with 2 types.

The island landscape sub-class has 1 type, representing the tropical vegetated island/cay landscape for both natural and artificial features. The offshore shallow marine landscape sub-class (0 to 100m depth) has 6 types which are differentiated by the distribution characteristics of organism communities and oceanographic conditions of the open water and inside the sheltered lagoon of atolls. 3 landscape types of the offshore shallow marine landscape sub-class include corals, reef fish communities and seagrass meadows that are distributed seaward of atolls. The mesopelagic (200-1,000m) and bathypelagic (1,000-4,000m) have 3 and 2 landscape types, respectively. Those landscape types are distributed on the western slope and rise of the Truong Sa (Dangerous Ground) mini-plate, on the plateau and plain of Sinh Ton - Co Rong region (Union Bank – Reed Bank/Tablemount region). The abyssal landscape sub-class (greater than 4,000m depth) includes 2 types, which are the assemblage of deep-sea organism communities distributed on the western slope and the rise of the Truong Sa (Dangerous Ground) mini-plate and deep-sea organisms living in the Sinh Ton - Co Rong region (Union Bank – Reed Bank/Tablemount region).

3.1.2. Characteristics and units of landscape zonation

a) Principles: The landscape zonation is based on the principles of landscape genetics objectivity, complexity, relative uniformity and common territory to establish a landscape map at the scale of 1/250,000.

b) Criteria: A 2-grade hierarchy system is applied: Landscape region and subregion, with a sub-grade of landscape secondary subregion. Accordingly, the homogeneity of landscape types, including geographical location, and thermal-salinity characteristics which affect the

establishment of marine organism communities, is used to zone a landscape region. Accordingly, surface salinity is divided into 3 levels: < 33‰, 33‰ - 33.5‰ and > 33.5‰; surface temperature: < 26°C, from 26 to 27 ^{o}C; above 27 ^{o}C.

Landscape region and sub-region are divided according to similar characteristics of bottom topography, which determines the characteristics of major organism groups in each landscape type. Accordingly, in the research area, there are four types of seabed morphology: i) Coral plateau; ii) plain; iii) Continental rise; iv) marginal depression.

c) Landscape zonation units:

Based on principles, criteria and landscape classification maps at 1/250,000 scale, the Truong Sa Islands area is zoned into 3 regions, 6 subregions and 2 secondary subregions of the landscape. The hierarchy, distribution characteristics and statistics result of landscape zonation for the study area are described in Table 1 and Figure 2 below.

Table 1. Landscape zoning units of the Truong Sa Islands area

Symbol	Landscape zoning units	Acreage (ha)
I	Landscape region on the western slope and rise of Truong Sa (Dangerous Ground) mini-plate	14,527,111
I.1	The landscape subregion of Truong Sa - Chu Thap (Spratly Island Reef - Fiery Cross Reef) plateau and plain	8,095,191
I.2	Landscape subregion on the northwest rise and marginal depression of Truong Sa (Dangerous Ground) mini-plate	6,431,920
II	Landscape region of Sinh Ton - Co Rong (Union Bank - Reed Bank) plateau and plain	11,121,701
II.1	Landscape subregion of Nam Yet - Song Tu (Tizard Bank - North Danger Reef) atolls	6,932,008
II.1.1	*Landscape secondary subregion of Nam Yet - Sinh Ton atolls*	779,471
II.1.2	*Landscape secondary subregion of Song Tu - Loai Ta depression*	1,009,408
II.2	Landscape sub-region of Co Rong (Reed Bank) plateau and plain	2,400,814
III	Landscape region of Tham Hiem - Trang Khuyet (Investigator Shoal - Half Moon Shoal) depression	11,019,551
III.1	Landscape subregion of Tham Hiem (Investigator Shoal) atoll and inclined depression	6,317,825
III.2	Landscape subregion of Binh Nguyen (Flat Island Bank) atoll and depression	4,701,727

- Landscape region on the western slope and rise of Truong Sa mini-plate: this landscape region lies to the western part of Truong Sa Islands, and covers the largest area of 14,527,111 hectares, accounting for 39% of the study area. As the major organism groups are determined by the seabed morphology and water depth, this region is divided into 2 subregions, including the landscape subregion of (I.1) Truong Sa - Chu Thap plateau and plain; (I.2) northwest rise and marginal depression of Truong Sa mini-plate (Figure 2).

The landscape region of Sinh Ton - Co Rong plateau and plain: distributed on the northeastern part of Truong Sa Islands, with an area of 11,121,701 hectares (30% of the study

area). The region is divided into 2 subregions and 2 special secondary subregions, which are the landscape subregion of (II.1) Nam Yet - Song Tu atolls include 2 secondary subregions (II.1.1) secondary subregions of Nam Yet - Sinh Ton atolls; (II.1.2) secondary subregion of Song Tu - Loai Ta depression; and (II.2) a sub-region of Co Rong plateau and plain (II.2) (Figure 2).

- Landscape region of Tham Hiem - Trang Khuyet depression: located on the southeast part of the Truong Sa Islands, with an area of 11,019,551 hectares. This region includes 2 subregions, (III.1) Tham Hiem atoll and inclined depression; and Binh Nguyen atoll and depression (III.2) (Figure 2).

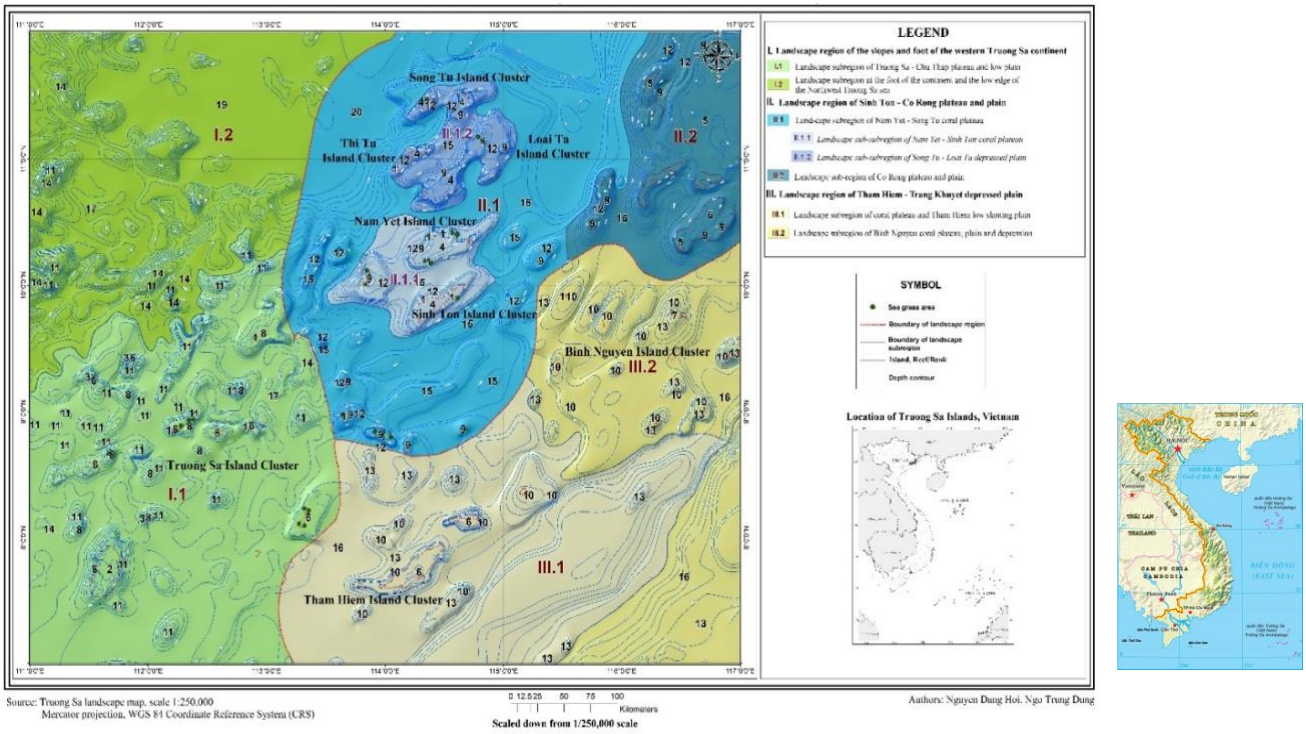


Figure 2. *Landscape zonation map of Truong Sa Islands, scaled at 1/250,000*

3.2. Landscape analysis and assessment

3.2.1. DPR analysis

The DPR method was applied to identify the status of influences, their pressure and corresponding response in the domain of the Truong Sa Islands for each landscape region. The results of the DPR analysis are summarized in Table 2.

Table 2. DPR analysis results for landscape regions of Truong Sa Islands

Landscape region	Dynamic	Pressure	Response
Region I	- Fishery yield increases over time, especially ocean tuna. - Intensive construction activities on islands, including	- Harsh living conditions on the island and over the seas, especially the limited land fund and fresh water resources.	- Response to drivers: Implementing policies to support fishermen; Expand and upgrade facilities on islands. - Respond to pressures: Invest and improve accommodation

	Fiery Cross Island. - Strengthen national defense, security, and sovereignty protection over sea and island territories.	- Ensure fishing output, limit destructive fishing methods, especially the use of chemicals and explosives. - Safeguard sovereignty over sea and island territories.	and production facilities on islands; Develop and expand Da Tay A logistics and service centre for the fishery.
Region II	- Fishery yield gradually increase with state support policies. - National defense, security, and sovereignty protection over sea and island territories. - Policies to support offshore seafood exploitation.	- Extreme weather events increase in number and magnitude. - Harsh living conditions on the island and over the seas. - Limited land available on the island landscape. - Intensive construction activities on islands, including Tu Nghia and Gac Ma reefs...	- Response to drivers: Implement policies to support fishermen in offshore fishing; Expand and upgrade dual-purpose facilities on islands. - Response to pressures: Invest and accomplish accommodation and production facilities on islands and low-tide elevations; Construct logistics service centre for the fishery for the central area of Truong Sa Islands, located on Nam Yet Island.
Region III	- Vast sea surface, fairly high biodiversity. - Advantages on national defense, military, and sovereignty protection over sea and island territories. - Area of many fish species with high conservation value.	- Distant island locations and fishery logistics service facilities; There are no storm shelters for boats in the area. - Sovereignty protection over sea and island territories; There are no floating islands in the area, only shallow beaches and underground beaches.	- Response to drivers: Apply regulations on resource management and biodiversity conservation to fishing vessels; Strengthen international cooperation in marine biodiversity conservation in companion with search-and-rescue service and safeguard other non-traditional security issues. - Response to pressures: Implement policies to support fishermen in offshore fishing.

3.2.2. SWOT analysis

The marine landscape of the Truong Sa Islands area was classified into 3 regions, 6 subregions and 2 secondary subregions. The SWOT analysis method was applied for each landscape subregion to simultaneously analyze strengths, weaknesses, opportunities and threats. Table 3 briefly represents the results of the SWOT analysis for a landscape subregion (I.1) - Landscape subregion of Truong Sa - Chu Thap plateau and plain.

Table 3. SWOT analysis of the landscape subregion of Truong Sa - Chu Thap plateau and low plain (I.1)

Landscape subregion	Results of SWOT analysis	
I.1. Landscape subregion of Truong Sa - Chu Thap plateau and plain (of landscape Region I)	*Strengths* - Large area, lies at the centre of Truong Sa Islands, with an airfield and logistics service centre for fishery. - Has high biodiversity coral reef and seagrass ecosystems with many species that have conservation value. - Has adequate potential capability in defense and security, with favourable factors for a defensive formation	*Weaknesses* - Scattered islands, shoals and low-tide elevation; limited technical infrastructure, energy and water resources. Access to An Bang Island is burdensome due to the complicated reef terrain - Regularly affected by extreme weather events. - The environmental protection and sea rescue forces are not strong.
	Opportunities - Could be the development centre of the Truong Sa Islands area, located adjacent to international maritime routes. - Has abundant economic fishing grounds and many favourable conditions to support fishery - Availability in international cooperation on biodiversity conservation, non-traditional security assurance, especially search and rescue activities, and marine environment protection.	*Threats* - Influences from harsh weather conditions. - Illegal movements of foreign military and civil forces (e.g. Fiery Cross Reef area,...). - Direct and indirect involvement of major countries and other countries in the region without Vietnam's permission.

A similar procedure was applied to analyze strengths, weaknesses, opportunities and threats for the remaining subregions based on the characteristics of natural factors and natural resources of each subregion; conservation value; internal – domestic – international influences on the regions.

3.3. Spatial orientation and solutions for resource management and biodiversity conservation associated with national defense and security

3.3.1. Basis to propose orientation and solutions

Spatial orientation for resource management, economic development, environmental protection, and biodiversity conservation in the Truong Sa islands area is based on the following: i) Characteristics of the landscape classification and zonation units; ii) Analysis results of landscape characteristics and attributes, including DPR and SWOT; iii) Position and role of the Truong Sa Islands in the comprehensive development at the national and local scale (Khanh Hoa province), concerning international factors. Therefore, a space for environmental protection and biodiversity conservation, considering the participation of

parties and international organizations, is essential as it demonstrates Vietnam's opinion and responsibility to safeguard Truong Sa Islands in authority and harmony.

3.3.2. Priority areas for development and solutions

We delineated 17 priority areas focused on resource use, environmental protection, and biodiversity conservation for the Truong Sa Islands territory based on landscape subregions (Figure 3).

a) Priority areas for administrative, economic and fishery logistics development

** Central administrative, economic and fishery logistics development in Truong Sa Island- Da Tay atoll area (I.1.a)*

- Economic development and resource management: Strengthen the role of Truong Sa Island as an administrative headquarters of the whole Islands to develop fishery logistics services, general services for the western part of Truong Sa Islands, as well as maritime tourism (eco-tourism, cultural- spiritual tourism).

- Environmental protection and biodiversity conservation: Preserving landscape, coral reef ecosystems, seagrass meadows on low-tide elevations, especially the fairly pristine ecosystems surrounding Da Lat (Dallas) Reef; Strengthen observation and monitoring landscape dynamic and marine-island environments in damaged or under the heavy influence of anthropogenic agents (Truong Sa Island, Da Tay A reef).

** Fishery logistics service centre development in the Northern Truong Sa Islands area (II.1.2.a)*

- Economic development and resource management: Establish facilities to develop fisheries logistics services and general services for the northern territory of Truong Sa Islands located on Song Tu Tay Island. Promote maritime tourism (eco-tourism and cultural-spiritual tourism).

- Environmental protection and biodiversity conservation: Conservation of landscape, coral reef ecosystems on islands and low-tide elevations; Strengthen observation and monitoring of landscape drivers and marine-island environments in damaged areas due to anthropogenic agents, including destructive activities to coral reefs by foreign forces.

b) Priority areas for marine biodiversity conservation and limited fishery activities

** Thuyen Chai Reef marine biodiversity conservation area (I.1.b) and Toc Tan - Phan Vinh Reefs marine biodiversity conservation area (II.1.a):*

- Economic development, and resource management: promote fishery logistics services in the southern area, including Phan Vinh, Toc Tan and Thuyen Chai reefs; Limit fishery activity, avoid the breeding season of species, especially the seagrass meadow ecosystem on Thuyen Chai Reef; Developing recreational diving eco-tourism (SCUBA diving, freediving and snorkelling) in Toc Tan and Thuyen Chai reefs.

- Environmental protection and biodiversity conservation: Strengthen conservation of natural landscapes and ecosystems, especially the coral reef ecosystem of Toc Tan Reef, the seagrass meadow ecosystem and the shallow-sea coral reef landscapes of Thuyen Chai Reef. Preservation focuses on precious and rare species, including the *Hippopus hippopus* and other giant clams of the *Tridacna* genus.

** Priority area for international cooperation for marine biodiversity conservation in the Nam Yet - Sinh Ton Reefs (II.1.1.a):*

- Economic development and resource management: Establish a fishery logistics service centre and general services in the central area of the Truong Sa islands, located on the Nam

Yet Island as the hub for administration and economic development, resource management; develop maritime tourism (eco-tourism, diving, cultural-spiritual tourism).

- Environmental protection and biodiversity conservation: Strengthen conservation of natural landscapes and ecosystems, especially coral reef ecosystems, seagrass meadows on the reefs of Nam Yet, Son Ca, Da Lon, ... and shallow water coral reef landscapes in this area. Establish a world biosphere reserve for the area of Nam Yet - Sinh Ton Reefs; Promote conservation of typical marine and island ecosystems.

** Nam Yet - Sinh Ton fishery restricted area (II.1.1.b):*

- Economic development and resource management: Limited fishing on economic fish species in deep-sea landscapes and marine landscapes with depths of over 100m; Strengthen cooperation in marine resource management, with the Nam Yet - Sinh Ton area as the central hub for international cooperation for biodiversity conservation.

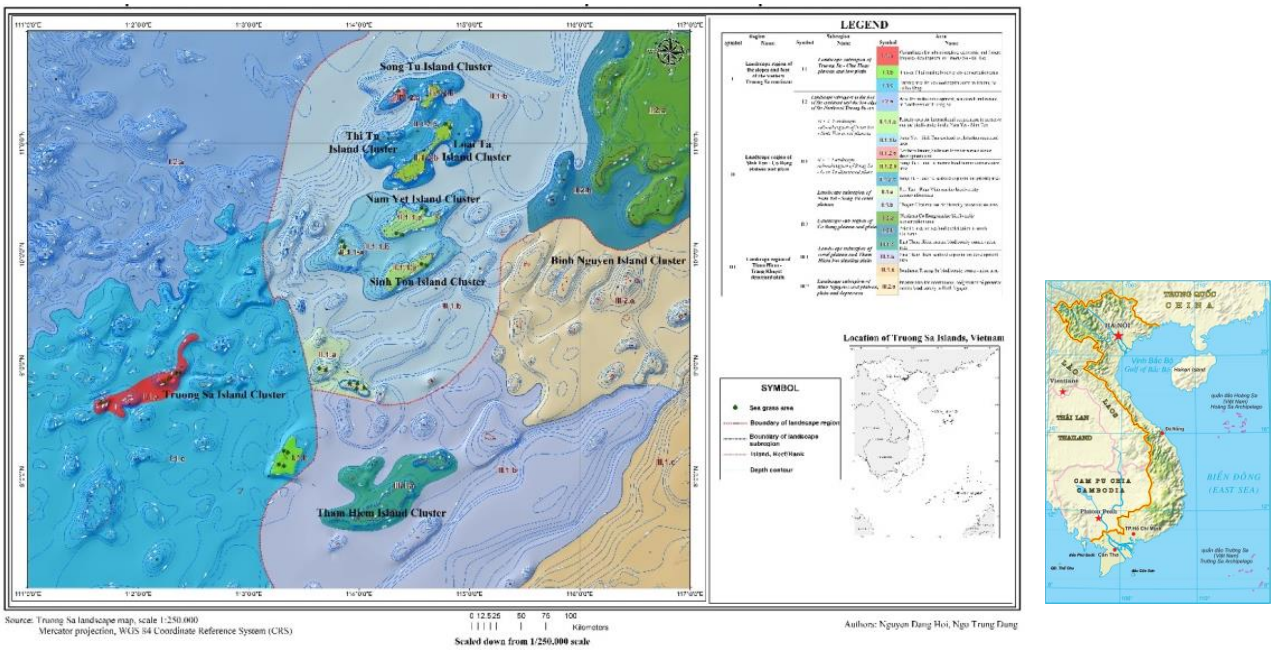


Figure 3. *Spatial orientation map for resource management, environmental protection and biodiversity conservation associated with national defense and security in the Truong Sa islands*

Environmental protection and biodiversity conservation: Establish buffer zone and transition zone of the Nam Yet - Sinh Ton World Biosphere Reserve. Implement spatial zonation to create management areas according to the criteria of the World Biosphere Reserve. The conservation area includes the entire space of the area, regardless of the current managing entity.

* Song Tu - Loai Ta Reefs marine biodiversity conservation area (II.1.2.b); Northern Co Rong Reefs marine biodiversity conservation area (II.2.a); East Tham Hiem Reefs marine biodiversity conservation area (III.1.a); Southeast Truong Sa Islands biodiversity conservation area (III.1.c); Binh Nguyen Reef Priority area for international cooperation to preserve marine biodiversity (III.2.a):

- Economic development and resource management: Manage marine biological resources according to subregions; establish seasonal restricted fishery activity from January to June each year on some economic fishes such as yellowfin tuna, king mackerel, and scad, ...

- Environmental protection and biodiversity conservation: Strengthen biodiversity conservation for typical shallow water marine ecosystems such as coral reefs and seagrass

meadows. Promote international cooperation in marine biodiversity conservation at East Tham Hiem Reef marine biodiversity conservation area and a priority area for international cooperation to preserve marine biodiversity in Binh Nguyen Reef.

c) Priority areas for fishery and maritime traffic

Includes *Priority areas for the fishery in Truong Sa - Chu Thap Reefs (I.1.c), Song Tu - Loai Ta Reefs (II.1.2.c), southern Co Rong Reef (II.2.b), and East Tham Hiem Reef (III.1.b); and marine biodiversity conservation area on Thuyen Chai Reef (II.1.b)*;

- Economic development and resource management: Prioritize the development of fishery activities, focusing on economic fishes such as *Katsuwonus pelamis*, *Auxis thazard*, *Euthynnus affinis*, *Thunnus tonggol*, *Thunnus obesus*, *Cacharinus sorah*, *Thunnus albacares*, *Acanthocybium solandri*, *Istiophorus orientalis*. Strengthen cooperation in joint marine exploitation in areas III.1.b and II.2.b.

- Environmental protection and biodiversity conservation: Develop a policy framework for fishery activities, with a focus on regulations of requirements and equipment toward sustainable fishery. Preserve precious and rare marine species such as dolphins and rays, ...

** Area for maritime transportation development, sea search and rescue in the Northwestern part of Truong Sa Islands (I.2.a)*:

- Economic development and resource management: Prioritize development of maritime transportation, and search and rescue cooperation. Promote seasonal fishery for the period of January to June each year, with an intensive focus from February to May, to avoiding the spawning season of economic fish species (yellowfin tuna, king mackerel, scad...).

- Environmental protection and biodiversity conservation: protect the marine environment, build response scenarios for maritime incidents such as oil spills, oil pollution, etc. Preserve precious and rare marine species such as dolphins and sea turtles. A sustainable fishery to avoid fish stock degradation and exhaustion.

4. CONCLUSIONS

The marine landscapes of the Truong Sa Islands feature warm water and tropical coral reef landscapes. The differentiation of physical components and anthropogenic agents has formed a diverse landscape taxonomy with 1 system, 1 sub-system, 4 classes, 7 sub-classes and 20 kinds of landscape, distributed on 6 subregions and 2 secondary subregions of 3 marine landscape types.

Analysis outcomes using DPR and SWOT methods on landscape region and subregion, respectively represented priority areas designated for resource management and biodiversity conservation in the Truong Sa Islands area. The spatial scheme prioritises 3 purpose groups (i) Administrative, economic and fishery logistics service developments; (ii) Marine biodiversity conservation and restrict fishery activities; (iii) Fishery and maritime transportation.

In correspondence to each purpose group, we propose a combination of solutions for 2 aspects as the following: Economic development and resource management; Environmental protection and biodiversity conservation. Implementation of solutions is recommended to be designated according to specific features of each landscape region/subregion.

REFERENCES

[1] Central Executive Committee of the Communist Party of Vietnam (2018). *Strategy for sustainable development of Vietnam's marine economy to 2030, vision to 2045*, Hanoi.

[2] Burke L., Selig E., Spalding M., McManus J. (2002). "Reefs at Risk in South East Asia", *The Future of Coral Reefs as Whole Systems under Climate Change*, 72 p.

[3] Dang Thi Ngoc, Nguyen Cao Huan, Nguyen Dang Hoi, Tran Van Truong, Ngo Trung Dung (2020). "*Classification system and landscape characteristics of the coastal zone of Quang Ngai province*". VNU Journal of Science: Earth and Environmental Sciences, Volume 36, No. 4(2020):52-63.

[4] English S., Wilkinson C. and Baker V. (1997). *Survey Manual for Tropical Marine Resources*. Australian Institute of Marine Science. Townsville. 390p.

[5] Gürel E. (2017). "SWOT analysis: a theoretical review", *Journal of International Social Research*, Vol. 10, pp. 994-1006.

[6] Hamdi A., Populus J., Piel S. (2021). "Marine landscape maps: methodology and potential use", *CoastGIS07*, 18 p, ifremer.fr.

[7] Kurniawan F., Adrianto L., Bengen D., Prasetyo L. (2016). "Patterns of Landscape Change on Small Islands: A Case of Gili Matra Islands, Marine Tourism Park, Indonesia", *Procedia - Social and Behavioral Sciences*, Vol. 227, pp. 553-559.

[8] Licht F.P. (1990). "*Atlas of underwater landscapes of the Japanese sea*". Moscow science 224.

[9] Mimura N. (2008). *Asia-Pacific Coasts and Their Management: States of Environment*, Springer, The Netherlands, 367 p.

[10] Ngo Trung Dung, Nguyen Dang Hoi, Nguyen Quoc Khanh, Nguyen Cao Huan, Dang Thi Ngoc, Vu Le Phuong (2022). Multidisciplinary approach in marine landscape study: A case study of marine landscape mapping scaled at 1/50.000 for remote maritime region of Nam Yet - Sinh Ton cluster, Truong Sa Islands, Vietnam, Proceedings of the 5th Aasian Conference on Geography Thai nguyen University, p.15-31.

[11] Nguyen Dang Hoi, Ngo Trung Dung, Kuznetsov A. N. and Vu Le Phuong (2022). "*Classification and mapping of marine-island landscape in Nam Yet Island, Truong Sa Islands, Vietnam"*. Vietnam Journal of Earth Sciences. p. 1-21.

[12] Nguyen Ngoc Khanh, Nguyen Cao Huan, Pham Hoang Hai (1996). "*Research on Vietnam landscape classification units at scale 1:1,000,000 (land and sea)*". VNU Journal of Science, Geography Issue, 30th-anniversary issue of Geography, Hanoi: 15-21.

[13] Nguyen Thanh Long, Nguyen Van Vinh (2012). "*Initial classification of Vietnam's sea and island landscapes*". Proceedings of the 6th National Geoscience Conference. Publishing House for Science and Technology, p. 107-115.

[14] Tran Anh Tuan (2013). "*Scientific basis and methodology for complex assessment of natural conditions and resources to serve the development guidances of offshore areas and islands, applied to Truong Sa islands*". Journal of Marine Science and Technology, Volume 13, No4: 324-334.

[15] Preobrazhensky B.V. et al (2000). *Fundamentals of underwater landscape science*. Dalnauka. Vladivostok**:** 351p.

CLIMATE CHANGE AND DISASTER MITIGATIONINNOVATION MEASURES FOR EARTH, MINING AND ENVIRONMENTAL SCIENCES
(Innovative measures for earth, mining and environment sciences to meet sustainable development goals)

FLOOD EARLY WARNING SYSTEMS IN HO CHI MINH CITY, VIETNAM: CURRENT STATUS, CHALLENGES AND WAY AHEAD

Anh Cao[1]*, Vo Le Phu[2,4], Luu Dinh Hiep[2,4], Nguyen Danh Thao[3,4], Yoshimura Kei[1]

[1] Institute of Industrial Science, The University of Tokyo, 5-1-5 Kashiwanoha, Kashiwa, Chiba, Japan

[2] Faculty of Environment & Natural Resources, Ho Chi Minh City University of Technology (HCMUT), 268 Ly Thuong Kiet street, District 10, Ho Chi Minh City, Vietnam

[3] Faculty of Civil Engineering, Ho Chi Minh City University of Technology (HCMUT), 268 Ly Thuong Kiet street, District 10, Ho Chi Minh City, Vietnam

[4] Vietnam National University Ho Chi Minh City, Linh Trung ward, Thu Duc District, Ho Chi Minh City, Vietnam

*Corresponding author: anh-cao@iis.u-tokyo.ac.jp

Abstract: Flood early warning systems (FEWS) are the crucial tool for reducing flood loss and damage, especially under increasing flood risks due to climate change. FEWS has four elements, namely Risk knowledge, Monitoring and forecasting, Warning dissemination, and Response capability. Despite existing global surveys on FEWS providing an overview of FEWS adequacy, there is a limited in-depth understanding of the current status of FEWS operations and challenges when implementing FEWS, particularly at the local government level. Ho Chi Minh City, Vietnam has been identified as one of the cities that are most vulnerable to increasing flood risks due to urbanization and climate change. In this study, in-depth interviews with various stakeholders were conducted at both national and local levels to reveal the currentstatus and challenges in operating FEWS in Ho Chi Minh City, Vietnam. The results indicated that although risk factors and socio-economic factors were well understood at relevant departments, the lack of coordination between them hindered the development of comprehensive vulnerability assessment. The government invested in various monitoring equipment and started initiatives to incorporate forecasting technology. However, more observation data and financial resources are necessary to improve model accuracy and to implement it at a larger scale. The current dissemination of warnings is merely at delivering hydro-meteorological information. Action-oriented information needed to be disseminated to enhance response capability of both the government and residents. Stronger commitment in communication programs can improve knowledge and response capability in residents. This study unveiled various challenges in developing an adequate and people-centred FEWS in Vietnam, particularly at the local level including lack of coordination between agencies, scattered initiatives, inadequate financial resources and observation data.

Keywords: *flood risk, early warnings, risk assessment, risk information, flood response*

1. INTRODUCTION

Flood risk in urban areas has significantly drawn extensive attention of the governments and authorities worldwide due to its costly damages and increasing extreme weather events. Floods are the most common disaster and have affected more than two billion people, causing over one million deaths and economic loss of US$80 billion [1, 2]. Vietnam is among the 10 countries most affected by climate risk and related extreme events in the period of 1999 – 2018 with total losses of US$ 2,018, equivalent to 0.47% per unit of GDP

[3]. Flood damage and loss account for about 2.5% of total annual household income in the Mekong Delta [4]. Flood damage has been growing exponentially due to increased flood risk induced by climate change, urbanization, and development practices. In coping with such risk, flood early warning systems (FEWS) are crucial and have been successfully implemented in numerous areas globally to prevent loss and damage from flooding, especially extreme events such as storms and heavy rainfalls.

Early warning is defined by the International Strategy for Disaster Reduction as "the provision of timely and effective information, through identified institutions, that allows individuals exposed to hazard to take action to avoid or reduce their risk and prepare for effective response" [5]. FEWS is more than just a prediction, it is an integrated system of four key elements, namely Risk Knowledge, Monitoring and Forecasting, Warning Dissemination, and Preparedness and Response Capability [6].

Risk knowledge refers to systematically collecting data and undertaking risk assessment, specifically the identification of flood risks and related threat, and the consolidation of such risks into hazard maps. Vulnerability assessment involves overlaying hazard exposures with socio-economic factors such as population density, infrastructure, or economic sectors. Risk assessment and hazard maps are useful in planning for preparedness and responses in the event of disaster and in long-term development planning, which determines community resilience to disasters. Risk knowledge can also help to increase risk awareness in residents, directly influencing individual preparedness and response to warnings.

Monitoring and Forecasting refers to the observation of hazards and provision of warning services using hydrological models with observed data. Forecasting model must have a strong scientific base to provide reliable and timely warnings, which is the core of early warning systems. Continuous, long-term observation data is crucial in improving accuracy of forecasting models.

Warning Dissemination refers to risk information and early warning communication to those at risk in a timely and effective manner. Warnings must include useful information of coming hazards, be clear, easy to understand to motivate population at risk to take proper actions to prepare and respond to risks. It is important to make sure that the population at risk can timely receive warnings. Consideration of vulnerable groups must be integrated as they usually have limited access or exposure to receive warnings.

The last key element of FEWS is *Preparedness and Response Capability*. Disaster preparedness and response plans must be created and implemented at both national and local levels to mitigate flood impacts and respond effectively when they occur. These plans must be well practiced and incorporate a participatory approach to include communities' perspectives to better enhance their capabilities. Communities should be well informed of what to prepare and what actions to take in the event of disasters. These require strong preparedness education programs, training activities, and evacuation drills. Such efforts can help increase risk perception and disaster (response) awareness, informing their actions and behaviours when receive flood early warnings.

Strong integration of these four key elements builds a people-centred FEWS, which motivates people and communities at risks to timely take proper actions to protect their lives and livelihoods, which in long-term build resilience to disasters.

Despite the recognized importance of FEWS, there are limited literature investigating all component of FEWS as most existing studies have focused on the technical aspect of providing warning services (i.e., forecasting technology or crucial role of community engagement and preparedness) [7, 8]. In 2005, a global survey reviewed early warning systems in 122 countries and indicated that there was significant development of knowledge and technical tools for risk assessment, generation of forecasts, and communication of warnings [6]. Especially forecasting technologies had been available for all types of hazards. The results pointed out an unequal focus on generating and issuing warnings and the three other elements were absent or weak. This imbalance was an attribute to factors such as the lack of political commitment in developing and operating integrated early warning systems, lack of coordination between stakeholders, lack of public awareness and participation. In 2019, Perera et al. provided an overview of FEWS availability in 47 developing countries and six developed countries [9]. The survey indicated that developing countries made continuous progress in implementing FEWS, but least developing countries only have basic warning systems. Although the survey provided insights into the current status and challenges in operating forecasting centre, it overemphasized the technical aspects (Monitoring and Forecasting element of FEWS) over the community response and preparedness. This is because the target respondents are national-level forecasting centre, which is crucial but only one of the actors involving in the integrated FEWS. NeuBner examined warning alerts in practice, covering 110 warning schemes and emphasized on consistent warning schemes across different hazards and even in different countries, which can be useful considering that global trades and international immigrants are increasing [10]. Aguirre-Ayerbe et al. took a step further in examining all key elements of FEWS in Maldives, Sri Lanka, Myanmar, and the Philippines [11]. However, its scope is still limited to at the national scale despite the involvement of different stakeholders. Garcia and Fearnley investigated the interlinkages of the four key elements of early warning systems, highlighting the importance of all four key elements [12].

While existing studies have provided a global overview of the availability, adequacy, and various challenges of FEWS, all of them addressed FEWS at the national level through involving national forecasting centres or high-level decisionmakers. Such studies provided merely the surface of FEWS implementation process. There is a lack of in-depth understanding of FEWS operation at the local level, where local governments play a crucial role in operating FEWS. Local governments involve in most key elements of FEWS, particularly Risk Knowledge as they have the most understanding of the local context. Additionally, local governments directly communicate with residents and have the responsibilities to implement disaster risk preparedness and response measures to ensure residents' safety.

Addressing this research gap, this study conducted in-depth interviews with various stakeholders to understand the current status and challenges of FEWS operation at the local level with a case study of Ho Chi Minh City (HCMC), Vietnam. HCMC was selected as the city is among the most vulnerable cities to increasing flood risks due to urbanization and climate change [13].

The present paper firstly provides an overview on flooding situation in HCMC and FEWS operation in Vietnam, which sets the background to identify stakeholders for FEWS operations in HCMC. The study area is briefly described to capture the context of natural

conditions and fast urbanisation and population growth in HCMC which result in flood risks. Then, this section provides details of in-depth interviews conducted to collect data for content analysis for the research objective. The section of Results presents and synthesizes the interview results, organized according to the four key elements of FEWS. Future policy implications were discussed and proposed to provide recommendations for ways to address operational challenges and move forward. The paper then concludes on key findings and suggestions for future research directions.

2. MATERIALS AND METHODS

2.1. Description of the study area

Ho Chi Minh City (HCMC) is the largest commercial city in Vietnam, located at the downstream area of Sai Gon and Dong Nai rivers. Naturally, HCMC is vulnerable to floods because of its low-lying topography. The elevation of approximately 65% of the city's areas is lower than 1.5m, which has been experiencing flooding frequently due to heavy rains and high tides [14]. Adding to the flood issue, rapid urbanization in the city significantly decreased its drainage capacity through filling up natural waterways with concrete-built environment and increased population overloading the aging drainage system constructed since the French colonization [15]. Furthermore, land subsidence also contributes to this complexed problem. Extensive groundwater extraction and heavy construction on soft soil led to an accumulation of 0.5 m of land subsidence in some parts of the city [16, 17].

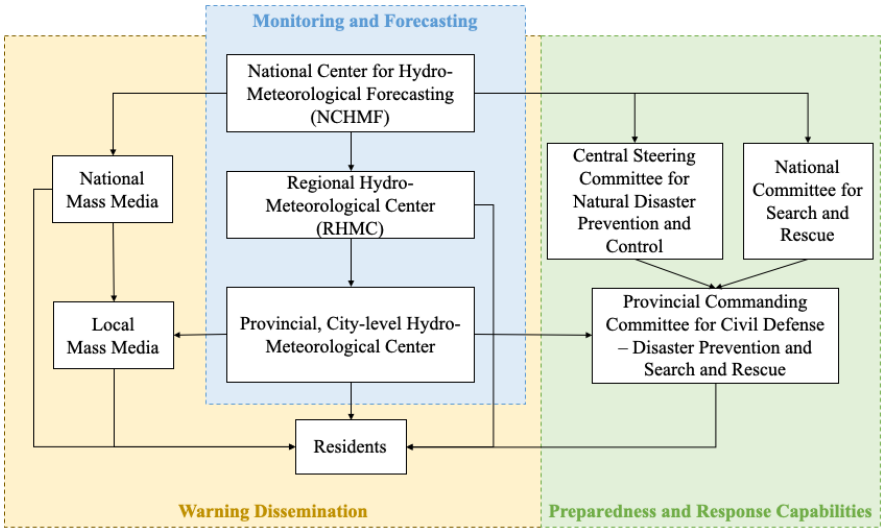


Figure 1. *Key stakeholders of flood early warning systems in Vietnam*

Hence, HCMC is among the most vulnerable cities to the impacts of climate change, particularly to increased precipitation, sea level rise, and extreme weather events [13].

To understand FEWS operation in HCMC, it is also important to grasp the overall structure of information flows at and from the national level. Literature reviews and in-depth interviews were carried out to map the FEWS scheme at the national level and to identify challenges in implementing FEWS at the local level in HCMC. Figure 1 depicts the stakeholder map for FEWS in Vietnam. Large flood forecasts are performed at the National Centre for Hydro-Meteorological Forecasting (NCHMF), which will be disseminated to the Central Steering Committee for Natural Disaster Prevention and Control, the National Committee for Search and Rescue, and Regional Hydro-Meteorological Centres (9 regional forecasting centres). The

regional forecasting centres further disseminate warnings to Provincial Hydro-Meteorological Centres, who will then inform the Provincial Steering Committee for natural Disaster Prevention and Rescue for preparedness and response. Moreover, warnings from NCHMF are also sent directly to National Mass Media for broadcasting to residents, which will be disseminated through the local news channels as well.

2.2. Stakeholders in operating FEWS in HCMC

Based on this understanding of information flow structures, stakeholders for the in-depth interviews are identified. The Southern Regional Hydro-Meteorological Centre is in charge of performing forecasts for 18 provinces in the southern Vietnam and directly for HCMC and disseminating warnings to other in line government bodies and agencies as described in Table 1. The Sub-Institute for Hydrometeorology and Climate Change and HCMC Space Technology Application Center conduct research projects that are requested by the National government or HCMC People's Committee. Division of Infrastructure and Planning and Urban Infrastructure Construction – Project Management Unit utilizes and provide data relevant to flood risk and vulnerability assessment. Division of Meteorology, Hydrology, and Climate Change collects hydrometeorological data from other stakeholders and organizes such information. The city's Commanding committee for Civil Defense – Disaster Prevention and Search and Rescue is responsible for developing disaster response plan for the People's Committee, raising public awareness and building response capabilities in the communities.

Table 1. Government Agencies for in-depth interviews regarding flood early warning systems in Ho Chi Minh City

National Agency	Regional Agency	Local (City) Agency
National Centre for Hydro-Meteorological Forecasting (NCHMF)	- Southern Regional Hydro-Meteorological Centre. - Sub-Institute for Hydrometeorology and Climate Change	- HCMC Space Technology Application Centre. - HCMC Department of Planning and Architecture – Division of Infrastructure and Planning. - HCMC Urban Infrastructure Construction – Projects Management Unit. - HCMC Sub-Department of Irrigation and Flood and Storm Prevention. - HCMC Department of Natural Resources and Environment (DONRE) – Division of Meteorology, Hydrology, and Climate Change. - Commanding Committee for Civil Defense – Disaster Prevention and Search and Rescue of HCMC.

2.3. Data collection

In-depth interviews were conducted in Vietnamese, lasting 30 minutes to one hour from June 28th – July 7th 2023. The key questions for in-depth interviews with stakeholders in HCMC were based on the World Meteorological Organization (WMO) checklist for a people-centered multi-hazard early warning system, covering all four areas of Risk knowledge, Monitoring and Forecasting, Warning Dissemination, and Preparedness and Response capability. These questions are shown in Figure 2. The interviews were transcribed and qualitatively analyzed based on the key themes of the FEWS and challenges.

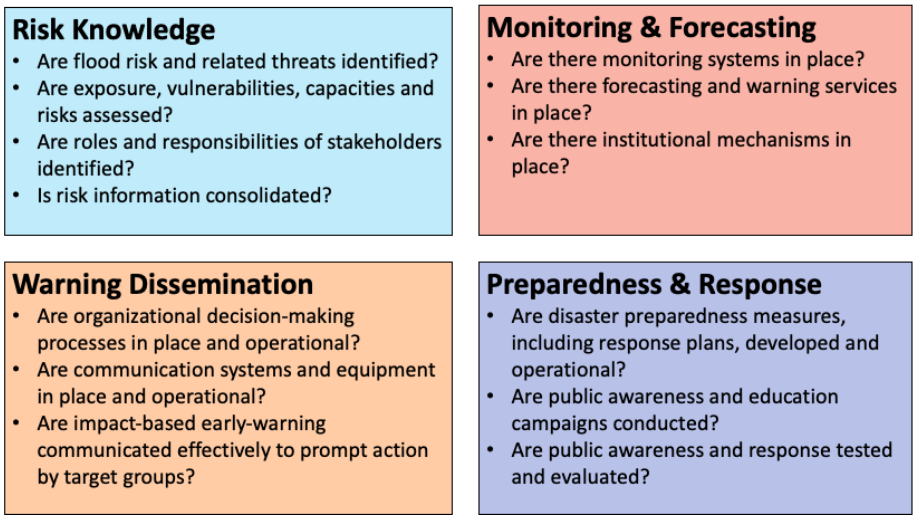


Figure 3. *Multi-Hazard Early Warning Systems: A Checklist [18].*

3. RESULTS

Table 2 summarises the key findings of the interviews with stakeholders, including current status and challenges in operating FEWS regarding to the four key elements. Detailed results are described in the following sections.

Table 2. Summary of current status and challenges in operating FEWS in HCMC

	Current Status	Challenges
Risk Knowledge	- Flood characteristics are well understood. - Overall vulnerability assessment was conducted but comprehensive assessment is missing. - Role and responsibilities in creating risk knowledge are not yet clearly defined. - Hazard maps are not yet developed.	- Complicated procedures to incorporate socioeconomic data. - Coordination and knowledge exchanges between agencies are inadequate. - Hazard maps are project-based.
Monitoring and Forecasting	- Monitoring systems are in place but still insufficient. - Several projects conducted to implement forecasting models. - Warning information focuses on weather forecast.	- Limited observation data. - Limited financial resources. - Aging combined drainage system - Public awareness (littering into the drainage pipes). - Scattered project targeting only

	- Institutional mechanisms are in place.	certain areas of the city. - Complicated and time-consuming institutional procedures. - Forecasting model uncertainties.
Warning Dissemination	- Top-down information flow from national to city level warning center and then to other local government agencies. - Communication systems and equipment are in place (TV, radio, bulletin, websites. - Warnings are not communicated on impact-based.	- Lack evaluation on effective communication channel. - Lack action-oriented warnings. - Specific affected areas are unidentified.
Preparedness and Response	- Disaster preparedness and response plans are developed and operational. - Public awareness programs are conducted (TV programs and radio broadcast, community-based program). - Public awareness and responses are not evaluated.	- Heavy schoolwork hinders disaster education. - Low risk perception due to limited experience with extreme events. - Lack equipment for emergency response. - Confusing and time-consuming procedures to obtain financial resources. - Coordination between agencies is missing or delayed.

3.1. Risk Knowledge

The interview results indicated that at the local level of HCMC, flooding characteristics are identified and well understood, together with the city context of nature topography and urbanization process. Rainfall historical data has been recorded and evaluated since the 1960s, providing a comprehensive understanding of the city's exposure to different types of floods. An overall vulnerability assessment of the city was conducted and provided risk levels for flood hazards. However, more detailed vulnerability assessments have not been implemented yet in HCMC. To conduct vulnerability assessment, socio-economic data such as population density, infrastructure maps, and development of economic sectors are important to overlay with exposure to floods. However, such data required official purchases from the General Statistics Office of Vietnam for usage, which hindered the vulnerability assessment scheme.

Roles and responsibilities of stakeholders involving the creation of risk knowledge are not yet clearly defined although stakeholder roles regarding other elements (Monitoring and Forecasting, Warning Dissemination, Preparedness and Response) are already identified in administrative decisions and publicly stated in the official websites of the stakeholders. Moreover, coordination and knowledge exchanges between different city division were more frequent before Covid19 pandemic. At the time of this study, such activities between stakeholders have not fully resumed.

Regarding the creation and dissemination of hazard maps, these maps are not yet developed to identify the geographical areas and population that could be affected by floods. Currently, HCMC has numerous flood hotspots, recorded based on traffic roads. A city-wide assessment of flooding areas has not yet been implemented because such hazard maps are usually project-based when financial resources are available.

3.2. Monitoring and Forecasting

Monitoring systems are in place for all weather regions in Vietnam, including HCMC. There are six meteorological stations (three are automatic), four hydrological stations (two are automatic), and 15 rain gauge stations (eight are automatic) equipped for HCMC. Himawari-8 Satellite images are also utilized for monitoring and forecasting.

The Southern Regional Hydrometeorological Centre (SRHMC) provides weather and flood forecasting services and warnings of severe weather. However, flood forecast in HCMC remains at weather forecast information such as warnings about heavy rains, wind or high tides. There are no early warnings providing details of areas that will be flooded and level of flood depths. There are several projects have been conducted to implement forecasting models such as WRF, Flood4Cast by Hydroscan, or combining WRF with hydrometeorological data, radar data and traffic cameras to provide to detailed warnings but only limited to certain districts in the city. Besides, these projects are scattered, there lacks systematic implementation to advance the forecasting model on the city scale. The officers indicated that institutional procedures for implementing such projects are also complicated and time-consuming. Hence, projects related to flooding have been moving slowly.

The interview results indicated various challenges in predicting floods in HCMC. Firstly, there are limited observation data (ex. Lack of real-time rainfall data) and limited financial resources for investing in more monitoring equipment. Secondly, there lacks comprehensive understanding of existing drainage system and infrastructure that influence the drainage capacity of the city. Further, the complexity of urban drainage systems is an additional hurdle to flood mitigation and prediction. There is the fact that the drainage systems in HCMC is a combination of sewerage system which was designed to convey both domestic wastewater and rainwater. More importantly, the previous design of drainage systems did not include the scenario of high rainfall due to extreme weather events. Social norms also add to this problem. Most of residents throw their daily garbage into drainage pipes or canals, which further reduce the already limited capacity of the drainage system. Finally, uncertainties of rain forecasting models and urban flood models limit the accuracy of flood predictions.

3.3. Warning Dissemination

Flood forecast is provided to mass media including TV and radio broadcasting channels and central newspaper. Warnings and forecasts are posted on the website of the National Centre for Hydro-Meteorological Forecasting, which is also disseminated to Regional and Provincial Hydro-Meteorological Forecasting centres (RHMC and PHMFC). The RHMC and PHMFC provide further detailed forecasts to the Provincial Flood and Storm Control Committees, the local TV channels, radio broadcasting channels with forecasting bulletin. The Steering Committee for Natural Disaster Prevention and Control also launch a mobile application for residents to get access to flood warnings, raise public awareness and build

capability for preparedness and response. However, the effectiveness of these strategies is not yet evaluated.

Rainfalls are forecasted with lead time of 2-3 days and used as inputs for hydrological forecasts. If river water levels are forecasted to exceed alarming level II, flood warnings are disseminated twice a day. If the river water levels are forecasted to exceed alert level III, flood warnings are disseminated three times per day. However, flood warnings information primarily focuses on hazard characteristics such as rainfall amount, wind speed. Hazard characteristics are categorized into warning levels. However, such levels are not directed linked to preparedness and response actions. Furthermore, warnings currently do not provide specific areas that will be affected by floods. For example, daily warnings of flood in HCMC provide observation rainfall data and tide water levels of the previous day and forecasts of the water levels for the next day with warning level but there is no information regarding which areas will be affected.

3.4. Preparedness and Response Capabilities

Disaster preparedness and response measures are already developed at national level and local level. For HCMC, detailed of disaster preparedness and response plan are determined in the administrative decision No.1337, Ho Chi Minh City and operational in HCMC Steering Committee for Natural Disaster Prevention and Control.

Public awareness programs are an important strategy that are recognized and developed in Decision No. 553 and Decision No. 3089, HCMC. Every year, the city radio broadcasts around 104 shows, the city TV channel broadcasts 15 shows to communicate weather and hydrological knowledge to raise public awareness of heavy rainfall, floods, and high tides. Besides, detailed plans to increase public awareness of flood knowledge and preparedness are developed in Plan No. 35 and Plan No.24 and operational in HCMC. Community-based awareness programs are implemented but there is no evaluations or reports on its effectiveness on the target population. Disaster education campaigns are developed but has encountered difficulties in implementation due to the heavy work load that students have to take in school.

Risk perception and response perception in residents in HCMC are not as high as in other regions such as in the northern or central Vietnam due to limited experience with extreme flood events that requires evacuation. Houses in HCMC are also less sturdy, making them vulnerable to floods and storm events. Further efforts are necessary to increase preparedness and response capabilities of residents. In some cases, affected residents did not follow evacuation orders even though security to their assets were provided.

Regarding capability to response to floods, HCMC military forces are trained for emergency response and rescue. However, the officers indicated that necessary equipment for emergency response is inadequate. There lacks financial resources for purchasing rescue equipment. Besides, institutional procedures for financial decisions are confusing and time-consuming, which hinder the response and rescue process when disaster happens. Adding to this, existing facilities and built environment also hinder the disaster response process. For example, rescue vehicles and fire truck have difficulties in accessing narrow streets. The preparedness and response process in the local government involves various stakeholders including high-level Party Agency, the Red Cross, and the Woman Association. However,

coordination between these agencies is missing or delayed, which influence the response capability of the local government.

4. DISCUSSION AND FUTURE DIRECTIONS OF FEWS

The early warning system is in place in Vietnam. However, the implementation of FEWS scheme in HCMC remains fragmented performance, including unavailable hazard map of flood risk, insufficient data for flood forecasting, and the lack of coordination between local government agencies. There are several published studies on creating flood loss analysis for HCMC (and other cities) [19] [20] [21] [22] [23], but not systematically conducted at the local level across Vietnam. Moreover, these studies were not utilized in flood risk management, city planning or in communicating to residents. Such fragmentation suggests that an integrated approach to flood risk governance is needed to improve the coordination of various stakeholders from central to local level and within the local level [24]. The existing involvement of stakeholders in FEWS (as shown in Figure 1) indicates that among the four key FEWS's elements, roles of stakeholders in relation to Risk knowledge component have not been implicit yet. Risk profiles and vulnerability assessment set the crucial contexts for the local areas, providing critical information for other FEWS elements. Enhanced risk knowledge, particularly developing comprehensive vulnerability assessment can contribute to long-term resilience when incorporated into development pathways [25]. To achieve that, the city government should establish a department dedicated to collecting and storing data regarding historical flood events, creating hazard maps, and conducting vulnerability assessment to provide to other governmental agencies involving in flood forecasting, city planning and flood preparedness and response, and the general public. Such department requires financial resources, human resources, and coordination with other governmental agencies to function and effectively contribute to the FEWS operation.

Risk knowledge of the flood characteristics and factors that attribute to vulnerability to floods were well identified and assessed at relevant departments. However, the lack of coordination between them hindered the development of comprehensive vulnerability assessment. To further enhance risk knowledge in HCMC, the need for integrated flood risk governance is vital. Existing literature suggested that establishing collaborative mechanism can enhance integrated flood risk governance and local knowledge, local agencies and trusts between stakeholders are enablers of such collaborative mechanism [26]. Furthermore, hazard map has not been developed to be disseminated to relevant agencies and residents. This should be the priority of the city government, which can significantly increase public awareness of their own vulnerabilities and can be useful for city planning for long-term resilience.

The government invested in various monitoring equipment and started initiatives to incorporating forecasting technology. However, more observation data and financial resources are necessary to improve model accuracy and to implement it at a larger scale. Reliable global real-time simulation model such as Today's Earth will be useful to provide data such as river discharge even in areas that lack monitoring equipment, which can be used to produce detailed forecasts [27].

Flood forecasting in HCMC has encountered various challenges due to the complexity of local context, which is exposed to various hazards such as heavy rainfalls, storm surges, and

relative sea level rise (including land subsidence). The current forecast technology can only provide hydro-meteorological information of hazardous events and accuracy of flood forecasts needs further improvement due to lack of observation data, uncertainties of forecasting models, and other factors such as knowledge of existing drainage systems.

Warning dissemination has been implemented through mass media (TV and radio) and websites of forecasting agencies, and disaster prevention and control agencies. There lacks evaluation of whether information actually reaches population at risk. Such evaluation is crucial to measure the effectiveness of dissemination and identify vulnerable groups that do not have access or means to receive warnings. Similar to existing FEWS in many other countries, FEWS in Vietnam is implemented in a typical top-down approach, where the national forecasting centres issues warnings to national authorities and regional warning centres, who in turn communicate to provincial and local authorities. The interview results highlighted the lack of effectiveness assessment of current warning dissemination approach. Especially, this top-down approach has been revealed to be insufficient and unable to timely reach population at risks. Furthermore, dissemination means such as TV or radio broadcast have limited ability to reach vulnerable group such as impoverished population, women, children, or the elderly [28] [6].

Besides, the current dissemination of warnings is merely at delivering hydro-meteorological information. Action-oriented information needed to be disseminated to enhance response capability of both the government and residents. Risk perception was indicated as a challenge, which influences residents' attitude towards warnings. Similar to the finding of Perera et al., sometimes residents do not take actions even when evacuation orders are issued [9]. Understanding public risk perception is important to tailor communication strategies [12]. Therefore, stronger commitment in communication programs can improve knowledge and response capability in residents.

Lastly, various efforts to increase the preparedness and response capabilities of residents have been implemented in HCMC. However, these also lack evaluation on effectiveness of these efforts. Such evaluation should be prioritized to identify what is working well and what needs improvements. This goes together with understanding public risk perception to tailor communication strategies and capacity building campaigns accordingly.

5. CONCLUSION

This study investigated the FEWS implementation at the local level through in-depth interviews with various stakeholders in HCMC. The results provided an overview of current status of operating FEWS in HCMC regarding key elements of Risk Knowledge, Monitoring and Forecasting, Warning Dissemination, and Preparedness and Response Capabilities. All key elements of FEWS in HCMC are established and operational. However, there lacks systematic evaluation of their effectiveness. Major challenges in operating FEWS at the local level were discussed to be fragmented efforts in building risk knowledge, insufficient observation data, complexities of local context, and lack of coordination between government agencies.

This study is the first to investigate all four key elements of FEWS implemented at the local level, which provides insights into various challenges that governments are encountering. Other cities in the region might encounter the same challenges. Future research should aim to set up an integrated approach to flood risk governance and a nation-

wide survey of FEWS implementation at the local level to quantify if similar challenges persist in other contexts.

ACKNOWLEDGMENTS

This study was supported by the JST-Mirai program, "New Social Challenges" mission area – "Advance practice of watershed flood management using surface hydrological prediction system", grant number JPMJMI21I6. We thank the government officers in Ho Chi Minh city who supported and coordinated the interviews conducted in this study. We also acknowledge the support of time and facilities from Ho Chi Minh City University of Technology (HCMUT), Vietnam National University, Ho Chi Minh for this study.

REFERENCES

[1] World Health Organization. Floods [Internet]. www.who.int. World Health Organization; 2021. Available from: https://www.who.int/health-topics/floods#tab=tab_1

[2] Floods [Internet]. public.wmo.int. 2021. Available from: https://public.wmo.int/en/resources/world-meteorological-day/previous-world-meteorological-days/climate-and-water/floods

[3] Eckstein D, Künzel V, Schäfer L and Winges M 2019 Global Climate Risk Index 2020: Who Suffers Most from Extreme Weather Events? Weather-Related Loss Events in 2018 and 1999 to 2018 (Bonn: Germanwatch)

[4] Chinh DT, Dung NV, Gain AK and Kreibich H 2017 Flood loss models and risk analysis for private households in Can Tho City, Vietnam *Water* **9** 313.

[5] Terminology: Basic terms of disaster risk reduction [Internet]. Available from: https://www.unisdr.org/files/7817_7819isdrterminology11.pdf

[6] Global Survey of Early Warning Systems [Internet]. Available from: https://www.unisdr.org/2006/ppew/info-resources/ewc3/Global-Survey-of-Early-Warning-Systems.pdf

[7] Schröter K, Ostrowski M, Velasco C, Torres DS, Nachtnebel HP, Kahl B, Beyene M, Rubin C, Gocht M, Aqua-Water&Finance P 2009 First Crue Era-Net Common Call Effectiveness and Efficiency of Non-Structural Flood Risk Management Measures. Bundesministerium für bildung und Forschung, Minsterio de educación y ciencia, Darmstadt University of Technology-IHWP, Universitat Politècnica de Catalunya-GRAHI-UPC, University of Natural Resources and Applied Life Science (BOKU), Pro Aqua-Water & Finance: London, UK.

[8] Rogers D, Tsirkunov V. Global Assessment Report on Disaster Risk Reduction: Costs and benefits of early warnings systems [Internet]. World Bank; 2010. Available from: https://documents1.worldbank.org/curated/en/609951468330279598/pdf/693580ESW0P1230aster0Risk0Reduction.pdf

[9] Perera D, Seidou O, Agnihotri J, Rasmy M, Smakhtin V, Coulibaly P, Mehmood H 2019 Flood early warning systems: a review of benefits, challenges and prospects. UNU-INWEH, Hamilton.

[10] Neußner O Early warning alerts for extreme natural hazard events: A review of worldwide practices. *International Journal of Disaster Risk Reduction***60** 102295.

[11] Aguirre-Ayerbe I, Merino M, Aye SL, Dissanayake R, Shadiya F, Lopez CM 2020 An evaluation of availability and adequacy of Multi-Hazard Early Warning Systems in Asian countries: A baseline study. *International journal of disaster risk reduction* **49** 101749.

[12] Garcia C, Fearnley CJ 2012 Evaluating critical links in early warning systems for natural hazards. *Environmental Hazards* 11(**2**) 123-37.

[13] Revi A, Satterthwaite DE, Aragón-Durand F, Corfee-Morlot J, Kiunsi RB, Pelling M, Roberts DC, Solecki W 2014 Urban areas Climate Change 2014: Impacts, Adaptation, and Vulnerability. Part A: Global and Sectoral Aspects. Contribution of Working Group II to the Fifth Assessment Report of the Intergovernmental Panel on Climate Change ed CB Field et al. Field, CB, Barros, VR, Dokken, DJ et al. 2014:535-612.

[14] Vachaud G, Quertamp F, Phan TS, Ngoc TD, Nguyen T, Luu XL, Nguyen AT, Gratiot N 2019 Flood-related risks in Ho Chi Minh City and ways of mitigation. *Journal of Hydrology***573** 1021-7.

[15] Nguyen QT 2019. The main causes of land subsidence in Ho Chi Minh City. *Procedia engineering* **142** 334-41.

[16] Trung LV, Viet VQ 2012 Impacts of the land subsidence on sustainable urban development. In 2nd International Engineering Symposium–IES 2012.

[17] Minh DH, Van Trung L, Le Toan T 2015 Mapping ground subsidence phenomena in Ho Chi Minh City through the radar interferometry technique using ALOS PALSAR data. *Remote sensing*7(**7**) 8543-62.

[18] Multi-Hazard Early Warning Systems: A Checklist [Internet]. public.wmo.int. 2018. Available from: https://public.wmo.int/en/our-mandate/focus-areas/natural-hazards-and-disaster-risk-reduction/mhews-checklist

[19] Couasnon A, Scussolini P, Tran TV, Eilander D, Muis S, Wang H, Keesom J, Dullaart J, Xuan Y, Nguyen HQ, Winsemius HC 2022 A flood risk framework capturing the seasonality of and dependence between rainfall and sea levels—An application to Ho Chi Minh City, Vietnam. *Water Resources Research* 58(**2**) e2021WR030002.

[20] Tran TN. Improvement of flood risk assessment under climate change in Ho Chi Minh City with GIS applications (Doctoral dissertation, BTU Cottbus-Senftenberg).

[21] Duy PN, Chapman L, Tight M. Resilient transport systems to reduce urban vulnerability to floods in emerging-coastal cities: A case study of Ho Chi Minh City, Vietnam. Travel behaviour and society. **15** 28-43.

[22] Apel H, Martínez Trepat O, Hung NN, Chinh DT, Merz B, Dung NV 2016 Combined fluvial and pluvial urban flood hazard analysis: concept development and application to Can Tho city, Mekong Delta, Vietnam. *Natural Hazards and Earth System Sciences*16(**4**) 941-61.

[23] Chinh DT, Dung NV, Gain AK, Kreibich H 2017 Flood loss models and risk analysis for private households in Can Tho City, Vietnam. *Water* 9(**5**) 313.

[24] Koop S, Gomes FM, Schoot L, Dieperink C, Driessen P and Van Leeuwen K 2018 Assessing the capacity to govern flood risk in cities and the role of contextual factors *Sustainability* **10** 2869.

[25] Mizutori M 2019 From risk to resilience: Pathways for sustainable development *Progress in Disaster Science* **2019** 100011

[26] Ishiwatari M 2019 Flood risk governance: Establishing collaborative mechanism for integrated approach *Progress in Disaster Science* **2019** 100014.

[27] Ma W, Ishitsuka Y, Takeshima A, Hibino K, Yamazaki D, Yamamoto K, Kachi M, Oki R, Oki T, Yoshimura K. Applicability of a nationwide flood forecasting system for Typhoon Hagibis 2019. Scientific reports. 2021 May 13;11(1):10213.

[28] Perera D, Agnihotri J, Seidou O, Djalante R 2020 Identifying societal challenges in flood early warning systems. *International Journal of Disaster Risk Reduction* **51** 101794.

THE STATUS OF KARST SPRINGS DEGRADATION IN THE WATER-SCARCE HIGH MOUNTAIN AREAS OF NORTHERN VIETNAM AND SOLUTIONS TO MANAGEMENT FOR SUSTAINABLE DEVELOPMENT

Dao Duc Bang[1,*], Tran Thi Thanh Thuy[2], Nguyen Van Trai[3], Nguyen Minh Viet[3], Vu Thu Hien[1] and Duong Thi Thanh Thuy[1]

[1] Faculty of Geosciences and Geoengineering, Hanoi University of Mining and Geology, Hanoi, Vietnam

[2] Faculty of Environment, Hanoi University of Mining and Geology, Hanoi, Vietnam

[3] Vietnam Academy for Water resources, Hanoi, VietNam

E-mail: daoducbang@humg.edu.vn

Abstract: Alongside the rapid economic development, the quality of life of people in high mountain and border areas has received increasing attention in various aspects, with household water supply being one of the top priorities. Since the 2000s, the government and non-governmental organizations from abroad have invested in numerous domestic water supply projects. Due to both human activities and natural factors, climate change has been reducing the efficiency of these projects over time. This decline results from both the deterioration of the infrastructure and the water sources themselves. Research findings from a study of 408 karst springs in the water-scarce high mountain areas of the Northern Vietnam indicate signs of depletion in the quantity and quality of these water sources. Through field investigations and interviews with residents, flow measurements and water sampling in the study area, the karstic springs have been categorized into nine groups based on varying levels of decline in water reserves and quality. Group I is the lowest level of degradation, which accounts for 6.6% of the total, followed by groups IIa and IIb, IIIa and IIIb, and IVa, IVb, and IVc. Group V represents the highest level, at 9.6%. These results serve as a foundation for managers to formulate digital transformation, green development, circular economy, and climate change adaptation solutions aimed at enhancing the efficiency of domestic water supply models for the region.

1. INTRODUCTION

The Northern mountainous region of Vietnam has the basic characteristic of an arc facing away from the sea, with quite strong cleavage and eroded karst terrain erosion in the Northeast and Northwest regions, featuring high mountain ranges extending towards the Northwest - Southeast, strongly dissected, creating the largest and most dangerous terrain difference in our country (Nguyen Kim Ngoc et al., 2003). Alongside this topographic condition, the geological and hydrogeological structure is quite complex with 3 porous aquifers, 25 fracture aquifers and 05 fracture - karst aquifers, making water supply difficult (Nguyen Van Lam et al., 2018). This complexity poses significant challenges to the provision of domestic water supply in the region, especially in water-scarce high mountain and border areas.

Water-scarce high mountain areas, characterized by an area of 4,451.94 square kilometers, exhibit challenging terrain with steep slopes ranging from 7.4% to 52.0%. Inhabitants are predominantly ethnic minorities, facing economic constraints and relying

heavily on nature. Livelihoods are sustained through small-scale, self-sufficient livestock farming, with water primarily utilized for dietary and household purposes. According to surveys, the daily water consumption for domestic use in the region ranges from 50-60 liters per person, resulting in a total demand of 16,392 cubic meters per day for the entire area (Do Ngoc Anh et al., 2019).

Government and non-governmental organizations have implemented various water supply projects, primarily sourcing from springs, caves, or surface water flows, catering to several dozen to a few hundred households. Some recent projects have incorporated effective water treatment systems; however, a significant portion of water remains untreated or undergoes only preliminary filtration. Regular quality checks and evaluations are limited. These water supply projects have partly fulfilled the demand for domestic water needs of the population. However, after several years of operation, the effectiveness of these projects has still not reached the expected level. In high mountainous communes, the sustainability of the water supply model is not high, with many degraded and damaged constructions (Do Ngoc Anh et al., 2019). This unsustainability is due to many different reasons, notably the deterioration of water reserves and quality. Therefore, conducting an assessment of water resource degradation is necessary to find out the appropriate solutions to help improve the effectiveness of water supply models for highly mountainous, water-scarce areas in the Northern region, ensuring water supply to serve residents.

2. METHODS

The degradation of water resources includes both reserve (quantity) and quality degradation. In the case of springs, the degradation of water reserves is assessed through a reduction in flow rates. The degradation of water quality is approached from two distinct perspectives. The first perspective argues that water resources are degraded when the quality exceeds a specific threshold in predefined standards. The second viewpoint posits that water resources are degraded when they surpass their natural background values (Nguyen Van Lam et al., 2020). The study area spans 15 northern mountainous provinces, focusing on high mountainous areas with water scarcity. There are currently no monitoring projects or documentation within the research area that carry out multi-year monitoring to evaluate flow changes in terms of time series. Therefore, to evaluate the possibility of water resource degradation and depletion, the research team implemented the following specific methods:

- Conducted monitoring and measurement of water flow in 408 springs in communes in 15 provinces to evaluate water reserves capable of supplying local people and changes in water flow in the study area. Assessing flow degradation requires measurements and observations over a long time series, however, within the scope of the study, we only measured flow in 2 periods that is two dry seasons in 2022 and 2023. The flow rate is determined using methods such as volumetric tanks, floatboards, or by measuring the cross-sectional area and flow velocity, depending on the actual conditions of each watercourse.

- Carry out quickly measuring total dissolved solids (TDS) parameters in the field at karst springs sources to evaluate the water quality using the Hanna HI 9034 meter.

Because the number of springs sources in the study area is very large and the rapid measurements in the field will help to assess the overall water quality of the study area. Rapid measurement of TDS was also carried out in 2 survey periods with a total number of measurement points of 408 points distributed on springs in communes in 15 provinces.

- Sampling to analyze water quality in karst springs sources in communes of 15 provinces with signs and potential quality deterioration. The total samples are 84 samples in the dry season in 2022 and 84 samples in the dry season in 2023. Analytical criteria of water quality assessment include Turbidity, Ammonium, Arsenic, Iron, Manganese, E.coli, and Coliforms. The result analysis was performed at the High-Tech Analysis Center, Hanoi University of Mining and Geology.

- Investigation, field surveys, consultation community, and information collection from local authorities and residents who use karst springs sources about changes in the water quality and reserves over time, interviewing 10-15 people in each surveyed area.

This information can be used to assess the possibility of water resource degradation. Besides, conduct surveys in water recharge areas to assess waste sources that have the potential to affect the quality of karst springs sources such as waste discharge from daily life, industrial and agricultural production, tourism, and trade in services,…

- Synthesize and build criteria to evaluate the water quality degradation, including:

+ *Assessing the degradation of reserve water (quantity):* The degradation in quantity water for karst springs is the decline in flow. Here, the degradation is understood as a decrease in quantity water value and it is determined when the observed flow of monitoring period 2 is smaller than monitoring period 1. During the monitoring process, some margin of error is inevitable, the flow measurements in the first and second phases always show differences. According to the circular No. 17/2021/TT-BTNMT on monitoring the exploitation and use of water resources issued by the Ministry of Natural Resources and Environment, effective from November 30, 2021, 'the relative error shall not exceed 5% compared to the measured value for flow parameters". Therefore, using the result comparing the quantity in the first and second phases as a basis for assessing degradation, if the quantity in the second period is less than 95% of the quantity in the first period, the water source is considered to have a degraded flow according to this criterion.

Based on the two criteria mentioned above, we classify the water quantity degradation into three levels: (1) Not experiencing quantity degradation, (2) Quantity degradation, but signs not clear and (3) Clear signs of quantity degradation (see table 1)

Table 1. Criteria for evaluating the water quantity degradation.

The quantity degradation level	The basis for assessing the level of quantity degradation	
	The reduction quantity of water according to the interviews and information collected from residents	Expression of quantity degradation according to the measurement results of period 1 (Q_1) and period 2 (Q_2)
Not experiencing quantity degradation	Not degradation	Not Degradation
Quantity degradation, but signs not clear	Not degradation	Degradation
	Degradation	Not degradation
Clear signs of quantity degradation	Degradation	Degradation

Note: Signs of quantity degradation, based on the flow rate results of period 1 (Q_1) and period 2 (Q_2), are determined as "Degradation" when 95% of $Q_1 > Q_2$, and vice versa.

+ *Assessing the degradation of quanlity water:* The quality degradation is assessed based on the results of the analysis from period 1 and period 2, which are determined as "Degradation" when at least 4 out of 7 water quality indicators from period 1 are lower than those from period 2 (for water sources with water sample analysis results) and the result of TDS in period 1 is lower than TDS in period 2 (for water sources without water sample analysis results), and vice versa. In addition, water sources show signs of quality deterioration when the regional level has activities that have the potential to adversely affect water quality. Based on the two criteria mentioned above, we classify water quality degradation into three levels: (1) Not experiencing quality degradation, (2) Quality degradation, but signs not clear, and (3) Clear signs of quality degradation (see table 2).

Table 2. Criteria for evaluating the water quality degradation.

The quality degradation level	The basis for assessing the level of quanlity degradation	
	Activities that have the potential to adversely affect water quality	Signs of water quality degradation according to the analysis results of period 1 and period 2
Not experiencing quality degradation	Not degradation	Not degradation
Quality degradation, but signs not clear	Degradation	Not degradation
	Not degradation	Degradation
Clear signs of quality degradation	Degradation	Degradation

3. RESULTS AND DISCUSSION

Based on the criteria for assessing water resource degradation in terms of both flow rate and quality, we have categorized water resource degradation into 9 groups. Specifically, group I consists of karst springs sources that have not experienced degradation in terms of both quantity and quality, while group V includes conduits with the most significant degradation in both flow and quality. Groups IIb and IVc are primarily associated with flow degradation, while froups IIIb and IVb are primarily related to quality degradation. The remaining groups exhibit unclear signs of degradation in both flow and quality (see table 3).

Table 3. Grouping degradation of karst springs sources according to quantity and quality.

Group	The quantity degradation level			The quality degradation level		
	Not experiencing quantity degradation	Quantity degradation, but signs not clear	Clear signs of quantity degradation	Not experiencing quality degradation	Quality degradation, but signs not clear	Clear signs of quality degradation
I	x			x		
IIa		x		x		
IIb			x	x		
IIIa	x				x	
IIIb	x					x
IVa		x			x	

Group	The quantity degradation level			The quality degradation level		
	Not experiencing quantity degradation	Quantity degradation, but signs not clear	Clear signs of quantity degradation	Not experiencing quality degradation	Quality degradation, but signs not clear	Clear signs of quality degradation
IVb		x				x
IVc			x		x	
V			x			x

Given the interview results and information collected from water users in the study area, it was found that out of 408 surveyed water sources, 181 (44.4%) experienced a decrease in flow rates in recent years. Flow rate measurements during two periods in two dry seasons showed that the first period's flow rate ranged from 0.03 to 75.2 L/s, with an average of 1.16 L/s. The second period's flow rate ranged from 0.02 to 64.7 L/s, with an average of 1.08 L/s. Among the 408 water sources, 216 (52.9%) exhibited reduced flow rates (see table 5).

Surveying in the water source replenishment region revealed that out of 408 water sources, 200 (49%) were at risk of being affected by human activities. Analysis of 84 water samples during the second period, using seven parameters, indicated that some samples exceeded the water quality standards for domestic use set by the Ministry of Health (QCVN 01-1:2018/BYT). Parameters such as turbidity (29 samples), ammonium (37 samples), iron (10 samples), and manganese (9 samples) were found to exceed the standards. Turbidity ranged from 0 to 5 NTU, iron concentrations ranged from 0.02 to 2.38 mg/L (average 0.221 mg/L), ammonium ranged from 0.03 to 0.62 mg/L (average 0.252 mg/L), and Coliforms ranged from 0 to 3 CFU/100mL. Comparing these results with the data from the first period, 22 out of 408 sources experienced an increase in turbidity, 28 saw an increase in ammonium, and 50 exhibited an elevated iron concentration, while E.coli levels showed almost no variation (refer to table 4). The rapid TDS measurements during the second period at the field indicated variations in levels ranging from 6.2 to 347.7 mg/L, with an average of 101.7 mg/L. The combined analysis of water sample results and on-site TDS measurements revealed that 238 out of 408 water sources showed signs of deterioration in water quality (58.3% of total sources), (see table 5).

Table 4. The number of water sources exceeding standards and showing signs of declining quality.

Water quality indicators	Unit	Min	Max	Average	Water quality standards	Number of samples exceeds the standard	Number of samples has a higher concentration than period 1
Turbidity	NTU	0	5	-	2	29	22
Ammonium	mg/L	0.02	0.62	0.252	0.3	37	28
Arsenic	mg/L	0	0.075	0.0055	0.01	4	11
Iron	mg/L	0.02	2.38	0.221	0.3	10	50
Manganese	mg/L	0.01	0.64	0.066	0.1	9	9
E.colie	CFU/100mL	0	0	0	<1	0	0

Water quality indicators	Unit	Min	Max	Average	Water quality standards	Number of samples exceeds the standard	Number of samples has a higher concentration than period 1
Coliforms	CFU/100mL	0	3	-	<3	0	21

Table 5. The number of water sources experiencing a decrease in flow rate and quality

Province	Number of karst springs	The reduction quantity of water according to the interviews and information collected from residents	Expression of quantity degradation according to the measurement results of period 1 (Q_1) and period 2 (Q_2)	Activities that have the potential to adversely affect water quality	Signs of water quality degradation according to the analysis results of period 1 and period 2
Son La	20	12	12	10	11
Dien Bien	11	6	5	7	6
Lai Chau	34	15	17	17	21
Yen Bai	48	20	21	26	28
Ha Giang	34	13	17	16	19
Bac Can	35	16	18	21	24
Cao Bang	91	42	51	41	53
Hoa Binh	19	7	10	8	11
Phu Tho	3	2	3	1	1
Lao Cai	9	5	6	5	5
Tuyen Quang	5	1	2	1	3
Thai Nguyen	4	1	2	1	2
Lang Son	82	35	45	40	47
Bac Giang	8	3	4	3	6
Quang Ninh	5	3	3	3	1
Total	408	181	216	200	238

Based on the results of field surveys at the karst springs sources in the study area and according to the basis for constructing groupings in Table 3, synthesize and group the degraded karst springs sources according to both quantity and quality. Detailed grouping degradation of karst springs is in Table 6. The research results show that the largest number of karst springs sources are exploited and used in Cao Bang province with 91 sources, Lang Son province with 82 sources and Yen Bai province with 48 sources. The number of exploited and used underground Karst water sources is the lowest in Phu Tho province with

03 sources. In particular, the greatest level of degradation and depletion of karst springs sources is in Lang Son province with 24 sources belonging to group IVc - V, accounting for about 29.3% of the karst springs sources in this province, followed by Cao Bang province with 24 sources, accounting for about 26.4% of the province's total springs sources. Particularly in Son La province, although springs sources are low with only 20 sources, the proportion of water sources belonging to groups IVc - V is high, accounting for 40% of the total spring sources of the province. This shows that karst water spring sources are currently facing the risk of degradation and depletion and need to be protected.

Table 6. Results of grouping degradation of karst springs in the water-scarce high mountain areas of Northern Vietnam

Province	Number of karst springs	Number of karst springs according to the degradation level groups								
		Group I	Group IIa	Group IIb	Group IIIa	Group IIIb	Group IVa	Group IVb	Group IVc	Group V
Son La	20	1	2	1	3	1	3	1	5	3
Dien Bien	11	1	0	1	1	2	2	1	2	1
Lai Chau	34	1	4	2	6	4	6	4	4	3
Yen Bai	48	4	2	3	8	9	9	2	7	4
Ha Giang	34	3	2	2	7	5	6	0	6	3
Bac Can	35	2	2	1	4	6	7	3	4	6
Cao Bang	91	6	5	9	17	8	16	6	15	9
Hoa Binh	19	2	1	1	4	2	3	1	4	1
Phu Tho	3	0	0	1	0	0	1	0	1	0
Lao Cai	9	0	1	1	1	1	1	1	2	1
Tuyen Quang	5	1	0	0	2	0	1	0	1	0
Thai Nguyen	4	1	0	0	1	0	1	0	1	0
Lang Son	82	4	5	6	17	11	13	2	17	7
Bac Giang	8	0	1	1	2	1	1	1	0	1
Quang Ninh	5	1	0	0	1	0	0	0	3	0
Total	**408**	**27**	**25**	**29**	**74**	**50**	**70**	**22**	**72**	**39**

The research result shows that the number of karst springs sources in group IIIa is the highest in the karst water sources found in 15 provinces in the water-scarce high mountain areas of Northern Vietnam with 74 sources, accounting for 18%, proving that these water sources have not degraded in reserve but have shown signs of deterioration in water quality. The number of springs sources that are degradated in both quality and quantity is high with 142 sources belonging to groups IVa and IVc, accounting for nearly 35% of the total karst water sources in the study area (see table 6).

The classification results indicate that, across the entire research area, out of a total of 408 karst springs sources, a small proportion remains unaffected by degradation which is 6.6%, while a larger proportion experiences both quantity and quality degradation is 9.6%.

Karst springs with degradation in either flow rate or water quality, or both, represent a higher percentage, over 17% which is groups IIIa, IVa, and IVc (see figure 1).

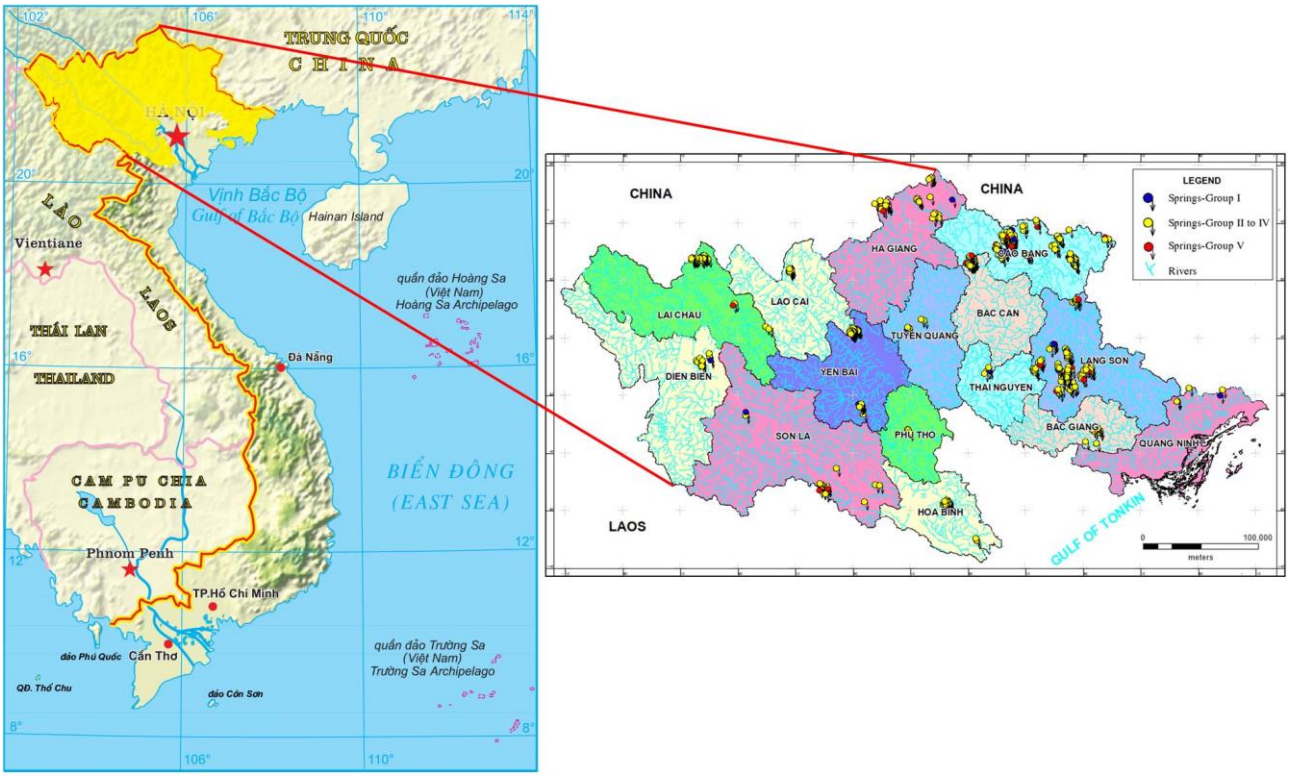


Figure 1. *Map of karst springs degradation groups in the study area.*

The degradation of water sources is caused by various factors. For the reduction in water flow, there are three main reasons: (i) climate change, (ii) deforestation at the headwaters reducing water supply, and (iii) forest conversion and changes in crop structure. Climate change leads to a significant decrease in rainfall, especially during the dry season, resulting in a reduction in water supply. According to surveys, most water channels experience decreased flow during the dry season, with many channels showing a reduction of over 60% (such as in Tua Thang, Ho Mit, Quoc Toan commune, etc.). Deforestation at the source region prevents rainwater from being retained, diminishing the underground water supply. In the research area, the headwaters are largely unprotected or poorly protected (61%) (Do Ngoc Anh et al., 2019). Deforestation often occurs on a small scale, driven by the needs of local residents. Some areas have converted natural forest into flower cultivation, fruit-bearing crops such as maize and acacia (Ha Giang, Dien Bien, Tuyen Quang, Quang Ninh, etc.), tea plant (Thai Nguyen, Son La), litchi tree (Bac Giang), leading to a decrease in forest cover and water retention capacity.

Concerning the decline in water quality, factors include: (i) agricultural activities, livestock farming, and residential construction in the upper region, (ii) mineral exploitation, (iii) inadequate construction and protection of surrounding areas. In many regions, due to economic difficulties and insufficient awareness, people use pesticides, herbicides, and chemical fertilizers when cultivating crops (maize, tea, oranges, litchi), affecting water quality. In some areas, ethnic minorities in water replenishment regions dispose of livestock and household waste, posing a risk of water pollution. Waste mud from mineral exploitation is often untreated, or poorly placed, posing a potential threat to water sources. During field

studies in some locations, locals reported issues, such as in Pung Ho Cave, Vu Nong commune, Nguyen Binh district, Cao Bang province, where the discharge of mining mud turned the water yellow and turbid, making it unsuitable for local households and the elementary school. In Coc Phat 1 stream, Pac Vo hamlet, Quoc Toan commune, Quang Hoa district, Cao Bang province, concerns were raised about the ore processing plant upstream potentially affecting the water source. However, visible signs were not evident, requiring more detailed studies in this area for accurate conclusions. Moreover, the awareness of water source protection among the local residents is limited, and lax management practices in localities contribute to the decline in both water quantity and quality.

Based on the assessment of the current situation and grouping of water resource degradation according to both quantity and quality, the authors propose the solutions to manage, protect, and rationally exploit water resources belonging to the groups that ensure sustainable development as follows:

(1) For areas without any signs of water resource degradation (Group I): To ensure sustainable exploitation in the future, it is essential to protect the source buffer zones by clearly defining these areas, setting up protective boundaries, and limiting or prohibiting activities such as deforestation, livestock grazing, the use of fertilizers, pesticides, herbicides, and construction. Additionally, afforestation in areas with low vegetation coverage can enhance water resources.

(2) For areas with degradation primarily in quantity rate (Groups IIb, IVc): Combining solutions like digging retention ponds, small infiltration tanks, and creating parallel ditches at the contour to temporarily reduce flow velocity, retain water, and supplement water during the dry season. Expanding forest cover to increase the vegetation areas and government mechanisms policy to relocate the land of residents in the buffer zone to maintain their livelihoods while preserving water resources are also recommended.

(3) For areas with degradation primarily in quality water (Groups IIIb, IVb): need to cease mining operations immediately with the areas affected by mineral mining activities, environmental treatment and penalties for waste discharge activities. For areas where residents use pesticides, raising awareness among residents to avoid or use environmentally friendly pesticides to prevent water quality deterioration is crucial. Local authorities should have policies to convert the land of residents and crops to suitable locations to ensure their livelihoods while returning the source buffer area for recovery and protection.

(4) For areas with degradation in both quantity and quality water (remaining groups): A comprehensive approach combining solutions from groups (2) and (3) is necessary. Furthermore, raising awareness and knowledge among residents about the importance of water resources and related issues is essential, ensuring that every resident takes responsibility for protecting and developing water resources for sustainable exploitation in the future.

In addition, in the coming time, as the economic conditions of the region improve, it is necessary to research and apply digital technology solutions for monitoring and data collection on flow rate and water quality to implement timely measures and ensure the sustainable development of karst springs sources.

The research area comprises high mountain villages with scarce water resources, lacking long-term quantity and quality water monitoring projects. In the current conditions, the authors have conducted surveys and measurements in two periods (corresponding to two dry

seasons) to establish initial groupings of water resource degradation. These are preliminary results providing an overview of the entire research area. Therefore, long-term monitoring of quantity and quality water over several years, during different seasons is necessary to refine the classifications.

4. CONCLUSION

The water-scarce high mountain areas of Northern Vietnam face significant challenges in terms of domestic water supply. However, signs of water resource degradation are becoming evident in the karst spring sources in this area. Based on the field surveys, consultation community, flow rate measurements, sampling and water sample analysis, the research team has evaluated the degradation of water resources and classified karst springs sources into nine groups. The study of 408 karst springs sources has revealed signs of both quantity and quality degradation in the water sources. The degradation levels are as follows: Group I has the lowest degradation rate (6.6%), followed by Groups IIa, IIb, IIIa, IIIb, and then Groups IVa, IVb, and IVc, with the highest degradation in Group V (9.6%). The classification results serve as a foundation for proposing measures to restore and protect water resources, ultimately improving the efficiency of the domestic water supply model in the region. However, the survey data from this study were collected during only two dry seasons. Therefore, the classification is preliminary and needs more comprehensive data collected over years, spanning various seasons to establish more specific groups.

REFERENCES

[1] Do Ngoc Anh et al., 2019 Research and propose models and technological solutions to exploit and protect sustainable development of Karst water sources to serve domestic water supply in water-scarce high mountain areas of Northern Vietnam. Final Report Project, Hanoi.

[2] Nguyen Van Lam et al, 2018 Groundwater potential in water-scarce high mountain areas of Northern *Journal of Mining and Earth Sciences and Technology* vol 59, Issue 3, pp 1-9.

[3] Nguyen Van Lam et al, 2018 Evaluating and selecting models and technological solutions for sustainable exploitation and use of karst water resources in high mountainous and water-scarce areas in the Northern region *Journal of Mining and Earth Sciences and Technology* Water Resources Science and Technology Journal vol 43, ISSN: 1859-4255/04-2018, pp 30-39, Hanoi.

[4] Nguyen Van Lam et al, 2020 Hydrogeological contamination *Transport Publishing House*, pp 8-10, Hanoi.

[5] Nguyen Kim Ngoc et al, 2003 Hydrogeology and groundwater resources of Vietnam territory *Transport Publishing House*, pp 44-51, Hanoi.

ACKNOWLEDGMENTS

I would like to express my sincere gratitude to the Hanoi University of Mining and Geology and the project DTDL-CN.66/21 which was led by the Vietnam Academy for Water resources, as well as the local authorities and the residents of the water-scarce high mountain areas of Northern Vietnam. Your support and cooperation have been invaluable in providing the conditions and assistance needed for the authors to complete this research.

ASSESSMENT OF MARINE POLLUTION LOADS FROM LAND-BASED ACTIVITIES: A CASE STUDY IN HAI AN DISTRICT, HAI PHONG CITY

Dao Van Hien [1], Nguyen Thi Ngoc Huong [1] Nguyen Manh Khai [1] and Bui Dac Thuyet[2]

[1]Faculty of Environmental Sciences, University of Science, Vietnam National University, Hanoi, Vietnam, 334 Nguyen Trai Street, Hanoi, Vietnam

[2]Faculty of Marine Science, Hanoi University of Natural Resources and Environment, 41A Phu Dien, Bac Tu Liem, Hanoi, Vietnam.

Email: hiendv@hus.edu.vn; hiendv@vnu.edu.vn

Abstract: The marine environment of Hai An district in Hai Phong city has been seriously affected by socio-economic activities. Therefore, assessment of marine pollution sources and pollutant loads to Hai An district coastal area is vital for environmental protection and sustainable development in Hai Phong city. The research used pollution load assessment method, combined with field survey, synthesis and analysis of data to identify pollution sources and assess marine pollution load to Hai An coastal area. The results showed that the total pollutant load was 16,702 tons in 2021, of which 14,545 tons were discharged into the sea. Of all the marine pollution sources, the residential and tourism activities contribute the most pollutant loads, followed by livestock farming, industry and aquaculture. The forecasted pollutant loads for 2025 and 2030 are 18,026 tons and 21,230 tons - an increase of 8% and 28% compared to 2021, respectively. Accordingly, the pollutant loads into the coastal area for 2025 and 2030 are forecasted to be 15,705 tons and 18,512 tons, respectively. The assessment of marine pollution load in that area also contributes to Sustainable Development Goal (SDG) indicator 14.1.1 on “prevent and significantly reduce marine pollution of all kinds, in particular from land-based activities" under SDG 14 on conservation and sustainable use of oceans, seas and marine resources for development.

1. INTRODUCTION

The marine pollution has received increasing attention due to its effects on marine species, human health and many related economic sectors, such as fishery, aquaculture, maritime and tourism. The United Nations Convention on the Law of the Sea 1982 regulates that there are five main sources of marine pollution, including: land - based activities; exploration and exploitation of marine resources on the continental shelf and seabed; toxic substances; cargo transportation at sea; and air pollution [4]. Of which, land-based sources account for more than 75% of the pollutants going into the sea ([2], [3]). Therefore, qualifying and estimating the pollution sources and pollutant loads are vital for proposing appropriate measures in pollution control and reduction. There have been numerous research attempts to estimate the land-based pollution loads in coastal areas or bays around the world [10-16]. Based on the research results, a number of measures, including regulations and programs (e.g., the Total Maximum Daily Load program, Best Management Practices, the European Water Framework Directive etc.) have been taken to control the land-based pollution in many countries.

In Vietnam, several studies have been conducted to estimate marine pollutant loads in Nghi Son, Thanh Hoa Province [18], Tam Giang Cau Hai lagoon of Thua Thien Hue City

[19], Da Nang Bay in Da Nang City [20], Truong Giang river basin of Quang Nam Province [21].

As with many coastal areas, socio-economic development in Hai An District, Hai Phong City may have increasing pressure on surrounding marine environment. There are many socio-economic development activities in the district, such as agriculture, fishing and marine exploitation, transportation - ports, tourism - services. Waste from domestic and economic activities (i.e., industrial waste, effluent from aquaculture ponds, livestock waste, chemicals used in agriculture, effluent from hotels and restaurants) can be easily discharged into the sea since the district is surrounded by the system of Lach Tray and Cam rivers with Nam Trieu estuary flowing into the Gulf of Tonkin (Figure 1). In addition, Hai An district is near Cat Ba Biosphere Reserves and thus pollutant loads from the district may affect this valuable ecosystem. However, there have been no studies to estimate and forecast pollutant sources and loads into the coastal area of Hai An district. Therefore, it is important to identify the land-based pollution sources and estimate the pollution loads to the coastal area. Based on collected data, the study identified the main sources of marine pollution as local residents, tourism, industry, aquaculture, livestock and accordingly calculated the pollutant loads generated from the above sources in 2021 and forecast for 2025 and 2030. The findings of this study can be used for investigating the self-cleaning capacity and marine environment capacity of the area. The assessment of marine pollution load also contributes to SDG indicator 14.1.1 on “prevent and significantly reduce marine pollution of all kinds, in particular from land-based activities" under SDG 14 on conservation and sustainable use of oceans, seas and marine resources for development.

2. MATERIAL AND METHODS

2.1. Study area

The study area is Hai An district, in Hai Phong city, Figure 1.



Figure 1. *Location of the study area - Hai An district, Hai Phong city.*

2.2. Data collection and analysis

Secondary data were collected from several sources, including: documents and reports of socio-economic activities (e.g., aquaculture, livestock, tourism), development planning of economic sectors up to 2030 and environmental state of Hai Phong for the period 2016-2020 from responsible agencies such as Hai Phong Statistics Department, Hai Phong Department of Natural Resources and Environment and Hai An district [22], [23], [24], [25], [26].. In addition, the study conducted surveys and fieldtrips to assess and identify sources of coastal pollution in Hai An district. From the identification of pollution sources, the study calculated the pollutant loads from the mainland discharged into the marine environment. The pollutant load coefficients are taken according to the studies of UNEP (1984) [27], San Diego - McGlone (2000) [28], Tran Van Nhan, Ngo Thi Nga (2002) [29], Tran Duc Thanh et al., (2012) [17]. This method has been used to assess the pollutant loads into the coastal area of Nghi Son, Thanh Hoa [18], Da Nang Bay [20] in Vietnam, Quanzhou Bay in China [15] and Tokyo Bay in Japan [30], the Niger Delta [31] and the Black Sea of Turkey [11].

2.3. Estimation of pollutant loads

2.3.1. Pollutant load from domestic sources, including local residents and tourists

The pollutant load from domestic source (Q_{sh}) is equal to the total pollutant load from local residents (Q_{dc}) and pollutant load of tourists (Q_{dl}).

$$Q_{sh} = Q_{dc} + Q_{dl} \text{ (tons/year) [17]} \quad (1)$$

The pollutant load from local residents was calculated based on the population of the area and the pollutant load coefficient per capita [15]:

$$Q_{dc} = P.\ Q_i\ .\ 10^{-3} \text{ [17]} \quad (2)$$

In which:

Q_{dc}: Pollutant load from local residents(tons/year).

P: Population of the area (people).

Q_i: Pollutant load coefficient per capital of substance i (kg/person/year).

The pollutant load from tourists was estimated based on the total number of days of stay per year of the tourist, and the pollutant load coefficient from domestic sources.

$$Q_{dl} = n\ .\ Q_i\ /365\ x\ 10^{-3} \text{ [17]} \quad (3)$$

In which:

Q_{dl}: Pollutant load from tourists (tons/year).

Q_i: Pollutant coefficient of substance i (kg/person/year).

n: Total number of days of tourist stay in the year (day/year).

Pollutant load coefficient from domestic sources is referred from Tran Duc Thanh et al., 2012 [17].

2.3.2. Pollutant load from industrial activities

The industrial pollutant load in the area was calculated based on the industrial output in the area multiplied by the pollutant load coefficient of that type of industry according to the formula:

$$Q_{ij} = \Sigma V_j \times C_{ij} \times 10^{-6} (j = 1, n) \text{ [17]} \quad (4)$$

Q_{ij}: Pollutant load i from industrial source j (tons/year).

V_j: Annual volume of wastewater from industrial source j (m3/year).

C_{ij}: Concentration of substance i in the wastewater of industrial source j (mg/l).

n: Number of industrial factories in the region.

2.3.3. Pollutant load from livestock

Pollution load from livestock was calculated by the number of livestock and the pollutant load unit.

$$Q_{cn} = n \times Q_i \times 10^{-3} \quad (5)$$

Q_{cn}: Pollution load from livestock (tons/year).

n: Number of livestock (head).

Q_i: the pollutant load unit (kg/per head/year).

The number of cattle was taken from the Hai Phong Provincial Statistical Yearbook 2021 [22]. The pollutant load coefficient per animal was taken from [17,18,20].

2.3.4. Pollutant load from aquaculture

The pollution source generated by aquaculture was calculated based on the aquaculture production in the area multiplied by the pollutant load coefficient for each type of fishery production. The amount of waste generated depends on the type and species of farming, in which industrial shrimp farming and fish cage culture have the most significant loads. Pollutant load coefficients are referred from research [17, 18, 20].

2.4. Estimation of pollutant load into the marine environment in Hai An district

Study on the current status of wastewater treatment found that only 13% of wastewater from domestic, tourist and service were treated and that the remaining 87% was directly discharged to the environment without treatment. The same figure was found from livestock waste. For aquaculture, 100% of wastewater were discharged into the sea without treatment. Wastewater from industry activities was collected and treated at a standard wastewater treatment plant (Column A, QCVN 40:2011/BTNMT) before releasing into the marine environment. Thus, wastewater after treatment met QCVN 40 column A and was discharged 100% into the sea.

3. RESULTS AND DISCUSSION

3.1. Pollutant loads generated in Hai An district

In 2021, there were 137 thousand people living in Hai An district [1, 2]. The district also hosted 182,000 visitors. However, in 2022, due to the Covid-19 pandemic reduction, Hai Phong hosted 7 million guests, including 350,000 visitors to Hai An district. By 2025, with a natural growth rate of about 0.92%, the district's population is estimated at 143 thousand people and by 2030 it is 149 thousand people. Besides, the tourism growth rate of the district is forecasted to be 16% [23] after the end of the Covid-19, then the number of tourists staying overnight will be 532,000 visitors in 2025 and about 1.07 million visitors in 2030.

Industrial production in the district in 2021 maintained a high growth rate, increasing by 18.15% compared to 2020. There were some industrial zones in areas including Dinh Vu,

South Dinh Vu, Deep C [26]. In 2021, Hai An district also has a livestock with buffalo herd (29 heads); cows (22 heads); pigs (230 heads); poultry (26800 heads) [1,2]. Agricultural activities are relatively stable and less affected by the Covid-19 pandemic. The livestock is expected to increase in the coming years, accounting for a high proportion of the total GDP of the fisheries - agriculture - forestry sector. In addition, Hai An district has 603.1 ha aquaculture area in 2021, producing 350 tons of commercial shrimp and 302 tons of fish from marine cages [25]. The growth rate of shrimp production, fish production and livestock production is 0.98%/year, 2.94%/year and 28%/year, respectively [22,23,24]. The growth rate of wastewater from industrial source is 15% [22,23,24].

The results showed that the socio-economic activities of Hai An district in 2021 generated 7.7 thousand tons of COD, 3.5 thousand tons of BOD_5, 583 tons of N-T (Total Nitrogen), 162 tons of P-T (Total Phosphorous) and 4.3 thousand tons of TSS. The total pollutant load was 16702 tons (Table 1). In which, domestic source was the highest, accounting for 92.86 to 97.99%, followed by livestock, industry and aquaculture sources (Figure 2). The reason is that most of the wastewater from domestic and livestock is not treated. However, wastewater from industrial activities was collected and treated to meet corresponding national standard before being discharged into the environment. The pollution load from aquaculture was low due to the aquaculture area in the district was small.

Table 1. Total pollutant load generated from various sources in Hai An District, Hai Phong City in 2021

	Pollutant load (tons/year)					
Parameter	**Resident**	**Tourism**	**Industry**	**Livestock**	**Aquaculture**	**Total**
COD	7560.25	27.90	35.82	101.87	14.75	7740.59
BOD_5	3436.48	12.68	11.94	41.68	4.20	3506.98
N-T	549.84	2.03	7.16	22.16	2.70	583.88
P-T	151.20	0.56	1.43	7.21	2.43	162.84
$NO_2^- + NO_3^-$	5.50	0.02	0.07	0.22	0.03	5.84
NH_4^+	302.41	1.12	2.39	5.32	0.65	311.88
PO_4^{3-}	81.65	0.30	0.64	2.62	1.13	86.35
TSS	4123.77	15.22	23.88	141.41	-	4304.28

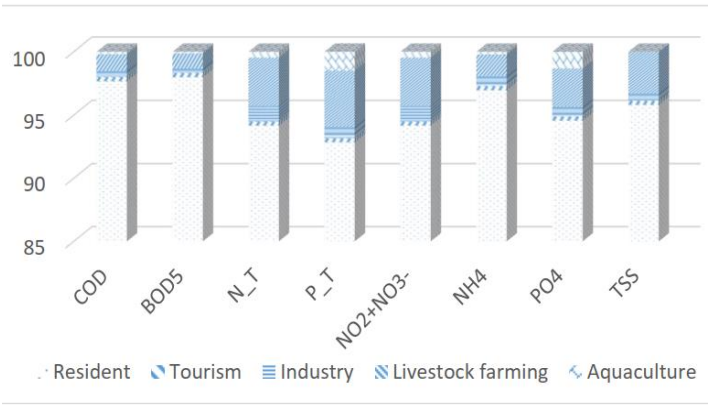


Figure 2. *The percentage of pollution source (%) in Hai An district, Hai Phong City in 2021.*

It is forecasted that, in 2025, socio-economic activities in Hai An district will generate around 8.3 thousand tons of COD, 3.7 thousand tons of BOD5; more than 650 tons of N-T and more than 183 tons of P-T; more than 4.7 thousand tons of TSS and total pollutant load is 18026 tons, Table 2. Compared to 2021, the pollutant load increases about 1.08 times. Of which, the domestic source of pollution accounts for 86-95%, followed by livestock, industry and aquaculture. The percentage of pollution sources from livestock is forecasted to increase by more than 10% compared to that in 2021 for pollutants such as N-T, P-T, NO_2^- + NO_3^-or TSS.

Table 2. Total pollutant load generated from various sources in Hai An district, Hai Phong City in 2025

	Pollutant load (tons/year)					
Parameter	Resident	Tourism	Industry	Livestock	Aquaculture	Total
COD	7842.33	81.32	62.66	272.6	15.48	8274.39
BOD_5	3564.69	36.97	20.89	111.54	4.40	3738.49
N-T	570.35	5.91	12.53	59.29	2.83	650.92
P-T	156.85	1.63	2.51	19.3	2.55	182.83
NO_2^- + NO_3^-	5.70	0.06	0.13	0.59	0.03	6.51
NH_4^+	313.69	3.25	4.18	14.23	0.68	336.03
PO_4^{3-}	84.70	0.88	1.13	7.02	1.18	94.91
TSS	4277.63	44.36	41.77	378.41	-	4742.17

In 2030, socio-economic development activities in Hai An district will generate 9,449.16 tons of COD; 4234.62 tons of BOD_5; 840 tons of N-T; 241.33 tons of P-T; more than 5,946 tons of TSS. The total amount of waste is 21230 tons. In which, organic substances and nutrients arise mainly from domestic sources (68.04 - 86.88%) and livestock (9.02 - 27.37%). The amount of total suspended solids mainly generated from domestic sources (resident and tourism) (75.31%) and followed by livestock (21.78%). Compared to 2021, the pollutant load increases by about 28% and domestic waste is still the most predominant source (Table 3).

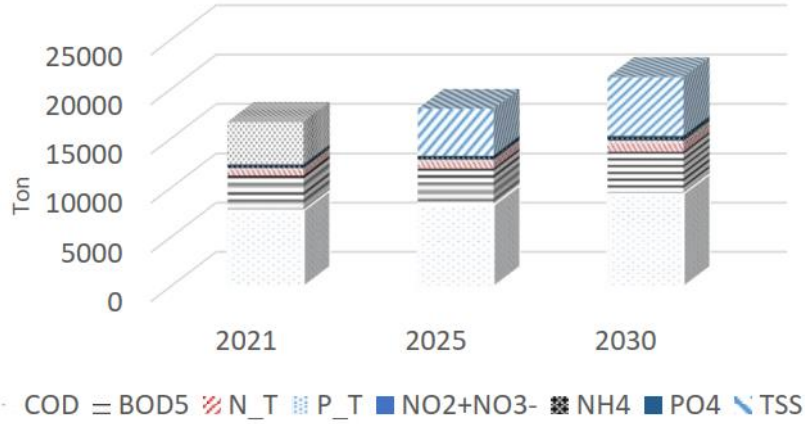


Figure 3. *Load of pollutants in 2021 and forecast for 2025 and 2030 (tons)*

Table 3. Total pollutant load generated from various sources in Hai An district, Hai Phong city in 2030

	Pollutant load (tons/year)					
Parameter	Resident	Tourism	Industry	Livestock	Aquaculture	Total
COD	8209.77	163.57	126.02	932.98	16.81	9449.16
BOD_5	3731.71	74.35	42.01	381.77	4.78	4234.62
N-T	597.07	11.90	25.20	202.92	3.07	840.17
P-T	164.20	3.27	5.04	66.05	2.77	241.33
$NO_2^- + NO_3^-$	5.97	0.12	0.25	2.03	0.03	8.40
NH_4^+	328.39	6.54	8.40	48.7	0.74	392.78
PO_4^{3-}	88.67	1.77	2.27	24.01	1.28	117.99
TSS	4478.06	89.22	84.01	1295.13	-	5946.42

The pollutant load forecast in 2025 and 2030 will be 18026 tons and 21230 tons, respectively, which increase of about 8% and 28% compared to 2021. Thus, the total pollution load increases gradually over the years (Figure 3).

3.2. Pollutant load into the marine environment in Hai An district

Based on the pollutant load generated in Hai An district, the total pollutant load to the marine environment was calculated and presented in Table 4.

Table 4. Total pollutant load into the sea in Hai An district, Hai Phong city from various sources in 2021

	Pollutant load (tons/year)					
Parameter	Resident	Tourism	Industry	Livestock	Aquaculture	Total
COD	6577.41	24.27	35.82	88.62	14.75	6740.88
BOD_5	2989.73	11.03	11.94	36.26	4.20	3053.17
N-T	478.36	1.77	7.16	19.28	2.70	509.26
P-T	131.55	0.49	1.43	6.27	2.43	142.17
$NO_2^- + NO_3^-$	4.78	0.02	0.07	0.19	0.03	5.09
NH_4^+	263.10	0.97	2.39	4.63	0.65	271.73
PO_4^{3-}	71.04	0.26	0.64	2.28	1.13	75.35
TSS	3587.68	13.24	23.88	123.03	-	3747.83

The load of pollutants from Hai An district into the marine environment was 6,740.88 tons of COD; 3,053.17 tons BOD_5. Total nitrogen and total phosphorus loads discharged into the area were estimated at 509.26 tons and 142.17 tons, respectively. The total pollutant load from Hai An district into the sea was 14,545 tons in 2021.

According to the forecast scenario to 2025, the estimated pollutant load into the sea in Hai An district in 2025 is 7,208.87 tons of COD, 3,255.77 tons of BOD_5, 568.3 tons of N-T, 159.72 tons of P-T, 5.68 tons of NO_2+ NO_3-, 292.98 tons of NH_4^+, 82.87 tons of PO_4^{3-}, and more than 4,131 tons TSS. The total pollutant load into the sea is estimated at 15,705 tons (Table 5).

Table 5. Forecasted pollutant load into the sea from various sources in Hai An district, Hai Phong city in 2025

	Pollutant loads (tons/year)					
Parameter	Resident	Tourism	Industry	Livestock	Aquaculture	Total
COD	6822.82	70.75	62.66	237.16	15.48	7208.87
BOD_5	3101.28	32.16	20.89	97.04	4.40	3255.77
N-T	496.21	5.15	12.53	51.58	2.83	568.30
P-T	136.46	1.42	2.51	16.79	2.55	159.72
$NO_2^- + NO_3^-$	4.96	0.05	0.13	0.51	0.03	5.68
NH_4^+	272.91	2.83	4.18	12.38	0.68	292.98
PO_4^{3-}	73.69	0.76	1.13	6.11	1.18	82.87
TSS	3721.54	38.59	41.77	329.22	-	4131.12

Table 6. Forecasted pollutant load into the sea from various sources in Hai An district, Hai Phong city in 2030

	Pollutant load (tons/year)					
Parameter	Resident	Tourism	Industry	Livestock	Aquaculture	Total
COD	7142.50	142.31	126.02	811.69	16.81	8239.33
BOD_5	3246.59	64.69	42.01	332.14	4.78	3690.21
N-T	519.45	10.35	25.20	176.54	3.07	734.62
P-T	142.85	2.85	5.04	57.46	2.77	210.97
$NO_2^- + NO_3^-$	5.19	0.10	0.25	1.77	0.03	7.35
NH_4^+	285.70	5.69	8.40	42.37	0.74	342.90
PO_4^{3-}	77.14	1.54	2.27	20.89	1.28	103.12
TSS	3895.91	77.62	84.01	1126.76	-	5184.31

Compared to the findings of other studies, such as [19], [20], it is reported that the main pollution sources are from domestic sources including residents and tourists and livestock farming, which is similar to the findings of this study.

4. CONCLUSION

The study found that domestic sources (residents and tourists), industry, livestock and aquaculture were the main pollution sources in coastal and marine environment in Hai An district, Hai Phong city. In 2021, the total pollutant load was 16,702 tons, of which, 14,545 tons were discharged into the coastal area of Hai An district. The domestic sources (residents and tourism) was the main pollutant source (93-98%), followed by livestock farming, industry and aquaculture.

The forecast scenario on pollutant load from Hai An district for 2025 and 2030 found that the pollutant load will be 18,026 tons in 2025 (an increase of about 8% compared to 2021) and 21,230 tons in 2030 (an increase of about 28% compared to 2021). The pollutant load into the marine environment in Hai An district for 2025 and 2030 are 15,705 tons and

18,512 tons, respectively. The findings of this study provide an overall picture of marine pollution in the area and this will provide help local government and policy makers to have appropriate measures in order to reduce land-based pollution to the coastal area of Hai An and to protect the Cat Ba Biosphere Reserves.

REFERENCES

[1] UNEP/GPA 2006 Protecting coastal and marine environments form land-based activities – A guide for national action, UNEP.

[2] GESAMP 1990 The State of the Marine Environment. IMO/FAO/UNESCO/WMO/IAEA/UN/UNEP Joint Group of Experts on the Scientific Aspects of Marine Pollution. UNEP Regional Seas Reports and Studies No. 115. UNEP, Nairobi.

[3] Goudie, A 2000 The Human Impact on the Natural Environment. Blackwell, Oxford.

[4] Laurence, D.M 1992 The Black Sea in crisis: a need for concerted international action. AMBIO: *A J. Hum. Environ*. 21 (4), 278-286.

[5] Higashi, H., Koshikawa, H., Murakami, S., Kohata, K., Mizuochi, M., Tsujimoto, T. 2012 Effects of land-based pollution control on coastal hypoxia: a numerical case study of integrated coastal area and river basin management in Ise Bay, Japan. *Procedia Environ. Sci*. 13 (0), 232-241.

[6] Li, D., Dag, D. 2004 Ocean pollution from land-based sources: East China Sea, China. AMBIO: *A J. Hum. Environ*. 33 (1), 107-113.

[7] Edinger, E.N., Jompa, J., Limmon, G.V., Widjatmoko, W., Risk, M.J., et al. 1998, Reef degradation and coral biodiversity in Indonesia: effects of land-based pollution, destructive fishing practices and changes over time. *Mar. Pollut. Bull*. 36 (8), 617-630.

[8] Williams, C. 1996 Combating marine pollution from land-based activities: Australian initiatives. *Ocean Coast. Manag*. 33 (1), 87-112.

[9] Islam, S., Tanaka, M. 2004 Impacts of pollution on coastal and marine ecosystems including coastal and marine fisheries and approach for management: a review and synthesis. *Mar. Pollut. Bull*. 48 (7), 624-649.

[10] Jarvie, H.P., Neal, C., Tappin, A.D., 1997 European land-based pollutant loads to the North Sea: an analysis of the Paris commission data and review of monitoring strategies. *Sci. Total Environ*. 194, 39-58.

[11] Tuncer, G., Karakas, T., Balkas, T.I., Geokçay, C.F., Aygnn, S., Yurteri, C., Tuncel, G. 1998 Land-based sources of pollution along the Black Sea coast of Turkey: concentrations and annual loads to the Black Sea. *Mar. Pollut. Bull*. 36 (6), 409-423.

[12] Asmah, R., and Biney, C. A. 2001 Assessment of air, water and land-based sources of pollution in the coastal zone of the Accra-Tema metropolitan area. *Journal of the Ghana Science Association*, 3(3), 126–135. DOI: 10.4314/ jgsa. v3i3.17775.

[13] Huang, J.-L., Li, Q.-S., Tu, Z.-S., Pan, C.-M., Zhang, L.-P., Ndokoye, P., Lin, J., Hong, H.-S. 2013 Quantifying land-based pollutant loads in coastal area with sparse data: methodology and application in China. *Ocean Coast. Manag*. 81, 14-28.

[14] Hosseini-Zare, N., Gholami, A., Panahpour, E., and Jafarnejadi, A. 2014 Pollution load assessment in the soil and water resources: a case study in Karun river drainage basin, southwest of Iran. *European Online Journal of Natural and Social Sciences*, 3(3(s)), 427–434.

[15] Zhao, W. L., Yang, S. Y., Wang, J., Xiao, J. M., Lu, X. X., Lin, J., Huang, P., and Cai, M. G. 2015 Load estimation and assessment of land-based pollution for Quanzhou bay and their relevance to the Total Quantity Control of Pollutants Discharged into the Sea (TQCPS) Program in China. *Estuarine, Coastal and Shelf Science*, 166, 230–239. https://doi.org/10.1016/j.ecss.2015.06.026.

[16] El-Nakib, S., Alameddine, I., Massoud, M., and Abou Najm, M.2020 Nutrient pollutant loading and source apportionment along a Mediterranean river. *Environmental Monitoring and Assessment*, 192, 1–1. https://doi.org/10.1007/s10661-020-8220-7.

[17] Tran, D.T, Tran V,M, Cao, T.T.T, Vu, D.V, Tran,A.T. 2012. Environmental Carrying Capacity of Ha Long Bay - Bai Tu Long Bay. Publishing House for Science and Technology, 297 p. (in Vietnamese).

[18] Cao,T.T.T, Dinh, H.N, Nguyen,V.T.2020. Assessment of pollution load from industrial activities of Nghi Son Economic Zone (Thanh Hoa province). *Vietnam Journal of Marine Science and Technology*, 20(3), 297–308.

[19] Cao T.T.T, Tran, D.T., Le,X.S. 2013. Assessment of pollution load into Tam Giang - Cau Hai lagoon and a prediction to 2020. *Vietnam Journal of Marine Science and Technology*, 13(3), 276–283.

[20] Le, X.S, Le, V.N. 2015. Assessment of pollution load into Da Nang Bay. *Vietnam Journal of Marine Science and Technology*, 2(15), 165–175.

[21] Mai, T.H, Ngo,X.N, Tran, V.T, Mai,T.H 2018 Determination of pollution load into Truong Giang river, Quang Nam province. VNU Journal of Science: Earth and Environmental Sciences, 34(4), 71– 79. DOI: https://doi.org/10.25073/2588-1094/vnuees.4303.

[22] Hai Phong City Statistical Office 2021 Hai Phong City Statistical Yearbook 2021, Statistical Publishing House.

[23] Hai Phong. 2019 Statistical report on the socio-economic situation of Hai Phong city in 2019., https://thongkehaiphong.gov.vn/thong-tin-king-te-xa-hoi/tinh-hinh-king-te-xa-hoi -thanh-pho-hai-phong-nam-2019-51.html.

[24] Hai An District People's Committee 2020 Situation and results of the implementation of socio-economic development tasks in 2020; Objectives, directions, tasks, and solutions in 2021.

[25] Hai An District People's Committee 2021 Situation and results of the implementation of socio-economic development tasks in 2021; Goals, directions, tasks, and solutions in 2022.

[26] Hai Phong City People's Committee 2020 Report on the State of the Environment in Hai Phong for the period 2016-2020.

[27] UNEP 1984 Pollutants from land-based resources in the Mediterranean. UNEP Regional Seas Reports and Studies No. 32.

[28] San Diego-McGlone, M. L., Smith, S. V., and Nicolas, V. F. 2000. Stoichiometric interpretations of C: N: P ratios in organic waste materials. *Marine Pollution Bulletin*, 40(4), 325-330.

[29] Tran, V. N, Ngo, T. N. 2002. Textbook on Wastewater Treatment Technology. Publishing House for Science and Technology.

[30] Tsuzuki, Y., 2006 An index directly indicates land-based pollutant load contributions of domestic wastewater to water pollution and its application. *Sci. Total Environ*. 370, 425-440.

[31] Ajao, E.A., Anurigwo, S. 2002 Land-based sources of pollution in the Niger Delta, Nigeria. Ambio *A J. Hum. Environ*. 31 (5), 442-445.

APPLICATION OF DEEP LEARNING AND REMOTE SENSING TO ASSESS THE RIVERBANK CHANGE: A CASE STUDY AT NHAT LE RIVER MOUTH, VIET NAM

Doan Quang Tri[1*], Nguyen Van Nhat[1] and Vu Dinh Cuong[2]

[1] Journal of Hydro-Meteorology, Information and Data Center, Viet Nam Meteorological and Hydrological, Hanoi, Vietnam

[2] Key Laboratory of River and Coastal Engineering, Vietnam Academy for Water Resources, Hanoi, Vietnam; E-mail: [1*]doanquangtrikttv@gmail.com

Abstract: The accretion-erosion process not only causes damage to the environment but also affects people's livelihoods and the economy. Nowadays, there is a lot of research related to this issue with different methods such as using the empirical formula, using model to simulate… This study uses remote sensing (Landsat-8 and Sentinel-1 in 2018) and deep learning to analyse the riverbank changes in Nhat Le River, Quang Binh province. Unsupervised classification and spectral water indexing method Normalized Difference Water Index (NDWI) for extraction of water bodies from Landsat-8. Deep learning technology is used to analyse and calculate the riverbank by Sentinel-1 images. The study results show that the Sentinel-1 image analysis from deep learning technology gives high-resolution and accuracy than the extraction of water-body analysis from Landsat images. This method could be useful for detecting and extracting (decreasing or increasing) open water surface area and study related issues: Calculating reservoir capacity according to the water levels, accretion - erosion in large rivers.

Keywords: *Deep learning, remote sensing, riverbank change, NDWI, DeepLab model*

1. INTRODUCTION

Water is a vital resource, essential not just for humans, but for all life forms on our planet. The careful stewardship and management of water resources play a crucial role in supporting and nurturing life, as well as in averting its potential destruction. The scope of water management is broad, encompassing the monitoring of changes in rivers and streams, regional planning, flood control, and agriculture, among other things. These activities necessitate meticulous surveying and planning, which includes the creation of precise maps of water bodies and shorelines. Therefore, extracting water bodies and shorelines from remote sensing data is crucial to document these changing dynamics and map their current patterns. But there are many causes such as natural currents and human activities that lead to shoreline changes.

Currently, there are many methods that allow shoreline extraction from satellite image data. There are many classification and spectral water indexing methods such as Normalized Difference Vegetation Index (NDVI), Normalized Difference Moisture Index (NDMI), Normalized Difference Water Index (NDWI), and Modified Normalized Difference Water Index (MNDWI) 0. In addition to Landsat images, many studies have now used Sentinel images to analyze water areas [2], [3]. With the development of current artificial intelligence technology, using R-CNN to extract shorelines from Landsat images has also achieved much success [4].

Numerous studies have been carried out in recent decades focusing on the erosion of riverbanks, specifically pertaining to rivers, chars (river islands), and char inhabitants, with a particular emphasis on the morphological evolution of the Padma River [5]]–[[7]. Additionally, the study [8] have been carried out on the Padma River using satellite imagery to examine the dynamics of the river and its chars (islands). The study [9] used remote sensing (RS) and geographical information systems (GIS) to present the movement of river channels on Padma and Jamuna. It showed [9] that RS and GIS are an effective tool for both quantitative and qualitative analysis of river morphology. A study [10] showed at quantifying riverbank erosion and bar deposition in the Sirajganj District revealed a significant decrease in human settlements, forests, seasonal crops, and agricultural features, while the river coverage dramatically increased. Furthermore, [11] conducted an observation of the channel changes in the Ganges-Padma River system, revealing substantial land loss on both banks of the Ganges-Padma River. [12] employed machine learning as the primary method for land cover classification using individual remote sensing images. However, these single RS images only offer momentary spectral information of the Earth's surface, which limits the features available for classification [13]. This limitation often results in subpar classification outcomes, particularly when distinguishing between different types of crops and vegetation [14]. Furthermore, the classification outcomes derived from single images are influenced by various factors such as seasonal changes, weather conditions, and more. This makes the method less suitable for comprehensive studies on land cover alterations [16]–[20]. Compared to single images, multitemporal remote sensing images offer a more abundant set of spatial features and a variety of temporal profiles [17]–[23]. This richness enables them to cater to more complex tasks and yield more consistent classification results. In recent times, there has been a widespread application of multitemporal images in the creation of time series images (TSIs), which has significantly advanced the field of land cover classification research [23], [24]. In recent times, deep learning algorithms have increasingly gained prominence in the field of remote sensing [25], [26]. Recent advancements in AI reveal that data-driven deep neural networks are effective in discerning fundamental sequential dependencies from multitemporal RS observations [15], [27]–[29]. Recurrent neural networks (RNNs), convolutional neural networks (CNNs), self-attention networks, and their variations are widely recognized deep learning architectures used for processing time-series satellite data. The ability of deep neural networks to learn features end-to-end significantly reduces the burden of manual feature engineering, enhancing the model's performance and generalizability. Prior research has provided a comprehensive overview and future outlook on the application and development of deep learning across various application fields and types of RS data. For instance, [29] provided a comprehensive overview of the application of deep learning technology in the detection of agriculture through airborne imagery.

For instance, [30] provided a comprehensive review of the current advancements in deep learning for remote sensing, highlighting that remote sensing is also benefiting from the wave of deep neural networks. This trend mirrors other fields where deep nets are proving to be robust models that tend to outperform traditional approaches that use hand-crafted features. A study conducted by [31] aimed to understand the processes of riverbank erosion in Bangladesh by employing numerical modelling and deep learning techniques on satellite images. This research, conducted on a pilot basis, focused on a specific stretch of the Jamuna River. The study area encompassed an 80 km reach of the river, starting just

downstream of the Bangabandhu bridge and ending approximately 15 km downstream of the confluence of the Jamuna and the Ganges. The riverbank erosion in this area causes significant distress to thousands of people living along the banks each year. The findings of this study were used to develop a tool for predicting bank erosion in the study area.

In pixel classification, Deeplab is currently one of the most famous and widely used models. Developed from DeeplabV1 solves the problem of information loss and reduced resolution of fully convolutional neural networks (FCN) using atrous convolution and fully connected conditional random field (CRF). The version DeepLabV3 uses an improved ASPP module by including batch normalization and image-level features and removes CRF in previous versions [32]. [33] showed that the DeepLabV3 model improves accuracy and extracts more detailed images. Therefore, the study objective uses a deep learning method with the DeepLabV3 model to extract the shoreline from Landsat-8 and Sentinel-1 images for the Nhat Le River estuary.

2. MATERIALS AND METHODS

2.1. Description of study area

Nhat Le River flows into the East Sea at Nhat Le mouth. The river has two main tributaries, Kien Giang and Long Dai branches. The river basin has geomorphology that is favorable for concentrating rainwater and is influenced by tides from the sea, so the downstream part of the river is often flooded during the annual rainy season. Nhat Le estuary is located in Dong Hoi City, Quang Binh province, with geographical coordinates 17°29' North latitude and 106°38' East longitude (Figure 1). The river section flowing through Quan Hau-Dong Hoi city area has a South-North direction along the coast and the river turns to the southwest-northeast direction when flowing into the sea. The interaction between the river and the sea has created a natural dynamic balance system in the estuary with the existence of deltas, tidal flats, sand dunes, sand bars, sedimentation and erosion that made dynamic balance process. In recent years, Nhat Le estuary has been experiencing coastal erosion, especially in the area north of Nhat Le estuary in Hai Thanh ward and Bao Ninh commune south of the estuary. Coastal erosion has caused direct damage to construction works, and beach erosion has greatly affected Nhat Le beach tourism activities. Meanwhile, the Nhat Le River mouth is accreted due to the development of sandspit from the south of the river mouth, affecting navigation and flood drainage ability.



Figure 1. *Study area.*

2.2. Data collection

Bathymetry data were collected in April 2018 from the research project "Study of erosion - accretion processes for coastal and estuarine areas from Quang Binh to Thua Thien Hue province taking accounts of upstream activities and proposing countermeasures for

stabilization", coded KC.08-16/16-20 - Key Laboratory for River and Coastal Engineering (KLORCE) (Figure 2).

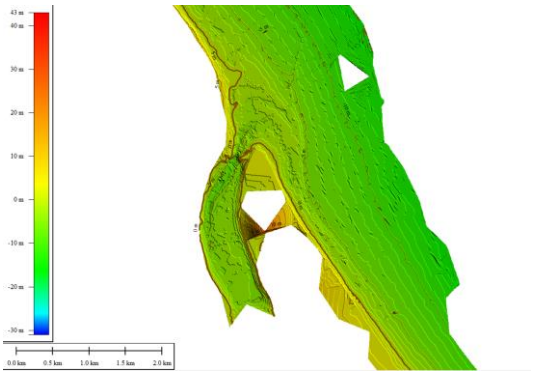


Figure 2. *Observed bathymetry at the Nhat Le estuary.*

The water level at Nhat Le River mouth selects Landsat 8 and Sentinel images with the water level closest to the 0 m mark and close to the time of field measurement in April 2018 (Figure 3). The study selects Landsat 8 level 1 images on April 13, 2018 at 03:00 with a water level of 0.125 m, Land Cloud Cover = 12.19% and Sentinel-1_IW_GRD on April 12, 2018 at 22:00 because of the actual measured data in April 2018 and this is the time when the water level is closest to chart zero (0.019 m) among the photos taken at the location during April 2018.

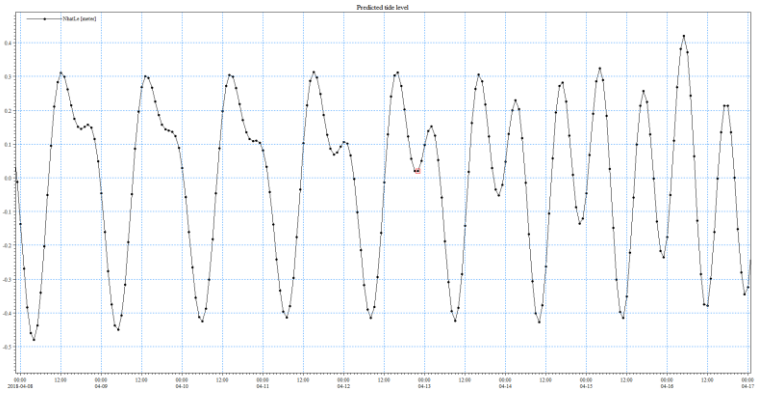


Figure 3. *The water level at Nhat Le.*

2.3. Methodology

The study uses Landsat 8 multi-spectral satellite image interpretation method and deep learning technology to analyze Sentinel-1 images to interpret the shoreline of the Nhat Le estuary area. The interpretation results of two methods will be compared with actual topographic data measured in the area inherited from... The flowchart of the study structure is presented in Figure 4.

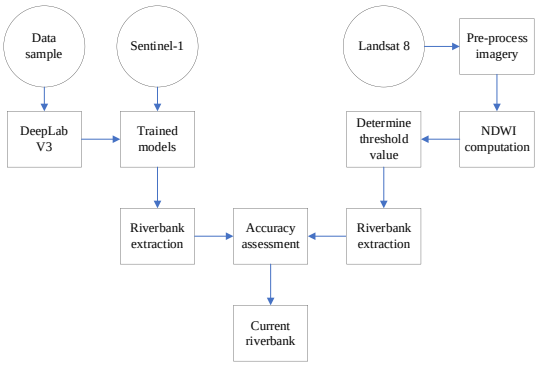


Figure 4. *The flowchart of study structure.*

2.3.1. Landsat satellite

The Landsat program provides the most extensive ongoing global record of our planet's surface, consistently supplying images that are both visually captivating and scientifically

valuable (Table 1, Figure 5). The unparalleled changes observed in land cover and usage have far-reaching implications, affecting weather patterns and climate change, ecosystem functionality and services, carbon cycling and sequestration, resource management, national and global economies, human health, and societal structures.

Table 1. Satellite chronology [34].

Name	Launched	Terminated	Instrument	Spatial and spectral resolution
Landsat 1	1972	1978	Multispectral Scanner (MSS)	0.5 to 1.1 µm (60m)
Landsat 2	1975	1982	Multispectral Scanner (MSS)	0.5 to 1.1 µm (60m)
Landsat 3	1978	1983	Multispectral Scanner (MSS)	0.5 to 1.1 µm (60m)
Landsat 4	1982	1993	MSS and Thematic Mapper (TM)	1.55 to 2.35 µm (30m)
Landsat 5	1984	2013	MSS and Thematic Mapper (TM)	1.55 to 2.35 µm (30m)
Landsat 7	1999	2022	Enhanced Thematic Mapper Plus (ETM+)	1.55 to 2.35 µm (30m)
Landsat 8	2013	active	Operational Land Imager (OLI) and Thermal Infrared Sensor (TIRS)	0.43 to 12.51 µm (30m)
Landsat 9	2021	active	Operational Land Imager (OLI) and Thermal Infrared Sensor (TIRS)	0.43 to 12.51 µm (30m)

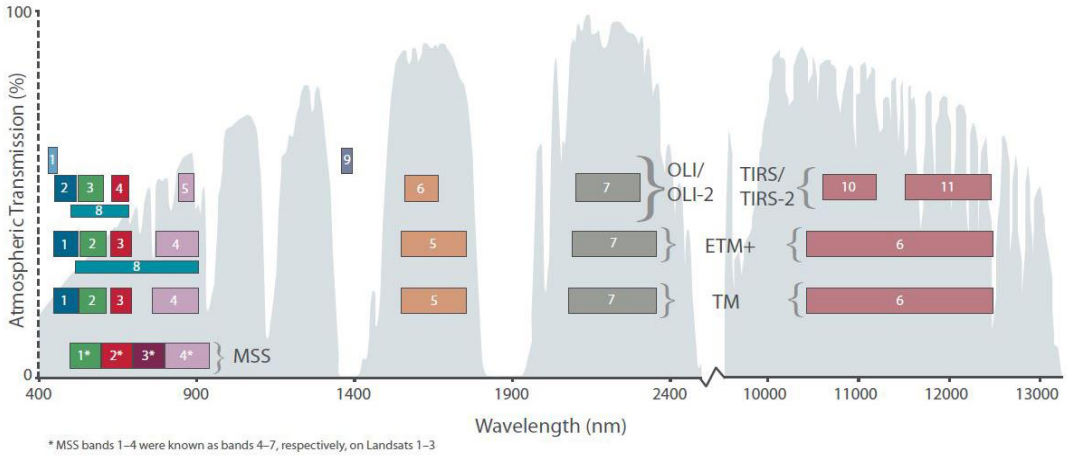


Figure 5. *Spectral Band passes for all Landsat Sensors [Usgs.gov].*

2.3.2. Sentinel-1

The Sentinel-1 mission encompasses C-band imaging that operates in four unique imaging modes, each offering different resolutions (as fine as 5 m) and coverage (up to 400 km) (Figure 6, Table 2) [35]. It boasts dual-polarization capability, extremely short revisit times, and quick product delivery. Additionally, for each observation, accurate measurements of the spacecraft's position and attitude are readily available. Synthetic Aperture Radar (SAR) holds the distinct advantage of functioning at wavelengths that are not hindered by cloud cover or lack of light, enabling it to gather data over any location, regardless of the time of day or weather conditions. The Sentinel-1 mission, equipped with its C-SAR instrument, can provide consistent and repeated wide-area surveillance. Sentinel-1 images are used in the following activities: Agriculture, forestry, subsidence, flooding, landslides, volcanism, and monitoring the changing flow of rivers and streams.

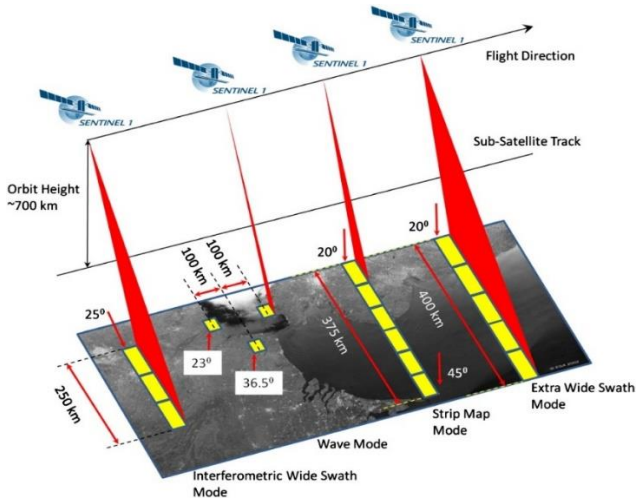


Figure 6. *Sentinel-1 Modes [sentinels.copernicus.eu].*

Table 2. Sentinel-1 operates in four exclusive acquisition modes.

Name	Resolution	Usage
Strip map (SM)	5m × 5m	Monitor small islands as well as emergency management for extraordinary events upon request.
Interferometric Wide swath (IW)	5m × 20m	Operational mode over land.
Extra-Wide swath (EW)	5m × 40m	Monitor wide coastal areas for phenomena such as shipping traffic and potential environmental hazards like oil spills or changes in sea ice.
Wave mode (WV)	5m × 5m	Operational mode over open ocean.

2.3.3. Normalized Difference Water Index (NDWI)

NDWI method is a popular method to identify water bodies, its formula is as follows:

$$NDWI = \frac{(GREEN - NIR)}{(GREEN + NIR)} \quad (1)$$

where NDWI is the normalized difference water index; GREEN is the band that includes reflected green light; NIR is the near-infrared radiation.

The selection of these wavelengths is intended to maximize the typical reflectivity of water features, representing high reflectivity of the NIR band by vegetation and soil spots while water bodies have low NIR reflectivity [36].

Hence, the NDWI can effectively differentiate between water and vegetation, enabling the extraction of water bodies. However, some minor water bodies may appear as fragmented water channels, which necessitates their removal through thresholding [37].

2.3.4. Deep learning

Machine learning, a subset of artificial intelligence, leverages structured data and algorithms to solve complex problems. Deep learning, a further subset of machine learning, employs a multi-layered approach in the form of neural networks to analyze input data. Each layer of the network identifies specific features and patterns within the data. Present-

day intelligence technologies have been trained to classify images, recognize objects, and enhance the clarity of the original image.

Not only successful in image processing, but deep learning is also currently being developed in spatial analysis problems in the GIS platform. When combined with remote sensing images, artificial intelligence can classify objects (such as roads, houses, forests, and water bodies), and can create maps [38]. ArcGIS pretrained models automate the task of digitizing and extracting geographical features from imagery and point cloud datasets.

The process of manually extracting features from raw data, such as digitizing footprints or creating land-cover maps, can be quite labor-intensive. Deep learning, however, automates this process, significantly reducing the amount of manual intervention required. Training a deep learning model can be complex, necessitating large volumes of data, substantial computing resources, and a thorough understanding of deep learning principles.

With ArcGIS's pretrained models, the need to invest time and effort into training a deep learning model is eliminated. These models have been trained on data from diverse geographies and perform well across various regions. As new imagery becomes accessible, you can extract features and generate layers of GIS datasets for mapping, visualization, and analysis. The pretrained models are readily available on the ArcGIS Living Atlas of the World to anyone with an ArcGIS account.

This model has the following characteristics:

- Input: Sentinel-1 C band SAR VH polarization band raster.

- Output: Binary raster representing water and non-water classes.

- Compute: This workflow is computed intensive and a GPU with compute capability of 6.0 or higher is recommended.

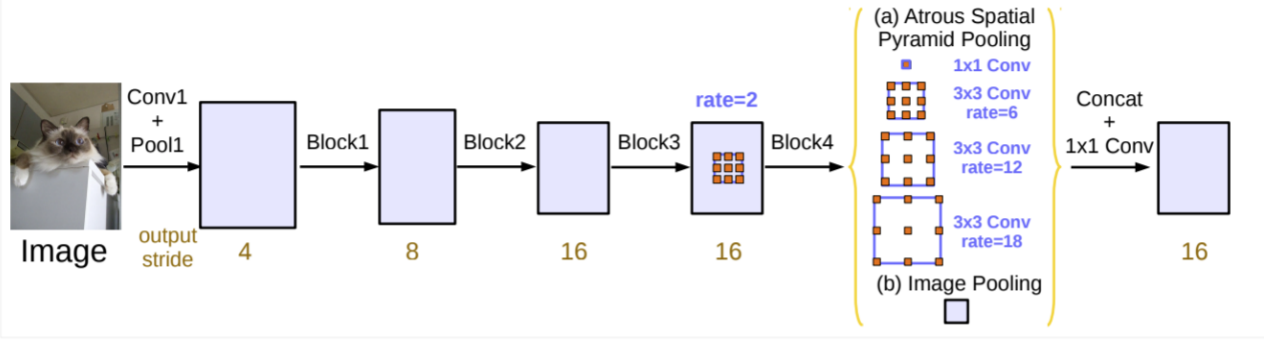


Figure 7. *DeepLabV3 Model Architecture [arcgis.com].*

- Applicable geographies: This model is expected to work well on Sentinel-1C band VH band raster for the United States.

- Architecture: This model uses the DeepLab model architecture implemented in ArcGIS API for Python.

- Accuracy metrics: This model has a precision of 0.945, recall of 0.92, and F1-score of 0.933.

- The DeepLabV3 model has the following architecture:

- Features are extracted from the backbone network (VGG, DenseNet, ResNet).

- To control the size of the feature map, atrous convolution is used in the last few blocks of the backbone.

- On top of extracted features from the backbone, an ASPP network is added to classify each pixel corresponding to their classes.

- The output from the ASPP network is passed through a 1 × 1 convolution to get the actual size of the image which will be the final segmented mask for the image.

1) Results

The results show that the riverbank line of the Nhat Le estuary has been successfully analyzed. Analysis results from Landsat 8 images show jagged lines, due to the resolution of Landsat-8 being 30 m, and at locations with structures such as bridges, they are still defined as riverbank. The shoreline in the Nhat Le estuary area analyzed from Sentinel images matches the measured topographic data. Not only that, DeepLab technology in the deep learning process also uses interpolations to improve the original resolution and smooth the output contour. However, there are still many erroneous locations due to many reasons such as: Insufficient number of pixels at small river locations, river structures, and sandy beaches on the coastline.

Figures 8 and 9 show the results of image extract from Landsat 8 and Sentinel -1 in 2018. The results show that images extracted from Sentinel -1 using Deep learning technology give smooth, high-quality results. High resolution, shoreline boundaries are smooth and even instead of jagged like the results of Landsat 8 extract using Normalized Difference Water Index (NDWI).

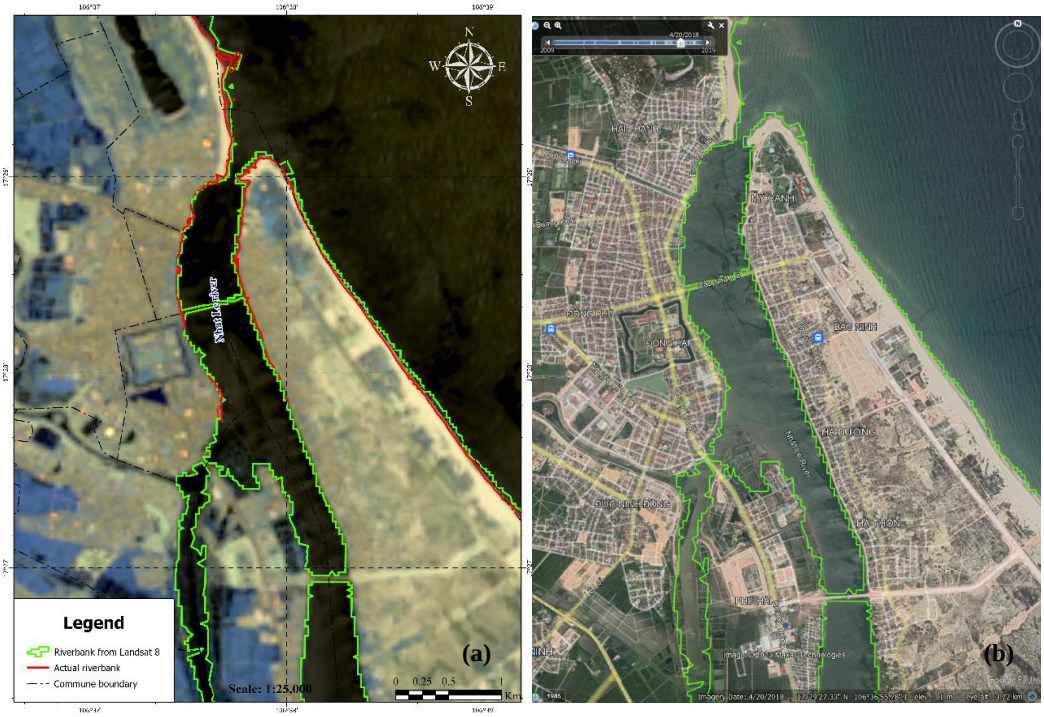


Figure 8. *Riverbank extract from Landsat 8 2018:*
(a) Landsat 8 basemap, (b) Satellite basemap.

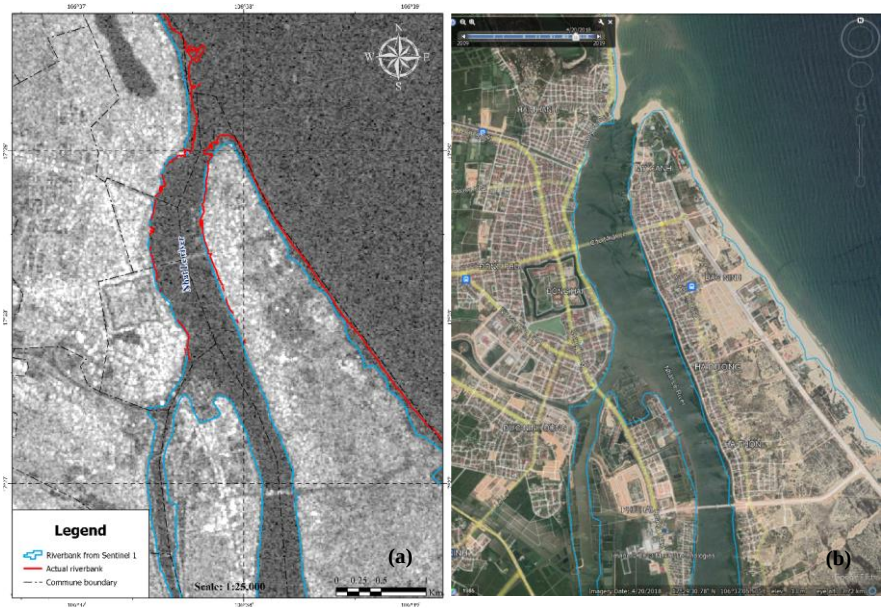


Figure 9. *Riverbank extract from Sentinel-1 2018: (a) Sentinel-1 basemap, (b) Satellite basemap.*

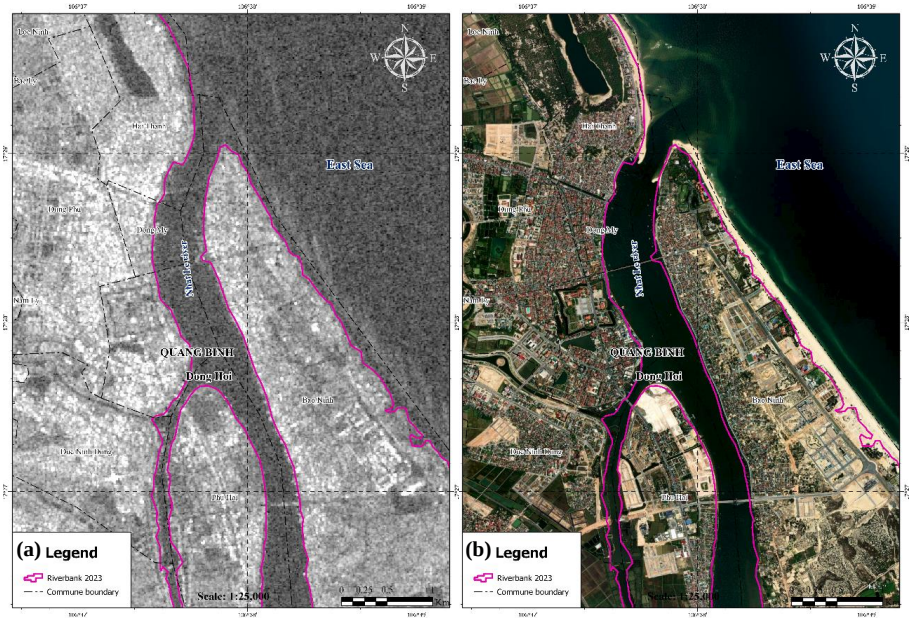


Figure 10. *Riverbank extract from Sentinel-1 2023:*
(a) Sentinel -1 basemap, (b) Satellite basemap.

The results of the 2023 Sentinel -1 extracting are shown in Figure 10 on the Sentinel -1 basemap (a) and on the Satellite basemap (b). The results of Sentinel -1 show riverbank change clearly and smoothly. To evaluate the water level change of riverbank in the study area, the study combined the analyzed riverbank change from these images from 2018-2023 image in Figure 11.

There is a clear change in the riverbank line in the northern area of Phu Hai commune. In 2023, the riverbank line covers the entire northern area of Phu Hai commune. This is reasonable because in 2018 that area is still aquaculture area. However, According to Decision No. 1778/QD-UBND dated June 16, 2021, the land use purpose change 5,748.5 m^2 of Phu Hai commune from agricultural land to urban land [39].



Figure 11. *Riverbank change between 2018 and 2023: (a) basemap 2018; (b) basemap 2023.*

2) Conclusion

Assessing riverbank changes is extremely important in planning work. Previously, performing this work depended on field measurement data. However, this method can only measure at a few monitoring locations and cannot measure the entire region or over a long period of time. In recent times, remote sensing technology has developed and been used as a useful solution to provide spatial and temporal image data with high resolution.

This article uses Deep learning algorithm to extract the riverbank of the study area from Sentinel-1, then use NDWI to threshold classification from Landsat 8. Then this study compares the results from two images with measurement data for the study area in 2018. Results show that Sentinel-1 gives more accurate and smooth results than Landsat 8. Finally, this research uses the 2023 Sentinel-1 to evaluate riverbank changes in the study area. The study shows that the application of DeepLab technology in determining riverbank is suitable for large river and lake areas. These results can be applied in other basins to assess riverbank erosion and monitor reservoir water levels.

3. REFERENCES

[1] Naik B C and Anuradha B 2018 Extraction of water-body area from high-resolution Landsat imagery *Int. J. Electr. Comput. Eng.* **8** 4111–4119

[2] Guo J, Luan Y, Li Z, Liu X, Li C and Chang X 2021 Mozambique flood (2019) caused by tropical cyclone Idai monitored from Sentinel-1 and Sentinel-2 images *IEEE J. Sel. Top. Appl. Earth Obs. Remote Sens.* **14** 8761–8772

[3] Shen G, Fu W, Guo H and Liao J 2022 Water body mapping using long time series Sentinel-1 SAR data in Poyang Lake *Water* **14**(2) 1902

[4] Gharbia R 2023 Deep learning for automatic extraction of water bodies using satellite imagery *J. Indian Soc. Remote Sens.* **51** 1511–1521

[5] Billah M M 2018 Mapping and monitoring erosion-accretion in an alluvial river using satellite imagery – The riverbank changes of the Padma river in Bangladesh *Quaestiones Geographicae* **37**(3) 87–95

[6] Sarker M H, Huque I and Alam M 2003 Rivers, chars and char dwellers of Bangladesh *Int. J. River Basin Manage.* **1**(1) 61–80

[7] CEGIS (Center for Environmental and Geographic Information Services) 2003 Ganges River: Morphological evolution and predictions. Prepared for Water Resources Planning Organization (WARPO), Dhaka, Bangladesh

[8] EGIS (Environmental and GIS Support) 2000 Riverine Chars in Bangladesh: Environmental Dynamics and Management Issues. The University Press Limited, Dhaka, Bangladesh

[9] Islam M T 2009 Bank erosion and movement of river channel: A study of Padma and Jamuna Rivers in Bangladesh using remote sensing and GIS. Division of Geoinformatics, Royal Institute of Technology, Stockholm, Sweden

[10] Hassan M S and Mahmud-ul-Islam S 2016 Quantification of riverbank erosion and bar deposition in Chowhali Upazila, Sirajganj District of Bangladesh: A remote sensing study *J. Geosci. Environ. Prot.* **4**(1) 50–57

[11] Dewan A, Corner R, Saleem A, Rahman M M, Haider M R, Rahman M M and Sarker M H 2016 Assessing channel changes of the Ganges–Padma River system in Bangladesh using Landsat and hydrological data *Geomorphology* **276** 257.

[12] Cheng X, Sun Y, Zhang W, Wang Y, Cao X and Wang Y 2023 Application of deep learning in multitemporal remote sensing image classification *Remote Sens.* **15** 3859

[13] Gomez C, White J C, Wulder M A 2016 Optical remotely sensed time series data for land cover classification: A review *ISPRS-J. Photogramm. Remote Sens.* **116** 55–72

[14] Tsai Y H, Stow D, Chen H L, Lewison R, An L, Shi L 2018 Mapping vegetation and land use types in Fanjingshan national nature reserve using google earth engine *Remote Sens.* **10** 927

[15] Zhong L, Hu L, Zhou H 2019 Deep learning based multi-temporal crop classification *Remote Sens. Environ.* **221** 430–443

[16] Flamary R, Fauvel M, Mura M D, Valero S 2015 Analysis of multitemporal classification techniques for forecasting image time series *IEEE Geosci. Remote Sens. Lett.* **12** 953–957

[17] Lyu H, Lu H, Mou L, Li W, Wright J, Li X, Li X, Zhu X X, Wang J, Yu L, Gong P 2018 Long-term annual mapping of four cities on different continents by applying a deep information learning method to Landsat data *Remote Sens.* **10**(3) 471

[18] Xie S, Liu L, Zhang X and Chen X 2019 Annual land-cover mapping based on multi-temporal cloud-contaminated Landsat images. *Int. J. Remote Sens.* **40** 3855–3877

[19] Ienco D, Gaetano R, Dupaquier C and Maurel P 2017 Land cover classification via multitemporal spatial data by deep recurrent neural networks. *IEEE Geosci. Remote Sens. Lett.* **14** 1685–1689

[20] Pelletier C, Webb G.I and Petitjean F 2019 Temporal convolutional neural network for the classification of satellite image time series *Remote Sens.* **11** 523

[21] Fang F, McNeil B E, Warner T A, Maxwell A E, Dahle G A, Eutsler E and Li J L 2020 Discriminating tree species at different taxonomic levels using multi-temporal WorldView-3 imagery in Washington DC, USA *Remote Sens. Environ.* **246** 111811

[22] Whelen T and Siqueira P 2018 Time-series classification of Sentinel-1 agricultural data over North Dakota. *Remote Sens. Lett.* **9** 411–420

[23] Kumar P, Gupta D K, Mishra V N and Prasad R 2015 Comparison of support vector machine, artificial neural network, and spectral angle mapper algorithms for crop classification using LISS IV data. *Int. J. Remote Sens.* **36** 1604–1617

[24] Shukla G, Garg R D, Srivastava H S, Garg P K 2018 An effective implementation and assessment of a random forest classifier as a soil spatial predictive model *Int. J. Remote Sens.* **39** 2637–2669

[25] Castro J B, Feitosa R Q, Happ P N 2018 An hybrid recurrent convolutional neural network for crop type recognition based on multitemporal SAR image sequences. In Proceedings of the IGARSS 2018-2018 IEEE International Geoscience and Remote Sensing Symposium, Valencia, Spain, 22–27 July 2018; pp. 3824–3827.

[26] Russwurm M and Korner M 2018 Multi-temporal land cover classification with sequential recurrent encoders *ISPRS Int. J. Geo-Inf.* **7** 129

[27] Russwurm M and Korner M 2020 Self-attention for raw optical satellite time series classification *ISPRS-J. Photogramm. Remote Sens.* **169** 421–435

[28] Teixeira I, Morais R, Sousa J J and Cunha A 2023 Deep learning models for the classification of crops in Aerial imagery: A review *Agriculture* **13** 965

[29] Sheykhmousa M, Mahdianpari M, Ghanbari H, Mohammadimanesh F, Ghamisi P and Homayouni, S 2020 Support vector machine versus random forest for remote sensing image classification: A meta-analysis and systematic review *IEEE J. Sel. Top. Appl. Earth Observ. Remote Sens.* **13** 6308–6325

[30] Zhu X X, Tuia D, Mou L, Xia G S, Zhang L, Xu F and Fraundorfer F 2017 Deep learning in Remote Sensing: A Review *IEEE Geosci. Remote Sens. Mag.* pp. 60

[31] Ali M and Zobeyer H 2021 Project "Research on river bank erosion dynamics using numerical modelling and deep learning techniques".

[32] https://developers.arcgis.com/python/guide/how-deeplabv3-works/

[33] Chen L, Papandreou G, Papandreou G, Schroff F and Adam H 2017 Rethinking atrous convolution for semantic image segmentation *arXiv:1706.05587v3*

[34] https://www.usgs.gov/faqs/what-are-band-designations-landsat-satellites.

[35] https://sentinels.copernicus.eu/web/sentinel/missions/sentinel-1/overview.

[36] McFeeters S K 1996 The use of the normalized difference water index (NDWI) in the delineation of open water features *Int. J. Remote Sens*. **17** 1425–1432.

[37] Ji L 2009 Analysis of dynamic thresholds for the normalized difference water index *Photogramm. Eng. Remote Sens.* **75** 1307–1317.

[38] https://www.esri.com/about/newsroom/arcwatch/where-deep-learning-meets-gis/

[39] https://nhadautu.vn/son-hai-group-duoc-quang-binh-giao-dat-thuc-hien-du-an-dia-oc-2200-ty-d53742.html.

Acknowledgments

Authors would like to thank the funding of ministerial-level project of MoNRE "Study on the scientific basic and establishing a warning system for the risk of landslide, subsidence due to the drought and underground water exploitation at Ca Mau peninsula", grant number: TNMT.2023.06.12 during 2023-2025. The ministerial-level key science and technology program on forecasting and warning of hydro-meteorological disasters for disaster prevention and control in the 2021-2025 period. Program code: TNMT.06/21-25. The methodology used in this study is one of the methods applied in building maps to identify landslide areas of the project.

INVENTORY OF LANDSLIDES TRIGGERED BY EXTREME RAINFALL IN AUGUST 2023 ALONG THE NATIONAL ROAD NO. 32, MU CANG CHAI DISTRICT, YEN BAI PROVINCE

Duong Thi Toan[1], Oneta Soulinthone[2], Nguyen Trung Thanh[3], Nguyen Viet Ha[4], Dang Quang Khang[1], Bui Van Dong[1], Do Minh Duc[1]

[1] University of Science, Vietnam National University, Hanoi, Vietnam

[2] PhD student at Vietnam Academy of Science and Technology, Vietnam

[3] Hanoi University of Mining and Geology, Vietnam

[4] Viet Anh-Hanoi Construction Investment and Consulting Company, Vietnam

E-mail: duongtoan@hus.edu.vn

Abstract: Landslides, debris flash floods, and riverbank erosion are common geo-hazards in mountain areas in Vietnam. In August 2023, Mu Cang Chai district, Yen Bai province was affected by heavy rain, and those geo-hazards destroyed hundreds of houses and damaged several kilometres of roads. This paper aims to investigate and classify landslides along 32 km of the National Road No. 32 from Mu Cang Chai town to Ho Bon commune in Mu Cang Chai district. The total number of landslides in the study area is 46 landslide blocks, divided into 7 types, including rock fall (6/46), debris and soil fall (5/46), debris and soil translational sliding (17/46), soil flow (8/46), soil rotational sliding (5/46), and complex sliding (5/46). The volume of slides ranged from very small (1-20m^3), which is 33.6% of the total, small (20-100 m^3) is 23.9%, small – medium (100-500m^3) is 21.7%, medium –large (100-500 m^3) is 8.7%, and large and very large (>1,000 m^3) is 13.0%.

1. INTRODUCTION

Mu Cang Chai is a high mountain area in Yen Bai province in the northwest region of Vietnam. The National Road No. 32 (NR.32) runs through Yen Bai province from Van Chan district, Nghia Lo, and Mu Cang Chai district goes to Lai Chau province. A series of geo-hazards such as landslides, debris flash floods, and riverbank erosion happened the early August 2023, especially along NR.32. The hundreds of village houses in Mu Cang Chai district were destroyed and strongly affected. The NR.32 was broken some segments in Ho Bon commune, Mu Cang Chai district.

This paper reviews the consequences of geo-hazard problems that happened in the Mu Cang Chai area during the rainfall event in August 2023. The main aim is to build the geo-hazards database and concentrate inventory of landslides. This paper will collect the types of geohazards, the number of landslide locations, types of landslide materials and movement, and the volume of landslide blocks. This paper also metion on the relationship landslide with the natural condition and human activities. These data will help further analysis, building an understanding cause of landslides as well as building warnings for this area. The study area focuss on along and surrounding region of NR.32 from Mu Cang Chai Town Ho Bon commune, belong to Km300 – Km332 (Figure 1). This road segment belongs to Mu Cang Chai town and 3 communes Ho Bon, Khao Mang, and Lao Chai.

In the previous publication, Mu Cang Chai also was a warning area with a high risk of geo-hazards. The flash flood and debris landslide happened several times. The recent flash flood occurred in 2017 at Mu Cang Chai town and Kim Noi commune 0. Study landslides in Yen Bai province and the Mu Cang Chai area were also performed and analyzed in some projects. In these publications, Ho Bon, Lao Chai, and Khao Mang were also recommended as general high risk of landslide and geo-hazards [2].

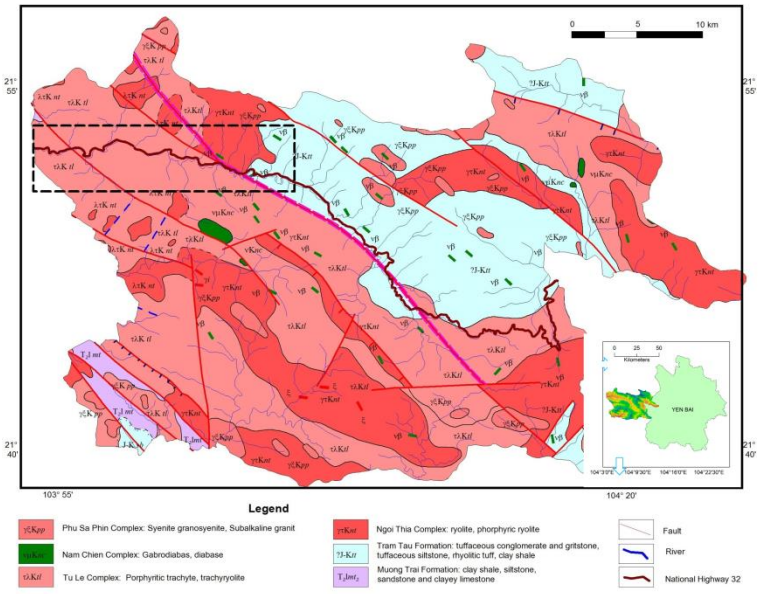


***Figure 1**. The study area and geological settings*

Mu Cang Chai is in a high hilly area. This area are ranging from 280 m to 2820 m in the elevation. The geological condition formed by main of the eruptive complexes such as Ngoi Thia, Tu Le, Phu Sa Phin. The sedimentary rocks can found in the Tram Tau formation. The main fault can find in this area are Nghia Lo, Nam Co Minh and Phong Tho – Yen Van fault. These geological conditions on the petrographic original and fault are factors having strong effects on the slope stability in the Mu Cang Chai area [2].

The evelation in the NR.32 from Mu Cang Chai town to Ho Bon (Km 300 to Km 332) ranges from 500 m to 1530 m above sea level. The low area is along NR.32 and the high area is in some villages in Lao Chai and Ho Bon commune. Along NR.32, the altitude ranges from 500 – 700 in Km332-Km325, and ranges from 700 – 950 in Km 324 – Km 300. In the high mountain area, the altitude ranges up to 1530 m such as in Ho Bon and Lao Chai commune. The surface is covered dominantly by eruptive magma of the Ngoi Thia, Tu Le, and Nam Chien geological complexes, Tram Tau formation. The sub-complex Ngoi Thia includes acidic and alkaline volcanic rocks with the main composition as rhyolite in blocky structure, and flow-like sharp in some places. The rhyolite in sub-complex Ngoi Thia has porphyritic architecture, quartz phenocrysts predominate, with less potassium feldspar. Ryolite is mostly light-coloured, coloured minerals are very few and usually only contain biotite. The sub-complex Tu Le includes almost acid-neutral sub-alkaline and alkaline volcanic rocks. That component is occupied by the main part of the Tu Le volcanic basin area. The petrographic composition of volcanic rocks mainly corresponds to ryodacite rhyolite, trachy-ryolite, and a lesser extent porphyry trachyte. Nam Chien complex includes gabbro amphibole and gabrodiabas bodies. Tram Tau formation includes gray, light gray

phylite tuff schist, containing thin strips of red-brown, light gray or light green volcanic glass fragments and opaque white quartz and feldspar grains. The gray tuff sandstones is thick layer, mainly quartz, feldspar. The phylitized tuff shale interbedded with limestone lenses, light gray tuff sandstone, tuff siltstone with gray sericite, fractal medium layer, limestone mixed with clay and quartz grains, sometimes in the form of macadam. These complexes and formations appeared to cut slopes along NR.32 and the local roads with different levels of weathered rock. These rocks are covered at the top of the slope by a thin-filled layer. Landslides occurred often in the slope with high weathered levels and or in the fill layer by heavy rain.

3. AUGUST 2023 EXTREME RAINFALL AND CONSEQUENCES IN THE MU CANG CHAI DISTRICT

Figure 2 shows the change in the accumulated rainfall by a day in August 2023. From the end of July to early August (before 5 August), rainfall with small intensity, less than 15 mm/day. From 4 August, rainfall increased to nearly 40 mm/day and rapidly up to 120 mm/day and 160 mm/day on 5 and 6 August, respectively. The series of landslides and flash floods in Ho Bon happened on the evening of 5 August, after 2 days of heavy rainfall. The heavy rainfall was continually in 6-7-8 August causing severe damage and isolation in the study area until August 8, 2023. Figure 3 shows the characteristics of rainfall in the August 2017 event. In 2017, the flash flood happened in Mu Cang Chai two when the rainfall accumulated was 140mm (Figure 3) nearly the same trigger threshold in 2023. However, the rainfall continued heavy until 8 August, when the accumulation reached 350mm.

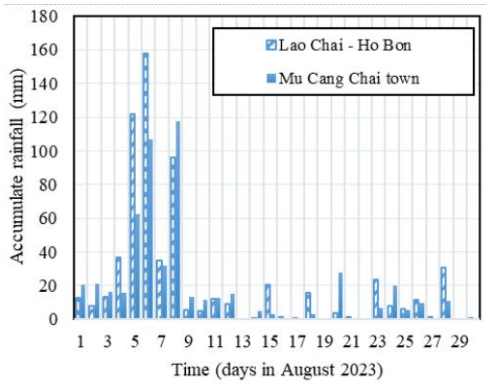


***Figure 2**. The rainfall characteristic in August 2023*

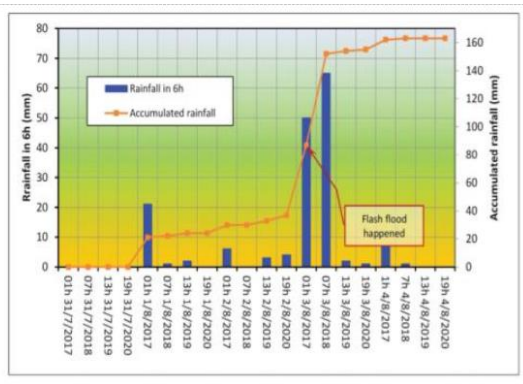


***Figure 3**. The rainfall characteristic in August 2017 0*

Ho Bon, Lao Chai communes were strongest affected durring rainfall event in August 2023, especially by a debris flash flood and landslide on 5 August. Figures 4 and 5 show the status at NR.32 from Km 325 to Km 328 at the center of Ho Bon commune. That area is in the highest density of houses, having the heath station center, commune People's Committee, and school. The NR.32 is in between of the positive talus of the steep slope and Nam Kim river. Then this aree were attacted by landslide, riverbank erosion and debris flash flood simultaneously.

Figure 4 shows the area near the Ho Bon Health Centre at Km325 at NR.32. The high velocity water flow bring the huges rock from the oposite spring to Nam Kim river. The 72m NR.32 and 4 houses near the health center were completely destroyed. An old man in

the Health Centre was swept. Along Km325 to Km328, the Ho Bon commune People's committee building, the NR.32 suffered by landslide in the positive talus slope and riverbank collapse in the negative talus (Figure 5). Material included rock, soil, mud, mixing of trees and material of broken house filled and spreaded to the NR.32. There werre 20 houses were completely destroyed and collapsed in this area.

Table 1 summarizes the damage consequences at Ho Bon, Khao Mang, Lao Chai communes. The consequence in terms of the types of facilities affected (e.g. local houses, roads, public buildings such as schools, and health centers…) and land used for agriculture. Which, 57 houses completely collapsed, 12 km of roads including both NR.32 and the local inter-commune roads, 200 ha corn, and 161,9 ha rice were impacted (Table 1).

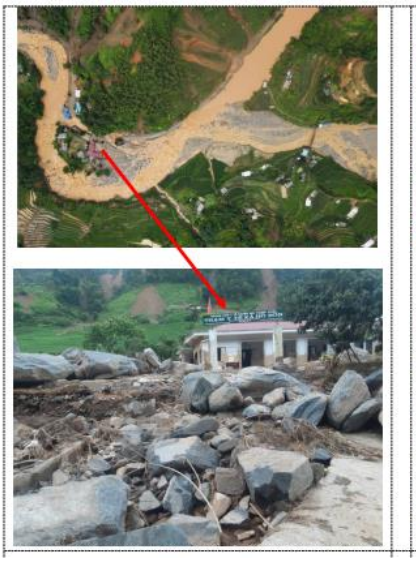


Figure 4. *The area surrounding the Ho Bon Health Center area (Sources of upper figure [3])*



Figure 5. *The Ho Bon center area and commune People's Committee.*

Table 1. The consequences in Mu Cang Chai

Types of Affected Facilities	Ho Bon	Lao Chai	Khao Mang	Mu Cang Chai district
Number of people killed	1		2	3
Number of houses completely collapsed	21	35	1	68
Number of houses evacuated	13	53	11	147
Number of houses need recovered	23	40	57	35
Other building affected (school, health station...)	1 primary school 1 Health station	1 primary school	0	2 primary shools 1 Health station
Highway and local roads destroyed and filled (km)	24	83	20	72 m NR.32 surface erosion Drainage: Km324 - Km329.
Agricultural damage	200 ha corn and 110 ha rice			200 ha corn and 161.9 ha rice

Source of data	*Stastified by local commune committee staff*	*[4]*

4. LANDSLIDE INVENTORY AND CLASSIFICATION

4.1. Methodology

The impact of geo-hazards was recorded and described by the field investigation during August 8-10. Equiments were used in the field including GPS garmin, demension measurement of Nikon Laser 550A, UAV photographs and describing landslide status by an information sheet, interviewing the local authorities and local people. The data measured and described in the field were used to evaluate the status and classify the landslide. Using the updated verion of the Varnes*'* 1978 classification system for classifing the type landslide based on the material and type of failure surface movement (Table 2).

Table 2. ***A summary of Varnes' 1978 classification system (update version [5])***

Movement type	Rock	Debris	Earth
Fall	1. Rock fall	2. Debris fall	3. Earth fall
Topple	4. Rock topple	5. Debris topple	6. Earth topple
Rotational sliding	7. Rock slump	8. Debris slump	9. Earth slump
Translational sliding	10. Block slide	11. Debris slide	12. Earth slide
Lateral spreading	13. Rock spread	–	14. Earth spread
Flow	15. Rock creep	16. Talus flow	21. Dry sand flow
		17. Debris flow	22. Wet sand flow
		18. Debris avalanche	23. Quick clay flow
		19. Solifluction	24. Earth flow
		20. Soil creep	25. Rapid earth flow
			26. Loess flow
Complex	27. Rock slide-debris avalanche	28. Cambering, valley bulging	29. Earth slump-earth flow

Calculating the volume of landslide block in the field is determined approximately by following equation (Eq. 1). Where *Dr* the vertical deformation; *Wr* is the maximum width of slope; *Lr* is the minimum distance from toe to top of landside block [6][7]:

$$V = \frac{1}{6}\pi . D_r . W_r . L_r \quad (1)$$

The landslide classification by the volume is modified from the classificate from International
Consortium on Landslides and V. Đ.Lômtadze [8].

4.2. Types of landslides

From the survey results, here are the preliminary assessments for landslide status along and surrounding NR.32 from Mu Cang Chai town to Ho Bon commune. There were 46 landslide blocks were recorded with 43 blocks along NR. 32, and 5 blocks at Trong La village – Ho Bon commune and at Hu Tru Linh village – Lao Chai commune (Figure 6). The type of landslide was determined by Varnes's 1978 classification system based on the type of material and movement as shown in Table 3. There were classified into 7 types, including (1) Rock falls; (2) Debris and earth fall; (3) Debris and earth translation sliding; (4) Soil (earth) flow; (5) Soil rotational sliding; (6) Complex (Debris and soil translation sliding and flow); and (7) Complex (Risk of large and soil rotational sliding). Which, the

majority of sliding blocks are mainly shallow sliding blocks, falling in (1) rockfall, (2) Debris and earth fall, and (3) Debris and earth translational sliding. Three of these shallow slides occupied 60.9% (28/46 slides); the soil slope failure type as (4) soil flow and (5) soil rotational sliding occupied 28,2%; and the two last types of complex type only 10.9%.

Tables 4 and 5 show the type of slope failure with the volume and the slope forming. Three groups as the very small volume (0-20 m^3), small (20-100 m^3) and small–medium (100-500 m^3) volume have a high number of failure slopes (10-11/46 blocks). These groups were mainly occupied by the type of shallow sliding (rock fall, debris and soil fall, translational sliding) as described in part 4.1. The large volume (>1000 m^3) presented in the complex types. In terms of slope forming (Table 5), there are three types natural slope, cut slope, and fill slope. Because the area is studied along national and local roads, slope failure falls into the cut slope (37/48). The slope forming by cutting may be one of the factors affecting the instability of the slope.



***Figure 6**. Location of sites of slope failure in the study area*

Table 3. Type of failure applied Varnes 1978 classification

No.	Types of Slope Failures	Numbers	Percentage (%)
1	Rock falls	6	13.0
2	Debris – soil (earth) falls	5	10.9
3	Debris and earth translational sliding	17	37.0
4	Soil (earth) flow	8	17.4
5	Soil Rotational Sliding	5	10.9
6	Complex (Debris and soil sliding and flow)	3	6.5
	Complex (Risk of large and soil rotational sliding)	2	4.3
	Total	46	100

Table 4. Slide volumes and types of failure distribution

Types	Volume of Failure	Numbers	Type of slope failures						
			Rock fall	Debris-soil fall	Translational sliding	Soil flow	Soil Rotational Sliding	Complex (translation and flow)	Complex (Risk of large sliding)
Very small	0 - 5 m^3	10	5	2	3	0	0	0	0
	5 - 10 m^3	0	0	0	0	0	0	0	0
	10 - 20 m^3	5	0	1	3	1	0	0	0

Small	20 - 100 m^3	11	1	0	6	4	0	0	0
Small-Medium	100 - 500 m^3	10	0	1	3	3	3	0	0
Medium Large	500 - 1000 m^3	4	0	1	0	0	2	1	0
Large	>1000 m^3	4	0	0	2	0	0	2	0
Risk of huge failure		2	0	0	0	0	0	0	2
Total		46	6	5	17	8	5	3	2

Table 5. Type of failure classified by volume and type of slope forming

Types	Volume of Failure	Numbers	Natural Slope	Cut Slopes	Fill Slopes	Percentage (%)
Very small	0 - 5 m^3	10	0	12	0	21.7
	5 - 10 m^3	0	0	0	0	0.0
	10 - 20 m^3	5	1	4	0	10.9
Small	20 - 100 m^3	11	1	10	0	23.9
Small-Medium	100 - 500 m^3	10	1	8	1	21.7
Medium-Large	500 - 1000 m^3	4	0	3	0	8.7
Large	>1000 m^3	4	3	0	0	8.7
Huge	Risk of large failure	2	2	0	0	4.3
	Total	46	8	37	1	100

4.3. Disscusion characteristics of failure slopes

4.3.1. Rock falls

Figure 7 shows a example of a rock fall type in cut slope along NR.32 in Ho Bon, Mu Cang Chai. Rock falls occupied 1-2m of the road, destroyed the water drainage, dangerous for traffic people on the roads.



Figure 7*. Rock fall at MCC 26, Ho Bon commune*

At point MCC31, a rock mass from the slope at the right slide (direct from Ho Bon to Khao Mang) fell and rolled across the road, attacked through the wood wall, and rolled until the bed in the house. That rock mass killed 2 kids sleeping in the bed. The distance from the foot of the slope to the stopping position was about 25m (Figure 8 a, b, c).

The rock fall and roll type happen at 6 sites (MCC03, MCC06, MCC07, MCC11, MCC 16, and MCC31) with 5 sites in Ho Bon commune and 1 site in Khao Mang commune. All sites are cut slopes and have very small volumes (less than 20m^3). Almost the failure slope fell down from the lateral slope surface at the low elevation (1-3m). The slopes are high

steep slopes with the angle of slope as 80-90 degrees. The lateral slopes are rough after failure. These slopes are cracked weathered rocks, and rocks fell down and spread to 1-2m NR.32 causing dangerous traffic.

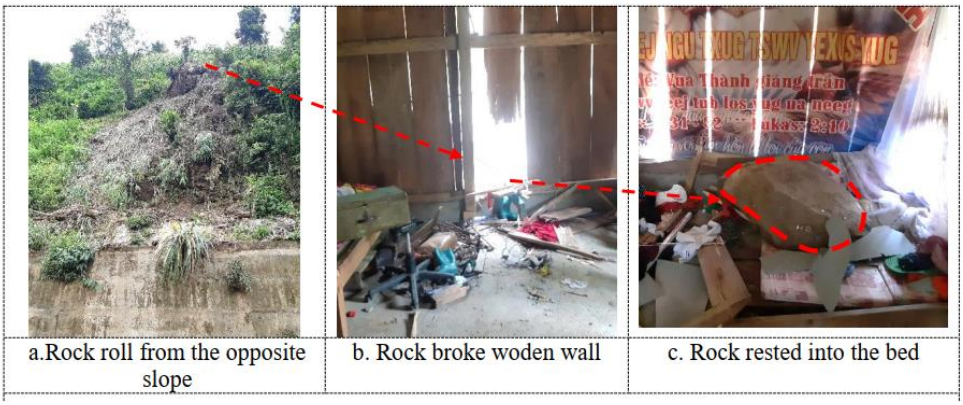


Figure 8. *Pathway of the rock fall and roll at MCC 31, Khao Mang commune*

4.3.2. Debris - soil (earth) falls and translational sliding

Figure 9,10 show types of the debris-soil fall and translational sliding. Almost landslide blocks of these types have very small volumes. The 3/5 the debris-soil fall and 12/17 translational slides are small volume (Table 3).



a. Debris fall at MCC02



b. Debris and soil at MCC10

Figure 9. *Debris and soil falls*



a. Debris fall at MCC01



a. Debris and soil at MCC27

Figure 10. *Debris and soil translational sliding*

The material of debris–soil fall occurred from the thin layer at the top of the slope, and may sweep some rock in the lateral slope surface (Figure 6a). The failure material almost fell down from the high elevation 14 – 25m. The translational sliding blocks happen at soil

layer at the top and lateral slope surfaces. The materials in this case often are a mixing of soil, mud, and rock known as debris, filling. The failure material spread to all surfaces of the road causing dangerous for transportation in the roads.

4.3.3. Soil flow and rotational sliding

Figures 11 and 12 show types of soil flow and rotational sliding. These types happen along the slope surface, having small, small – medium volumes. The soil flow blocks were often located in the same place as the water drainage of the slope. By the pressure of water, the soil at the top and slope surface was saturated swept into the toe and spread to the roads. The material of soil flow affected longer road distances than other types of failure blocks. Soil, water and rock, trees together create a mixing fill to the road with a layer thick of 0,5 m to 1m, and spread the hundred-meter length on the road (Figure 11). The rotational sliding happens in slopes having thick soil – completely weathered rocks (Figure 12)



a. Soil flow at MCC14



b. Soil flow at MCC24

***Figure 11**. Soil flow failure slopes*



a. Soil rotaional slide at MCC42



b. Soil rotaional slide at MCC46

***Figure 12**. Soil rotational sliding*

4.3.4. Complex failure slopes

The complex landslide is the combination of some types of landslide failure in a site. These slopes often have thick soil layers and have water drainage line on body landslide blocks. The volume of this type is from medium to large volume, larger than 500 m^3. The complex landslide of soil flow and sliding happened in both natural slopes (MCC18, MCC19) and in cut slopes (MCC21). Figure 13 shows an example of the types of complex sliding and soil flow happened in Trong La village, Ho Bon commune. The rainfall water and drainage water infiltrate to landslide blocks through the tension crack. By changing saturated soil properties, and by pressure of water flow, the large material failure. In this site (MCC19), the surface of the slope was used for growing rice. The water flow line and water stored in the rice fields as factors that promote the development of the water drainage in this area. During heavy and long day rainfall, the water continues drainage in this way causing the move down of slope.



***Figure 13**. An example of complex type of soil sliding and flow (MCC19 and model)*

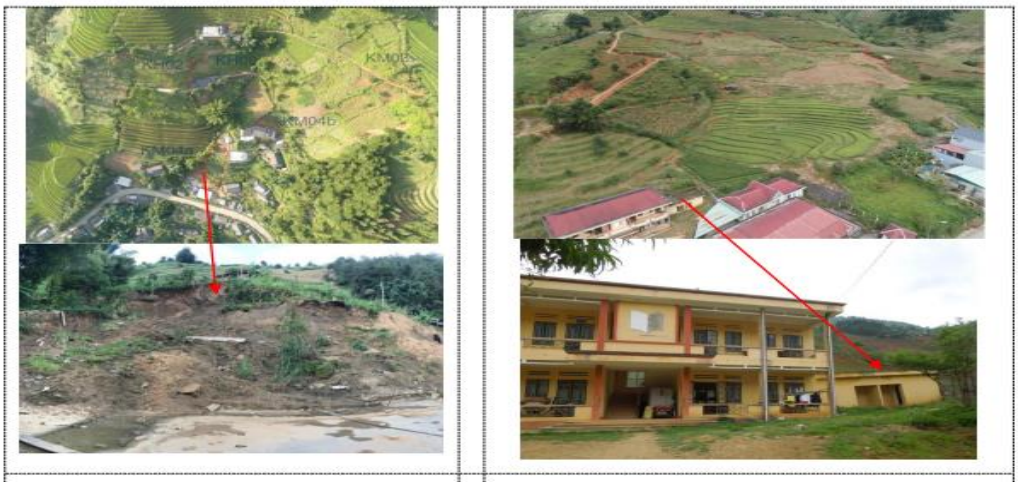


***Figure 14.** The high risk of large and deep landslide at Khao Mang commune*

***Figure 15.** The high risk of large and deep landslide at Mu Cang Chai town*

Two locations were determined may have a high risk of the large and deep driving surfaces along. These two landslide locations are in Khao Mang (MCC 36), at Km 317 H1 (Figure 14), and at Mu Cang Chai town (MCC48) at Km300H4 (Figure 15). At Khao Mang, the area terrain is low mountainous with slope elevation from 770 to 960 m, slope varying from 15 – 25 degrees, width 150 m, height 127 m, and length from top to bottom of slide block 370 m, as known the complex landslide block. About 20 houses will affected when landslides occur. In August 2023, two houses at the toe of the area were filled by soil material of failure slope. The volume of landslide failure was 842,55 m^3 with the dimensions 8m in height, 45m in length, and 4 m in depth. Two houses near the toe of the landside failed to have to move to another place. Two houses in the upper middle of the slope also need to move and recover. The reason of this failure is mainly due to activities of cutting steep slopes to build roads and houses. The soils at the toe and body slope surface are poorly cohesive and easily permeable to water. At site of MCC48 in the Mu Cang Chai town is shown in Figure 15. The NR.32 is along the toe of this landslide block about 200m (Km300H4-H6), and local houses were built in high density in both sites of NR.32 near the toe of the landslide block. A new building Mu Cang Chai as the people's Procuracy was a settlement and must moved to another place (from 2017). The slope surface has an altitude of 960 m to 1100 m. The sliding block has a width of about 250 m, a height of 110 m, and a length from the top to the bottom of the sliding block of 400 m. The slope surface is used for terraced fields. The failure of this landslide block will affect to many house in both site of NR.32. Both these large-scale landslides need further and detail study.

5. IMPACTS FROM OTHER GEO-HAZARDS

Besides the impact of landslides and flash flood hazards, the riverbank collapsing and the instability of the Hydraulic plants along the Nam Kim River were also serious problems. Figure 16 shows the impaction of riverbank erosion and landslide material fill to the Hydraulic Plant. The NR.32 here runs along the Nam Kim River connecting Yen Bai and Lai Chau. Landslides happen in the positive talus, and riverbank erosion and collapse in the negative talus. The NR 32 was strongly destroyed and stopped the escape way of people in this area. In this area, there are two Hydraulic plants along Nam Kim River, geo-hazard destroyed a lot of power transformer stations (Mu Cang Chai district lost power 80 transformer stations), filled material into the control house, and lost power in some days. Moreover, the materials of landslide blocks, debris flow, and flash floods accumulated in Nam Kim River caused a risk to the water storage lake, and the strength of the dam. The risk of overpressure and dam may affect further areas downstream of the Nam Kim River.



Negative talus or riverbank erosion *The control house of Hydraulic plant*

***Figure 16**. Consequence along Nam Kim riverbank*

6. CAUSES OF GEO-HAZARDS

In general, the consequence of these geohards in this August caused the heavy damage to Mu Cang Chai area. According to local people, they have never witnessed such heavy rain and damage in the past. In fact, no strong and combined geo-hazars have occurred in the past hundred years in the Ho Bon area. In 2017, Mu Cang Chai also experienced similar geohazards but only occurred in the central area of Mu Cang Chai district, Kim Noi commune and Mu Cang Chai town.

Heavy rain was the main cause of damage but some problems were related to the conditions and activities of the area. Some problems can be noticed: First, the local people often concentrate on living and building houses near streams and areas with drainage ditches. When geohazards occur, this area suffers the most damage, for example in the center of Ho Bon commune (Figures 4-5). At the same time, areas with the flow landslide mostly have drainage ditches from the slopes. At some similar locations, large-scale flows have occurred, endangering buildings, such as the MCC 14 area (Figure 11a) and the area near the center of Ho Bon commune health station (Figure 4). These are places where houses should not be built. The second problem is the excavation of slopes to build roads, which are the areas with the highest concentration of landslides. The third problem is that farming on terraced fields decreases the forest area and increases the seepage deformation of

the slope, easily causing landslides. More specific recomments require further detailed research.

7. CONCLUSIONS

During the rainfall event in August 2023, Mu Cang Chai district was affected strongly by people, the local infrastructure, and facilitation (houses, roads, schools, health centers, power system…). Ho Bon, Khao Mang, and Lao Chai were three communes that were impacted the strongest, 3 people died, 254 houses were broken, evacuated, and needed to be recovered; 2 schools 1 health center, and 127 km of local and highway were destroyed. This paper not only inventory the landslide blocks but also covers the other geo-hazards (flash floods, riverbank erosion, and the instability of hydraulic plant construction). Along NR.32 from Ho Bon commune to Mu Cang Chai town, 46 landslide blocks were recorded, classified into 7 types. The volume of the landslide block changes from less than 1 m^3 to higher 1000 m^3. The characteristics of types of landslide blocks in this area are as follows:

- The rock fall, debris – soil fall often occured in the weathered rock and very steep slope with the thin fill layer on the top. The failure material fall in very small to small volumes. The rock fall from the lateral slope, and the debris–soil fall is from the fill layer at the top of the slope. For these locations, building-protected walls should be applied to prevent landslides from filling the roads.

- The types of debris and soil translational have the highest number in this area. Slopes here often have diluvial layers at both the top of the slope and the lateral slope. The type of soil flow also has the same slope characteristic, but often occurs at a location having water drainage, in a high elevation slope, with a small–medium volume of mixing soil, mud, tree…

- The complex type as combining of translational, rotational slides and soil flow in a site. In that, the slope is often formed by thick wreathed soil. This type of landslide happens in the long term. The mechanics of this type are complex and need to more studied further.

- The risk of geo-hazards in this area continually happens and needs further study in more detail. The contents and problem should be of concern in further research: (1) Extending the survey area to both sites of NR.32, following the boundary of the watershed; (2) Assess the natural condition (geology, geotechnics, hydro-geology, geography…) and building the relationship with landslide factors; (3) Checking location and infrastructure where having the high risk to geo-hazards as well as condition enhancing the geo-hazards; (4) Designing the landslide mitigation techniques to protect the slope along the roads; (5) Building the early warning system for this area.

REFERENCES

[1]. Minh Tuyen H, Huu Dung L, Tuan Nghia L 2017. Flash flood events in Mu Cang Chai and Muong La on August 2017 – Cause and prevention meaures. *Journal of Climate Chang Science 3-2017:61-67.*

[2]. Phong Tung N, Tuyen TT, Shirzadi A, Binh Thai P, Shahabi H, Omidvar E, Amini A, Entezami H, Prakash I, Phong TV, Thao BV, Thanh T, Lee S, Tien Dieu B 2019 Development of a novel hybrid intelligence approach for landslide spatial prediction. *Applied Sciences*. 2019 Jul 15;9(14):2824.

[3]. https://afamily.vn/gan-100-diem-sat-lo-3-vi-tri-mat-duong-do-mua-lu-tren-quoc-lo-32-qua-yen-bai-20230807100449777.chn

[4]. https://kttv.yenbai.gov.vn/bao-cao-thiet-hai/bao-cao-so-18bc-bch-ngay-1182023 (Vietnamese).

[5]. Hungr O, Serge L, and Luciano P 2014 The Varnes classification of landslide types, an update. Landslides 11 (2014): 167-194.

[6]. Cooper RG 2007 Mass Movements in Great Britain, Geological Conservation Review Series, No. 33, Joint Nature Conservation Committee, Peterborough, 348 pp.

[7]. Parkash S 2019 Landslide preparedness guidelines for safety of buildings on slopes; published by national institute of disaster management. Ministry of Home Affairs, Government of India, New Delhi-110001, India. 2019:80.

[8]. Minh Duc D 2023 Study on the charateristic of the causes and development for the large landslide blocks in the Northern Viet Nam (Case study at Xin Man district, Ha Giang province). The geological thesis, Vietnam Academy of Science and Technology 2023 (Vietnamese).

ACKNOWLEDGMENTS

This paper was supported by project code ĐTĐL.CN-37/23, the authors appreciate this support.

MONITORING LAND COVER CHANGE BASED ON MULTI-SCALE ANALYSIS: A CASE STUDY IN LAO CAI PROVINCE, VIETNAM

Hoang Thi Thu Huong[1, *], Vu Kim Chi[2], Anton Van Rompaey[3]
[1] Faculty of Geography, VNU-University of Science, Vietnam
[2]VNU – Institute of Vietnamese studies and Development Science, Vietnam
[3]Department of Earth and Environmental Sciences, KU Leuven, Belgium
*Email: huonghtt@hus.edu.vn

Abstract: Land Use/Land Cover Change (LUCC) is the result of processes that act at different spatial scales and organizational levels. It is not only triggered by exogenous factors such as land policies, economic modernization and globalization but also by endogenous drivers such as livelihood decisions and dynamics that are taking place at household level. Spatial scale and levels are important in identifying relations. In this paper, land cover data from different sources were compared to resume the historical land cover dynamics (1950s-now) at multiple spatial scales. Lao Cai province in Northern Vietnam was selected for the analysis at province level and SaPa district (located within Lao Cai province) was selected for the analysis at the district and village level. The study relies primarily on high to very high-resolution remote sensing images. The results show that when considering the long-term period (1952 to 2012), a net loss of forest area occurred in the study area. However, when considering the short-term period (2000-2014), the land cover data all show an increase of forest cover at village, district and provincial level. The largest increase in forest cover is observed at the province level, with an increase of 8630ha/year. The forest cover dynamics in SaPa district and the five selected communes was much lower with rates of 440ha/year and 65ha/year, respectively. The trends of land cover change that are observed in the study area are roughly similar to what is reported at the national scale and for other regions in Northern Vietnam. However, the land cover conversions are smaller in SaPa district, compared to the other regions in Northern Vietnam.

Key words: *Remote sensing, Land cover change, Multi-scale, Lao Cai*

1. INTRODUCTION

As many tropical countries, Vietnam was characterized by a net deforestation during the period 1950s-1990s [1]. Since the 1990s, Vietnam has experienced a net increase in forest cover as a result of forest policies, economic growth, and market integration [2]. However, forest cover dynamics vary locally, and national-scale inventories mask disparities that might exist at local scales [2-5]. Single-scale analyses of land cover change might not be enough to reflect the complexity of mountainous regions in e.g. northern Vietnam [6, 7].

The integration of multi-source data is necessary to monitor land cover change at various spatial scales [8-12]. Aerial photographs and Very High-Resolution SPOT images (VHR-SPOT) are known to be highly accurate for investigating historical land cover, but cover only limited area. Aerial photos are therefore often used to detect long-term land cover change (spanning 50 to 60 years) at local scale, covering individual villages or clusters of households. This approach has been successfully applied in previous studies by [13, 14]. Landsat images cover large areas (170 by 183 km), and offer up-to-date and costly-effective

information on the earth surface [10]. As the image availability is limited to the past 30 or 40 years (or even less for specific regions), Landsat images are suitable for investigating short-term land cover change at larger spatial scale such as provinces or districts [2, 15]. In addition, in Vietnam, the land cover maps established by specialized agencies such as the Forest Inventory and Planning Institute of Vietnam (FIPI, belonging to Ministry of Agriculture and Rural Development) and the General Department of Land Administration (belonging to Ministry of Natural Resources and Environment) are available at national and regional scale and cover the period from the early 1990s to 2010. These maps have been used to investigate forest cover change at national scale [12]. To study land cover changes at different scales for long-term period, it is necessary to use different remote sensing data. This method has been applied in previous studies in the world and Vietnam [16-25]**.**

In this paper, land cover data from different sources were compared to resume the historical land cover dynamics (1950s-now) at multiple spatial scales. Lao Cai province in Northern Vietnam (ca.6000 km^2) (Figure 1) was selected for the analysis at province level and Sa Pa district (ca.700 km^2, located within Lao Cai province) was selected for the analysis at the district and village level. The study relies primarily on high to very high-resolution remote sensing images (Landsat, VHR-SPOT4, 5), aerial photographs and FIPI data. The following three research questions are addressed: (1) What are the major trends of land cover change over 60 years? (2) Can these changes robustly be detected using multi-source datasets? and (3) How do recent land cover changes (10-20years) fit with longer term trends (50 years)?

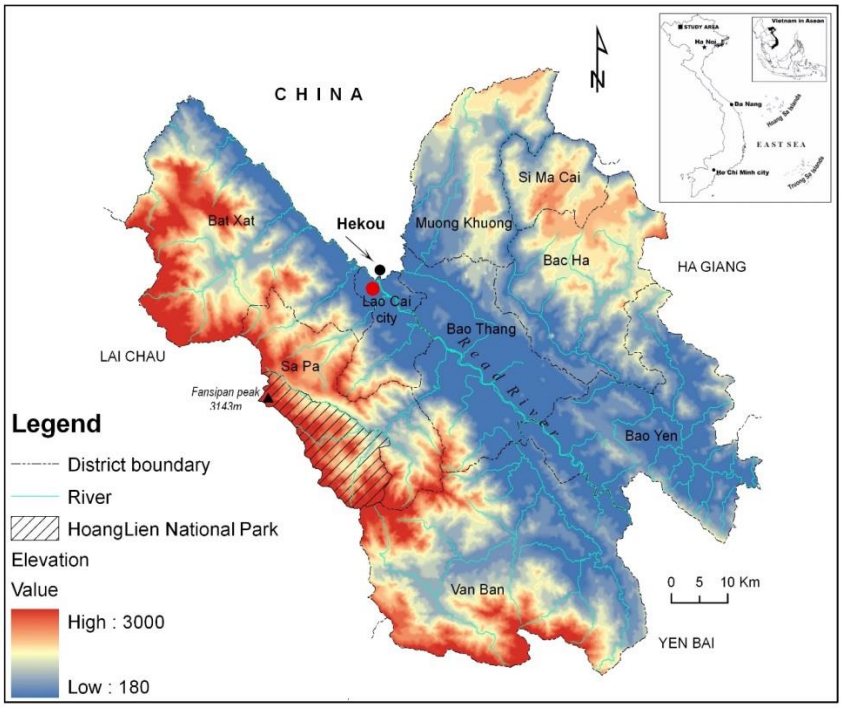


Figure 1. *Map of Lao Cai province*

2. Materials and methods

2.1. Materials

Table 1 gives an overview of the data that were used for the land cover analysis. The data span a time period of 60 years, and data are available at relatively regular time intervals.

Table 1. Characteristics of the data used for the land cover analysis (Aerial photographs, VHR-SPOT, Landsat images and FIPI data)

Characteristics	Aerial photographs	VHR-SPOT	Landsat	FIPI
Year	1952, 1993, 2002	2006, 2012	1993, 2006, 2014	1993, 2000, 2010
Type	Black and white	4 bands	7 bands	Digital maps
Size	60km^2	1569 km^2	31110 km^2	330,000 km^2
Scale (or resolution)	1/38,180; 1/47,500; 1/47,500	5m x 5m; 2.5m x 2.5m	30m x 30m	30m x 30m
Image quality	Good	Good	Good	Good
Covering	5 communes[1]	Sa Pa district	Sa Pa district	Lao Cai province
Land Cover categories	Closed canopy forest, Open canopy forest, Shrub, Paddy field, Upland field, Water body, Residential area, Road.	Closed canopy forest, Open canopy forest, Shrub, Paddy field, Upland field, Water body, Residential area, Road,	Closed canopy forest, Open canopy forest, Shrub, Paddy field, Upland field, Water body, Residential area.	Natural forest, Planted forest, Shrub, Arable land, Water body, Residential area,

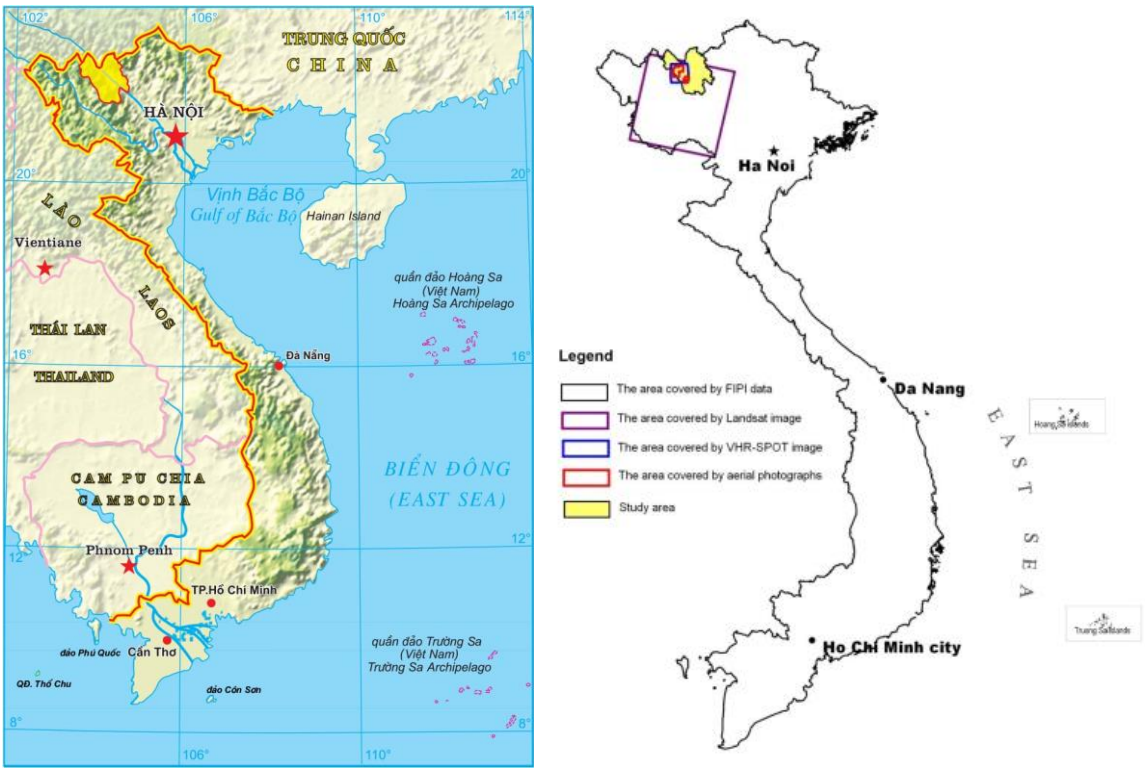


Figure 2. *The delineation of the area covered by FIPI, Landsat, VHR-SPOT images and aerial photographs for this analysis*

[1]Trung Chai, Ta Phin, San Sa Ho, Lao Chai and Nam Cang

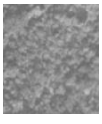
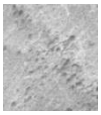
2.2. Land cover classification on very high-resolution images

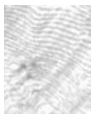
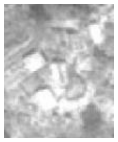
At small spatial scale, very high-resolution satellite images (VHR-SPOT) and aerial photographs were used. The time series spans the period from 1952 to 2012, and covers part of SaPa district (Table 1, Figure 2).The aerial photographs were obtained as scanned files from the Agency for Survey and Mapping, Ministry of Natural Resources and Environment, Vietnam [26-28]. The three sets of aerial photographs were extracted for five communes within the SaPa district: (1) Trung Chai, (2) Ta Phin, (3) San Sa Ho, (4) Lao Chai and (5) Nam Cang (Figure 6). The first set of aerial photographs was taken between 1952 and 1954 and its printing scale is approximately 1/38,180. The second and third sets were taken in 1993 and 2002 respectively, and their printing scale is approximately 1/47,500. The photographic quality of the three series of photos is acceptable. The aerial photos were orthorectified and georeferenced using Photomod software [29].

The land cover maps of 2006 and 2012 were based on visual interpretation of VHR-SPOT satellite images of 2006 and 2012 with a resolution of 5 by 5m and 2.5 by 2.5m, respectively. All SPOT images were obtained in orthorectified and georeferenced format from the Ministry of Natural Resources and Environment, Vietnam [30, 31].

For all images (three sets of aerial photographs and two VHR-SPOT images), image segmentation was carried out with the eCognition Professional 6.0 software. As such, the digital image was segmented into a set of non-superimposable, discrete regions on the basis of their internal homogeneity criterion [32, 33]. Land cover maps were produced by grouping manually the segments based on a visual interpretation. Eight categories were used (Table 2): (1) closed canopy forest, (2) open canopy forest, (3) paddy field, (4) upland field, (5) shrub, (6) residential area, (7) water body, and (8) road.

Table 2. Short description of the eight land cover types, as they were detected on aerial photographs and VHR-SPOT images

Land cover type	Terrestrial picture	VHR-SPOT image	Aerial photograph	Characteristics
Closed canopy forest				Closed canopy forests are distinguished on the aerial photos and VHR-SPOT by a dark tone, the 'cauliflower' texture, and most of the time by their specific location on steep slopes, at high altitudes and/or in gullies [11].
Open canopy forest				Open canopy forests have a more open cauliflower texture than closed canopy forests
Shrub				Shrub is distinguished by a lighter tone than forest. The texture still shows some patterns, but does not show the 'cauliflower' pattern typical of a continuous cover of trees [11].

Paddy field				Paddy fields are recognized by their light (almost white) tone, by their steps and by their location in the valleys near rivers.
Upland field				Upland fields are recognized by the light, homogeneous tone and the texture. Upland fields often have angular forms.
Residential area				Residential areas were easily distinguished by the shape of the houses, by their location near infrastructure and by their non-uniform pattern [11].
Water body				Water body (rivers) and roads are easily recognized through their curved lines and light color. Roads are typically smoother and more uniform than rivers
Road				

2.3. Land cover classification on high resolution images

Three land cover maps were produced based on LANDSAT images that covers the SaPa district with a spatial resolution of 30m by 30m. The Landsat images were taken from Feb 1, 1993; Nov 4, 2006 and Jan 01, 2014 in the post-harvest period when the agricultural land is mostly bare. All Landsat images are orthorectified and corrected for atmospheric and topographic effects [34, 35].

Then, a supervised maximum likelihood classification was applied to classify the Landsat images into 7 land cover categories: closed canopy forest, open canopy forest, shrubs, paddy field, upland field, water body and residential area (including paved roads). Interpreted patterns for the different land cover types were identified based on field work carried out in 2010.

2.4. Land cover maps based on Forest Inventory and Planning Institute of Vietnam (FIPI)

The land cover data used at province level were collected from the Forest Inventory and Planning Institute of Vietnam (FIPI) for the years 1993, 2000 and 2010. The FIPI maps were produced by supervised classification of Landsat satellite images that were validated by field inventories, and have a spatial resolution of 30m by30m. According to Meyfroidt and Lambin [12], FIPI maps can be considered as the most consistent maps at national level compared to other datasets, such as the IGBP [36], AARS (Asian Association of Remote Sensing) [37], UNEP (United Nations Environment Programme) [38], or VCF (Vegetation Continuous Fields) [39]. The original land cover classification (13 classes) was generalized into 5 land cover categories to facilitate comparison with our land cover classification from Landsat images and aerial photographs: Natural Forest, planted forest, shrubs, arable land (including paddy and upland fields), water body, residential area (including paved roads) (Figure 10).

2.5. Accuracy assessment

In this study, we assumed that the land cover maps derived from aerial photographs and VHR-SPOT image are more accurate (because of their smaller spatial resolution) than the land cover maps derived from a supervised classification of Landsat images and FIPI data. Therefore, we used these land cover maps (derived at very high spatial resolution) to evaluate the quality of the high-resolution land cover maps derived from Landsat and/or FIPI. For the land cover maps at high resolution of 1993 and 2000, the comparison was done with the information at very high resolution derived from aerial photographs of 1993 and 2002. For the HR information of 2006, 2010 and 2014, the comparison was done with a VHR-SPOT image of 2006 and 2012. A total 200 validation points were randomly selected with 10 to 78 sample points per land cover class, depending on the areal cover of the classes.

2.6. Land cover change analysis

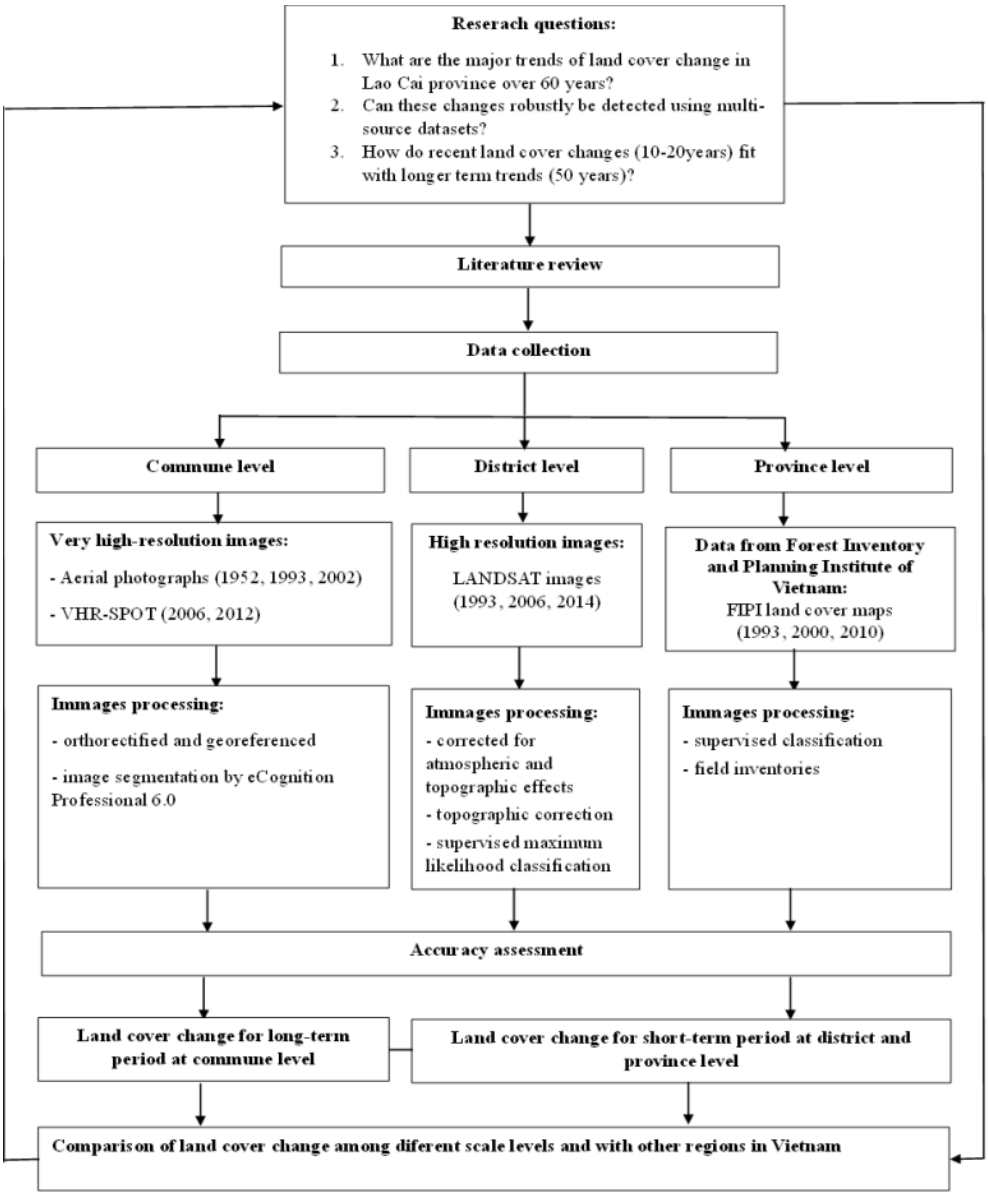


Figure 3. *Flowchart of the study*

The land cover maps derived from aerial photos (1952, 1993, 2002), VHR Spot images (2006, 2012), HR Landsat images (1993, 2006, 2014) and FIPI data (1993, 2000, 2010) were compared to calculate land cover changes. This was done by performing an overlay of two raster maps so that a cross-tabulation can be carried out by the raster calculator tool in ArcGIS 9.3. Flowchart of the study is shown in Figure 3.

3. RESULTS

3.1. Accuracy assessment

The overall accuracy of the land cover classification from Landsat images was assessed at 71%, 83% and 82% (quantity disagreement of 5%, 4%, 5% and allocation disagreement of 24%, 13%, 13%) for the land cover maps of 1993, 2006 and 2014, respectively. The main errors result from confusion between (i) closed and open canopy forest, (ii) shrubs and open canopy forest, (iii) paddy fields and upland fields. Differentiation between closed and open canopy forests is difficult based on the pixel reflectance of Landsat images, and it is not straight forward to make the differentiation in the field neither. Besides, upland fields on steep slopes were hardly identified on the satellite images, as parcels as very small and have mixed spectral reflectance values. Therefore, we merged closed and open canopy forests into one ‘forest class’ and ‘paddy field’ and ’upland field’ into one ‘arable land’ class.

The overall accuracy, quantity and allocation disagreement were computed for the two classifications (with/without regrouping) (Table 3). The overall accuracy increased substantially while quantity and allocation disagreement decreased after regrouping, as the overall accuracy was assessed at 80%, 86% and 85% (quantity disagreement of 5%, 3%, 4% and allocation disagreement of 15%, 11%, 11%) for the land cover maps of 1993, 2006 and 2014, respectively (Table 3). For this reason, we only analyzed ‘forest’ and ‘arable land’ in the later sections.

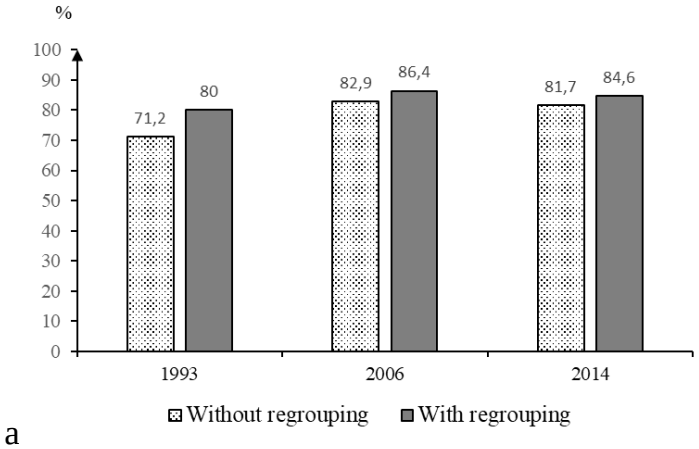
Table 3. Results of accuracy assessment of land cover classifications from Landsat images in Sa Pa district

Land cover	Without regrouping			With regrouping		
Year	*1993*	*2006*	*2014*	*1993*	*2006*	*2014*
Overall accuracy (%)	71.2	82.9	81.7	80.0	86.4	84.6
Quantity disagreement (%)	5.0	4.4	5.2	5.0	2.8	4.4
Allocation disagreement (%)	23.8	12.7	13.1	15	10.8	11

With the configuration of the initial seven classes, the accuracies may seem low but the spatial pattern of land cover types is consistent with field observations [7]. This suggests that the results of Landsat classification maybe useful to assess land cover changes for which no (complete) sets of aerial photographs are available.

For FIPI maps, the overall accuracy is much lower having values of 62%, 67% and 65% (quantity disagreement of 12%, 13%, 15% and allocation disagreement of 26%, 20%, 20%) for the land cover maps of 1993, 2000 and 2010, respectively. The low accuracy can be explained by classification system that was used for FIPI data. Aerial photo interpretation was based on the current status of the land surface to classify forests into closed and open canopy forests, while FIPI maps were based on the purposes of forest exploitation and

divided forests into natural and planted forests. The difference in classification systems may be solved by grouping the two forest classes.



a

Figure 4. *Results of accuracy assessment of land cover classifications from Landsat images in Sa Pa district with and without regrouping*

The overall accuracy, quantity and allocation disagreement were computed for the two classifications (with/without regrouping) (Table 4). The overall accuracy is increasing substantially, while quantity and allocation disagreement decrease after regrouping. The regrouped data have an overall accuracy of 69%, 73% and 71% (quantity disagreement of 10%, 8%, 14% and allocation disagreement of 21%, 19%, 15%) for the land cover maps of 1993, 2000 and 2010, respectively.

Table 4. Results of accuracy assessment of land cover maps from FIPI in Lao Cai province

Land cover	Without regrouping			With regrouping		
Year	*1993*	*2000*	*2010*	*1993*	*2000*	*2010*
Overall accuracy	62%	67%	65%	69%	73%	71%
Quantity disagreement	12%	13%	15%	10%	8%	14%
Allocation disagreement	26%	20%	20%	21%	19%	15%

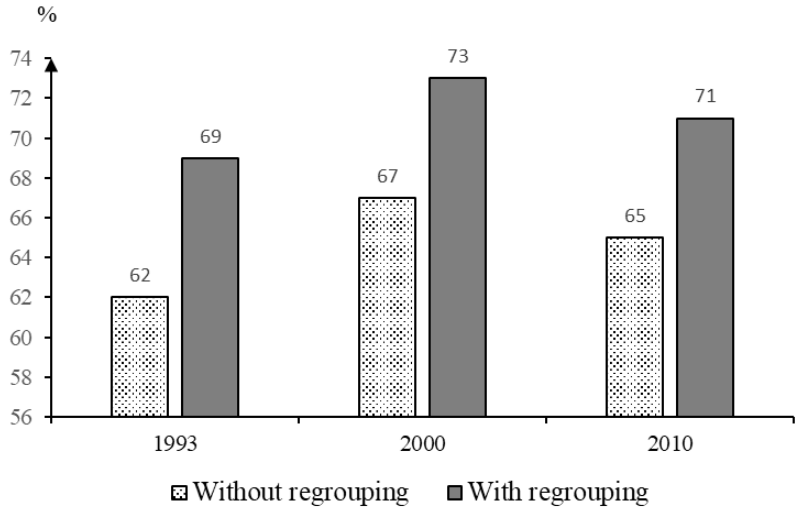


Figure 5. *Results of accuracy assessment of land cover maps from FIPI in Lao Cai province with and without regrouping*

3.2. Land cover change based on VHR data

The land cover maps obtained from aerial photographs and VHR-SPOT images for the years1952, 1993, 2002 and 2012 are shown in Figure 6A, B, C, D. Table 5 presents land cover changes between 1952 and 2012 in 5 selected communes. The area of forest has decreased by 9% between 1952 and 2012 while shrubs, arable land and residential area increased by 11%, 20% and 42%, respectively (Table 5).

Table 5. Land cover and land cover changes in the period 1952 –2012

Land cover	Area (ha)				Change 1952-2002		Change 2002-2012		Change 1952-2012	
	1952	1993	2002	2012	Differences	%	Differences	%	Differences	%
Forest	14602	12712	12583	13232	-2019	-14	649	5	-1370	-9
Arable land	2127	2657	2656	2367	529	25	-289	-11	240	11
Shrub	5264	6535	6719	6332	1455	28	-387	-6	1068	20
Residential area	149	181	184	211	35	23	27	15	62	42

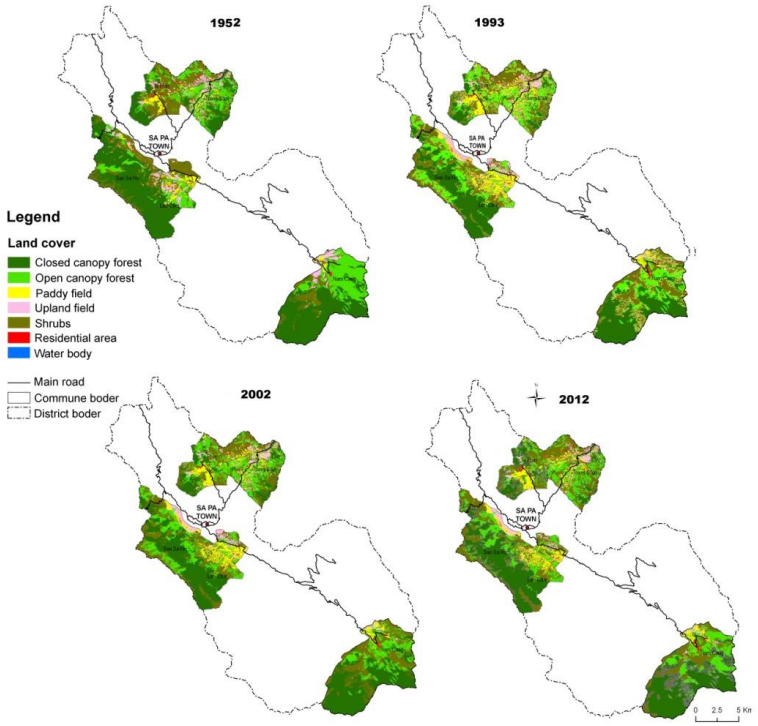


Figure 6. *Land cover maps of 5 selected communes in 1952, 1993, 2002 and 2012 (from aerial photographs and VHR-SPOT image)*

Table 6 shows the major land cover conversions in the selected communes for overall period 1952-2012. In this table, the grey cells are the unchanged areas, while the major changes are highlighted in bold. The major changes were the reduction of the forest area and the expansion of arable land. The conversion from shrub to forest and from arable land to shrubs is also remarkable. Over the last 60 years, 80% of the forest remained intact, while 18% has been transformed to shrubs and 2% to arable land. Similarly, only 59% of shrubs in 1952 remained: 25% was converted to forest and 15% to arable land (Figure 7).

Table 6. Absolute land cover changes between 1952 and 2012 for selected communes (ha)

2012-1952	Forest	Shrub	Arable land	Residential area
Forest	11719	**2563**	295	25
Shrub	**1347**	3100	**793**	24
Arable land	166	**665**	1278	18
Residential area	0	0	0	144

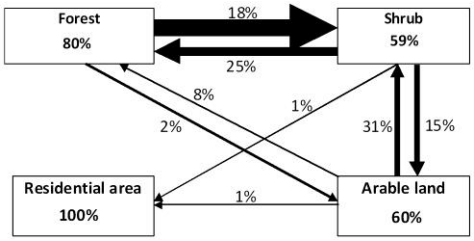


Figure 7. *Synthesis of the major land cover changes between 1952 and 2012 (The width of arrows represents the area of each conversion)*

3.3. Land cover change based on HR satellite data

Figure 8 shows the land cover maps for the years 1993, 2006 and 2014 as derived from Landsat image classification. Table 7 presents land cover changes between 1993 and 2014 in SaPa district, which were calculated from the land cover classifications of 1993, 2006 and 2014. Between 1993 and 2014, the overall forest and arable land increased by respectively 7% and 17% while shrubs decreased by 32%. However, these trajectories mask substantial inter-interval differences. Between 1993 and 2006 forest decreased slightly by 1% while arable land increased by30%. But deforestation tendency seems to have reversed since 2006 in SaPa district. Forest increased by 8% while arable land decreased by 10% between 2006 and 2014. The shrubs decreased continuously between 1993 and 2014 (Table 7).

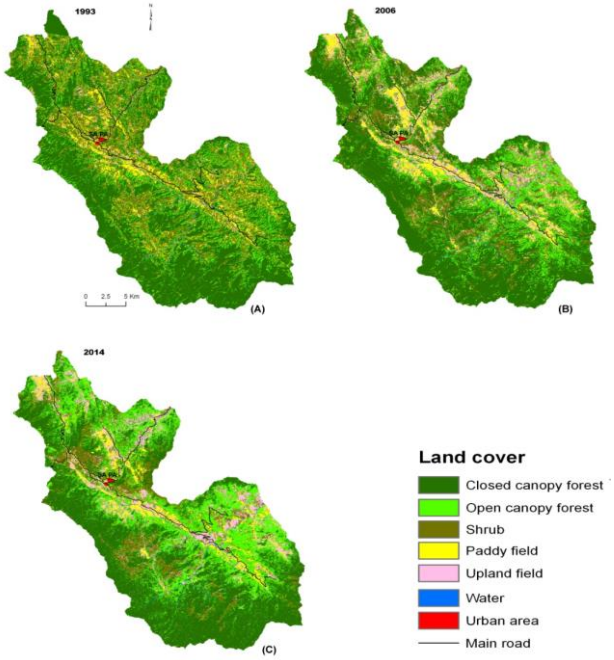


Figure 8. *Land cover maps of Sa Pa district in 1993, 2006 and 2014 (from Landsat images)*

Table 7. Land cover and land cover changes in the period 1993 –2014 for SaPa district

Land cover	Area (ha)			Change 1993-2006		Change 2006-2014		Change 1993-2014	
	1993	2006	2014	Differences	%	Differences	%	Differences	%
Forest	45641	45209	48734	-432	-1	3525	8	3093	7
Arable land	8294	10751	9677	2457	30	-1074	-10	1383	17
Shrub	13696	11639	9277	-2057	-15	-2362	-20	-4419	-32

Figure 9 show the major land cover conversions in SaPa district between 1993 and 2014. It can be seen that the major changes were conversion from shrubs to forest and from shrubs to arable land. Over the last 21 years, 85% of the forest remained intact, while 9% were transformed to shrub and 6% to arable land. Only 25% of shrubs remained, 50% were converted to forest and 25% to arable land.

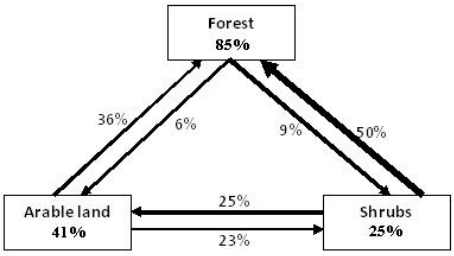


Figure 9. *Synthesis of the major land cover changes between 1993 and 2014 for Sa Pa district (The width of arrows represents the area of each conversion)*

3.4. Land cover change based on FIPI data

Figure 10 shows the land cover maps for the year 1993, 2000 and 2010 of Lao Cai province that were collected from FIPI data. Across all three dates, forest is dominant in the high mountains in the eastern and western parts of the province. Overall, for the period from 1993 to 2010, there is a clear trend of reforestation as forest cover increased from 31% in 1993 to 41% in 2000 and 54% in 2010. For the period 1993-2010, the forest increased by 75%. More specifically, the area covered by shrubs decreased in Lao Cai province over the last 17 years by 56%, while the residential area increased 160% between 1993 and 2010. Arable land increased by 26% between 1993 and 2000 and then decreased by 15% between 2000 and 2010. For overall period 1993-2010, the arable land increased only by 8% (Table 8).

Table 8. Land cover and land cover changes in the period 1993 –2010 of Lao Cai province

Land cover	Area (ha)			Change 1993-2000		Change 2000-2010		Change 1993-20110	
	1993	2000	2010	Differences	%	Differences	%	Differences	%
Forest	197799	258989	345292	61190	31	86303	33	147493	75
Arable land	127576	161353	137550	33777	26	-23803	-15	9974	8
Shrub	296161	198986	130390	-97175	-33	-68596	-34	-165771	-56
Residential area	7476	13583	19418	6107	82	5835	43	11942	160

Table 9 and Figure 11 show the major land cover conversions in Lao Cai province between 1993 and 2010. The major changes were conversion from shrub to forest and arable land. Over the last 17 years, only 24% of the shrubs remained unchanged, while 48% were

transformed to forest, and 25% to arable land. Similarly, 76% of forest in 1993 remained intact: 16% was converted to shrub and 8% to arable land (Figure 11). Only 33% of arable land remained, 41% has been converted to forest, 22% to shrub and 4% to residential area.

Table 9. Absolute land cover changes between 1993 and 2010 in Lao Cai province (ha)

2010-1993	Forest	Shrub	Arable land	Residential area
Forest	148501	31180	16980	0
Shrub	**142239**	71465	**74564**	7816
Arable land	**50765**	26954	41393	4602
Residential area	0	200	276	7000

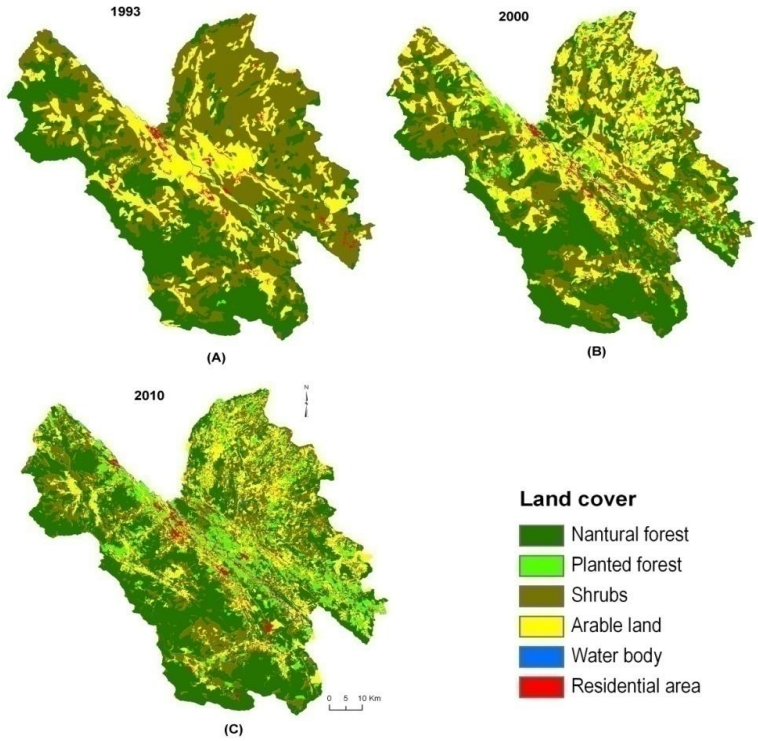


Figure 10. *Land cover maps of Lao Cai province collected from FIPI for 1993, 2000 and 2010*

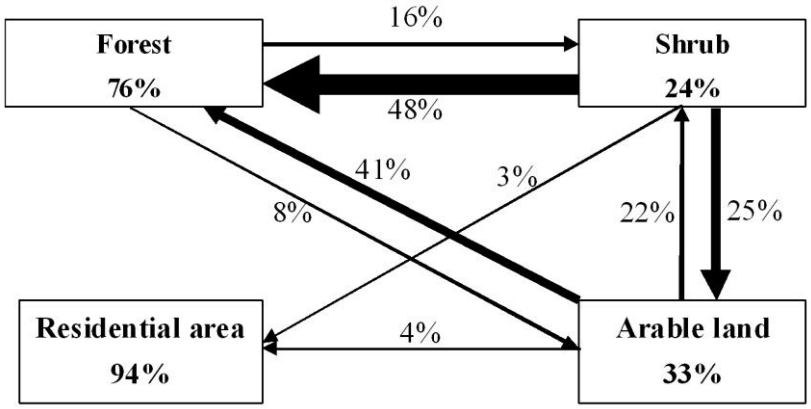


Figure 11*. Synthesis of the major land cover changes between 1993 and 2010 in Lao Cai province (The width of arrows represents the area of each conversion)*

4. DISCUSSION

4.1. Land cover change over last 60 years (1952-2012)

Figure 12 presents the trends of land cover change over the past 60 years for 5 selected communes. The trends are based on the best available land cover data, i.e. the very high resolution aerial photographs and VHR SPOT images. For overall period (1952-2012), the major trends are the expansion of arable land and shrubs; and reduction of forest. The overall area covered by forest decreased by 9% while area covered by shrubs and arable land increased by 11% and 20%, respectively during last 60 years. However, these trajectories mask substantial inter-interval differences. The tendency of forest cover change seems to have reversed since 2002, some years after the implementation of forest policies and the introduction of tourism in SaPa district. The area covered by forest increased slightly after 2002 by 5% while shrubs and arable land decreased by 6% and 11%, respectively during the period 2002-2012 (Table 5). A forest transition occurred in the study area at the beginning of the 2000s.

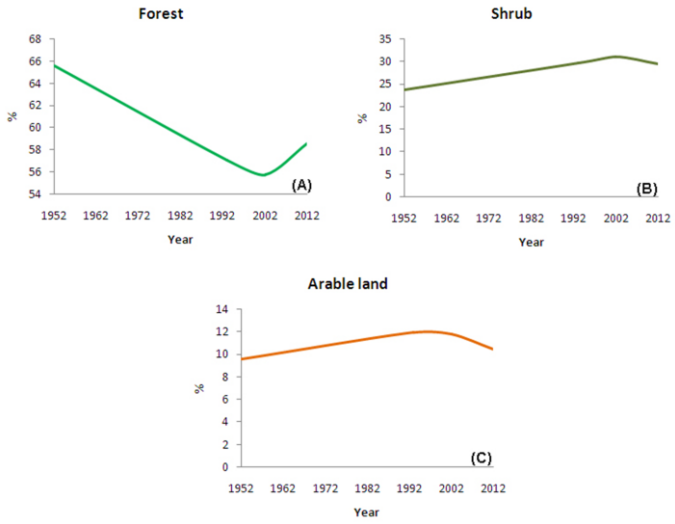


***Figure 12**. The trends of main land cover categories over the past 60 years in the case study: (A) Forest, (B) shrubs and (C) arable land*

Table 10 presents the conversion rate calculated for the different time periods. The conversion from forest to shrubs peaked during 1952-1993 with the rate of 70 ha/year while the conversion from shrub to forest peaked recently during 2002-2012 with the rate of 132 ha/year. This reveals a trend of deforestation before 2000s and a recent phase of reforestation. The conversion from shrub to arable land peaked during first period (1952-1993) while the conversion from arable land to shrub reached highest rate during 2002-2012. This result shows a trend of land expansion during the first period and recent trend of land abandonment. The first period (1952-1993) was remarkable with the highest rate of conversion from forest to shrub and shrub to arable land while the third period (2002-2012) was characterized with the highest rate of conversion from shrub to forest and from arable land to shrub. The mid-period (1993-2002) is characterized by lower land cover change rates.

Table 10. Overall land cover change rate at different periods (ha/yr)

Major land cover changes	1952-1993	1993-2002	2002-2012
Forest to shrub	70	14	65
Forest to arable land	6	2	5
Shrub to forest	27	2	132
Shrub to arable land	21	6	11

Arable land to forest	4	0	4
Arable land to shrub	11	8	41

4.2. Comparison of data from different sources

From the accuracy assessment, it is clear that image classification for land cover mapping is associated with a relatively large degree of error, even if the best available methods are used. In order to compare the data from different sources, we extracted the land cover maps derived from the Landsat classification and the FIPI data for the 5 communes within Sa Pa district where very high-resolution land cover data are available (Figure 13). The comparison was carried out for the period 1993-2014. The land cover categories were regrouped as follows: forest (including closed and open canopy forest, or natural and planted forest), arable land (including paddy and upland fields). For internal consistency, the comparisons were carried out for three land cover categories: forest, arable land and shrubs.

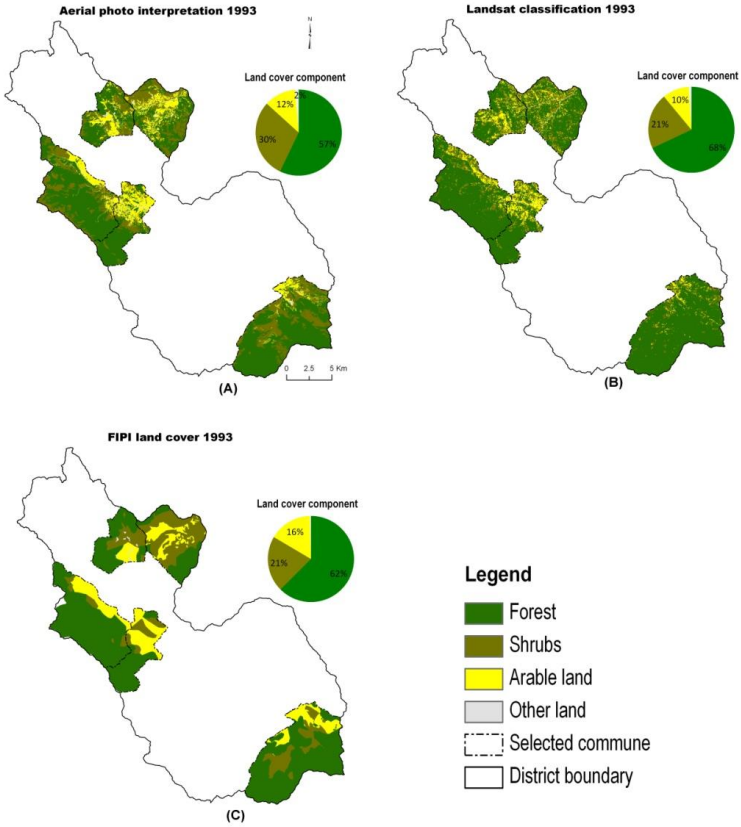


Figure 13. *Land cover map of 1993 for 5 selected communes derived from (A) Aerial photographs, (B) Landsat images, and (C) FIPI data*

Figure 14 presents the trends in land cover change for the 5 communes from the different datasets. There are clearly differences in the amount of land cover change that is derived from different data sources, but the trends in land cover change are roughly the same. Generally, we can observe an expansion of forest area with the rate of 0.1 to 0.5%/year, and a reduction of shrubs (with the rate of 0.1 to 0.4%/year) and arable land (with the rate of ca.0.1%/year) (Figure 14). The area covered by forest and arable land on the maps derived from Landsat images and FIPI data seems to be overestimated, as compared to the land cover mapping from aerial photos. On the other hand, the area covered by shrubs seems to

be largely underestimated compared to the results from the aerial photos. This might be related to confusion between forests and shrubs, and arable land and shrubs.

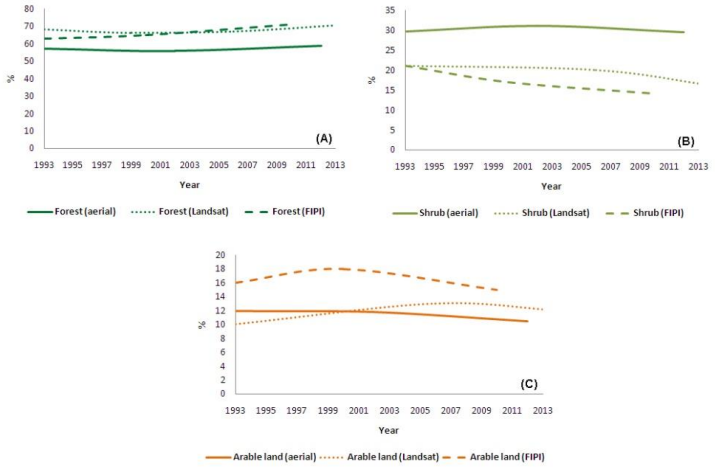
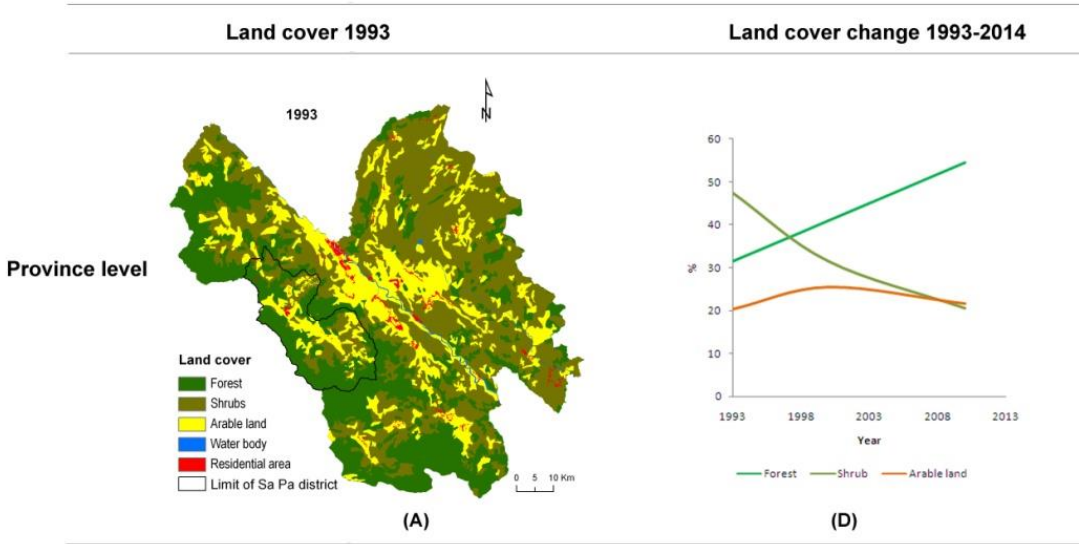


Figure 14. *Comparison of land cover change (1993-2014) for 5 selected communes based on three different datasets: (A) forest, (B) shrubs, (C) arable land (The continuous lines show the information derived from aerial photographs, the dotted lines from Landsat images and the dashed lines from FIPI data).*

4.3. Land cover change at province, district and village level

Figure 15 shows the land cover maps for different administrative levels (province, district, village) for the year 1993. The land cover data at the provincial level are derived from FIPI, at district level from Landsat classification, and at village level from aerial photographs or VHR SPOT images.

The comparison of the trajectories of land cover change at different administrative levels is shown in Figure 15D, E and F. Although the trends in land cover change are somehow similar at the different administrative levels, it is clear that the largest forest cover dynamics were observed at the provincial level (Figure 15 D). These data suggest that land cover dynamics within the mountainous SaPa district are slower than the ones observed in the central part of the Lao Cai province.



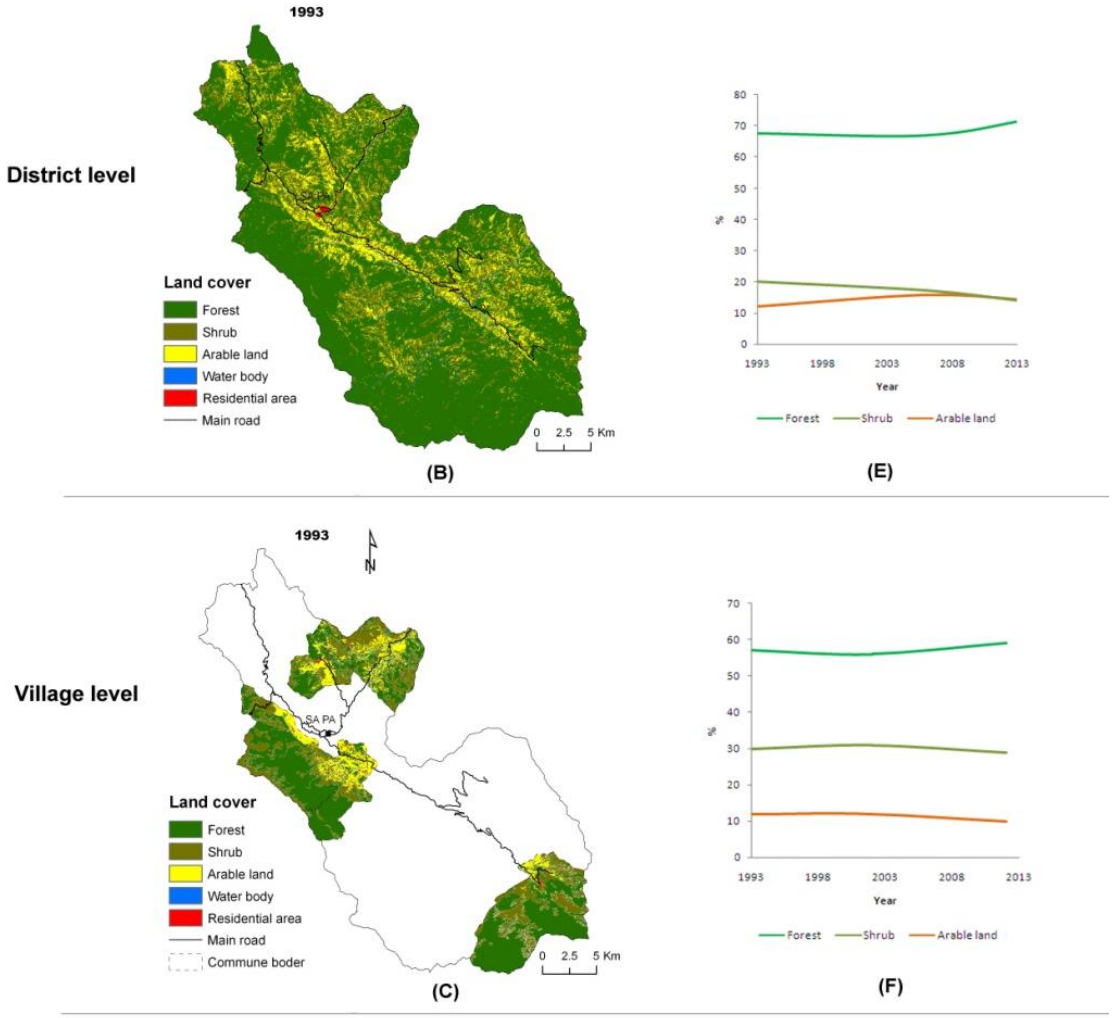


Figure 15. *Comparison of land covers (A, B, C) and land cover change (D, E, F) from different administrative levelsin the study area*

4.4. Comparison with national-scale land cover dynamics

In Figure 16, the land cover dynamics in SaPa district are compared with those of other northern provinces and with national-scale land cover dynamics. The overall trends of forest cover change are similar at regional and national scale. All figures show a decrease of forest cover between 1952 and 1990s and a recent phase of forest cover increase. However, in Sa Pa district (Lao Cai province), the forest increase started in the early 2000s (Figure 16A), some years later than what has been observed at national scale and in other regions. This might be due to the fact that the impact of land use policies and socio-economic transformation is spatially variable [40]. Lao Cai and Bac Kan province have abundant forest resources, and they were covered for 54% and 58% resp.by forests in 2010 [41]. Their forest cover is high compared to 40% forest cover at the national level [41], and 40% in the Son La province [41].

The changes in arable land are different between the three regions (Figure 16 A, B, C). In Lao Cai and Bac Kan province (northeast Vietnam), shrubs and arable land increased between 1950s and 1990s and decreased in recent years. While in Suoi Muoi catchment (Son La province, northwest Vietnam), arable land increased continuously from the 1950sto

recent years. The recent decrease of arable land and shrubs in the northeastern provinces is probably associated with a reduction in shifting cultivation [13]. Most swidden rice fields with low yields have been left fallow to regenerate into shrubs and/or forest [5]. In contrast, in Suoi Muoi catchment, shifting cultivation is still observed in some ethnic minority communities such as Thai, Khang, Hmong and Khomu [45]. In this region, the conversion of shrubs to arable land (and vice versa) occurred, something which is typical for shifting cultivation practices. In a shifting cultivation system, farmers create temporary upland fields by cutting and burning off the vegetative cover. After a few years of intensive cultivation, the soil is depleted and the upland fields are taken out of production in order to allow a natural recover of shrubs and forests [11].

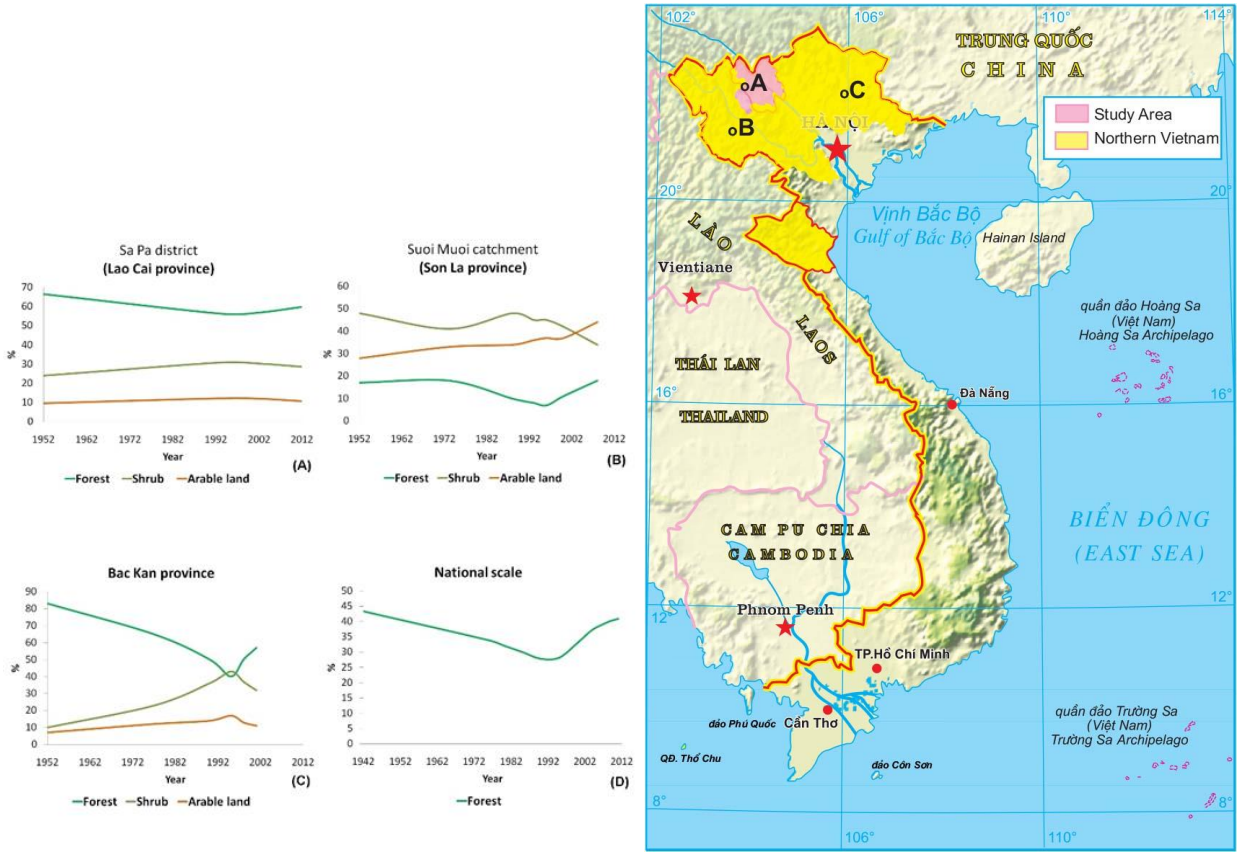


Figure 16. *Comparison land cover change trajectories among national scale and different regions in Northern Vietnam: (A) Sa Pa district, Lao Cai province; (B) Suoi Muoi catchment, Son La province [11]; (C) Bac Kan province [13, 42], and (D) Trajectory of forest cover change at national scale [43, 44].*

In comparison with the study of Vu [11] for Son La province and Castella et al [13] for Bac Kan province, the land cover dynamics in SaPa district are small (Figure 16 A, B, C). In SaPa district, the forest cover between 1952 and 2012 changed of only -9% in favor of shrubs and arable land that changed of +20% and +11% (percentage of category). These rates were much higher in Bac Kan province, where forest cover changed of -31% while shrubs and arable land changed of +220% and +57% resp. between 1952 and 2001. Similarly, in Suoi Muoi catchment, where the forest and arable land changed of+6% and +57% resp. while shrubs changed of -29% between 1952 and 2008 (Figure 16 B). Furthermore, the percentage of forest that remained intact between 1952 and 2012 in SaPa district is about 80-85%, in contrast to only 35% in Suoi Muoi catchment [11].

5. CONCLUSION

This study used multi-temporal remote sensing data to evaluate land cover changes in Lao Cai province at different scale levels. This method proves effective to resume the history of land cover in the study area over the past 60 years in the context that remote sensing data in Vietnam is not continuous in time and does not cover all the space. This method can be applied in studying land cover changes in mountainous areas like Lao Cai province. When comparing different data sources, clear differences were obtained in the land cover change rates. This is mostly associated with the different classification system that was used for aerial photographs, Landsat images and FIPI data. The accuracy of the land cover maps improves after regrouping land cover classes. The major trends inland cover change obtained from the different datasets are roughly similar. As we are not much interested in the exact classification of individual pixel, but rather in the broad patterns and trends of land cover, we can consider that the three datasets are complementary.

The research results show that when considering the entire time period 1952 to 2012, the land cover data at very high-resolution shows that a net loss of forest area occurred in the five selected communes in SaPa district. Between 1952 and 2012, the overall forest cover decreased by 9% in favor of shrubs and arable land that increased by 20% and 11%. When considering only the last 15 years (2000-2014), the land cover data all show an increase of forest cover by about 3 to13% at village, district and provincial level. The largest increase in forest cover is observed at the province level, with an increase of 8630ha/year. The forest cover dynamics in SaPa district and the five selected communes was much lower with rates of 440ha/year and 65ha/year, respectively. The trends of land cover change that are observed in the study area are roughly similar to what is reported at the national scale and for other regions in Northern Vietnam. However, the land cover conversions are smaller in SaPa district, compared to the other regions in Northern Vietnam.

At national-scale, it is documented that deforestation happened between 1952 and 1990, and that this was followed by a recent phase of forest increase. In the study area, forest cover increased was observed only from the early 2000s, some years later than that was reported for the national level and other regions in Northern Vietnam. The trends of arable land and shrubs in the study area were characterized by an increase of shrubs and arable land during the period 1952 to 2002, and a reversal of these trends since the 2000s. These trajectories are similar to what has been reported for Bac Kan province, where a reduction in shifting cultivation was reported. However, they are different to Suoi Muoi catchment, a place in the northwest region where shifting cultivation is still practiced.

REFERENCES

1. Lang, C., *Deforestation in Vietnam, Laos and Cambodia*, in *Deforestation, Environment, and Sustainable Development: A comparative analysis*, V. DK, Editor. 2001: Praeger, Westport, CT, USA. p. 111-137.

2. Meyfroidt, P. and E.F. Lambin, *The causes of the reforestation in Vietnam.* Land Use Policy 2008. **25**(2): p. 182-197.

3. Clement, F. and J.M. Amezaga, *Linking reforestation policies with land use change in northern Vietnam: Why local factors matter.* Geoforum, 2008. **39**: p. 265-277.

4. Clement, F., et al., *Drivers of afforestation in Northern Vietnam: Assessing local variations using geographically weighted regression.* Applied Geography, 2009. **29**(4): p. 561-576.

5. Sowerwine, J., *Territorialisation and the Politics of Highland landscapes in Vietnam: Negotiating property relations in policy, meaning and practice.* Conservation and Society, 2004. **2**(1): p. 98-117.

6. Castella, J.C., et al., *Scaling up local diagnostic studies to understand development issues in a heterogeneous mountain environment: An introduction to the SAM Program*, in *Doi Moi in the mountains*, J.C. Castella and D.Q. Dang, Editors. 2002, The Agricultural Publishing House: Hanoi, Vietnam. p. 149-173.

7. Jadin, I., V. Vanacker, and T.T.H. Hoang, *Drivers of Forest Cover Dynamics in Smallholder Farming Systems: The Case of Northwestern Vietnam.* AMBIO, 2013. **42**(3): p. 344-356.

8. Petit, C. and E.F. Lambin, *Integation of multi-source remote sensing data for land cover change detection.* International Journal of Geographical Information Science, 2001. **15**: p. 785-803.

9. Zhao, X., *Integation of multi-source data for the detection and analysis of long term land cover change*, in *International Institute for Geo-Information Science and Earth Observation*. 2007: Enschede, The Netherlands.

10. Balthazar, V., *Remote sensing of forest cover change and ecosystem dynamics in mountain areas*, in *Faculté des sciences*. 2014, Université Catholique de Louvain: Louvain-La-Neuve, Belgium.

11. Vu, K.C., *Land use change in the Suoi Muoi catchment*. 2007, KULeuven: Leuven, Belgium.

12. Meyfroidt, P. and E.F. Lambin, *Forest transition in Vietnam and its environmental impacts.* Global Change Biology 2008. **14**(6): p. 1319–1336.

13. Castella, J.C., et al., *Analysis of village accessibility and its impact on land use dynamics in a mountainous province of northern Vietnam.* Applied Geography 2005. **25**: p. 308-326.

14. Vanacker, V., *Geomorphic Response to Human Induced Environmental Change in Tropical Mountain Areas. The Austro Ecuatoriano as a Case-study*. 2002, Katholieke University Leuven.

15. Dasgupta, S., U. Deichmann, and D. Wheeler, *Where is the Poverty–Environment Nexus? Evidence from Cambodia, Lao PDR, and Vietnam.* World Development, 2005. **33**(4): p. 617–638.

16. Rembold, F., et al., *Use of aerial photographs, Landsat TM imagery and multidisciplinary field survey for land-cover change analysis in the lakes region (Ethiopia).* International Journal of Applied Earth Observation and Geoinformation, 2000. **2**(3): p. 181-189.

17. Petit, C.C. and E.F. Lambin, *Integration of multi-source remote sensing data for land cover change detection.* International Journal of Geographical Information Science, 2001. **15**(8): p. 785-803.

18. Chen, B., B. Huang, and B. Xu, *Multi-source remotely sensed data fusion for improving land cover classification.* ISPRS Journal of Photogrammetry and Remote Sensing, 2017. **124**: p. 27-39.

19. Li, Q., et al., *Mapping the Land Cover of Africa at 10 m Resolution from Multi-Source Remote Sensing Data with Google Earth Engine.* Remote Sensing, 2020. **12**(4): p. 602.

20. Khanh Ni, T.N., et al., *Mapping Submerged Aquatic Vegetation along the Central Vietnamese Coast Using Multi-Source Remote Sensing.* ISPRS International Journal of Geo-Information, 2020. **9**(6): p. 395.

21. Guo, X., J. Ye, and Y. Hu, *Analysis of Land Use Change and Driving Mechanisms in Vietnam during the Period 2000–2020.* Remote Sensing, 2022. **14**(7): p. 1600.

22. Price, K.P. and M.D. Nellis, *Development of a Land Use Mapping and Monitoring Protocol for the High Plains Region: A Multitemporal Remote Sensing*

Application. 1996, NASA Technical Reports Server.

23. Symeonakis, E., et al. *A landuse change and land degradation study in Spain and Greece using remote sensing and GIS*. in *Proceedings of XXth ISPRS Congress, Istanbul, Turkey, http://www. isprs. org/istanbul2004/comm7/papers/110. pdf,(15 January, 2006)*. 2004. Citeseer.

24. Reis, S., *Analyzing land use/land cover changes using remote sensing and GIS in Rize, North-East Turkey.* Sensors, 2008. **8**(10): p. 6188-6202.

25. Dewan, A.M. and Y. Yamaguchi, *Land use and land cover change in Greater Dhaka, Bangladesh: Using remote sensing to promote sustainable urbanization.* Applied geography, 2009. **29**(3): p. 390-401.

26. MONRE, *Aerial photos*. 1952: Department of Survey and Mapping, Ministry of Natural Resources and Environment (MONRE).

27. MONRE, *Aerial photos*. 1993: Department of Survey and Mapping, Ministry of Natural Resources and Environment (MONRE).

28. MONRE, *Aerial photos*. 2002: Department of Survey and Mapping, Ministry of Natural Resources and Environment (MONRE).

29. Racurs, *Photomod 4.4 Overview. User manual*. 2009, Moscow.

30. MONRE, *VHR-SPOT image 2006*. 2006: Remote Sensing Center, Ministry of Natural Resources and Environment, Vietnam (MONRE).

31. MONRE, *VHR-SPOT image 2012*. 2012: Remote Sensing Center, Ministry of Natural Resources and Environment, Vietnam (MONRE).

32. Ruelland, D., et al., *Comparison of methods for LUCC monitoring over 50 years from aerial photographs and satellite images in a Sahelian catchment.* International Journal of Remote Sensing, 2011. **32**(6): p. 1747-1777.

33. Devereux, B.J., G.S. Amable, and C.C. Posada, *An efficient image segmentation algorithm for landscape analysis.* International Journal of Applied Earth Observation and Geoinformation, 2004. **6**: p. 47-61.

34. Richter, R., *Atmospheric/Topographic Correction for Satellite Imagery—ATCOR-2/3 User Guide, Version 8.0*. 2011, Switzerland: ReSe Applications Schla¨pfer.

35. Balthazar, V., V. Vanacker, and E. Lambin, *Evaluation and parametrization of ATCOR3 topographic correction method for forest cover mapping in mountain areas.* International Journal of Applied Earth Observation and Geoinformation, 2012. **18**: p. 436-450.

36. Loveland, T.R., et al., *Development of a global land cover character istics database and IGBP DISCover from 1km AVHRR data.* Inter national Jour nal of Remote Sensing 2000. **21**(6-7): p. 1303-1330.

37. Wen, C.G. and R. Tateishi, *30-second degree grid land cover classification of Asia.* International Journal of Remote Sensing, 2001. **22**: p. 3845-3854.

38. Giri, C., P. Defourny, and S. Shrestha, *Land cover characterization and mapping of continental Southeast Asia using multi-resolution satellite sensor data.* International Journal of Remote Sensing, 2003. **24**: p. 4181-4196.

39. DeFries, R.S., et al., *A new global 1-km dataset of percentage tree cover derived from remote sensing.* Global Change Biology, 2000. **6**: p. 247-254.

40. Castella, J.C., N.R. Tronche, and V. Nguyen, *Landscape changes in Cho Don District during the doi moi era (1990-2000) and their implications for sustainable natural resource management in Vietnam's mountainous provinces* in *Doi Moi in the mountains*, J.C. Castella and D.Q. Dang, Editors. 2002, The Agricultural Publishing House: Hanoi, Vietnam. p. 149-173.

41. GSO, *Vietnam statistical year book 2010*. 2011, Statistical publishing house: Hanoi, Vietnam.

42. Fatoux, C., et al., *From rice cultivator to agroforester within a decade: the impact of Doi Moi on agricultural diversification in a mountainous commune of Cho Moi District, Bac Kan Province, Vietnam*, in *Doi Moi in the Mountains. Land use changes and farmers's livelihood stratergies in Bac Kan province Vietnam*, J.C. Castella and D.D. Quang, Editors. 2002, The Agricultural Publishing House: Hanoi. p. 73–98.

43. De Jong, W., D.D. Sam, and T.V. Hung, *Forest rehabilitation in Vietnam: histories, realities and future*. 2006, Bogor Barat 16680, Indonesia: Center for International Forestry Research (CIFOR).

44. GSO, *Vietnam statistical year book 2011*. 2012, Statistical publishing house: Hanoi, Vietnam.

45. Vu, K.C., et al., *Land Transitions in Northwest Vietnam: An Integrated Analysis of Biophysical and Socio-Cultural Factors.* Human Ecology, 2013. **41**(1): p. 37– 50.

ACKNOWLEDGMENTS

This research was funded by the Vietnam National Foundation for Science and Technology Development (NAFOSTED) (grant number NCUD.05-2022.04). We are thankful to all ministries and institutions in Vietnam which provided the necessary data to undertake this research.

APPLYING 3D GEOSPATIAL DATA AND PROPOSED SOLUTIONS TO SUPPORT THE ADMINISTRATION, MANAGEMENT, AND MONITORING OF COASTAL SMART CITIES ADAPTING TO CLIMATE CHANGE IN VIETNAM

L T T Ha[1,2], N V Trung[1,2], N Q Long[1]

[1] Faculty of Geomatics and Land Administration, Hanoi University of Mining and Geology, No. 18 Pho Vien, Duc Thang Ward, North-TuLiem District, Ha Noi city, Vietnam.

[2] Geomatics in Earth Sciences Research Group, Hanoi University of Mining and Geology, No. 18 Pho Vien, Duc Thang Ward, North-TuLiem District, Ha Noi city, Vietnam.

Email: lethithuha@humg.edu.vn

Abstract: The development of smart cities in Vietnam's coastal urban areas faces unique challenges in addressing issues such as the consequences of climate change, rising sea levels, urban floods, storms, marine pollution, and other related factors. To meet this demand, in addition to developing urban infrastructure systems, there needs to be an information infrastructure and data system that allows policymakers, administrators, and residents to connect and formulate preparedness and response plans, minimizing risks during extreme events. The most crucial information resource for a smart coastal city is the 3D geospatial data of the city. The 3D geospatial data of Halong city was established based on the geospatial technologies with popular software such as Excel, ArcMap, Sketchup, FME. Based on the results we have developed for the Ha Long coastal area, we will make recommendations on using 3D geospatial data to enhance governance, management, manage and monitor coastal smart cities as they adapt to climate change in Vietnam.

1. INTRODUCTION

3D geospatial data is a geographic information system (GIS) database system where each geographical entity is treated as a presence situated in a three-dimensional (3D) space. These databases are designed for efficient storage and retrieval of information pertaining to objects within a geospatial model. Numerous 3D database models exist, and one of the exemplary models is characterized by having just two primary components: spatial data and attribute data. Spatial data represents an assembly of objects within 3D space, consisting of points defined by a three-dimensional coordinate system (x, y, z), accompanied by 3D geographical entities and their associated property information.

In the development of smart cities in coastal urban areas, there are distinctive features that address challenges like the impacts of climate change, elevated sea levels, urban flooding, storms, hurricanes, and marine environmental pollution. Coastal cities, characterized by significant population density, face the crucial objective of constructing smart urban environments to safeguard residential communities from the consequences of extreme events. To fulfill this need, beyond constructing urban infrastructure, establishing information and data systems is crucial. These systems assist policymakers, managers, and residents in collaborating to devise strategies for readiness and response, reducing risks during extreme events. The primary information system in a smart coastal city is its 3D geospatial data (Anilkumar, 2014).

In developed nations, the use of 3D geospatial information and geospatial technologies in constructing intelligent coastal cities to tackle climate change and rising sea levels has been put into practice. Meanwhile, the utilization of LiDAR data to generate 3D geospatial information has offered solutions in crafting flood geospatial data for a city in Honduras (Haile and Rientjes, 2005). UAV data was utilized to develop a 3D coastal map for Pusan, Korea, aiding its adaptation to climate change (Yoo, Oh, and Choi, 2018). Additionally, (Papakonstantinou et al., 2015) delineated coastal regions and crafted 3D maps using UAV data for the advancement of smart city initiatives in Lesvos Island and the Eressos coast, Greece. These studies highlight the capability of geospatial data in constructing 3D geospatial information for smart cities, specifically in adapting to coastal regions within developed nations.

Presently, our country is advancing towards smart city development, with approximately 30 cities already in the process. Among these cities are Hanoi, Ho Chi Minh City, Ha Long, Hai Phong, Thai Nguyen, Da Nang, Hue, Da Lat, Binh Duong, Can Tho, and more…Vietnam is currently adopting a fresh strategy for organizing and overseeing marine areas through a geospatial database system. This system aims to detail the positions and spatial boundaries of marine entities while directing oceanic courses. It assists in coastal and marine area planning, shaping legal frameworks, and offers a foundation for users and stakeholders to depict, visualize, and recognize spatial data pertaining to the sea and coastal regions, presented as 3D geospatial information. Creating 3D geospatial data demands consideration of Vietnam's coastal city features amid climate change. This involves using existing data and incorporating new, location-specific data tailored to each area within the country's localities.

In our study, we have used a technique to integrate the different data acquisition techniques, including terrestrial laser scanner, terrestrial photogrammetry, and unmanned aerial system. The project has built a 3D geospatial data set for the coastal smart city of Ha Long city, Quang Ninh province. This study focuses on recommendations on using 3D geospatial data to enhance governance, management, manage and monitor coastal smart cities as they adapt to climate change in Vietnam.

2. CREATING THREE-DIMENSIONAL GEOSPATIAL INFORMATION FOR HA LONG CITY'S COASTAL REGION

2.1. Study Area



Figure 1: *The study site*

2.2. Data and research methods

Data acquisition techniques DJI Phantom 4 Pro V2.0, FARO FOCUS^{3D} X130 TLS, and Sony DSCF828



Figure 2: *Data collection by using the UAV, FARO FOCUS^{3D} X130 TLS, and Sony DSCF828*

The methodology of this study can be categorized into three phases: data acquisition, data processing, and the results (fig.3).

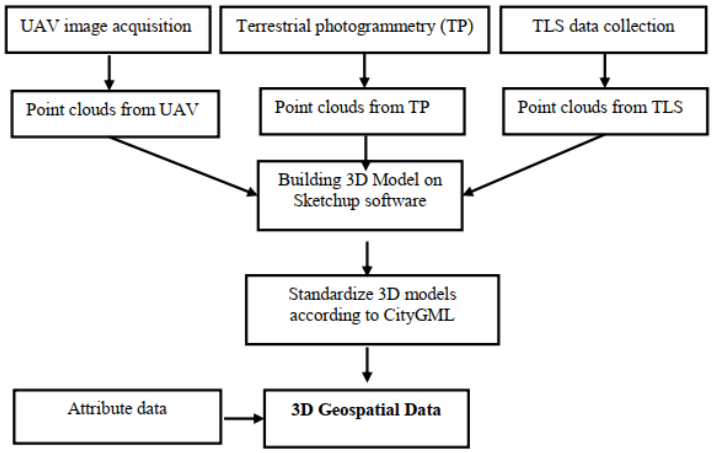


Figure 3: *Flowchart in data processing phase*

2.3. The results

After being satisfied with the integration result obtained, the integrated data is utilized to generate a 3D model as a final product of this study. Figure 4,5 shows the 3D model as a final product of integration points cloud process.



Figure 4: *The 3D Lod-2 point cloud in the experimental area*

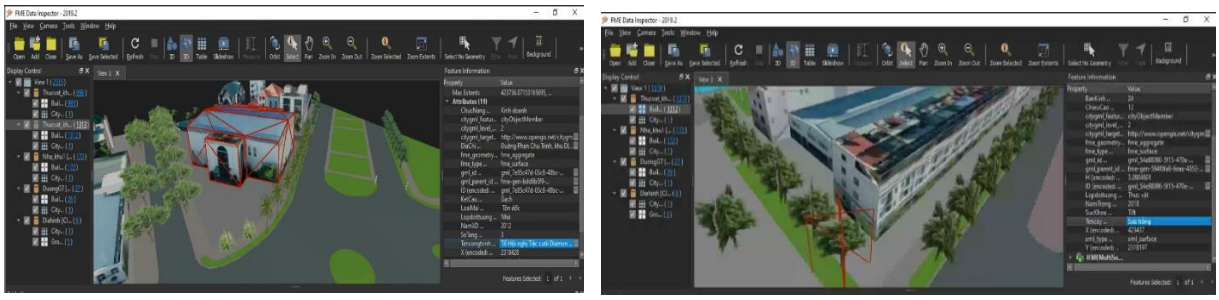


Figure 5: *The 3D geospatial data of buildings and trees*

3. PROPOSE SOME SOLUTIONS APPLYING 3D GEOSPATIAL DATA TO SUPPORT THE ADMINISTRATION, MANAGEMENT, AND MONITORING OF COASTAL SMART CITIES ADAPTING TO CLIMATE CHANGE IN VIETNAM

3.1. Solutions for Applying 3D Geographic Spatial Data in Smart Coastal Urban Space Management

To plan and manage smart cities, a variety of modern technologies must be employed, with a critical element being geospatial data. It is estimated that nearly 80% of decisions in urban planning and management rely on the analysis of geospatial data and information. When we talk about smart cities, we're referring to electronic service systems based on various modern technologies, with information and communication technologies (ICT) being a prime example. Geospatial data plays a vital role and serves as the foundation for developing different types of ICT systems.

3D geographic spatial data can be utilized for urban planning. Using the X, Y coordinates of the data and the descriptive information, leaders at various levels can combine 3D visualization to gain a comprehensive overview of the current urban planning zones and anticipated future development areas for the city. 3D geographic spatial data facilitates visual and vivid urban planning, enabling managers, investors, and residents to envision the new layout of functional planning areas.



Figure 6: *Application of 3D Geographic Spatial Data in Urban Planning and Management*

The planning can include:

- Opening new roadways for the city;
- Expanding existing road networks;
- Establishing economic zones such as coastal and inland economic zones.

Furthermore, 3D geographic spatial data of the city provides the capability to display visuals with precise geographic coordinates and dimensions relative to reality. This allows designers and planners to efficiently develop and integrate their design proposals directly onto models for evaluation (Figure 3). When designing transportation routes through an area, 3D urban spatial data also serves as crucial documentation for assessing impact levels, calculating information, estimating relocation and compensation costs, and determining

traffic density. It also provides the optimal conditions for planning amusement parks, greenery planting, and landscape design for research areas.

3D geographic spatial data of the city provides information to support urban real estate management. A 3D spatial information system is an essential foundation for the management of real estate, including land and buildings. In addition to traditional documents like land records and cadastral maps, which show the ground layout of land and buildings, today, 3D geographic spatial data with different levels of detail (LoD) offers more specific and visually detailed technical drawings of urban real estate objects (Figure 7).

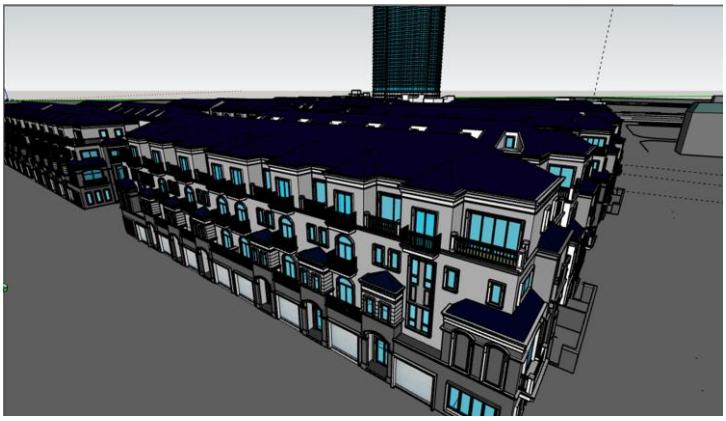


Figure 7: *Application of 3D Geographic Spatial Data in Real Estate Management*

3D geographic spatial data provides information for managing incidents, emergencies, and urgent responses. In densely populated urban areas, incidents related to traffic, medical emergencies, fires, and crimes occur frequently, necessitating swift and timely interventions. Thanks to spatial information about street networks, addresses, buildings, traffic routes, and both industrial and residential structures, experts can quickly identify and access the locations of incidents.

Furthermore, through spatial data analysis, it is possible to determine the shortest or most sensible route to make decisions regarding the most advantageous approach to an object or incident. Spatial information about housing density, infrastructure systems, the likelihood of crime occurrence serves as a foundation for urban authorities to devise preventive measures against fires, traffic incidents, and criminal activities.

3.2. Solution applying 3D geographic spatial data in smart risk alert management for coastal cities ensures adaptation to climate change

The integration of information technology facilitates the real-time connection of data between monitoring locations and the center. Data from specialized automated monitoring stations are continuously updated online and shared with 3D geographic spatial data. With applications on mobile devices, technical staff can extract all the needed information, and some criteria are even automatically alerted by the system. In addition to automatic updates from monitoring stations, risk information data can also be contributed by the community in real-time to the relevant authorities.

By combining 3D geographic spatial data with real-time models and figures, the analysis, calculation, and statistical assessment of damages (if any) during risks or natural disasters are conducted. Real-time updates of parameters and the construction of models are performed using 3D geographic spatial data, which includes the positions of real-time monitoring stations. This is combined with expert knowledge to provide forecasts for the monitored areas in the near future. Based on actual data and forecasts, leaders can make quick decisions to minimize damages as much as possible.

3D geographic spatial data of the city provides information about buildings in the form of visual 3D data with real dimensions. In addition to calculating damages and assessing risks from natural disasters such as earthquakes, tsunamis, etc., it also aids in developing preventive measures, such as evacuation and rescue plans during disasters. The 3D geographic spatial data is constructed on a terrain with real photo overlays, assisting in choosing optimal evacuation locations in the event of flooding. In densely populated urban areas, incidents such as traffic accidents, emergency medical responses, fires, crimes, etc., occur frequently and require prompt and timely handling.



Figure 8: *Application of 3D Geographic Spatial Data to identify and timely access the locations of incidents*

Furthermore, 3D geographic spatial data provides information about the street network, buildings, roads, infrastructure, enabling experts to quickly identify and timely access the locations of incidents (Figure 8). Moreover, it helps determine the shortest or most reasonable route for approaching objects or incidents in the most advantageous way. In the case of fires, the 3D model serves as a basis for pre-selecting the location to place firefighting ladders while the firefighting team is en route to the scene.

3.3. The solution applying 3D geographic spatial data in smart water management for coastal cities involves several aspects

The 3D geographic spatial data helps city managers have an overview of the city's water supply and drainage system, enabling them to plan renovations, upgrades, and new installations in a synchronized manner, while meeting the requirements of a smart city.

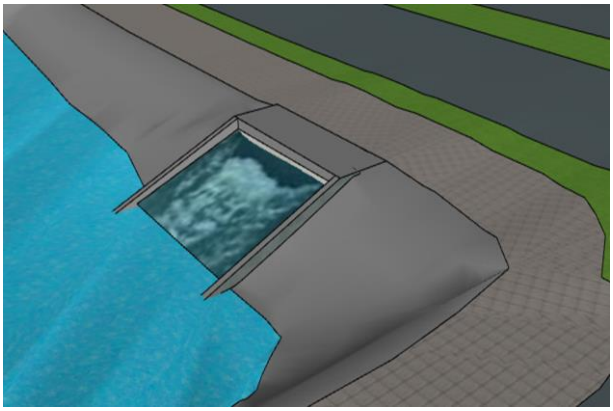


Figure 9:*3D spatial data of the urban drainage system*

3D geographic spatial data in smart cities is used for storing, managing, manipulating, and analyzing spatial information. This data can be used to create specialized maps, enabling the design and operation of a unified water supply and drainage system for the entire city (Figure 9).

Smart cities around the world have successfully implemented water supply and drainage models. However, applying these models, managing operations, adopting new technologies, and developing smart coastal cities in Vietnam face many challenges and difficulties during

implementation. Smart drainage systems in coastal cities provide real-time water level results on the 3D spatial data model accurately and instantly. This real-time model helps operators and managers know precisely when to control the system for optimal operation. Combined with e-governance in providing new clean water services, operators can use the existing 3D spatial data of the city to make the most optimal choices during real-world deployments based on operational requirements.

3.4. Solution for applying 3D geographic spatial data in smart transportation management for coastal cities for economic and social development

Detailed 3D geographic spatial data on traffic, this data serves as a convenient and fast management foundation (Figure 10). It includes:



Figure 10: *3D geographic spatial data in smart transportation management for coastal cities*

- Smart camera data: Supports the city's smart traffic management system in monitoring and handling violations of traffic safety regulations.

- Smart streetlight data: Involves automatic lights that adjust according to ambient light or pedestrian movement, contributing to the city's illumination.

- Data for lane management: Covers traffic lane management, parking lot management, non-stop toll booth management, smart load weigh station management, road management, and road quality.

- Sensor and traffic alert system data: Assists managers in monitoring and alerting for traffic hazards involving different vehicles.

- Detailed navigation map data: Includes road classifications, road types, speed limits for road segments, aiding vehicles during transit.

- Intelligent signage and warning system data: Covers data related to intelligent traffic signs and warnings.

- Road infrastructure data: Supports monitoring, analyzing situations, maintenance, and managing road infrastructure for various activities.

This comprehensive 3D geographic spatial data facilitates the implementation of a smart road transportation system, contributing to the economic and social development of coastal cities.

3.5. Solution for Applying 3D Geographic Spatial Data in Smart Waste Collection and Management for Urban Environmental Protection

Identifying environmental issues and managing the urban environment, one significant concern in large cities is urban waste. The results of spatial data analysis from 3D geographic spatial data enable the determination of landfill locations, assessing their volume and optimizing waste collection routes for cost efficiency and increased effectiveness. The

landfill location depends on various criteria, such as the distance to the city center, residential areas, locations of water wells, and groundwater sources.

Analyzing multiple criteria allows identifying the optimal landfill location. Spatial data analysis helps determine the optimal collection routes for waste transportation within the urban area. Optimized collection routes contribute to cost savings in transportation, fuel efficiency, and time.

The application of 3D database for managers and government authorities enables the identification and planning of centralized waste treatment areas using modern technology to minimize the impact on the surrounding environment. Around islands and coastlines, sensors can be placed to determine the flow of waste in the sea, allowing for quick remedies. Remote-controlled robots can also be deployed to access areas that are inaccessible to humans.

4. CONCLUSION

Based on the findings of the research into solutions that utilize spatial data to aid in the oversight and administration of smart cities, the article arrives at the subsequent conclusions:

3D geographic spatial data consists of layers of information about buildings, greenery, hydrology, traffic, and topography. It provides 3D objects with spatial information regarding height and attribute. These object attributes serve as input requirements to support the management, administration, and supervision of urban space. The calculations aid in alerting the impacts of natural disasters, smart drainage management, operation and monitoring of intelligent transportation, and waste collection. These are essential tasks in the construction, operation, and management of smart cities.

5. REFERENCE LISTS

[1] Anilkumar, P. P. (2014). Geographic Information System for Smart Cities. India, Copal Publishing Group.

[2] Biljecki, F., J. Stoter, H. Ledoux, S. Zlatanova and A. Çöltekin (2015). "Applications of 3D City Models: State of the Art Review." ISPRS International Journal of Geo-Information 4(4): 2842-2889.

[3] Yalcin, G. and O. Selcuk (2015). "3D City Modelling with Oblique Photogrammetry Method." Procedia Technology 19: 424-431.

[4] Yoo, C. I., Oh, Y. S., and Choi, Y. J. (2018). COASTAL MAPPING OF JINU-DO WITH UAV FOR BUSAN SMART CITY, KOREA, Int. Arch. Photogramm. Remote Sens. Spatial Inf. Sci., XLII-4, 725-729, https://doi.org/10.5194/isprs-archives-XLII-4-725-2018, 2018

[5] OGC City Geography Markup Language (CityGML) Encoding Standard," Open Geospatial Consortium: Wayland, USA, 2012.

[6] OGC IndoorGML-with Corrigendum, Open Geospatial Consortium: Wayland, USA, 2018.

[7] OGC CityGML 3.0 Conceptual Model, [Online]. Available: https://github.com/opengeospatial/CityGML-3.0CM. [Accessed 14 June 2020].

[8] T. Kutzner, K. Chaturvedi and T. Kolbe, "CityGML 3.0: New Functions Open Up New Applications," Photogramm. Remote Sens. Geoinf. Sci, vol. 88, p.43-61, 2020.

[9] Góźdź, K., Pachelski, W., Oosterom, P.O., Coors, V. (2014). The possibilities of using CityGML for 3D representation of buildings in the cadastre. In Proceedings of the 4th International Workshop on 3D Cadastres, p.339-362.

[10] Komninos, N., (2021). Developing a policy roadmap for smart cities and the future internet. eChallenges e-2011 Conference Proceedings.

[11] Kozłowski, W., and K. Suwar, (2021). Smart City: Definitions, Dimensions, and Initiatives. European Research Studies Journal. XXIV(3), p.509-520.

COUPLED EVALUATION OF POLYMER-CEMENT MODIFIED SOIL MIXTURE USED FOR THE IMPROVEMENT OF HAUL ROAD PERFORMANCE AT A COAL MINING SITE

Lam Phuc Dao[1], Hung Trong Vo[2], Manh Van Nguyen[2], Thuc Van Luu[3], Tuoc Ngoc Do[3], Khoa Cong Dam[3], Piotr Osinski[4] and Duc Van Bui[2]

[1] Faculty of Civil Engineering, University of Transport Technology, Vietnam

[2] Faculty of Civil Engineering, Hanoi University of Mining and Geology, Vietnam

[3] Institute of Mining Science and Technology, Hanoi City, Vietnam

[4] Institute of Civil Engineering, Warsaw University of Life Sciences (SGGW), Poland

E-mail: buivanduc@humg.edu.vn

Abstract: The performance of haul roads is considered one of the crucial factors affecting the efficiency of mining site management. Due to heavy dynamic loads, and the frequency of passes, it is important to provide safe and reliable working conditions for the haul roads on mining sites. Since the technology of road construction in mining areas is well established, it is the construction material that is still a matter of scientific research. The aim of the study is to address the issue of poor haul road performance at a mining site in Quang Ninh province, Vietnam, due to construction material properties used. The present research conducted a laboratory and field test for haul road natural and modified soil mixed with different ratios of polymer-cement additives. The laboratory tests aimed at identifying the most effective material composition for this case study. The major part of laboratory tests comprised compaction behavior, unconfined compressive strength (UCS), and indirect tensile strength (ITS). The laboratory test results proved that the samples prepared on modified soil of 5% polymer and 7% cement gave the highest values of UCS (> 5MPa) and ITS (> 1.2MPa). To confirm the most effective ratios in situ conditions, the study was extended by performing field tests on already constructed roads filled with materials of different compositions. The field test comprised a dynamic cone penetrometer (DCP) and lightweight deflectometer. The results confirmed the conclusions from the laboratory tests. The largest values of the modulus of deformation (> 400MPa), as well as the DCP depth (>30mm), were achieved for soil mixtures as tested in the laboratory. As expected, the lowest values were obtained for untreated material. The research study allowed proposing the most effective solution for the road construction material used for the haul road, so the management and safety of the mining site could be improved.

1. INTRODUCTION

Transportation management in the open pit mines industry in Vietnam continues to develop by improving the technologies of road contraction procedures and materials used. The transportation management expenses encompass a range of costs, including fuel and equipment maintenance that according to available reports [1] contribute to over 65% of total transportation costs. The haul road systems are usually planned and managed based on practical local engineering experience. The increasing demand for development requiring conventional resources of energy requires of larger scale of transportation vehicle employment which leads to burdened road performance, insufficient maintenance planning, and higher overall costs associated with demanding conditions of technological road

exploitation. The planning of mine haul roads involves considering structural, functional, and maintenance aspects [2, 3]. While there is a significant connection between the structural and functional performance of roads and the safe, cost-effective operation of mining transport, it's essential to recognize that the maintenance component of haul road design cannot be treated as distinct from the structural and functional aspects because they are interrelated [4, 5]. The expenses associated with designing and constructing most haul roads make up only a small part of the total costs for operation and maintenance. An ideal functional design will incorporate a specific level of maintenance, including activities like grading, conducted at intervals that align with the required road performance standards and the aim of minimizing both vehicle operating costs and road maintenance costs. In engineering practice, the design and construction of haul roads is only a minor part of the expenses and deserves more attention [2, 6]. Following the common rule, "it is better to prevent than to cure" more consideration needs to be paid when it comes to planning the construction, focusing more on the material used in road works. The factors influencing the open mine management systems are fuel consumption, vehicle operating costs, and maintenance, which are directly related to transport infrastructure conditions [7]. Thus the quality of the road pavement plays a crucial role when the economy is considered. Currently, Vietnamese open-pit mines follow the standards outlined in Article 11 of TCVN 5326: 2008, which focuses on open-pit mining techniques. The transportation standards closely resemble those found in TCVN 4054: 2005, intended for road design and limited to roads accommodating a maximum load of 10 tons. Such standards differ from the reality of Vietnamese open pit mines, where transportation equipment with considerably larger capacities, ranging from 55 to 130 tons, is employed. The mining sites of Vietnam are usually located in mountainous regions with uneven sections and steep slopes, making the site's safety and economy of transport even more challenging. The most efficient means of providing safe and low-maintenance pavements is to establish a permanent road structure using materials like asphalt or concrete, similar to regular highways. However, applying this concept to mining haul roads can be challenging due to their temporary nature and the frequent alterations required to accommodate mining operations [8, 9]. Due to economic factors, haul road construction at the mining sites is usually performed using the natural soil material available and from the excavation works [10].

The present research aims to analyse and propose the optimum soil and additive mixtures used in haul road construction that would allow for improving transport performance and decrease the expenses associated with the maintenance of transportation equipment. For that purpose, soil samples of natural soil available at the site mixed with polymer and cement in different ratios were laboratory tested to verify the mechanical and physical parameters of the proposed mixtures. Based on the results observed in the laboratory, the sections of the haul road were constructed using the mixtures. Then the efficiency of the proposed building material was monitored and tested in situ. Such an approach allowed the adoption of recommendations for the transportation network at the mining site also contributing to the reduction of dust emissions due to the bonding characteristics of polymers and their moisture content containment properties.

2. PRESENTATION OF CASE STUDY

The haul road in the present case study is located in an open pit mine site of Cao Son Coal Join Stock company, Cam Pha city, Quang Ninh province. There are two critical

sections that were studied, namely Section No. 1 and Section No.2. The total lengths of the sections are 2,2km and 0,5km, respectively. The plan view of both sections is presented in figures 1 and 2. Prior to the haul road improvement works, the site condition was investigated using both visual monitoring and in-situ testing methods. The in-situ tests consisted of Light Weight Deflectometer (LWD) Test and Dynamic Cone Penetrometer (DCP) tests. The investigation results indicated that due to improperly adopted design solutions a series of issues, like uneven surface deformations causing potholes, extensive dusting, and surface erosion were identified. The haul road conditions and associated issues are presented in figure 3.

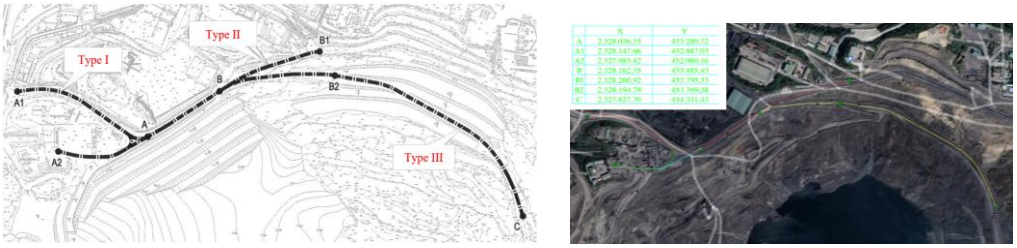


Figure 1. *Plan view of Section No. 1 including subsections ($A_1 \div A$), ($A_2 \div A$), ($A \div B$), ($B \div C$), ($B \div B_1$).*



Figure 2. *Plan view of Section No. 2.*



(a) Potholes formed on the haul road



(b) Post mining rock material used for road construction



(c) Dusting issues during transport

Figure 3*. Haul road conditions and issues caused by improperly adopted design solutions.*

3. MATERIALS AND IMPROVEMENT CONCEPTS

3.1. Materials

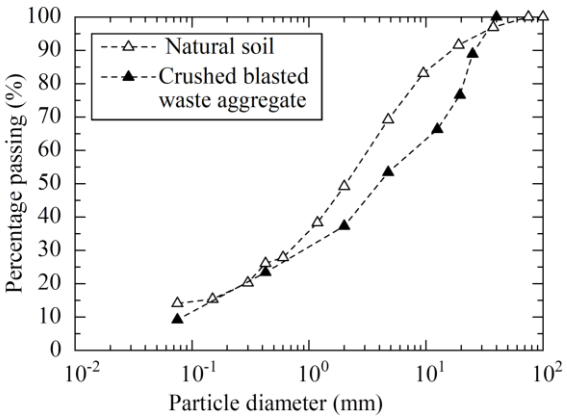


Figure 4. *Grain size distribution of soil and rock materials used in the study.*

Since the purpose of the study was to determine the most efficient soil mixture to improve the driving performance of the haul road the first step was to prepare several samples of different material composition and content ratios. The laboratory testing was performed using the following materials natural soil available at the site (originally used for haul road in section No. 2), blasted residual rock material (used for both surface and base layers in section No. 1), polymer additive (GeoStab^{TM}), and Portland Cement PCB40. The soil and rock samples (exploitation residual material) were collected from an open pit mine of Cao Son Coal company in Cam Pha, Quang Ninh province in Vietnam. The samples were transported to the construction laboratory LAS-XD 1679, weighed, and oven dried in 40^0C for 4-5 days. The geotechnical and chemical characteristics of samples of different content and compositions were determined using laboratory equipment following current testing standards i.e. AASHTO T88 (Standard Test Method for Particle-Size Analysis of Soils), AASHTO T90 (Standard Method of Test for Determining the Plastic Limit and Plasticity Index of Soils), AASHTO T 267 (Standard Method of Test for Determination of Organic Content in Soils by Loss on Ignition), AASHTO T85 (Standard Method of Test for Specific Gravity and Absorption of Coarse Aggregate), AASHTO T180-19 (Method of Test for Moisture-density Relations of Soils), AASHTO T193-13 (Standard Method of Test for California Bearing Ratio), ASTM D1633-17 (Standard Test Methods for Compressive Strength of Molded Soil-Cement Cylinders), TCVN 8862:2011 (Standard test method for indirect tensile strength of aggregate material bonded by adhesive binders). The soil samples for laboratory testing were prepared according the characteristics provided in Table 1. The grain size distribution curves for natural soil and the aggregates used for laboratory testing are presented in Figure 4.

Table 1. Profile of soil specimens for the compaction tests.

Soil samples	Descriptions
SP1	Natural soil (including particle size greater than 19 mm in diameter: occupied 8,4% in mass)
SP2	Natural modified soil where a smaller particle size (4,75-19mm in diameter) was used to replace the larger size of 19mm
SP3	SP2+ 5% Geostab + 5% Cement
SP4	SP2 + 5% Geostab + 7% Cement

3.2. Haul road improvement concepts

The major part of the research was to suggest the most effective material mixture to improve the transport conditions of the haul road. Although equally important was to propose the road construction design so the optimised soil mixtures could meet performance properties obtained in the laboratory. To do so, the authors proposed three different road design approaches, distinguished by the thickness of layered and engineered material, their composition and the location of application to make the results more representative.

The method used to improve the transport condition and the quality of the existing mine haul road for each segment in sections No.1, No.2 was chosen mainly based on the observation and monitoring of the damages caused by heavy vehicles and the erosion effect of the haul road, as well as their functional design in the study mining site. Detail of 3 different concepts of road conditions improvement and the approach used for the two study sections is shown in Figure 5. The mixtures (1, 2, 3) used for different sections and different concepts (1, 2, 3) presenting their particle size composition is given in Table 2.

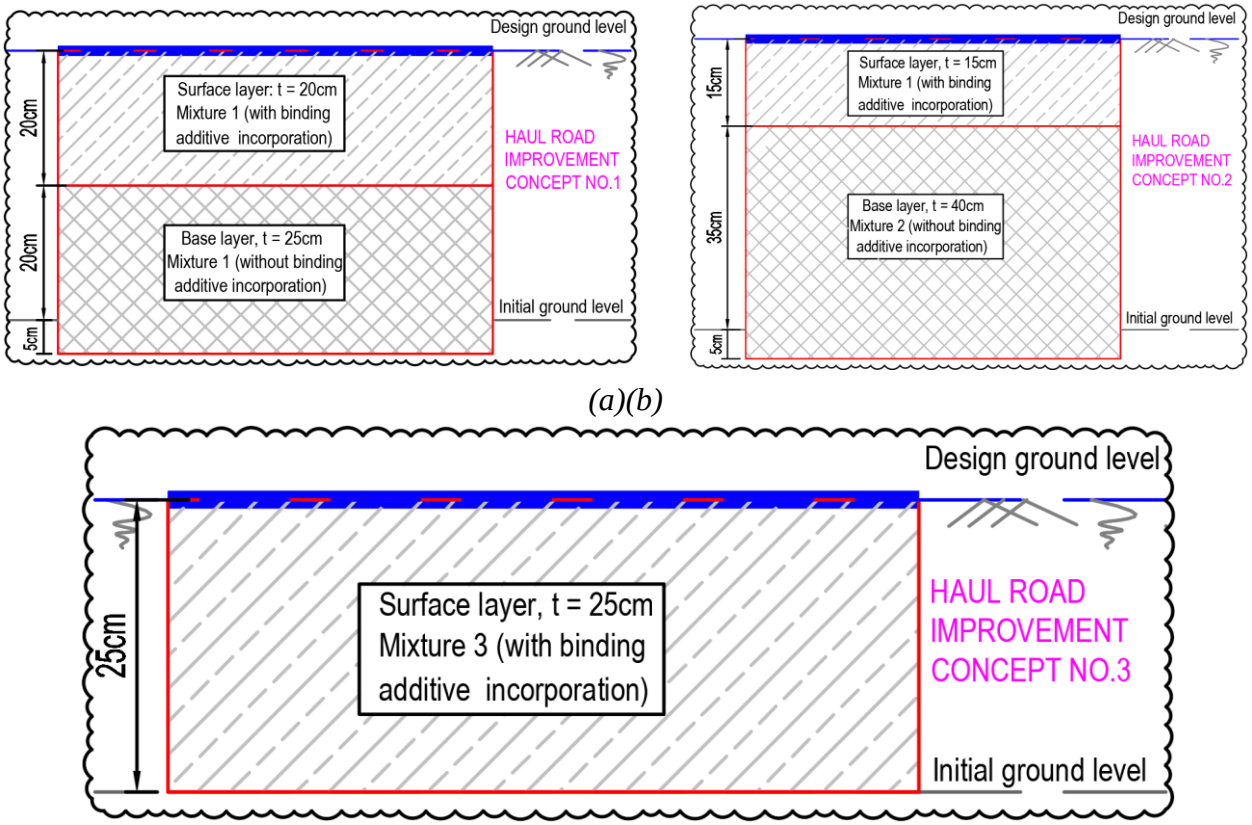


Figure 5. *Design concepts for improving the quality of haul roads in each section: (a) Concept 1 for segments ($A_2 \div A$) for section No. 1; (b) Concept 2 for segments ($A_1 \div A$), ($A \div B$), ($B \div C$), ($B \div B_1$) for section No. 1; Concept 3 used for entire section No. 2.*

Table 2. Material's characteristics used in mixtures.

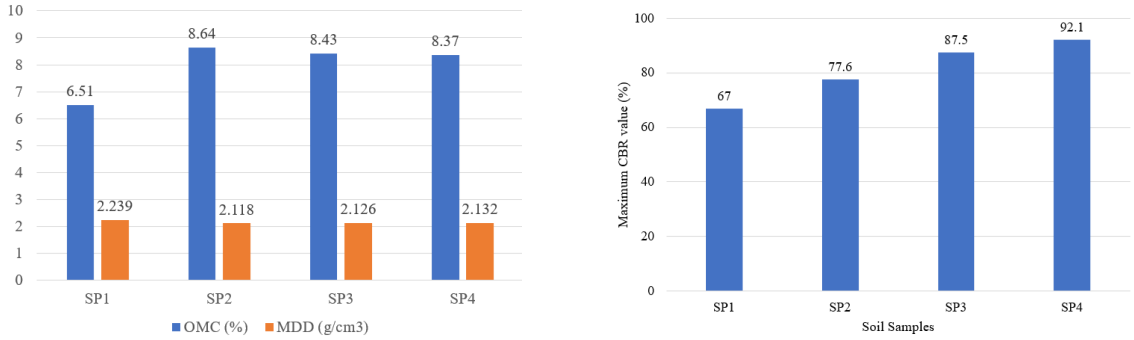
Descriptions	Maximum size of grain, mm	Group coefficient	Passing 2mm sieve (%)
Mixture 1	40	20-35	n/a
Mixture 2	150	n/a	< 20
Mixture 3	Modified natural soils (grain size from fig 4)		

4. RESULTS AND DISCUSSIONS

4.1. Laboratory tests

4.1.1 Compaction characteristics

A series of laboratory compaction tests were performed to evaluate the compaction characteristics of both soil and rock materials, such as maximum dry density and optimum moisture content. For the crushed blasted waste aggregate, the optimum moisture content was about 8%. The soil material's compaction characteristics of all test samples are shown in Figure 6 a and b. The composition of the tested samples is presented in Table 1. Figure 6 a presents the lowest value of the organic matter content (OM) observed for SP1, with the lowest maximum dry density (MDD) which is for the sample consisting of natural soil (including particle size greater than 19 mm in diameter: occupied 8,4% in mass) and the highest MDD for SP2 consisting of modified natural soil where a smaller particle size (4,75-19mm in diameter). The compaction test was performed applying national standards using California Bearing Ration (CBR) and is represented by giving the maximum CBR values. The highest value is obtained for SP4 samples which consist of modified natural soil where a smaller particle size (4,75-19mm in diameter) was used to replace the larger size of 19mm, with 5% addition of Geostab and 7% content of cement, while the lowest is obtained for SP1 sample.



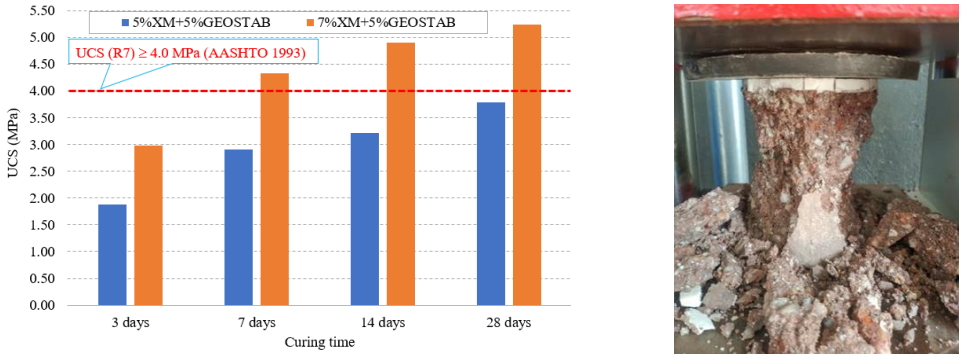
(a) *(b)*

Figure 6. *Compaction characteristics of soil samples*
a) organic matter content and maximum dry density b) CBR values.

4.1.2. Unconfined Compressive Strength

The unconfined compression test is a common method to determine the strength of the bonded mixtures used for road construction subbase. The unconfined compressive strength (UCS) in the present study was adopted as a parameter reflecting best mixture design for stabilising the natural modified soil that was considered for further application in reinforcing the haul road sub base.

The test was performed for two sample types, SP3 (consisting of SP2 soil+ 5% Geostab + 5% Cement) and SP4 (consisting of SP2 + 5% Geostab + 7% Cement), the UCS was determined at 4 different curing times (3, 7, 14 and 28 days.). The maximum unconfined compressive strength was achieved for the SP4 sample (5% of Geostab and 7% of cement), while the UCS maximum value for the same texting conditions for sample SP3 (5% of Geostab and 5% of cement was found to be below the required standard. The compressive strength results of tested samples at different curing time are presented in Figure 7.

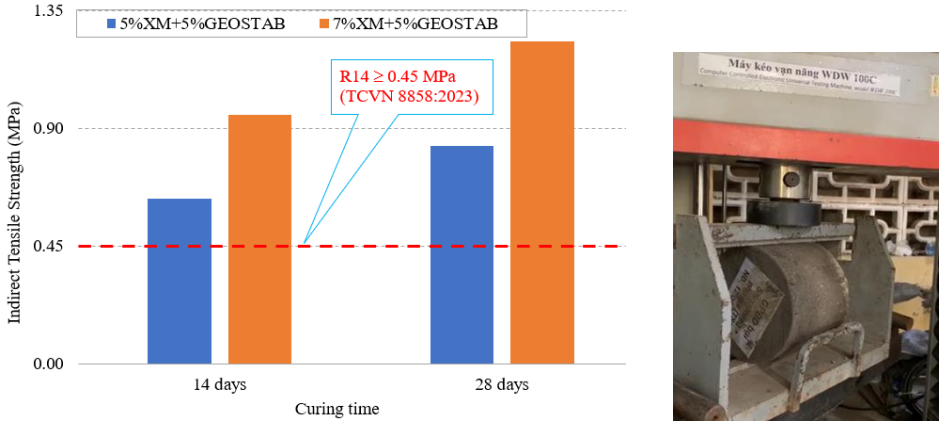


(a) *(b)*

Figure 7. *Unconfined compressive strength test a) results, b) tested sample.*

4.1.3. Indirect tensile strength

The test involves loading a cylindrical specimen with compressive loads distributed along two opposite generators. The advantage of the test is that the failure is not seriously affected by the surface condition and is initiated in a region of relatively uniform tensile stress. The test allows capturing the peak compressive load applied transversely to a cylindrical specimen prior to or on the onset of cracking. The test was performed according AASHTO. Since the used standard does not recommend any particular value for Indirect Tensile Strength (ITS) of cement-treated aggregate base for road pavement, the Vietnam national standard (TCVN 8858:2023), was used as the reference, where the minimum value of ITS at the curing time of 14 days is 0,45 MPa. Figure 8 shows the results for ITS test indicating that all soil samples met the standard value. As expected the highest values (1.20MPa) were obtained for SP4 sample (consisting of modified natural soil with 5% additive of Geostab and 7% of cement), and only half that strength (0.65 MPa) was achieved for SP3 at 14 day curing time.



(a) *(b)*

Figure 8. *Indirect tensile strength of treated soils SP3 and SP4 a) results b) test in progress*

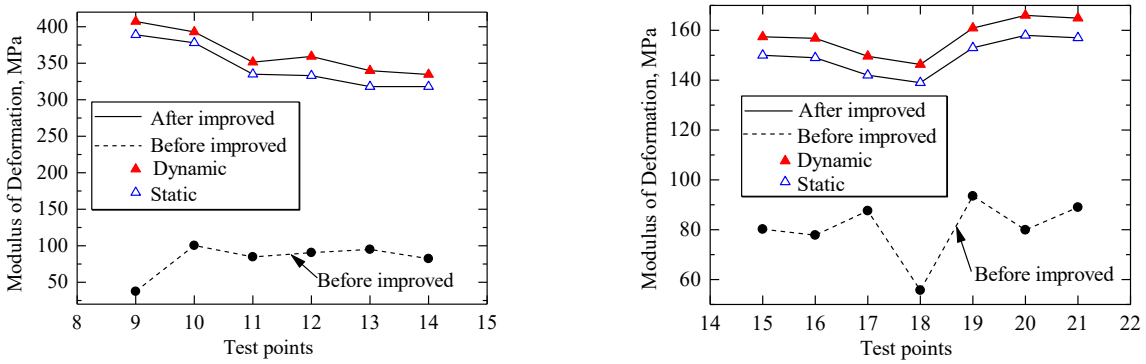
4.2. In situ Assessment

4.2.1. Light Weight Deflectometer (LWD) Test

The present research study aimed also at verifying the laboratory test by performing in-situ investigation before the haul road improvement works and after the new construction approach was implemented. One of the most common on-site test to determine the stiffness of unbound materials (subgrade/subsoils and base layers, granular layers & backfilling

materials) is Light Weight Deflectometer (LWD). The LWD is a lightweight portable tool used for measuring the bearing capacity (deflection) of subgrade/subsoils and unbound base layers. The zone of influence for the test typically extends to between 1 and 1.5 times the plate diameter. It is designed to provide a quick and non-destructive method for determining the load-bearing capacity of soil and assessing its stiffness.

The primary interest in the present study was the determination of Modulus of Deformation. For that purpose, LWD was performed meeting ASTM E2583-27(2015) standard requirements. The part of results of deformation modulus values from point 9 to point 21 representing segments A-A2 and A-B, is shown in figure 9a, b.



(a) segment (A-A2) *(b) segment (A-B)*

***Figure 9**. Improvement of modulus of deformation after improvement (stabilised with 7% cement- Concept 1).*

The testing procedure was started by selecting 32 test to determine the deformation modulus of the mining road before and after the improvement works (using laboratory-tested mixtures) were executed. There were, 8 testing points in segment (A-A1), 6 points in A-B0, 7 points in A-A2 and 11 points (B-C). In these locations Concept 1 of improvement was used, layering in particular thicknesses soil mixture containing modified natural soil with 5% Geostab and 7% cement. It is clear that the increase in the modulus of deformation is significant for stabilizer-improved soil mixture conditions.

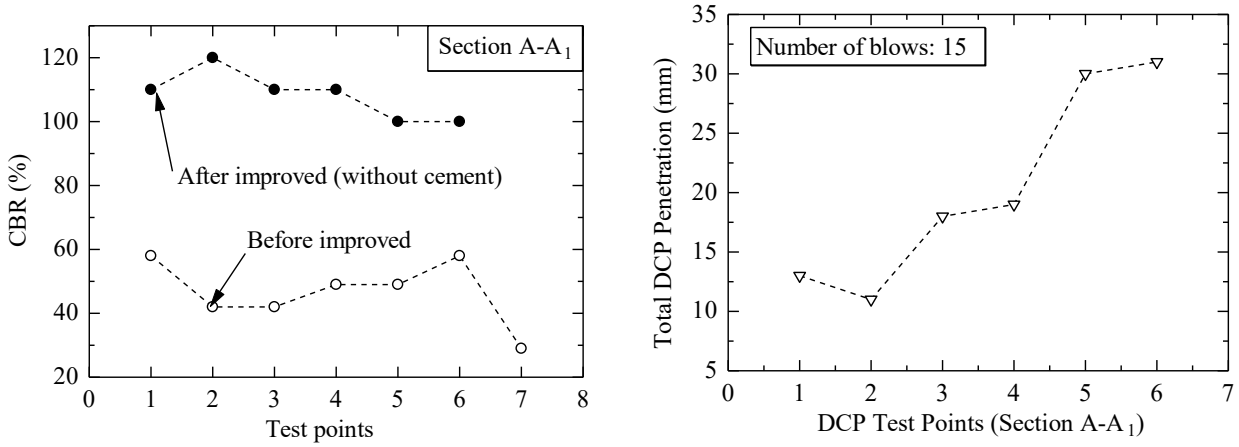
4.2.2. Dynamic Cone Penetrometer (DCP) Test

Another type of test used for coupled verification of results and to confirm best performing results of soil mixture used for haul road improvement was Dynamic Cone Penetrometer (DCP) Test.

The method is used to determine underlying soil strength by measuring the penetration of the device into the soil after each hammer blow. test is conducted by lifting and dropping the hammer onto the anvil, and measuring the penetration of the DCP cone into the pavement layers. Data are typically collected by measuring the penetration after every 5 blows, up to a total depth of 800 mm. The interpretation of DCP test is usually expressed in penetration depth in (mm). However, for comparison with laboratory test purposes, the DCP values could correlated and expressed using CBR approach. The values obtained from DCP test and presented both in CBR values (%) and depth (mm) are given in figure 10 a and b.

Figure 11a shows the CBR values of the haul road in section A-A1 obtained from DCP test, and Figure 11b shows the total DCP penetration. It is noted that the highest values of CBR were obtained for testing point 2 in section A-A1 and the deepest penetration depth

(30mm) was reached for the location of point 6 at the same section. The CBR values presenting the conditions before improvement works are significantly lower, by as much as 50% and more for test point no 2.



(a) *(b)*

***Figure 10**. DCP test results a) CBR correlated values before and after improvement b) penetration depth.*

5. CONCLUSIONS

The current study involved both laboratory and field experiments to assess the performance of haul road surfaces made from a combination of natural and treated soils, with varying ratios of polymer-cement additives. In the laboratory experiments, the primary goal was to determine the most efficient material composition specifically designed to meet the requirements for improving the road conditions presented in the present case study. The primary focus of the laboratory tests involved examining the compaction characteristics, unconfined compressive strength (UCS), and indirect tensile strength (ITS) of the materials under investigation. The laboratory test outcomes demonstrated that the specimens prepared using modified soil with a composition of 5% polymer and 7% cement exhibited the most substantial values for unconfined compressive strength (UCS) exceeding 5MPa, indirect tensile strength (ITS) exceeding 1.2MPa. To validate the optimal ratios under in situ conditions, the study was extended to include field tests on existing roads constructed using materials with various compositions. The field testing involved the use of a dynamic cone penetrometer (DCP) and a lightweight deflectometer. The outcomes validated the findings derived from the laboratory experiments. The highest values for modulus of deformation (> 400MPa) and DCP depth (> 30mm) were attained in the soil mixtures tested in the laboratory. As anticipated, the untreated material yielded the lowest values. The research study facilitated the formulation of the most efficient solution for the construction material employed in haul road design, thereby enhancing both the management and safety of the mining site.

REFERENCES

[1] Dang L N and Chuc A T 2019. Attaining Energy Security In Viet Nam: Impediments And Policy Implications. In *Achieving Energy Security in Asia Divers Int and Pol Imp*, 183-218.

[2] Thompson R Peroni R and Visser A T 2019. *Mining haul roads: Theory and practice*. CRC Press.

[3] Rupprecht S M 2019. Surface haul road design considerations in mine planning. *In Mine Planner's Colloquium p 1.*

[4] Thompson RJ and Visser A 2000. The functional design of surface mine haul roads. *Journal of the Southern African Institute of Mining and Metallurgy,* **100**(3), 169-180.

[5] Medinac F Bamford T Hart M Kowalczyk M & Esmaeili K 2020. Haul road monitoring in open pit mines using unmanned aerial vehicles: A case study at Bald Mountain Mine Site. *Mining, Metallurgy & Exploration*, **37**, 1877-1883.

[6] Alegre D de Lemos Peroni R da Rosa Aquino E & Dille F 2021. A method to assess haul roads rolling resistance using dispatch system data. *Mining Technology,* **130**(3), pp.176-187.

[7] Golbasi O & Kina E 2022. Haul truck fuel consumption modeling under random operating conditions: A case study. *Transportation Research Part D: Transport and Environment*, **102**, p.103135.

[8] Kashi V K Karmakar N C Krishnamoorthi S Adhikary P & Sahu A R 2023. A Laboratory Study on Application of Synthesised Amylopectin-grafted-Polyacrylamide AP-g-PAM on Coal Mine Haul Road Dust Emission at Different Atmospheric Temperatures. *Journal of The Institution of Engineers (India)* In D 1-8.

[9] Hajarian A & Osanloo M 2020. A New Developed Model to Determine Waste Dump Site Selection in Open Pit Mines: An Approach to Minimize Haul Road Construction Cost. *International Journal of Engineering*, **33**(7), 1413-1422.

[10] Hao S & Pabst T 2021. *Estimation of resilient behavior of crushed waste rocks using repeated load CBR tests.* Transportation Geotechnics **28**, 100525.

SHORELINE CHANGES FROM QUANG NINH TO THAI BINH IN THE PERIOD 1987 TO 2021 USING GIS TECHNOLOGY AND REMOTE SENSING DATA

Nguyen Thi Anh Nguyet[1], Tran Tuan Duong[1], Nguyen Dac Ve[2], Tran Anh Tuan[1], Pham Viet Hong[1]

[1] Institute of Marine Geology and Geophysics, Hanoi, Vietnam

[2] Institute of Marine Environment and Resources, Hai Phong City, Vietnam

E-mail: nguyet.imgg@gmail.com

Abstract: The article analyses the process of shoreline changes in the region from Quang Ninh to Thai Binh using different Normalized Difference Water Indices (NDWIs) to separate the boundary between the coastal area and the water bodies on sattelite images from 1987 to 2021. The calculation of the shoreline change rate for accretion/erosion processes was performed using the DSAS tool and was validated by Linear Regression Rate (LRR), End Point Rate (EPR) and Net Shoreline Movement (NSM) methods on cross sections along the region. The shoreline in study area was divided into two sub-regions: South Do Son (112 sections) and North Do Son (97 sections). The results from 209 cross-sectional lines show that modern shoreline displacement in the period 1987-2021 in the South Do Son area was alternating processes, both erosion and accretion. Sections at the outer bank of Van Uc estuary showed erosion process with a speed of 14.2m/year. However, the sedimentation process tends to take place strongly at the outer bank of Van Uc river to Thai Binh river with a speed of up to 72.66m/year. The shoreline of the North Do Son sections showed clearer trend in accretion process with an accumulated area of 3,889.67 ha (1987-2003) and 4,179.93 ha (2003-2021). This trend follows the long-term shoreline displacement during the Middle-Late Holocene to present day.

Keywords: *Shoreline changes, GIS, remote sensing, Quang Ninh - Thai Binh*

1. INTRODUCTION

The changes in the topography of the coastline have a great impact on the communities and shoreline ecosystems. The results of the study of topographic changes both on land as well as at the coast are recognized as one of the important sources of documents to develop planning for development and environmental management of the shore zone. Many studies attempted to use remote sensing and geographic information systems as useful tools for monitoring coastline changes in terms of erosion and accretion. A study of shoreline change for over 9000 islands in South East Asia showed that approximately 12% of the total islands had undergone changes in coastlines, resulting in about 251km^2 decrease in area (Zhang et al., 2021). However, another study by Cui et al. (2022) indicated the length of shorelines around the South East Asia maintained growth, especially in the 1990s, which increased by 734.8 km, from 28,243.8 km (1990) to 28,978.6 km (2000). The increase of artificial shorelines was mostly driven by the expansion of constructed and aquaculture dikes but the proportion of natural shorelines decreased from 92.4% to 73.3% during the past 40 years. Recent study in Phuket, Thailand (Nidhinarangkoon, 2023), also indicated that eight of the study site's locations were under mild erosion from 2013 to 2021. The average shoreline change varied between -4.10 and 5.47m/year.

In Vietnam, the erosion of coastal area is occurring very strongly in all 28 coastal provinces, but at different levels. On the entire coastline of Vietnam, there are about 249 eroded shore sections, with a total length of about 400km. The erosion process is taking place in almost all types of coastal materials such as bedrock, sandy gravel, clay, clay mud, sandy mud... in which sand banks are accounting for 82% of the total number of eroded sections. There are 30% of sections eroding at a fast speed of 10m-30m/year and there are many areas where the erosion speed is up to 100m/year (Nguyen Thi Thu Ha, 2015). The erosion process along Sam Son - Quang Xuong section of Thanh Hoa province, takes place under conditions of sediment deficiency combined with the active activity of sea currents. This trend is accompanied by human activities such as the exploitation of coastal mangrove forests, hydroelectric dams upstream, reduction of the sedimental supply... (Nguyen Thi Thu Ha et al., 2015). Analysis of element at risk at Hai Hau county, Nam Dinh province, showed that areas with dense population, infrastructure such as road networks, resident houses and mangrove sites are relatively high vulnerability (Nguyen Dinh Bac et al., 2020).

This study aims to evaluate shoreline changes from Quang Ninh to Thai Binh provinces, using the public-access satellite data and estimate different change rates with field observation data. Moreover, the present coastal management strategies will be discussed with the results of shoreline changes to propose appropriate future adaptation management strategies.

2. MATERIALS AND METHODS

2.1. Study area and data

In study area, the shoreline from Cua Luc - Quang Ninh to Diem Dien estuary - Thai Binh is about 190km long, with many large rivers flowing into the sea, carrying a lot of alluvium, so the shoreline fluctuates sharply. The development is extremely complicated and the speed is not uniform in space and time. In this study, we divided the shoreline of the above study area into two regions, the South Do Son region and the North Do Son region as a basis for calculating the shoreline changes in the period 1987-2003 and 2003-2021. In the South Do Son area (the shoreline from along the Diem Dien estuary up to Bang La commune - Do Son district) and the North Do Son area (the shoreline from along the Lach Tray river mouth to the Bach Dang river mouth, Phu Long - Cat Hai and Cua Luc - Ha Long).

The study conducted surveys and collected relevant documents for shoreline change assessment including Landsat satellite images in 1987 (Landsat 5 TM), 2003 (Landsat5 TM), and 2021 (Landsat8 OLI). All selected scenes have low cloud coverage (<10%), images are downloaded from the website: http://earthexplorer.usgs.gov (Table1). The shoreline is referenced to a certain extent, the area along the Quang Ninh-Thai Binh coast, the water level at the mouth of the river, and the sea at the time of taking pictures range from 0.77 to 2.2m according to the altitude conversion.Therefore, tidal fluctuations greatly affect the water shorelines extracted from satellite images in 3 time periods, in the years of 1987, 2003 and 2021. For the determination of variation, the shoreline is converted to the general tidal level by interpolation method usually applied to the contour line at some standard elevation [20]. In this study, the tidal level of 0.77m in 2003 was chosen as the standard level to refer to different times.

Table 1. Satellite image used in this study.

	Resolution (m)	Shooting date	Tide level
Landsat 5 TM	30	07/03/1987	0.83 m
Landsat 5 TM	30	06/05/2003	0.77 m
Landsat 8 OLI	30	01/12/2021	2.20 m

2.2. Methods

In this study, the remote sensing method is used to extract the shoreline over the years. To extract the shoreline from remote sensing data, the Landsat 5 TM and Landsat 8 OLI satellite images are atmospherically corrected. In this study, using NDVI, and NDWI indices in shoreline separation gives high results due to the effective discriminant between land and water [4],[8], [22], calculation of shoreline change is done by the DSAS5 tool [34].This method effectively handles noise caused by breaking waves, clarifies the coastline, and creates a complete boundary between the shore and the water. The process of classifying satellite images is carried out on ENVI software. After classification, raster images will be converted to vector images. Once the complete shoreline layers are obtained, apply different GIS methods to calculate the final result.

$$Coastline = \frac{\rho_{Green}}{\rho_{NIR}} \times \frac{\rho_{Green}}{\rho_{SWIR}} + NDWI \quad (1)$$

$$Coastline = \frac{\rho_{Green}}{\rho_{SWIR}} + NDVI \quad (2)$$

$$NDWI = \frac{(\rho_{Green} - \rho_{NIR})}{(\rho_{Green} + \rho_{NIR})} \quad (3)$$

$$NDVI = \frac{(\rho_{NIR} - \rho_{Red})}{(\rho_{NIR} + \rho_{Red})} \quad (4)$$

Where: ρ_{Green} is Green spectrum channel; ρ_{Red}: Red spectrum channel; ρ_{NIR}: Near-infrared spectrum channel; ρ_{SWIR}: Short spectrum infrared channel.

In the study, each section is spaced 500m apart, transects are built along the shoreline from Quang Ninh to Thai Binh and divided into two sub-regions: South Do Son and North Do Son. The transects are numbered in ascending order from Nam Do Son to North Do Son, and the total number of sections is 209 (the South Do Son area has 112 sections, the North Do Son area has 97 sections). From transect 1 to transect 112 is the coastline from Diem Dien estuary ward to Bang La commune - Do Son district (South Do Son area),transects 113 to 209 are the coastline from Lach Tray estuary to Bach Dang estuary, Phu Long - Cat Hai and Cua Luc - Ha Long (Northern Do Son).

Analysis of shoreline change with 03 different parameters selected as follows: SCE (Shoreline Change Envelope), NSM (Net Shoreline Movement), and EPR (End Point Rate).

$$EPR = \frac{NSM}{n} \quad (5)$$

Where: n is the number of years in the calculation period.

In the shoreline areas of Hai Phong, Thai Binh, and Quang Ninh, there are many socio-economic activities affecting the shoreline area such as reclaiming the shoreline area to build aquaculture ponds, encroaching on the sea for tourism, and encroaching on the sea, port making and port logistics... These are objects that cause noise in automatic image

processing, distorting the results from reality. In this study, we decided that in places with strong human impacts such as the shores of farming lagoons and embankments, tourist areas to the sea will be artificialshoreline. From there, the automatic shoreline interpretation results that are deviated from reality will be re-calibrated for the best results before being included in the calculation of the accretion and erosion results.

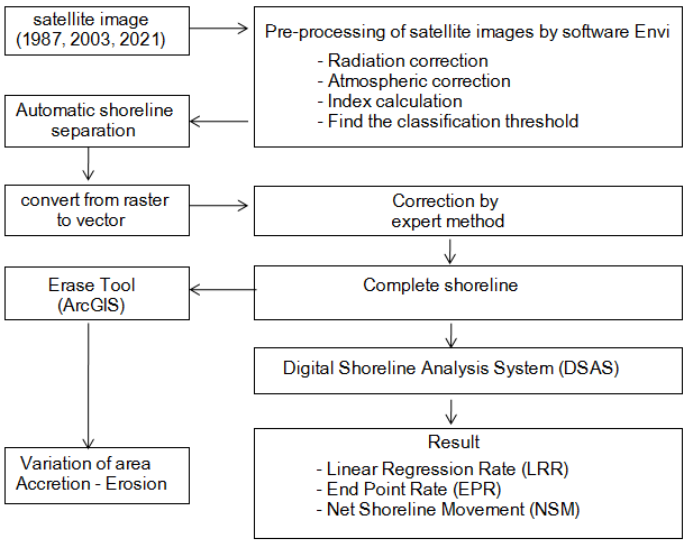


Figure 1. *Flowchart of shoreline change calculation.*

3. RESULTS AND DISCUSSION

3.1. Shoreline changes of the Quang Ninh-Thai Binh area in the period of 1987-2021

The shoreline results of each year 1987, 2003, and 2021 are separated and adjusted for estuaries with lower water than other shore estuaries.In order to facilitate the calculation of fluctuations and describe the results, the limestone structures due to very small fluctuations will be ignored and not calculated in this study.

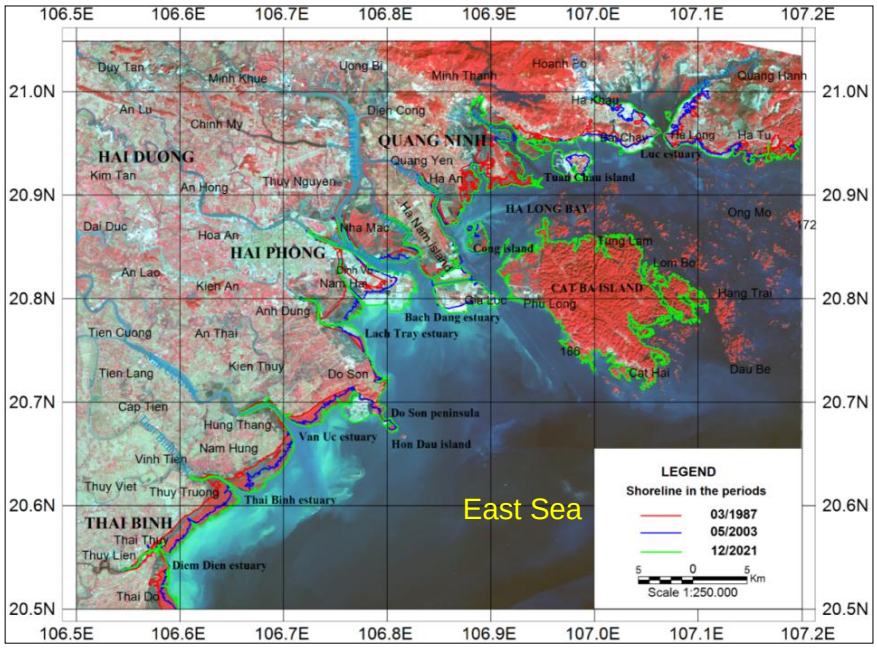


Figure 2. *Study area's shoreline in 1987, 2003 and 2021.*

3.2. The accretion/erosion area of the shoreline in the period of 1987-2021

The process of accretion-erosion through these two stages is different throughout the South Do Son and North Do Son regions, the accretion area converges more than the erosion area (Figure 3, Figure 4). In 16 years from 1987-2003, the South Do Son shoreline accreted to the sea 3,354.5ha, of which the North Do Son area accreted to the sea 3889.67 ha. In the 18-year period from 2003-2021, the South Do Son area accreted to the sea 2564.59ha, while the North Do Son area accreted to the sea with an area of 4179.93ha. (Table 2).

Table 2. Parameters of shoreline accretion-erosion of Quang Ninh-Thai Binh in the period of 1987-2021.

Shoreline	Accretion / Erosion (ha)	1987-2003	2003-2021
South Do Son	Accretion	3,356.14	2,606.80
	Erosion	1.64	42.21
	Accretion/Erosion Difference	3,354.50	2,564.59
North Do Son	Accretion	4,228.46	4,644.31
	Erosion	338.79	4,64.38
	Accretion/Erosion Difference	3,889.67	4,179.93



Figure 3. *Shoreline accretion/erosion of Quang Ninh - Thai Binh in the period of 1987-2003.*



Figure 4. *Shorelineaccretion/erosion of Quang Ninh-Thai Binh in the period of 2003-2021.*

3.3. The process of shoreline change of the Quang Ninh - Thai Binh area in the period of 1987-2021

In the period 1987-2021, the shoreline of the South Do Son area, the accretion distance to the sea from the mouth of Thai Binh River to the bank of Dong Hung Tien Lang commune, 0.47m (section 55) gradually increased to 2436.2m. (section number 68). The smallest NSM has a value of -473.6m (at the cross-section of 94 Van Uc estuary) showing that in 1987 compared with 2021, a slight erosion occurred 473.6m inland and the NSM had a large value. 2436.2m (at section 68 of the East Hung-Tien Lang bank) shows that the accretion is quite strong. (Figure5, Figure 6, Table 3).

On the shoreline of the North Do Son region, the SCE value ranges from 3.57m (at section 133 of Lach Tray estuary) to 3082.3m (at section 148, from Lach Tray to Dinh Vu) showing that the accretion distance to the sea from the bank of Lach Tray river mouth up along the shore towards Dinh Vu tends to increase from 3.57m to 3082.3m. NSM has the smallest value -295.12m (at the cross-section 201 at Phu Long - Cat Hai) showing that in 2021, the erosion inland is 295.12m and the NSM has the largest value of 3082.3m (at cross-section 148).) shows that the accretion is quite strong up to 3082.3m at the bank from Lach Tray estuary to Dinh Vu. (Figure 5, Figure 6).

Table 3. Values of SCE, NSM shorelinecross-sections from Quang Ninh to Thai Binh in the period 1987-2021.

Shoreline	Value	SCE (m)	NSM (m)
South Do Son	Min	0.47	-473.6
	Max	2,436.2	2,436.2
	Average	836.4	806.6
North Do Son	Min	3.57	-295.12
	Max	3,082.3	3,082.3
	Average	623.5	547.6

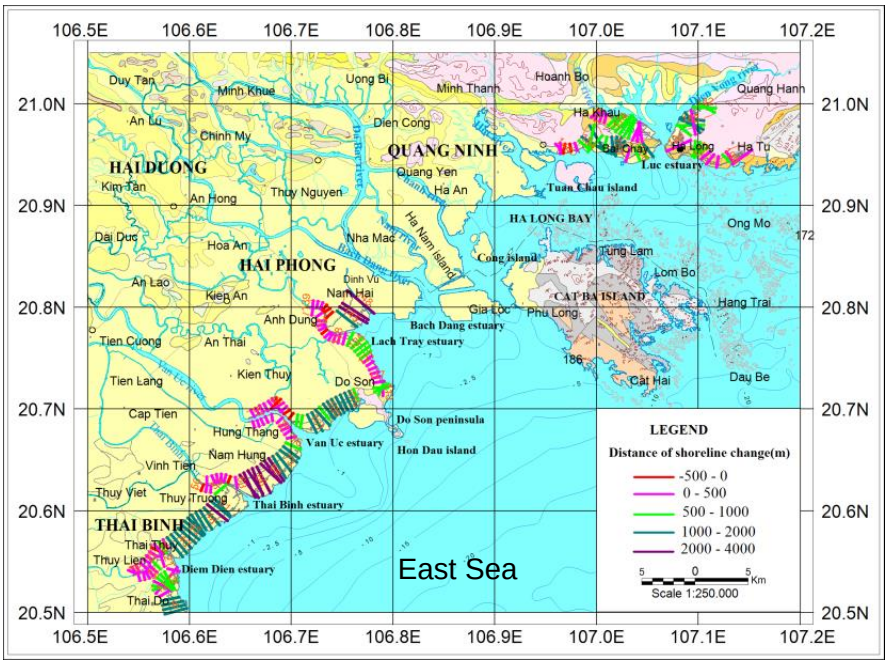


Figure 5. *Distance of shoreline change from Quang Ninh to Thai Binh in the period of 1987-2021.*

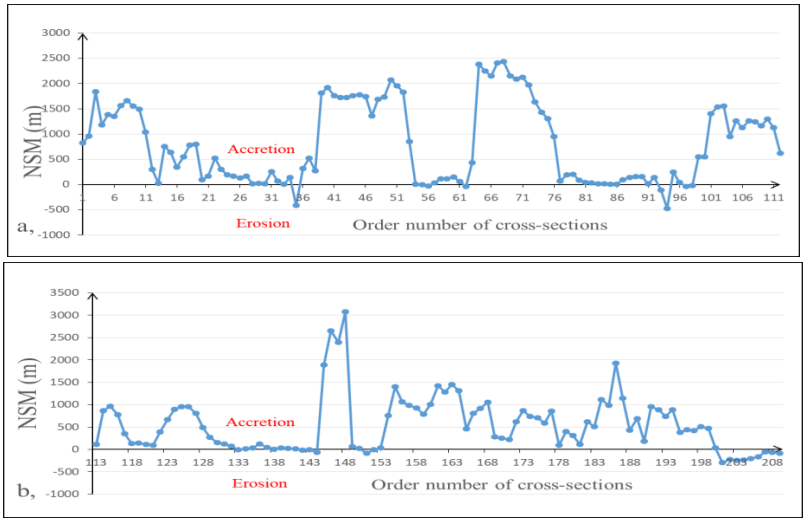


Figure 6. *Distance of shoreline change on cross-sections from Quang Ninh to Thai Binh in the period of 1987-2021: a) Southern Do Son area; b) Northern Do Son area.*

3.4. The change rate of the Quang Ninh-Thai Binh shoreline in the period 1987 - 2021

In the period 1987-2021, in the South Do Son area, the accretion phenomenon dominates.The average annual shoreline change rate (EPR value) at the cross-sections of the South Do Son occurs from moderate to strong accretion (0-72.66m/year) from section 1 to section 112. The bank section from Thai Binh estuary to Van Uc estuary has a strong convergence rate (50-72.66m/year), in which the highest accretion rate occurs at section 68, the bank between Thai Binh estuary and Van Uc estuary, at Van Uc estuary there is moderate to quite strong erosion, in which erosion is greatest at section 94 (Van Uc estuary), the erosion rate is up to 14.2m/year. (Figure 7, Figure 8)

The bank sections from the Van Uc river mouth up to the Bach Dang river mouth and the banks on both sides of Luc's mouth have accretion at a rate of 0.16-91.93m/year.The strongest accretion rate occurs at section 148 (Dinh Vu bank section) up to 91.93m/year.Contrary to the above accretion phenomenon, erosion at Phu Long Cat Hai bank (from section 201 to 209) during this period, the rate of erosion is from 1.57m/year to 8.8m/year.

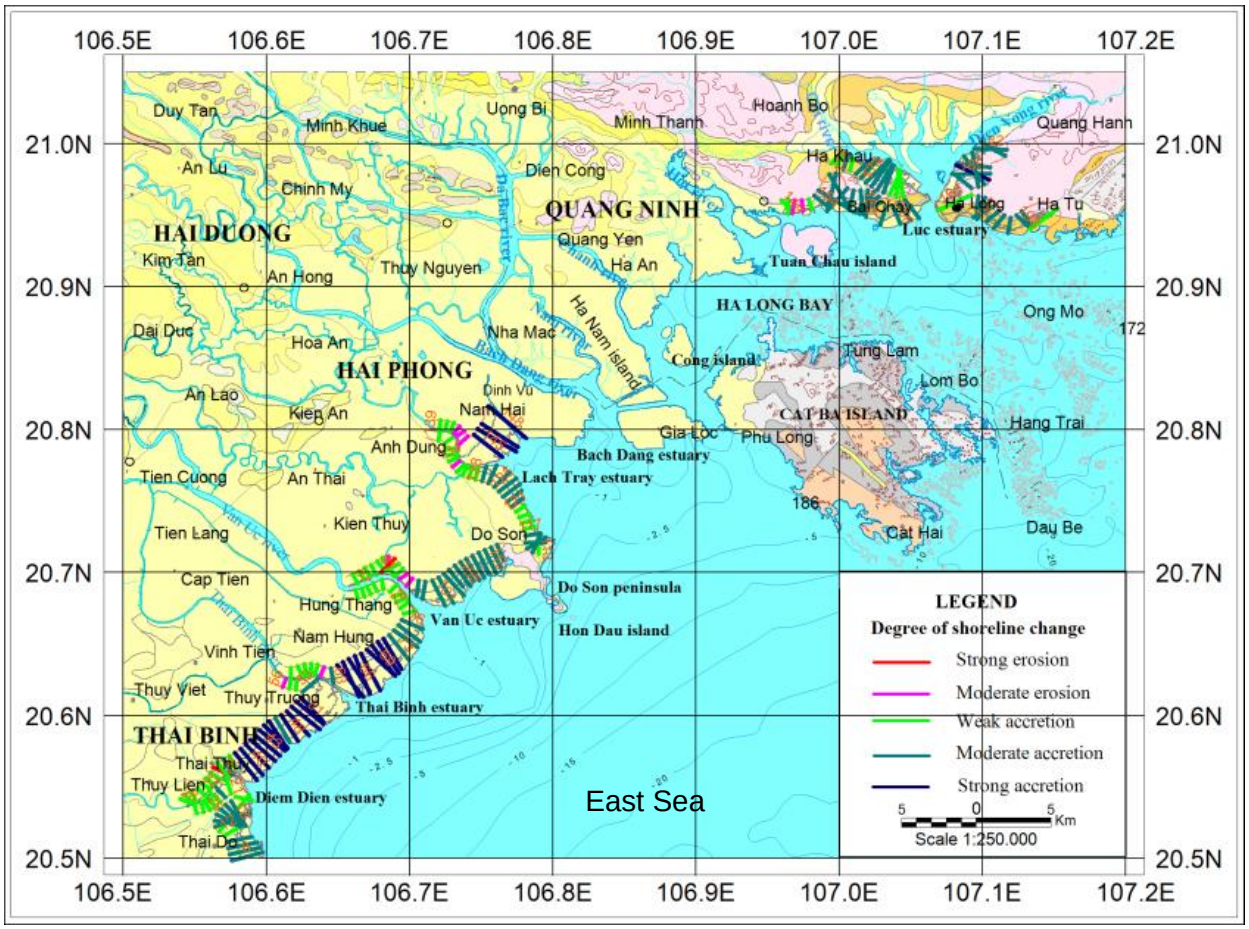


Figure 7. *Degree of shoreline change from Quang Ninh to Thai Binh in the period of 1987-2021.*

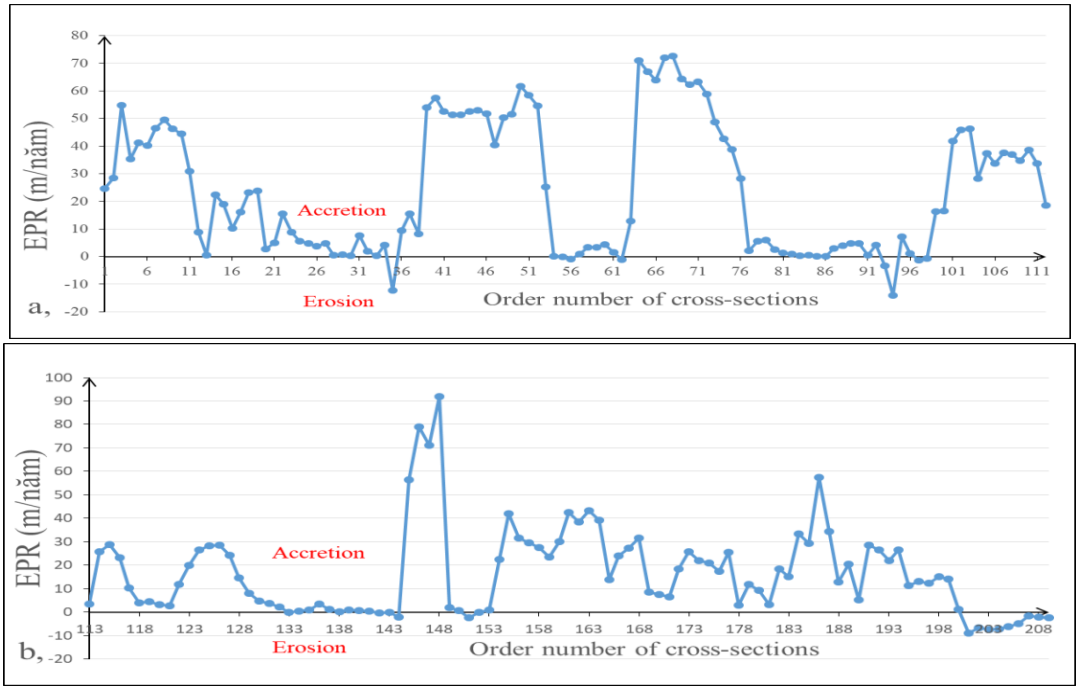


Figure 8. *Degree of shoreline change on cross-sections from Quang Ninh to Thai Binh in the period of 1987-2021: a) Southern Do Son area; b) Northern Do Son area.*

Several factors, such as beach slope, sediment grain size, and wave climate, can contribute to shoreline changes in terms of erosion and accretion. Human activities can also change beach morphology, mainly through coastal development, pollution, and recreational activities. Coastal urbanization can result in drainage channels leading directly to the sea, as well as other coastal structures developed by humans to protect the areas behind the shores.

4. DISCUSIONS AND CONCLUSION

During the early Holocene period about 8.000 years ago, the shoreline receded inland in the southwestern region (study area), due to the high terrain of the Northeast, the displacement of the coastline deep inland during this period is not significant. In the mid-late Holocene period, the strong encroachment of the Red River Delta towards the sea caused the shoreline in the Southwest region to shift rapidly and have a delta-like coastline with a tendency to encroach on the sea.

Modern shoreline displacement from multi-temporal remote sensing data shows in the period 1987-2021, The shoreline in the Nam Do Son area has alternating erosion and accretion. The part of the bank inside the Van Uc estuary has erosion with a speed of 14.2 m/year. However, in the South Do Son area, the accretion phenomenon still prevails, the sedimentation process tends to take place strongly at the outer bank of the Van Uc river mouth to the Thai Binh river mouth with a speed of up to 72.66 m/ year and accretion area up to 3354.50 ha (1987-2003) and 2564.59 ha (2003-2021). The shoreline of the North Do Son area used to have erosion and accretion in the period 1987 - 2021, in the section of Phu Long - Cat Hai, the erosion process took place with the maximum speed of 8.8m/year.However, the accretion process still dominates with an area of 3889.67 ha (1987 - 2003) and 4179.93 ha (2003 - 2021).

In general, the trend of the shoreline in the southwestern part of the Red River Delta is accretion and displacement towards the sea.This trend is determined by the long-term

shoreline displacement trend during the Middle-Late Holocene, combined with studies on shoreline displacement and erosion using remote sensing data. However, additional analyses and data are needed to establish a causal relationship between these factors and changes in shoreline. A comprehensive analysis of shoreline changes, including a detailed assessment of costs and benefits associated with potential adaptations, should be undertaken before undertaking any management decisions or adaptation plans.

ACKNOWLEDGMENTS

The authors wish to thank the Institute of Marine Geology and Geophysics-VAST for supporting the necessary conditions to complete this research.

REFERENCES

[1]. Benjamin J., Rovere A.,et al., 2017. Late Quaternary sea-level changes and early human societies in the central and eastern Mediterranean Basin: An interdisciplinary review. Quat. Int. 449, 29-57.

[2]. Boyd R., Dalrymple R., Zaitlin B. A., 1992. Classification of Elastic Coastal Depositional Environments, Sedimentary Geology 80, 139-150.

[3]. Carr A. S., Bateman M. D., Roberts D. L., Murray-Wallace C. V., Jacobs Z., Holmes P. J., et al., 2010. The last interglacial sea-level high stand on the southern Cape coastline of South Africa. Quat. Res. 73, 351-363.

[4]. Cassé C., Viet P. B., Nhung P. T. N., Phung H. P., Nguyen L. D., 2012. Remote Sensing Application For coastline Detection In Ca Mau, Mekong Delta, in: Proceeding of International Conferance on Geometics for Spatial Infrastructure Development in Earth and Allied Science-GIS IDEAS 2012. 199-204.

[5]. Cui Y., Yan F., He B., Ju C. and Su F., 2022. Characteristics of shoreline changes around the South China Sea from 1980 to 2020. Frontiers in Marine Science 9:1005284. doi: 10.3389/fmars.2022.1005284.

[6]. Doan Dinh Lam, 2003. Development history of sediment in Red river delta. PhD thesis of Geology, Vietnam National University, Hanoi. (inVietnamese)

[7]. Doan Dinh Lam, 2008. Delta lobes of the Red River Delta. Journal of Geology, series A, No. 308, 9-10/2008, 59-67. (inVietnamese)

[8]. Dung B. V., Stattegger K., Unverricht D., Phach P. V., Thanh N. T., 2013. Late Pleistocene-Holocene seismic stratigraphy of the Southeast Vietnam Shelf. Global and Planetary Change 110, 156-169.

[9]. Fan D., Nguyen D. V., Su J., Bui V. V., Tran D. L., 2019. Coastal morphological changes in the Red River Delta under increasing natural and anthropic stresses. Anthr. Coasts 2, 51-71. https://doi.org/10.1139/anc-2018-0022.

[10]. Funabiki A., Haruyama S., Quy N. V., Hai P. V., Thai D. H., 2007. Holocene delta plain development in the Song Hong (Red River) delta. Vietnam. Journal of Asian Earth Sciences 30, 518-529.

[11]. Grant K. M., Rohling E. J., Bar-Mathews M., Ayalon A., Medina-Elizalde M., Ramsey C. B., Satow C., Roberts A. P., 2012. Rapid coupling between ice volume and polar temperature over the past 150,000 years. Nature 491, 744-747.

[12]. Hanebuth T. J. J., Stattegger K. 2004. Depositional sequences on a late Pleistocene-Holocene tropical siliciclastic shelf (Sunda shelf, southeast Asia). Journal of Asian Earth Sciences 23, 113-126.

[13]. Hanebuth T. J. J., Saito Y., Tanabe S., Vu Q. L., Ngo Q. T., 2006. Sea levels during late marine isotope stage 3 (or older ?) reported from the Red River delta (northern Vietnam) and adjacent regions. Quat. Int. 145-146, 119-134.

[14]. Hanebuth T. J. J., Stattegger K., Bojanowski A., 2009. Termination of the Last Glacial Maximum sea-level lowstand: The Sunda-Shelf data revisited. Global Planet. Change 66, 76-84.

[15]. Hanebuth T. J. J., Voris H. K., Yokoyama Y., Saito Y., Okuno J., 2011. Formation and fate of sedimentary depocentres on Southeast Asia's Sunda Shelf over the past sealevel cycle and biogeographic implications. Earth Sci. Rev. 104, 92-110.

[16]. Hanebuth T., Stattegger K., Grootes P. M., 2000. Rapid flooding of the Sunda Shelf: a late-glacial sea-level record. Science 288, 1033-1035.

[17]. Hori K., Tanabe S., Saito Y., Haruyama S., Nguyen V., Kitamura., 2004. Delta initiation and Holocene sea-level change: example from the Song Hong (Red River) delta, Vietnam. Sedimentary Geology 164, 237-249.

[18]. Lam D. D, Boyd W. E., 2000. Holocene coastal stratigraphy and model for the sedimentary development of the Hai Phong area in the Red River delta, north Viet Nam. Journal of Geology (Series B) 15-16, 18-28.

[19]. Lambeck K., Chappell J., 2001. Sea level change through the Last Glacial Cycle. Science 27, 679-686.

[20]. Lieu N. T. H., 2006. Holocene evolution of the Central Red River delta, Northern Vietnam. PhD thesis of lithological and mineralogical in Germany, 130 pp.

[21]. Nguyen Dinh Bac, Nguyen Quoc Phi, Nguyen Thi Cuc, 2020. Assessment of elements at risk by coastal erosion of Hai Hau, Nam Dinh province. Proceedings of the Conference on Earth Sciences and Natural Resources for Sustainable Development (ERSD 2020). Transport Publishing House, Hanoi, Vietnam, p.16-22. ISBN: 978-604-76-2277-1.

[22]. Nguyen Ngoc Tien, Cuong D. H., et al., 2018. Shoreline change analysis with remotesensing sensed data in the Hau river mouth area. Vietnam Journal of Marine Science and Technology 17, 386-392. https://doi.org/10.15625/1859-3097/17/4/8858.

[23]. Nguyen Thi Thu Ha, Nguyen Hoai Nam, Nguyen Phuong Thao, Dinh Thu Thuy, Vu Thu Trang, Le Hai Hoan, Nguyen Quoc Phi, 2015. Coastal erosion susceptibility from Sam Son city to Quang Xuong county, Thanh Hoa province. Proceedings of GIS Conference 2015, Hanoi, p.187-192.

[24]. Nidhinarangkoon P., Ritphring S., Kino K. and Oki T., 2023. Shoreline Changes from Erosion and Sea Level Rise with Coastal Management in Phuket, Thailand. Journal of Marine Science and Engineering 11:969. https://doi.org/10.3390/jmse11050969.

[25]. Pan T., Murray-Wallace C. V., Dosseto A., Bourman R. P., 2018. The last interglacial (MIS 5e) sea level highstand from a tectonically sBång far-feld setting, Yorke Peninsula, southern Australia. Mar. Geol. 398, 126-136.

[26]. Pham Thi Phuong Thao, Ho Dinh Duan, Dang Van To, 2008. Integrated remote sensing and GIS for calculating shoreline change in Phan-Thiet coastal area. Int. Symp. Geoinformatics Spat. Infrastruct. Dev. Earth Allied Sci. 1-6.

[27]. Phung Van Phach et al., 2018. Comparative study on the evolution of Holocene sediments of the Red River Delta and the Truong Giang River Delta. Proceeding solutions to protect and exploit the Red River Delta coastal strip. NĐT.01.CHN/15.

[28]. Ping Yin, Phung Van Phach, Dinh Lan Tran, Xiaoyong Duan et al., 2018. Introduction to the China-Vietnam Cooperation Project: A Comparative Study of the Holocene Sedimentary Evolution of the Yangtze and Red River Deltas. Journal of Ocean University of China 17, 1269-1271.

[29]. Rohling E. J., Fenton M., Jorissen F. J., Bertrand P., Ganssen G., Gaulet J. P., 1998. Magnitute of sea-level lowstands of the past 500,000 years. Nature 394, 162-165.

[30]. Rovere A., Raymo M. E., Vacchi M., Lorscheid T., Stocchi P., Gomez-Pujol L., Harris D. L., Casella E., O'Leary M. J., Hearty P. J., 2016. The analysis of Last Interglacial (MIS 5e) relative sea-level indicators: Reconstructing sea-level in a warmer world. Earth Sci. Rev. 159, 404-427.

[31]. Saito Y., Katayama H., Ikehara K., Kato Y., Matsumoto E., Oguri K., Oda M., Yumoto M. 1998. Transgressive and highstand systems tracts and post-glacial transgression, the East China Sea. Sedimentary Geology 122, 217-232.

[32]. Sato H., Ban F., Katoh S., Hyodo M., 2017. Sea-level variations during Marine Isotope Stage 7 and coastal tectonics in the eastern Seto Inland Sea area, western Japan. Quat. Int. 456, 102-116.

[33]. Stattegger K., Tjallingii R., Saito Y., Michelli M., Thanh N. T., Wetzel A., 2013. Mid to late Holocene sea-level reconstruction of Southeast Vietnam using beachrock and beach-ridge deposits. Global Planet. Change 110, 214-222.

[34]. Tanabe S., Hori K., Saito Y., Haruyama S., Doanh L. Q., Sato Y., Hiraide S., 2003a. Sedimentary facies and radiocarbon dates of the Nam Dinh-1 core from the Song Hong (Red River) delta, Vietnam. Journal of Asian Earth Sciences 21, 503-513.

[35]. Tanabe S., Hori K., Saito Y., Haruyama S., Phai V. V., Kitamura A., 2003b. Song Hong (Red River) delta evolution related to millennium-scale Holocene sea-level changes. Quaternary Science Reviews 22, 2345-2361.

[36]. Tanabe S., Saito Y., Lan V. Q., Hanebuth T. J. J., Lan N. Q., Kitamura A., 2006. Holocene evolution of the Song Hong (Red River) delta system, northern Vietnam. Sedimentary Geology 187, 29-61.

[37]. Tjallingii R., Stattegger K., Stocchi P., Saito Y and Wetzel A., 2014. Rapid flooding of the southern Vietnam shelf during the early to mid-Holocene. Journal of Quaternary Science 29, 581-588.

[38]. USGS, 2018. Digital Shoreline Analysis System (DSAS). Open-File Rep. 2018-1179.

[39]. Waelbroeck C., Labeyrie L., Michel E., 2002. Sea level and deep water temperature changes derived from benthonic foraminifera isotopic records. Quat. Sci. Rev. 21, 295-305.

[40]. Zhang Y. X., Li D., Fan C., Xu H. and Hou X. Y., 2021. Southeast Asia island coastline changes and driving forces from 1990 to 2015. Ocean & Coastal Management 215:105967. doi: https://doi.org/10.1016/j.ocecoaman.2021.105967.

INTERACTION OF SURGE AND WAVE ON STRONG/SUPER TYPHOON IN THE NORTHERN COASTAL AREA OF VIETNAM

Pham Van Tien[1*], Nguyen Ba Thuy[2], Pham Khanh Ngoc[2], Bui Manh Ha[3], Vu Hai Dang[4], Nguyen Kim Cuong[5], Nguyen Viet Hang[5]

[1] Vietnam Institute of Meteorology, Hydrology and Climate change;
No. 23/62 Nguyen Chi Thanh, Lang Thuong, Dong Da, Hanoi.

[2] Vietnam National Hydrometerological Forecasting Center Hanoi,
No 8, Phao Dai Lang, Dong Da, Ha Noi

[3] Oceanography center, No 8, Phao Dai Lang, Dong Da, Ha Noi

[4] Institute of Marine Geology and Geophysics, VAST, 18 Hoang Quoc Viet St,
Hanoi, Vietnam Type the author addresses here

[5] VNU University Of Science, 334 Nguyen Trai, Hanoi, Vietnam

[6]Center for Environmental Fluid Dynamics, University of Science,
Vietnam National University, Hanoi

Email: phamvantienbn@gmail.com[2]; thuybanguyen@gmail.com[1];
ngocpkchibo@gmail.com[1]; manhhamhc@gmail.com[1]; vuhaidang@hotmail.com[4];
cuongnk@hus.edu.vn[5]; viethang1485@gmail.com

Abstract: In this study, the interaction of surge and wave in strong/supper typhoon in the North Central coastal area of Vietnam was investigated by a coupled model of surge wave and tide (called: SuWAT). The numerical model then applied to simulate storm wave and surge for the cases of typhoon, Wukong (2000) and Talas (2017). The super typhoon case was assumed by keeping the track and landfall time of typhoon Talas but increasing the intensity up to the level of 16 (Beaufort scale). The numerical results showed good agreement with observation data on storm surge and wave height. In general, the wave height is higher near the coast and lower off shore in considering the interaction of tide and storm surge on storm wave. The results also indicated that the surge-wave interaction is crucial to the both storm surge and wave simulation. In the case of super typhoon, the difference results between the case with and without considering the interaction of wave and storm surge of 40% and 50%, respectively. This study is usefull for improving the technology of storm wave prediction in this area.

1. INTRODUCTON

History has recorded many storms that generated high surge and large waves causing severe damage to the North Central coastal area such as Dan (1989), Wukong (2000), Damrey (2005), and Doksuri (2017). Previous studies have shown that the North Central Coast area in Vietnam may experience super typhoon up to level 16 [7]. This suggests that the region is susceptible to extremely powerful and destructive storms, which could have significant impacts on the area.

Storm surge and waves are processes that occur simultaneously in a storm, with a strong interaction between them. The interaction between storm surge and waves is a complex phenomenon that occurs due to the combined effects of storm surge and wind-generated waves, which can amplify the impact on coastal areas. Changes in water level and flow field

affect wave propagation, wave breaking process, and other wave characteristics. At the same time, the surface and bottom stresses are regulated by the waves, and the radiation stress generated by the waves affects the water level and flow field. The mechanism of the interaction between surge and waves are studied using a coupled model. The ability to easily modify the component forces in the simulation allows for a detailed analysis of how surges and waves interact.

Several studies have examined the impact of surface stress due to waves, showing that the integrated model has significantly improved the storm surge calculation results when compared to monitoring data, especially for coastal areas. Funakoshi et al (2008) combined the ADCIRC storm surge simulation model and the SWAN wave model and showed that wave surges can contribute 10-15% to the extreme storm surge levels [6]. Research by Chen et al (2010) concluded that, during Hurricane Katrina in 2005 in the United States, surge due to coastal wave effects accounted for 80% of the extreme water level rise while other influences such as Tides, surface waves and wind surges contribute only 20% [2]. Kim et al (2008) built an integrated model of surge, waves and tide (Surge Wave and Tide - SuWAT), with a caged grid design to calculate storm surge in Tosa Bay - Japan. and gave results that were very consistent with the measurement data. The study also shows that the results of calculating surge due to wave radiation stress depend on spatial resolution, and the height of surge becomes larger as the spatial resolution increases [10]. Xinru Feng et al (2011) evaluation of the impact of wave-induced radiation stress on storm surge during Typhoon Saomai using a coupled wave-current model based on the ROMS ocean model and the SWAN wave model. The results show that radiation stress can cause both set-up and set-down in the storm surge. The maximum wave-induced set-up occurs on the right side of the Typhoon path, whereas the maximum wave induced set-down occurs on the left side [4]. Marsooli and Lin (2018) utilized the ADCIRC-SWAN coupled model to simulate sea level extremes induced by tropical cyclones in the western North Atlantic from 1988 to 2015. The study discovered that in most coastal areas, peak wave surges were about tens of centimeters, and the contribution of wave surges to peak water levels caused by the most extreme storm events was less than 17% [12]. Li et al (2020) investigated the impact of storm scale and intensity on the interaction between storm surge and waves in the northeast East Sea using the coupled ADCIRC-SWAN model. As storm intensity or size increased, both the maximum value and spatial extent of simulated significant wave height and storm surge increased significantly [11]. The contribution of wave surge to peak storm surge increased nonlinearly as storm intensity and scale increased. In Vietnam, the influence of grid resolution on surge results due to wave radiation stress is also discussed in some studies [3, 17, 15, 16]. These studies have shown that the impact of the interaction between surge, waves and tide on storm surge in the northern coastal region of Vietnam, helps improve the accuracy of storm surge simulation up to 30%. It also shows that the wave-induced radiation stress is an important factor and depends on the spatial resolution. Surge-wave interaction combined wave-dependent drag and radiation stress contributed to a 25% increase in total surge levels during storms Ketsana (2009) and Nary (2013) [17].

In general, studies on coupled models and interaction mechanisms between storm surge and waves have been developed but there is still a lack of evaluation and comparison in strong/super storm conditions. In this study, we selected the North Central coastal region of Vietnam (Figure 1) to conduct a systematic comparative study of the interaction between

surge and waves caused by strong storms/super storms. First, the coupled model was verified with observational data in the cases of typhoons Wukong (2000) and Talas (2017). Then, the numerical model is applied to simulate for the cases of strong/super typhoons. The super typhoon cases was assumed by keeping the track and landfall time of typhoon Talas but increasing the intensity up to the level of 16 (Beaufort scale).

2. DATA AND METHOD

2.1. Data

The study used four level grid system. The outermost domain D1 covers the whole Gulf of Tonkin and the northern coast of Vietnam, domain D2 was set to cover the coast from Thanh Hoa to Ha Tinh provinces of Vietnam, domain D3 covered the coast of Nghe An and Ha Tinh provinces and the innermost domain D4 is focused on Hon Ngu station (Figure 1 (a), (b)). Seabed topographic maps at scales of 1/50,000, 1/100,000, 1/200,000, and 1/500,000 published by the Vietnam General Administration of Seas and Islands were used. The spatial resolution for D1, D2, D3, and D4 in both X and Y directions is 11,000m, 5,500m, 1,100m, and 220m.

The least squares method was used for tidal harmonic analysis to predict the tides, and then the tides were removed from the observed water levels of Hongu station to obtain the sea surges (Huan, 2011).

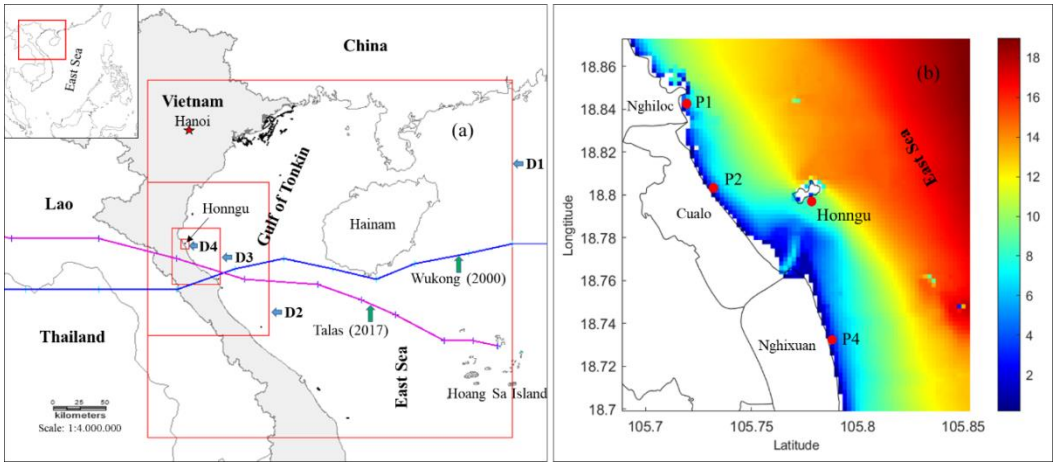


Figure 1. *(a) The location map of four domains, the typhoons track of Wukong (2000) (blue line) and Talas (2017) (purple line); (b) Bathymetry domain D4 and location of four points P1, P2, Honngu station and P4.*

Typhoon Wukong (2000) and Typhoon Talas (2017) were selected for validating the model, and the parameters of both storms were collected from the Digital Typhoon Dataset [18]. Typhoon Wukong formed in the eastern region of the East Sea on September 6, and it intensified into a storm, reaching its maximum intensity with a maximum wind speed of 75 knots (level 13 of the extended Beaufort scale) at 06:00 on September 8. Subsequently, Typhoon Wukong weakened and made landfall in Ha Tinh province of Vietnam at 03:00 on September 10 with a maximum wind speed of 45-50 knots (level 10 of the Beaufort scale). Typhoon Talas formed on July 13, and it intensified into a storm before making landfall in Vietnam's Ha Tinh province at its maximum intensity, with a maximum wind speed of 50 knots (level 10 on the Beaufort scale).

2.2. Method

The coupled model of surge, wave and tide (called SuWAT), developed by Kim et al. (2008, 2010, 2015) was used. SuWAT is capable of doing parallel computations for an arbitrary number of domains using the Message Passing Interface (MPI). In this study, two modules of surge and wave are integrated into SuWAT as shown in Figure 2 that reveals the information of the flow among the modules and the domains. Coupling parameters include open boundary values, internal exchange among modules and domains in a machine. The calculations are sequentially carried out from the higher level domain to the lower level; the rest of the lower level domains wait for the completion of the higher level domain at a time step. This modeling system has been implemented and verified in other studies [10, 3, 17, 16].

Surge model: The surge model solves the depth-averaged, nonlinear shallow-water equations using the staggered Arakawa C grid in space and the leapfrog scheme in time. The explicit finite difference scheme is used with the upwind method. The solid boundary condition is adopted at land boundaries for no inundation conditions. The radiation condition along open boundaries is given by following Flather's method (1994) in all domains. The current and sea surface level in the coarse grid domain are transferred to the nested open boundaries in the fine grid domain at each time step of 1 s. The time step is 1 s for the surge model.

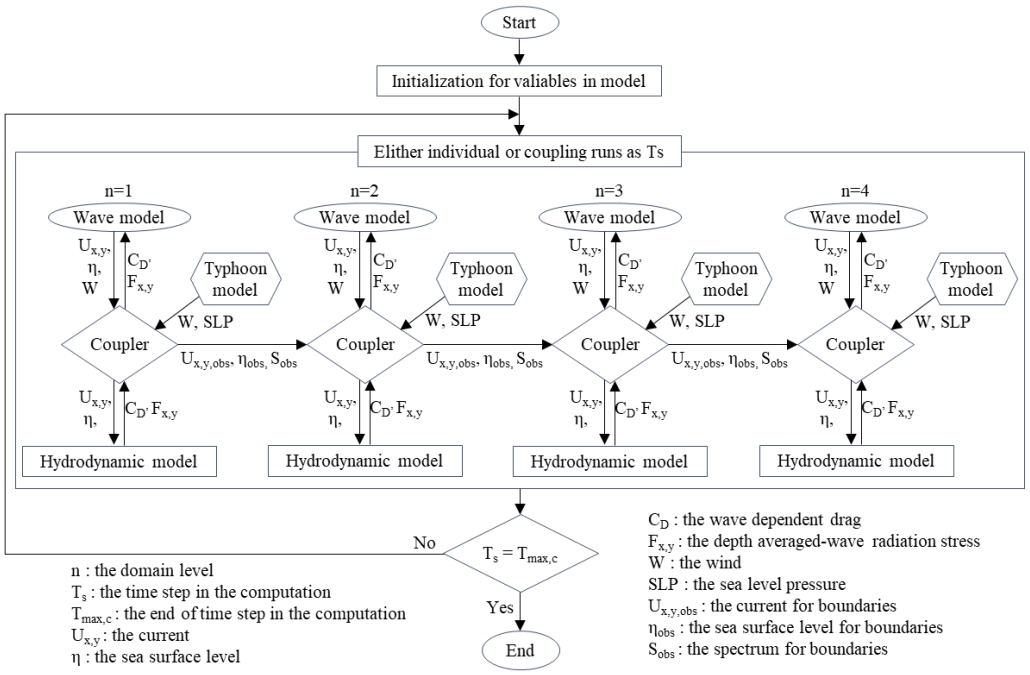


Figure 2. *Framework of SuWAT for four level domains that shows the information flow between surge and wave modules in each domain.*

Wave model: The simulating waves nearshore (SWAN) model [1] version 40.41 has been integrated into SuWAT as the wave module [10]. An Ursell number of 10 is used for the limit of the quadruplet interaction, with a factor of 1.0 for the fraction of breaking waves. The following discretizations were used: the direction resolution is 108, and the frequency range is 0.05 to 1.00 Hz. In the outermost domain, the wave spectrum along open boundaries is estimated by the Joint North Sea Wave Project spectrum, with a peak enhancement parameter of 3.3, the peak period, and a directional width of 108. The wave

spectrum in the coarse grid domain is transferred to the open boundaries in the fine grid domain at each time step of 900 s. The time step is 900 s for the wave model.

Typhoon model (parametric wind and pressure):

A parametric wind and pressure model implemented in the SuWAT model is used to estimate typhoon wind and pressure fields. Schloemer's formula (1954) is used for the pressure [14]:

$$P = P_c + \Delta P exp\left(\frac{r_0}{r}\right) \quad (1)$$

where P is the atmospheric pressure at distance r from the center, P_c is the central atmospheric pressure, ΔP is the difference between P and P_c, and r_0 is the radius to the maximum wind.

Fujii and Mitsuta's formula (1986) for the surface wind is written as follows [5]:

$$V_{gr} = r_t\left(\sqrt{\frac{f^4}{r} + \frac{r_0 \Delta P}{\rho_a r^2 r_t} exp\left(\frac{r_0}{r}\right)} - \frac{f}{2}\right) \quad (2)$$

where V_{gr} is the geostrophic wind and r_t is the following relation:

$$r_t = r/\left(1 + \frac{U_{10}}{V_{gr}} sin\beta\right) \quad (3)$$

In Equation (3), V_{gr} and U_{10} are at the previous time step. Here, b is the degree between the typhoon moving direction and the direction to r in the anticlockwise direction. U_{10} is calculated by multiplying V_{gr} by G(x) as follows:

$$G(x) = G(\infty) + \left[G(x_p) - G(\infty)\right]\left(\frac{x}{x_p}\right)^{k-1} exp\left(1 - \frac{1}{k}\right)\left[1 - \left(\frac{x}{x_p}\right)^k\right] \quad (4)$$

$$U_{10} = V_{gr} G(x) \quad (5)$$

where $x = r/r_0$, k = 2.5, xp = 0.5, $G(x_p) = 1.2$, and $G(\infty) = 0.667$ are given by Fujii and Mitsuta (1986). In the wind model, the geostrophic wind is reduced by a factor of G(∞). Finally, the wind at a 10-m height is obtained from the vector sum of the wind at a 10-m height calculated by Equation (5) and the typhoon moving speed. In the present model, deformation of the core structure in the typhoon is not considered.

A series of numerical simulations is summarized in Table 1. For the historical storm surge simulations of typhoons Wukong (2000) and Talas (2017) and hypothetical typhoon level 16, the cases of uncoupled and coupled surge with wave ware executed. In the uncoupled case surge with waves, storm surge is calculated using Honda and Mitsuyasu's (1980) conventional drag coefficient. In the coupled case surge with waves, both the drag coefficient dependent on waves by Janssen (1989, 1991) and wave radiation stress are used in storm surge simulation [17].

For the surge model, the Manning number (n = 0.025) is used in all four domains. For the wave model, the wave breaking coefficients (α = 1.0, γ = 0.73), rough layer length (kn = 0.05), and diffraction coefficient (cgmod = 1) are used in all four domains.

Simulation parameters for two storms, including time, longitude, latitude, and pressure at the center (Pc), were collected from [18]. For a hypothetical super typhoon level 16, the pressure at the center Pc is 930 mb, and the maximum wind speed is 105 knots. For all storms, the maximum wind radius (r_o = 45 km) and travel speed (V_m = 15 km/h).

Table 1. List of the numerical experiments.

Typhoons	Simulation Case	Conventional the Drag Coefficien (without wave effect)	Wave-Dependent Drag	Wave Radiation Stress
Historical typhoons: Wukong (2000) and Talas (2017)	Uncoupled surge with wave (Uncoupled)	Yes	No	No
	Coupled surge with wave (Coupled)	No	Yes	Yes
Hypothetical super typhoon up to level of 16	Uncoupled	Yes	No	No
	Coupled	No	Yes	Yes

3. RESULTS

3.1. Model calibration and validation

The SuWAT model was calibrated and validated for surges caused by Typhoon Wukong (2000) and Typhoon Talas (2017). The results show that, in the coupled case, both the drag coefficient dependent on waves and wave radiation stress, the surge peak levels at Hon Ngu station match the observations better than in the uncoupled case, only the conventional drag coefficient, in both storms (Figure 3). The difference in the largest surge between these two cases in typhoon Wukong and typhoon Talas is 0.2 cm and 0.15 cm, respectively. It can be said that the surge-wave interaction improves the surge height (Thuy et al, 2017).

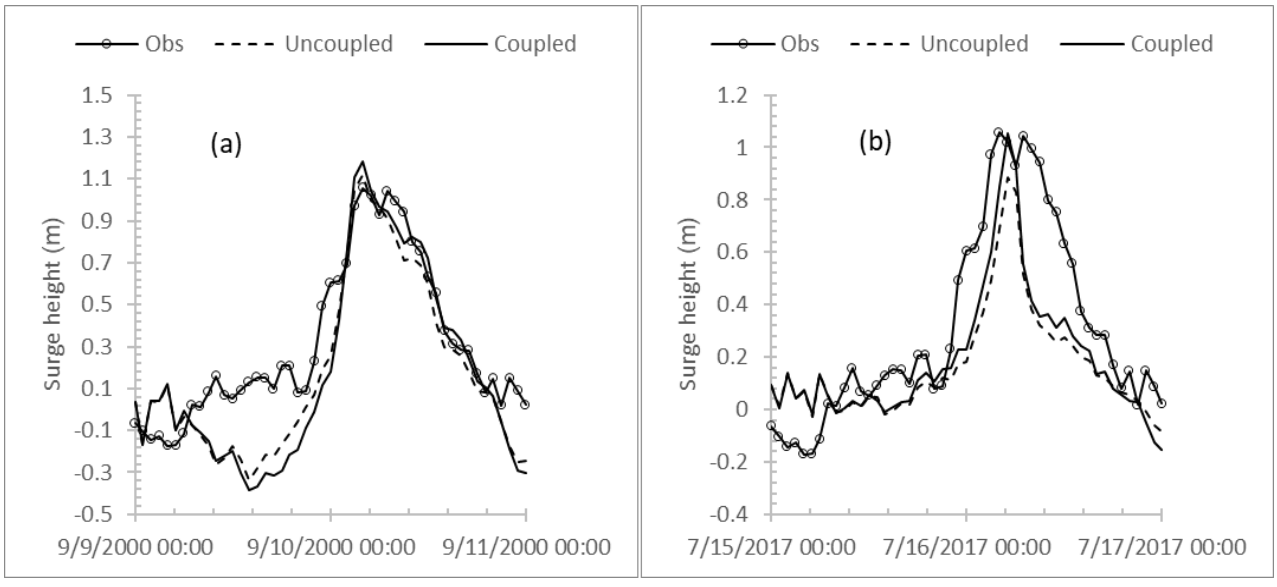


Figure 3. *Time series of calculated and observed surge heights at Honngu station because typhoons of Wukong (a) and Talas (b).*

To evaluate the model, statistical criteria such as the Coefficient of Correlation (R), the Mean Error (ME), and The Root Mean Squared Error (RMSE) are used. The criteria analysis results are very good, as shows in the Table 2.

Table 2. The coefficients of the model calibration and validation.

Typhoons	Simulation Case	R	ME	RMSE
Wukong (2000)	Uncoupled	0.91	-0.13	0.18
	Coupled	0.89	0.20	0.25
Talas (2017)	Uncoupled	0.81	-0.29	0.32
	Coupled	0.82	-0.27	0.30

The spatial distribution of the peak surges because of Typhoon Wukong and Typhoon Talas is depicted in Figures 4 and 5. The maximum surges in the coupled case (Figure 4 (b) and Figure 5 (b)) is higher and shows a greater distribution in both along-shore and cross-shore directions compared to the uncoupled case (Figure 4 (a) and Figure 5 (a)). This confirms the important role of surge-wave interaction in storm surges.

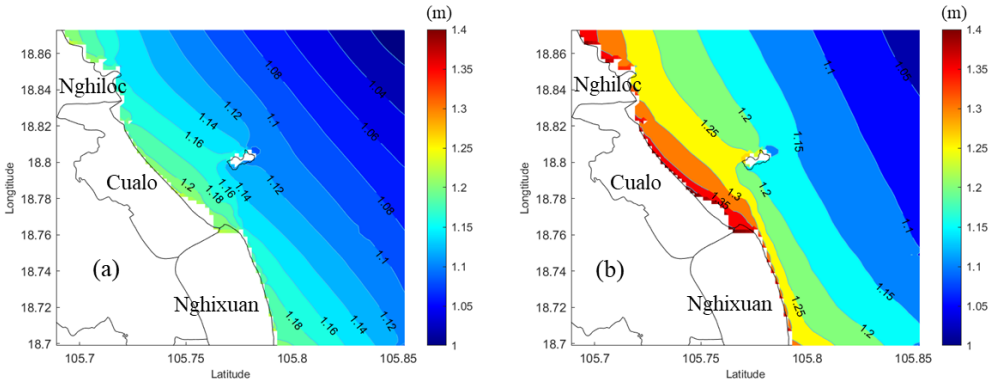


Figure 4. *Spatial distributions of the peak surge levels because of the typhoon Wukong (2000): (a) case uncoupled; (b) case coupled*

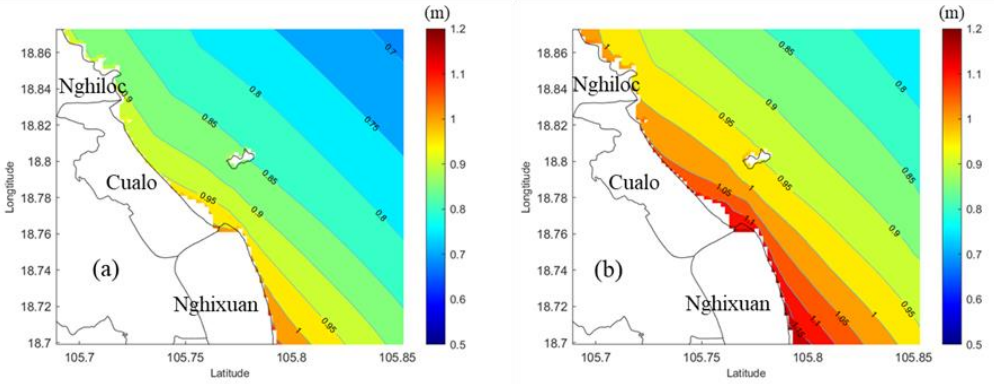


Figure 5. *Spatial distributions of the peak surge levels because of the typhoon Talas (2017): (a) case uncoupled; (b) case coupled*

3.2. Interaction of surge and wave on super typhoon

To evaluate the storm surge-wave interaction of a super typhoon, we assume that a super typhoon with level 16 (Beaufort scale) has the track and landfall time of Typhoon Talas (2017), and calculate for the case of uncoupled only considers the normal drag coefficient and the case of coupled considers both the drag coefficient and wave radiation stress. The influence of surge-wave interaction is considered by subtracting in the case of uncoupled from the maximum storm surge and significant wave height in the case of coupled, this difference is normalized in percentage compared to the uncoupled case. Changes in peak

surge and maximum significant wave height due to the superstorm are presented in Figures 6 and 7. The results show that, at 4 points along the coast P1, P2, Honngu and P4 (Figure 1b), the maximum storm surge in the case of coupled is greater than in the case of uncoupled in the order of 1.51 m, 1.47 m, 1.36 m and 1.38 m, corresponding to 46.08%, 42.64%, 42.33% and 36.35% (Figure 6). For waves, this difference is 0.82 m, 0.78 m, 0.66 m and 0.78 m, corresponding to 40.08%, 33.40%, 23.29% and 38.92% (Figure 7). The degrees behind the 4 points are -1 m, -1.8 m, -3.4 m and -1 m, respectively. These show that, at the Honngu point with the maximum depth of -3.4 m, the surge-wave interaction has less influence on the significant wave height than at points with smaller depths.

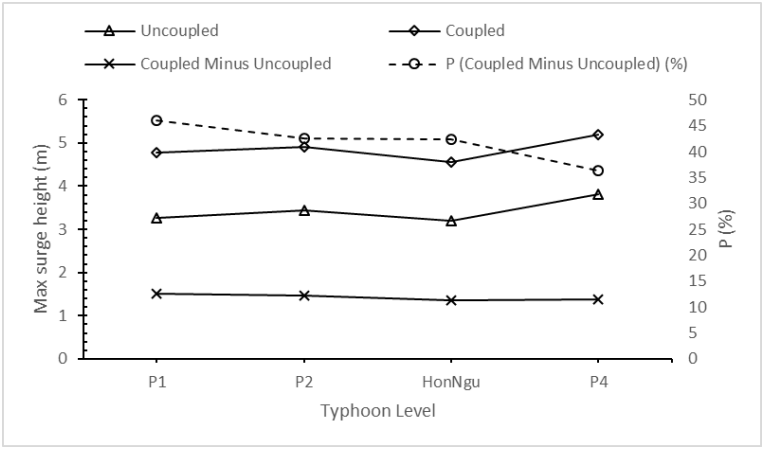


Figure 6. *Changes of peak surge because of hypothetical super typhoon level 16: (a) the uncoupled case, (b) the coupled case, (c) coupled minus uncoupled, (c) coupled minus uncoupled displayed as percentages.*

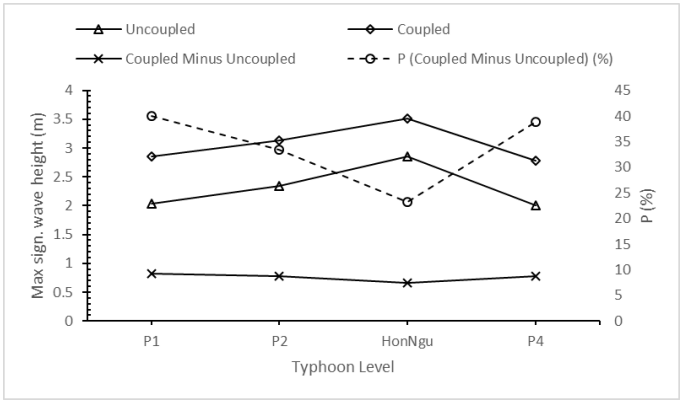


Figure 7. *Changes of maximum significant wave height because of hypothetical super typhoon level 16: (a) the uncoupled case, (b) the coupled case,, (c) coupled minus uncoupled, (c) coupled minus uncoupled, displayed as percentages.*

When considering the entire D4 calculation domain, the difference in the surge in the two cases can be up to 1.5 m, corresponding to a ratio of approximately 50% (Figure 8 (c) and (d)). It is worth noting that the surge improved most significantly in Nghiloc in the northern, gradually decreased in Cualo, and finally in Nghixuan in the south (Figure 8 (c)). Meanwhile, the largest surge in the case of uncoupled has the opposite distribution, gradually increasing from north to south (Figure 8 (a)). At the same time, the distribution of maximum significant wave height between regions is quite similar because it depends mainly on the impact of wind and terrain (Figure 9 (a)). These show that surge-wave

interaction improves maximum surge height most strongly in areas with lower surge height but equivalent wave height. For significant wave height, this interaction improves wave height significantly most strongly in shallow water areas, where there is a significant change in water depth caused by surge (Figure 9(c)).

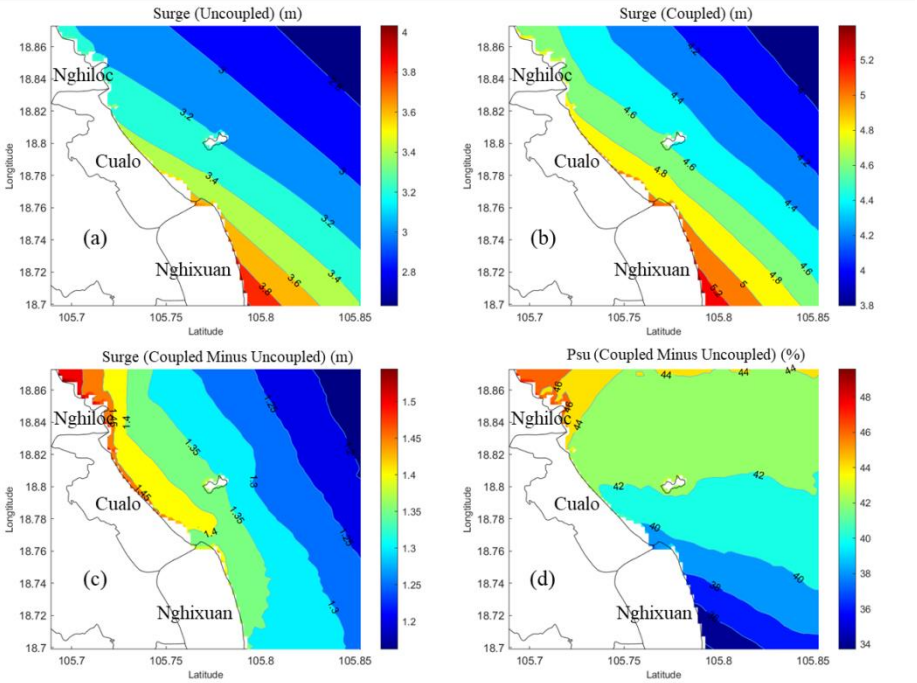


Figure 8. *Spatial distributions of the peak surge levels because of hypothetical super typhoon level 16: (a) the uncoupled case, (b) the coupled case, (c) coupled minus uncoupled, (d) coupled minus uncoupled displayed as percentages.*

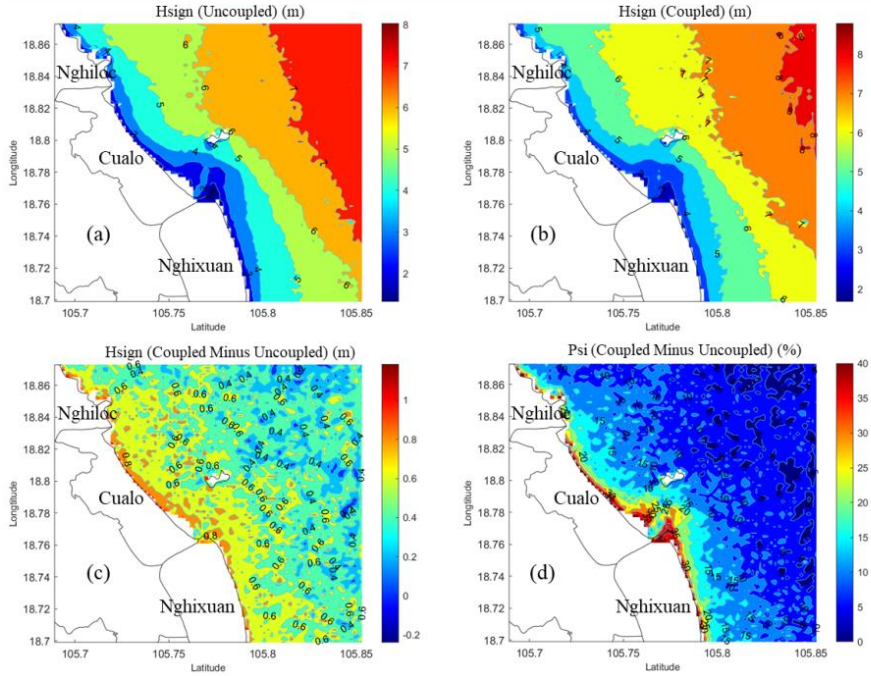


Figure 9. *Spatial distributions of maximum significant wave height because of hypothetical super typhoon level 16: (a) the uncoupled case, (b) the coupled case, (c) coupled minus uncoupled, (d) coupled minus uncoupled displayed as percentages.*

4. CONCLUSIONS

This study examined the impact of surge-wave interaction on surge height and significant wave height during a superstorm using the SuWAT coupled model. Model validation was based on surge observations at Honngu station during Typhoon Wukong (2000) and Typhoon Talas (2017). In the case of coupled, both the drag coefficient and the wave radiation stress were considered, the simulation results have a closer correlation with the observations than in the case of uncoupled, only the normal drag coefficient was considered. Simulated two cases coupled and uncoupled to evaluate surge-wave interaction in a super typhoon. The results show that surge-wave interaction plays an important role in the distribution of surge height and significant wave height. This interaction can contribute up to 50% of total nearshore storm surge and more than 40% of significant wave height. Overall, the study results are consistent with some previous research [2, 6, 17]. However, this study only evaluated the case of a super typhoon level 16, so further studies are needed to evaluate in detail the surge-wave interaction at different levels of typhoons.

ACKNOWLEDGEMENTS

This research is funded by the Ministry of Science and Technology of Vietnam under grant number ĐTĐL_CN-46/22, which the authors gratefully acknowledge.

REFERENCES

[1] Booij N, Ris RC and Holthuijsen L.H. A third-generation wave model for coastal regions, part I, model description and validation. Journal of Geophysical Research 1999; 104 (C4), 7649–7666.

[2] Chen, X.; Ji, P.; Wu, Y.; Zhao, L (2010). Coupling simulation of overland flooding and underground network drainage in a coastal nuclear power plant. Nucl. Eng. Des. 2017, 325, 129–134.

[3] Chien, D.D., 2015. Researching the Scientific Basis to Assess the Storm Surge in the Sea Areas from Quang Binh to Quang Nam. Hanoi, Vietnam: University of Science–Vietnam National University, Ph.D. dissertation, 117p [in Vietnamese].

[4] Feng, X., Yin, B.S., Dezhou, Y., Perrie, W. (2011). The effect of wave-induced radiation stress on storm surge during Typhoon Saomai (2006), Acta Oceanol. Sin., 2011, Vol. 30, No. 3, p.20-26.

[5] Fujii, T. and Mitsuta, Y., 1986. Synthesis of a stochastic typhoon model and simulation of typhoon winds. Annuals of the Disaster Prevention Research Institute, 29(B-1), 229–239 [in Japanese].

[6] Funakoshi, Y., Hagen, S.C., Bacopoulos, P. (2008). Coupling of hydrodynamic and wave models: case study for Hurricane Floyd (1999) Hindcast, Journal of Waterway, [3] Port, Coastal and Ocean Engineering, (134), pp. 321 – 335.

[7] Nguyen Xuan Hien, Nguyen Van Thang, Tran Thuc, Nguyen Van Hiep, Huynh Thi Lan Huong, Mai Van Khiem. Study of typhoon zoning and determination of typhoon and storm surge risks during super typhoon landing. Journal of climate change science. No. 17 – March 2017.

[8] Huan, P.V. Tide forecasting by harmonic analysis. Science and Technology Publishing House, Hanoi, 2011.

[9] Janssen, P.A.E.M., 1989. Wave-induced stress and the drag of air flow over sea waves. Journal of Physical Oceanography, 19, 745–754.

[10] Janssen, P.A.E.M., 1991. Quasi-linear theory of wind-wave generation applied to wave forecasting. Journal of Physical Oceanography, 21, 1631–1642.

[11] Kim SY, Yasuda T, and Mase H (2008). Numerical analysis of effects of tidal variations on storm surges and waves. Applied Ocean Research 2008; 30, 311-322.

[12] Kim SY, Yasuda T and Mase H. Wave set-up in the storm surge along open coasts during Typhoon Anita, Coastal Engineering 2010; ASCE, 57, 631–642.

[13] Kim SY, Matsumi Y, Yasuda T and Mase H. Storm surges along the Tottori coasts following a typhoon, Ocean Engineering 2014; 91, 133-145

[14] Kim SY, Mori N, Mase H and Yasuda T. The role of sea surface drag in a coupled surge and wave model for Typhoon Haiyan 2013, Ocean Modelling 2015;.doi:10.1016/j.ocemod.2015.06.004.

[15] Li, A.; Guan, S.; Mo, D.; Hou, Y.; Hong, X.; Liu, Z. Modeling wave effects on storm surge from different typhoon intensities and sizes in the South China Sea. Estuar. Coast. Shelf Sci. 2020, 235, 106551.

[16] Marsooli, R.; Lin, N. Numerical Modeling of Historical Storm Tides and Waves and Their Interactions Along the U.S. East and Gulf Coasts. J. Geophys. Res. Ocean. 2018, 123, 3844–3874.

[17] Mastenbroek, C., Burgers, G., Janssen, P.A.E.M., (1993). The dynamical coupling of a wave model and a storm surge model through the atmospheric boundary layer, Journal of Physical Oceanography, (23), pp. 1856-1866.

[18] Schloemer, R.W., 1954. Analysis and Synthesis of Hurricane Wind Patterns over Lake Okechobee. Washington, D.C.: U.S. Government Printing Office, Report No. 31, 49p.

[19] Thai T.H., Thuy N.B., Dang V.H., Kim S., Hole L.R. (2017). Impact of the interaction of surge, wave and tide on a storm surge on the north coast of Vietnam. Procedia IUTAM, 25 , pp. 82-91.

[20] Pham Van Tien, Pham Khanh Ngọc, Pham Quoc Hung, Nguyen Kim Cuong, Nguyen Ba Thuy. Effect of waves during the storm on coastal inundation in Thai Binh province. Journal of Hydro-Meteorology 2021, 724, 72-81; doi:10.36335/VNJHM.2021(724).72-81

[21] Thuy, N.B., Kim, S., Dang, V.H., Cuong, H.D., Wettre, C., Hole, L.R. (2017), Assessment of Storm Surge along the coast of Central Vietnam. Journal of Coastal Research, 33, 518-530.

http://agora.ex.nii.ac.jp/digital-typhoon/

PREDICTION OF INCREMENTAL CASES OF DEATH DUE TO HIGH TEMPERATURE IN HO CHI MINH CITY, VIETNAM BASED ON RCP4.5 AND RCP8.5 SCENARIOS

Phung Duc Nhat[1*], Tran Ngoc Dang[2], Duong Thi Minh Tam[1], Dang Van Chinh[3], Phu L Vo[4,5*]

[1] University of Medicine Pham Ngoc Thach, 2 Duong Quang Trung street, District 10, Ho Chi Minh City, Vietnam

[2] University of Medicine and Pharmacy Ho Chi Minh City, 217 Hong Bang Street, District 5, Ho Chi Minh City, Vietnam

[3] Institute of Public Health, 159 Hung Phu Street, District 8, Ho Chi Minh City, Vietnam

[4] Faculty of Environment and Natural Resources, Ho Chi Minh City University of Technology (HCMUT), 268 Ly Thuong Kiet Street, District 10, Ho Chi Minh City, Vietnam

[5] Vietnam National University Ho Chi Minh City, Linh Trung ward, Thu Duc District, Ho Chi Minh City, Vietnam

Corresponding authors: nhatphd@pnt.edu.vn; volephu@hcmut.edu.vn

Abstract: Climate change is leading cause of an increase in average temperature. The number of heat waves led to a harmful effect on the community health. In general, it will cause an increase in mortality caused by high temperature. This study predicts the number of incremental deaths by high temperature in Ho Chi Minh City (HCMC) by an interval decade of 2020 - 2050. Data of death cases was registered in 322 community health centers of 24 districts of HCMC (A6 logbook). The results showed that the incremental cases of death with the RCP4.5 scenario for the decades of 2020s, 2030s and 2040s are 4619, 2828 and 3248, respectively. With the RCP8.5 scenario for decades of 2020s, 2030s and 2040s, the incremental cases are predicted consecutively as 3070, 7259 and 3569, respectively. This study provided useful information on the impact of high temperature on number of deaths in HCMC. This finding implies that the City's authorities need to have policies to reduce the number of deaths and to adapt with an increase in high temperature impact due to climate change to people's health.

Keywords: *High temperature, heat wave, mortality, incremental death, Ho Chi Minh City, Viet Nam*

1. INTRODUCTION

On the report of International Panel on Climate Change (IPCC), developing countries were addressed as the most affected by global climate change [1]. Accordingly, Vietnam is the seventh countries out of ten most suffered from climate change impacts [2].

The heat waves can increase in hospital admission and deaths especially in the elderly and chronic diseases patients. In 2003, heat waves in Europe have caused 70,000 cases of death [3]. In May and June 2015, the heat waves attacked India and Pakistan and temperature raised to 49°C leading to nearly 5,000 deaths [4,5]. The cause of immediately deaths by heat stroke mostly were congestive heart failure because these patients are more prone to die due to extreme high temperature [6,7].

A recent meta-analysis study by Nu Quy Linh Tran et al. in Vietnam indicated that a 1°C above the 19°C increase the hospitalization risk at 0-3 days' lag for all causes and infectious diseases by 0.8% and 2.4%, respectively [8]. Kristie L Ebi et al. studied health risk of hot

weather and heat extremes revealed that extreme heat can cause over-sweating which can lead to kidney injuries and failure, a concern for outdoor workers in mesoamerica, India, and other regions [9]. Ollie Jay et al. in a study on reducing the health effects of hot weather and heat extremes showed that air-conditioning was not a good solution. In heat extreme situation, when peak demand of electricity supply exceeded maximum supply by electricity grid, power disruption occurred and contributed to heat-related mortality increase in Pakistan in 2015 and 2018, and in Australia, due to the prevalence of household air conditioning [10].

In 2013, IPCC announced a report of updated Representative Concentration Pathways (RCP) on the concentration of greenhouse gas distribution graph to use for prediction of global warming on different scenarios. The Ministry of Natural Resources and Environment (MONRE) of Vietnam also used these scenarios for climate change prediction in Vietnam.

Table 1. RCP scenarios till the year 2100.

RCP	Degree of radiation by the year 2100.
RCP 8.5	8.5 W/m^2
RCP 6.0	6.0 W/m^2
RCP 4.5	4.5 W/m^2
RCP 2.6	2.6 W/m^2

Source: [11]

In this study, we evaluate and predict the impact of high temperature (heat waves and high temperature) on death cases in Ho Chi Minh City, Vietnam. The prediction is carried out in a decade interval from 2020s to 2040s with a reference of Honda's prediction method based on two climate change scenarios of medium scenario RCP4.5 and high scenario RCP 8.5.

2. MATERIALS AND METHODS

A study conducted by Honda et al. (2014) to predict cases of deaths attributable to high temperature reported that this incremental number would be 19,662 cases by the year 2030 if there were no measure to adapt with the impact of climate change [12]. He also proclaimed his method on predicting of incremental of deaths cause by weather factors, especially by high temperature [12].

Data of deaths were collected from daily death reports from all health centers (322 community health centers) of all districts (24 districts) of Ho Chi Minh City by an official system set up by the national death registered system (logbook A6) for 3 years from 1st January 2010 to 31st December 2013. We also collected data of hospitalized cases of some diseases that can be affected by weather such as pulmonary diseases and heart diseases reported by Ho Chi Minh City Center for Diseases Control (HCDC) and Department of Health, HCMC.

Weather data was from stations of the whole city. Daily weather data from 1st January 2010 to 31st December 2013 were collected in the same period as mortality data. Those collected weather factors were temperature (minimum, maximum, and average), temperature range, humidity, wind speed, and rainfalls. We also use Global Climate Model (GCM) to estimate daily weather data. Scenarios of climate change of RCP4.5 and RCP8.5 were inherited from MONRE.

2.1. Method of prediction

We applied the model of heat-related mortality risk under climate change impact. This model was proclaimed by Honda et al. (2014). The procedure was conducted in two steps. The first step, we analysed and find out the short-term relation between weather factors and health outcome (mortality and morbidity of pulmonary and cardiac diseases and heat extremes). In the second step, we used GCM to estimate and anticipate the weather of HCMC in the future by an interval of decade (till 2030s and 2040s) and then predict incremental deaths due to high temperature in the future weather conditions.

The study used distributed lag non-linear model (DLNM) time-series method to forecast and considered the non-linear relation between temperatures and health outcomes, we used a cross-basis function of multiple lag-day temperatures [13]. The quasi-Poisson time series regression model were used to link daily hospitalization (outcomes or responses) with daily average weather factors (exposure) [14]. Furthermore, we analysed and adjusted for the long-term trend and seasonality.

Other studies showed that the relationship between high temperature and deaths had two features, non-linear relation and a lag time which means the relation could be demonstrated by a V- or U-shape line [15, 16]. The lag affect meant exposure to temperature could cause an immediate effect, but the effect could also happen in days after the exposure [17,18]. Therefore, the distributed lag non-linear model (DLNM) was used recently to describe and to create a model of the relation between temperature and health effect [19].

Figure 1 below shows a relation between temperature and health. The DLNM was deployed for the analysis of this study.

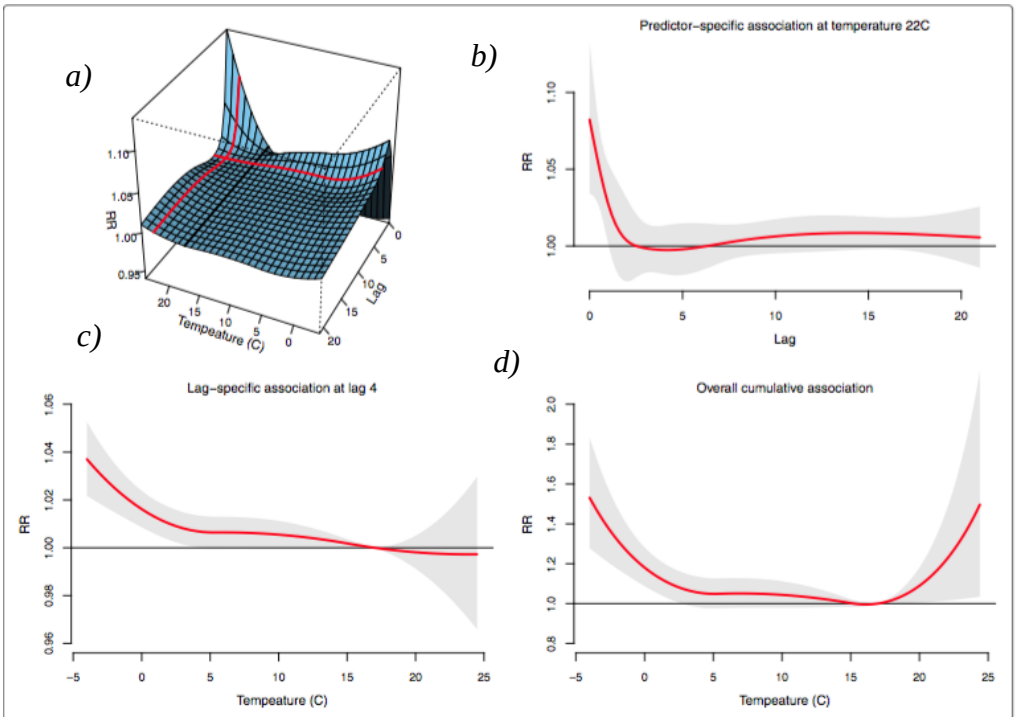


Figure 1. *Application of DLNM in studying relation of temperature and health*

Figure 1a is a 3D image of impact of lag, temperature on risk of death. Fig.1b is the impact of temperature on different lag times. Fig.1c is the impact of temperature on a fixed lag (4 days). Fig.1d is the general relationship between temperature and death risk.

3. RESULTS AND DISCUSSION

We analyzed data from this study and found out that total of deaths from 2010 to 2013 in HCMC was 101,959; 22,218 deaths by heart diseases (21.8%), 8,804 deaths by pulmonary diseases (8.63%). The highest group of deaths (58.2%) was the more than 65-year-olds elderly people. In terms of gender, the proportion of deaths for male was 54.6% and female was 45.4%.

Table 2. Duration of heat waves and median temperature in HCMC, 2010-2013

Begin-end mm/dd/yyyy	Timing (by days)	Intensity (°C) Median (min-max)
04/24 – 04/26/2010	2	31.20 (31.07 – 31.25)
05/5 – 05/21/2010	16	31.75 (30.95 – 32.10)
05/23 – 05/27/2010	4	31.12 (30.92 – 32.12)
05/30 – 06/2/2010	3	31.23 (31.02 – 31.30)
03/31 – 04/6/2013	6	31.40 (30.90 – 32.0)

During the summer time from 2010 to 2013, the basic temperature was really high (the average temperature was 31^0C and sometimes reached 32^0C) and there were heat waves during these times. Observation showed that the number of deaths also increased in these times which meant there could be a relationship between deaths and high temperature and heat waves increased risk of death. These data are shown below.

Figure 1 depicts daily hospitalization, daily mortality, daily mean temperature over time and we can recognised a slightly increase in mean temperature and death cases in summers (March to May).

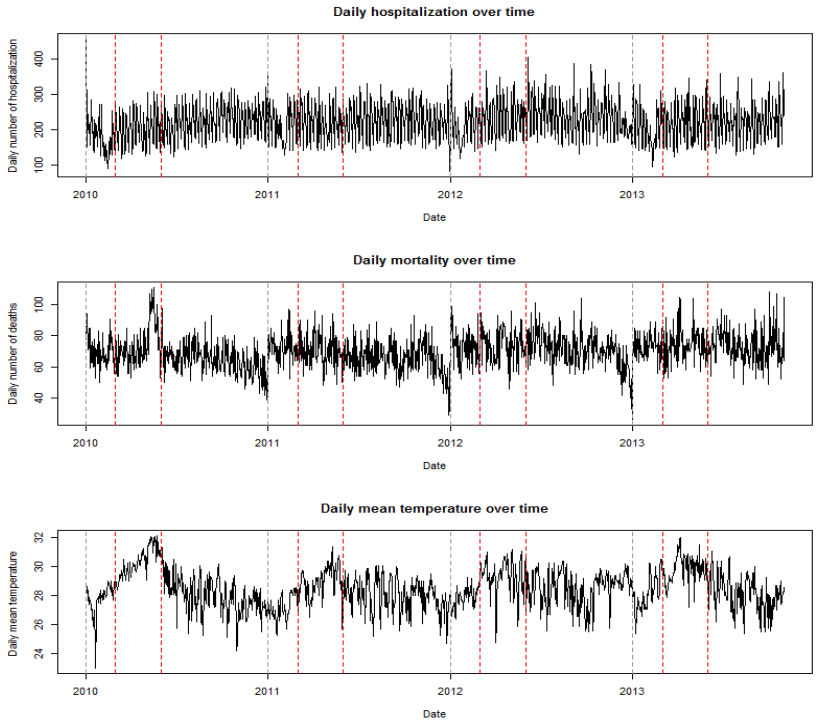


Figure 2. *Time series of daily deaths by all causes and daily hospital admission vs. mean temperature of HCMC from 2010-2013*

On the first step, we calculated the short-term relationship between temperature, deaths, and hospital admission in HCMC. This step is quite important for the long-term prediction of the relationship between these factors in mortality. Data showed that there was relationship between temperature and deaths when the mean temperature was higher than 30^0C. However, there is the lag effect when the mortality increased under a specific lag time in the period of 2010 – 2013 as shown in Figure 3.

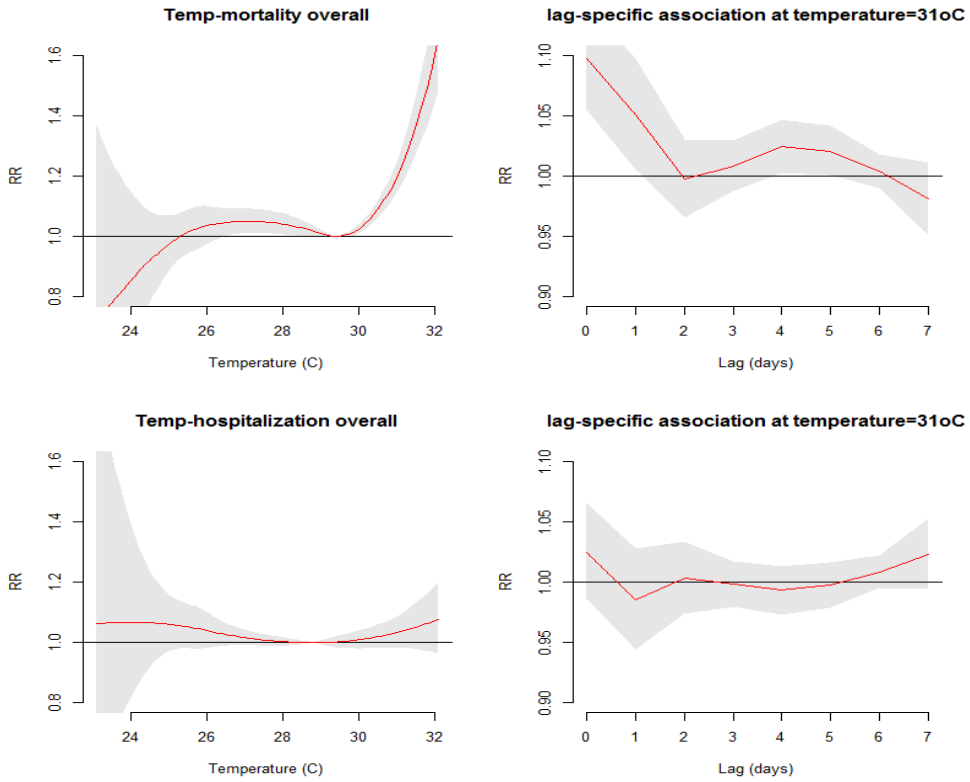


Figure 3. *Short term relationship among temperature, hospital admission, and deaths in HCMC from 2010-2013.*

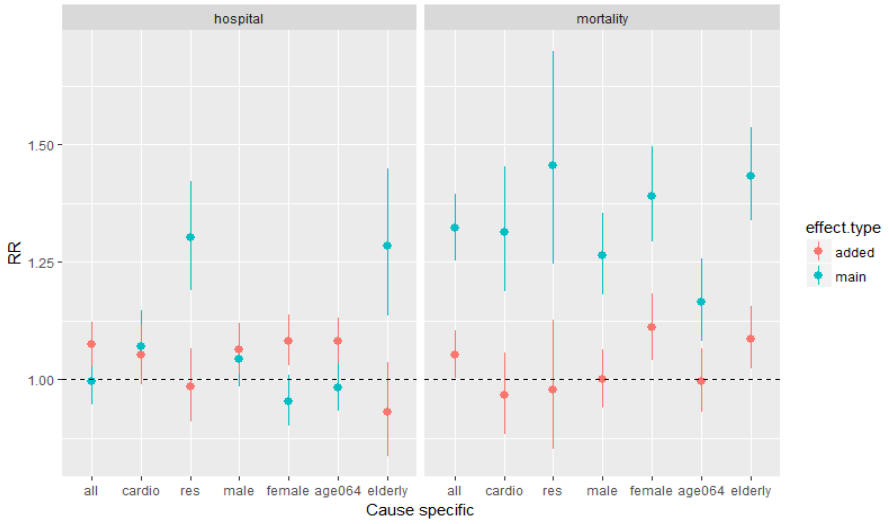


Figure 4. *Main effect and added effect of heat waves on number of deaths and hospital admission in HCMC from 2010-2013.*
age064: group from 0 to 64 years of age; cardio: cardiac diseases; res: respiratory diseases.

To measure the two effects of heat waves on deaths and admission to hospital, the main effect and the added effect, we analysed these effects of heat wave on public health. Figure 4 illustrates the two effects. Main effect increased dramatically death risk of cardiac diseases, pulmonary diseases in which death relative risk (RR) were highest for respiratory patients and the elderly (respiratory diseases, RR = 1.45, 95%CI: 1.25-1.70; the elderly RR = 1.43, 95%CI: 1.34-1.53). The added effect led to an increase in death risk for female group only, with RR = 1.11, 95%CI: 1.04-1.18.

We predicted temperature increase based on the historical temperature by decades. With basic time for temperature (historical baseline) in the period of 2006-2015 (one decade), we predicted future temperature till the end of the century (2100) on two different climate change scenarios (RCP 4.5 and RCP 8.5). Figure 5 shows that the RCP 8.5 scenario is worse than the RCP 4.5 scenario.

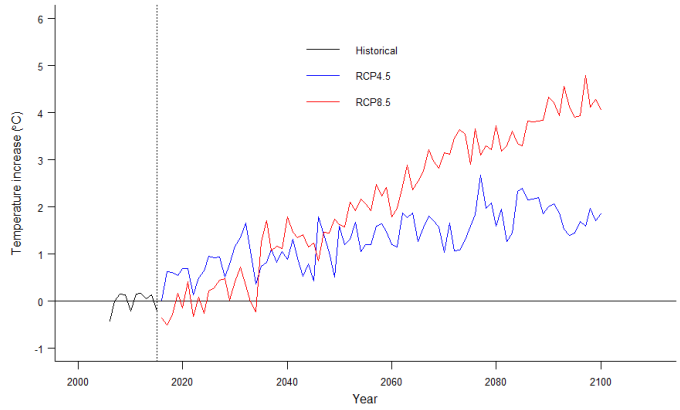


Figure 5. *Difference of temperature compared to the basic average temperature during the period of 2006-2015 of HCMC on two scenarios RCP4.5 and RCP8.5*

Figure 6 below shows basic data of daily deaths in HCMC, analysed for the period 2010 - 2013. It showed average number of deaths by day during the period of study (2010-2013) with daily deaths ranged between 60-80 cases/day during most of the time of the year and dropped at the end of the year.

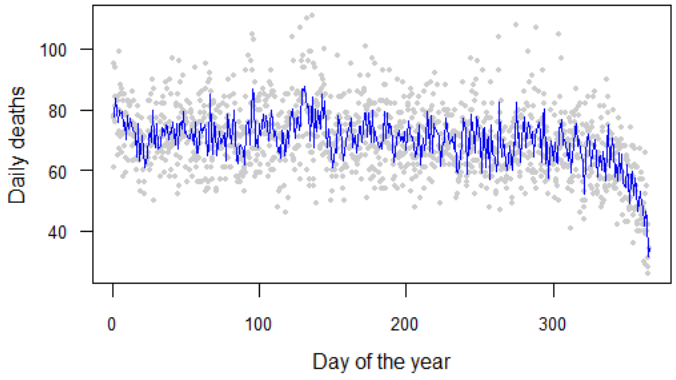


Figure 6. *Average daily number of deaths in HCMC (2010-2013).*
The dot depicts the average of daily deaths in HCMC during 2010-2013.

Data of weather in HCMC also adjusted based on GCM. The left side of Figure 7 showed observed data in a higher peak and GCM in a lower peak. The right side of Figure 7 depicted observed line compared to GCM and GCM calibrated. The black dotted line is of HCMC, the grey curve line is of GCM, and the dotted grey line is the adjusted data of HCMC after adjusted with GCM.

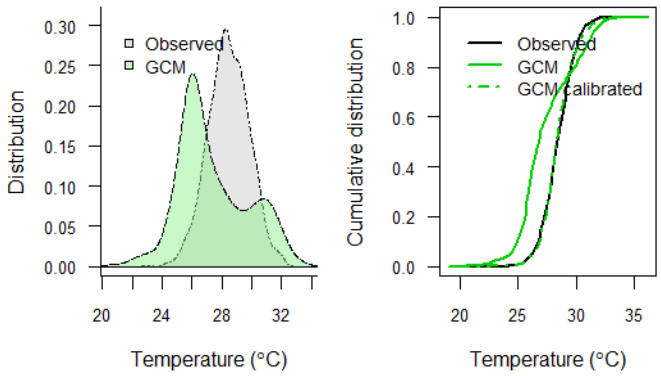


Figure 7. *Adjustment of data of HCMC using data from GCM (Global Climate Model).*

Figure 8 below shows 3D and the graph of relationship between temperature and deaths in HCMC with a U-shape relation.

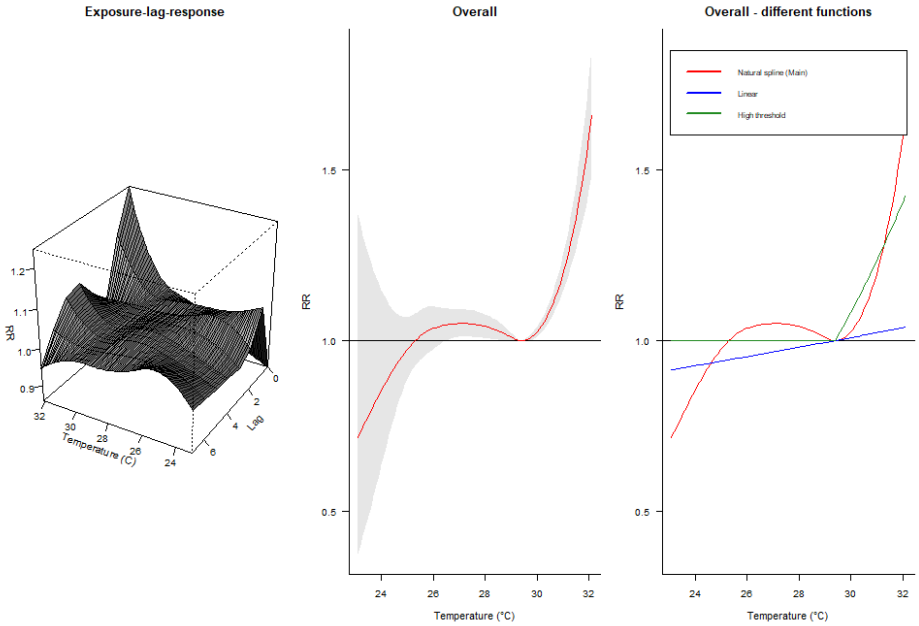


Figure 8. *Relationship between temperature and deaths in HCMC.*

The number of incremental deaths attributable to high temperature were presented in Table 3 below.

Table 3. Number of predictive of deaths attributable to high temperature during 2010-2050 on scenarios RCP4.5 and RCP8.5.

No	Decade	RCP4.5		RCP8.5	
		Number of incremental deaths attributable to high temperature	Relative increased proportion of deaths attributable to high temperature (%)	Number of incremental deaths attributable to high temperature	Relative increased proportion of deaths attributable to high temperature (%)
1	2010-2019 (baseline scenario)	600	0.2	616	0.2
2	2020-2029	4,619	1.8	3,070	1.2

3	2030-2039	2,828	1.1	7,259	2.8
4	2040-2049	3,248	1.3	3,569	1.4

4. CONCLUSION

Global climate change will lead to an increase in average ambient temperature. This will sooner or later increases the number of heat waves and extreme weather which can cause bad health impact for people living in Ho Chi Minh city.

The study predicts the incremental deaths attributable to high temperature in Ho Chi Minh city, Vietnam. The projection was calculated for two scenarios of RCP 4.5 and RCP 8.5. During the period of 2020-2050, the total number of incremental deaths attributable to hot weather and heat extremes for scenarios of RCP 4.5 and RCP 8.5 will be 10,695 and 13,898, respectively.

The groups most likely affected by heat waves were the elderly, women, those who suffered from pulmonary and/or cardiac diseases. To protect these prone groups, the formulation of public health policy and resilient approach to climate change is needed.

The city government can develop strategies such as green city, zero emission of carbon to protect people from hospitalization and death due to heat waves. Besides, there should be campaigns on health education to warn the high risk groups (the elderly, women, pulmonary patient, and cardiac patients) on the bad impact on health of heat waves and extreme hot weather so that they can protect themselves when these extreme weather conditions occur. They should stay home or use method to cool the in-house temperature to keep them safe whenever heat waves and hot temperature attack the city. Especially, adaptation measures for urban citizens are in imperative to protect community health from high temperature and heat waves.

ACKNOWLEDGEMENTS

The authors acknowledge the support of time and facilities from Ho Chi Minh City University of Technology (HCMUT), VNU - HCM for this study. We thank to Ho Chi Minh City Department of Science and Technology for its funding under the contract No.43/2018/HĐ-SKHCN.

SKHCNREFERENCES

[1] IPCC 2014 Climate Change 2014: impacts, adaptation and vulnerability. Contribution of working group II to the fifth assessment report of the Intergovernmental panel on climate change UK: Cambridge University Press.

[2] Kreft S et al. 2015 Global Climate Risk Index 2015: Who Suffers Most From Extreme Weather Events? Weather-related Loss Events in 2013 and 1994 to 2013. pp. 1-31.

[3] Robine J M et al. 2008 Death toll exceeded 70,000 in Europe during the summer of 2003 *C R Biol*. **331**(2) 171-8.

[4] Ho H C, Knudby A, Walker B B and Henderson S B 2016 Delineation of Spatial Variability in the Temperature-Mortality Relationship on Extremely Hot Days in Greater Vancouver, Canada *Environmental Health Perspectives* **125**(1) 66-75.

[5] Ho H C, Knudby A and Huang W 2015 A Spatial Framework to Map Heat Health Risks at Multiple Scales *International Journal of Environmental Research and Public Health* **12**(12) 16110-16123

[6] Argaud L 2007 Short- and long-term outcomes of heatstroke following the 2003 heat wave in Lyon, France. *Arch Intern Med.* **167**(20) 2177–2183.

[7] Stafoggia M, Forastiere F, Agostini D, Caranci N, de'Donato F, Demaria M, Michelozzi P, Miglio R, Rognoni M, Russo A and Perucci C A 2008 Factors affecting in-hospital heat-related mortality: a multi-city case crossover analysis. *J Epidemiol Community Health* **62** 209–215.

[8] Nu Linh Quy Tran, Hieu K T Ngo, Tran Ngoc Dang, Son Nghiem, Huu Quyen Nguyen and Dung Phung 2023 The association between high ambient temperature and risk of hospitalization: a time-series study in eight regions in Vietnam *Environ Res: health 1 045003*

[9] Kristie L Ebi et al Hot weather and heat extremes: health risks *Lancet 2021; 398: 698-708*

[10] Ollies Jay et al Reducing the health effects of hot weather and heat extremes: from personal cooling strategies to green cities *Lancet 2021; 398: 709-24*

[11] MONRE 2016 Climate change scenario for Vietnam Vietnam Map, Resource and Environment Publisher.

[12] Honda Y, Kondo M, McGregor G, Kim H, Guo Y-L, Hijioka Y, Yoshikawa M, Oka K, Takano S, Hales S and Kovats R S 2013 Heat-related mortality risk model for climate change impact projection *Environ Health Prev Med* **19**(1) 56-63.

[13] Gasparrini A, Armstrong B and Kenward M G 2010 Distributed lag non-linear models *Statist. Med.* **29**(21) 2224-2234.

[14] Bhaskaran K 2013 Time series regression studies in environmental epidemiology *Int J Epidemiol* **42** 1187-95

[15] Basu, R. and J.M. Samet, *Relation between elevated ambient temperature and mortality: a review of the epidemiologic evidence.* Epidemiol Rev, 2002. 24(2): p. 190-202

[16] Basu R 2009 High ambient temperature and mortality: a review of epidemiologic studies from 2001 to 2008 *Environmental Health* **8** 40.

[17] Muggeo V M and Hajat S 2009 Modelling the non-linear multiple-lag effects of ambient temperature on mortality in Santiago and Palermo: a constrained segmented distributed lag approach *Occup Environ Med* **66**(9) 584-591

[18] Baccini, M, Biggeri A, Accetta G, Kosatsky T, Katsouyanni K, Analitis A, Anderson H R, Bisanti L, D'Ippoliti D, Danova J, Forsberg B, Medina S, Paldy A, Rabczenko D, Schindler C and Michelozzig P2008 Heat effects on mortality in 15 European cities *Epidemiology* **19**(5) 711-719.

[19] Gasparrini A 2014 Modeling exposure-lag-response associations with distributed lag non-linear models *Statist. Med.* **33**(5) 881-899.

DATA PROCESSING IN ANALYSING LANDSLIDE IN THE MOUNTAINOUS AREA BY GEODETIC METHODS

Quoc Khanh Pham[1] and Thi Kim Thanh Nguyen[1]
[1]Falculty of geomatics and land aministration, University of Mining and Geology, Hanoi, Vietnam

Abstract: The task of processing displacement monitoring data and conducting deformation analysis presents a significant challenge. It necessitates not only precise data processing but also the application of an appropriate adjustment method that is in compliance with a specific process related to construction. Although adjustment methods share a common correction number for the measured values, the resulting adjusted coordinates or height differ. This paper employs landslide simulation data from the Mong Sen Bridge in Sa Pa, Lao Cai, and various adjustment methods to process the data. The outcomes of the displacement calculations are then compared to validate the aforementioned issue. However, an accurate comparison and analysis of displacement can only be achieved when the same adjustment method is consistently applied across all cycles. The results of the analysis are also precise and reliable. Furthermore, it is crucial to consider the size of the monitoring region when selecting an adjustment method to ensure that the simulation results and the trend of the landslide closely resemble reality.

1. INTRODUCTION

The system for monitoring networks, such as those used for landslide monitoring, can be structured as either a one-level or two-level network, comprising the base network and the monitoring network. The style of work and monitoring plan dictate whether data processing (adjustment) is conducted using a relative or absolute network [1]. Adjustment methods, including dependent network adjustment, free network adjustment with some stable points, and free network adjustment based on all points, are implemented through the principle of least squares [2,3].

The results obtained from these adjustment methods differ if the adjusted coordinates of points are selected as parameters, due to the varying systems of benchmarks. Utilizing the adjusted coordinates in a network without a consistent system of benchmarks for structural displacement analysis often yields incorrect results, leading to inaccurate conclusions about the state of the work [4,5,6]. Furthermore, displacement analysis also relies on the trend of structural displacement to provide a reliable evaluation.

This paper conducts an experiment to analyze the displacement results in the landslide area at Mong Sen Bridge, Sapa, Lao Cai, demonstrating that different adjustment methods yield varying results. This underscores the necessity of unifying the adjustment method across all cycles and selecting the relative or absolute method based on the scale of the construction to ensure that the results align with the displacement trend. In the experiment conducted for this paper, given the relatively extensive area of the landslide, we opted for a free grid variance model encompassing all grid points. The variance results yielded by this method are consistent, with the grid's weakest point being 7,2mm, which is the smallest in comparison to other models.

2. THEORETICAL BASE AND THE MONITORING METHOD

2.1. The process of geodetic network adjustment

When a network of displacement monitoring is adjusted with the indirect adjustment method, the process of calculation includes the following steps [7]:

Choose the adjusted coordinates of points without coordinates to be the unknown, symbol the unknown vector as $_{\delta X}$, proximate coordinate vector as X_0

Establish the system of correction equations as follows :

$$A\delta X + L = V \tag{1}$$

Where: *A* is the coefficient matrix, $_{\delta X}$ is the unknown vector, *V*, *L* are the correction vector and free number vector. If the network is free, there is lack of positioning elements, so the equation system (1) has dependent columns (the number of dependent columns equal the missing number d)

Based on the least square principle to transit the correction equation system to the standard system:

$$R\delta X + b = 0 \tag{2}$$

With $R = A^T PA; \quad b = A^T PL$

Matrix *R* depending on the adjustment method is calculated as follows:

If the network is dependent or has enough original data, *R* is non-degenerate matrix, *Det (R) # 0*, solutions of equation (2) :

$$\boldsymbol{\delta X = -R^{-1}b} \tag{3}$$

If the network is free, *R* is degenerate matrix, *Det (R) = 0* so it is unable to solve the system by normal method because equations has infinitely many solutions

To determine the unique solution vector, add a binding condition system of the unknown vector, as form:

$$C^T \delta X = 0 \tag{4}$$

The system (4) has to satisfy two conditions:

The number of conditions equal the missing number

Rows in the matrix $\boldsymbol{C^T}$ are linear independence to rows in matrix *A*

Combine (2) and (4), based on the indirect adjustment method with conditions, a expand standard system is established

$$\begin{bmatrix} R & C \\ C^T & 0 \end{bmatrix} \times \begin{bmatrix} \delta X \\ K \end{bmatrix} + \begin{bmatrix} b \\ 0 \end{bmatrix} = \begin{bmatrix} 0 \\ 0 \end{bmatrix} \tag{5}$$

The coefficient matrix in (5) can be inverted normally and has form of block matrix.

$$\begin{bmatrix} R & C \\ C^T & 0 \end{bmatrix}^{-1} = \begin{bmatrix} R^{\sim} & T \\ T^T & 0 \end{bmatrix} \tag{6}$$

Solution of system (5) is determined by the formula:

$$\delta X = -R^{\sim} b \tag{7}$$

There are many ways of calculating the pseudo-inverse matrix, for example as:

$$R^{\sim} = (R + CP_0C^T)^{-1} - TP_0^{-1}T^T \quad (8)$$

$$\boldsymbol{T = B(C^T B)^{-1} T} \quad (9)$$

Where B is Helmet coordinate transition matrix

In the plane network with $d = 4$, matrix B is calculated as follows:

$$B_i = \begin{bmatrix} 1 & 0 & y_i & x_i \\ 0 & 1 & -x_i & y_i \end{bmatrix} \quad (10)$$

$$B = \begin{bmatrix} B_1 & B_2 & .... & B_k \end{bmatrix}^T$$

Notes: formula (9) is right for the plane network (x, y, □, m) - free, if an original element is definite, the corresponding column no exists in the mentioned formulas.

Accuracy evaluation is implemented through normal formulas of the indirect adjustment method with conditions

Mean square error of unit weight is calculated as:

$$\mu = \sqrt{\frac{V^T PV}{n - k + d}} \quad (11)$$

Where: n is sum of the measured values, k is the essential value

2.2. Establishment of the landslide displacement monitoring network

The deformation monitoring network is able to be established as two formats: the relative network and the absolute network. The absolute network comprises points situated outside the deformation area, which serve as benchmarks. The relative network includes all points lying in the deformation area. In instances where the deformation region and its impact are minimal, the monitoring network is typically constructed as an absolute network, as exemplified in hydroelectric dams, construction sites, and small landslide areas, as depicted in Figure 1. However, when the deformation area is exceptionally large or undefined, a relative network is established, resulting in a network devoid of benchmarks. This is often the case in scenarios involving crustal deformation, geological fissure monitoring, and the effects of earthquakes and volcanoes, as illustrated in Figure 2 [1].

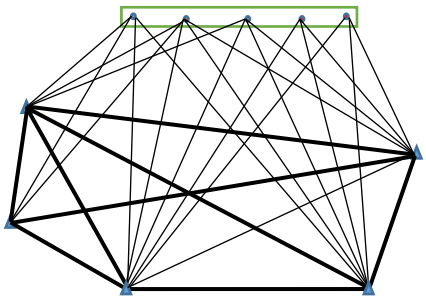


Figure 1. *The hydroelectric dam monitoring network*

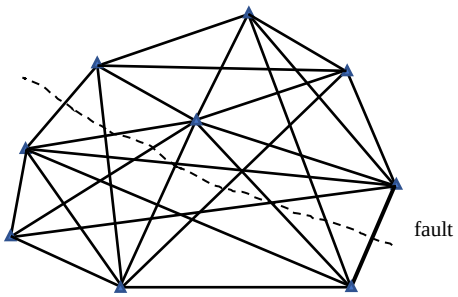


Figure 2. *The fault monitoring network*

In the context of an absolute network, points are situated outside the landslide area and are referred to as benchmarks or reference points. These points facilitate the determination of the absolute displacement of points within this area. Consequently, these benchmarks are strategically positioned on stable geological locations, distanced from the landslide area, or embedded within the original rock layer. This arrangement ensures that the displacement

values obtained from the monitoring points within the landslide area represent absolute displacement.. However, benchmarks may also experience displacement due to various factors, such as being placed on unstable strata or being affected by external conditions. In monitoring process, to detect the unstable benchmarks, a large number of benchmarks should be layout to form the framework. This framework is measured in cycles to evaluate the stability of the benchmarks, followed by the correction of any unstable benchmarks. In contrast, with a relative network, all points are located within the landslide area, and only the application of the entirely free adjustment method can yield reliable results [4].

3. EXPERIMENT MODEL

3.1. Desctiption of case study

Area at Mong Sen bridge, Sapa, Lao Cai has weak geological condition, always happen landslide in the rainy season. This place has strongly divided terrain with steep banks and dangerous 3-level bends on national highway 4D connecting Lao Cai to Sapa. Lao Cai province has just allowed to clear the bridge that is across the valley and has the highest pillar in the north in August, 2023 to avoid the 3-level bends, reduce risks and shorten the moving time of vehicles. Image of the landslide area at Mong Sen bridge from Google Earth, the base points (triangular) and monitoring points (square) are shown in Figure 3.



Figure 3. *The landslide region at Mong Sen bridge (Source: Google Earth)*

3.2. Calculation and analysis of the landslide data

3.2.1. Accuracy estimation. With Mong Sen monitoring area as figure 3, the article designs the absolute network including 5 benchmarks (MC1-MC5) that are far from landslide region, 9 monitoring points are located in the landslide region (QT1-QT9). Firstly, accuracy estimation for the monitoring network needs implementing to choose equipment and instrument in order to ensure the requirement accuracy. The allowance error of position is 15 millimetres [8]. Therefore, according to [7] mean square error of position of the base network and the monitoring network is calculated, respectively as follows:

$$\boldsymbol{m_I = \frac{m_p}{\sqrt{1+k^2}} = \frac{15}{\sqrt{1+4}} = \frac{15}{\sqrt{5}} = 6.7m} \quad (12)$$

$$\boldsymbol{m_{II} = \frac{2\times m_p}{\sqrt{1+k^2}} = \frac{2\times 15}{\sqrt{1+4}} = \frac{30}{\sqrt{5}} = 13.2mm} \quad (13)$$

Using two adjustment methods for four models to compare and choose the suitable one with real displacement. The adjustment methods are given in table 1, where the adjustment

method for the fourth model is the one for the relative network, in which equipment is no put at monitoring points to measure.

Table 1. Expected adjustment models

N^o	The adjustment methods	Notes
1	Adjustment for the dependent network	the side measuring network
2	Free adjustment with origin as central point of three stable benchmarks	the side measuring network
3	Free adjustment with origin as central point of five stable benchmarks	the side measuring network
4	Free adjustment with origin as central point of all points	the side measuring network

Implement accuracy estimation for four mentioned cases, equipment is an electronic total station with error of side measurement m_s*=3+2ppm*. The designed network is the side measuring ones so that measurement is swift, no affected by environment. In case 1, all base points are entirely stable, measure 38 sides. The other cases measure 56 sides as figure 4. Results of estimation are represented in table 2.

Table 2. Results of accuracy estimation

N^o	points	Coordinate X(m)	Coordinate Y(m)	error of position m_p(mm)			
				Case 1	Case 2	Case 3	Case 4
1	QT1	9321.0	6770.0	5.0	5.1	5.1	4.6
2	QT2	9230.0	6838.0	9.0	9.6	9.6	8.6
3	QT3	9231.0	6740.0	5.3	5.6	5.6	5.3
4	QT4	9157.0	6704.0	4.3	4.5	4.4	4.3
5	QT5	9179.0	6780.0	3.7	3.8	3.7	3.7
6	QT6	9151.0	6870.0	7.1	7.6	7.6	7.1
7	QT7	9143.0	6635.0	4.3	4.5	4.5	4.4
8	QT8	9101.0	6706.0	3.3	3.4	3.3	3.3
9	QT9	9111.0	6811.0	3.4	3.5	3.4	3.4
10	MC1	8815.0	6617.0	0.0	2.4	1.7	2.0
11	MC3	8866.0	6793.0	0.0	2.3	1.7	1.8
12	MC2	9067.0	6567.0	0.0	1.2	1.4	2.1
13	MC4	8927.0	6974.0	0.0	1.5	1.7	2.1
14	MC5	8719.0	6788.0	0.0	1.5	1.6	1.8

The table 2 shows that the weakest point in all cases is QT2, the weakest error of position is 9.6 millimetres in the second and the third model. All cases satisfy error of position of the monitoring network in formula (12). This proves that electronic total station with medium accuracy can be used to monitored.

3.2.2. Results of model calculation

The designed network, comprising 56 measured values of side, was assessed using the electronic total station TC703, which has a side measurement error of m_s *= 3+2ppm*.

Subsequent data processing was conducted for the four models under consideration. If the coordinates listed in columns 3 and 4 of Table 2 are regarded as the adjusted coordinates from the previous cycle, the coordinate correction number equates to the displacement of points. Table 3 presents the displacement of points in the coordinate axis, while Table 4 provides information on the smallest positional error. Figure 4 illustrates the error ellipse of points across all models.

Table 3. Adjustment results

N^o	Point	Displacement in coordinate axis (mm)							
		Case 1		Case 2		Case 3		Case 4	
		δX	δY	δX	δY	δX	δY	δX	δY
1	QT1	1.5	3.8	1.6	3.8	1.6	3.8	1.5	3.5
2	QT2	1.8	4.1	2.0	7.7	2.0	7.7	1.9	6.9
3	QT3	1.8	3.3	2.0	4.3	1.9	4.3	1.8	4.1
4	QT4	1.6	2.7	1.9	3.4	1.8	3.4	1.7	3.4
5	QT5	1.7	3.4	1.7	2.7	1.7	2.7	1.6	2.7
6	QT6	1.8	2.3	1.9	6.2	1.9	6.2	1.8	5.8
7	QT7	1.7	2.3	1.8	3.6	1.8	3.6	1.6	3.5
8	QT8	1.9	7.2	1.9	2.3	1.8	2.3	1.7	2.3
9	QT9	1.9	5.8	1.8	2.4	1.7	2.4	1.6	2.4
10	MC1	0.0	0.0	1.2	1.7	0.8	1.2	1.0	1.3
11	MC3	0.0	0.0	0.7	0.8	0.9	0.8	1.2	1.3
12	MC2	0.0	0.0	1.2	1.5	0.9	1.1	0.9	1.2
13	MC4	0.0	0.0	0.8	1.0	1.0	1.1	1.3	1.2
14	MC5	0.0	0.0	0.9	0.9	0.8	1.2	0.8	1.3

Table 4. The position error of the weakest point

N^o	Point	*The position error of the weakest point* mm)			
		Case 1	Case 2	Case 3	Case 4
(1)	(2)	(3)	(4)	(5)	(6)
1	QT2	7.5	8.0	8.0	7.2

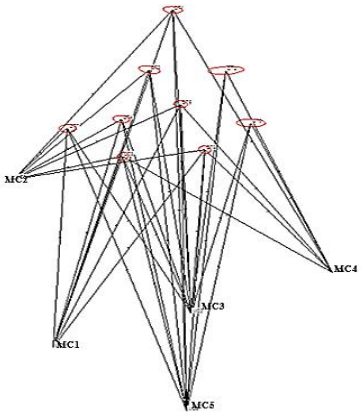


Figure 4a. *Case 1 (5 fixed original points)*

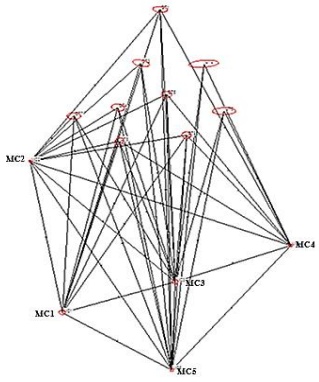


Figure 4b. *Case 2 (origin is center of three stable benchmarks)*

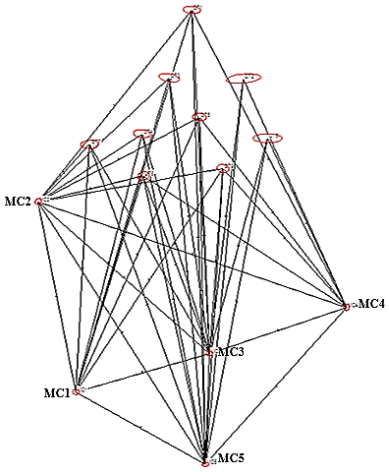


***Figure 4c**. Case 3 (origin is center of five stable benchmarks)*

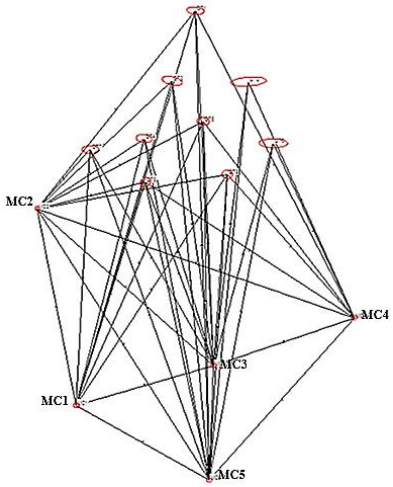


***Figure 4d.** Case 4 (origin is center of all points)*

***Figure 4.** Error Ellipse of all points*

4. DISCUSSION

Upon analyzing a single cycle of data, it is observed that the four adjustment models yield equivalent positional errors, thereby ensuring a similar estimation problem. However, several distinctions are noted:

In the first model, 'dependent network adjustment', the network comprises two ranks, whereas the other models feature a one-rank network.

In the first model, benchmarks are assumed to be entirely stable, hence exhibiting no displacement. Consequently, data processing is primarily conducted for the base network, with benchmarks remaining stable and error-free. In the second and third models, if data processing is performed separately as per the calculation process, these revert to the first model. Post-adjustment, it is observed that the correction values increase with the distance of the monitoring points from the origin. However, the calculated displacement values closely resemble the actual values.

In the second, third, and fourth models, the correction values of the benchmarks represent the displacement of these points. If these displacement values exceed the permissible error, calculated using the stability standard $\mathbf{k} * \mathbf{m_I}$ (k=3, $\mathbf{m_I}$ as per formula (12)), the benchmark is deemed unstable and is subsequently removed from the system. If the unstable benchmark continues to be used for calculating the displacement of monitoring points, it necessitates correction, followed by readjustment.

In the fourth model, the positional errors of all points are relatively equal, given that the origin is the central point of all points. This validates that for large monitoring areas, this model yields the most uniform displacement result in the landslide region, as the center of this region is selected as the origin.

The displacement of monitoring points calculated using different methods varies, indicating that the number of benchmarks chosen for adjustment influences the displacement values. Therefore, to accurately calculate the displacement of monitoring points, the number of benchmarks needs to be consistent across cycles used for displacement comparison. This ensures that the analysis and assessment are reliable.

5. CONCLUSIONS

For smaller monitoring regions, the use of an absolute network, which includes two ranks, is recommended as it yields more accurate results. If a free network is employed, the stability of benchmarks must be analyzed. Stable benchmarks, which are devoid of error, necessitate the application of a calculation process for the absolute network.

For larger monitoring regions, the relative network is advised. The most suitable method in this scenario is the free adjustment method, with the central point of all points serving as the origin.

The selection of the adjustment method in the processing of monitoring data significantly influences the calculated displacement values. Therefore, to ensure reliable results, it is essential to maintain consistency in the adjustment method across all cycles.

REFERENCES

[1] Huang S, Yin H, Jiang Z 2012 *Deformation data processing* (publisher of science and technique) p 117-120.

[2] Pham Q K and Tran Q A 2017 Free network adjustment using the generalized inverse matrix. *Geo-spatial Technologies and Earth Resources (GTER 2017)*, p 301-306.

[3] Tao B 2017 *Free adjustment and deformation analysis* (Publisher of Resources-Environment and Map Vietnam) p 75-88.

[4] Pham Q K 2021 *Data processing and structural deformation prediction (*publisher of science and technique) p 24-27; 98-105.

[5] Pham Q K 2011 Choosing the reference system for the base network in structural deformation monitoring *J. Min & Geo Sci tech.* 34 p 95-98.

[6] Pham Q K and Tran N D 2019 The integrated method in monitoring displacement of retaining walls on soft ground in Vietnam *Con. Nat Sci VietGeo* p 137-144.

[7] Tran K and Nguyen Q P 2010 *Structural deformation monitoring* (Publisher of transportation).

[8] Vietnamese standard 9399:2012 Houses and construction works-horizontal displacement monitoring by geodetic methods.

MONITORING ENVIRONMENTAL RECLAMATION AT COAL MINES IN THE TERRITORY OF HA LONG CITY USING LANDSAT DATA

Quyet Chien NGUYEN[1], Vu Khac DANG[1*], Thi Anh Cuc NGUYEN[1], Thi Huong Giang CHU[1], Quynh Trang PHUNG[1]

[1]Faculty of Geography, Hanoi National University of Education,
136 Xuan Thuy, Cau Giay, Hanoi, Vietnam

*Email: dangvukhac@gmail.com

Abstract: Ha Long is one of the coastal cities, that are closely connected to the coal mining industry of Vietnam Coal and Mineral Group (TKV). Together with the green growth strategy of Quang Ninh People's Committee – which emphasizes the need for environmental protection alongside the exploitation of natural resources, coal mining production must comply with environmental reclamation efforts. This study evaluates the ability to use satellite imagery to monitor environmental reclamation by mapping land cover changes associated with coal mining activities. Object-oriented classification methods using support vector machine algorithms (SVMs) were applied to Landsat 8 images captured from 2013 to 2022. The accuracy of the classification results was independently validated through visual interpretation of Google Earth satellite images captured during the same period. The validation indicated that these classification results were consistent with the Overall Accuracy > 87.67% and the Kappa coefficient > 0.81. Statistical data from the classified maps presented the mutation of vegetation, coalfield, and bare soil at the Suoi Lai coal mine in the territory of Ha Long City. The mutation shows that the vegetation area in this site has significantly increased from 16.21% in 2013 to 44.64% in 2022; while the bare soil area has gradually decreased from 54.08% in 2013 to 36.19% in 2022 and was converted into other types of land cover, especially vegetation. Otherwise, the values of NDVI and NDSI at the quadrats in the Suoi Lai coal mine show two opposite tendencies: NDVI values have increased continuously while NDSI values have decreased. This fact proves that the environmental reclamation at this coal mine has been well deployed by the Hon Gai Coal Company, and the mentioned approach could support authorities to monitor the reclamation implementation of coal mining companies in order to limit its impact on adjacent residential settlements.

Keywords*: environmental reclamation, Landsat 8, object-oriented classification, SVMs, spectral index, land cover*

1. INTRODUCTION

Ha Long City is situated in the North Eastern region of Vietnam, where many coal seams have been explored since the 19th century with the biggest reserves. Due to its contribution to thermal power, metallurgy, boiler combustion, chemical production, paper, glass production, etc. coal yield in this territory has rapidly increased significantly contributing to the country's economic development in recent decades. However, mining activities including drilling, blasting, rock breaking, loading, transporting, and dumping waste rock during coal production have induced great pressure on the environment. This impact is not limited to the coalfields but also extends to the surrounding residential areas of Ha Long City, resulting in the degradation of natural ecosystems at various scales. For example, open-pit coal mining with the removal of waste rock causes environmental problems such as

water pollution, air pollution, landslides, debris flow, and even landscape modification (Vu *et al.*, 2018). Therefore, environmental reclamation is considered as one of the mandatory tasks together with coal production, and it is widely implemented in many countries worldwide to restore the natural environment, re-establish ecosystems, and improve the function of specific ecosystems, conserve biodiversity, mitigate impacts, and adapt to climate change, etc. (Starzomski, 2014; Vaughn *et al.*, 2010).

The in-situ monitoring of environmental reclamation faces various difficulties because many coal mines are usually dispersed in expansive and remote areas. However, researchers have noted that this process can be described and traced via land cover change detection (Szostak *et al.*, 2020). The spectral variations between different acquisition dates due to the modification of land cover are utilized for identifying the changes when its amplitude is more significant than any noises (Ingram *et al.*, 1981). Thus, the application of remote sensing technology based on measuring reflected and emitted values in different wavelengths to establish a land cover map with appropriate classification techniques will provide reliable results to efficiently manage this reclamation process (Al-doski *et al.*, 2020; Kavitha *et al.*, 2021). These classification techniques have been strongly developed in the past decades to process multispectral images with pixel-based or object-based classification techniques (Alberto *et al.*, 2017; Ebong *et al.*, 2019; Kobayashi *et al.*, 2020; Piekkoontod *et al.*, 2020). Pixel-based classification techniques can distinguish land cover categories based on the reflectance values of objects in several bands of the spectrum without regard to spatial information. Therefore, digital image processing based purely on reflectance values does not always allow to accurately discriminate different land cover categories because various features on the ground can have identical spectral behaviours causing spatial fragmentation in the classification results (Igoniye *et al.*, 2015; Santillan and Makinano-Santillan, 2018). Object-based classification techniques have been recently developed and they take advantage of combining both spectral and spatial information to group the clusters of pixels into different land cover categories. The second technique implies pixels based on their spectral responses, texture, shape, and spatial relationship with surrounding pixels. Thus, they reduce confusion between land cover categories, and avoid spatial fragmentation, although they require satellite images with high spatial resolution (Yu *et al.*, 2006; Xu *et al.*, 2018). There have been many works using Landsat images to exploit spatial information with object-based classification techniques for mapping land cover (Shang *et al.*, 2019; Yang *et al.*, 2021).

In fact, reclamation monitoring has been promoted with the deployment of Earth Observation satellites for spatially and temporally determining land cover changes (location, intensity, period) via satellite data processing (Gómez *et al.*, 2016; Kantakumar and Neelamsetti, 2015; Sun and Ongsomwang, 2020). Studying land cover change over the last decades demands a historical series of satellite images. The Landsat program can satisfy these conditions owing to the consecutive launches of some Landsat satellites from 1 to 9 (except Landsat 6 due to the failure) since the 1970s by the collaborative mission between the United States Geological Survey (USGS) and the National Aeronautics and Space Administration (NASA) (Goward *et al.*, 2006). This Landsat program might be recognized as a potential source of data in comparison to traditional in situ methods for supporting environmental management at a regional scale (Kloiber *et al.*, 2002) due to its wide

observation coverage with medium spatial and temporal resolutions (Wulder *et al.*, 2019). Otherwise, Landsat satellites improve the probability of taking images without cloud cover and it could be considered as suitable and consistent datasets for analyzing land cover change in a more timely and cost-effective manner (Markham *et al.*, 2018). Therefore, Landsat images have been used to detect where, when, and how the ground surface has been changing owing to over 50 years of archived data. Although the number of studies using Landsat images has considerably increased since the opening of all Landsat collections for download at no charge in 2008 (Wulder *et al.*, 2012). However, the studies on land cover change have been limited with an inadequate amount in which the methods of change detection have evolved depending on the number of treated images (Hemati *et al.*, 2021b).

Several scientists recognized that change detection is the process of identifying variation in the situation of an object or phenomenon by concurrently processing a couple or several images of the same geographic region (Singh, 1989). Meanwhile, Radke et al. noted that change detection was considered the process of determining significant differences in pixels that appear consecutively on satellite images due to the appearance, disappearance, or variation in the shape of objects on the ground (Radke *et al.*, 2005). Such changes in land cover can be determined by comparing satellite images acquired at two different times - the bi-temporal approach, which is simpler but less comprehensive in terms of dynamics than the multi-temporal approach (Coppin *et al.*, 2004). However, in recent multi-temporal approaches, a set of satellite images taken at many different times provides a larger amount of information than a single image pair in the context of local change over time (Réjichi and Chaabane, 2015). Despite these advantages, it remains some specific challenges that relate to temporally anomalous signals of different land covers, inadequate sampling to train supervised classification, or the lack of satellite data. To determine land cover change, many issues are discussed and summarized in the overview section of the articles. Among them, Hemati et al. (Hemati *et al.*, 2021a) and Zhu (Zhu, 2017) have proposed the groups of method such as thresholding, differentiation, segmentation, classification, regression, etc. which are applied in various applications using satellite data to observe the dynamics caused by human activities (Liu *et al.*, 2020).

Although environmental reclamation has recently become a question of interest in Vietnam, and the aspects of environmental management and the solutions of environmental reclamation relating to open-cast coal mining activities in Quang Ninh province have been considered by several researchers (Ngô, 2013; Phạm, 2014). However, the application of remote sensing technology into observing the progress of reclamation process at coal mines is still missing. Therefore, our research aims to evaluate the possibility of using Landsat satellite images captured at different times to monitor the environmental reclamation at the Suoi Lai coal mine of Hon Gai Coal Company and its surrounding areas via the changes of some land cover categories, as well as the variable tendency of some typical spectral index at three quadrats during the period of 2013-2022. The obtained results will create a reliable basis to evaluate the proper implementation of environmental reclamation, to perform environmental protection plans, and to organize environmental management at coal mining companies in this coastal area.

2. CONTENT

2.1. Study area

The Suoi Lai coal mine commenced operation since 2017 and it closed on December 2022. Its territory comprises some main sections: coalfield, dumped area, warehouse, overburden, etc. in which dumped area has been replanted for environmental reclamation during the coal exploitation process and coalfield will be transformed to either dumped area or other occupations at the closure of mine. This Suoi Lai coal mine spreads over urban wards such as Ha Khanh, Ha Lam, Cao Xanh, etc. of Ha Long City, Quang Ninh province where diverse landscapes present: mountainous terrain with many coal mines in the northern part; narrow alluvial plains in the middle. The remaining part in the south is predominant by marine environment with hundreds of small limestone islands.

As illustrated in Figure 1, the development of Ha Long City over the past three decades has experienced some periods: it was established on December 27, 1993 on the basis of Hon Gai town; recognized as a class II urban center on September 26, 2003 and a class I urban center on October 10, 2013. However, urban development during these former periods expands toward shallow tidal flats due to the constraint of topographic and geologic conditions (Nguyen *et al.*, 2022). Most recently, its administrative boundary was expanded on December 17, 2019 toward higher fluvial terraces in Hoang Bo district. Local authorities have reorganized urban settlements, improved urban infrastructures, developed public utilities, and improved environmental sanitation for creating the enormous urban centers of the region.

In 2019, the population of Ha Long City reached 322710 people, distributed over a territory of 1119 km^2, spreaded across 21 wards and 12 communes. This territory is influenced by a tropical monsoon climate, in which the average annual temperature has ranged from 22.6 to 24.4°C and the average annual rainfall has approximately attained from 2200 to 2700 mm (Hoang *et al.*, 2018). The climate is divided into two distinct seasons: hot summer (lasting from May to October) with heavy rainfall (accounting for 80% to 85% of the total yearly rainfall) and cold winter (lasting from November to April) with low rainfall (accounting for 15% to 20% of total annual rainfall) (Huynh, 2002). The hydrological system consists of small, short rivers originating from the northern mountainous districts with characteristics of rapid flow and rapid drainage into the sea due to steep terrain and heavy precipitation in the rainy season. On the one hand, major rivers flowing across the city include Dien Vong, Vu Oai, Man, and Troi rivers. These four rivers pour their water into Cua Luc Bay and then into Ha Long Bay. On the other hand, streams in Ha Long City are small, short and they course along the southern slopes of Hong Gai, Ha Tu, and Ha Phong wards with low water debit (Tran, 2022).

Many coal seams are located in the Hon Gai Formation, distributed in the central part of the city.

Residential areas are developed on both sides of national road No.18 with many different man-made structures extending along the coast. Meanwhile, tropical rainforests still dominate in the northern part. In addition, carbonate sediments with thick limestone layers develop in the marine environment, creating unique landscapes with high geomorphological value. That is the reason why Ha Long Bay has been recognized twice as a World Natural Heritage by the United Nations Educational, Scientific and Cultural Organization

(UNESCO) since 1994. These resources give several advantages for developing economic sectors, such as coal mining, aquaculture, tourism, forestry, etc. For instance, the total number of tourist arrivals reached about 21.78 million and the tourism industry contributed 8% to the total GDP of Quang Ninh province in the period of 2013–2015, and Ha Long City is their destination (Phuong, 2021). On the other hand, in the coal mining sector, 80000 workers operate in 23 large coal mines with an output of more than 38.5 million tons of raw coal in 2020 (Pham, 2021).

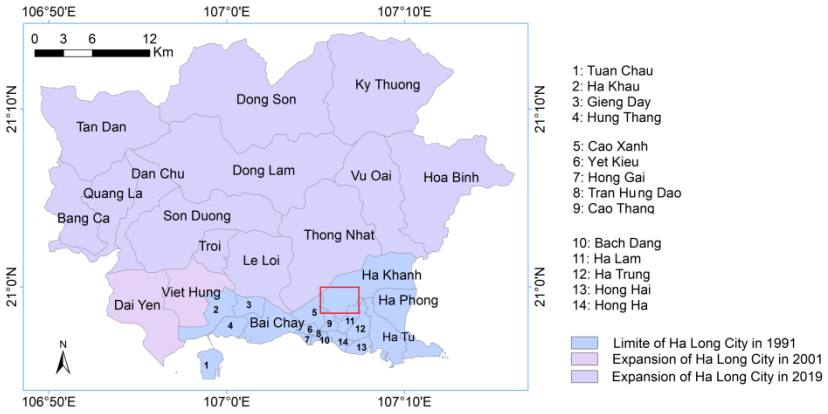


Figure 1. *Modification of administrative boundary of Ha Long City during the last decades. Red box presents the position of Suoi Lai coal mine and its surroundings.*

2.2. Method and used data

2.2.1. Data

2.2.1.1. Landsat 8 images. In this study, satellite images are collected for free of charge from the website of the United States Geological Survey (USGS): https://earthexplorer.usgs.gov/. These Landsat 8 satellite images captured from 2013 to 2022 were selected during the dry season when rice and crops were harvested to increase the ability to separate reclaimed plants from other vegetation. Some image scenes have relatively high cloud cover while the study area was not affected.

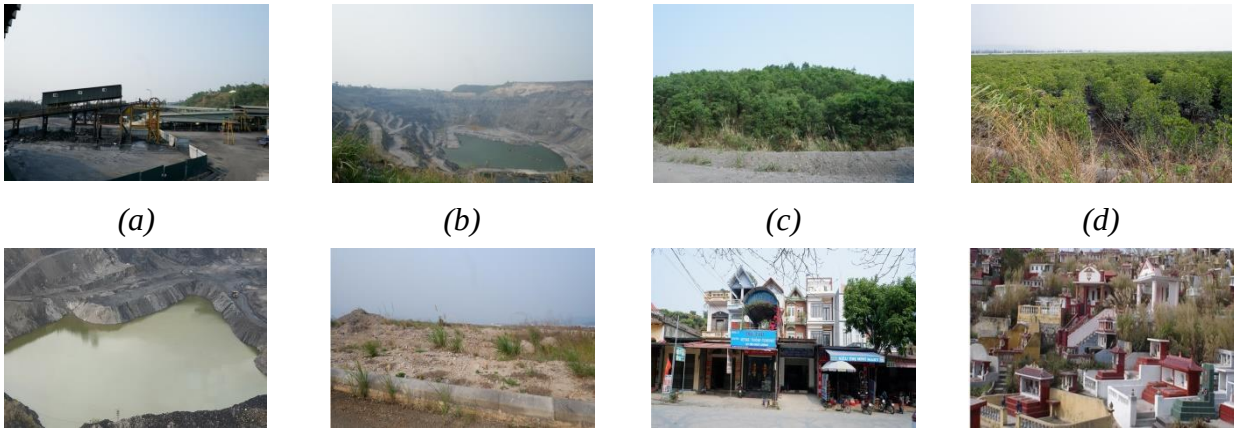
Table 1. Parameters of Landsat 8 images used in this study

Nomenclature	Acquisition date	Path; Row	Cloud cover %
LC08_L2SP_126045_20131008_20200913_02_T1	08/10/2013	126; 45	12.53
LC08_L2SP_126045_20141230_20200910_02_T1	30/12/2014	126; 45	0.03
LC08_L2SP_126045_20150928_20200908_02_T1	28/09/2015	126; 45	32.99
LC08_L2SP_126045_20160930_20200906_02_T1	30/09/2016	126; 45	20.12
LC08_L2SP_126045_20171206_20200902_02_T1	06/12/2017	126; 45	20.24
LC08_L2SP_126045_20181006_20200830_02_T1	23/11/2018	126; 45	0.95
LC08_L2SP_126045_20191110_20200825_02_T1	10/11/2019	126; 45	0.36
LC08_L2SP_126045_20201112_20210317_02_T1	12/11/2020	126; 45	7.02
LC08_L2SP_126045_20211201_20211209_02_T1	01/12/2021	126; 45	0.51
LC08_L2SP_126045_20221017_20221031_02_T1	17/10/2022	126; 45	5.78

Landsat 8 satellite images are recorded on 11 spectral bands, including 9 shortwave bands and 2 thermal infrared bands with different spatial resolutions: 15 m, 30 m, 100 m.

2.2.1.2. High-resolution images from Google Earth. Google Earth integrates spatial data such as: satellite images in the form of natural color composite, aerial photos, and geographic information data, etc. Satellite images are historically archived, meaning images can be displayed at the present or at a time in the past. Google Earth images are provided with a super high spatial resolution (<1m), so users can easily recognize objects on the ground at an appropriate scale (Malarvizhi *et al.*, 2016). Images of each year in the period of 2013-2022 are exploited to visually interpret and select validation samples via recognition from field surveys (Lesiv *et al.*, 2018).

2.2.1.3. Field survey. The identification of land cover categories is difficult due to the ambiguity of objects on Landsat images from the early years of the researched period. Therefore, the selection of training samples for supervised classification is carried out independently on each Landsat image, which needs to be supported by visual interpretation of super-high resolution Google Earth images and field surveys to determine land cover categories in the study area. A field survey was realized on 5th March 2023, and eight different categories of land cover have been recognized in this study area such as: urban residence, vegetation, mangrove, bare soil, warehouse, water body, coalfield, and cemetery.



(a) *(b)* *(c)* *(d)*

(e) *(f)* *(g)* *(h)*

***Figure 2**. Pictures of several land cover categories at Hon Gai coal mine: (a) Warehouse, (b) Coalfield, (c) Vegetation, (d) Mangrove, (e) Water body, (f) bare soil, (g) residence, (h) cemetery*

2.2.2. Method

Zhu (Zhu, 2017) argues that regardless of the different change detection approaches: bi-temporal or multi-temporal, the changes are commonly identified using images captured on different days. The spatiotemporal patterns of changes in land covers will be determined by finding differences in classification results or in other words, post-classification comparisons. This principle has been applied to identify urban development since the early 1970s, and it requires the comparison of classified images corresponding to spectral changes over time due to land cover changes (Dueker and Horton, 1972). In recent years, many advanced classification algorithms have been developed for handling satellite image, and image classification methods can be grouped into several categories: supervised and unsupervised, or with parametric and non-parametric, or hard and soft, or pixel-based and object-based. For detailed information about each category, readers can refer to the work of Lu and Weng (Lu and Weng, 2007). In general, each algorithm has its own advantages and disadvantages, and choosing the appropriate classification method depends on the selection

of training samples, the distribution of objects on the ground, and the spatial resolution of satellite images, the availability of image processing software. In this study, the land cover maps were established using an object-oriented classification method, with the Support Vector Machine (SVMs) algorithm because this approach is highly effective, widely used in many land cover change studies.

2.2.2.1. Processing steps. Landsat 8 images are atmospherically corrected by USGS with surface reflectance at 2A level, georeferenced to the UTM coordinate system (WGS84). Some key preprocessing steps are presented below. The multispectral bands of image with the spatial resolution of 30 m are then processed according to the procedure illustrated in Figure 3.

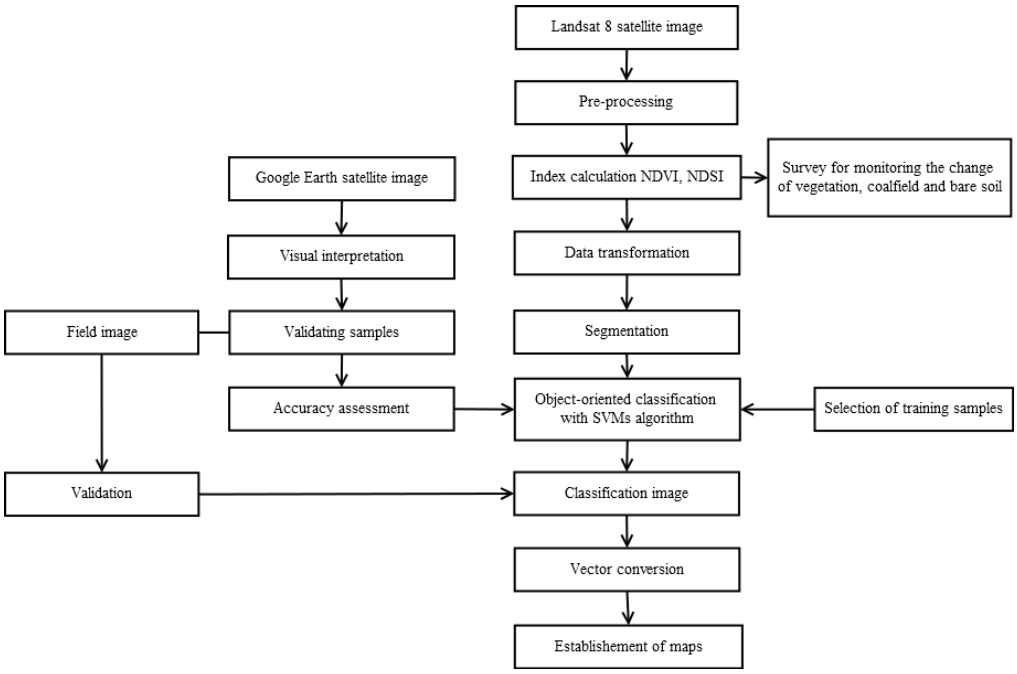


Figure 3. *Processing steps of satellite images in this study*

- Registering two or more images to a reference image for ensuring that the images are geometrically aligned so that all objects on each image overlap themselves on the other images. This coregistration step is a prerequisite for accurately extracting features and can then provide results that compare land cover maps with each other.
- Image cropping aims to remove unwanted parts outside the area of interest from the Landsat scene to preserve the important part - the study area (Figure 1).
- Merge layers for stacking multiple Landsat bands with the same reference system, so multiple bands can be processed later in an image processing software.
- Convert the reflectance values in the integer format to decimal format according to formula (1) for each captured image.

$$Ref_n = (B_n \times 0.0000275) - 0.2 \quad (1)$$

Here, Ref_n is the reflectance value of band n in a decimal number, B_n is the apparent value of band n in an integer number (Sayler, 2020)

2.2.2.2. Spectral index. The spectral index is calculated based on the normalized difference between 2 or more original spectral bands. There are many different types of spectral index that could serve to highlight different land cover categories. Spectral index

bands are widely used in remote sensing applications, and they often support to isolate vegetation, to analyze vegetation changes, to distinguish water bodies, or bare soil, etc. This is because each land cover category in the spectral index band has distinct values compared to other land cover categories. On the one hand, the spectral index bands are integrated with the original bands during the classification process for increasing the ability to separate land cover categories from each other. This approach thus allows to reduce confusion between land cover categories, which have similar reflectance signatures, and to avoid spatial fragmentation in classification results.

Table 2. Formulas for calculating spectral index NDVI and NDSI (NIR – near-infrared band, R – red band, SWIR2 – Shortwave infrared band, G – Green band)

Index	Formulas	For Landsat 8	Reference	
NDVI	= (NIR-R)/(NIR+R)	= (B5-B4)/(B5+B4)	(Rouse *et al.*, 1974)	(2)
NDSI	= (SWIR2-G)/(SWIR2+G)	= (B7-B3)/(B7+B3)	(Deng *et al.*, 2015)	(3)

On the other hand, change detection is indirectly investigated by the mutation of vegetation, and bare soil at the coalfield during the reclamation process. Hence, the index related to vegetation: NDVI (normalized difference vegetation index), and to bare soil: NDSI (normalized difference soil index) are exploited to assess the mutation of this reclamation process in this area. If it is well implemented, the value of the NDVI index will continuously increase over time and inversely for the NDSI index.

2.2.2.3. Segmentation and selection of training samples. Image segmentation is applied based on the color composite of each Landsat 8 image for dividing them into image objects. This is an optimization process, for a given number of image objects, that minimizes their average heterogeneity and maximizes their respective uniformity. The segmentation process starts with single image objects of a pixel and continuously merges them in several pairwise iterations into larger units as long as it does not exceed the upper threshold of local uniformity (Trimble, 2010). This uniformity criterion is defined as the combination of spectral uniformity and conformational uniformity. The ‘scale’ parameter affects this calculation, high ‘scale’ values create large image objects, while small ‘scale’ values create small image objects. This classification method is based on the object’s reflectance values and spectral characteristics and it considers other parameters such as: shape, size, compactness, and connection with adjacent objects to set up the training process. In this study, the relevant parameters are sequentially selected as follows: Scale = 2, Shape = 0.01, Compactness = 0.05 to perform object-oriented classification.

Next step, the visual interpretation of color composite images determines several types of land covers: water body, vegetation, mangroves, cemetery, residence, bare soil, warehouse, and coalfield in the study area. Google Earth images are also used to identify land cover categories through some elements that are difficult to obtain from Landsat images. To conduct supervised classification, a set of training samples is determined by selecting directly on the screen based on segmented image objects that correspond to the land cover types defined above. For each category of land cover, 5 samples are selected, with an average size of 200 pixels/sample. The Figure 4 below shows the differences in color and texture of each land cover category in the study area.

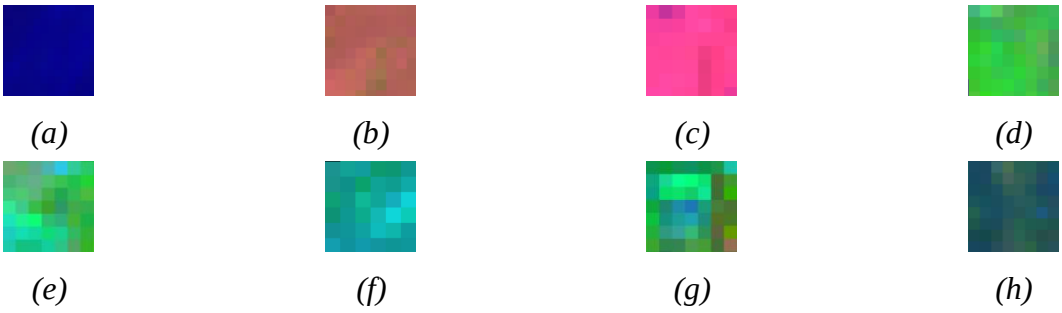


Figure 4. *Training samples of main land cover categories issued from Landsat 8 images (colour composite): (a) Water body; (b) Vegetation; (c) Mangrove; (d) Cemetery; (e) Residence; (f) Bare soil; (g) Warehouse; (h) Coalfield*

2.2.2.4.Object-based classification. Image classification is a suitable method for identifying land cover categories and provides the possibility of establishing a series of land cover maps at different times. Object-based image classification for land cover mapping from satellite images has attracted attention in recent years. Many studies performed over the past decades have considered the variety of sensors on board different satellites, the selection of classification algorithms, and other elements, etc. (Ma *et al.*, 2017). In this study, we applied an object-oriented classification with the Support Vector Machines (SVMs), a supervised classification algorithm developed by Cortes and Vapnik (Cortes and Vapnik, 1995). It was initially applied to machine vision fields such as handwritten digits and text recognition based on Statistical Learning Theory. It was then deployed in satellite image classification (Hermes *et al.*, 1999).

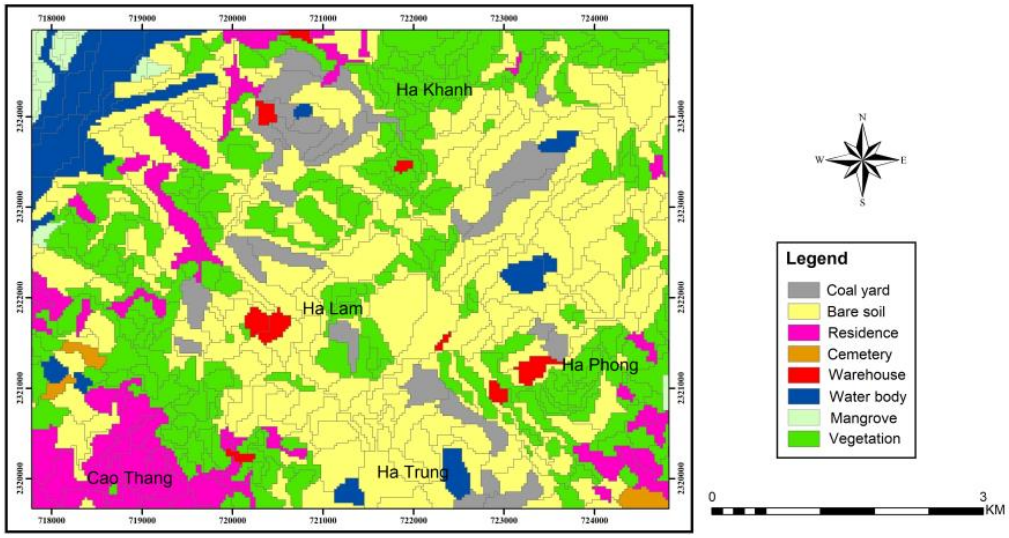
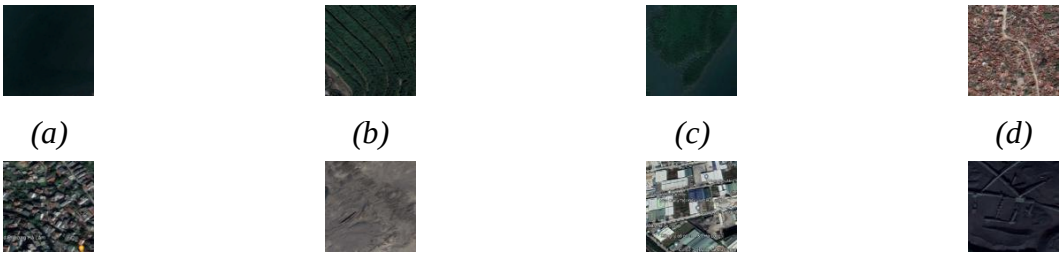


Figure 5. *Land cover classification issued from Landsat 8 image captured on 28/09/2015*

Although this algorithm has been developed for three decades, the results of recent studies have demonstrated the effectiveness of SVMs due to its ability to generalize events despite a limited training samples (Devadas *et al.*, 2012). Otherwise, Tzotsos and Argialas (2008) argue that SVMs outperforms several other algorithms in establishing an accurate method of mapping land covers in a large, heterogeneous tropical area (Tzotsos and Argialas, 2008). The object-oriented classification result for the image captured on 28 September 2015, is presented with the land cover situation as shown in Figure 5.

2.3. Results, discussion

2.3.1. Validation. The analysis of land cover change depends on the accuracy of satellite image classification results, which can be affected by many reasons such as: the classification method, the algorithm used, the spatial resolution, the amount of training samples, etc. In this study, the accuracy of Landsat image classification however was evaluated using validation samples, which were obtained by visual interpretation. Accordingly, the selection of validation samples for each land cover category is realized on Google Earth images due to its super high resolution, which helps to clearly identify objects with different characteristics and together with knowledge from field surveys.



(a) *(b)* *(c)* *(d)*

(e) *(f)* *(g)* *(h)*

Figure 6. *Training samples of land cover categories issued from Google Earth: (a) Water body; (b) Vegetation; (c) Mangrove; (d) Cemetery; (e) Residence; (f) Bare soil; (g) Warehouse; (h) Coalfield*

The confusion matrix includes many different parameters such as: User's Accuracy, Producer's Accuracy, Overall Accuracy and Kappa index which present the accuracy of image classification results. For instance, 32 samples were selected on Google Earth images captured on 19 December 2022 corresponding to 8 land cover categories to conduct random validation of Landsat 8 image classification results captured on 17 October 2022. Overall accuracy achieved = 87.67% and Kappa = 0.85. Thus, the object-oriented classification method with SVMs algorithm provides appropriate accuracy and validation approach is also similarly applied to the classification results of other years and their parameters are showed in Table 3.

Table 3. Accuracy parameters

No	Date	OA (%)	Kappa	No	Date	OA (%)	Kappa
1	08/10/2013	91.27	0.84	6	23/11/2018	93.01	0.88
2	30/12/2014	92.61	0.87	7	10/11/2019	88.02	0.81
3	28/09/2015	90.71	0.91	8	12/11/2020	92.09	0.90
4	30/09/2016	89.57	0.86	9	01/12/2021	92.72	0.87
5	06/12/2017	91.36	0.86	10	17/10/2022	87.67	0.85

2.3.2. Land cover maps

Object-oriented classification method with Support Vector Machine algorithm is applied to separate pixel images into different object classes. This classification process is also assigned to all images captured during the period of 2013-2022. Then 3 groups of land cover: coalfield, bare soil, and vegetation were kept on the maps to analyze the change for monitoring the implementation of reclamation at Suoi Lai coal mine of Hon Gai Coal Company during this period (Figure 7).

These maps visually show the change in land cover at the coalfield, illustrating the transition from bare soil to vegetation with the increase of vegetation areas and the reduction in coalfield and bare soil areas in the central part of the study area. This fact demonstrates the positive progress of the environmental reclamation process at the Suoi Lai coal mine.

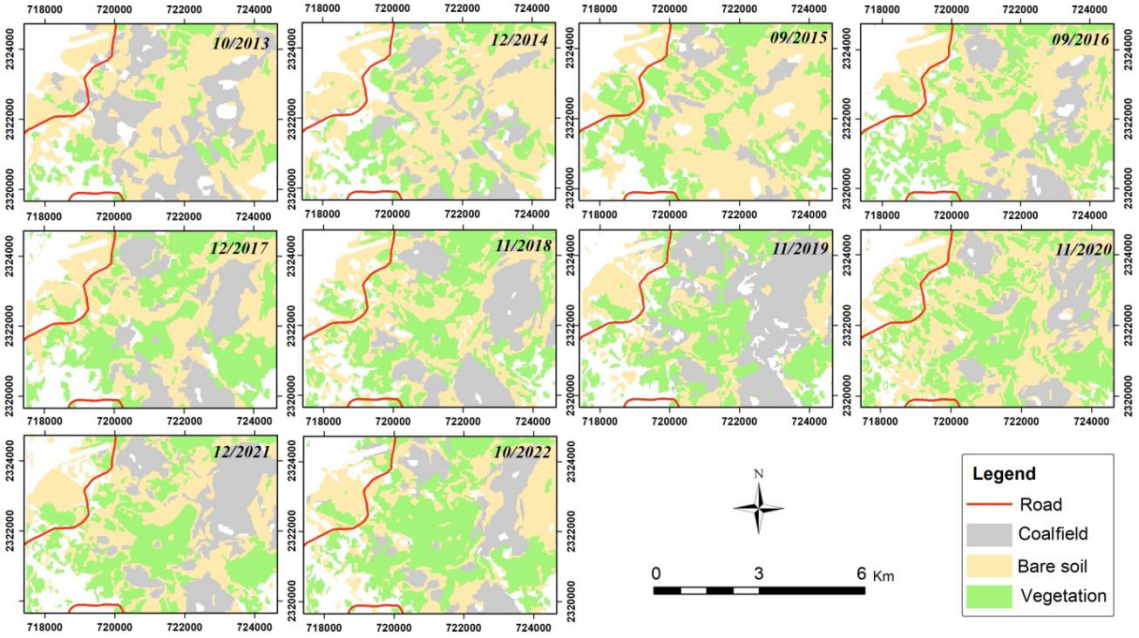


Figure 7. *Land cover maps during the period of 2013-2022*

2.3.3. Analysis of land cover changes

The quantitative analysis of change for main land cover categories is performed by overlaying the classification results for 2 years: 2013 and 2022. Thereby the change of 3 main land cover categories at the coalfield during this period is established and presented in Table 4.

Table 4. Changes of main land cover categories for the period of 2013 - 2022

Land covers	2013		2022		Mutation	
	Area (m^2)	Percentage (%)	Area (m^2)	Percentage (%)	Area (m^2)	Percentage (%)
Coalfield	9238500	29.71	6047100	19.17	-3191400	-10.54
Bare soil	16817400	54.08	11414700	36.19	-5402700	-17.89
Vegetation	5041800	16.21	14083200	44.64	+9041400	+28.43

Obtained statistics show that vegetation area tends to increase sharply to 9041400 m^2, equivalent of 28.43 %. Meanwhile, the area of coalfield and bare soil decreased relatively strong, especially the area of bare soil decreased by 5402700 m^2, equivalent of 17.89 %. The achieved results are due to the strict adherence of the Hon Gai Coal Company by the direction of local authorities in planting trees at waste dumps and surrounding areas to thereby narrow the area of bare soil. Besides, these changes can also be proven by calculating the vegetation normalized difference index (NDVI) and soil normalized difference index (NDSI) at 3 quadrats which locate in the dumped area of Suoi Lai coal mine as presented in the next section.

2.3.4. NDVI, NDSI index

The calculation of NDVI and NDSI index for the entire study area are presented in Figure 8. However, the values of these indices are also extracted corresponding to three quadrats mentioned above and they are averaged for monitoring the variation during the period of 2013-2022.

2.3.4.1. Variation of NDVI. The NDVI is calculated to highlight the difference of vegetation in the near-infrared and red bands. Based on the average of NDVI values at quadrats for establishing the graph of NDVI mutation during the period of 2013 - 2022. The results show that the average of NDVI values varies at different levels around the trend line. However, in general it has a continuously increasing form (Figure 9). This proves that the trees in the quadrats are growing better year after year.

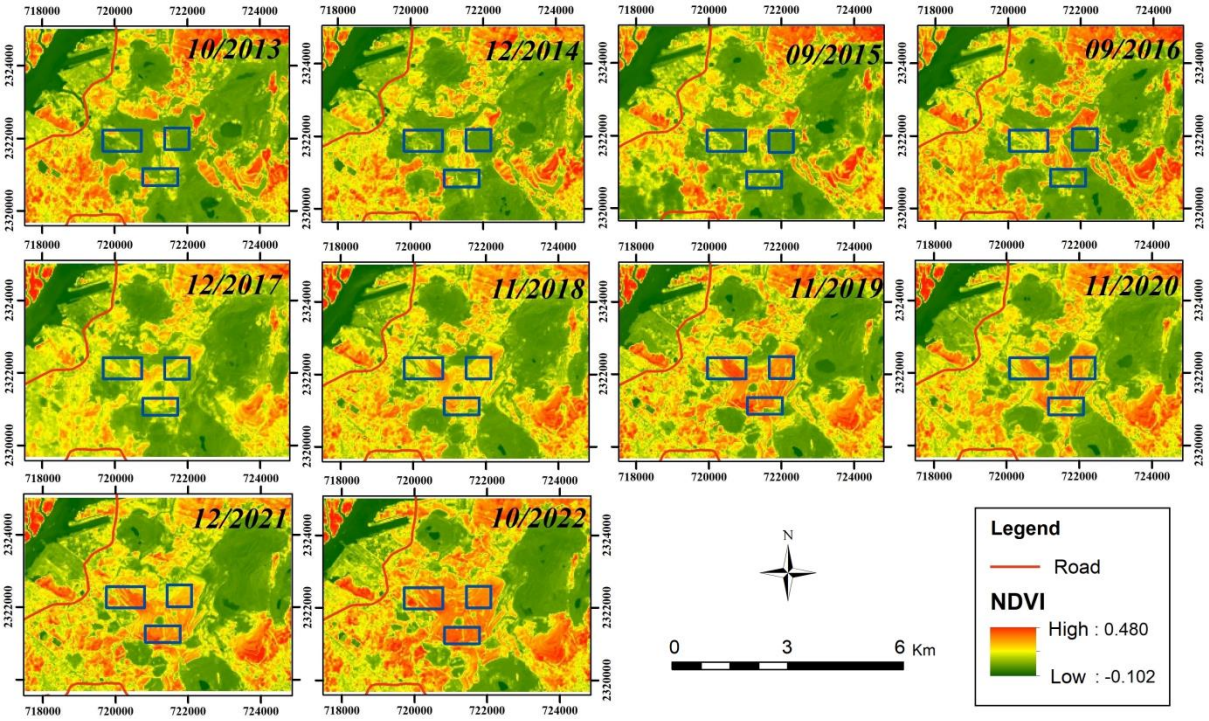


Figure 8. *Distribution of NDVI index during the period of 2013-2022. Blue boxes correspond to the quadrats*

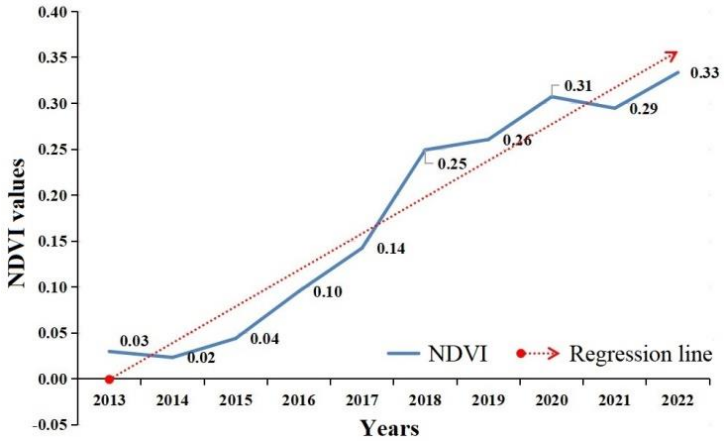


Figure 9. *NDVI average values of 3 quadrats during the period of 2013-2022*

The graph 9 shows that in 2013, the average of NDVI values at quadrats was still low (0.03 in 2013) and it tended to decrease slightly in the following year (0.02 in 2014). However, the NDVI values rapidly increased in the next years. In the period 2016-2022, the planting of new trees has significantly increased the area of vegetation.

2.3.4.2. Variation of NDSI:

The NDSI is calculated to highlight bare soil differences in the green and shortwave infrared band. Based on the average of NDSI values at the quadrats for establishing the graph of NDSI mutation during the period of 2013 - 2022. The results show that the average of NDSI value varies at different values around the trend line of NDSI. However, in general it has a continuous decreasing trend (Figure 10). This proves that bare soil in the quadrats is increasingly disappearing.

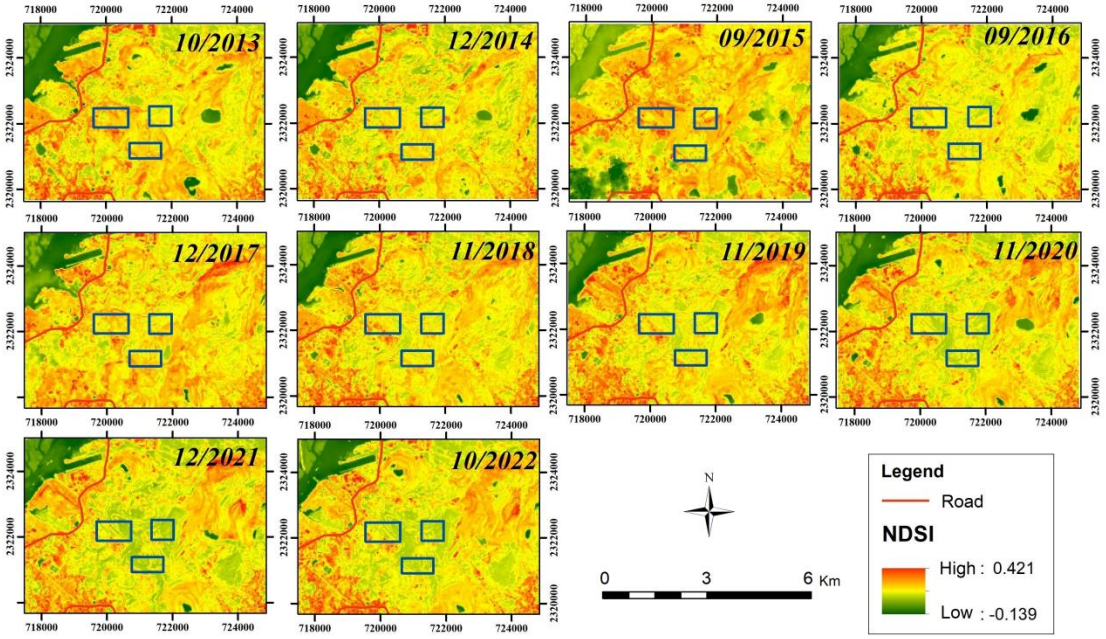


Figure 10. *Distribution of NDSI index during the period of 2013-2022. Blue boxes correspond to the quadrats.*

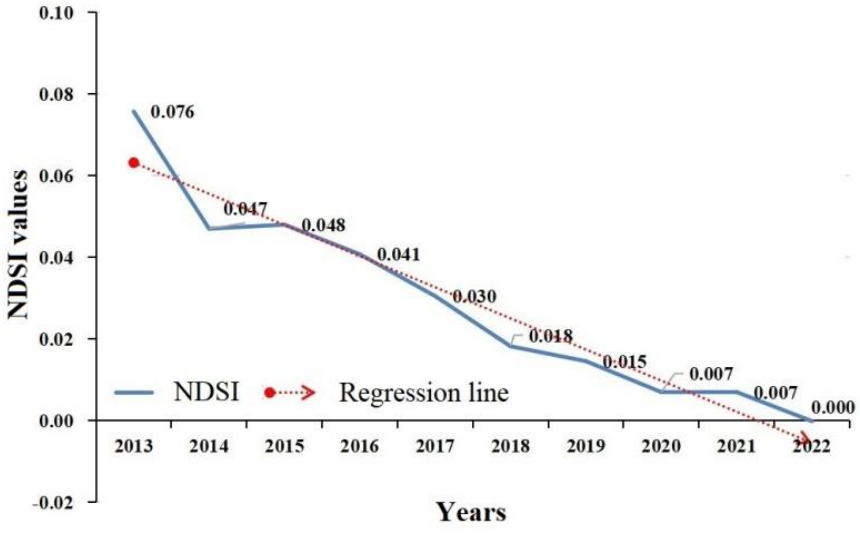


Figure 11. *NDSI average values of 3 quadrats during the period of 2013-2022*

The graph 11 shows that at the beginning, the ground was covered by bare soil so it had a quite high NDSI index of 0.07. However, as time goes on, the value of NDSI gradually decreases and reaches the negative threshold in 2022. That means that the bare soil in the quadrats has been replaced by trees, or in other words, the reclamation work has gradually transformed bare soil into vegetation.

2.4. Discussion

Remote sensing technology is used to monitor the process of environmental reclamation because satellite images are intuitive and objective for observing objects on the ground at different times of the year. Due to the wide coverage of images, information on the change of objects is consistent. Landsat satellite images are a source of data to analyze the process of environmental reclamation via variation on the ground and the spatial distribution of mainland covers at coalfields such as: vegetation, coalfield, and bare soil. The supervised classification method is realized for identifying land covers based on the object classification of Landsat images and the accuracy was assessed through validation samples issued from the visual interpretation of super-high resolution Google Earth images and on-the-ground knowledge. In addition, NDVI and NDSI spectral indices were also calculated to monitor mutation in vegetation and bare soil at quadrats in the Suoi Lai coal mine over 10 years. The obtained NDVI and NDSI values show their close relationship with each other, where the increase/decrease of either index clearly reflects the reclamation process at this coal mine. In addition, the image classification results recognize an increase in the area of vegetation cover, which means a decrease in the area of bare soil and coalfield. The continuous decreasing trend of the NDSI value and the continuous increase of the NDVI value demonstrate the efforts of local governments in general and coal mining companies for reclaiming the environment and transitioning from “brown” to “green” models of economic development. This fact accordingly manifests the activity of Vietnam National Coal and Mineral Industries Group (TKV) when they reclaimed and replanted nearly 200 hectares of trees within the territory of Ha Long city such as the Western section (Hon Gai Coal Company), South-eastern section (Ha Lam Coal Joint Stock Company), Eastern section (Ha Tu Coal Joint Stock Company) and Northern section (Giap Khau area) during the period from 2017 to the present (Pham, 2020).

3. CONCLUSION

The availability of Landsat images has offered a valuable data source for mapping land covers in the study area. It is possible then to evaluate the reclamation process via land cover changes over many years. The accuracy has been independently validated for all classification results using high resolution satellite images in Google Earth database and it attained appropriate with OA > 87.67% and Kappa coefficient > 0.81. Although, the errors have remained in the classification results due to the selection of samples from the Landsat images with medium spatial resolution (30 m). However, several land cover categories such as urban residence, coalfield, warehouse, and bare soil are clearly separated even they have identical reflectance signatures. This fact proves that remote sensing technology is a highly efficient and objective tool in managing resources and environment. Monitoring the environmental reclamation process in coal mining production is an extremely necessary duty, that contributes to improve the direct impact on human being and natural environment.

The results of this research provide accurate information, based on which authorities and coal mining companies can prepare appropriate plans for a sustainable environment.

ACKNOWLEDGEMENTS

The authors wish to acknowledge assistance from colleagues and support from the Hanoi National University of Education for deploying this research.

REFERENCE

1. Al-doski J, Mansor S B, San H n P and Khuzaimah Z 2020 Land Cover Mapping Using Remote Sensing Data *American Journal of Geographic Information System* **9** 33-45.

2. Alberto R T, Serrano S C, Damian G B, Camaso E E, Biagtan A R, Panuyas N Z and Quibuyen J S 2017 Extraction of inland Nypa fruticans (Nipa Palm) using Support Vector Machine. In: *Fifth International Conference on Remote Sensing and Geoinformation of the Environment*, ed K Themistocleous, *et al.* (Paphos, Cyprus: SPIE) p 1044406

3. Coppin P, Jonckheere I, Nackaerts K, Muys B and Lambin E 2004 Review ArticleDigital change detection methods in ecosystem monitoring: a review *International Journal of Remote Sensing* **25** 1565-96.

4. Cortes C and Vapnik V 1995 Support-vector networks *Marchine Learning* **20** 273-97.

5. Deng Y, Wu C, Li M and Chen R 2015 RNDSI: A ratio normalized difference soil index for remote sensing of urban/suburban environments *International Journal of Applied Earth Observation and Geoinformation* **39** 40-8.

6. Devadas R, Denham R and Pringle M 2012 Support vector machine classification of object-based data for crop mapping, using multi-temporal landsat imagery *ISPRS - International Archives of the Photogrammetry, Remote Sensing and Spatial Information Sciences* **XXXIX-B7** 185-90.

7. Dueker K J and Horton F E 1972 Urban-change detection systems: Remote-sensing inputs *Photogrammetria* **28** 89-106.

8. Ebong M S, Esin J, Ubong D E and Nsidibe M S 2019 Assessing The Presence of Nipa Palm in Qua Iboe River Estuary and Cross River Estuary: A Brackish Water Environment of Akwa Ibom State, South Nigeria *Euro Afro Studies International Journal* **1** 56-69.

9. Gómez C, White J C and Wulder M A 2016 Optical remotely sensed time series data for land cover classification: A review *ISPRS Journal of Photogrammetry and Remote Sensing* **116** 55-72.

10. Goward S, Arvidson T, Williams D, Faundeen J, Irons J and Franks S 2006 Historical record of Landsat global coverage: Mission operations, NSLRSDA, and international cooperator stations *Photogrammetric Engineering and Remote Sensing* **72** 1155-69.

11. Hemati M, Hasanlou M, Mahdianpari M and Mohammadimanesh F 2021a A Systematic Review of Landsat Data for Change Detection Applications: 50 Years of Monitoring the Earth *Remote Sensing* **13** 1-33.

12. Hemati M A, Hasanlou M, Mahdianpari M and Mohammadimanesh F 2021b A Systematic Review of Landsat Data for Change Detection Applications: 50 Years of Monitoring the Earth *Remote Sensing* **13** 2869.

13. Hermes L, Frieauff D, Puzicha J and Buhmann J 1999 Support vector machines for land usage classification in Landsat TM imagery. In: *International Geoscience and Remote Sensing Symposium (IGARSS),* (Hamburg, Germany: IEEE) pp 348-50 vol.1.

14. Hoang T V, Chou T-Y, Fang Y-M, Chen M, Yeh M and Nguyen X L 2018 Evaluation Vulnerability of Climate Change Impacts to Quang Ninh Province, Vietnam *International Journal of Advanced Remote Sensing and GIS* **7** 2758-81.

15. Huynh S 2002 Hydrodynamic study of Ha Long Bay. In: *Department of Environmental Engineering,* (Perth, Australia: University of Western Australia) p 81.

16. Igoniye W, Okujagu C and Ayirite A 2015 Synthesis and Characterisation of Nipa Palm Extract as a Potential Emitting Material for Organic Light Emitting Diode *Journal of Natural Sciences Research* **5** 152-7.

17. Ingram K, Knapp E and Robinson J 1981 *Change Detection Technique Development for Improved Urbanized Area Delineation* (Springfield, USA: Computer Sciences Corporation).

18. Kantakumar L N and Neelamsetti P 2015 Multi-temporal land use classification using hybrid approach *The Egyptian Journal of Remote Sensing and Space Science* **18** 289-95.

19. Kavitha A V, Srikrishna A and Satyanarayana C 2021 A Review on Detection of Land Use and Land Cover from an Optical Remote Sensing Image *IOP Conference Series: Materials Science and Engineering* **1074** 012002.

20. Kloiber S M, Brezonik P L and Bauer M E 2002 Application of Landsat imagery to regional-scale assessments of lake clarity *Water Research* **36** 4330-40.

21. Kobayashi N, Tani H, Wang X and Sonobe R 2020 Crop classification using spectral indices derived from Sentinel-2A imagery *Journal of Information and Telecommunication* **4** 67-90.

22. Lesiv M, See L, Bayas J C L, Sturn T, Schepaschenko D, Karner M, Moorthy I, McCallum I and Fritz S 2018 Characterizing the Spatial and Temporal Availability of Very High Resolution Satellite Imagery in Google Earth and Microsoft Bing Maps as a Source of Reference Data *Land* **7** 118.

23. Liu S a, Li X, Chen D, Duan Y, Ji H, Zhang L, Chai Q and Hu X 2020 Understanding Land use/Land cover dynamics and impacts of human activities in the Mekong Delta over the last 40 years *Global Ecology and Conservation* **22** e00991.

24. Lu D and Weng Q 2007 A survey of image classification methods and techniques for improving classification performance *International Journal of Remote Sensing* **28** 823-70.

25. Ma L, Li M, Ma X, Cheng L, Du P and Liu Y 2017 A review of supervised object-based land-cover image classification *ISPRS Journal of Photogrammetry and Remote Sensing* **130** 277-93.

26. Malarvizhi K, Kumar S V and Porchelvan P 2016 Use of High Resolution Google Earth Satellite Imagery in Landuse Map Preparation for Urban Related Applications *Procedia Technology* **24** 1835-42.

27. Markham B L, Arvidson T, Barsi J A, Choate M, Kaita E, Levy R, Lubke M and Masek J G 2018 *Comprehensive Remote Sensing,* ed S Liang (Oxford: Elsevier) pp 27-90.

28. Ngô T S 2013 Environmental management during the mining and reclamation process at Hong Thai coal mine, Quang Ninh province. In: *Faculty of Environment,* (Hanoi: University of Science) p 82.

29. Nguyen G C, Dang K V, Vu T A, Nguyen A K and Weber C 2022 Ha Long—Cam Pha Cities Evolution Analysis Utilizing Remote Sensing Data *Remote Sensing* **14** 1241.

30. Pham T 2020 TKV: Greening the environment of coal mines. In: *Quang Ninh News,* (Ha Long: Quang Ninh people's Committee).

31. Pham T 2021 Quang Ninh - coal mining sector: closely sticking In: *The information gate of Quang Ninh province,* (Ha Long: Quang Ninh people's Committee).

32. Phạm T H N 2014 Research on environmental reclamation solutions in open-cast coal mining activities in Quang Ninh province. In: *Faculty of Economy and Management,* (Hanoi: Thuy Loi University) p 98.

33. Phuong T 2021 Quang Ninh tourism: Efforts to revive after a long hibernation due to Covid 19. In: *Trade Mark and Public Opinion,* (Hanoi: Vietnam Association for Anti-Counterfeiting and Trademark Protection).

34. Piekkoontod T, Pachana B, Hrimpeng K and Charoenjit K 2020 Assessments of Nipa Forest Using Landsat Imagery Enhanced with Unmanned Aerial Vehicle Photography *Applied Environmental Research* **42** 49-59.

35. Radke R, Andra S, Al-Kofahi O and Roysam B 2005 Image change detection algorithms: A systematic survey *IEEE transactions on image processing : a publication of the IEEE Signal Processing Society* **14** 294-307.

36. Réjichi S and Chaabane F 2015 Satellite image time series classification and analysis using an adapted graph labeling. In: *8th International Workshop on the Analysis of Multitemporal Remote Sensing Images (Multi-Temp),* (Annecy, France: IEEE) pp 1-4.

37. Rouse J W, Haas R H, Schell J A and Deering D W 1974 Monitoring vegetation systems in the Great Plains with ERTS. In: *Third Earth Resources Technology Satellite (ERTS) Symposium,* (Texas, USA: NASA) pp 309-17.

38. Santillan J R and Makinano-Santillan M 2018 Analysis of in-situ spectral reflectance of sago and other palms: implications for their detection in optical satellite images. In: *Developments, Technologies and Applications in Remote Sensing,* (Beijing, China: ISPRS) pp 185-91.

39. Sayler K 2020 Landsat 4-7-8 Collection 2 (C2) Level 2 Science Product (L2SP) Guide. (South Dakota: US Geological Survey) p 43.

40. Shang M, Wang S, Zhou Y, Du C and Liu W 2019 Object-based image analysis of suburban landscapes using Landsat-8 imagery *International Journal of Digital Earth* **12** 720-36.

41. Singh A 1989 Review Article Digital change detection techniques using remotely-sensed data *International Journal of Remote Sensing* **10** 989-1003.

42. Starzomski B 2014 *Encyclopedia of Quality of Life and Well-Being Research,* ed A C Michalos (Dordrecht: Springer Netherlands) pp 3205-9.

43. Sun J and Ongsomwang S 2020 Multitemporal Land Use and Land Cover Classification from Time-Series Landsat Datasets Using Harmonic Analysis with a Minimum Spectral Distance Algorithm **9** 67.

44. Szostak M, Pietrzykowski M and Likus-Cieślik J 2020 Reclaimed Area Land Cover Mapping Using Sentinel-2 Imagery and LiDAR Point Clouds *Remote Sensing* **12** 261.

45. Tran T H 2022 Introduction to Ha Long City. (Ha Long City: Ha Long City Ha Long People's Committee).

46. Trimble 2010 *eCognition® Developer 8.64.0 Reference Book* (München, Germany: Trimble Germany GmbH).

47. Tzotsos A and Argialas D 2008 *Object-Based Image Analysis: Spatial Concepts for Knowledge-Driven Remote Sensing Applications,* ed T Blaschke, *et al.* (Berlin, Heidelberg: Springer Berlin Heidelberg) pp 663-77.

48. Vaughn K J, Porensky L M, Wilkerson M L, Balachowski J, Peffer E, Riginos C and Young T P 2010 Restoration Ecology *Nature Education Knowledge* **3** 66-70.

49. Vu T P, Do N H and Vo T C 2018 Impacts of coal mining on landscape, environment, and land use at Ha Long City (Quang Ninh province) *Vietnam Journal of Agricultural Sciences* **16** 351-63.

50. Wulder M A, Loveland T R, Roy D P, Crawford C J, Masek J G, Woodcock C E, Allen R G, Anderson M C, Belward A S, Cohen W B, Dwyer J, Erb A, Gao F, Griffiths P, Helder D, Hermosilla T, Hipple J D, Hostert P, Hughes M J, Huntington J, Johnson D M, Kennedy R, Kilic A, Li Z, Lymburner L, McCorkel J, Pahlevan N, Scambos T A, Schaaf C, Schott J R, Sheng Y, Storey J, Vermote E, Vogelmann J, White J C, Wynne R H and Zhu Z 2019 Current status of Landsat program, science, and applications *Remote Sensing of Environment* **225** 127-47.

51. Wulder M A, Masek J G, Cohen W B, Loveland T R and Woodcock C E 2012 Opening the archive: How free data has enabled the science and monitoring promise of Landsat *Remote Sensing of Environment* **122** 2-10.

52. Xu Y, Wu L, Xie Z and Chen Z 2018 Building Extraction in Very High Resolution Remote Sensing Imagery Using Deep Learning and Guided Filters *Remote Sensing* **10** 144.

53. Yang D, Wu D and Ding H 2021 Study on land use change detection based on Landsat data with object-oriented method. In: *International Conference on Computer Information Science and Artificial Intelligence (CISAI),* (Kunming, China: IEEE) pp 268-72.

54. Yu Q, Gong P, Clinton N, Biging G, Kelly M and Schirokauer D 2006 Object-based Detailed Vegetation Classification with Airborne High Spatial Resolution Remote Sensing Imagery *Photogrammetric Engineering and Remote Sensing* **72** 799-811.

55. Zhu Z 2017 Change detection using landsat time series: A review of frequencies, preprocessing, algorithms, and applications *ISPRS Journal of Photogrammetry and Remote Sensing* **130** 370-84.

IDENTIFICATION OF WEIGHTING EVENT CAUSED BY UNDERGROUND COAL MINING AT QUANG NINH COAL FIELD, VIETNAM

T D Le[1,2] and P H Nguyen[1,2]

[1] Faculty of Mining, Hanoi University of Mining and Geology, Hanoi, Vietnam

[2] Research Group: Sustainable Development of Mining Science, Technology and Environment (SDM), Hanoi University of Mining and Geology, Hanoi, Vietnam

E-mail: t.d.le@humg.edu.vn

Abstract: Underground mining is one of the prevalent technologies that matches the national government's attitude towards the Vietnam coal industry. It is considered as a critical component of the brown-to-green transition strategy. One of the problems dealing with sustainable underground coal mining in Vietnam is to exploit the seams in unfavourable ground control conditions. Although a large proportion of national coal reserves is distributed in these conditions, its exploitation remains limited and unsafety due to the critical geo-mechanical associated risks such as roof fall or weighting event. This paper presents an identification on the cause and solution of the weighting event occurring in Vietnam geological-mining conditions. Using collected field measurement, computational modelling and expert methods, the weighting event is found to commonly occur in two typical stratigraphic settings. Corresponding technological solutions to minimising the event are theoretically proposed, contributing to the safe, fully exploited, and efficient mining of Vietnam coal industry.

1. INTRODUCTION

Weighting event is the great concentration and rapid release of roof pressure at underground exploiting face (workplace). This is commonly associated with the overhanging and breakage of roof strata portion at initial face advance (first weighting) and/or after a certain distance of face advance (periodic weighting, Figure 1). This portion of roof strata is the lower part of main roof, has sparse geological structures (e.g., joint, bedding), and typically occurs within 50–70 m above seam floor. This roof is called massive roof (in academic research) or competent strata (in industry report), which are normally stable. Along with the main roof strata conditions, the immediate roof should be of insufficient thickness that cannot fill the mined-out void. This enables the massive roof to directly impact the working face. Weighting is a critical event in underground coal extraction because when occurs, it causes great force that destroys face equipment and injures workers. Weighting may also cause roof cavities and face spall that interrupt normal production, requiring significant time and cost for remedy.

A precursor for identification of the weighting event at Quang Ninh coal field is to classify the stability of roof rock strata in the field. Unfortunately, there have been limited studies in the literature and all are in Vietnamese [2, 3]. According to Pham [3], Vietnam Mining Science and Technology Association (VMST) developed a system for classification of Vietnam roof rock strata stability (Table 1). It is stated that for the gently inclined to inclined coal seams at Quang Ninh coal field, in period of 2021–2025 the proportion of industrial reserves classified as stable, medium and unstable is 25, 69 and 6%, respectively.

The result indicates that the VMST system is basically similar to VNIMI system. The main difference is the reduction of bedding thickness, while the addition of GIG index appears to insignificantly affect the classification result. It is the thinner bedding that results in a significant proportion of medium stable roof (69%) and very small proportion of unstable roof (6%) compared to the classification result in a 10-year earlier research [2]. A common agreement between the two studies is that the roof rock of Quang Ninh underground coal mines is mainly in class of medium-to-stable strata. This facilitates the occurrence of weighting event when mining in such strata, as mentioned earlier in this section.

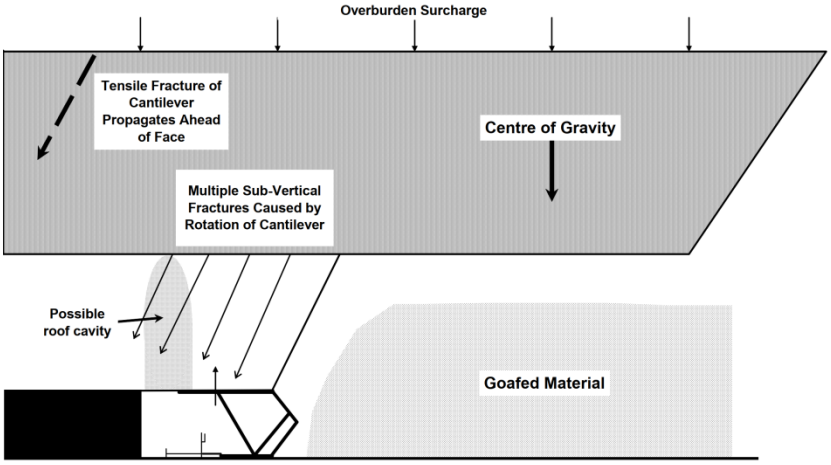


Figure 1. *Concept of weighting event [1].*

Table 1. Stability classification of roof rock strata in Quang Ninh coal field [3].

Rock composition and strength			GIG index	Classification of roof stability			Classification of roof caving	
Composition	Compressive strength (MPa)	Bedding thickness (m)		Class	Exposed area (m^2)	Exposed time (hour)	Class	Caving span (m)
Conglomerate-gritstone, sandstone, thickly bedded siltstone	60–80	> 0.3	> 280	Stable	> 15	> 2	Very hard to cave	> 12
							Hard to cave	6–12
Sandstone, averagely bedded siltstone	30–60	0.1–0.2	60–280	Medium stable	10–15	0.5–2	Medium to cave	2–6
Thinly bedded siltstone, thinly bedded claystone	20–40	0.1–0.15	32–60	Unstable	5–10	< 0.5	Easy to cave	1–2
Claystone, coal-claystone, thinly bedded	10–20	0.05–0.1	< 32	Very unstable	< 5	~ 0	Very easy to cave	< 1

Because Quang Ninh underground coal mines started exploitation under medium-to-stable roof strata, the identification of potential weighting event in this coal field is of practical needs and great importance. Apart from the above two studies, there are only a few others investigating the weighting event for Quang Ninh condition. Vu [4] studied the

parameters affecting the characteristics and breakage ability of massive strata in steep condition, which is seam V15, zone III, Quang Hanh coal mine. Also in steep seam condition, Luong [5] proposed the room mining method combined with strip coal pillar for minimization of weighting event. Le et al. [6] computationally modelled the mine pressure law and behaviour of hard-to-cave roof of face TT7.9, zone Nga Hai, Quang Hanh coal mine. Using similar method, Pham and Nguyen [7] studied the effect of weighting on roadway stability. Although all these studies interpreted some characteristics of weighting in Quang Ninh coal field, no generalized cause and solution of the event in the field was identified. This paper aims to identify the typical types of the weighting event in Quang Ninh mining condition. The study results can guarantee the exploitation safety and productivity in the largest coal field of Vietnam, satisfying the requirements from Vietnam practice and government.

2. ANALYSIS OF WEIGHTING EVENTS AT QUANG NINH COAL FIELD

According to Pham [3], the Quang Ninh coal measures have an average sedimentation thickness of 200–1280 m. The measures consist of coal-claystone, claystone, siltstone, sandstone, gritstone, and conglomerate. The rock size increases as its relative location to coal seam increases. In the order of stratigraphic column, roof rocks are usually thickly-to-thinly bedded siltstone overlain by sandstone strata. Sometimes there exists a thin layer of claystone or coal-claystone of 0.3–0.5 m between seam and siltstone. This is called the false roof. The immediate roof is thinly (< 15 cm) to medium (15–30 cm) bedded siltstone. The main roof is commonly sandstone and/or thickly bedded siltstone.

Mining practice in Quang Ninh shows that under hard-to-cave roof, an exploitation panel has a typical overhanging roof of 2–6 m length behind face support. The overhanging roof breaks periodically and causes weighting event at face. Due to the use of hydraulic support and mechanised support, the panel has low risk of face breakdown. However, face spall and roof cavity (roof fall) do occur, especially in top-coal caving mining method. Some examples of hard-to-cave roof panel can be analysed as follows. In 1991, Ha Lam coal mine exploited Seam 10 at section of medium thickness. The roof did not cave after some face advances, and the mine had to change the mining method to maintain safety and recover production. It was reported that in that section, the immediate roof consisted of claystone, coal-claystone, and siltstone (Figure 2a). The claystone had an average caving span of 1–2 m, but it was thinly (0.1–1.5 m) and unevenly distributed in the roof. The siltstone had an average caving span of 6–8 m while the main roof was very competent. As the siltstone was evenly distributed with a thickness of 3–14 m, it made the immediate roof stable and overhanging. It was also reported that the caving thickness of immediate roof was not sufficient to fill the goaf. The competent main roof therefore also contributed to the weighting event at face. A similar problem occurred at Seam 15 Bac Bang Danh coal mine. The seam's immediate roof was of 3–3.5 m thickness and overlain by a competent main roof (Figure 2b).

In 1999, Uong Bi coal mine exploited Seam 46, Trang Khe area at level +350/+390. The first caving in the panel did not occur although the face had advanced 30 m. It was reported that the seam's roof consisted of 0.3–0.7 m of claystone and coal-claystone (false roof) and competent main roof interbedded by thin siltstone layers (Figure 2c). It was believed that due to the absence of sufficient immediate roof, the main roof acted as a massive roof that

resulted in the weighting event at area. A similar stratigraphic column setting was seen at Seam 5, Canh Ga area, Vang Danh coal mine (Figure 2d).

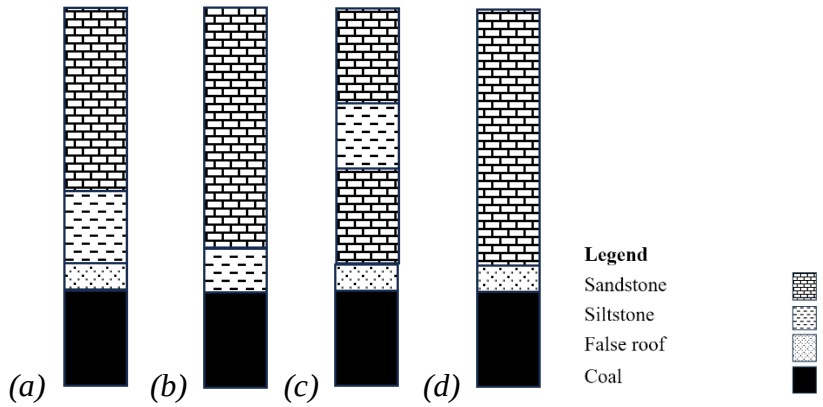


Figure 2. *Stratigraphic column at (a) Seam 10 Ha Lam, (b) Seam 15 Bac Bang Danh, (c) Seam 46 Trang Khe, Uong Bi, and (d) Seam 5 Canh Ga, Vang Danh coal mines (modified from [3]).*

3. MODELLING OF WEIGHTING EVENT AT MONG DUONG COAL MINE

3.1. Model construction

Mong Duong coal mine is located in Mong Duong ward, Quang Ninh province, Vietnam. Using the VMST classification system, the mine is found to have 19 panels under stable and hard-to-cave roof condition [3]. At present, the mine has exploited Seam M6 East Wing where weighting events are reported to occur irregularly. According to the company report [8], for Panel M6 No.2 level -190/-130, the seam has a total thickness of 2.2 m, average dip angle of 34 degrees, and strength index of 1–2. The immediate roof has an average thickness of 4.5 m, compressive strength of 594.7 kG/cm^2, and tensile strength of 91.05 kG/cm^2. The main roof has an average thickness of 22 m, compressive strength of 522.8 kG/cm^2, and tensile strength of 60.23 kG/cm^2.

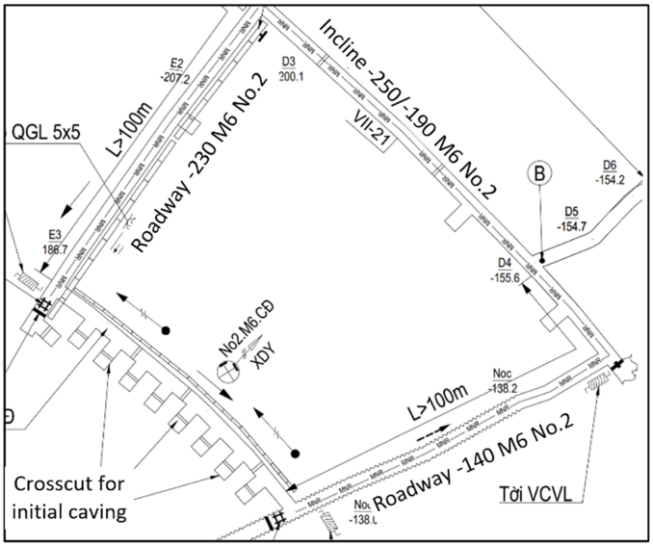


Figure 3. *Location of cross-section for modelling.*

To understand the mechanisms of the weighting event at Panel M6 No.2 level -190/-130, a simplified computational model of the panel along its strike is developed (Figure 3). Based on the above geological conditions, the model consists of a 2.2 m seam thickness, overlain by a 4.5 m immediate roof thickness and a 22 m main roof thickness (Figure 4). Above the main roof is an overburden strata of 40 m thickness. Similarly, below the seam is a floor strata of 40 m. The total model height is 108.8 m. Along the direction of face

advance, the modelled exploitation length is 55 m. This corresponds to the practical length in Phase 1 of panel exploitation. The total model width is 220 m.

The altitude of surface is +97.5 and the seam has a cover depth of 257.5 m. Because a strata portion of 68.7 m is explicitly modelled, the remaining portion of 188.8 m is modelled by a boundary stress of 5.02 MPa applied on top of model. The stress regime is modelled with a ratio of vertical stress to horizontal stress of one.

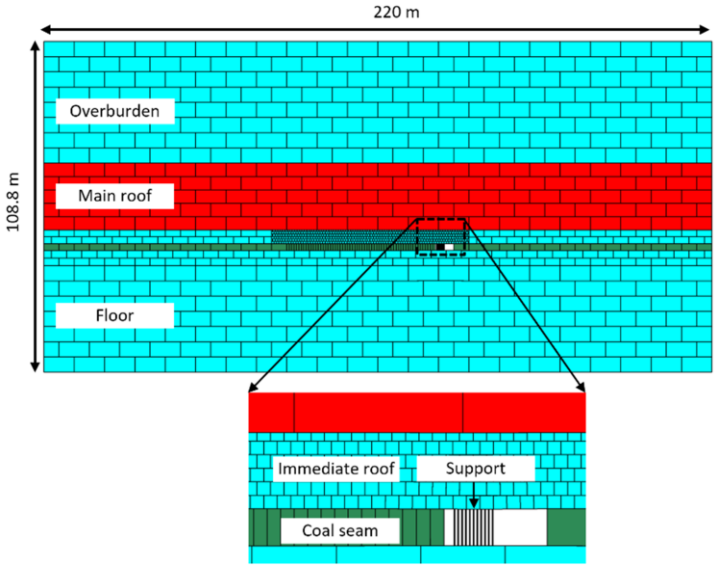


Figure 4. *Computational model of Panel M6 No.2 level -190/-130.*

The available information on engineering geology is at regional scale. Therefore, detailed geological structures at the mine are referred from similar mines. For example, as the coal seam is fully exploited in single cut, the vertical joints are modelled with a spacing of 0.8 m, which is equivalent to one web cut. For the immediate roof, typical sedimentary structures such as joints and beddings are modelled. The spacing between beddings is 0.8 m, which is equal to the lowest bedding thickness. The spacing between joints is 0.8 and 1.6 m, representing two scenarios of medium jointed and sparsely jointed strata. For the strata outside the area of interest, the geological structures are modelled with an increasing spacing of from 2.5 to 10 m.

The two dimensional discontinuum-based code UDEC is used [9]. The plastic model is assigned to intact rock. The Coulomb slip model is assigned to joints and beddings. The input parameters of intact rock for modelling are presented in Table 2. The support is modelled as a set of spring elements with a total width of 2.26 m and a loading capacity of 1.8 MN (Figure 4).

Table 2. Input parameters of intact rock for modelling.

Strata	Volume weight (kg/m^3)	Compressive strength (MPa)	Tensile strength (MPa)	Compressive elastic modulus (GPa)	Tensile elastic modulus (GPa)	Cohesion strength (MPa)	Internal friction angle (degree)
Coal seam	1600	15	4.3	-	-	4.8	25
Immediate roof	2660	59	9.1	0.35	0.12	16	33
Main roof	2630	79	15.3	0.45	0.15	20.6	35

3.2. Model analysis

For the scenario of medium jointed immediate roof (spacing of 0.8 m), the model result shows that when the face advances 20 m (25 web cuts), this roof is visually separated from

the main roof (Figure 5a). Within the immediate roof, the layers are also separated from each other, especially for the lower layer. The separation is clearly seen in the middle of hanging roof. At both ends of the hanging roof, the joints and bedding fail, mostly in tension mode. At the same time, Figure 5b shows that the intact rock fails very little in the immediate roof. Intact rock mostly fails in coal seam in shear mode. The hanging roof caves as the face advances 20.8 m (26 web cuts). This is called the first caving or initial caving of immediate roof. The numerical results from Figure 5 confirm that the immediate roof of Panel M6 No.2 level -190/-130 is stable and hard to cave.

After the first caving, the immediate roof caves periodically. The roof caves after one to two web cuts (0. 8–1.6 m), as shown in Figure 6a and Figure 6b. It sometimes caves after three cuts (3.4 m, Figure 6c). These results indicate that for the scenario of medium jointed strata, the immediate roof can cave immediately or overhang after the advance of face support.

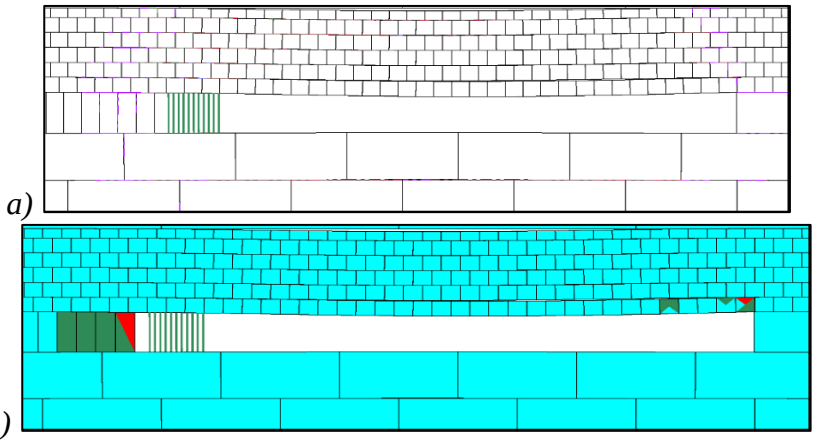


Figure 5. *First caving of medium jointed immediate roof.*

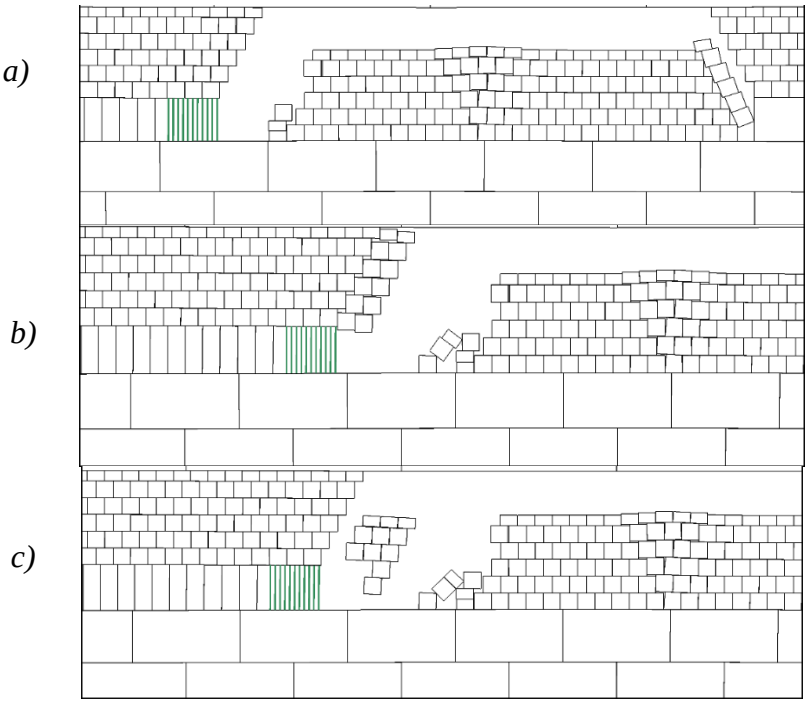


Figure 6 *Periodic caving of medium jointed immediate roof.*

For the scenario of sparsely jointed immediate roof (spacing of 1.6 m), the model results show that when the face advances 28 m (35 web cuts), the roof starts to cave its lowest layers (Figure 7a). The above layers of the roof complete caving after next two cuts (29.6 m). After the first caving, the immediate roof caves periodically along the vertical joints. However, due to the large spacing between the joints, the immediate roof normally caves after two web cuts, which is 1.6 m of face advance. Furthermore, the broken part may not completely detach from the immediate roof due to insufficient void space. This results in the overhanging roof of 4–5 m behing face support (Figure 7b).

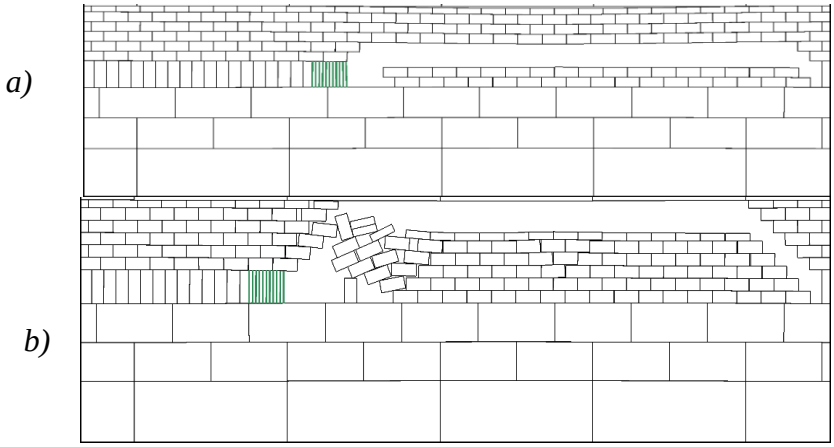


Figure 7 *(a) First caving and (b) overhanging of sparsely jointed immediate roof.*

4. PROPOSAL OF TECHNOLOGICAL SOLUTIONS

As analysed in Section 2, when a face enters hard-to-cave roof condition, most mines in Quang Ninh coal field have to change the mining method (mining system). In particular, the fully caving method (the prevalent ground control technique in coal field) is replaced by the room-and-pillar method. The roof strata are naturally lowered on strip pillars between the room without caving. Although this technological solution enables a mine to safely exploit through difficult mining condition, it results in low production rate (2.000–5.000 tons/month), low labour productivity (1.6–2.2 tons/manshift), high roadway development cost (30–42 m/1000 tons), and high resources loss (33–40%) [10]. In order to minimise the resources loss for sustainable coal industry and based on the literature review [3], this paper proposes a solution approach in which the hard-to-cave roof is first weakened and then caves behind face support. The weakening solution can be implemented by pre-blasting of advancing borehole ahead of face, post-blasting of short holes behind face, and hydraulic fracturing. The solutions are applicable to current Vietnam coal industry but require detailed investigation to interpret the advantages, disadvantages, and conditions for use. For example, the solution of drilling long borehole can be quickly used in practice. However, it requires a significant volume of explosives and thus needs careful consideration. It should be noted that apart from mining method, other solutions such as panel design or operational parameter design (e.g., speed of face advance, setting value and/or yield value of support) can be considered in separate studies.

5. CONCLUSIONS

This paper presents an identification on the cause and solution of the weighting event occurring in Quang Ninh geological-mining conditions—the largest coal field in Vietnam. Using collected field measurement, computational modelling and expert methods, the

weighting event is found to commonly occur in two typical stratigraphic settings of roof strata: (i) insufficient immediate roof overlain by massive strata and (ii) false immediate roof overlain by massive strata. The results from modelling confirm that the geological structures (i.e., joints) greatly contribute to the stability of roof strata (manifested as overhanging and caving) and accordingly to the risk of weighting event. Based on the literature review, technological solutions to weakening the roof are proposed for the exploitation in Quang Ninh coal field conditions. Future studies are required for the detailed application of the solutions.

REFERENCES

[1] Frith R 2005 Half a career trying to understand why the roof along the longwall face falls in from time to time? *Proc. 24th Int. Conf. on Ground Control in Mining* (West Virginia: West Virginia University) pp 33–43

[2] Pham D H 2012 *Development of geo-mechanical database for mechanisation of coal industry in Vietnam* (Hanoi: Vietnam Institute of Mining Science and Technology)

[3] Pham D T 2022 *Research and selection of technological solution for ground control in conditions of hard-to-cave roof and weak roof* (Hanoi: Vietnam Mining Science and Technology Association)

[4] Vu V H 2013 *Research and proposal of proper ground control for hard-to-cave roof condition at Seam 15, zone III - Quang Hanh coal company* (Hanoi: Hanoi University of Mining and Geology)

[5] Luong M H 2017 *Research and selection of proper roof control method for hard-to-cave roof condition of Seam 11(46) - Uong Bi coal mine* (Hanoi: Hanoi University of Mining and Geology)

[6] Le Q P, Zubov V P, Dao V C and Vu T T D 2018 The rules apparition mine pressure and transfigure stone roof in the longwall mechanized furnace TT7.9 – area Nga Hai, Quang Hanh coal company *Proc. Conf. Earth Sciences and Natural Resources for Sustainable Development* (Ha Noi: Transport Publishing House) pp 124–129

[7] Pham T N and Nguyen V N 2021 The effects of dynamic pressure on the stability of prepared drifts near the working surface areas *J. of Mining and Earth Sciences* **62** pp 85–92

[8] Mong Duong Coal Company 2022 *Technical design of Panel M6 CĐ-2 level -190/-130* (Quang Ninh: Mong Duong Coal Company)

[9] Itasca Consulting Group 2019 *UDEC – Universal Distinct Element Code Ver. 7.0* (Minneapolis: Itasca)

[10] Truong D D, Dao H Q, Vu V H and Hoang K H 2014 Assessment of controlling solution to hard-to-cave roof at some Quang Ninh underground mines. *Mining Industry J.* **2** pp 58–62

ACKNOWLEDGMENTS

This research is funded by Vietnam Ministry of Education and Training (MOET) under grant number B2023-MDA-05. Mong Duong Coal Company is thanked for providing field data.

DETERMINATION OF THE ROCK PRESSURE BY NUMERICAL MODELING METHOD WHEN DIGGING ROADWAYS UNDER THE OPEN-PIT MINE AREA AT THE HA LAM COAL MINE, QUANGNINH

Tien Trung Vu[1*], Doan Viet Dao[2], Son Anh Do[1]

[1] Faculty of Mining, Ha Noi University of Mining and Geology, Ha Noi City, Vietnam

[2] Faculty of Civil Engineering, Ha Noi University of Mining and Geology, Ha Noi City, Vietnam

*Email: vutrungtien@humg.edu.vn

Abstract: Currently, Ha Lam Coal Mine is exploiting a number of the longwalls that are located under the open-pit mine area. Therefore, it is very difficult and complicated to calculate the rock pressure when digging the roadways under the open-pit mine area. The potential risks of unsafety are huge. It can be the risk of water flowing into the roadways or the occurrence of water cracking and mud, which is a very dangerous phenomenon in mining.

In this research, the numerical method was used. Based on Phase2 software and geological conditions of the Ha Lam Coal Mine, the authors built a simulation model to determine the rock pressure acting on the roadways that are located underneath the open-pit mine area. Through the actual study at Ha Lam Coal Mine, the authors calculated the rock pressure when digging the roadways underneath the open-pit mine area of Seam 14 at the West Side at level -54. This open-pit mine is located on the longwall in Seam 11, the stratigraphic distance from the longwall to the bottom of the open-pit mine is about 100 ÷ 120 m.

The findings of the study serve as the foundation for the practical application of production methods at the Ha Lam Coal Mine. Based on calculating the rock pressure acting on the roadways at Seam 11, from which the support plan has been developed. The research result of the article will also serve as a basis for other underground mines with similar geological conditions in Quang Ninh province to consider and apply.

Keywords: *rock pressure, roadways, numerical method, open-pit mine, Ha Lam Coal Mine.*

1. INTRODUCTION

The process of exploiting the longwalls of the coal seams located underneath the open-pit mine area is extremely difficult and complicated [1]. To ensure the safe and effective exploitation of these longwalls, we need a reasonable solution for excavation and protection, as well as calculating the rock pressure acting on the tunnels under this area. Currently, calculating the rock pressure acting on the tunnels are done using many different methods [2]. Depending on each specific condition, we can select a reasonable method to calculate the rock pressure acting on the tunnel. If the calculation of rock pressure acting on the tunnel is more accurate, the more reasonable the choice of support will be, the tunnel will be well protected and meet the requirements for use in actual mine production [3; 4].

When digging and supporting, as well as calculating the rock pressure acting on the tunnels that are located under the open-pit mining area (completed or under exploitation), it is necessary to pay attention to potential risks unsafe which is related to the amount of water contained in the open-pit mine. Thus, the water is one of the factors affecting on the rock pressure, as well as the stability of the tunnels during the exploitation of coal seams underneath the open-pit mine area. From the actual survey, it has been shown that, although open-pit mining has ended, but according to calculations, the open-pit area still contains a very large amount of water, especially in the rainy season [5]. Therefore, during the excavation process, it can lead to the risk of water cracking and mud. This phenomenon is very complicated, if it occurs, it will disrupt the production of the entire mine, threatening the safety of workers as well as destroying equipment in the mine, leading to economic loss of the mine [6; 7].

Ha Lam Mine is one of the mines exploited by underground mining method with a big capacity in the Quang Ninh coalfield of Vietnam. Currently, in some mines in the Quang Ninh province, including Ha Lam Mine, which is facing many difficulties in exploitation the seams, the coal reserves located underneath the open-pit mine area have finished exploitation. This problem is not only concerned by the leaders of the underground mines, but also by the leaders of the Vietnam National Coal – Mineral Industries Holding Corporation Limited [8].

The longwall in Seam 11 at the Ha Lam Coal Mine is located underneath the of Seam 14 open-pit mine area of Nui Beo Coal Mine, including open- pit at levels -54; -80; -60. The stratigraphic distance to the bottom of the ope- pit is about 100 ÷ 120 m, the stratigraphy consists of a layer of siltstone with a thickness of about 5 ÷ 6m, sandstone with a thickness of about 5 ÷ 18m, gravel with a thickness of about 15 ÷ 35m, and siltstone mixed with sandstone with a thickness of about 12 ÷ 40 m [9]. Digging the roadways in the coal Seam 11 will result the rock pressure in the mining area affecting these roadways are very complicated, as well as the influence of the water contained in the open-pit mine area on the underground mining is very large, the risk of the water cracking and mud in the mine. In order to avoid potential water risks, it is necessary to forecast and calculate the rock pressure acting on the tunnel that has been dug in coal Seam 11 at the Ha Lam Coal Mine [9]. On this basis, it is possible to assess the level of influence of water on digging the roadways. In this research, the authors uses the numerical method, by using Phase2 software to calculate the rock pressure acting on the tunnel that was dug in coal Seam 11 at Ha Lam Coal Mine under the Seam 14 open-pit area of Nui Beo Coal Mine. Input parameters of rock and coal conditions were collected from the actual mine, build a model and analyze model results based on the excavation plan corresponding to the longwall mining process. Research result of this article is also the basis for the Ha Lam

Mine to be proactive in deploying and selecting a reasonable support plan for the current conditions of this Coal Mine.

2. THEORETICAL BASIS AND RESEARCH METHODS

2.1. Introduction of the Ha Lam Coal Mine and typical cross-section of the study site

+ Introduction of the Ha Lam Coal Mine

Ha Lam Coal Mine is located in Ha Tu - Ha Lam mineral deposits, about 7 km east - northeast from Ha Long city [9].

- The East borders Nui Beo Coal Mine.
- The West borders Binh Minh Coal Mine.
- The South borders Road 18A.
- The North borders Suoi Lai Coal Mine.



***Figure 1**. The geographic location of Ha Lam Coal Mine area [10]*

The boundary of Ha Lam Coal Mine has been approved by the Ministry of Natural Resources and Environment according to Decision No. 2497/GP-BTNMT November 28th, 2008. According to this decision, Ha Lam Coal Joint Stock Company - Vinacomin belongs to the Vietnam National Coal – Mineral Industries Holding Corporation Limited is allowed to exploit coal seams V.14(10), V.11(8), V.10(7), V.7(4), V.6(3), V5 (2) from level -50 to level -300 by underground mining method. Those coal seams belong to Ha Lam Coal Mine, Ha Lam ward, Ha Long city, Quang Ninh province. Location of the Ha Lam Coal Mine is shown in figure 1.

+ The typical geological cross-section of the study site.

Based on the typical geological cross-section in the Seam 14 open-pit mine area of the Nui Beo Coal Mine, it can be shown that the bottom of its stops mining at the West Side at the -54 level. The Nui Beo Coal Mine has dumped waste rock in that open-pit mine. Because of a long time of dumping, the waste rock in the Seam 14 open-pit mine has been stabilized, but the porosity coefficient is still very large. So , the amount of water trapped in the waste rock of the Seam 14 open-pit mine is also very large. That is one of the potential causes of the risk of water cracking when digging the roadways in the coal seams at the edge and bottom of the Seam 14 open-pit mine. Simultaneously, the water contained in the waste rock of the Seam 14 open-pit mine is also one of the causes of the rock pressure acting on the roadway support structure in digging it under the open-pit mine area. The typical geological cross-section in the Seam 14 open-pit mine is shown in figure 2.

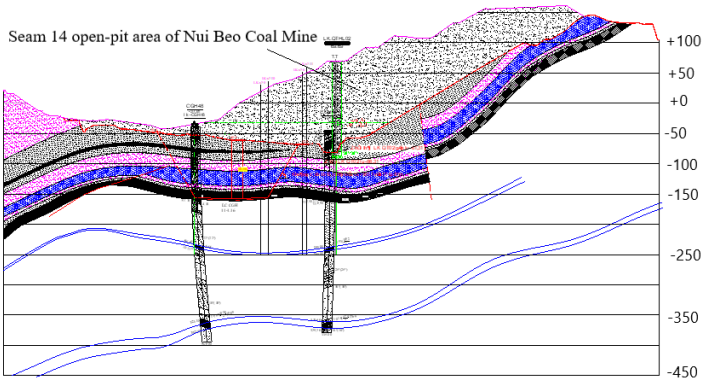


Figure 2. *The typical geological cross-section of the Seam 14 open-pit mine filled with waste rock [11]*

2.2. Geological conditions of the study site

The study site includes layers of rocks including cobblestone, gravelstone, sandstone, siltstone, claystone, and coal [11; 12].

- *Gravelstone:* This type of rock accounts for 19% of the rocks in the area. It is white-gray to ash-gray in color, mostly distributed far from the coal seam roof and floor. Its grain composition is selected quartz, cementitious cement is silica, quartz sand. The gravelstone usually have a lenticular structure or with thin to medium-thickness layers. The layers of gravelstone are strongly fractured and irregular, the exposed part of the seam is weathered and fractured with a yellow-gray color.

- *Sandstone:* This type of rock accounts for 25% of the rocks in the area. It is relatively widely distributed in the mine, the rock has coarse to fine grain, white gray to dark gray color. Its grain composition is mainly quartz sand, cementitious cement is silica clay. The rock has a blocky structure, thick to medium layers, and is heavily fractured. Distributed both on the roof and under the floor of the coal seam, but not continuously. The cracks develop from moderate to strong, the change in the degree of cracking with depth is not clear. Along with the gravelstone, sandstone can store and conduct water.

- *Siltstone:* This type of rock accounts for 33% of the rocks in the area, it is ash gray, and dark gray. Its main component is clay, but also mixed with plant humus. The siltstone is widely distributed throughout the mine and is often located near the roof and floor or interbedded within coal seams. The siltstone layer has a relatively stable thickness of 3 to 5 m, with special places having a thickness of up to 70 m. The siltstone is a type of rock commonly found in coal seam roof and floor and is the main roof. Its degree of cracking ranges from moderate to strong and is non-directional.

- *Claystone:* This type of rock accounts for 9% of the rocks in the area, it is dark gray in color. Distributed directly on the roof and under the floor of coal seams and interbedded within coal seams, thin layers, sometimes soft and friable. The claystone is often a false roof of coal seams and often collapses during mining.

- *Coal clay:* This type accounts for about 1% of the area. It is dark gray in color, thinly layered, soft, and swells when exposed to water. The coal clay is often found on the roof and floor of coal seams and interbedded within coal seams.

- *Coal:* This type accounts for about 12% of the area, black, metallic, broken in the form of shells and stairs.

- Parameters of the rock mass has been analyzed and shown in Table 1.

Table 1. Input parameters of the simulation model [12]

Descriptions	Unit	Value	Descriptions	Unit	Value
Model size parameter			*Roadway size parameter*		
Width	m	471	Width	m	3.69
Height	m	680	Height	m	3.17
Depth of digging roadway	m	120	Radius	m	
Conglomerate mass parameters			*Sandstone mass parameters*		
Compression resistane strength	kG/cm^2	1595.49	Compression resistane strength	kG/cm^2	927.35
Tensile strength	kG/cm^2	118.26	Tensile strength	kG/cm^2	93.64
Volumetric weight	g/cm^3	2.58	Volumetric weight	g/cm^3	2.65
Poisson's coefficient	-	0.2	Poisson's coefficient	-	0.2
Siltstone mass parameters			*Claystone mass parameters*		
Compression resistane strength	kG/cm^2	521.78	Compression resistane strength	kG/cm^2	206.22
Tensile strength	kG/cm^2	55.38	Tensile strength	kG/cm^2	27.35
Volumetric weight	g/cm^3	2.66	Volumetric weight	g/cm^3	2.70
Poisson's coefficient	-	0.2	Poisson's coefficient	-	0.2
Coal mass parameter			*Interbedded rock mass parameters*		
Compression resistane strength	kG/cm^2	222.270	Compression resistane strength	kG/cm^2	363.65
Tensile strength	kG/cm^2	27.223	Tensile strength	kG/cm^2	42.67
Volumetric weight	g/cm^3	1.361	Volumetric weight	g/cm^3	2.64
Poisson's coefficient	-	0.12	Poisson's coefficient	-	0.12

2.3. Hydrogeological conditions around the area of the longwall in coal Seam 11

- The Seam 14 open-pit mine at West Side at level -54 (Figure 3). This open-pit mine is located on the longwall in Seam 11, the stratigraphic distance from the longwall to the bottom of the open-pit mine is about 100 ÷ 120 m, and the stratigraphy consists of a siltstone layer lying on the coal seam with a thickness of about 5 ÷ 6 m, followed by a sandstone layer with a thickness of about 5 ÷ 18 m, above the sandstone layer is a layer of gravel with a thickness of about 15 ÷ 35 m, above the gravel layer is a layer of siltstone mixed with sandstone with a thickness of about 12 ÷ 40 m.

The progress of dumping waste at this landfill in recent years has been carried out in the form of a circumference, dumping in the order of exploitation (when the mining was finished, dump the waste there), the height of the waste layer is from 30÷50 m, almost no floor has entered the end position [11; 13].

In the study area, the reserves of the coal Seam 14 were exploited by the open-pit mining method of the Nui Beo Coal Mine. Open-pit mining activities had destroyed the original

topography, creating on the topography open-pit mine and dumps that can be placed for water to accumulate. The reserve of coal Seam 11 below the upper open-pit mine has been mobilized by Ha Lam Coal Mine to exploit by the underground mining method according to the planning of the build mining investment project below the -50 level of Ha Lam Coal Mine. The coal Seam 11 belongs to the type of thick and gentle seam, exploited and using the roof control method by full caving. Thus creating collapsed and fractured areas capable of developing from the mining area to the topographic surface, if the mining depth is not too large [15; 16; 17].



Figure 3*. The bottom of Seam 14 open-pit mine at West Side at level -54} of Nui Beo Coal Mine (it shows that before dumped waste) [14]*

Synthesized hydrogeological information in the area shows that the water source affecting underground mining is mainly water from open-pit mines that have been exploited with a flow of about 500 000 m^3 [18]. So, in the process of digging and exploiting the longwall in coal Seam 11 at Ha Lam Coal Mine located underneath the coal Seam 14 open-pits mine of Nui Beo Coal Mine, it is necessary to have solutions to prevent the risk of water cracking into the roadways. In order to select reasonable solutions, it is necessary to study and assess the risk of water cracking from the upper open-pit mine into the longwall in coal Seam 11.

2.4. Establishing a numerical model

+ Modeling establishing steps

Numerical analyses in plane strain were conducted using the finite element Phase2 software. Modeling establishing steps to simulate rock pressure acting on the roadway include [19].

- Step 1. Determination of the study site (the roadway and the surrounding boundary);
- Step 2. Meshing the finite element and establishing the initial boundary conditions (conditions for limiting displacement at the model boundary);
- Step 3. Determination of the primary stress field conditions and groundwater level;
- Step 4. Determination of the properties of materials (Characteristics of rock mass types);
- Step 5. Digging the rock inside the roadway boundary.

+ Simulation model

Based on the typical geological cross-section of the Seam 14 open-pit mine of the Nui Beo Coal Mine in Figure 2, based on a parametric analysis in Table 1, a numerical

simulation model with dimensions of 471 x 680 m has been established and is shown in Figure 4. The water level in the Seam 14 open-pit mine is at -50.

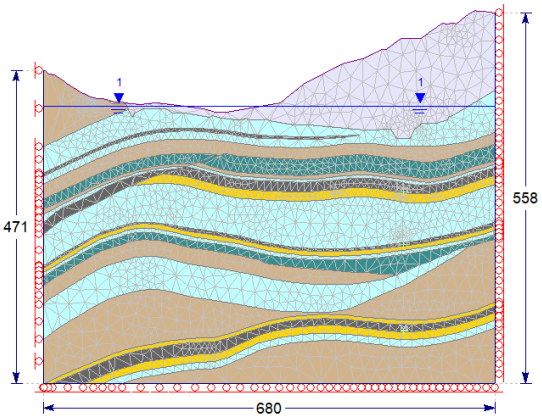


***Figure 4**. Layout of numerical simulation model*

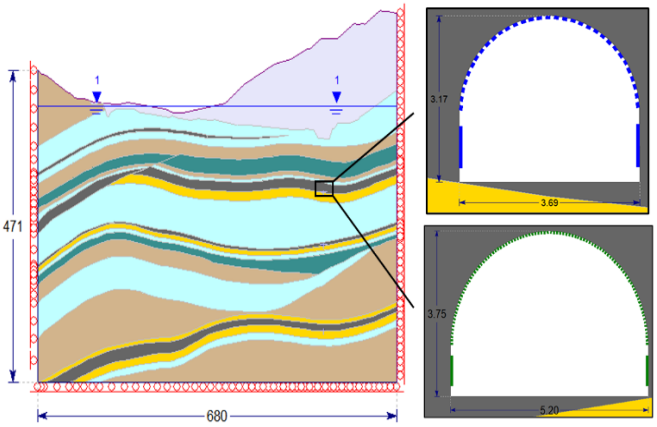


***Figure 5**. Position and size of roadway in the numerical simulation model*

The roadways cross-section was assumed as vertical sidewalls with dimensions of 3.69 m wide, 3.17 m high (corresponding to an area of 9.6 m^2, and it is also a single railway roadway) and 5.2 m wide,

3.75 m high (corresponding to an area of 17.9 m^2, and it is also a double railway roadway). The roadways have been dug at a depth of 120 m from the ground surface. The location and size of the roadway in the numerical model are shown in Figure 5. To be able to calculate the rock pressure acting on these roadways, we continue to use the computer to run the simulation model, the analysis results from the models are the basis for allowing calculation and selection the best.

3. RESULTS AND DISCUSSION

3.1. Analyze the maximum stress acting on the roadways

The maximum principal stress in the rock mass around the single railway roadway is shown in Figure 6, the double railway roadway is shown in Figure 7.

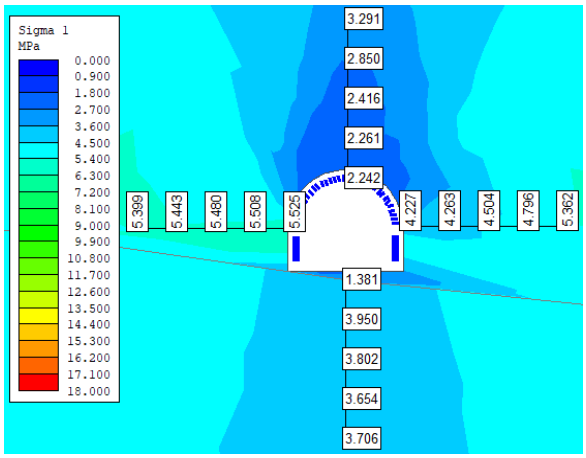


***Figure 6.** The maximum principal stress in the rock mass around the single railway roadway*

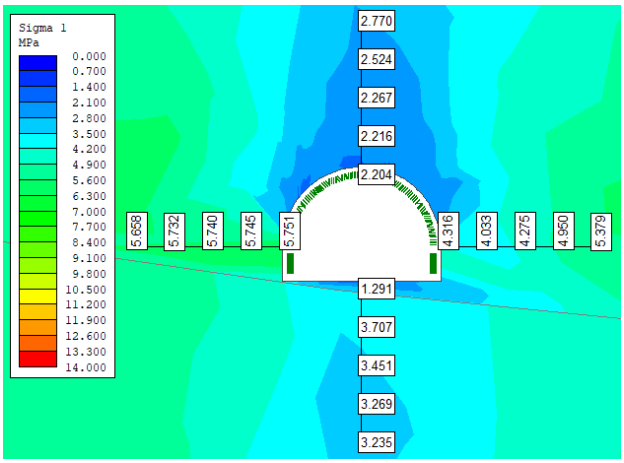


***Figure 7.** The maximum principal stress in the rock mass around the double railway roadway*

Analyzing the simulation model results from Figure 6 and Figure 7 shows that the maximum principal stress (Sigma 1) is distributed according to the law of decreasing from the rock mass to the roadway boundary. In other words, the observed principal stress on the roadway boundary has the minimum value. It is explained that when performing the digging roadway process, the primary stress in the rock mass is released, and the rock mass tends to move inside the tunnel space. At the same time, when digging the tunnel, the primary stress state of the rock mass is broken, forming a secondary stress state, the rock mass is redistributed in its stress state. As the tunnel is dug deeper into the rock mass, the influence of stress distribution gradually decreases, and the rock mass returns to its original state of primary stress.

Furthermore, when the tunnel size changes, the level of impact on the rock mass also changes, leading to stress differences. Specifically, it can be seen that the maximum principal stress at the roof and floor area of the single railway roadway is bigger than the maximum principal stress of a double railway roadway. This is explained as follows, because the roof and floor of the roadway are mainly subject to compression, the larger the cross-section of the roadway, the greater the degree of displacement of the rock mass into the roadway space. In other words, the degree of stress release is bigger than that of a roadway with a smaller cross-section.

3.2. Analyze the minimum stress acting on the roadways.

The minimum principal stress in the rock mass around the single railway roadway is shown in figure 8, the double railway roadway is shown in Figure 9.

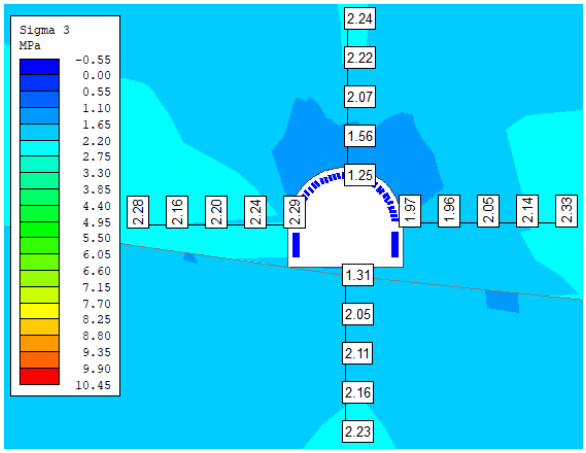


Figure 8. *The minimum principal stress in the rock mass around the single railway roadway*

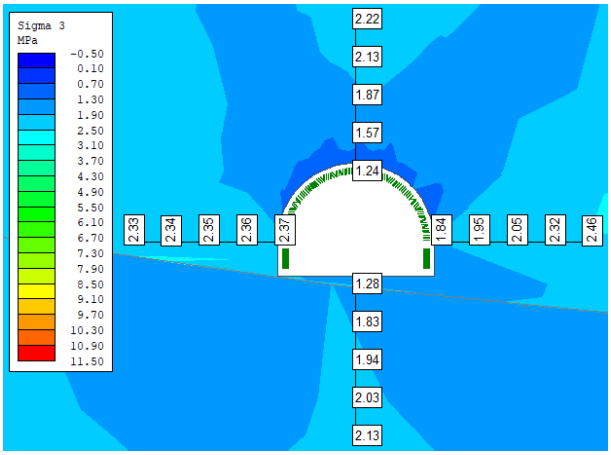


Figure 9*. The minimum principal stress in the rock mass around the double railway roadway*

Analyzing the results of the simulation model in figure 8 and figure 9, it can be seen that the minimum principal stress (Sigma 3) is distributed in the rock mass around the roadway gradually increases from the roadway boundary to deeper inside rock mass, but bigger than 15 m from the roadway boundary, the stress begins to decrease and gradually returns to the primary stress state. This can be explained that when digging the tunnel, the rock mass around the tunnel is divided into 4 zones including: crumbling zone, this area has a strong decrease in stress; plastic zone, this area the stress begins to increase; the elastic region, this

region increases stress; primary stress zone, this zone is the rock mass area that is not affected by the digging work of the tunnel. Analysis results from figures 8 and 9 can be seen that the stress of the roadway boundary is biggest at the roaway roof position is 1.25 MPa, the stress on both sides of the roadway is 1.84 MPa, and the furnace floor stress is 1.31 MPa. However, analysis results from the model also show that the deeper inside the rock mass, the biggest principal stresses appear on both sides of the tunnel. This is explained that when digging the tunnel, the rock mass under the roof of the tunnel space was taken away, so the load on the roof of the tunnel is not supported by the rock mass below, but the load on the roof is transferred to the rock mass on both sides of the tunnel, so the rock mass on both sides of the tunnel are subjected to large concentrated stress.

3.3. Analyze the vertical stress acting on the roadways

The vertical stress in the rock mass around the single railway roadway is shown in Figure 10, the double railway roadway is shown in Figure 11.

Analyzing the results of the simulation model in figure 10 and figure 11, it can be seen that the vertical stress (Sigma Z) is distributed in the rock mass around the roadway also tends to increase gradually from from the roadway boundary to deeper inside rock mass, but bigger than 15 m from the roadway boundary, the stress begins to decrease and gradually returns to the primary stress state. Analysis results from figures 10 and 11 can be seen that the stress of the roadway boundary is biggest at the roaway roof position is 1.24 MPa, the stress on both sides of the roadway is 3.11 MPa, and the furnace floor stress is 1.29 MPa. However, analysis results from the model also show that the deeper inside the rock mass, the biggest principal stresses appear on both sides of the tunnel. This is explained that when digging the tunnel, the rock mass under the roof of the tunnel space was taken away, so the load on the roof of the tunnel is not supported by the rock mass below, but the load on the roof is transferred to the rock mass on both sides of the tunnel, so the rock mass on both sides of the tunnel are subjected to large concentrated stress.

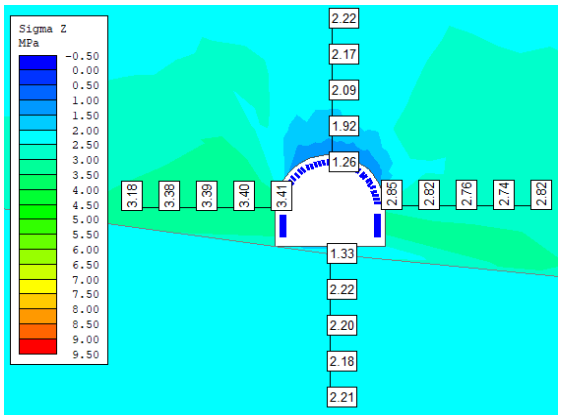


Figure 10. *The vertical stress in the rock mass around the single railway roadway*

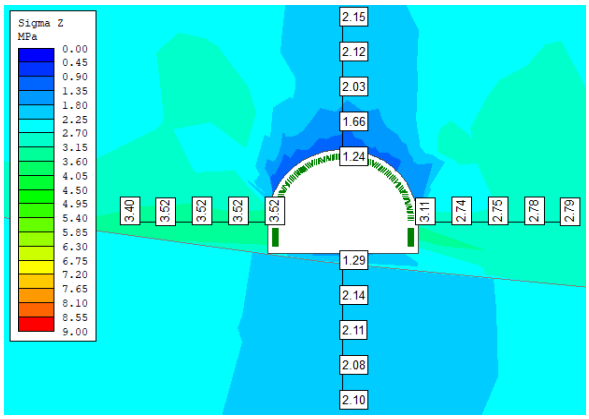


Figure 11. *The vertical stress in the rock mass around the double railway roadway*

4. CONCLUSIONS

These authors have generalized the geological conditions, hydrogeological conditions, and topography of the Seam 14 open-pit mine area of Nui Beo Coal Mine. The selection of numerical method is Phase2 software to build numerical simulation model to calculate rock pressure acting on the roadway under the Seam 14 open-pit mining area.

Based on geological conditions, topographical conditions, and groundwater conditions, the authors have built a model to calculate rock pressure acting on the roadway when exploiting coal seam 11 of Ha Lam Coal Mine under the Seam 14 open-pit mining area of Nui Beo Coal Mine. The authors have chosen a typical size to simulate and calculate the rock pressure acting on the roadway, including two types of areas: the cross-sectional size of the roadway of 9.6 m^2 (for single railway roadway) and the cross-sectional size of the roadway of 17.9 m^2 (for double railway roadway).

From the selected size, proceed with modeling to simulate the stress acting on the tunnel with the size of a single railway roadway and the tunnel with the size of a double railway roadway when digging the tunnels under the Seam 14 open-pit mining area of Nui Beo Coal Mine. Analysis results from the model show that the maximum principal stresses, minimum principal stresses, and vertical stresses all have the rule of gradually increasing from the roadway boundary to deeper inside the rock mass and decreasing gradually return to the state of primary stress at the location of the rock block more than 15 m from the roadway boundary.

ACKNOWLEDGEMENTS

The authors express their gratitude to the staff of the Department of Engineering and Technology of two Ha Lam and Nui Beo Coal Mines, Vietnam for creating favorable conditions for data collection and field survey for the authors to complete this study. Simultaneously, the authors would like to thank for the Organizing Committee of the GREEN EME 2023 conference.

REFERENCES

[1] T.T. Vu, S.A. Do. (2023). Determination of the rock mass displacement zone by numerical modeling method when exploiting the longwall at the Nui Beo Coal Mine, Vietnam. Mining of Mineral Deposits, 17(1), 59-66. https://doi.org/10.33271/mining17.01.059.

[2] H. Yang, X. Jiang, C. Wen, J. Yang et al., 2013. Yin Modeling the deformation of tunnel excavations in layered rock masses Electronic Journal of Geotechnical Engineering, 18 (2013), pp. 723-734.

[3] Dao Viet Doan, 2022. Research on the stability of surrounding coal rock mass roadway excavation in coal seam with soft clay interlayer. National conference of Earth science and natural resources for sustainable development (ERSD 2022), Hanoi, 761-769.

[4] Yan, Z.G. (2011). Study on deformation of tunnel with underlying coal mining. Applied Mechanics and Materials, (105-107), 1295-1298. https://doi.org/10.4028/www.scientific.net/amm.105-107.1295.

[5]Ha Lam Coal Company - Department of Geodesy and Mine Geology 2015 R*eport on assessment of hydrogeological and engineering geological conditions for mechanized mining projects at two Seams 11 and 7* (Quang Ninh) p 107 *(Vietnamese).*

[6] Zheng, G., Yang, P., Zhou, H., Zhang, W., Zhang, T., and Ma, S. (2021). Numerical Modeling of the Seismically Induced Uplift Behavior of Twin Tunnels. International Journal of Geomechanics, 21(1), 04020240.

[7] Vu, T.T., & Dao, V.D. (2022). Assessing the impact of underground working (tunneling) in the ii section of seam 14 on surface construction works at Ha Lam coal mine (Vietnam). Naukovyi Visnyk Natsionalnoho Hirnychoho Universytetu, (4), 39-44. https://doi.org/10.33271/nvngu/2022-4/039.

[8]Ha Lam Coal Company - Department of mining technology 2021 *Mining passport for fully mechanized longwall in Seam 11 and Seam 7* (Quang Ninh) p 43 *(Vietnamese).*

[9]Ha Lam Coal Company - Department of Geodesy and Mine Geology 2019 *Report on assessment of geological conditions at Ha Lam coal mine for deep mining project* (Quang Ninh) p 143 *(Vietnamese).*

[10] *https://www.google.com/maps/place/C%C3%B4ng+Ty+Cp+Than+H%C3%A0+L%E1%BA%A7m++Tkv/@20.966128,107.1095612,153m/data=!3m1!1e3!4m6!3m5!1s0x314a57faf816bf9f:0x5845426396fa711!8m2!3d20.9662318!4d107.1097956!16s%2Fg%2F1hc1grvl3?hl=en&entry=ttu*

[11]Nui Beo Coal Mine - Department of Geodesy and Geology 2021. *Report of geological conditions of Nui Beo coal mine.* Quang Ninh, Vietnam.

[12]Ha Lam Coal Company - Department of mining technology 2017 *Explanation, design drawings for the construction of the crosscuts at +75 and -300 levels. Quang Ninh (Vietnamese).*

[13] Report of geological conditions of Nui Beo coal mine. (2021). Nui Beo Coal Mine. Quang Ninh, Vietnam: Department of Geodesy and Geology.

[14] Vu Trung Tien, 2022. Determination of the movement and deformation areas of strata when exploiting longwall of Seam 11 under the open-pit mine at Ha Lam Coal Mine, Vietnam. IOP Conf. Series: Earth and Environmental Science, (1049) 012009. doi:10.1088/1755-1315/1049/1/012009.

[15] Dao, V. D., Xia, B., & Dinh, V. D. (2019). Control technology for coal roadway with mudstone interlayer in Nui Beo coal mine. Geomate Journal, 17(60), 259-266.

[16] Hu, J., Chen, Q., and Liu, H. (2018). Relationship between earthquake-induced up lift of rectangular underground structures and the excess pore water pressure ratio in saturated sandy soils. Tunnelling and Underground Space Technology, 79, 35-51.

[17] Dang, K.Van, Vo, H.Trong, Ngo, H.Doan and Tran, H.Xuan 2022. An experimental study on the use of fly ash for making concrete lagging of SVP steel arches in underground coal mines in Quang Ninh area (in Vietnamese). Journal of Mining and Earth Sciences. 63, 3a (Jul, 2022), 103-111. DOI:https://doi.org/10.46326/JMES.2022.63(3a).12.

[18]Institute of Mining Science and Technology 2017 *Report the results of determining the water flow in the open pit level -54; -60; -80 at Nui Beo coal mine* (Ha Noi) p 129 *(Vietnamese).*

[19] Tien Trung Vu, Doan Viet Dao, 2023. Determination of steel arch support distance for roadways under the open-pit mine: a case study at the Mong Duong Coal Mine (Vietnam). Naukovyi Visnyk Natsionalnoho Hirnychoho Universytetu, (3), 39-45. https://doi.org/10.33271/nvngu/2023-3/039.

MANAGING ENVIRONMENTAL CONFLICTS FOR SUSTAINABLE TOURISM DEVELOPMENT

Tran Duy Minh[1]
1 University of Social Sciences and Humanities,
Viet Nam National University Ho Chi Minh City, Vietnam
E-mail: tdminh@hcmussh.edu.vn

Abstract: The process of tourism development often gives rise to environmental conflicts when the expansion of tourism activities is perceived as a threat to the natural environment. Resolving these conflicts is an important requirement for sustainable tourism development. This article analyzes the common environmental conflicts that arise in tourism development and the strategies for managing these conflicts in the context of sustainable tourism development. The document analysis method was used to review relevant literature on environmental conflicts in tourism development and the approaches used to manage them. The analysis revealed that common environmental conflicts in tourism development include issues related to resource use, land use, pollution, and wildlife conservation. Strategies for managing these conflicts include collaborative decision-making, community engagement, environmental impact assessments, and regulatory frameworks. The article concludes by emphasizing the importance of prioritizing environmental conflict management in sustainable tourism development and highlighting the need for further research in this area. The outcomes of this research are available for utilization by tourism industry stakeholders to develop effective approaches to managing environmental conflicts and promoting sustainable tourism practices.

1. INTRODUCTION

In the context of the robust development of global tourism, ensuring the sustainability of the developmental process has become a paramount and crucial principle. As the tourism industry continues to expand, the intricate interplay between economic development and environmental conservation is becoming increasingly intricate. A key challenge in this context is the effective management of environmental conflicts that arise from the negative impact of tourism activities on both natural and human ecosystems. The objective of this article is to analyze common environmental conflicts that emerge in tourism development and strategies for managing these conflicts within the framework of sustainable tourism development (STD).

The primary methodology employed in this study involves the synthesis and analysis of pertinent literature. The sources reviewed consist of relevant literature on environmental conflicts in tourism development and the approaches used to manage them. Through the conducted analyses, the discussion centers initially on the imperative nature of rigorously managing environmental conflicts as an integral aspect in promoting STD. By exploring the relationships between tourism activities and environmental factors, the article seeks to explicitly delineate prevalent environmental conflicts in current tourism development. Consequently, the article synthesizes appropriate strategies and frameworks to manage these conflicts, with the aim not only of resolving conflicts but also contributing to the potential

for long-term ecological restoration and the socio-economic benefits closely associated with sustainable tourism.

2. THE NECESSITY OF ENVIRONMENTAL CONFLICT MANAGEMENT IN SUSTAINABLE TOURISM DEVELOPMENT

STD refers to the approach of tourism planning and management that aims to optimize the economic, social, and environmental benefits while minimizing the adverse effects of tourism on the natural and cultural resources of a destination. The concept of STD is increasingly being embraced by tourism destinations, policymakers, and industry stakeholders as a way to balance economic growth, environmental conservation, and cultural preservation. Sustainable tourism is defined as "all forms of activities, management and development of tourism that preserve natural, economic and social integrity and guarantee maintenance of natural and cultural resources" [1].

Some potential benefits of STD include economic growth and job creation, preservation of natural and cultural resources, and enhanced quality of life for local communities. For example, a study conducted by the World Travel and Tourism Council (WTTC) found that the tourism industry generated 10.4% of global GDP and supported 319 million jobs in 2018 [2]. Additionally, STD can help protect and conserve natural and cultural resources, such as wildlife, biodiversity, and historic sites, which can provide long-term economic and social benefits to a destination.

A study by the United Nations Environment Programme (UNEP) found that STD in the Galapagos Islands helped to reduce the negative impacts of tourism on the fragile ecosystem and supported conservation efforts. Furthermore, STD can enhance the quality of life for local communities by fostering employment opportunities, bolstering local businesses, and preserving cultural heritage [3]. According to research conducted by the European Travel Commission, the promotion of sustainable tourism in rural regions can contribute to the rejuvenation of local economies and the strengthening of social bonds [4].

All in all, STD has the potential to generate significant economic, social, and environmental benefits for tourism destinations. By adopting sustainable tourism practices, destinations can ensure the long-term viability of their tourism industry while also preserving and enhancing their natural and cultural resources.

Managing environmental conflicts is essential for STD as it helps to balance the economic benefits of tourism with the protection and conservation of natural resources. Environmental conflicts can arise when tourism activities negatively impact the environment or when environmental protection measures hinder the growth of the tourism industry. Managing these conflicts requires effective communication and collaboration among tourism stakeholders, local communities, and environmental organizations.

One of the primary reasons for managing environmental conflicts is to ensure the long-term sustainability of tourism destinations. Environmental degradation, such as habitat destruction and pollution, can reduce the attractiveness of a destination and negatively impact the local economy. The World Tourism Organization (UNWTO) report has pointed out that tourists are ready to spend additional funds on environmentally sustainable tourism products, indicating that there is a growing demand for sustainable tourism experiences [5].

Furthermore, managing environmental conflicts can help to build positive relationships between tourism stakeholders and local communities. By involving local communities in

tourism planning and decision-making, stakeholders can ensure that their interests and concerns are taken into account. This can help to build trust and support for tourism development and minimize the potential for conflict.

Effective management of environmental conflicts also requires the implementation of environmentally sustainable practices in the tourism industry. For example, the use of renewable energy sources, waste reduction and recycling programs, and sustainable transportation options can help to minimize the negative impacts of tourism on the environment.

The goal of sustainability in tourism is to acknowledge all impacts of tourism and minimize the negative effects while maximizing the positive ones. Sustainable tourism practices aim to ensure that the tourism industry maintains a viable support system for the environment in and around the destination, prioritizing the ecological well-being of the area [6]. Managing environmental conflicts is essential for STD as it helps to ensure the long-term viability of tourism destinations while protecting and conserving natural resources. By involving local communities and implementing sustainable tourism practices, stakeholders can minimize the adverse effects of tourism on the environment and build positive relationships with local communities.

3. COMMON ENVIRONMENTAL CONFLICTS IN TOURISM DEVELOPMENT

Sustaining tourism is an ongoing endeavor that necessitates continuous monitoring of its effects [1]. When tourism arrivals exceed capacity, it can lead to problems rather than benefits. This includes depletion of natural resources, leaving behind soil erosion, accumulation of waste, water and air pollution, as well as endangering biodiversity and the decomposition of socio-cultural habitats. Such uncontrolled tourism can also lead to damage to the virginity of land and sea [6]. Environmental conflicts can arise in the tourism industry when tourism activities negatively impact the natural environment or when environmental protection measures hinder the growth of the tourism industry.

Environmental conflicts manifest as political, social, economic, ethnic, religious or territorial conflicts, conflicts over resources or national interests, or any other type of conflict. They are contradictions arising from man-made environmental degradation. Environmental conflict is characterized by degradation in one or more of the following areas: overuse of renewable resources; pollution that exceeds the cleaning capacity of the environment; living space degradation [7]. The growth of tourism can exacerbate the strain on natural resources in regions already facing scarcity, as it leads to increased consumption. Additionally, tourism can contribute to various types of pollution, such as air emissions, noise, solid waste, littering, and releases of sewage, oil, and chemicals, including architectural and visual pollution, similar to other industries. Environmental conflicts in the tourism industry can manifest through specific environmental issues as follows:

Overuse of natural resources: Tourism can put a significant strain on local resources, such as energy, food, and other raw materials, which may already be in short supply [8]. Tourism activities such as water sports, hiking, and wildlife viewing can lead to the overuse of natural resources, which can lead to environmental degradation. For example, in the Galapagos Islands, the increase in tourism activities has led to the overuse of water resources and damage to fragile ecosystems [3].

Habitat destruction and wildlife disturbance: Tourism activities such as construction of hotels and resorts, road development, and wildlife viewing can lead to habitat destruction and disturbance of wildlife. The use of air travel and vehicles for transportation is a significant contributor to the rise of greenhouse gas emissions worldwide. This, in turn, leads to the loss of biodiversity caused by habitat destruction, resource depletion, and degradation of different ecosystems such as coastal regions, mountains, rural areas, wilderness areas, and small islands. The consequences of these activities can be seen in the form of environmental changes affecting the air, land, and water [9]. According to World Wildlife Fund (WWF), tourists and suppliers introducing exotic species may introduce non-native insects, wild and cultivated plants, and diseases to the local environment. This can cause significant disruption and even destruction of ecosystems [8].

Waste management: The increase in tourism activities can lead to increased waste generation, which can lead to pollution of natural resources such as water bodies and soil. Tourist destinations that have a high concentration of activities and natural attractions often face significant challenges with waste disposal. Improper disposal of waste can have a severe impact on the natural environment, including rivers, scenic areas, and roadsides [8].

Climate change: Tourism activities, such as transportation and energy consumption, can contribute to greenhouse gas emissions, which can exacerbate the effects of climate change. Studies revealed that the combined effects of air and road travel associated with tourism contribute to the overall impact of global climate change. This, in turn, has adverse effects on tourism, particularly in alpine regions and numerous small islands [9]. For example, the melting of glaciers in the Swiss Alps due to climate change has reduced the attractiveness of the region for winter tourism [10]. Previous studies have also shown that international tourism and the resulting surge in tourist arrivals and energy consumption lead to increased carbon dioxide (CO_2) emissions and air pollution, ultimately contributing to climate change [6].

Altogether, tourism activities can lead to negative impacts on the natural environment and local communities. It is these impacts that give rise to conflicts in the relationship between parties related to resources and the local environment due to differences in interests, goals, roles, etc. Effective management of these conflicts requires collaboration and communication among tourism stakeholders, local communities, and environmental organizations, and the implementation of sustainable tourism practices.

The nature of environmental impacts is complex, with many having non-linear characteristics that can make them difficult to predict. Some impacts may accumulate gradually over time, leading to long-term and significant changes that may not become apparent until it is too late to reverse them [9]. The impacts of environmental conflict in the tourism industry are often easily seen in the basic elements of the industry such as local communities, ecosystems, tourists and tourism operators.

Local Communities: The negative environmental impacts of tourism include overcrowding, traffic gridlock, air pollution, noise pollution, degradation of the natural environment, and the loss of landscaping for both local communities and tourists [6]. Environmental conflicts in the tourism industry can negatively impact local communities by reducing their access to natural resources, reducing the availability of jobs, and leading to social and cultural changes. For example, in Bali, Indonesia, the increase in tourism

activities has led to the displacement of local communities and the loss of access to coastal resources, which are essential for their livelihoods [11].

Ecosystems: Environmental conflicts can lead to damage and degradation of ecosystems, which can have negative impacts on biodiversity and ecosystem services. For example, the overuse of water resources in the Galapagos Islands has led to the decline of biodiversity in the region [3] or other studies have shown that tourism and recreational activities threaten endangered species and biodiversity in Australia [12]. The destruction of habitats and disturbance of wildlife can also have long-lasting impacts on ecosystem function and biodiversity.

Tourist: Environmental conflicts can result in restricted or reduced access to natural and cultural attractions. For example, conflicts over land use, resource extraction, or conservation measures may lead to temporary or permanent closures of tourist sites, limiting tourists' opportunities to visit and enjoy these attractions. Environmental conflicts may lead to changes in tourists' travel behavior. For example, tourists may choose to avoid destinations associated with environmental issues or boycott destinations or tourism operators perceived to be contributing to environmental degradation [13].

Tourism operators: Environmental conflicts can also impact tourism operators by reducing their revenue and creating negative perceptions of their destinations [6]. Indications propose that tourists highly prioritize air quality when choosing travel destinations, and past research has demonstrated that subpar air quality adversely affects tourist arrival numbers [14].

On the whole, environmental conflicts in the tourism industry can have far-reaching impacts on the natural ecosystems, local communities, tourists and tourism operators. This situation will negatively affect the sustainability of tourism development. Effective management of these conflicts requires collaboration and communication among tourism stakeholders, local communities, and environmental organizations, and the implementation of sustainable tourism practices.

4. STRATEGIES FOR MANAGING ENVIRONMENTAL CONFLICTS

Tourist destinations often experience various types of pollution, including littering, solid waste, , sewage, air emissions, noise, oil and chemical pollution, architectural and visual pollution, and increased car use. However, the negative impact on the environment is not limited to pollution. Poorly planned and overcrowded tourism can also lead to overconsumption of natural resources, a decline in service quality, and a skyrocketing surge in waste and pollution, all of which have significant adverse effects on the environment [6]. These things have made the problem of environmental conflict even more complicated.

There is no single framework for managing environmental conflicts in tourism development, as various approaches may be needed depending on the situation. Commonly used approaches include collaborative decision-making, community engagement, environmental impact assessments, and regulatory frameworks.

Collaborative decision-making: In the past few decades, when conflicts related to the environment or natural resources have arisen, various parties such as government agencies, stakeholder organizations, and citizens have often sought alternatives to adversarial battles. Collaboration has been the preferred approach, with an attempt to work through conflicts and find common ground to make sound decisions [15]. Collaborative decision-making

involves bringing together stakeholders from different sectors to participate in the decision-making process. This approach can help to build trust and foster cooperation among stakeholders, resulting in more sustainable outcomes [16]. For example, the Great Barrier Reef Marine Park Authority in Australia, the utilization of collaborative processes facilitated policy actors in mediating conflicts and addressing power imbalances. These processes were also employed by policy actors to negotiate compromises with stakeholders regarding new policies. Besides, they used collaboration to help make complex decisions, secure resources, and mobilize effort [17].

Community engagement: The local community is encouraged to be involved in the development and management of grassroots tourist attractions and services that showcase the community's culture, heritage, and environmental assets [18]. Community engagement involves involving local communities in the decision-making process. This approach can help to build support for sustainable tourism practices and address concerns and conflicts related to tourism development [19]. For example, the Maasai Mara Wildlife Conservancies Association in Kenya has implemented community engagement processes to manage conflicts between tourism operators and local communities [20].

Environmental impact assessments: The Environmental Impact Assessment (EIA) is the principal tool used for the purposes of planning, evaluating, and managing development projects. Its purpose is to support sustainable and resilient development goals and green growth outcomes. When used effectively, EIA can help support governments in achieving green growth goals and enhancing resilience to climate change, and Sustainable Development Goals [21]. EIA's role is to identify and assess significant project impacts on the environment and population, using scientific knowledge, to mitigate them, inform decision-makers, and promote public participation and dialogue, potentially reducing conflicts [22]. For example, the Galapagos National Park in Ecuador has implemented an EIA process to manage conflicts between tourism operators and environmental groups [3].

Regulatory frameworks: Regulatory measures can help mitigate the negative impacts of tourism. For example, Restricting tourist activities and visitor mobility within protected areas can effectively reduce the ecological impacts, preserving the site's integrity and vitality. These limitations also contribute to minimizing the negative impact on resources [8]. Regulatory frameworks involve the implementation of laws and policies to manage conflicts related to tourism development. These frameworks can help to ensure that tourism development is sustainable and does not negatively impact the natural environment or local communities. For example, the European Union has implemented regulations to manage conflicts related to tourism development, such as the EU Water Framework Directive, which aims to protect water resources [10].

In general, there are different approaches to effectively manage environmental conflicts in tourism development, including collaborative decision-making, community engagement, environmental impact assessment and regulatory frameworks. Depending on the specific environmental context, managers need careful consideration to choose appropriate approaches.

5. CONCLUSION

Tourism growth and environmental pollution are global phenomena that have been observed in various regions around the world. These two aspects often go hand in hand.

Following the growth of tourism, environmental degradation has also increased. This problem seriously threatens the sustainability of tourism development.

As stated above, environmental conflicts in tourism development are common and can have significant impacts on local communities, ecosystems, and tourism operators. Strategies for managing these conflicts include collaborative decision-making, community engagement, environmental impact assessments, and regulatory frameworks. It is crucial for tourism industry stakeholders to prioritize environmental conflict management in STD to ensure long-term sustainability and benefits for all stakeholders involved.

There is a need for further research in this area, particularly in understanding the effectiveness of different approaches to managing environmental conflicts and their impact on the sustainability of tourism development. Research can also focus on identifying emerging conflicts and developing proactive strategies for conflict prevention in tourism development.

In summary, managing environmental conflicts is a critical aspect of STD that requires the cooperation and participation of all stakeholders involved. It is important to prioritize sustainable practices to ensure the long-term sustainability of the tourism industry while balancing the needs of local communities and ecosystems. Only through effective management of environmental conflicts can we create a sustainable future for the tourism industry and protect our planet's natural resources for generations to come.

REFERENCES

[1] Niedziółka I 2012 Sustainable Tourism Development *Regional Formation and Development Studies* **8** 157–66.

[2] World Travel and Tourism Council 2019 Travel & Tourism Economic Impact 2019.

[3] United Nations Environment Programme and World Tourism Organization 2012 *Tourism in the Green Economy – Background Report* (Marid: UNWTO).

[4] European Tourism Manifesto 2017 *Background document: The European Tourism Manifesto for Growth and Jobs* (Brussels, Belgium.

[5] World Tourism Organization (UNWTO) 2018 UNWTO Tourism Highlights, 2018 Edition. (Madrid).

[6] Baloch Q B, Shah S N, Iqbal N, Sheeraz M, Asadullah M, Mahar S and Khan A U 2023 Impact of tourism development upon environmental sustainability: A suggested framework for sustainable ecotourism *Environmental Science Pollution Research* **30** 5917-30.

[7] Libiszewski S J J o p r 1991 What is an environmental conflict **28** 407-22.

[8] Sunlu U 2003 *Local resources and global trades: Environments and agriculture in the Mediterranean region,* ed D Camarda and L Grassini: Bari : CIHEAM) pp 263-70.

[9] Belsoy J, Korir J and Yego J 2012 Environmental impacts of tourism in protected areas *Journal of Environment Earth Science* **2** 64-73.

[10] Scott D, Hall C M and Stefan G 2012 *Tourism and climate change: Impacts, adaptation and mitigation*: Routledge).

[11] Kinseng R A, Nasdian F T, Fatchiya A, Mahmud A and Stanford R J 2018 Marine-tourism development on a small island in Indonesia: blessing or curse? *Asia Pacific Journal of Tourism Research* **23** 1062-72.

[12] Pickering C M and Hill W 2007 Impacts of recreation and tourism on plant biodiversity and vegetation in protected areas in Australia *Journal of environmental management* **85** 791-800.

[13] Kemperman A D 2021 *Women's voices in tourism research-Contributions to knowledge and letters to the next generation.*, pp 266-73.

[14] Su Y and Lee C-C 2022 The impact of air quality on international tourism arrivals: a global panel data analysis *Environmental Science and Pollution Research* **29** 62432-46

[15] Walker G B and Daniels S E 2019 Collaboration in environmental conflict management and decision-making: comparing best practices with insights from collaborative learning work *Frontiers in Communication* **4** 2.

[16] Melo V 2018 *Collaborative Efforts for Sustainable Development: Surveying the Literature on Multi-Stakeholder Initiatives to Realize the Sustainable Development Goals*

[17] Vella K and Baresi U 2017 Understanding How Policy Actors Improvise and Collaborate in the Great Barrier Reef *Coastal Management* **45** 487-504.

[18] Curcija M 2016 Conflict management within the context of community based tourism: An exploratory study. UQ Business School, The University of Queensland).

[19] Buckley R 2012 Sustainable tourism: Research and reality *Annals of tourism research* **39** 528-46

[20] Bedelian C 2014 Conservation, tourism and pastoral livelihoods: wildlife conservancies in the Maasai Mara, Kenya. UCL (University College London)).

[21] Secretariat of the Pacific Regional Environment Programme 2018 *Environmental impact assessment : guidelines for coastal tourism development in Pacific island countries and territories* (Apia, Samoa: SPREP).

[22] Larsen S V, Hansen A M and Nielsen H N 2018 The role of EIA and weak assessments of social impacts in conflicts over implementation of renewable energy policies *Energy Policy* **115** 43-53.

ASSESSMENT OF OIL DEGRADING ABILITY IN DRILLING MUD BY BIOSURFACTANTS OF STRAIN *BREVIBACTERIAN CELERE*

Tran Thi Thu Huong[1,2*]

1 1Faculty of Environment, Ha noi University of Mining and Geology, Vietnam

2 Innovations for Sustainable and Responsible Mining (ISRM) Research Group, Hanoi University of Mining and Geology, Hanoi, 100000, Vietnam

E-mail: tranthithuhuong@humg.edu.vn /huonghumg@gmail.com

Abstract. Environmental pollution from waste sources of oil and gas extraction industry is facing many challenges. Particularly, the drilling mud from the mining process at sea is very difficult to handle because it is generated in conducting exploratory drilling and mine development, consisting of a mixture of soil and rock contaminated with oil, chemicals, and drilling fluid. The treatment technology using biosurfactant is receiving much attention due to biosurfactant is a bipolar compound that allows the dissolution of insoluble substances in water, creating an emulsion that helps microorganisms better contact the oil and easily decomposes the contaminated oil. Therefore, this study was carried out to assessment of oil degrading ability in drilling mud by biosurfactants produced from microbial strain *Brevibacterian celere* M150. The results showed that strain *B. celere* could generate biosurfactants under conditions: pH = 7; [NaCl] = 1%; temperature 30°C and the carbon source is diesel oil. The amount of diesel and saraline added to the culture medium degraded by 82.6% and 74.5%, respectively; Surface tension also decreased from 36.5 mN/m to 29.7 mN/m for diesel and from 29.2 mN/m to 27.6% mN/m for saraline oil. This indicates that the biosurfactants produced by this strain are a potential source of materials for environmental pollution treatment in the Petroleum industry in particular and in sea environmental pollution in general.

Key word: *Biosurfactants, Brevibacterium celere, Drilling mud, Microbial strain, Petroleum industry.*

1. INTRODUCTION

Petroleum and its products are source of nessessary energy for many countries around the world in general and Vietnam in particular. The oilfield industry plays an important role in our country's economic development. Besides the great benefits, the activities in the Oil and Gas industry also cause serious ecological pollution to both water, land, and air environments. The oil and gas drilling process releases a large amount of drilling mud, it will cause serious pollution if it is not treated and discharged directly into environment [1]. Drilling mud is generated during exploratory drilling and oilfield development, and consists of a mixture of soil, rock contaminated with oil, chemicals, and drilling fluid [2]. The pollution status is even greater if drilling fluids contained oil. According to Vietnamese regular, this waste source must be brought ashore for treatment. However, is very difficult and expensive to treat them so contractors often neglect it. There are many physicochemical methods proposed to solve the pollution status derived from drilling mud discharge, but they are not very effective and are expensive. Recently, the biological method is being widely applied due to its outstanding advantages, in which the use of biosurfactant of microorganisms to decompose oil in petrolium drilling mud is being interesting of researchers.

Biosurfactants are natural hydrocarbon emulsions produced by some of bacteria fungi and yeast strains. They are extracellular polymers, with a bipolar structure consisting of two parts: hydrophobic moiety and hydrophilic moiety, forming micelles concentrated inside the surface of the liquid layer between different polars such as water and oil. Therefore, it has the ability to reduce surface tension between molecules, create hydrogen bridges and interactions between hydrophobic and hydrophilic substances, helping microorganisms have better contact with oil and more easily decomposition of contaminated oil [2, 3]. It also has antibiotic properties such as gramicidin S or polymicin and reducing the surface tension [4]. Biosurfactants have very different characteristics in both chemical structure and molecular size, from very simple structure like fatty acids to complex like polymer compounds. On the other hand, biosurfactant is easily biodegradable, non-toxic and can be produced from cheap substrates such as industrial waste, thereby completely solving the problem of pollution caused by these waste sources. Therefore, this study was conducted to evaluate the oil decomposition ability of biosurfactant produced by the microbial strain B. celere.

2. METHODOLOGY

2.1. Setup the experiments

The bacterial strain *Brevebacterium cerere* (species has been identified) received from the Petroleum Microbiology Department - Institute of Biotechnology was used for further experiments in this study.

The experimental medium is Gost 1% mineral medium with the following ingredients ($g.L^{-1}$): Na_2HPO_4 = 0.7; KH_2PO_4 = 0.3; KNO_3 = 3; $MgSO_4$ = 0.4 and tap water 1 L. Shake the solution at pH = 7.5; v = 200 rpm and continuously monitored for 5 days.

2.2. The analysis methods

2.2.1. Evaluate the biosurfactant producing capacity by Pruthi method

The capacity for producing biosurfactant was evaluated by the emulsification index E24 [5]. The emulsification index E24 characterizes the emulsification ability of metabolic products produced by microorganisms in xylene solvent after 24 h at 4°C. Take 1 ml of culture solution, centrifuge to remove cells, add 1 ml of xylene into the test tube and voltex for 1 min at 2000 rpm. Samples were kept at 4°C for 24 h and then measured the height of emulsion column. The emulsion stability was determined and calculated after 24 h according to formula as follow [4]:

E24 = (Emulsion layer (height)/Solution (height)) x 100% (Height: mm)

2.2.2. Evaluate the effect of environmental factors to create the biosurfactant

The ability to produce biosurfactant of microbial strains is influenced by many environmental factors such as pH, temperature, carbon source and salt concentration. In this study, the conditions for conducting survey experiments are conducted as follows [5]:

- Effect of temperature: The experimental medium was conducted at 1% NaCl concentration; pH = 7.5; The carbon source is DO oil with temperatures of 22, 28, 30 and 37°C.

- Effect of pH: The experimental medium was prepared with pH values of 6.5; 7; 7.5 and 8 were supplemented with 5% (v/v) DO oil, shaken at a speed of 200 rpm and temperature of 30°C.

Effect of NaCl concentration: The experimental medium was conducted with a NaCl concentration range of 0, 1, 2 and 3% with carbon source as DO, pH = 7.5, at temperature condition of 30°C.

- Effect of carbon source: The experimental medium was conducted with DO oil, saraline, glycerin, olive oil at 1% salt concentration; pH = 7.5; The temperature condition is 30°C.

After 120 hours (5 days) of shaking culture, the optimal biosurfactant production ability will be evaluated through the emulsification index E24.

2.2.3. Evaluate the oil decomposition ability of biosurfactant

a) Evaluate the oil decomposition ability of biosurfactant to number of microbial cells

The influence of biosurfactant on microorganisms is evaluated through fluctuations in the number of microbial cells. Prepare the flasks containing of Gost 1% NaCl mineral medium, add 5% saraline oil (v/v) and 0.5ml *B. celere* bacteria fluid into the flasks. Then, add biosurfactant to every flask according to ratio 1, 2 and 3ml respectively and one flask control (without adding biosurfactant). Shake all flasks at conditions: speed of 200 rpm, temperature of 30°C. Count and compare the number of microbial cells at D0 and D5.

b) Measure the surface tension and the viscosity of oil

The determining surface tension process is measured in a thermostat mechanic. The viscosity was measured by using Ostwald viscometer. These experiments were conducted in Center of additivies and petrolium products, Vietnam Institute of Industrial Chemistry

c) Analyze oil content by gas chromatography instrument system

The oil degrading ability by biosurfactant depends on the amount of oil decomposed during the shaking process. In this study, the remaining oil content in the sample after 5 days was analyzed by gas chromatography at Laboratory Chemistry Department 5 - Technical Center for Standards, Metrology and Quality 1 - General Department of Standards, Metrology and Quality.

2.3. Statistics analysis

All experiments were meticulously conducted in triplicate. Subsequently, the data obtained was processed using the software Sigmaplot 14.

3. RESULTS AND DISCUSSION

3.1. Effect of some environmental factors on the biosurfactant producing capacity of B. celere strain

3.1.1. Effect of pH on the biosurfactant producing capacity

Effect of pH on the biosurfactant producing capacity in Figure 1 showed that pH = 7.5 is the optimal value for *B. celere* strain producing biosurfactant. Especially, the emulsification index E24 of this strain achieved 72% after 72 hours. These results also indicated that pH range for bacteria growth is fairly wide. The bacteria growth at pH values 6.5; 7 and 8 was recorded but not as high as at pH = 7.5. Normally, neutral pH is the best value for the bacteria to grow. Morever, this bacteria strain is isolated from seawater so the pH 7.5 is also a suitable pH for the seawater environment. Therefore, pH 7.5 is a suitable value for the bacterial strain to grow and produce amounts of biosurfactant high.

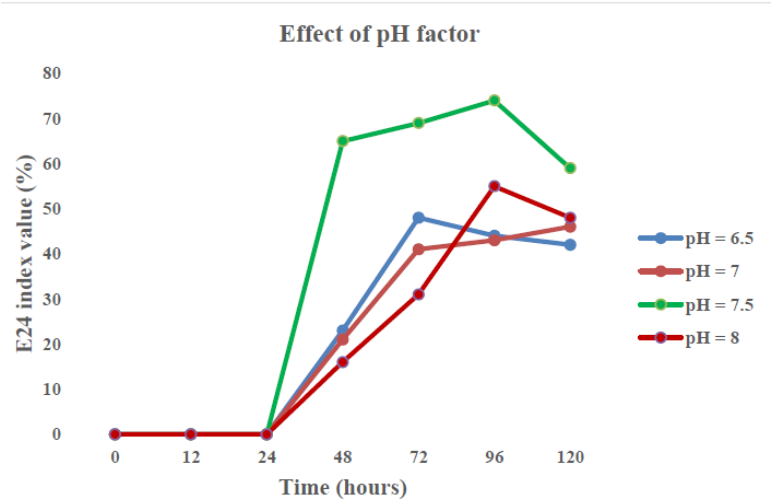


Figure 1. *Effect of pH on the biosurfactant producing capacity of B. celere strain*

3.1.2. Effect of temperature on the biosurfactant producing capacity

Similarly, the result in figure 2 showed that *B. celere* strain has a wide temperature range for biosurfactant production. The emulsification index E24 at four temperature value is stable and at the temperature 30°C reached the highest emulsification index E24 (67% after 120 hours). Therefore, the temperature of 30°C is the appropriate temperature for the bacterial strain producing amounts of biosurfactant high.

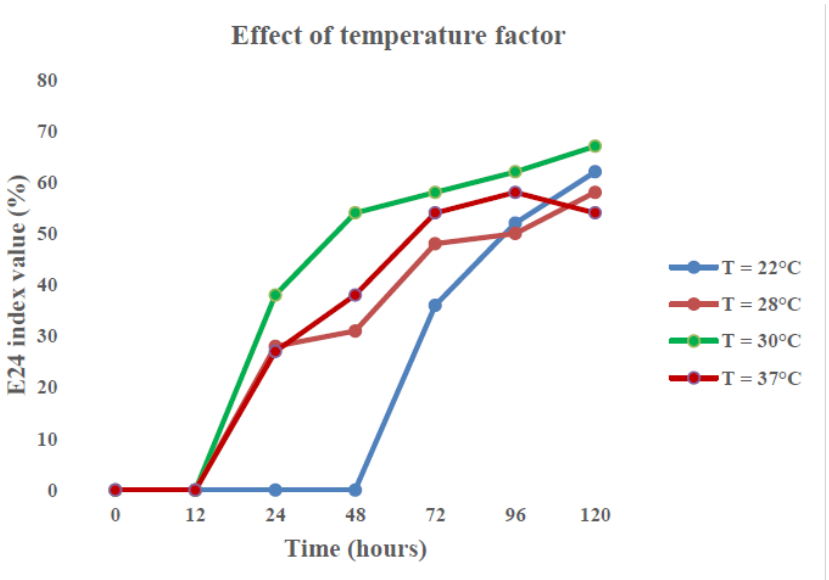


Figure 2. *Effect of temperature on the biosurfactant producing capacity of B. celere strain*

3.3.3. Effect of NaCl concentration on the biosurfactant producing capacity

The oil pollution often occurs at the sea and the experimental bacterial strain isolated from coastal areas, so testing how salinity effect bacterial growth is very important for future applications. The experimental results showed that the appropriate salt concentration for the producing biorsurfactant of 1% (Fig. 3). The *B. celere* strain can grow with a wide range of salt concentrations from 0% - 3%, however, this strain achieves the highest emulsification index of 67% at a concentration NaCl 1%. Therefore, concentration NaCl 1% is the best suitable concentration for *B. celere* strain to grow and develop.

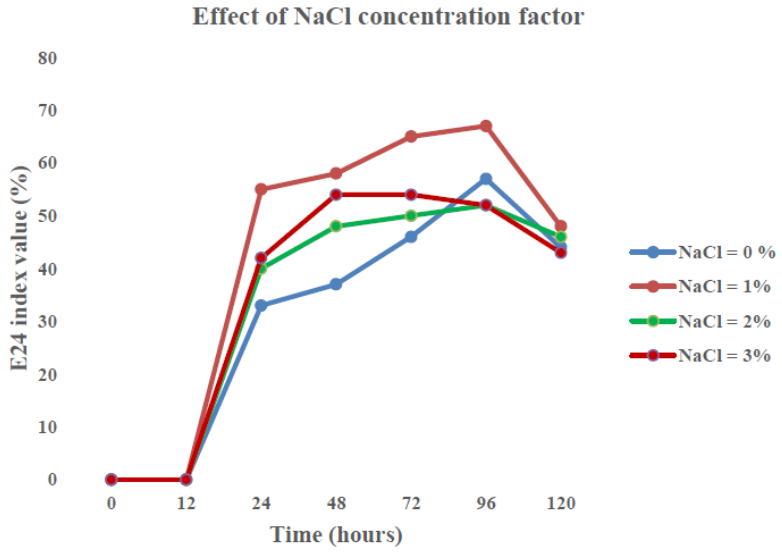


***Figure 3**. Effect of NaCl concentration on the biosurfactant producing capacity of B. celere strain*

3.3.4. Effect of carbon source on the biosurfactant producing capacity

The carbon source is also a very important factor affecting the biosurfactant producing capacity. Currently, oil spills at sea often contain saraline, DO oil and paraffin. Especially in drilling mud, saraline oil often accounts for a large amount. The technical requirements for petroleum oil exploitation are deep drilling and oblique drilling into the ground, so the drilling fluid commonly used contains the oil (saraline). Therefore, the selection of carbon sources suitable for biosurfactant production in this study is presented in Figure 4. The analysis results showed that *B. celere* strain is the ability to produce biosurfactant and decompose oil strongly, the highest decomposing carbon source is saraline and DO oil.

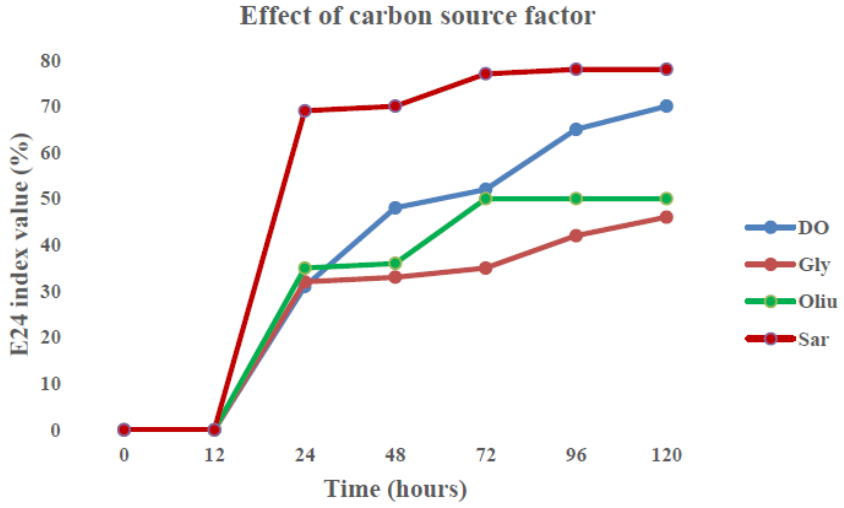


***Figure 4.** Effect of carbon source on the biosurfactant producing capacity of B. celere strain*

3.4. Evaluate the effect of biosurfactant on oil decomposition ability

3.4.1. Effect of biosurfactant on the microbial population in drilling mud

The effect of biosurfactant is evaluated through its impact on changing the number of microorganism in drilling mud. When the number of cell increases, it means that these

strains use oil as a source of nutrition and leading to reduce the amount of oil. This is a way to treat oil pollution by biostimulation method - taking the local biome as the center of the pollution treatment process [4]. The variation in the number of bacteria cell is shown in Table 1.

Table 1. Effect of biosurfactant on the number of bacteria cell in drilling mud

Volume of biosurfactant added (ml)	Number of bacteria cell (CFU/ml)	
	Before	After
0 ml	4.27×10^3	6.2×10^2
1ml	4.27×10^3	1.7×10^6
2ml	4.27×10^3	7.8×10^8
3ml	4.27×10^3	1.1×10^9

The results showed that the biosurfactant increased the number of bacteria cells in oil-contaminated drilling mud. The number of microorganisms in shaking culture flasks grow and change the medium colour from white to brown, yellow brown or red brown. Oil decomposes to form a solution and dissolves in the culture medium. There are cases where bacteria thrive and form a membrane between the oil and water phases. The number of bacteria cells on average increased from 10^3 to 10^9 cells/ml. When adding 2ml to 3ml biosurfactant, the number of bacteria cells increase significantly. The number of cells also increased greatly by 70.9% and up to 10^9 CFU/ml when adding 2 and 3 ml biosurfactant, respectively. In the control sample (without adding biosurfactant), the number of bacteria cells decreased by nearly 10 times. In addition, the number of M150 strain cells in all shaking culture flasks containing DO, glycerin, and olive oil grew well. The analysis results showed that biosurfactant of strain M150 has a stimulating effect on microorganism population in drilling mud. The number of cells increases the most obvious when the amount of biosurfactant added is 3 ml.

3.4.2. Effect of biosurfactant on viscosity and surface tension of oil

The effect of biosurfactant on viscosity and surface tension of oil is shown in Table 2. The analysis result showed that both the surface tension and viscosity of the experimental sample adding biosurfactant decreased compared to the control sample without biosurfactant.

Table 2. Results of measuring viscosity and surface tension of bacterial fluid samples

Type of oil	Samples	Temperature (25^0C)	
		Tension (mN/m)	Viscosity (cst)
DO	Control	36.5	0.93
	Add biosurfactant	29.7	0.91
Saraline	Control	29.2	0.92
	Add biosurfactant	27.6	0.91

3.4.3. Effect of biosurfactant on the ability to decompose oil in drilling mud

Conduct the experiments with M150 strain in mineral medium Gost 1% NaCl, supplemented with 5% DO and saraline oil. The bacterial culture samples after 5 days were analyzed on a gas chromatograph (Gas Chromatography - Shimazdu). The results are shown in table 3.

Table 3. Effects of biosurfactant on the composition of DO and saraline oil

No.	Before	After	Amount of oil used (%)
DO oil (g/50ml)	1.95 g	1.0231 g	82.6
Saraline oil (g/50ml)	2.075 g	0.6775 g	74.5

The result in Table 3 showed that the research strain used 82.6% and 75.4% saraline and DO oil, respectively. The obtained data demonstrated that the research strain can create biosurfactant and decompose oil in drilling mud within 5 days and the maximum decomposition efficiency reached 82.6%.

Our results have a number of similarities with Shah et al., (2016), Barakat et al., (2017), Joshi et al., (2014) findings [6-8]. Shah et al., (2016) showed that the biossurfactant produced by *Pseudomonas aeruginosa* can decompose the crude oil [6]. In the medium supplemented with 1% crude oil (TAPIS), the emulsification index E24 of Rhamnolipids to TAPIS was maximum value of 42% [6]. The isolated result of Barakat et al., (2017) in Shalateen, Red Sea, Egypt showed that two strain *Bacillus amyloliquefaciens* SH20 and *Bacillus thuringiensis* SH24 can decomposed oil with the highest emulsification index (E24) 57 and 56%, respectively [7]. The fact that biosurfactant can reduce surface tension of both hydrocarbon mixtures and aqueous solutions [8]. Therefore, Joshi et al., (2014) indicated that microbial strain *Pseudomonas stutzeri* isolation from soil samples at petrol pumps and garages in Kalyan also have able produced biosurfactant [8]. The different microbial strains have the biosurfactant-producing capacity and degrading oil differently. The source of initial oil used in many studies is also very diverse, but mainly focus to use DO oil, saraline for lubricating the drill bit or increasing the pressure to push the oil. Thefore, the biosurfactant of *Brevebacterium cerere* strain is the potential compound for drilling mud treatment and oil pollution treatment.

4. CONCLUSION

This study determined that the condition for the highest biosurfactant production of *Brevebacterium cerere* strain is pH = 7.5; temperature 30°C; NaCl concentration is 1%, the carbon source is saraline and DO oil. The analysis result of the remaining oil content showed that the biosurfactant of strain M150 decomposed 82.6% and 74.5% of saraline and DO oil, respectively. The biosurfactant of this strain also decreased the surface tension and viscosity of oil in both experimental and the control sample. Simultaneously, this subtance also affects the biological community in drilling mud samples. These results indicated that the biosurfactants produced by *Brevebacterium celere* strain can be applied in drilling mud treatment and environmental pollution treatment.

REFERENCES

1. BH. Diem, DTT. Phuong, and TP. Hung, *Environment protection in oil and gas exploration and production activities, offshore Vietnam*, Journal of oil and gas, 12, 2022, pp. 45 – 49.

2. LT. Hien, *Lecture for master's in petroleum microbiology*, Science and Technology Publishing House, 1997.

3. JD. Desai, and IM. Banat, *Microbial production of surfactants and their commercial potential*. Microbiol Mol Biol R, 61(1), 1997, pp. 47-64.

4. M. S. Bami, P. Khazaeli, H. Forootanfar, G. Dehghannoudeh, and M. Ohadi, *Isolation and identification of biosurfactant producing bacterial strain from saline soil samples in Iran: Evaluation of factors on biosurfactant production*, Jundishapur Journal of Natural Pharmaceutical Products, 15 (4), 2020, pp. e96798.

5. LT. Hien, DV. Thang, NT. An, TC. Van, DT. Hoa, *Biosurfactant-producing bacteria isolated from Nha Trang sea*, Journal of Marine Science and Technology, 2, 2004, pp. 2- 13.

6. MUH. Shah, M. Sivapragasam, M. Moniruzzaman, and SB. Yusup, *A comparison of recovery methods of rhamnolipids produced by Pseudomonas aeruginosa*, Procedia Engineering, 148, 2016, pp. 494-500

7. KM. Barakat, SWM. Hassan, and O. M. Darwesh, *Biosurfactant production by haloalkaliphilic Bacillus strains isolated from red sea, Egypt*, The Egyptian Journal of Aquatic Research, 43(3), 2017, pp. 205-211.

8. PA. Joshi, and DB. Shekhawat, *Screening and isolation of biosurfactant producing bacteria from petroleum contaminated soil*, European Journal of Experimental Biology, 4(4), 2014, pp. 164-169.

PROCEEDINGS OF THE SIXTH INTERNATIONAL SCIENTIFIC CONFERENCE

EARTH AND ENVIRONMENTAL SCIENCES, MINING FOR DIGITAL TRANSFORMATION, GREEN DEVELOPMENT AND RESPONSE TO GLOBAL CHANGE

GREEN EME 2023

Chịu trách nhiệm xuất bản
Giám đốc - Tổng Biên tập
Bùi Minh Cường

Chịu trách nhiệm nội dung: TS. NGUYỄN HUY TIẾN
Biên tập và sửa bản in: TS. NGUYỄN HUY TIẾN
Họa sỹ bìa: NGỌC ANH

NHÀ XUẤT BẢN KHOA HỌC VÀ KỸ THUẬT
70 Trần Hưng Đạo - Hoàn Kiếm - Hà Nội

CHI NHÁNH NHÀ XUẤT BẢN KHOA HỌC VÀ KỸ THUẬT
28 Đồng Khởi - Quận 1 - TP. Hồ Chí Minh

Liên kết xuất bản: Công ty Cổ phần in và dịch vụ văn phòng Tân Đại Việt

---

In 100 bản, khổ 17x24cm, in tại Tại Công ty Cổ phần in và dịch vụ văn phòng Tân Đại Việt
Địa chỉ: 16 Đường Chùa Láng, P. Láng Thượng, Q. Đống Đa, Hà Nội
Số ĐKXB: 4525-2023/CXBIPH/01-253/KHKT
Quyết định xuất bản số: 196/QĐ-NXBKHKT, ngày 11 tháng 12 năm 2023
ISBN: 978-604-67-2826-9
In xong và nộp lưu chiểu năm 2023.